RNA Technologies

Volker A. Erdmann
Stefan Jurga
Jan Barciszewski *Editors*

RNA and DNA Diagnostics

Springer

RNA Technologies

More information about this series at
http://www.springer.com/series/8619

Volker A. Erdmann • Stefan Jurga •
Jan Barciszewski
Editors

RNA and DNA Diagnostics

Springer

Editors
Volker A. Erdmann
Free University of Berlin
Institute of Chemistry/Biochemistry
Thielallee 63, Berlin
Germany

Jan Barciszewski
Institute of Bioorganic Chemistry Polish
Academy of Sciences
Z. Noskowskiego 12/14 Poznań
Poland

Stefan Jurga
Nanobiomedical Center
Adam Mickiewicz University
Umultowska 85 Poznań, Poland

ISSN 2197-9731 ISSN 2197-9758 (electronic)
RNA Technologies
ISBN 978-3-319-17304-7 ISBN 978-3-319-17305-4 (eBook)
DOI 10.1007/978-3-319-17305-4

Library of Congress Control Number: 2015940998

Springer Cham Heidelberg New York Dordrecht London

Printed on acid-free paper

Springer International Publishing AG Switzerland is part of Springer Science+Business Media (www.springer.com)

Preface

The cell is the fundamental unit of life, composed of a large array of biomolecules: DNA, RNA, proteins, sugars, lipids, and small compounds which altogether define its biochemical properties and biological functions. Each cell is able to respond to its environment or stress and to communicate with other cells to create tissues, organs, and whole organisms. The question is how do these cellular constituents assemble to yield a cell with the ability to carry out different functions in response to its surroundings, which give the property of life? A detailed understanding of the chemistry of life, as well as the experimental tools to probe pathways and to restore deregulated states in human pathology, will stimulate their diagnosis and treatment. The basic units of inheritance (genes) are composed of nucleic acids. Even though nucleic acids represent less than 5 % of the dry mass of a typical cell, nucleic acids control for example the production of proteins that make up approximately 75 % of the dry mass. The information encoded in the nucleic acids influences when and how cells respond to environmental conditions through the production of proteins.

The structure, function, and reactivity of DNA and RNA are central to molecular biology and are crucial for the understanding of the complex biological processes. The central feature of nucleic acid technologies is the programmability of nucleic acid structures by Watson−Crick base pairs, which are responsible for the information content of all living systems. Nucleic acids may store additional information, like in epigenetics, for protein function. DNA and RNA, as well as their derivatives and analogues, can be used for a variety of applications ranging from gene regulation (RNA interference, RNA catalysis, antisense approach, etc.), the modulation of protein function by employment of aptamers, and to molecular diagnostics. These nucleic acid secondary and tertiary structure recognition interactions are reliable, reversible, and responsive, showing low error rates.

Since the early 1970s, the use of nucleic acid sequences for specific diagnostic applications has followed a dramatic development. Early methods for restriction enzyme digestion, as well as reverse transcription, were followed by Southern, Northern, and dot blotting, as well as DNA sequencing. The discovery of the

polymerase chain reaction (PCR) in 1985 and easy laboratory manipulation of sufficient quantities of DNA for diagnostics, as well as the development of real-time quantitative PCR and oligonucleotide microarrays, resulted in an explosion of knowledge in the field of molecular and cellular biology. This advancement continues with the development of methods for direct nucleic acid target detection from samples without in vitro amplification and enhanced transduction elements for improved sensitivity of nucleic acid detection. The existence and success of the field is clearly a consequence of the convenient availability of specific sequences of nucleic acids, owing to the development of their chemical synthesis. The binding of a probe molecule to the complementary nucleic acid target is the molecular basis for most of the current methods in DNA- and RNA-based diagnostics. With these tools one can detect, for example, the presence of a pathogen either by directly probing the presence of DNA or RNA nucleic acids in the host or by first amplifying the pathogen DNA or RNA. In the case of infectious diseases, nucleic acid-based diagnostics detect DNA or RNA from the infecting organism, but for noninfectious diseases, nucleic acid-based diagnostics may be used to detect a specific gene or the expression of disease associated genes. Nucleic acid-based diagnostics have an advantage over immunoassays in that they can detect genetic markers, such as those for drug resistance in bacteria, beyond detecting the presence of a pathogen. However, by infectious organisms that are able to hide in host organs, or other areas of the body, from which the extraction of an infected sample is difficult, nucleic acid-based diagnostics may fail to detect such a disease. Currently, nucleic acid-based diagnostics are used to detect a wide range of conditions, including cancer, genetic markers associated with a high risk of cancer, leishmaniosis, tuberculosis, HIV, genetic diseases (e.g., cystic fibrosis), and a variety of infectious diseases, including anthrax, *Clostridium difficile* (a common hospital acquired bacterial infection), chlamydia, and gonorrhea. Currently, there are many new and intelligent technologies under development for the specific detection of the nucleic acid sequences. These include biosensors, nanopores, and next-generation sequencing technologies. In the future, these technologies will move nucleic acid diagnostics away from centralized laboratory facilities and into locations such as emergency rooms, physician's offices, and even into the home. These technical developments will also provide systems for integrated information transfer from one location to another, allowing remote diagnosis by clinicians. Thus, DNA and RNA targeted analyses play an important role and are used in various clinical settings. There is no doubt that the field is approaching a certain level of maturity, but there are still many fundamental questions, which remain to be answered before its value to molecular medicine can be fully exploited.

In this book, one can see contributions showing the state of the art in nucleic acid diagnostics, its application, clinical practice, and the emerging technologies in the field. They discuss future trends and expected advances in the field of molecular medicine. The approaches presented and discussed are based on specific properties of nucleic acids as for example electrochemical features, fluorescence of different

nucleic acid analogues, aptamers, microchips, single-nucleotide strategies, and structural propensity of RNA and DNA.

Thus, in this new volume we will find most interesting contributions, which discuss challenges in translating nucleic acid diagnostic approaches to clinical applications.

Berlin, Germany — Volker A. Erdmann
Poznań, Poland — Stefan Jurga
Poznań, Poland — Jan Barciszewski

Contents

Electrochemical Biosensors for miRNA Detection

Diego Voccia and Ilaria Palchetti

Contents

Abstract MicroRNAs (miRNAs) are intensely studied as candidates for diagnostic and prognostic biomarkers. They are naturally occurring small RNAs (approximately 22 nucleotides in length) that act as regulators of protein translation. Because many diseases are caused by the misregulated activity of proteins, miRNAs have been implicated in a number of diseases including a broad range of cancers, heart disease, and immunological and neurological diseases. A great deal of effort, therefore, has been devoted to developing analytical methods for miRNA analysis. The consideration when selecting existing or designing new methods for miRNA analysis includes sensitivity and multiplexing capability without PCR. In this chapter, novel electrochemical strategies for miRNA detection and quantification will be reviewed.

Keywords Electrochemical biosensors • miRNA • Electrodes • Cancer • Biomarker • Limit of detection

D. Voccia • I. Palchetti (✉)
Dipartimento di Chimica "Ugo Schiff", Università degli Studi di Firenze, Via della Lastruccia 3, 50019 Sesto Fiorentino (Fi), Italy
e-mail: ilaria.palchetti@unifi.it

V.A. Erdmann et al. (eds.), *RNA and DNA Diagnostics*, RNA Technologies,
DOI 10.1007/978-3-319-17305-4_1

1 Introduction

In 1993, Victor Ambros and Gary Ruvkun reported that a small RNA, of about 20 nucleotides long, regulated another gene by base pairing to the other gene's mRNAs (Lee et al. 1993; Wightman et al. 1993). The gene for the small RNA was lin-4, and it was turning off the lin-14 gene after the mRNA was made to control developmental timing in the soil nematode *Caenorhabditis elegans*. This lin-4 small RNA was the first microRNA (miRNA) discovered, although it was not called that at the time. miRNA lin-4 was considered an anomaly until 2000, when Ruvkun group discovered another small RNA, called let-7 (Reinhart et al. 2000), which is complementary to parts of the 3′ untranslated regions of the heterochronic genes lin-14, lin-28, lin-41, lin-42, and daf-12, indicating that expression of these genes may be directly controlled by let-7. Moreover, the same lab identified let-7 homologues in many vertebrate species including humans (Pasquinelli et al. 2000), demonstrating that miRNAs are evolutionarily conserved across many species and are often ubiquitously expressed.

Since that time, it has become clear that this class of small noncoding RNAs plays an important role in many biological processes as modulator of gene expression.

miRNAs have a peculiar mechanism of action and biogenesis. The main biological role of miRNAs is to perform gene regulation either directly through cleavage of mRNA or indirectly through translational repression. In either case, miRNA hybridizes with its target mRNA strand at the mRNA's 3′ untranslated region. Initially, miRNA is part of a much larger piece of RNA with stem–loop structures, which may contain multiple potential miRNAs as reported in Fig. 1. This long strand of RNA, known as primary miRNA (pri-miRNA), is transcribed by RNA polymerase II in the nucleus of the cell (Lee et al. 2002). Next, the pri-miRNA is cleaved by an RNase III endonuclease known as Drosha, which cuts the RNA into an approximately 60-base stem–loop structure (Lee et al. 2003). This piece of RNA is known as pre-miRNA. The pre-miRNA is then exported to the cytoplasm via the carrier protein exportin-5 (Exp-5). Once the Exp-5 has mediated pre-miRNA delivery into the cytoplasm, the pre-miRNA separates from the Exp-5 and is cleaved by an RNase III enzyme known as Dicer, which results in the mature form of miRNA (Lund et al. 2004).

An abnormal miRNA expression (overexpression or downexpression) could be linked to many diseases, like cardiovascular pathologies (van Rooij et al. 2006), cancer (Calin and Croce 2006), and immunological (Pauley et al. 2009) and neurological (Hébert and De Strooper 2009) diseases. For instance, in cancer, miRNAs are implicated in each one of the main essential features of cancer progression (from cell proliferation to inhibition of cell apoptosis), and in the same cancer type, different miRNAs can be up- or downregulated with respect to a basal level.

The first evidence of involvement of miRNAs in human cancer came from molecular studies which revealed that two miRNAs, mir-15 and mir-16, were

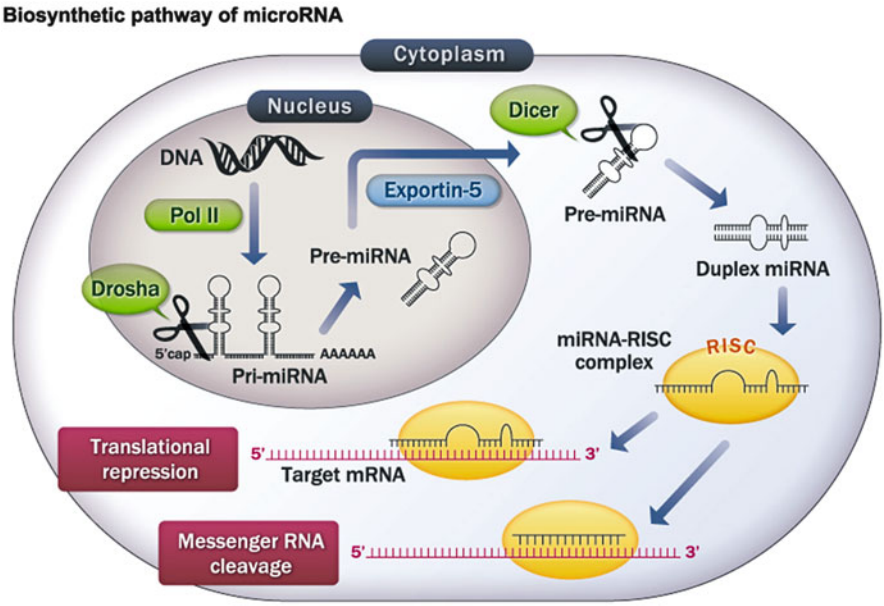

Fig. 1 Biosynthetic pathway of miRNA [Reproduced from Nohata et al. (2012)]

involved in chronic lymphocytic leukemias (CLL) (Calin et al. 2002). Particularly, these first studies were performed in an attempt to identify tumor suppressors at chromosome 13q14, frequently deleted in CLL. Indeed, as demonstrated later by the same group and other groups, chromosomal regions encompassing microRNAs involved in the negative regulation of a transcript encoding a known tumor suppressor gene can be amplified in cancer development. This amplification would result in the increased expression of the microRNA and consequent silencing of the tumor suppressor gene. Conversely, microRNAs repressing oncogenes are often located in fragile loci, where deletions or mutations can occur and result in reduced microRNA levels and overexpression of the target oncogene. microRNAs playing an oncogenic role by targeting oncosuppressor molecules are called oncomiRs; instead, microRNAs playing an oncosuppressive role by targeting oncogenes are tumor suppressor miRNAs.

In Table 1, some examples of miRNA expression deregulated in human cancer are reported. These deregulated miRNAs may function as either tumor suppressors or oncogenes by targeting each one of these features.

miRNA profiles can distinguish not only between normal and cancerous tissue and identify tissues of origin, but they can also discriminate different subtypes of a particular cancer or even specific oncogenic abnormalities. Gene expression profiling has already demonstrated its effectiveness at subtyping various cancers. However, miRNA profiles are equally discriminatory and can even be more informative, as expression changes can provide insights into the multitude of gene permutations observed in various cancer subtypes (Iorio and Croce 2012).

Table 1 Tumor suppressor and oncogene microRNAs

miRNA	Tumor associated	Type of targeting
miR-15/16	Chronic lymphocytic leukemia (Aqeilan et al. 2009)	Tumor suppressor gene
miR-17/92	Colon (Tsuchida et al. 2011)	Oncogene
miR-21	Cholangiocarcinoma (Lu et al. 2014)	Oncogene
miR-34	Gastric cancer (Ji et al. 2008)	Tumor suppressor gene
miR-155	Breast cancer (Jiang et al. 2010)	Oncogene
miR-200 family	Bladder cancer (Wiklund et al. 2011)	Tumor suppressor gene
miR-222/221	Glioblastoma (Zhang et al. 2010), prostate (Galardi et al. 2007), and thyroid carcinoma (Visone et al. 2007)	Oncogene

For all these reasons and considering that they are more stable than long mRNA, miRNAs are intensely studied as candidates for diagnostic, prognostic, and predictive tumor markers.

2 miRNA as Tumor Marker

Biological markers, better known as "biomarkers," refer to medical signs that are objective indications of a medical state and that are possible to measure accurately and reproducibly. It is important to note that medical signs are in contrast with symptoms that are instead indications of health or illness perceived by patients. There are several definitions of biomarkers in the literature, but in 1998, the National Institutes of Health Biomarkers Definitions Working Group defined a biomarker as "a characteristic that is objectively measured and evaluated as an indicator of normal biological processes, pathogenic processes, or pharmacologic responses to a therapeutic intervention" (Atkinson et al. 2001).

A biomarker associated with cancer is commonly defined *tumor or cancer marker*. Indeed, historically, the most important cancer diagnostic and prognostic indicators are morphological and histological characteristics of tumors. The use of tumor markers that produce "molecular signatures" provides the potential to identify a tumor and to tailor medical care, both at tumor and patient levels. Tumor markers are substances that are produced by malignant cells and that can be determined in body fluids or tissues. In order to evaluate a good candidate as tumor marker, it is important to know its sensitivity and specificity. Moreover, a major issue, in cancer, is clearly represented by the need of markers for an early diagnosis. This issue is extremely important considering that survival and prognosis of patients depend on the stage of the tumor at the time of detection, with an early diagnosis usually been associated with the best prognosis.

microRNAs have revealed a great potential as tumor markers and especially as early diagnosis markers. Indeed, they are able to discriminate tumor origins, subtypes, oncogenic mutations, and cancer predisposition. Moreover, since miRNAs regulate the most important cellular processes, they can be useful to predict also cancer prognosis and/or response to specific therapies. Furthermore, the presence of miRNAs not only in body cells and tissues but also in body fluids (circulating miRNAs) may be an important feature for minimally invasive analysis (Lawrie et al. 2008; Cortez et al. 2011). However, these circulating miRNAs are present at very low level and in some cases are secreted from cells packaged in microparticles (exosomes, microvesicles, and apoptotic bodies) or by their association with RNA-binding proteins, including Argonaute 2 or lipoprotein complexes such as high-density lipoprotein (HDL) (Di Leva et al. 2014). For these reasons, proper extraction procedures have to be performed. Moreover, the composition of these fluids is quite dissimilar, which implies that isolation methods cannot be directly transposed from one tissue/fluid to another (Moldovan et al. 2014). Obviously, these findings complicate the detection of miRNA in biological fluids.

Thus, to use miRNAs as reliable diagnostic, predictive, or prognostic tumor markers, the development or optimization of efficient, sensitive, and reproducible detection methods, including robust sample extraction selection or preparation procedure, is of primary importance (Iorio and Croce 2012).

3 miRNA Detection

Actually, there are different methods for the detection of miRNAs, each of them with their own unique advantages and disadvantages. Many detection methods rely on hybridization event with a complementary sequence. The hybridization event could occur either with solid-phase approach (a capture probe is adsorbed or bound to a solid surface for hybridization to the target) or with a solution-phase approach (target hybridization occurs in solution). Solution-phase methods often result in much more rapid analysis times, while solid-phase methods, in general, are more appropriate for high-throughput analysis. Once the hybridization event occurs, it is necessary to translate the event in something that is possible to detect.

Northern blotting is the most widely used miRNA detection method because it is generally a readily available technology for laboratories and does not require special equipment and technical knowledge. In general, target RNA runs on an electrophoresis gel, and then it is transferred, by blotting, onto a membrane to which the RNA is covalently bound. Finally, the membrane is incubated with a labeled probe, which is a single-stranded DNA, forming a duplex with its target. The hybrid can be revealed by a radioactive or by an enzyme label (e.g., alkaline phosphatase or horseradish peroxidase). However, this method is time-consuming and semi-quantitative and is characterized by a low sensitivity. In order to increase sensitivity, locked nucleic acid (LNA)-modified oligonucleotide probes were used to enhance the efficiency of hybridization (Válóczi et al. 2004).

The use of microarray is another classical detection method and requires immobilized oligonucleotides on a support with the same sequence as the target miRNA in order to detect cDNA from a sample (Barad et al. 2004). The cDNA is produced via reverse transcription from a sample's RNA using fluorescent- or enzyme-labeled primers. Recently, quantum dots (QDs) as fluorescent labels have been introduced because of the high extinction coefficient and high quantum yield, which should dramatically increase the sensitivity for microarray detection (Liang et al. 2005). Even if microarrays can analyze thousands of samples in a day, they are very expensive to fabricate. Thus, the high cost limits the wide applications of miRNAs microarray, especially in clinical diagnosis.

Another standard method of detection is the quantitative reverse transcriptase polymerase chain reaction (RT-PCR), which can detect miRNA in real time and is one of the most used due to the inherent sensitivity and reliability. Because of their small size (similarly to the primers), miRNA detection based on PCR is complicated (i.e., ligation is needed), has low throughput, and is time-consuming.

A great deal of effort, therefore, has been devoted to developing new analytical methods for miRNA analysis that possess appropriate sensitivity, appropriate dynamic range, and multiplexing capability without PCR.

Alternative methods include bioassays and biosensor based on surface-enhanced Raman scattering (SERS), surface plasmon resonance (SPR), surface plasmon resonance imaging, fluorescence, and bioluminescence-based techniques (Cissell et al. 2008). However, many of these methods are laborious and require the use of a well-equipped laboratory with specialized and well-trained personnel and are neither feasible for routine determination of miRNAs nor applicable for point-of-care (POC) testing.

Electrochemical biosensors are emerging options for miRNA detection. In comparison with other techniques, like optical methods, electrochemistry is considered as one of the most appealing techniques in terms of cost, ease of operation, and automation.

4 Electrochemical Biosensors for the Detection of miRNA

Electrochemical biosensors have emerged as particularly attractive options for miRNA detection in terms of simplicity of use, low assay time, and a small amount of sample required. The role of electrochemical biosensors for miRNAs detection has been reviewed recently (Hamidi-Asl et al. 2013; Campuzano et al. 2014a; Teo et al. 2014). In this section, the definition of electrochemical biosensors will be introduced, and examples of miRNA detection using electrochemical biosensor will be discussed.

4.1 Electrochemical Biosensor: Definition and Classification

According to the International Union of Pure and Applied Chemistry (IUPAC), an electrochemical biosensor is "a self-contained integrated device, which is capable of providing specific quantitative or semi-quantitative analytical information using a biological recognition element (biochemical receptor) which is retained in direct spatial contact with an electrochemical transduction element" (Thévenot et al. 2001). There are two classes of different biosensors classified according to the biologically active part: catalytic and affinity biosensors (Ronkainen et al. 2010). Catalytic biosensors are based on biological catalysts such as enzymes, cells, microorganisms, or biomimetic catalysts, which promote a specific reaction with the target analyte to produce a species to which the electrode responds (Cammann 1977). Because of their immediate application in clinical tests and ease of preparation, these biosensors have been very popular, with thousands of articles published. In particular, glucose oxidase-based biosensors have been commercialized for testing glucose levels in blood since decades (Luong et al. 2008). Affinity biosensors instead are based on biomolecules able to selectively and reversibly bind specific ligands (Leech 1994). In this way, it is possible to monitor and quantify the binding of antibodies to antigens, cell receptors to their ligands, and nucleic acid (DNA, RNA) with a complementary sequence. Biosensors based on antibodies and antigens, commonly known as immunosensors, have been the most investigated due to their high affinity, versatility, and commercial availability of the biological elements. However, the use of antibodies in biosensing has some limitations (Jayasena 1999): antibodies are labile, and the identification and selection of rare antibodies are laborious. In order to overcome these limitations, new biorecognition elements are under study, such as aptamers (Mascini et al. 2012), which offer new perspectives for the realization of affinity biosensors with higher selectivity, sensitivity, and stability.

An important class of affinity biosensors is genosensors (Labuda et al. 2010), which employ an oligonucleotide sequence as biorecognition element. In this case, recognition derives from complementary base coupling (hybridization).

In particular, genosensors are analytical devices that result from the integration of a sequence-specific probe, usually a short synthetic DNA oligonucleotide (Laschi et al. 2009; Ngo et al. 2013) and a signal transducer. The probe, immobilized onto the transducer surface, acts as the biorecognition molecule and recognizes the target DNA (or RNA), while the transducer is the component that converts the biorecognition event into a measurable signal (Laschi et al. 2006).

4.2 Electrochemical Genosensors: Key Aspects

Electrochemical genosensors monitor the reaction among capture probes with its target nucleic acid (Labuda et al. 2010). The reaction being monitored

electrochemically typically generates a measurable current (amperometry, voltammetry) and a measurable charge accumulation or potential (potentiometry) or alters the conductive properties of the medium between electrodes (conductometry). The use of electrochemical impedance spectroscopy (EIS) by monitoring both resistance and reactance in the biosensor is also becoming more common.

Amperometry is based on the application of a constant potential promoting a redox reaction, while in voltammetry, current is measured upon varying the potential in a proper range. In both techniques, the resulting current is proportional to the bulk concentration of electroactive species (Zanardi et al. 2012). Potentiometry measures the accumulation of a charge or a potential at the working electrode (usually known as indicator electrode) compared to the reference electrode when zero or no significant current flows between them. In other words, potentiometry provides information about the ion activity in an electrochemical reaction. Conductometric detection monitors changes in the electrical conductivity of the sample solution, as the composition of the solution changes in the course of the chemical reaction. EIS measures the resistive and capacitive properties of electrode materials upon perturbation of a system by a small amplitude sinusoidal ac excitation signal typically of 2–10 mV. The frequency is varied over a wide range to obtain the impedance spectrum. The in-phase and out-of-phase current responses are then determined to obtain the resistive and capacitive components of impedance, respectively. Impedance methods are powerful because they are capable of sampling electron transfer at high frequency and mass transfer at low frequency. Typically, this technique is used for the direct monitoring of the changes in conductivity or capacitance of an electrode as a result of the immobilization of DNA/RNA duplex, onto the electrode surface. In photoelectrochemical measurements, light is used to excite active species on the electrode, and photocurrent is obtained as the detection signal. A photoelectrochemistry-based analytical method has the advantages of both optical and electrochemical methods. Due to its separate source for excitation and detection, it is potentially very sensitive. As an additional benefit in comparison with all optical detection methods, such as fluorescence, that have to use complex and expensive optical imaging devices and sophisticated image recognition software, the low cost inherent to electronic detection makes the photoelectrochemical instrumentation simple and low cost (Bard and Stratmann 2002; Zhang et al. 2013). Despite the advantages mentioned above, only rather limited photoelectrochemical biosensors have been reported for nucleic acid determination in the past decade. The emergence of nanomaterials with enhanced photoelectrochemical properties (Derry et al. 2013; Chuang et al. 2014; Mettenbörger et al. 2014; Shon et al. 2014) shows great potential in the field of photoelectrochemical biosensors (Wang et al. 2012; Wenjuan et al. 2013; Liu et al. 2014c; Zhang et al. 2014b).

The probe immobilization step plays an important role in determining the overall performance of a genosensor. Both physical and chemical methods have been developed for immobilizing the capture probe on the sensor surface. Physical strategies comprise adsorption or entrapment in permeable membranes, while chemical methods rely on the covalent binding or cross-linking of reactive residues

present within the biomolecule such as amine, carboxylic, aldehydic, or thiolic groups. The probes have to be immobilized in a way that retains their stability, reactivity, and accessibility to target analyte and optimal orientation. Sensor surface coverage by DNA probes is also important in minimizing nonspecific binding.

The nature and the composition of the working electrode surface become important in order to choose the better immobilization procedure for a specific application. The achievement of high sensitivity and selectivity requires maximization of the hybridization efficiency and minimization of nonspecific adsorption, respectively. Several kinds of electrode surface have been investigated as electrochemical transducers in genosensor development: glassy carbon (Liu et al. 2014a), screen-printed carbon (Bettazzi et al. 2013), screen-printed gold (Farabullini et al. 2007; Bettazzi et al. 2008; Voccia et al. 2015), gold (Yu et al. 2014), and ITO electrodes (Patel et al. 2013). Generally, the use of disposable electrodes that avoid the regeneration step appears to be the most promising approach (Laschi et al. 2006). Depending on the electrode surface, the immobilization of the probe could occur in different ways. One of the most simple methods of immobilization on carbon-based electrodes is adsorption at controlled potential. The biggest advantage of this method is the possibility to avoid capture probe modifications. A pretreatment of the carbon surface is necessary in order to enhance the immobilization of the probe (Wang et al. 1995). However, in this immobilization procedure, washing steps must be performed carefully in order to avoid desorption. Moreover, immobilized DNA probe uses bases to interact with the surface, resulting not totally accessible for hybridization and, consequently, reducing hybridization efficiency. Another probe immobilization method with carbon-based electrodes requires the use of N-hydroxysulfosuccinimide (NHS) with ethyl(dimethylaminopropyl) carbodiimide (EDC) to activate carboxylate groups on the electrode surface in order to covalently immobilize single-stranded DNA probe (Millan and Mikkelsen 1993). The high stability of covalent bound allows the regeneration of the probe-modified surface denaturating the hybrid formed for the detection.

The use of gold electrodes for genosensor development is widely used. Residual contaminants on bare gold can be removed by repeated voltammetry cycling in diluted H_2SO_4 (Hashimoto et al. 1994) until stable voltammograms are obtained. Self-assembly provides one of the most elegant approaches to obtain well-defined and organized surfaces that can be an excellent platform for biosensor applications. One of the widely used approaches in literature involves the direct chemisorption of thiol-modified DNA probes onto gold surfaces. The self-assembly of thiolated molecules was characterized at the beginning of the 1980s (Nuzzo and Allara 1983). Sulfur-based molecules coordinate very strongly onto a variety of metals, but gold is the most favored, because it is reasonably inert. The assumed reaction between a thiolate compound and a gold substrate is:

$$\mathrm{RSH} + \mathrm{Au} \leftrightarrow \mathrm{RS\text{-}Au} + \mathrm{e}^- + \mathrm{H}^+$$

Chemisorption of thiolated single-stranded DNA (HS-ssDNA) probes onto gold substrates was extensively characterized using X-ray photoelectron spectroscopy (XPS), ellipsometry, ^{32}P-radiolabeling, neutron reflectivity, and electrochemical methods (Herne and Tarlov 1997; Levicky et al. 1998; Steel et al. 1998). The ionic strength of HS-ssDNA solutions was found to have an effect on surface coverage, with chemisorption greatly enhanced at high salt concentrations. The authors hypothesized that intermolecular electrostatic repulsion between neighboring DNA strands was minimized under the high ionic strength conditions, as the charged strands were better electrostatically shielded. More precise control over surface coverage and probe availability was achieved by creating mixed monolayers of the HS-ssDNA and a spacer thiol, like mercaptohexanol (MCH), by a two-step method, where first the gold substrate was exposed to a micromolar solution of HS-ssDNA, followed by exposure to a millimolar solution of MCH. The posttreatment with MCH allows DNA molecules to "stand up" from an initial disordered layer. Thus, the DNA strand is more accessible for specific hybridization.

As the specificity of the hybridization reaction is essentially dependent on the biorecognition properties of the capture oligonucleotide, the design of the capture probe is undoubtedly one of the most important pre-analytical steps. The probes can be linear oligonucleotides or structured (hairpin) oligonucleotides, which are being used with increasing frequency (Lucarelli et al. 2008; Jin and Grote 2012). The design of linear probes takes great advantage of many commercially available softwares which can design capture oligonucleotides within the hypervariable or highly conserved regions of different genomes after their assembly and alignment. Candidate sequences, usually 18–22 nucleotides in length, are finally tested for theoretical melting temperature (T_m), hairpins, and dimers formation and for homologies using a basic local alignment search tool (BLAST) search (Lucarelli et al. 2008).

The experimental variables affecting the hybridization event at the transducer–solution interface are referred to as stringency, and they generally include hybridization and post-hybridization-washing buffer composition and reaction temperature. When dealing with complex sets of probes, the basic requirement for a functional system is the ability of all the different probes to hybridize their target sequences with high affinity and specificity under the same stringency conditions.

In addition, a number of probes, variable for chemical composition and conformational arrangement, have been used to assemble genosensors. PNAs are DNA mimics in which the nucleobases are attached to a neutral N-(2-aminoethyl)-glycine pseudopeptide backbone. If compared to the conventional oligonucleotide probes, PNAs have appeared particularly interesting for the development of electrochemical genosensing, the main reason being the drastically different electrical characteristics of their molecular backbone. Moreover, some reports described the synthesis and hybridization of a novel nucleotide termed LNA (Obika et al. 1998; Laschi et al. 2009). LNA is a nucleic acid analogue of RNA, in which the furanose ring of the ribose sugar is chemically locked by the introduction of a methylene linkage between 2′-oxygen and 4′-carbon. The covalent bridge effectively "locks"

the ribose in the N-type (3-endo) conformation that is dominant in A-form DNA and RNA. This conformation enhances base stacking and phosphate backbone pre-organization and results in improved affinity for complementary DNA or RNA sequences, with each LNA substitution increasing the melting temperatures (T_m) by as much as 3.0–9.6 °C (Kvaerno and Wengel 1999). LNA bases can be interspersed with DNA bases, allowing binding affinity to be tailored for individual applications. Due to the very high affinity of the LNA molecules, it demonstrates that LNA probes hybridize with very high affinity to perfectly complementary targets and at the same time shows an extraordinary specificity to discriminate the targets that differ by a single base.

As well as specificity, sensitivity is also a key factor in the performances of a biosensor: sensitive detection of specific DNA/RNA sequence on the basis of the hybridization reaction can be achieved by increasing the immobilization amount and controlling over the molecular orientation of the probes. At this purpose, nanomaterials have been increasingly introduced in the fabrication of biosensors in order to increase the immobilization amount of the probe and to magnify the detection signal and lower the detection limit (Patolsky et al. 2006; Nair and Alam 2007; Merkoçi 2007; Zhang et al. 2014a).

Finally, the use of electroactive or enzymatic labels is a strategy widely performed to increase the sensitivity of the device, even if many examples of label-free format have been reported.

4.3 Application to miRNA Detection

Electrochemistry is an emerging technique for miRNA biosensing (Hamidi-Asl et al. 2013; Campuzano et al. 2014a; Teo et al. 2014). Electrochemical detection of miRNA was first reported by Gao and Yang (2006) using electrocatalytic nanoparticle tags (Fig. 2). The assay was based on a direct chemical ligation procedure involving a chemical reaction to tag miRNAs with OsO_2 nanoparticles. The nanoparticles catalyze the oxidation of hydrazine and enhance the detectability of miRNAs, thereby lowering the detection limit to femtomolar level.

Labeling of miRNAs for electrochemical assay is often necessary for miRNA sensitive detection. Gao and Yu reported an miRNA labeling procedure that utilizes a chemical ligation to directly label miRNA, via a covalent bond, to an isoniazid-substituted osmium complex (Gao and Yu 2007b). In a separate attempt, the same group made use of the $Ru(PD)_2Cl_2$ (PD = 1,10-phenanthroline-5,6-dione) electrocatalytic moiety to monitor the oxidation of hydrazine (Gao and Yu 2007a). Both these biosensors were applied to the quantitation of miRNA in total RNA extracted from HeLa cells.

Recently, it has been reported the use of ruthenium oxide (RuO_2) nanoparticle-initiated polymerization of 3,3′-dimethoxybenzidine and miRNA-templated deposition of an insulating poly(3,3′-dimethoxybenzidine) film (Peng and Gao 2011). In a separate work, RuO_2 nanoparticles tagged to target miRNA strands served as a

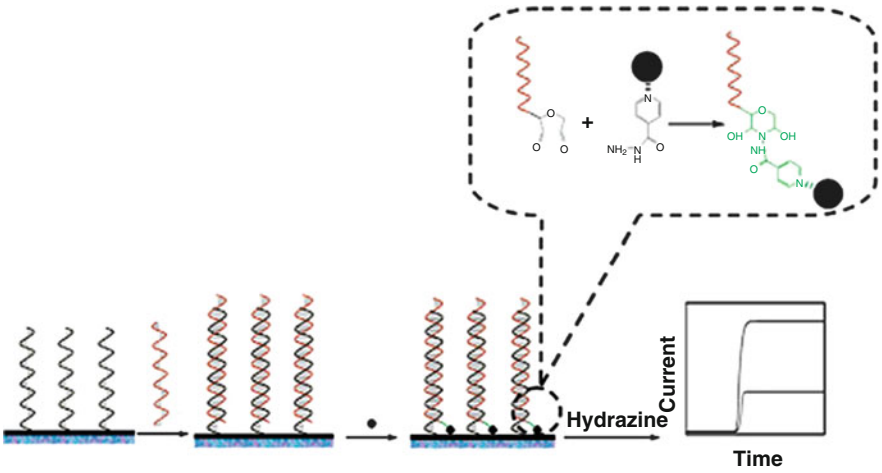

Fig. 2 Schematic illustration of miRNA assay using electrocatalytic OsO_2 nanoparticles [Reprinted with permission from Gao and Yang (2006)]

catalyst for polymerization of aniline, and the hybrid acted as templates for the deposition of polyaniline at the hybridized miRNA strands (Peng et al. 2010).

A biosensor based on palladium (Pd) nanostructured microelectrodes has been developed (Yang et al. 2009). Differential pulse voltammetry (DPV) was used to monitor the electrochemical reduction current of Ru^{3+} accumulated on the electrode surface after hybridization with the target miRNA. The signals observed with this reporter system (Ru^{3+}) are amplified by the inclusion of ferricyanide, which can regenerate Ru^{3+} chemically after its electrochemical reduction. After a 30 min hybridization, the detection of 10 aM of target was reported and the RNA extracted in a panel of RNA samples tested.

Enzymes have been used as label in many biosensor formats. The use of such a label greatly amplifies the hybridization signals, offering considerable promise for ultrasensitive electrochemical detection of DNA hybridization. An esterase as amplifier in a gap hybridization assay format was used (Pöhlmann and Sprinzl 2010). Another strategy for miRNA detection is through the use of an electrochemically activated glucose oxidase (GOx) tag/amplifier (Gao and Peng 2011; Gao 2012). An miRNA biosensor based on triple signal amplification due to the immobilized graphene and dendritic gold nanostructure and subsequent monitoring of the reduction current as a result of the oxidation of hydroquinone by H_2O_2 and horseradish peroxidase was also reported (Yin et al. 2012).

A horseradish peroxidase (HRP)-modified LNA hairpin probe was used by Zhou's group in order to detect miRNA 21 (Zhou et al. 2012). The LNA-incorporated hairpin probe was modified with biotin at its 5′-end and –SH at its 3′-end. After the probe hybridized with target miRNA-21, its loop-and-stem structure was unfolded to force the biotin away from the electrode surface. Through the specific interaction between biotin and streptavidin-HRP, a target can be

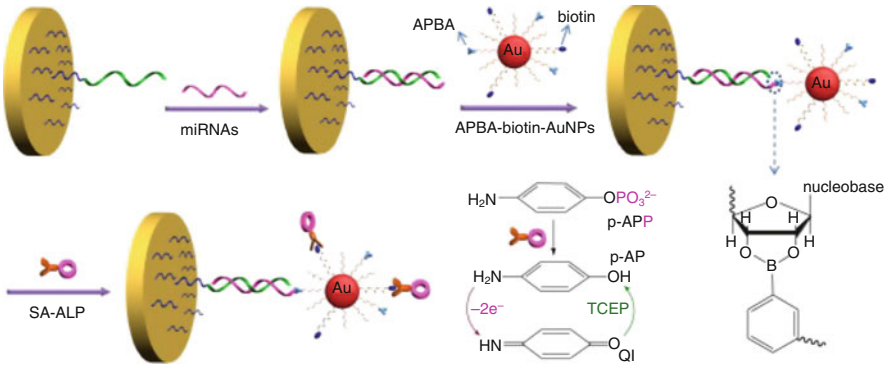

Fig. 3 Schematic representation of the label-free detection of miRNAs based on the triple signal amplification of APBA–biotin–AuNPs, SA-ALP, and the p-AP redox cycling reaction [Reprinted with permission from Liu et al. (2014b)]

quantified by electrochemical detection of the enzymatic product of benzoquinone in the presence of H_2O_2 and hydroquinone. Liu's group designed an enzyme-labeled amperometric genosensor based on streptavidin-conjugated alkaline phosphatase (SA-ALP) (Liu et al. 2014b). The analytical procedure consisted of six steps: (a) immobilization of 3′-thiolated DNA probe, (b) miRNAs were then captured forming a hybrid, (c) cis-diol group of ribose sugar at the end of the miRNAs chain allowed 3-aminophenylboronic acid (APBA)/biotin-modified multifunctional AuNPs (APBA–biotin–AuNPs) to be attached through the formation of a boronate ester covalent bond, (d) biotin in AuNPs facilitated the capture of SA-ALP via the biotin–streptavidin interaction, and (e) addition of the 4-aminophenylphosphate (p-APP) substrate in the presence of the enzyme that produces the conversion from p-APP to p-aminophenol (p-AP) occurred. The resulting p-AP could be cycled by a chemical-reducing reagent after its electrooxidation on the electrode (known as p-AP redox cycling), thus enabling an increase in the anodic current, obtaining a detection limit of 3 fM (Fig. 3).

Bettazzi et al. were the first to report an electrochemical method based on paramagnetic beads and alkaline phosphatase amplification for miRNA detection (Bettazzi et al. 2013).

Label-free detection schemes have been also reported. Such direct detection can be accomplished by monitoring the changes in some electrical parameter generated by the hybridization event. This approach greatly simplifies the sensing protocol, as they eliminate the use of indicators and labeling reaction in the real samples. Moreover, the assay safety is improved, since the indicators are usually toxic or carcinogenic compounds. The first indicator-free scheme in genosensors was described and consisted of the recognition of the hybridization event through the decrease of the guanine peak (that occurs around 1.0 V vs. SCE) of the immobilized probe (Wang et al. 1996). However, this procedure is not applicable in most cases (e.g., for guanine containing targets). This limitation has been overcome by developing a new approach, based on the use of inosine-modified (guanine-free) probes

(Wang et al. 1998; Lucarelli et al. 2002). The inosine still forms a specific base pair with the cytosine residue (Case-Green and Southern 1994), but its oxidation signal is well separated from that of guanine. This approach was also used for miRNA detection (Erdem and Congur 2014). A flat baseline (around +1.0 V) for the probe-modified electrode was observed. The hybrid formation was thus detected through the appearance of the guanine oxidation peak of the target sequence in DPV. A detection limit of 1.4 μM of oligonucleotide target sequence was reported for an indicator-free hybridization biosensor based on magnetic beads coated with streptavidin and screen-printed carbon electrode as transducer surface.

A different label-free approach, based on hybridized miRNA-templated deposition of an insulating polymer film and electrochemical impedance spectroscopic detection, was reported (Gao et al. 2013). The biosensor described in this work was based on an indium tin oxide (ITO)-coated glass slide modified with a DNA morpholino capture probe. After hybridization, the neutral surface of the biosensor is converted to anionic by the hybridized miRNA strands. The deposition of the insulating polymer film, poly(3,3′-dimethoxybenzidine) (PDB), is then carried out by the horseradish peroxidase (HRP)-catalyzed polymerization of 3,3′-dimethoxybenzidine (DB) in the presence of H_2O_2. Electron transfer resistance in the presence of a $Fe(CN)_6^{4-}/Fe(CN)_6^{3-}$ equimolar solution increased with the miRNA concentration and used as analytical signal. This occurs because of negative hybrid nature that interacts with DB producing a high density of monomer on the biosensor surface, and, consequently, this facilitates DB polymerization and the deposition of PDB in the presence of HRP and H_2O_2. A detection limit of 2.0 fM was reported. In 2007, Fan and colleagues introduced a strategy for sensitive and label-free detection of miRNA based on conducting polymer nanowires (Fan et al. 2007). In 2009, an miRNA biosensor based on PNA capture probes immobilized on silicon nanowire was proposed (Zhang et al. 2009). Resistance change measured before and after hybridization correlates directly to concentration of the hybridized target miRNA. A detection limit of 1 fM was obtained.

In addition to the common hybridization-based strategies employed to detect and quantify miRNAs, several peculiar approaches have also been reported in the literature. Recently, a three-mode electrochemical biosensor which exploited the strong and nonsequence-specific binding of a p19 fused dimer protein to double-stranded miRNAs was proposed incorporating three modalities based on hybridization, p19 protein binding, and protein displacement (Labib et al. 2013). Recently, an amperometric magneto-biosensors again involving protein p19 as a selective biorecognition element were reported (Campuzano et al. 2014b; Torrente-Rodríguez et al. 2014). These p19-based magneto-sensors were able to detect 0.04 nm of a synthetic target and endogenous miR-21 (selected as a model for its role in a wide variety of cancers) in total RNA extracted from cancer cells and human breast tumor specimens without PCR amplification and sample preprocessing.

5 Conclusions

The works reviewed show that electrochemical miRNA diagnostic is becoming an increasingly relevant field of application of biosensor technology. Typical levels of circulating miRNAs in serum were estimated to be in the aM to pM range (Hamidi-Asl et al. 2013; Campuzano et al. 2014a; Teo et al. 2014). As reported in this chapter, many electrochemical biosensors developed for miRNA detection allow detection limits in this concentration range to be achieved. Nevertheless, most of the current biosensor-based assays show a lack of reliable validation in clinical samples. A multitude of intriguing detection schemes has been reported. On the contrary, extensive validation in clinical samples is not always reported. To increase the reliability of genosensor in clinical diagnostic, there is the need to ensure robust technical and clinical validation of the developed bioassay and biosensor and preferably within the context of randomized clinical trials in which the detection of the clinical biomarkers by means of a particular methodology can be clearly linked to patient outcome.

Little attention has been also paid to stability of electrochemical genosensors for miRNA detection, which is of the utmost importance in routine and real diagnostic applications.

Some other significant challenges involve reliable microarray fabrication, integration into automated systems (essential to achieve widespread point-of-care use), and increased speed of analysis.

However, due to the effort devoted by the scientific community in this research field is unprecedented, the future is bright for producing microfluidic, multiplexed tool within the next decade that can be used for miRNA detection as early cancer diagnostics.

References

Aqeilan RI, Calin GA, Croce CM (2009) miR-15a and miR-16-1 in cancer: discovery, function and future perspectives. Cell Death Differ 17:215–220

Atkinson AJ, Colburn WA, DeGruttola VG et al (2001) Biomarkers and surrogate endpoints: preferred definitions and conceptual framework. Clin Pharmacol Ther 69:89–95

Barad O, Meiri E, Avniel A et al (2004) MicroRNA expression detected by oligonucleotide microarrays: system establishment and expression profiling in human tissues. Genome Res 14:2486–2494

Bard AJ, Stratmann M (2002) Semiconductor electrodes and photoelectrochemistry. In: Licht S (ed) Encyclopedia of electrochemistry, vol 6. Wiley, Weinheim

Bettazzi F, Lucarelli F, Palchetti I et al (2008) Disposable electrochemical DNA-array for PCR amplified detection of hazelnut allergens in foodstuffs. Anal Chim Acta 614:93–102

Bettazzi F, Hamid-Asl E, Esposito C et al (2013) Electrochemical detection of miRNA-222 by use of a magnetic bead-based bioassay. Anal Bioanal Chem 405:1025–1034

Calin GA, Croce CM (2006) MicroRNA signatures in human cancers. Nat Rev Cancer 6:857–866

Calin GA, Dumitru CD, Shimizu M et al (2002) Frequent deletions and down-regulation of micro-RNA genes miR15 and miR16 at 13q14 in chronic lymphocytic leukemia. Proc Natl Acad Sci USA 99:15524–15529

Cammann K (1977) Bio-sensors based on ion-selective electrodes. Frensius Z Anal Chem 287:1–9

Campuzano S, Pedrero M, Pingarron JM (2014a) Electrochemical genosensors for the detection of cancer-related miRNAs. Anal Bioanal Chem 406:27–33

Campuzano S, Torrente-Rodríguez RM, López-Hernández E et al (2014b) Magnetobiosensors based on viral protein p19 for microRNA determination in cancer cells and tissues. Angew Chem Int Ed Engl 53:6168–6171

Case-Green SC, Southern EM (1994) Studies on the base pairing properties of deoxyinosine by solid phase hybridisation to oligonucleotides. Nucleic Acids Res 22:131–136

Chuang H-Y, Hsu S-C, Lee P-I et al (2014) Synthesis and properties of a new conjugated polymer containing benzodithiophene for polymer solar cells. Polym Bull 71:1117–1130

Cissell K, Campbell S, Deo S (2008) Rapid, single-step nucleic acid detection. Anal Bioanal Chem 391:2577–2581

Cortez MA, Bueso-Ramos C, Ferdin J et al (2011) MicroRNAs in body fluids—the mix of hormones and biomarkers. Nat Rev Clin Oncol 8:467–477

Derry C, Wu Y, Zhu S et al (2013) Composite semiconductor material of carbon nanotubes and poly[5,5′-bis(3-dodecyl-2-thienyl)-2,2′-bithiophene] for high-performance organic thin-film transistors. J Electron Mater 42:3481–3488

Di Leva G, Garofalo M, Croce CM (2014) MicroRNAs in cancer. Annu Rev Pathol-Mech 9: 287–314

Erdem A, Congur G (2014) Label-free voltammetric detection of MicroRNAs at multi-channel screen printed array of electrodes comparison to graphite sensors. Talanta 118:7–13

Fan Y, Chen X, Trigg AD et al (2007) Detection of microRNAs using target-guided formation of conducting polymer nanowires in nanogaps. J Am Chem Soc 129(17):5437–5443

Farabullini F, Lucarelli F, Palchetti I et al (2007) Disposable electrochemical genosensor for the simultaneous analysis of different bacterial food contaminants. Biosens Bioelectron 22: 1544–1549

Galardi S, Mercatelli N, Giorda E et al (2007) miR-221 and miR-222 expression affects the proliferation potential of human prostate carcinoma cell lines by targeting p27Kip1. J Biol Chem 282:23716–23724

Gao Z (2012) A highly sensitive electrochemical assay for microRNA expression profiling. Analyst 137:1674–1679

Gao Z, Peng Y (2011) A highly sensitive and specific biosensor for ligation- and PCR-free detection of MicroRNAs. Biosens Bioelectron 26:3768–3773

Gao Z, Yang Z (2006) Detection of microRNAs using electrocatalytic nanoparticle tags. Anal Chem 78:1470–1477

Gao Z, Yu YH (2007a) Direct labeling microRNA with an electrocatalytic moiety and its application in ultrasensitive microRNA assays. Biosens Bioelectron 22:933–940

Gao Z, Yu YH (2007b) A microRNA biosensor based on direct chemical ligation and electrochemically amplified detection. Sens Actuators B Chem 121:552–559

Gao Z, Deng H, Shen W et al (2013) A label-free biosensor for electrochemical detection of femtomolar microRNAs. Anal Chem 85:1624–1630

Hamidi-Asl E, Palchetti I, Hasheminejad E et al (2013) A review on the electrochemical biosensors for determination of microRNAs. Talanta 115:74–83

Hashimoto K, Ito K, Ishimori Y (1994) Sequence-specific gene detection with a gold electrode modified with DNA probes and an electrochemically active dye. Anal Chem 66:3830–3833

Hébert SS, De Strooper B (2009) Alterations of the microRNA network cause neurodegenerative disease. Trends Neurosci 32:199–206

Herne TM, Tarlov MJ (1997) Characterization of DNA probes immobilized on gold surfaces. J Am Chem Soc 119:8916–8920

Iorio MV, Croce CM (2012) MicroRNA dysregulation in cancer: diagnostics, monitoring and therapeutics. A comprehensive review. EMBO Mol Med 4:143–159
Jayasena SD (1999) Aptamers: an emerging class of molecules that rival antibodies in diagnostics. Clin Chem 45:1628–1650
Ji Q, Hao X, Meng Y et al (2008) Restoration of tumor suppressor miR-34 inhibits human p53-mutant gastric cancer tumorspheres. BMC Cancer 8:266
Jiang S, Zhang H-W, Lu M-H et al (2010) MicroRNA-155 functions as an OncomiR in breast cancer by targeting the suppressor of cytokine signaling 1 gene. Cancer Res 70:3119–3127
Jin J, Grote J (2012) Materials science of DNA. CRC/Taylor & Francis, Boca Raton, FL
Kvaerno L, Wengel J (1999) Investigation of restricted backbone conformations as an explanation for the exceptional thermal stabilities of duplexes involving LNA (Locked Nucleic Acid):† synthesis and evaluation of abasic LNA. Chem Commun 7:657–658
Labib M, Khan N, Ghobadloo SM et al (2013) Three-mode electrochemical sensing of ultralow microRNA levels. J Am Chem Soc 135:3027–3038
Labuda J, Brett Ana Maria O, Evtugyn G et al (2010) Electrochemical nucleic acid-based biosensors: concepts, terms, and methodology (IUPAC technical report). Pure Appl Chem 82: 1161
Laschi S, Palchetti I, Marrazza G et al (2006) Development of disposable low density screen-printed electrode arrays for simultaneous electrochemical measurements of the hybridisation reaction. J Electroanal Chem 593:211–218
Laschi S, Palchetti I, Marrazza G et al (2009) Enzyme-amplified electrochemical hybridization assay based on PNA, LNA and DNA probe-modified micro-magnetic beads. Bioelectrochemistry 76:214–220
Lawrie CH, Gal S, Dunlop HM et al (2008) Detection of elevated levels of tumour-associated microRNAs in serum of patients with diffuse large B-cell lymphoma. Br J Haematol 141: 672–675
Lee RC, Feinbaum RL, Ambros V (1993) The C. elegans heterochronic gene lin-4 encodes small RNAs with antisense complementarity to lin-14. Cell 75:843–854
Lee Y, Jeon K, Lee JT et al (2002) MicroRNA maturation: stepwise processing and subcellular localization. EMBO J 21:4663–4670
Lee Y, Ahn C, Han J et al (2003) The nuclear RNase III Drosha initiates microRNA processing. Nature 425:415–419
Leech D (1994) Affinity biosensors. Chem Soc Rev 23:205–213
Levicky R, Herne TM, Tarlov MJ et al (1998) Using self-assembly to control the structure of DNA monolayers on gold: a neutron reflectivity study. J Am Chem Soc 120:9787–9792
Liang R-Q, Li W, Li Y et al (2005) An oligonucleotide microarray for microRNA expression analysis based on labeling RNA with quantum dot and nanogold probe. Nucleic Acids Res 33: e17
Liu L, Jiang S, Wang L et al (2014a) Direct detection of microRNA-126 at a femtomolar level using a glassy carbon electrode modified with chitosan, graphene sheets, and a poly (amidoamine) dendrimer composite with gold and silver nanoclusters. Microchim Acta 182: 77–84
Liu L, Xia N, Liu H et al (2014b) Highly sensitive and label-free electrochemical detection of microRNAs based on triple signal amplification of multifunctional gold nanoparticles, enzymes and redox-cycling reaction. Biosens Bioelectron 53:399–405
Liu Q, Cai J, Huan J et al (2014c) A visible light photoelectrochemical biosensor coupling enzyme-inhibition for organophosphates monitoring based on a dual-functional Cd0.5Zn0.5S-reduced graphene oxide nanocomposite. Analyst 139:1121–1126
Lu L, Byrnes K, Han C et al (2014) miR-21 targets 15-PGDH and promotes cholangiocarcinoma growth. Mol Cancer Res 12:890–900
Lucarelli F, Marrazza G, Palchetti I et al (2002) Coupling of an indicator-free electrochemical DNA biosensor with polymerase chain reaction for the detection of DNA sequences related to the apolipoprotein E. Anal Chim Acta 469:93–99

Lucarelli F, Tombelli S, Minunni M et al (2008) Electrochemical and piezoelectric DNA biosensors for hybridisation detection. Anal Chim Acta 609:139–159
Lund E, Güttinger S, Calado A et al (2004) Nuclear export of microRNA precursors. Science 303: 95–98
Luong JHT, Male KB, Glennon JD (2008) Biosensor technology: technology push versus market pull. Biotechnol Adv 26:492–500
Mascini M, Palchetti I, Tombelli S (2012) Nucleic acid and peptide aptamers: fundamentals and bioanalytical aspects. Angew Chem Int Ed 51:1316–1332
Merkoçi A (2007) Electrochemical biosensing with nanoparticles. FEBS J 274:310–316
Mettenbörger A, Singh T, Singh AP et al (2014) Plasma-chemical reduction of iron oxide photoanodes for efficient solar hydrogen production. Int J Hydrog Energy 39:4828–4835
Millan KM, Mikkelsen SR (1993) Sequence-selective biosensor for DNA based on electroactive hybridization indicators. Anal Chem 65:2317–2323
Moldovan L, Batte KE, Trgovcich J et al (2014) Methodological challenges in utilizing miRNAs as circulating biomarkers. J Cel Mol Med 18:371–390
Nair PR, Alam MA (2007) Dimensionally frustrated diffusion towards fractal adsorbers. Phys Rev Lett 99:256101
Ngo HT, Wang H-N, Fales AM et al (2013) Label-free DNA biosensor based on SERS molecular sentinel on nanowave chip. Anal Chem 85:6378–6383
Nohata N, Hanazawa T, Enokida H et al (2012) microRNA-1/133a and microRNA-206/133b clusters: dysregulation and functional roles in human cancers. Oncotarget 3:9–21
Nuzzo RG, Allara DL (1983) Adsorption of bifunctional organic disulfides on gold surfaces. J Am Chem Soc 105:4481–4483
Obika S, Nanbu D, Hari Y et al (1998) Stability and structural features of the duplexes containing nucleoside analogues with a fixed N-type conformation, 2′-O,4′- C-methyleneribonucleosides. Tetrahedron Lett 39:5401–5404
Pasquinelli AE, Reinhart BJ, Slack F et al (2000) Conservation of the sequence and temporal expression of let-7 heterochronic regulatory RNA. Nature 408:86–89
Patel MK, Ali MA, Srivastava S et al (2013) Magnesium oxide grafted carbon nanotubes based impedimetric genosensor for biomedical application. Biosens Bioelectron 50:406–413
Patolsky F, Zheng G, Lieber CM (2006) Nanowire-based biosensors. Anal Chem 78(13): 4260–4269
Pauley KM, Cha S, Chan EKL (2009) MicroRNA in autoimmunity and autoimmune diseases. J Autoimmun 32:189–194
Peng Y, Gao Z (2011) Amplified detection of microRNA based on ruthenium oxide nanoparticle-initiated deposition of an insulating film. Anal Chem 83:820–827
Peng Y, Yi G, Gao Z (2010) A highly sensitive microRNA biosensor based on ruthenium oxide nanoparticle-initiated polymerization of aniline. Chem Commun 46:9131–9133
Pöhlmann C, Sprinzl M (2010) Electrochemical detection of microRNAs via gap hybridization assay. Anal Chem 82:4434–4440
Reinhart BJ, Slack FJ, Basson M et al (2000) The 21-nucleotide let-7 RNA regulates developmental timing in Caenorhabditis elegans. Nature 403:901–906
Ronkainen NJ, Halsall HB, Heineman WR (2010) Electrochemical biosensors. Chem Soc Rev 39: 1747–1763
Shon JW, Ohta J, Ueno K et al (2014) Fabrication of full-color InGaN-based light-emitting diodes on amorphous substrates by pulsed sputtering. Sci Rep 4:5325
Steel AB, Herne TM, Tarlov MJ (1998) Electrochemical quantitation of DNA immobilized on gold. Anal Chem 70:4670–4677
Teo AKL, Lim CL, Gao Z (2014) The development of electrochemical assays for microRNAs. Electrochim Acta 126:19–30
Thévenot DR, Toth K, Durst RA et al (2001) Electrochemical biosensors: recommended definitions and classification. Biosens Bioelectron 16:121–131

Torrente-Rodríguez RM, Campuzano S, López-Hernández E et al (2014) Direct determination of miR-21 in total RNA extracted from breast cancer samples using magnetosensing platforms and the p19 viral protein as detector bioreceptor. Electroanalysis 26:2080–2087
Tsuchida A, Ohno S, Wu W et al (2011) miR-92 is a key oncogenic component of the miR-17–92 cluster in colon cancer. Cancer Sci 102:2264–2271
Válóczi A, Hornyik C, Varga N et al (2004) Sensitive and specific detection of microRNAs by northern blot analysis using LNA-modified oligonucleotide probes. Nucleic Acids Res 32:e175
van Rooij E, Sutherland LB, Liu N et al (2006) A signature pattern of stress-responsive microRNAs that can evoke cardiac hypertrophy and heart failure. Proc Natl Acad Sci USA 103:18255–18260
Visone R, Russo L, Pallante P et al (2007) MicroRNAs (miR)-221 and miR-222, both overexpressed in human thyroid papillary carcinomas, regulate p27Kip1 protein levels and cell cycle. Endocr Relat Cancer 14:791–798
Voccia D, Bettazzi F, Baydemir G et al (2015) Alkaline-phosphatase-based nanostructure assemblies for electrochemical detection of microRNAs. J Nanosci Nanotechnol 15:3378–3384
Wang J, Cai X, Wang J et al (1995) Trace measurements of RNA by potentiometric stripping analysis at carbon paste electrodes. Anal Chem 67:4065–4070
Wang J, Cai X, Tian B et al (1996) Microfabricated thick-film electrochemical sensor for nucleic acid determination. Analyst 121:965–969
Wang J, Rivas G, Fernandes JR et al (1998) Indicator-free electrochemical DNA hybridization biosensor. Anal Chim Acta 375:197–203
Wang W, Bao L, Lei J et al (2012) Visible light induced photoelectrochemical biosensing based on oxygen-sensitive quantum dots. Anal Chim Acta 744:33–38
Wenjuan Y, Le Goff A, Spinelli N et al (2013) Electrogenerated trisbipyridyl Ru(II)-/nitrilotriacetic-polypyrene copolymer for the easy fabrication of label-free photoelectrochemical immunosensor and aptasensor: application to the determination of thrombin and anti-cholera toxinantibody. Biosens Bioelectron 42:556–562
Wightman B, Ha I, Ruvkun G (1993) Posttranscriptional regulation of the heterochronic gene lin-14 by lin-4 mediates temporal pattern formation in C. elegans. Cell 75:855–862
Wiklund ED, Bramsen JB, Hulf T et al (2011) Coordinated epigenetic repression of the miR-200 family and miR-205 in invasive bladder cancer. Int J Cancer 128:1327–1334
Yang H, Hui A, Pampalakis G et al (2009) Direct, electronic microRNA detection for the rapid determination of differential expression profiles. Angew Chem Int Ed Engl 48:8461–8464
Yin H, Zhou Y, Chen C et al (2012) An electrochemical signal 'off-on' sensing platform for microRNA detection. Analyst 137:1389–1395
Yu Y, Chen Z, Shi L et al (2014) Ultrasensitive electrochemical detection of microRNA based on an arched probe mediated isothermal exponential amplification. Anal Chem 86:8200–8205
Zanardi C, Baldoli C, Licandro E et al (2012) Development of a gold-nanostructured surface for amperometric genosensors. J Nanopart Res 14:1–12
Zhang G-J, Chua JH, Chee R-E et al (2009) Label-free direct detection of miRNAs with silicon nanowire biosensors. Biosens Bioelectron 24:2504–2508
Zhang C-Z, Zhang J-X, Zhang A-L et al (2010) MiR-221 and miR-222 target PUMA to induce cell survival in glioblastoma. Mol Cancer 9:229
Zhang X, Guo Y, Liu M et al (2013) Photoelectrochemically active species and photoelectrochemical biosensors. RSC Adv 3:2846–2857
Zhang P, Wu X, Chai Y et al (2014a) An electrochemiluminescent microRNA biosensor based on hybridization chain reaction coupled with hemin as the signal enhancer. Analyst 139: 2748–2753
Zhang Y, Ge L, Li M et al (2014b) Flexible paper-based ZnO nanorod light-emitting diodes induced multiplexed photoelectrochemical immunoassay. Chem Commun 50:1417–1419
Zhou Y, Zhang Z, Xu Z et al (2012) MicroRNA-21 detection based on molecular switching by amperometry. New J Chem 36:1985–1991

Electrochemical Detection of RNA

Christopher Pöhlmann and Mathias Sprinzl

Contents

Abstract Over the past few decades, it was demonstrated that RNA plays a central role for a wide range of functions in living cells through control of the gene expression. This chapter focuses on different electrochemical detection approaches of RNA with applications in clinical diagnostics as well as in food and environmental analysis. Electrochemical biochips are an emerging tool for point-of-care diagnostic systems due to their inherent high sensitivity along with cost and time effectiveness. In this review, different strategies of electrochemical biosensors for direct RNA detection will be compared. Additionally, the implementation of nanotechnology as a powerful alternative to common detection approaches will be addressed. Specific detection of 16S ribosomal RNA allows species-specific identification of bacteria without a prior nucleic acid amplification step. Examples of 16S rRNA detection describe the analysis of pathogens in food samples,

C. Pöhlmann
Bruker Daltonik GmbH, Permoserstraße 15, 04318 Leipzig, Germany

M. Sprinzl (✉)
Laboratory of Biochemistry, University of Bayreuth, Universitätsstraße 30, 95440 Bayreuth, Germany
e-mail: Mathias.Sprinzl@uni-bayreuth.de

V.A. Erdmann et al. (eds.), *RNA and DNA Diagnostics*, RNA Technologies,
DOI 10.1007/978-3-319-17305-4_2

indicator bacterium *Escherichia coli* in water samples, or uropathogens in clinical samples. Additionally, messenger RNA-based bacteria detection was applied by several research groups for species-specific bacteria identification. Beside bacteria detection, direct detection of viruses that contain RNA as genetic material is feasible. Electrochemical messenger RNA detection enables the determination of mRNA levels in cells and, thus, the evaluation of different cell populations or cell status. The abnormal expression of microRNAs in malignant cells makes microRNAs promising biomarkers for cancer diagnostics. Therefore, different electrochemical biosensing strategies for direct microRNA profiling will be compared.

Keywords Electrochemical biosensor • Ribosomal RNA • Messenger RNA • microRNA • Bacteria • Viruses • Pathogens • Cancer

1 Introduction

Ribonucleic acid (RNA) is present in all living organisms. It transfers genetic information from DNA to proteins, serves as structural and catalytic molecule, and regulates gene expression. In some viruses, RNA fulfills the role as a sole carrier of genetic information. The size of naturally occurring RNA is strongly variable, ranging from small helical structures with about 20 base pairs up to long RNA chains composed of thousands of nucleotides. Large RNAs have complex tertiary structures composed of helical modules and different structural elements in the single-stranded regions connecting these helices (Moore 1999; Leontis et al. 2002; Westhof 2010).

Table 1 summarizes the most prominent types of RNA. Besides RNA detailed in this chapter, also other RNA types such as telomerase RNA (teloRNA), primary

Table 1 Different RNA types and their functions

Name	Abbreviation	Distribution	Function
Messenger RNA	mRNA	All organisms	Codes for proteins
Transfer RNA	tRNA	All organisms	Translation
Ribosomal RNA	rRNA	All organisms	Translation
Small nuclear RNA	snRNA	Eukaryotes and archaea	Splicing of pre-mRNA
Small nucleolar RNA	snoRNA	Eukaryotes and archaea	Nucleotide modification of mRNAs
microRNA	miRNA	Most eukaryotes	Regulation of mRNA stability, translation
Small interfering RNA	siRNA	Most eukaryotes	Posttranscriptional regulation of transcripts; transcriptional gene silencing

RNA (pri-RNA), guide RNA (gRNA), small nuclear RNA (snRNA), transfer messenger RNA (tmRNA), signal recognition particle RNA (srpRNA), vault RNA, and catalytic RNA (ribozyme) were described (Bratkovic and Rogelj 2011).

2 RNA as Biomarkers

Due to the various functions carried out by RNA in cells, different types of RNA are valuable *biomarkers* for the cell status. For example, elevated or decreased *messenger RNA* (mRNA) or *microRNA* (miRNA) levels in cells can be an indication for cancer or other diseases. On the other hand, sequence-specific detection of bacterial *ribosomal RNA* (rRNA) enables species-specific bacteria identification. Hence, analyzing the RNA present in biological cellular processes is essential to develop new methods of diagnosis.

In this chapter, we focus on the application of electrochemical techniques for direct (i.e., nucleic acid amplification-free) RNA detection with impact for clinical diagnostics, food testing, as well as environmental analysis.

3 Electrochemical Detection of RNA

Electrochemical biosensors have been the subject of basic as well as applied research as particularly attractive for bioanalysis because of their high sensitivity and selectivity, low cost, and ease of automatization (Drummond et al. 2003). In general, a biosensor consists of a biorecognition layer (e.g., DNA, RNA, antibodies, lectins, aptamers) generating substances for detection by the physicochemical transducer providing the measurable signal. Particularly, for electrochemical biosensors, the transduction element is an electrode (e.g., gold-coated electrode, indium tin oxide electrode, graphite electrode, silicon nanowire). The sensing principle of electrochemical biosensors specific for RNA mostly relies on the *hybridization* of RNA to complementary DNA oligonucleotides immobilized on the electrode. DNA/RNA hybridization results in measureable changes in the electrode or interfacial properties of the electrode. Transduction is based on either intrinsic nucleic acid electroactivity (guanine oxidation), redox indicators (e.g., groove binders, intercalators), covalently bound redox labels (e.g., organometallics, metal chelates, nanoparticles), or reporter enzymes coupled to nucleic acids (e.g., phosphatases, peroxidases) (Palecek and Bartosik 2012; Hartman et al. 2013). Transduction in electrochemical biosensors for RNA detection has been performed via amperometric, potentiometric, resistive, and impedance-based approaches (Johnson and Mutharasan 2014).

4 Electrochemical RNA Sensors for Microorganism and Virus Detection

4.1 Pathogen Detection Based on Ribosomal RNA as Target Molecule

Due to the fact that bacterial cells contain, depending on their physiological state, 5,000–75,000 ribosomes, each with one copy of rRNA, direct rRNA detection is sensitive without any prior nucleic acid amplification process (Bremer and Dennis 1996). Additionally, rRNA correlates better with vegetative properties of bacteria than the very stable DNA (Keer and Birch 2003). Ribosomal RNA sequences differ substantially from one species to the other. 16S and 23S rRNAs possess sequence regions which are invariable but also sequences which are specific for certain bacterial species (Nielsen et al. 2003). Furthermore, nucleotide sequences of 16S rRNA for most bacteria species are available in databases, which is a prerequisite for successful capture and detector probe design. Therefore, particularly sequences of 16S rRNA are mostly used as target molecules for pathogen detection based on electrochemical biosensors.

A general approach for species-specific bacteria detection applies single-stranded DNA capture and detector probes for hybridization to complementary regions of bacterial rRNA. This so-called sandwich hybridization assay was mostly applied for RNA detection. In this chapter, the characteristics of several electrochemical biosensors for direct rRNA-based pathogen detection are described. However, there are also several review articles summarizing biosensors for bacteria detection based on nucleic acid amplification or immunoassay-based methods (Kirsch et al. 2013; Arora et al. 2013).

Already in 2005, Metfies et al. developed an electrochemical biosensor for detection of toxic dinoflagellate *Alexandrium ostenfeldii* relying on sandwich hybridization. A biotinylated capture probe is immobilized onto an avidin-modified electrode surface. The target RNA was hybridized to complementary capture probe as well as helper oligonucleotides and digoxigenin (DIG)-labeled detector probe. The helper oligonucleotides resolve complex secondary structure of rRNA and improve hybridization efficacy of target rRNA to capture and detector probes. Finally, the enzyme-mediated electrochemical signal after addition of anti-DIG-horseradish peroxidase (HRP) was measured. The determined limit of detection for 18S rRNA of *Alexandrium ostenfeldii* was approximately 16 ng μL^{-1} (equals approximately 800 *Alexandrium ostenfeldii* cells) using an optimized hybridization protocol within a total assay time of approximately 70 min.

In 2005, LaGier et al. presented a proof-of-concept study of an electrochemical biosensor for monitoring waters for presence of fecal indicator bacteria *Escherichia coli*. DNA capture oligonucleotides immobilized on magnetic beads were hybridized to complementary regions of 16S rRNA from *E. coli*. After a series of washing

and magnetic separation steps to remove nonspecifically bound nucleic acids, guanine bases are released into the solution from DNA/RNA hybridization assemblies by treatment with sulfuric acid. Released guanine bases are detected by pulse voltammetry at a pencil graphite electrode. The resultant voltammograms display current peaks, resulting from the oxidation of guanine, whose height is proportional to the amount of RNA hybridized to DNA capture oligonucleotides. This technique allowed the detection of down to 10^7 colony-forming units (cfu) *E. coli* within 4 h.

Gabig-Ciminska et al. (2004) applied silicon-based biochips possessing interdigitated electrodes in combination with bead-based sandwich hybridization (BBSH) for 16S rRNA analysis. A sandwich hybridization assembly between a capture probe immobilized on *paramagnetic beads*, a single-stranded target RNA, and a DIG-labeled detector probe was produced. After enzyme labeling of the detector probe using anti-DIG-alkaline phosphatase conjugate, the enzymatic reaction produced electroactive *p*-aminophenol (pAP) which is detected by potentiometric measurement at the chip surface. In detail, pAP was oxidized at the anode of the chip to quinone imine that was reduced back to pAP at the cathode (*redox cycling*) (Niwa et al. 1993). This biosensor technology was applied for *E. coli* 16S rRNA detection with limit of detections ranging from 10^{11} to 10^{10} molecules with a total assay time of 4 h.

As an alternative to the previously described single-plex assays with long assay time, Elsholz et al. (2006) developed an automated analysis system based on biochips with 16 gold interdigitated electrodes for identification of five pathogens typically involved in urinary tract infections. The multiple cathode and anode fingers enable the redox cycling of an electroactive product generated by the reporter enzyme achieving signal amplification of resulting current (Fig. 1a) (Hintsche et al. 1997). Five different capture probes specific for *Staphylococcus epidermidis*, *Pseudomonas aeruginosa*, *E. coli*, *Staphylococcus aureus*, and *Enterococcus faecalis*, each of them on three array positions and a positive control capture probe on one array position were immobilized on the low-density biochip. A 3′-biotin-labeled detector oligonucleotide and supporting oligonucleotides (also called helper oligonucleotides) resolving secondary structure of 16S rRNA were hybridized to complementary regions of 16S rRNA (Fig. 1b). The biotin-labeled detector oligonucleotides allowed the binding of alkaline phosphatase conjugated to avidin. The reporter enzyme converted the electroinactive substrate *p*-aminophenyl phosphate into electroactive pAP which undergoes a redox cycling process due to interdigitated electrode structure (Fig. 1a). After substrate flow stops, the effective pAP concentration is permanently increased, provided the reporter enzyme is attached to the electrode. This leads to an increase of the measured current. The signal calculated from the slope of current vs. time indicates the existence of DNA/RNA hybridization (Fig. 1c). The position-specific readout signals were proportional to the 16S rRNA target concentration. The automated procedure allowed detection of 0.5 ng μL^{-1} total *E. coli* RNA (21 ng total RNA) corresponding to approximately 10^5 cfu mL^{-1} *E. coli* within an analysis time (RNA fragmentation and hybridization) of 60 min (without sample preparation). The

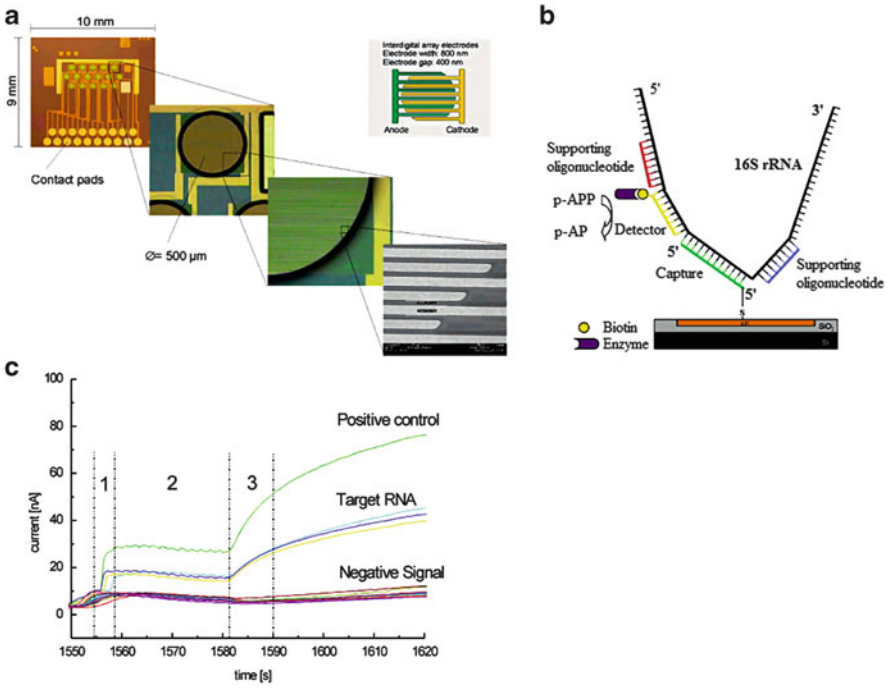

Fig. 1 Electrochemical 16S rRNA detection using interdigitated gold electrode biochip technology. (**a**) Photograph of biochip with gold interdigitated electrodes. (**b**) Scheme of sandwich hybridization assay consisting of immobilized capture probe, target 16S rRNA, supporting oligonucleotides, and biotinylated detector oligonucleotides. (**c**) Current vs. time plot of 16 gold electrodes of one biochip. In phase 1, substrate solution was introduced at a constant flow rate. In phase 2, the system was in an equilibrium phase, i.e., a constant current level was generated for all electrode positions in dependence of bound reporter enzyme. In phase 3, the substrate flow was stopped and positive positions showed a linear increase in current (Reprinted with permission from Elsholz et al. (2006), Automated detection and quantitation of bacterial RNA by using electrical microarrays. Anal Chem 78:4794–4802. Copyright (2006) American Chemical Society)

robustness of this strategy in the presence of real sample matrices (clinical samples) has to be proven in future studies.

Liao et al. (2006) developed also a sandwich hybridization assay for *uropathogen detection* using an array of 16 sensor positions, each consisting of three single-layer gold electrodes (working, reference, and auxiliary). Capture probes specific for clinically relevant bacterial urinary pathogens *E. coli*, *Proteus mirabilis*, *P. aeruginosa*, *Enterococcus* spp., and the *Klebsiella-Enterobacter* group were immobilized on the electrode array. Furthermore, a universal capture probe detecting all human uropathogens tested was immobilized as positive control. Bacterial 16S rRNA derived from single-step bacterial lysis was hybridized both to the biotin-modified capture probe on the sensor surface and to a second, fluorescein-modified detector probe. Detection of the target-probe hybrids was achieved through binding of an HRP-conjugated anti-fluorescein antibody to the

detector probe. Linking the enzymatic activity of HRP to amperometric current flow via oxidation and reduction of tetramethylbenzidine achieved species-specific detection of as few as 2,600 uropathogenic bacteria in culture, inoculated urine, and clinical urine samples within 45 min from the beginning of sample processing. During the following years, the assay procedure was substantially optimized in Haake's (Sun et al. 2005; Liao et al. 2006, 2007; Mastali et al. 2008; Mach et al. 2009) as well as in Wang's laboratories (Wu et al. 2009, 2010; Campuzano et al. 2011), e.g., the influence of gap distance between capture and detector oligonucleotides, the single-step bacterial cell lysis, and the new ternary *self-assembled monolayers* (SAMs) for preventing unspecific adsorption and reducing the noise were studied. Particularly, the introduction of new ternary SAMs consisting of coassembled thiolated capture oligonucleotides, mercaptohexanol, and dithiothreitol resulted in an impressive improvement of limit of detection to 40 zmol rRNA (corresponding to 1 cfu *E. coli* per sensor) using chronoamperometric detection (Wu et al. 2010). The composition of ternary SAMs was improved in further studies. Ternary SAMs consisting of coassembled thiolated capture oligonucleotide, mercaptohexanol, and hexanedithiol were resistant to nonspecific adsorption even in undiluted serum or urine. This improvement was an important step in application of this kind of biosensor in clinical *point-of-care* diagnostics (Campuzano et al. 2011). Finally, a biosensor cassette applying the biochip within an enclosed fluidic system was established. Alternating current (AC) electrokinetics enhanced molecular convection and hybridization efficacy through electrokinetics-induced fluid motion and Joule heating-induced temperature elevation (Bercovici et al. 2012). Using electrokinetic stringency control, the background noise due to the matrix effects of clinical urine samples can be reduced by 60 % and allowed single-base mismatch discrimination (Liu et al. 2014a). Additionally, the biosensor cassette was validated using patient-derived clinical urine samples (Bercovici et al. 2012; Mohan et al. 2011; Ouyang et al. 2013). Liu et al. (2014b) applied the electrokinetics-enhanced biosensor platform for rapid antimicrobial susceptibility testing.

Patel et al. (2011) introduced a target-specific capture sample preparation method enhancing sensitivity of electrochemical 16S rRNA detection. Therefore, biotinylated DNA probes were immobilized on streptavidin magnetic beads for binding complementary regions of target 16S rRNA. After washing the beads and removal of inhibiting substances in sample matrices, target RNA was eluted. The concentrated and purified target rRNA is detected electrochemically by linking the enzymatic activity of HRP to amperometric current flow via oxidation and reduction of tetramethylbenzidine. The implementation of target-specific capture increased detection sensitivity by a factor of approximately five and reduced the limit of detection from 3.6×10^4 to 4.7×10^3 cfu mL^{-1}. Furthermore, target-specific capture significantly improved sensor performance in a study of 52 clinical urine specimens. However, this particular sample preparation and concentration method extended the analysis time by 60 min, due additional steps of target-specific capture.

Pöhlmann et al. (2009a) established a biosensor based on DNA/RNA hybridization for monitoring of *E. coli* and other foodborne pathogens during food processing. Low-density biochips with four electrodes were used, and species-specific capture probes for *E. coli*, *Hafnia alvei*, *Listeria innocua*, and *Bacillus subtilis* were immobilized on the gold electrodes via thiol-gold linkage. The identification of bacteria relies on simultaneous hybridization between the 16S rRNA, capture oligonucleotide, a helper oligonucleotide, resolving secondary structure of 16S rRNA as well as allowing continuous base stacking, and a covalent *esterase 2* (EST2)-detector oligonucleotide conjugate. This so-called four-component hybridization causes the immobilization of the reporter enzyme in the vicinity of the particular electrode. Enzymatic hydrolysis of electroinactive substrate *p*-aminophenyl butyrate produces electroactive pAP used for the redox cycling process and results in a detectable amperometric signal. Electrochemical redox cycling was achieved through a cycle of voltage pulses instead of using interdigitated electrodes as applied, for example, by Elsholz et al. (2006). In contrast to previous approaches, a covalent EST2-detector oligonucleotide conjugate was applied instead of biotin- or fluorescein-labeled detector oligonucleotide probes and avidin or antibody reporter enzyme conjugates. The use of the covalent EST2-detector oligonucleotide conjugate simplified the procedure due to the minimizing of pumping and incubation steps. Furthermore, a thermostable reporter enzyme allows broader temperature variations during nucleic acid-based assays and is optimally suited for on-site applications. This biosensor achieved the detection of 500 cfu *E. coli* within less than 40 min and was further improved by establishing a rapid one-step lysis method allowing sample preparation suitable for an on-site application (unpublished results). Additionally, *signal amplification* was achieved by using multiple EST2 molecules conjugated via polyamidoamine dendrimer to single universal detector oligodeoxynucleotide (Humenik et al. 2008). This resulted in a detection limit of 50 cfu *E. coli* per electrode sensor within less than 40 min (Pöhlmann et al. 2009b). The method was validated using contaminated meat juice samples. The detection limit of the biochip applying this complex sample matrix was approximately 2,000 cfu mL^{-1} *E. coli* (Heidenreich et al. 2010).

Walter et al. (2011) described also an electrochemical biosensor for detection of *E. coli* 16S rRNA using pAP redox cycling by nicotinamide adenine dinucleotide (NAD). In analogy to previous studies, a sandwich-type hybridization assay using an immobilized capture probe and a biotin-labeled detector oligonucleotide as well as streptavidin-alkaline phosphatase as reporter enzyme were used. This electrochemical biosensor allowed the detection of down to 960 cfu *E. coli* per sensor (250 cfu μL^{-1}) within a total assay time of approximately 60 min. Yet, applicability of this biosensor for real sample testing (food samples, clinical samples) has still to be demonstrated.

Another approach for PCR-free testing of beer spoilage bacteria *Lactobacillus brevis* relies on the formation of sandwich hybridization assembly of capture oligonucleotide, 16S rRNA of *L. brevis*, and biotinylated reporter DNA on the

surface of magnetic beads. After labeling sandwich assembly with lipase, the lipase-labeled DNA-hybridized magnetic bead suspension was transferred to gold electrodes modified with a ferrocene-terminated SAM formed by aliphatic esters. Lipase hydrolysis of the ester bond released a fraction of the ferrocene molecules from the electrode surface and led to a decrease of electrochemical signal. Detection limit for purified *L. brevis* 16S rRNA was 16 amoles within a total analysis time of approximately 4.5 h. This corresponds to detection of 400 *L. brevis* cells isolated from 1 L beer (Shipovskov et al. 2012). Beside quite long analysis time, the signal-off character of this biosensor could be problematic in case of real sample testing due to possible matrix interference reactions.

Liu et al. (2011) applied *stem-loop structured probes* for enzymatic detection of *P. aeruginosa* 16S rRNA in composting degradation instead of linear capture oligonucleotides (Fig. 2). The stem-loop probe was modified with a 5′-thiol for immobilization on the gold electrode, whereas a 3′-biotin label allowed binding of streptavidin-HRP conjugate. In the "closed" state, the biotin moiety was not accessible for the bulky streptavidin-HRP conjugate. The hybridization with the target rRNA induced the conformational change of the stem-loop probe to the "open" state. The biotin moiety at the 3′-end was accessible for binding with streptavidin-HRP, and subsequent quantification of the target was accomplished by electrochemical detection of the enzymatic product. The determined limit of detection of this biosensor was 0.012 pg μL^{-1} *P. aeruginosa* 16S rRNA revealing a dynamic range from 0.3 to 600 pg μL^{-1}.

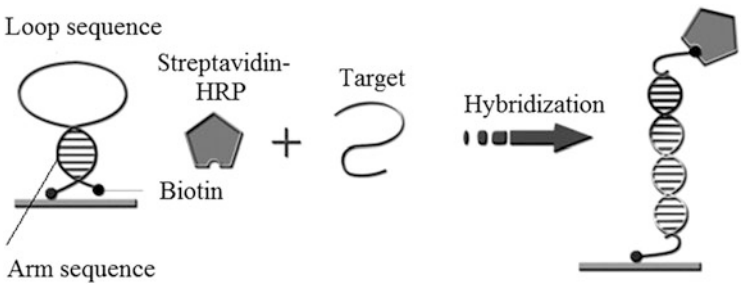

Fig. 2 Detection of 16S rRNA from *P. aeruginosa* using stem-loop structured probes. In the absence of target RNA, the stem-loop structure is closed, and biotin moiety is not accessible for binding to streptavidin-HRP conjugate due to close proximity to the electrode surface. In the presence of target RNA, immobilized stem-loop structure undergoes a conformational change, and biotin label becomes accessible for binding to streptavidin-HRP conjugate producing an enzyme-mediated electrochemical signal (Reprinted from Enzyme Microb Technol 49, Liu C, Zeng GM, Tang L, Zhang Y, Li YP, Liu YY, Li Z, Wu MS, Luo J, Electrochemical detection of Pseudomonas aeruginosa 16S rRNA using a biosensor based on immobilized stem-loop structured probe, 266–271, Copyright (2011), with permission from Elsevier)

4.2 mRNA-Based Bacteria and Protozoa Detection

Electrochemical biosensors targeting mRNA as the analyte offer an added advantage over conventional DNA-based detection methods, i.e., detection of only viable cells. In contrast to biosensors targeting rRNA, biosensors using mRNA as analyte can differentiate between closely related bacteria species via species-specific toxin, virulence, or antibiotic markers. However, the copy number of a specific mRNA in microorganisms varies drastically from one mRNA to another. In general, mRNA level is much lower than of rRNA. Hence, detection of mRNA without prior nucleic acid amplification is challenging. Additional disadvantages of biosensors applying mRNA as target molecule are the often limited life span of mRNA and the high susceptibility to degradation due to contaminants in sample matrices.

The interdigitated gold electrode array used by Elsholz et al. (2006) was also applied for monitoring mRNA levels of a focused set of selected genes of *B. subtilis* and *B. licheniformis* in order to provide a tool for an improved control of industrial bioprocesses (Jurgen et al. 2005; Pioch et al. 2007). For this purpose, the magnetic bead-based sandwich hybridization (BBSH) was established. Capture oligonucleotides immobilized on paramagnetic beads were hybridized to target mRNA molecules and simultaneously bound to DIG-labeled detector oligonucleotides. The sandwich hybridization assembly is detected using an anti-DIG-alkaline phosphatase conjugate producing electroactive pAP, which was detected amperometrically at the interdigitated electrodes of the biochip by redox cycling. After several optimization steps including a change from the bead-based to a solution-based sandwich hybridization (SBSH), the rearrangement of the probes and the introduction of a second detection probe significantly enhanced the hybridization signals. A specific mRNA of total RNA isolated from *B. licheniformis* could be detected within approximately 80 min (Pioch et al. 2008). The expression profiles determined using the electrochemical biochip assay were in good agreement with expression profiles determined by RT-PCR experiments.

A very promising approach for direct bacterial mRNA detection was invented by the group of Shanna Kelley by combining electrochemical sensors and *nanotechnology*. Originally, the sensor consists of *nanostructured microelectrodes* (Fig. 3a) as electrode platform and immobilized *peptide nucleic acids* (PNAs) as capture probes. PNA capture probes were used due to their higher affinity to mRNA as compared to DNA capture oligonucleotides earlier demonstrated for PNA-DNA interactions (Brandt and Hoheisel 2004). RNA hybridization to PNAs is detected using an electrocatalytic reporter system, namely, $Ru(NH_3)_6^{3+}$, a DNA-binding and cationic electron acceptor, and $Fe(CN)_6^{3-}$, an anionic electron acceptor. $Ru(NH_3)_6^{3+}$ is attracted by the RNA film at the electrode surface through electrostatic interactions with the negatively charged phosphate backbone. During a negative potential sweep, Ru(III) is reduced and regenerated by the Fe(III) oxidant for multiple turnovers (Fig. 3b). The multiple redox cycles of Ru(III) amplify the reduction signal, thus reporting on the amount of hybridization at the electrode surface (Fang et al. 2009). Recently, Lam et al. (2012) presented an integrated

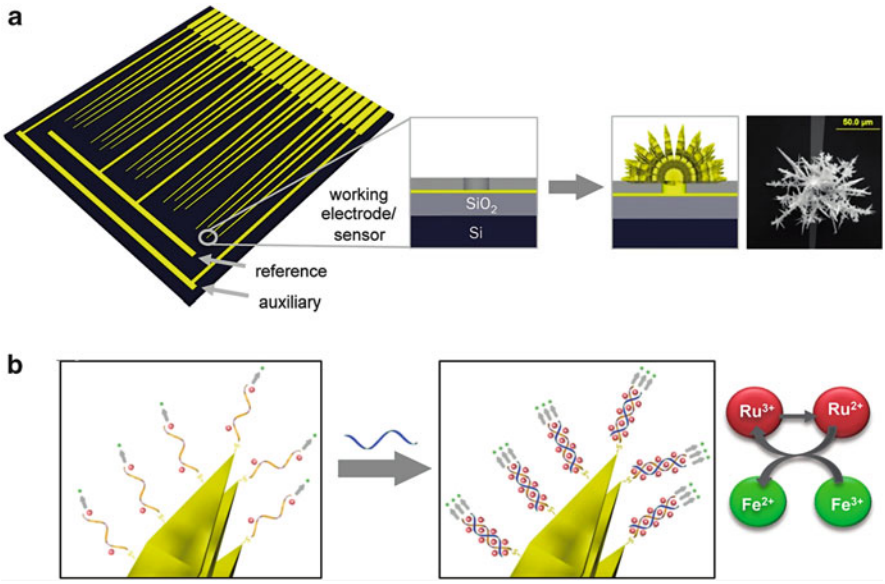

Fig. 3 Bacterial mRNA on nanostructured microelectrodes applying an electrochemical reporter system. (**a**) Schematic picture of the nanostructured microelectrodes. The Si chip consists of patterned Au working, Ag/AgCl reference, and platinum auxiliary electrodes. 5 µm apertures are etched at the tip of each working electrode. The substructures of the nanostructured microelectrodes were electroplated within each aperture, with a typical size of approximately 100 µm. (B) Ru(III) and Fe(III) electrocatalytic reporter pair for nucleic acid detection (Reprinted with permission from Lam et al. (2012), Polymerase chain reaction-free, sample-to-answer bacterial detection in 30 min with integrated cell lysis. Anal Chem 84:21–25. Copyright (2012) American Chemical Society)

platform for PCR-free bacterial detection with integrated cell lysis with a sample-to-answer time of 30 min. A sensor cartridge composed of a lysis chamber, a nanostructured microelectrode chip, and connection pads for readout was designed. After lysis of bacterial sample with an applied electric field, the sample is moved to the chip by injection of air with a syringe and mixed with electrocatalytic reporter groups. Electrochemical bacteria detection with high specificity and sensitivity based on described electrocatalytic reporter system was demonstrated achieving a limit of detection of 1 cfu μL^{-1}, i.e., clinical samples can be analyzed without a PCR step or a pre-cultivation step. The authors demonstrated direct detection of *rpoβ* mRNA isolated from *E. coli* or *Staphylococcus saprophyticus*, respectively, in urine samples. In the case of low concentrations of bacteria, diffusion for a dilute solution of target mRNA to the sensor can take hours or even days. Therefore, the authors improved the biosensor by introducing a new device capable of proximal electrochemical lysis and detection. This device achieved detection of *E. coli* down to 0.4 cfu μL^{-1} in 2 min (Besant et al. 2013).

Due to the fact that only viable oocysts can cause infection, detection of viable oocysts is mandatory in public water treatment systems. Therefore, mRNA is a

superior analyte in comparison to DNA because less stable mRNA allows the detection of only viable cells. Hence, Wongkaew et al. (2013) presented a novel multichannel poly(methyl methacrylate) microfluidic biosensor with interdigitated ultramicroelectrode arrays for electrochemical detection of mRNA from *Cryptosporidium parvum*. In this study, an mRNA for a heat-shock protein, hsp70, produced by *C. parvum*, was used as target molecule. As proof of principle, five microchannels were positioned over a large single interdigitated ultramicroelectrode. Target mRNA was hybridized to complementary capture oligonucleotides immobilized on paramagnetic beads and simultaneously to a cholesterol-labeled detector oligonucleotide coupled to *liposomes* encapsulating potassium ferri-/ferrocyanide as reporter molecules. Subsequently, the redox marker was detected over the interdigitated ultramicroelectrodes, generating a current proportional to *C. parvum* mRNA target concentration. In a final step, the magnet was removed and the sensor extensively washed for regeneration of the sensor. The established coulometric detection procedure revealed a limit of detection of 12.5 μM synthetic DNA target which used the authors as model target for the mRNA target.

4.3 *Electrochemical Biosensors for RNA-Based Detection of Viruses*

Beside bacteria detection, electrochemical biosensors have been developed for detection of viruses. Currently viruses with RNA genome, e.g., *hepatitis C virus* (HCV), are detected using immunoassays, and results are confirmed by conventional or real-time reverse transcriptase polymerase chain reaction (RT-PCR) or branched DNA-based assays (Scott and Gretch 2007). These assays exhibit high sensitivity and specificity; however, they are time consuming, labor intensive, and expensive and require specialized equipment. Interestingly, also most biosensors for rapid virus detection developed so far focused on immunoassay-based strategies or on PCR or RT-PCR amplification (Caygill et al. 2010). Hence, there is a need to develop simple and rapid assays for the direct detection of unamplified viral RNA (e.g., HCV, human immunodeficiency virus (HIV), dengue virus, influenza virus) with acceptable sensitivity and specificity, short turnaround time, and cost-effectiveness (Shawky et al. 2010).

Kwakye et al. (2006) designed an electrochemical biosensor with an integrated minipotentiostat for identification and quantification of dengue virus RNA. The detection is based on DNA/RNA hybridization and liposome signal amplification. Capture probes specific for *dengue virus* RNA were immobilized on paramagnetic beads, and following hybridization with target RNA as well as with detector oligonucleotide coupled to liposomes, hybridization assembly was separated using magnetic force. Liposomes entrapping the electrochemically active redox couple potassium ferri-/ferrohexacyanide were lysed to release the electrochemical redox markers that were detected on an interdigitated ultramicroelectrode array.

The electrochemical biosensor achieved a limit of detection of 0.01 μM synthetic DNA. Furthermore, the functionality of this biosensor was successfully demonstrated with the detection of dengue virus RNA obtained after nucleic acid sequence-based amplification (NASBA).

Park et al. (2010) introduced a label-free impedimetric sensor for detection of a target RNA sequence located on the internal ribosome entry site of HCV. As recognition element, PNA is immobilized via a well-defined self-assembled monolayer on a gold electrode. Hybridization events of the PNA capture probe with the target RNA were monitored by measuring charge-transfer resistances for the ferricyanide redox probe using Fourier transform electrochemical impedance spectroscopy. The authors determined a limit of detection of 23 pM in rat liver lysate applying this biosensor technique.

Krejcova et al. (2013) combined a fully automated paramagnetic particle-based isolation system and electrochemical detection of oligonucleotides labeled with quantum dots (QDs) for detection of point mutations in neuraminidase gene of *influenza virus* H5N1. The metal part of the oligonucleotide QDs was detected by differential pulse anodic stripping voltammetry. Within an assay time of less than 1 h, detection of subnanogram quantities of target RNA was achieved.

Most other electrochemical biosensors for virus detection described in literature used synthetic DNA oligonucleotides as model analytes instead of RNA or real samples (e.g., Ahour et al. 2013; Pournaghi-Azar et al. 2010; Rai et al. 2012). The applicability of these sensor principles with real samples has still to be demonstrated.

5 Electrochemical Biosensors for Clinically Relevant Biomarker Detection

5.1 Detection of mRNA as Disease Biomarkers

Beside mRNA detection for bacteria identification (see Sect. 4.2), mRNAs can serve as cancer biomarkers important for early *cancer diagnosis* and to predict prognosis and response to therapy. In contrast to mostly used conventional or RT-PCR assays, direct detection of mRNA allows the development of simple and rapid workflows as well as development of low-cost biosensors ideally suited for point-of-care applications.

One of the first reports applying electrochemical biosensors for direct mRNA detection was described by Xie et al. (2004a). Extracted total RNA from animal tissues was labeled with cisplatin-biotin conjugates *via* coordinative bonds with purine bases in the mRNA sequence. Subsequently, labeled mRNAs were hybridized, and glucose-oxidase-avidin conjugates were attached to biotin moieties. Then, the electrode surface was overcoated with a cationic redox polymer containing osmium-bipyridine enabling amperometric detection of the oxidation current of

glucose in solution. The method was applied for detection of breast cancer susceptibility genes, such as p53, hsp90, BRCA1, and histone H4 mRNA. The lowest detectable amount of a specific gene was found to be in the subfemtogram range, i.e., about 800 copies in 1.5 ng of total mRNA (Xie et al. 2004b). The method was later further improved and applied to point mutation detection of p53 tumor suppressor gene mRNA in rat liver tissue (Tansil et al. 2005).

Early, noninvasive diagnosis is an important factor to enhance effectiveness of disease treatment. Particularly, biomarker detection in saliva is a promising application of noninvasive biomarker detection. Using a hairpin probe (immobilized stem-loop oligonucleotide on gold electrode, similar to the arrangement depicted in Fig. 2), interleukin (IL)-8 mRNA (proposed as a salivary biomarker for oral cancer) could be detected amperometrically. *Molecular beacons* were immobilized via 5′-biotin modification of the stem to a gold electrode carrying streptavidin molecules. The 3′-end of the molecular beacon was labeled with a fluorescein moiety. In the absence of target mRNA, steric hindrance avoids binding of bulky anti-fluorescein-HRP conjugate to the fluorescein group in close vicinity of the electrode surface. Interaction with target mRNA opens the hairpin structure of the probe, and the reporter enzyme conjugate can bind to the then accessible fluorescein moiety. Enzymatic reaction of reporter enzyme HRP results in an electrochemically readable signal. This biosensor principle revealed a good correlation with quantitative PCR method and showed a limit of detection of approximately 0.4 fM applying only 5 min hybridization time (Wei et al. 2008). The promising application of a hairpin probe biosensor was further investigated for multiplex biomarker detection (Wei et al. 2009). The electrochemical sensor consisted of a 16-gold-electrode array. A conducting polymer was applied as the supporting film. Furthermore, to enhance biocompatibility, streptavidin-modified dendrimer nanoparticles were introduced into the polymer matrix using electropolymerization. Hairpin probes were immobilized via biotin-streptavidin interaction, and during hybridization with target mRNA (200 s), a cyclic square wave electrical field was applied. Detection of target mRNA was carried out as described above (Wei et al. 2008). Interestingly, in this work, the authors presented a multiplex study detecting IL-8 mRNA and IL-8 protein (immunoassay based) in parallel on the same biochip. Applying the multiplexing assay, limit of detection of salivary IL-8 mRNA reached to 3.9 fM in saliva, whereas limit of detection of IL-8 protein was 7.4 pg mL^{-1} in saliva. Parallel detection of both mRNA and protein biomarkers showed a better correlation with clinical data as compared to single biomarker. Similarly, a stem-loop oligonucleotide probe combined with a switchable “on-off-on” electrochemical technique for the direct detection of survivin mRNA in living cells was developed by Liu et al. (2012). Survivin mRNA becomes an important biomarker for early cancer diagnostics because elevated survivin mRNA levels were found in most human cancer cells.

Nanostructured microelectrodes developed by the group of Kelley (see Fig. 3) were also applied for analysis of mRNA levels in cancer cells (Vasilyeva et al. 2011). As model analyte, the *bcr-abl* gene fusion, which is specific to chronic myeloid leukemia (CML), was used. The authors applied large-footprint sensors

enabling the capture of large analytes. Amino acid/nucleic acid chimeras (ANAs) with good solubility and ability to form stable monolayers were used as capture molecules. The optimized sensor allowed detection of 1 pg μL^{-1} total mRNA, and the current signal increased in a linear manner over four orders of magnitudes of target concentration.

5.2 *Analysis of microRNA for Cancer Diagnostics*

microRNAs (miRNAs) are a class of small (21–25 nucleotides) endogenous non-coding RNAs that regulate gene expression posttranscriptionally in a sequence-specific manner and regulate gene expression by binding to complementary sequences of target mRNAs causing their degradation or translational repression (Bartel 2009). The first miRNA (lin-4) which regulates the gene lin-14 by binding to the 3′-untranslated region of lin-14 mRNA was discovered in *Caenorhabditis elegans* by Lee et al. in 1993. After several years of research, miRNAs are regarded as key posttranscriptional regulators of gene expression (Iorio and Croce 2012).

The public repository for all published miRNA sequences, miRBase, contains in the recent release (v20, June 2013) 24,521 miRNA loci from 206 species, processed to produce 30,424 mature miRNA products (Kozomara and Griffiths-Jones 2014). It was assumed that approximately 30 % of human genes are regulated by miRNAs (Lewis et al. 2005). Furthermore, miRNA dysregulation has been associated with the development and progression of cancer (Hayes et al. 2014; Calin and Croce 2006). Some miRNAs can function as tumor suppressors, whereas others act as oncogenes. Particularly, circulating miRNAs in the plasma and serum constitute a very promising class of biomarkers useful for noninvasive cancer diagnostics. Interestingly, miRNAs packaged in exosomes and microvesicles or bound to specific proteins such as Ago-2 remain rather intact and stable in biological fluids. Therefore, quantification of miRNA levels in peripheral blood has the potential for an early cancer diagnostics or to predict prognosis and response to cancer therapy (Schwarzenbach et al. 2014).

There are several excellent reviews describing traditional assays for miRNA detection covering RT-PCR, Northern blot, and microarrays (Wark et al. 2008; Nelson et al. 2004; Koshiol et al. 2010). However, these traditional molecular techniques require usually extensive sample preparation, including amplification steps elongating total analysis time and introducing measurement bias. Hence, novel methods based on colorimetric, fluorescence, electrochemical, and bioluminescence detection have been developed which reduce assay complexity, analysis time, and costs (Cissell and Deo 2009; Campuzano et al. 2014; Johnson and Mutharasan 2014).

Among label-free electrochemical detection methods, Lusi et al. (2009) developed a method based on G oxidation signal applying G-free inosine-modified DNA probes with potential for detection of miRNA-122 in serum and biopsies. This method revealed a detection limit of 0.1 pM. However, detection of miRNA in real

physiological samples has to be still demonstrated with this technique because the authors used for hybridization synthetic oligonucleotide models.

One very early report of miRNA detection relying on miRNA labeling with electrocatalytic nanoparticle tags was described by Gao and Yang, already in 2006. After treatment of total RNA extracts with periodate, hybridization of periodate-treated miRNA with complementary capture oligonucleotides immobilized on an indium tin oxide electrode was performed. Then, nanoparticle tags, isoniazid-capped OsO_2 nanoparticles, were brought to the electrode through a condensation reaction with the 3′-end of periodate-treated miRNA. The resulting miRNA-modified electrode showed an electrocatalytic activity toward the oxidation of hydrazine, drastically reducing its oxidation overpotential. The established optimized assay exhibited a limit of detection of 80 fM and a linear relationship between current and miRNA concentration up to 200 pM using 60 min hybridization time. The authors demonstrated specific detection of miRNAs in total RNA extracts of HeLa cells. The application of two different transition metal complexes as nanoparticle tags instead of OsO_2 nanoparticles was demonstrated in further studies. The electrocatalytic moiety was introduced either by coordinative bonds with purine bases in the miRNA (Gao and Yu 2007a) or by covalent ligation to the 3′-end of miRNAs (Gao and Yu 2007b). The optimized assay allowed the detection of miRNAs in the range of 0.50–400 pM with a limit of detection 0.2 pM (Gao and Yu 2007a). In 2011, Peng and Gao introduced a biosensor applying ruthenium oxide nanoparticle-initiated polymerization of 3,3′-dimethoxybenzidine and miRNA-templated deposition of an insulating poly(3,3′-dimethoxybenzidine) film. In this study, miRNA is labeled with ruthenium oxide nanoparticles. Electrochemical impedance spectroscopy revealed a linear relationship of charge-transfer resistance vs. concentration from 6.0 fM to 2.0 pM after 1 h hybridization and 1 h polymerization reaction. The performance of the developed biosensor was tested applying three different miRNAs (miR-720, let-7c, and miR-1248). However, described detection methods are based on direct labeling of miRNAs, thus, increasing the complexity of the assay due to mandatory labeling steps of miRNA. Hence, Dong et al. (2012) used oligonucleotide-encapsulated silver nanoclusters (Ag-NCs) as electrochemical tags for label-free miRNA detection. After hybridization of miRNA to an immobilized stem-loop structure, the oligonucleotide Ag-NCs are brought into the vicinity of the electrode. The efficient catalytic property of Ag-NCs toward H_2O_2 reduction resulted in a detectable electrochemical response down to 67 fM miRNA concentration.

A simple magnetic bead-based electrochemical assay for miRNA detection applying miRNA 3′-end labeling using osmium(VI) was reported recently (Bartosik et al. 2014). Already in 2010, a similar approach was proposed by the same group, while the new approach exhibits better sensitivity (Trefulka et al. 2010). A quick, two-step labeling procedure (approximately 25 min) of 3′-ribose of miRNA using osmium(VI) and 2,2′-bipyridine was established. Labeled miRNA was hybridized to biotinylated DNA capture probes bound to streptavidin magnetic beads and subsequently detected at hanging mercury drop electrode. A limit of detection in the femtomole range (approximately 10 nM) was achieved using miR-522. The

developed sensor showed capability of single-mismatch discrimination and was successfully applied to total RNA samples from *in vitro* cultured cancer cell lines.

Impressive sensitivity was achieved using an electrochemical miRNA biosensor applying nanostructured microelectrodes modified with PNA probes. PNA probes were used due to their higher affinity toward short miRNA sequences compared to DNA probes. After 30 min hybridization of unlabeled miRNA, duplex formation was electrochemically detected by electrocatalytic Ru(III) redox reporter system (see also Fig. 3). Ru(III) was accumulated on the electrode surface. Inclusion of ferricyanide was used to amplify the signals of the redox reporter system. Using miR-21 as model analyte, a limit of detection of 10 aM was achieved (corresponds to approximately ten molecules per μL sample). Additionally, the authors demonstrated application of the electrochemical biosensor for analysis of miRNA extracted from normal human cells as well as from human head and neck squamous cancer cells grown in culture (Yang et al. 2009).

Another strategy for miRNA detection utilized target-guided polymer wire formation in nano-gaps onto an array composed of up to 100 pairs of interlocking comblike microelectrodes. After hybridization of miRNA to PNA capture probe and addition of a mixture of aniline/HRP/H_2O_2 at pH 4.0, the protonated aniline molecules are concentrated around the negatively charged miRNA molecules resulting in polyaniline nanowires. A dynamic range from 20 pM to 10 fM and a limit of detection of 5 fM were achieved (Fan et al. 2007).

A rapid and simple enzyme-amplified electrochemical detection strategy for miRNA using a *gap hybridization assay* was developed by Pöhlmann and Sprinzl (2010). Only in presence of a specific miRNA binding between an immobilized capture oligonucleotide and an esterase 2-detector oligonucleotide conjugate, the reporter enzyme esterase 2 is brought in vicinity to the gold electrode and produced an enzyme-mediated electrochemical signal (Fig. 4). The authors demonstrated with miR-16 as model analyte selective detection of miR-16 within a mixture of other miRNAs, including discrimination of single-base mismatches. A limit of detection of 2 pM (or 2 amoles in 1 μL droplets) miR-16 was reported within a total analysis time of less than 30 min (without sample preparation). Additionally, miRNA expression analysis of two miRNAs miR-16 and miR-21 in human breast adenocarcinoma cells was demonstrated successfully.

A very interesting report relying on DNA nanostructure as recognition element for sensitive electrochemical analysis of miRNA was presented recently (Wen et al. 2012). Similar to the gap hybridization assay described above, the presented electrochemical miRNA sensor employed also a base-stacking strategy. A tetrahedron-structured probe containing three thiol groups is immobilized via thiol-gold linkage on a gold electrode. A capture DNA probe complementary to part of analyte miRNA is appended on a vertex of the tetrahedron-structure probe. A sandwich assay is performed by hybridization of a biotin-labeled detector probe complementary to the other part of the miRNA. Applying this assembly, the sandwich assembly is stabilized by the base pairing between the two oligonucleotide probes and the target miRNA as well as the base-stacking forces between the

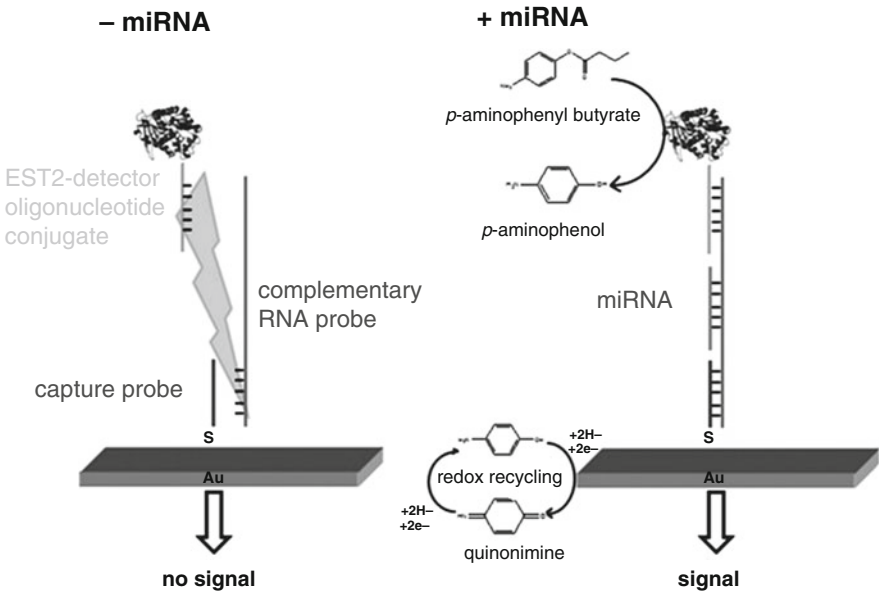

Fig. 4 Electrochemical gap hybridization assay for miRNA detection. In absence of specific miRNA, no hybridization assembly is achieved on the gold electrode due to lack of stabilizing coaxial base pairing. In presence of specific miRNA, a four-component hybridization assembly composed of immobilized capture oligonucleotide, miRNA, reporter enzyme-detector oligonucleotide, and complementary oligonucleotide is produced, and enzyme-mediated electrochemical signal is produced (Adapted with permission from Pöhlmann and Sprinzl (2010), Electrochemical detection of microRNAs via gap hybridization assay. Anal Chem 82:4434–4440. Copyright (2010) American Chemical Society)

padlock probes. An enzyme-mediated electrochemical signal is generated by addition of avidin-HRP catalyzing the reduction of hydrogen peroxide and generating quantitative electrochemical signal in the presence of the co-substrate 3,3′,5,5′-tetramethylbenzidine. This DNA nanostructure-based electrochemical biosensor achieved a limit of detection of 10 fM for model analyte miR-21. Significant signal amplification was shown employing a polymerized streptavidin-HRP conjugate (poly-HRP). This reporter enzyme conjugate contained up to 400 HRP molecules per conjugate. Applying this polymerized conjugate, the sensor could detect down to 10 aM miRNAs. Furthermore, the authors demonstrated the application of this sensor for analyzing miRNA expression levels in clinical samples from esophageal squamous cell carcinoma patients. An identical limit of detection (10 aM) was achieved by combining the use of tetrahedral DNA nanostructure probes as described above and hybridization chain reaction amplification within a total analysis time of more than 4 h. However, in this study, the authors showed no application of the biosensor with real samples (Ge et al. 2014). Labib et al. (2013a) developed a *DNA four-way junction*-based electrochemical sensor for miRNA analysis. The presented multicomponent sensor consisted of a universal interfacial

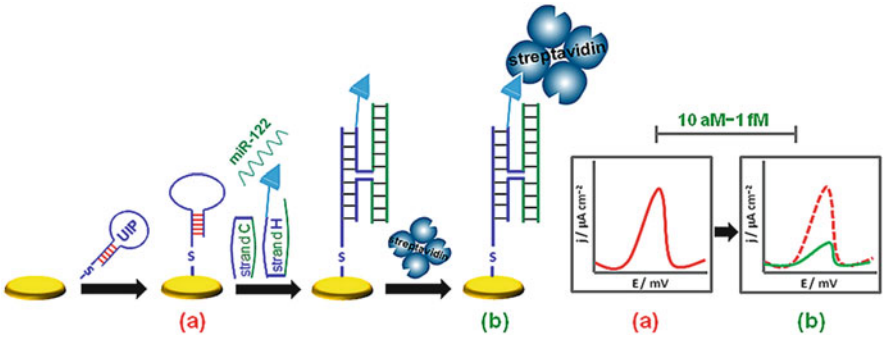

Fig. 5 Schematic representation of the DNA four-way junction-based electrochemical sensor (4J-SENS) for miRNA analysis. The universal interfacial probe (UIP) was immobilized on the gold electrode (**a**). The two DNA adaptor strands (strand C and strand H) cooperatively hybridize to complementary parts of miRNA and the immobilized universal interfacial probe (**b**). In a final step, tetrameric streptavidin can bind to biotinylated stand H resulting in a current decrease measured by square wave voltammetry (Reprinted with permission from Labib et al. (2013a), Four-way junction formation promoting ultrasensitive electrochemical detection of microRNA. Anal Chem 85:9422–9427. Copyright (2013) American Chemical Society)

probe (UIP) and two DNA adaptor strands which cooperatively hybridize to complementary parts of miRNA and the immobilized UIP. In the absence of target miRNA, the two adaptor strands cannot interact with the UIP due to the stable stem-loop structure of the UIP which is thermodynamically more stable than the assembly with the adaptor strands. However, in the presence of target miRNA, the two adaptor strands form a hybridization assembly with miRNA and the UIP, resulting in a quadripartite complex with a four-way junction structure (Fig. 5). Additionally, one of the two adaptor strands is biotin labeled and can bind a streptavidin to produce a significant increase in the interfacial resistance of the sensor surface (signal-off sensor). Application of this sensor for miR-122 detection revealed a dynamic range from 10 aM to 1 fM with a limit of detection of 2 aM within a total analysis time of approximately 90 min. The sensor was also employed for expression analysis of hsa-miR-122 in healthy human serum and chronic lymphocytic leukemia (CLL) patient serum. Obtained results were in good correlation with qPCR analysis. The same research group developed also a three-mode electrochemical sensor applying three different detection modalities (hybridization, p19 binding protein, and protein displacement) for miRNA quantification. This sensor allowed detection of 5 aM miRNA per 30 µL sample volume and could be operated within a dynamic range of 10 aM to 1 µM (Labib et al. 2013b).

Ramnani et al. (2013) used the RNA-binding protein p19 from Carnation Italian ringspot virus (CIRV) in combination with carbon-nanotube field-effect transistor (CNT-FET) transducer for sensitive and specific miRNA detection. After hybridization of miRNA to a complementary RNA probe, p19 fusion protein binds tightly to RNA/miRNA duplexes. This results in a change in conductance of the carbon nanotubes. This sensor detected miR-122a, a specific liver marker linked with lipid

metabolism, liver homeostasis, and hepatitis C virus replication, from 1 aM to 10 fM in the presence of a millionfold excess of total RNA and other miRNA sequences. Kilic et al. (2013) applied also viral protein p19 as a molecular caliper. The authors determined oxidation signal of p19 for detection of miR-21. Using this sensor, a limit of detection for miR-21 in the pmole range was possible because changes of intrinsic p19 oxidation signals were observed with differential pulse voltammetry.

Tran et al. (2013) proposed an electrochemical biosensor strategy based on antibodies directed to DNA/RNA hybrids for detection of miR-29b-1 and miR-141. A DNA probe complementary to target miRNA was covalently grafted on a conducted polymer/reduced oxide-modified electrode. After hybridization with target miRNA, square wave voltammetry was applied to record the redox signal (signal on). The dynamic range of this biosensor was from 1 fM to 1 nM. After addition of RNA/DNA duplex-specific antibodies, current decreased (signal off) which confirmed the presence of a specific miRNA with a limit of detection of 8 fM. Subsequently, addition of miRNA/DNA duplexes in solution caused a shift-back of the current signal (signal on). This on-off-on detection sequence guaranteed high reliability of miRNA detection. However, this biosensor was only tested with synthetic oligonucleotides, and robustness of on-off-on detection sequence toward real samples has still to be demonstrated.

Recently, a label-free approach for miRNA detection based on *isothermal amplification* was developed by Reni et al. (2013). After hybridization of target miRNA to complementary capture probe immobilized on a gold electrode, miRNA/DNA duplexes are cleaved off by a duplex-specific nuclease. Released target miRNAs are recycled for another round of hybridization offering an isothermal signal amplification cycle. The significant difference in electrochemical impedance between a duplex-specific nuclease cleaved and a not cleaved electrode enables miRNA detection down to 1 fM. Application of this electrochemical biosensor for detection of miRNAs in serum was successfully demonstrated. Advantages of this strategy are the simple assay protocol with minimal or no sample pretreatments as well as isothermal amplification process. An analogous approach, using T7 exonuclease for cleavage of miRNA/DNA duplexes instead of duplex-specific nuclease achieved a detection limit of 0.17 fM (Wang et al. 2014).

6 Future Perspectives of Electrochemical Biosensors for Direct RNA Detection

The development of electrochemical biosensors for direct RNA detection is still a challenging task due to the fact that high sensitivity has to be a mandatory characteristic of these techniques to meet the requirement of nucleic acid amplification-free concept. Current clinical diagnostic systems are mainly PCR based, limited for use in specialized laboratories in hospitals and clinics, and still

relatively complex and expensive. Therefore, most of these PCR-based techniques still require well-trained personnel and are not suitable for point-of-care diagnostics or on-site detection in settings outside clinics or specialized analytical laboratories. *Integrated sample preparation* with nucleic acid amplification and detection in a robust, cheap, and user-friendly manner still remains challenging. Therefore, biosensors enabling direct detection of RNA avoiding PCR-based nucleic acid amplification will be of substantial interest. The development of integrated devices combining sample preparation (cell lysis and RNA purification) and biochip detection is another field which is of utmost importance for robust applications of these biosensors as point-of-care devices. In the future, there will be ongoing research in overcoming mass transfer limitations because of the use of nanoscale sensing elements (Johnson and Mutharasan 2014). Another important parameter—particularly for application of biosensors in real scenarios—is the reduction of *nonspecific binding* effects and the generation of self-assembled monolayers avoiding nonspecific adsorption. Additionally, signal amplification technologies enhancing the reliability and improving the limits of detection of biosensor measurements are a very active research field.

7 Conclusions

Electrochemical biosensors are optimally suited for direct RNA detection due to their high sensitivity combined with high specificity and low-cost production. The resulting simple workflow requiring only minimal sample preparation simplifies the design of on-site detection devices for different applications such as clinical diagnostics, food pathogen identification, or environmental analysis. This chapter demonstrated various examples for successful direct RNA detection, e.g., the sensitive identification of bacteria based on 16S rRNA or mRNA detection, the detection of viral RNA sequences, or the quantification of mRNA or miRNA biomarkers relevant for cancer diagnostics.

References

Ahour F, Pournaghi-Azar MH, Alipour E et al (2013) Detection and discrimination of recombinant plasmid encoding hepatitis C virus core/E1 gene based on PNA and double-stranded DNA hybridization. Biosens Bioelectron 45:287–291

Arora P, Sindhu A, Kaur H et al (2013) An overview of transducers as platform for the rapid detection of foodborne pathogens. Appl Microbiol Biotechnol 97:1829–1840

Bartel DP (2009) MicroRNAs: target recognition and regulatory functions. Cell 136:215–233

Bartosik M, Hrstka R, Palecek E et al (2014) Magnetic bead-based hybridization assay for electrochemical detection of microRNA. Anal Chim Acta 813:35–40

Bercovici M, Han CM, Liao JC et al (2012) Rapid hybridization of nucleic acids using isotachophoresis. Proc Natl Acad Sci U S A 109:11127–11132

Besant JD, Das J, Sargent EH et al (2013) Proximal bacterial lysis and detection in nanoliter wells using electrochemistry. ACS Nano 7:8183–8189

Brandt O, Hoheisel JD (2004) Peptide nucleic acids on microarrays and other biosensors. Trends Biotechnol 22:617–622

Bratkovic T, Rogelj B (2011) Biology and applications of small nucleolar RNAs. Cell Mol Life Sci 68:3843–3851

Bremer H, Dennis PP (1996) Modulation of chemical composition and other parameters the cell by growth rate. In: Neidhardt FC, Curtiss R III, Ingraham JL, Lin ECC, Low KB, Magasanik B, Reznikoff WS, Riley M, Schaechter M, Umbarger HE (eds) Escherichia coli and Salmonella: cellular and molecular biology, vol 2, 2nd edn. ASM Press, Washington, DC, p 1553

Calin GA, Croce CM (2006) MicroRNA signatures in human cancers. Nat Rev Cancer 6:857–866

Campuzano S, Kuralay F, Lobo-Castanon MJ et al (2011) Ternary monolayers as DNA recognition interfaces for direct and sensitive electrochemical detection in untreated clinical samples. Biosens Bioelectron 26:3577–3583

Campuzano S, Pedrero M, Pingarrón JM (2014) Electrochemical genosensors for the detection of cancer-related miRNAs. Anal Bioanal Chem 406:27–33

Caygill RL, Blair GE, Millner PA (2010) A review on viral biosensors to detect human pathogens. Anal Chim Acta 681:8–15

Cissell KA, Deo SK (2009) Trends in microRNA detection. Anal Bioanal Chem 394:1109–1116

Dong H, Jin S, Ju H et al (2012) Trace and label-free microRNA detection using oligonucleotide encapsulated silver nanoclusters as probes. Anal Chem 84:8670–8674

Drummond TG, Hill GH, Barton JK (2003) Electrochemical DNA sensors. Nat Biotechnol 21:1192–1199

Elsholz B, Worl R, Blohm L et al (2006) Automated detection and quantitation of bacterial RNA by using electrical microarrays. Anal Chem 78:4794–4802

Fan Y, Chen X, Trigg AD et al (2007) Detection of MicroRNAs using target-guided formation of conducting polymer nanowires in nanogaps. J Am Chem Soc 129:5437–5443

Fang Z, Soleymani L, Pampalakis G et al (2009) Direct profiling of cancer biomarkers in tumor tissue using a multiplexed nanostructured microelectrode integrated circuit. ACS Nano 3:3207–3213

Gabig-Ciminska M, Holmgren A, Andresen H et al (2004) Electric chips for rapid detection and quantification of nucleic acids. Biosens Bioelectron 19:537–546

Gao Z, Yang Z (2006) Detection of microRNAs using electrocatalytic nanoparticle tags. Anal Chem 78:1470–1477

Gao Z, Yu YH (2007a) Direct labeling microRNA with an electrocatalytic moiety and its application in ultrasensitive microRNA assays. Biosens Bioelectron 22:933–940

Gao Z, Yu YH (2007b) A microRNA biosensor based on direct chemical ligation and electrochemically amplified detection. Sens Actuators B 121:552–559

Ge Z, Lin M, Wang P et al (2014) Hybridization chain reaction amplification of microRNA detection with a tetrahedral DNA nanostructure-based electrochemical biosensor. Anal Chem 86:2124–2130

Hartman MR, Ruiz RC, Hamada S et al (2013) Point-of-care nucleic acid detection using nanotechnology. Nanoscale 5:10141–10154

Hayes J, Peruzzi PP, Lawler S (2014) MicroRNAs in cancer: biomarkers, functions and therapy. Trends Mol Med 20:460–469

Heidenreich B, Pohlmann C, Sprinzl M et al (2010) Detection of Escherichia coli in meat with an electrochemical biochip. J Food Prot 73:2025–2033

Hintsche R, Paeschke M, Uhlig A et al (1997) Microbiosensors using electrodes made in Si-technology. Experientia Suppl 80:267–283

Humenik M, Pohlmann C, Wang Y et al (2008) Enhancement of electrochemical signal on gold electrodes by polyvalent esterase-dendrimer clusters. Bioconjug Chem 19:2456–2461

Iorio MV, Croce CM (2012) MicroRNA dysregulation in cancer: diagnostics, monitoring and therapeutics. A comprehensive review. EMBO Mol Med 4:143–159

Johnson BN, Mutharasan R (2014) Biosensor-based microRNA detection: techniques, design, performance, and challenges. Analyst 139:1576–1588
Jurgen B, Barken KB, Tobisch S et al (2005) Application of an electric DNA-chip for the expression analysis of bioprocess-relevant marker genes of Bacillus subtilis. Biotechnol Bioeng 92:299–307
Keer JT, Birch L (2003) Molecular methods for the assessment of bacterial viability. J Microbiol Methods 53:175–183
Kilic T, Nur TS, Ozsoz M (2013) A new insight into electrochemical microRNA detection: a molecular caliper, p19 protein. Biosens Bioelectron 48:165–171
Kirsch J, Siltanen C, Zhou Q et al (2013) Biosensor technology: recent advances in threat agent detection and medicine. Chem Soc Rev 42:8733–8768
Koshiol J, Wang E, Zhao Y et al (2010) Strengths and limitations of laboratory procedures for microRNA detection. Cancer Epidemiol Biomarkers Prev 19:907–911
Kozomara A, Griffiths-Jones S (2014) miRBase: annotating high confidence microRNAs using deep sequencing data. Nucleic Acids Res 42:D68–D73
Krejcova L, Hynek D, Kopel P et al (2013) Development of a magnetic electrochemical bar code array for point mutation detection in the H5N1 neuraminidase gene. Viruses 5:1719–1739
Kwakye S, Goral VN, Baeumner AJ (2006) Electrochemical microfluidic biosensor for nucleic acid detection with integrated minipotentiostat. Biosens Bioelectron 21:2217–2223
Labib M, Ghobadloo SM, Khan N et al (2013a) Four-way junction formation promoting ultrasensitive electrochemical detection of microRNA. Anal Chem 85:9422–9427
Labib M, Khan N, Ghobadloo SM et al (2013b) Three-mode electrochemical sensing of ultralow microRNA levels. J Am Chem Soc 135:3027–3038
LaGier MJ, Scholin CA, Fell JW et al (2005) An electrochemical RNA hybridization assay for detection of the fecal indicator bacterium Escherichia coli. Mar Pollut Bull 50:1251–1261
Lam B, Fang Z, Sargent EH et al (2012) Polymerase chain reaction-free, sample-to-answer bacterial detection in 30 minutes with integrated cell lysis. Anal Chem 84:21–25
Lee RC, Feinbaum RL, Ambros V (1993) The C. elegans heterochronic gene lin-4 encodes small RNAs with antisense complementarity to lin-14. Cell 75:843–854
Leontis NB, Stombaugh J, Westhof E (2002) Motif prediction in ribosomal RNAs Lessons and prospects for automated motif prediction in homologous RNA molecules. Biochimie 84:961–973
Lewis BP, Burge CB, Bartel DP (2005) Conserved seed pairing, often flanked by adenosines, indicates that thousands of human genes are microRNA targets. Cell 120:15–20
Liao JC, Mastali M, Gau V et al (2006) Use of electrochemical DNA biosensors for rapid molecular identification of uropathogens in clinical urine specimens. J Clin Microbiol 44:561–570
Liao JC, Mastali M, Li Y et al (2007) Development of an advanced electrochemical DNA biosensor for bacterial pathogen detection. J Mol Diagn 9:158–168
Liu C, Zeng GM, Tang L et al (2011) Electrochemical detection of Pseudomonas aeruginosa 16S rRNA using a biosensor based on immobilized stem-loop structured probe. Enzyme Microb Technol 49:266–271
Liu J, Zhou H, Xu JJ et al (2012) Switchable 'on-off-on' electrochemical technique for direct detection of survivin mRNA in living cells. Analyst 137:3940–3945
Liu T, Sin ML, Pyne JD et al (2014a) Electrokinetic stringency control in self-assembled monolayer-based biosensors for multiplex urinary tract infection diagnosis. Nanomedicine 10:159–166
Liu T, Lu Y, Gau V et al (2014b) Rapid antimicrobial susceptibility testing with electrokinetics enhanced biosensors for diagnosis of acute bacterial infections. Ann Biomed Eng. doi:10.1007/s10439-014-1040-6
Lusi EA, Passamano M, Guarascio P et al (2009) Innovative electrochemical approach for an early detection of microRNAs. Anal Chem 81:2819–2822

Mach KE, Du CB, Phull H et al (2009) Multiplex pathogen identification for polymicrobial urinary tract infections using biosensor technology: a prospective clinical study. J Urol 182:2735–2741
Mastali M, Babbitt JT, Li Y et al (2008) Optimal probe length and target location for electrochemical detection of selected uropathogens at ambient temperature. J Clin Microbiol 46:2707–2716
Metfies K, Huljic S, Lange M et al (2005) Electrochemical detection of the toxic dinoflagellate Alexandrium ostenfeldii with a DNA-biosensor. Biosens Bioelectron 20:1349–1357
Mohan R, Mach KE, Bercovici M et al (2011) Clinical validation of integrated nucleic acid and protein detection on an electrochemical biosensor array for urinary tract infection diagnosis. PLoS One 6:e26846
Moore PB (1999) Structural motifs in RNA. Annu Rev Biochem 68:287–300
Nelson PT, Baldwin DA, Scearce LM et al (2004) Microarray-based, high-throughput gene expression profiling of microRNAs. Nat Methods 1:155–161
Nielsen HB, Wernersson R, Knudsen S (2003) Design of oligonucleotides for microarrays and perspectives for design of multi-transcriptome arrays. Nucleic Acids Res 31:3491–3496
Niwa XY, Halsall HB, Heinemann WR (1993) Small-volume voltammetric detection of 4-aminophenol with interdigitated array electrodes and its application to electrochemical enzyme immunoassay. Anal Chem 65:1559–1563
Ouyang M, Mohan R, Lu Y et al (2013) An AC electrokinetics facilitated biosensor cassette for rapid pathogen identification. Analyst 138:3660–3666
Palecek E, Bartosik M (2012) Electrochemistry of nucleic acids. Chem Rev 112:3427–3481
Park JY, Lee YS, Chang BY et al (2010) Label-free impedimetric sensor for a ribonucleic acid oligomer specific to hepatitis C virus at a self-assembled monolayer-covered electrode. Anal Chem 82:8342–8348
Patel M, Gonzalez R, Halford C et al (2011) Target-specific capture enhances sensitivity of electrochemical detection of bacterial pathogens. J Clin Microbiol 49:4293–4296
Peng Y, Gao Z (2011) Amplified detection of microRNA based on ruthenium oxide nanoparticle-initiated deposition of an insulating film. Anal Chem 83:820–827
Pioch D, Jürgen B, Evers S et al (2007) At-line monitoring of bioprocess-relevant marker genes. Eng Life Sci 7:373–379
Pioch D, Jurgen B, Evers S et al (2008) Improved sandwich-hybridization assay for an electrical DNA-chip-based monitoring of bioprocess-relevant marker genes. Appl Microbiol Biotechnol 78:719–728
Pöhlmann C, Sprinzl M (2010) Electrochemical detection of microRNAs via gap hybridization assay. Anal Chem 82:4434–4440
Pöhlmann C, Wang Y, Humenik M et al (2009a) Rapid, specific and sensitive electrochemical detection of foodborne bacteria. Biosens Bioelectron 24:2766–2771
Pöhlmann C, Humenik M, Sprinzl M (2009b) Detection of bacterial 16S rRNA using multivalent dendrimer-reporter enzyme conjugates. Biosens Bioelectron 24:3383–3386
Pournaghi-Azar MH, Ahour F, Hejazi MS (2010) Direct detection and discrimination of double-stranded oligonucleotide corresponding to hepatitis C virus genotype 3a using an electrochemical DNA biosensor based on peptide nucleic acid and double-stranded DNA hybridization. Anal Bioanal Chem 397:3581–3587
Rai V, Hapuarachchi HC, Ng LC et al (2012) Ultrasensitive cDNA detection of dengue virus RNA using electrochemical nanoporous membrane-based biosensor. PLoS One 7:e42346
Ramnani P, Gao Y, Ozsoz M et al (2013) Electronic detection of microRNA at attomolar level with high specificity. Anal Chem 85:8061–8064
Reni Y, Deng H, Shen W et al (2013) A highly sensitive and selective electrochemical biosensor for direct detection of microRNAs in serum. Anal Chem 85:4784–4789
Schwarzenbach H, Nishida N, Calin GA et al (2014) Clinical relevance of circulating cell-free microRNAs in cancer. Nat Rev Clin Oncol 11:145–156
Scott JD, Gretch DR (2007) Molecular diagnostics of hepatitis C virus infection: a systematic review. JAMA 297:724–732

Shawky SM, Bald D, Azzazy HM (2010) Direct detection of unamplified hepatitis C virus RNA using unmodified gold nanoparticles. Clin Biochem 43:1163–1168

Shipovskov S, Saunders AM, Nielsen JS et al (2012) Electrochemical sandwich assay for attomole analysis of DNA and RNA from beer spoilage bacteria Lactobacillus brevis. Biosens Bioelectron 37:99–106

Sun CP, Liao JC, Zhang YH et al (2005) Rapid, species-specific detection of uropathogen 16S rDNA and rRNA at ambient temperature by dot-blot hybridization and an electrochemical sensor array. Mol Genet Metab 84:90–99

Tansil NC, Xie F, Xie H et al. (2005) An ultrasensitive nucleic acid biosensor based on the catalytic oxidation of guanine by a novel redox threading intercalator. Chem Commun (Camb) 8:1064–1066

Tran HV, Piro B, Reisberg S et al (2013) Antibodies directed to RNA/DNA hybrids: an electrochemical immunosensor for microRNAs detection using graphene-composite electrodes. Anal Chem 85:8469–8474

Trefulka M, Bartosik M, Palecek E (2010) Facile end-labeling of RNA with electroactive Os (VI) complexes. Electrochem Commun 12:1760–1763

Vasilyeva E, Lam B, Fang Z et al (2011) Direct genetic analysis of ten cancer cells: tuning sensor structure and molecular probe design for efficient mRNA capture. Angew Chem Int Ed Engl 50:4137–4141

Walter A, Wu J, Flechsig GU et al (2011) Redox cycling amplified electrochemical detection of DNA hybridization: application to pathogen E. coli bacterial RNA. Anal Chim Acta 689:29–33

Wang M, Fu Z, Li B et al (2014) One-step, ultrasensitive, and electrochemical assay of microRNAs based on T7 exonuclease assisted cyclic enzymatic amplification. Anal Chem 86:5606–5610

Wark AW, Lee HJ, Corn RM (2008) Multiplexed detection methods for profiling microRNA expression in biological samples. Angew Chem Int Ed Engl 47:644–652

Wei F, Wang J, Liao W et al (2008) Electrochemical detection of low-copy number salivary RNA based on specific signal amplification with a hairpin probe. Nucleic Acids Res 36:e65

Wei F, Patel P, Liao W et al (2009) Electrochemical sensor for multiplex biomarkers detection. Clin Cancer Res 15:4446–4452

Wen Y, Pei H, Shen Y et al (2012) DNA Nanostructure-based Interfacial engineering for PCR-free ultrasensitive electrochemical analysis of microRNA. Sci Rep 2:867

Westhof E (2010) The amazing world of bacterial structured RNAs. Genome Biol 11:108

Wongkaew N, He P, Kurth V et al (2013) Multi-channel PMMA microfluidic biosensor with integrated IDUAs for electrochemical detection. Anal Bioanal Chem 405:5965–5974

Wu J, Chumbimuni-Torres KY, Galik M et al (2009) Potentiometric detection of DNA hybridization using enzyme-induced metallization and a silver ion selective electrode. Anal Chem 81:10007–10012

Wu J, Campuzano S, Halford C et al (2010) Ternary surface monolayers for ultrasensitive (zeptomole) amperometric detection of nucleic acid hybridization without signal amplification. Anal Chem 82:8830–8837

Xie H, Yu YH, Xie F et al (2004a) A nucleic acid biosensor for gene expression analysis in nanograms of mRNA. Anal Chem 76:4023–4029

Xie H, Yu YH, Xie F et al (2004b) Breast cancer susceptibility gene mRNAs quantified by microarrays with electrochemical detection. Clin Chem 50:1231–1233

Yang H, Hui A, Pampalakis G et al (2009) Direct, electronic microRNA detection for the rapid determination of differential expression profiles. Angew Chem Int Ed Engl 48:8461–8464

DNA and PNA Probes for DNA Detection in Electroanalytical Systems

Benoît Piro, Vincent Noël, and Steeve Reisberg

Contents

Abstract There is a strong demand for sensitive DNA assays that are fast, simple to use, and inexpensive. Traditional approaches rely on labeled molecules, for example, fluorescent probes, providing an optical transduction. However, modern electroanalytical approaches have been described since the 1990s, involving electrochemical then transistor-based transductions. In addition to classical DNA probes, initially developed for other purposes, many forms of promising nucleic acid analogs and mimics were also involved in DNA sensors, such as locked nucleic acids (LNAs), peptide nucleic acids (PNAs), and other XNAs. More recently, transduction architectures based on nanometer-sized devices (not only nanoparticles but nanogaps, nanowires, nanopores, etc.) have been described, allowing exceedingly high sensitivities.

B. Piro (✉) • V. Noël • S. Reisberg
University Paris Diderot, Sorbonne Paris Cité, ITODYS, UMR 7086 CNRS, 15 rue J-A de Baïf, 75205 Paris Cedex 13, France
e-mail: piro@univ-paris-diderot.fr

V.A. Erdmann et al. (eds.), *RNA and DNA Diagnostics*, RNA Technologies,
DOI 10.1007/978-3-319-17305-4_3

Keywords Deoxyribonucleic acid (DNA) • Peptide nucleic acid (PNA) • Electrochemical sensors • Field-effect transistors • Electrochemical transistors • Lab-on-chips

1 Introduction

It makes no sense to discuss about deoxyribonucleic acid (DNA) generalities here. One may only remind readers that among all biomolecules, DNA is considered the easiest to detect because molecular recognition of the target single strand by a complementary capture strand is based on hybridization, a perfectly well-understood mechanism. Even if hybridization is known since 1953, it is not before the beginning of the 1990s that an electrochemical DNA detection was proposed and 4 years later for FET devices. Since these dates, progresses were extreme. These techniques are now ready for integration in chips and brought to the market.

2 Electrochemical Systems

2.1 DNA Probes

2.1.1 Generalities on Electrochemical Systems Using DNA Probes

Electrochemical detection of deoxyribonucleic acids seriously emerged in the early 1990s; a number of good reviews have been published since then (Willner et al. 1999; Drummond et al. 2003; Paleček and Jelen 2002; Fan et al. 2003; Kouřilová et al. 2005; Lucarelli et al. 2004; Odenthal and Gooding 2007; Rai and Toh 2013; Lazerges and Bedioui 2013; Paleček and Bartošík 2012). DNA-based electrochemical sensors use oligonucleotides (ODN), short single-stranded synthetic DNA molecules (10–40 bases, ssDNA) generally immobilized on a surface to hybridize a complementary target sequence generally in solution. Different kinds of electrochemical detections were developed, mainly using electrochemistry of DNA bases or labels such as organometallic complexes, electroactive organic molecules, or enzymes. Probes may be immobilized through self-assembled monolayers (SAMs), diazonium chemistry, or conducting polymers, on various surfaces from classical electrodes to nanostructured ones. Most of the transduction mechanisms rely on the fact that hybridization induces a conformational change which alters mass transport or charge transfer properties.

2.1.2 Organometallic Complexes

Organometallic complexes used as intercalators were recently reviewed (Wei et al. 2011). In the early 1990s, it was shown that organometallic complexes may be used to detect DNA hybridization using cyclic voltammetry (CV) (Millan and Mikkelsen 1993). Electroactive intercalator $Co(bpy)^{3+}$ and $Co(phen)^{3+}$ complexes associate with negatively charged dsDNA immobilized on the electrode and therefore give an electrochemical signal proportional to the quantity of hybrids. For example, using cobalt phenanthroline complexes (Niu et al. 2006) allows a limit of detection (LoD) of 27 pM using differential pulse voltammetry (DPV). $[Ru(NH_3)_6]^{3+}$ was also used (Zhang et al. 2006), with a LoD in fM range. Poly (4-vinylpyridine) (PVP) bearing an osmium complex, with a 1,000 times higher sensitivity (0.5 aM) than the monomeric complex, and which allowed discrimination of single- and double-base-mismatched DNA has been employed (Liu and Anzai 2004).

2.1.3 Electroactive Organic Molecules

On the same model, organic molecules were used as redox reporter. For example, 2-nitroacridone (binding constant of 3.19×10^5 L mol^{-1} for dsDNA) was used to detect DNA sequence related to chronic myelogenous leukemia with LoD of 6.7×10^{-9} M (Chen et al. 2008). A supramolecular approach was also followed by Li et al. (2007), where transduction is accomplished by aggregation of nucleic acid-functionalized gold nanoparticles (AuNPs) and intercalation of electroactive methylene blue (MB) in the aggregated DNA (Fig. 1).

2.1.4 Nanoparticles

Magnetic and electroactive nanoparticles were frequently used for detection of DNA hybridization, e.g., Wang et al.(2002), who described cadmium sulfide NPs

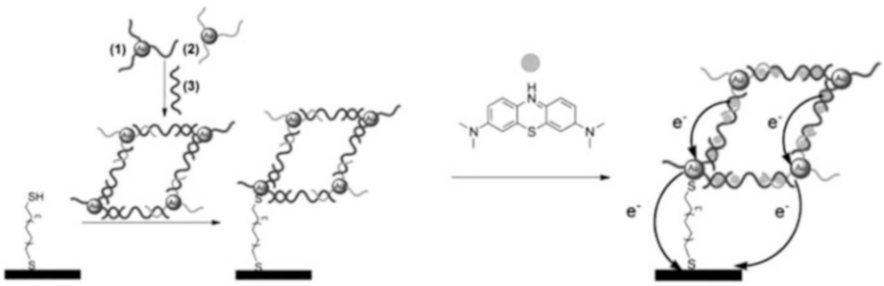

Fig. 1 *Left* Schematic representation of redox polymer association with hybrids followed by an electrochemical signal. *Right* Electrochemical detection of DNA through the aggregation of AuNPs and redox-active MB intercalator in the duplex-aggregated NPs [Adapted from Li et al. (2007), with permission of The Royal Society of Chemistry]

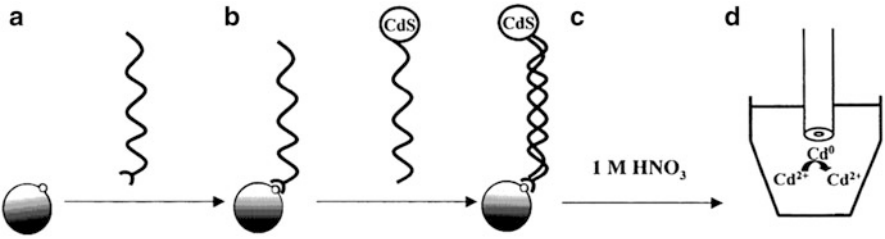

Fig. 2 (**a**) Binding of the target to the magnetic beads, (**b**) hybridization with the CdS-labeled probe, (**c**) dissolution of CdS tag, (**d**) potentiometric stripping detection at a mercury-film electrode [Reprinted from Wang et al. (2002). Copyright 2002, with permission from Elsevier]

combined to electrochemical stripping measurements of the cadmium and a "magnetic" collection of the magnetic-bead/dsDNA/CdS assembly, giving a LoD of 100 fM (Fig. 2). Reviews are available on this topic (Wang 2003; Zanoli et al. 2012).

2.1.5 Enzyme Labeling

DNA labeling with redox enzymes was extensively investigated (Paleček and Bartošík 2012). The general principle relies on a biotinylated target DNA, to allow an avidin-conjugated enzyme to bind to the hybrid. After addition of a substrate, the redox product of the enzyme is electrochemically detected. Two publications in the 2000s are particularly interesting, which take profit of redox dendrimers to enhance the catalytic amplification down to the fM level (Kim et al. 2003). Enzyme-amplified sandwich assays using redox hydrogels as mediators were also described, with a similar LoD (Zhang et al. 2004).

2.1.6 Molecular Beacons

The concept of DNA beacon was introduced by Fan et al. (2003) (Fig. 3 Left) and recently reviewed (Abi and Ferapontova 2013). The strategy involves a ferrocene (Fc)-tagged DNA stem–loop self-assembled on gold electrode. Hybridization induces a conformational change which alters the electron transfer rate, measured by CV. It was shown that single-nucleotide polymorphism (SNP) can be easily detected by this way (Farjami et al. 2011). Other DNA beacons were introduced with the concept of template-enhanced hybridization. Following this strategy, Zhang et al. (2009b) demonstrated that a template (the target) provokes the formation of a ternary complex ("Y" junction structure) with two other partially complementary sequences (Fig. 3 Right). This method is particularly sensitive to SNPs. Rolling circle amplification (RCA), a replication process able to synthesize multiple copies of circular molecules of DNA, was also investigated (Ji et al. 2012).

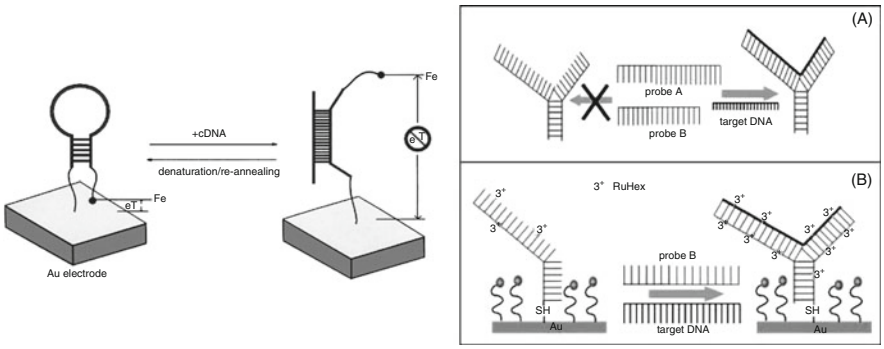

Fig. 3 *Left* DNA beacon [Reprinted from Fan et al. (2003), with permission. Copyright (2003) National Academy of Sciences, USA]. *Right* The concept of template-enhanced hybridization, using Ru complex as reporter [Reprinted from Zhang et al. (2009b). Copyright 2009 with permission from Elsevier]

2.1.7 Use of Carbon Nanotubes

As first proposed in the early 2000s (Wang et al. 2003), carbon nanotubes (CNTs) are promising for electrochemical DNA sensors due to their high surface-to-volume ratio and electron transfer (ET) properties (Balasubramanian 2012). For example, it was shown that multiwall carbon nanotubes (MWCNTs) facilitate adsorptive accumulation of DNA and enhance guanine electrooxidation for label-free detection (Erdem et al. 2006; Caliskan et al. 2009), allowing a LoD of 20 nM (Zhang et al. 2009c; Berti et al. 2009). CNTs were also embedded in conducting polymer, for example, in polypyrrole (Cai et al. 2003), chitosan (Li et al. 2005), polyaniline (Zhou et al. 2009), or quinone-based polymers (Acevedo et al. 2008; Tran et al. 2013b) in order to improve ET and increase surface area; LoDs in the fM range were obtained. Recently, Zhang et al. (2011) reported a new strategy where both redox indicator and DNA probe were grafted on SWCNTs to make a reagentless and label-free DNA sensor. Oxidized SWCNTs were first immobilized on a SAM of cysteamine; then, the redox and the DNA probes were grafted on the nanotube ends. Hybridization increases the redox kinetics of the probe, detected by square wave voltammetry (SWV) (Fig. 4).

2.1.8 Charge Transport in DNA

It was shown that the base pairs stack and allow charge transport (CT) through dsDNA. This is extremely sequence dependent, which makes sensors based on this principle highly sensitive to SNPs (Boon and Barton 2002; Boal and Barton 2005). This was also exploited with redox probe in solution or using redox-active intercalators (Wong and Gooding 2006).

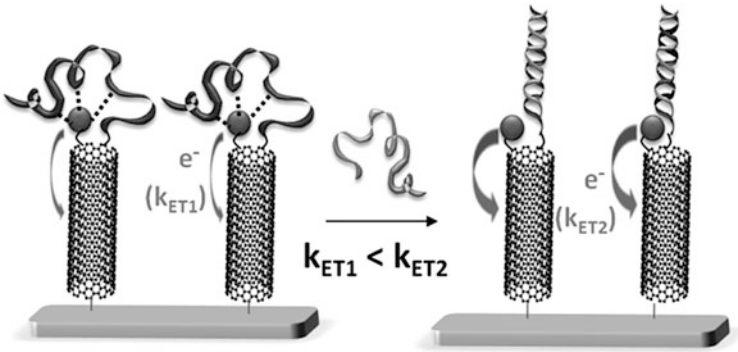

Fig. 4 Co-immobilization of a redox indicator and a DNA probe on a monolayer of *vertically aligned* SWCNTs. Before hybridization, the redox indicator forms hydrogen bonds with the DNA probe, whereas these bonds are broken upon hybridization, which causes an increase in the indicator's electroactivity [Reproduced from Zhang et al. (2011), with permission from The Royal Society of Chemistry]

2.1.9 Conducting Polymers, Self-Assembled Monolayers, and Other Thin Films

Conducting polymers (CPs) were extensively used for immobilization of DNA probes and electrochemical transduction of hybridization (Gerard et al. 2002; Peng et al. 2009). The first report in 1997 concerned ODN-functionalized polypyrrole; in the presence of the complementary target, the oxidation potential shifted to more positive potential, attributed to the bulkiness of the dsDNA. The LoD was 10^{-11} M, better than the 10^{-9} M limit achieved at this time by biosensors based on fluorescence (Korri-Youssoufi et al. 1997). Nanoparticles were later used in conjunction with CPs to enhance conductivity. For example, thiolated capture DNA strands were immobilized on AuNPs mixed with poly-3,4-ethylenedioxythiophene (PEDOT), leading to a LoD of 150 pM (Spain et al. 2013). When dealing with reagentless transduction, most CP-based electrodes present a signal decrease upon hybridization (signal-off), which impedes sensitivity and reliability, due in particular to false-positive responses from nonspecific adsorption. However, signal-on was demonstrated using quinone-modified electrodes (Pham et al. 2003; Piro et al. 2005; Reisberg et al. 2006), which exchange cations instead of anions during electrochemical doping process (Fig. 5).

The transduction mechanism was studied by investigating hybridization of target strands shorter than the probe strand (Reisberg et al. 2005). It was shown that the current depends on the length of the double strand, evidencing the importance of the change in conformation of the DNA strands upon hybridization, in the transducing mechanism (Piro et al. 2007). As it is illustrated on Fig. 6, ssODN behave as coils, hiding a bigger surface area on the electrode than straight dsODN.

Hydrogen bonds between 5-hydroxy-1,4-naphthoquinone and nucleobases were also investigated by Zhang et al. (2012b). They showed significant change in the

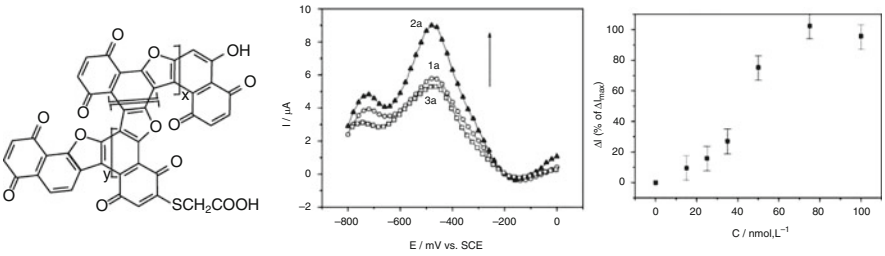

Fig. 5 *Left* Structure of an electroactive polymer carrying quinone moieties [Reprinted with permission from Reisberg et al. (2005). Copyright 2005 American Chemical Society]. *Center* SWV response of a corresponding polymer-modified electrode onto which a probe sequence is grafted (*plain squares,* curve 1a), after addition of a target sequence (*plain down-triangles*, curve 2a) or a noncomplementary random target (*open circles*, curve 3a). [target] = 100 nM. *Right* Corresponding calibration *curve* [Reprinted from Reisberg et al. (2006). Copyright 2006 with permission from Elsevier]

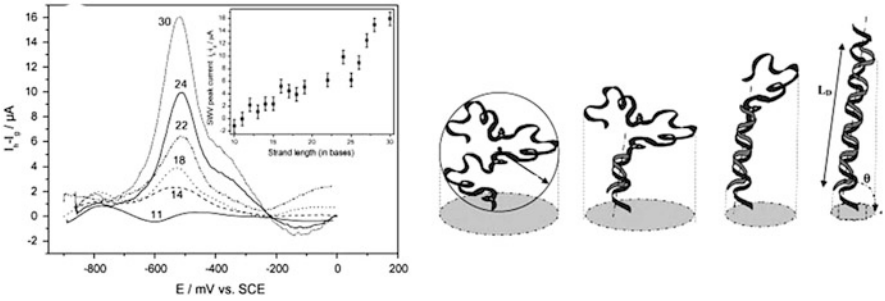

Fig. 6 *Left* SWVs for different target lengths (*inset*: current as a function of length). *Right* For uncompleted hybridization, one part of the probe is hybridized and rigid, while the other part is coiled. The hidden surface area is intermediate [Reprinted from Piro et al. (2007. Copyright 2007 with permission from Elsevier]

electrochemical behavior of the redox indicator upon interactions, as well as with homo-oligonucleotides (polyA, polyT, polyC, and polyG) (Fig. 7 Above). These interactions were exploited in an original strategy by Zhang et al. (2012b), where electroactive conjugated oligomers of 5-amino-1,4-naphthoquinone and DNA probes were grafted together on an electrode surface (Fig. 7 Middle).

Self-assembled monolayers (SAMs) for DNA immobilization were described soon, and several reviews are available (Paleček and Bartošík 2012; Samanta and Sarkar 2011). Among the first published works, Steel et al. (1998) and Sun et al. (1998) developed electrochemical methods to quantify DNA immobilized on monolayers of ssODN. As expected, the lower the density, the better the hybridization efficiency. It was also shown that the surface density of ssDNA probes decreases with respect to the DNA length (Steel et al. 2000). Co-immobilization of ssDNA strands and electroactive molecules was also described, for example, using a SAM of naphthoquinone derivative (March

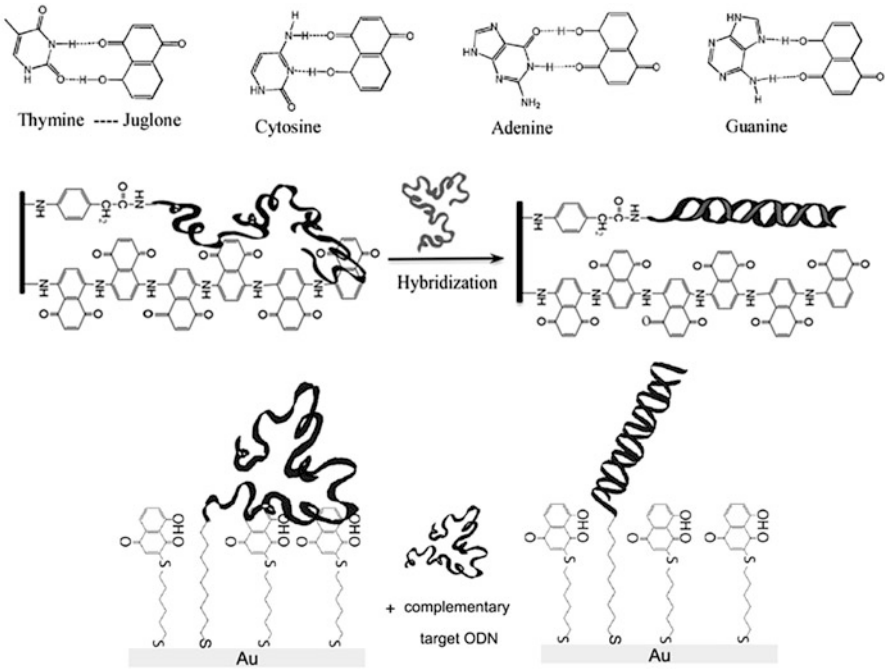

Fig. 7 *Above* Probable hydrogen bonds between the four nucleobases and the oxidized form of juglone [Reprinted from Zhang et al. (2012c). Copyright 2012 with permission from Elsevier]. *Middle* Schematic representation of the co-immobilization of electroactive oligomers and oligonucleotides [Reprinted from Zhang et al. (2012b). Copyright 2012 with permission from Elsevier]. *Below* Co-immobilization of DNA and electroactive molecules in a mixed SAM monolayer [Reprinted with permission from March et al. (2008). Copyright 2005 American Chemical Society]

et al. 2008). Before hybridization, ssDNA can interact with quinone, which slows down the redox reaction. When the complementary target is added, the formation of the double helix eliminates ssDNA/quinone interactions, and the electron transfer rate increases, hence the current (Fig. 7 Below). The sensor achieved a LoD of 300 pM on real PCR products related to *Mycobacterium tuberculosis* strains (Zhang et al. 2012a). Electroactive thin films obtained by diazonium electroreduction are also particularly efficient for application in DNA sensors (Gooding 2008). For example, a mixed monolayer obtained by electroreduction of 5-hydroxy-1,4-naphthoquinone and 4-aminobenzoïc acid diazonium derivatives was used by Hai et al. (2014), for DNA grafting and electrochemical detection, with a LoD of 10 pM (Fig. 8).

2.1.10 Graphene and Graphene Oxide

Advances in graphene- and graphene oxide-based DNA electrochemical sensors were reviewed (Gao et al. 2014; Shao et al. 2010). Recently, a type of direct DNA

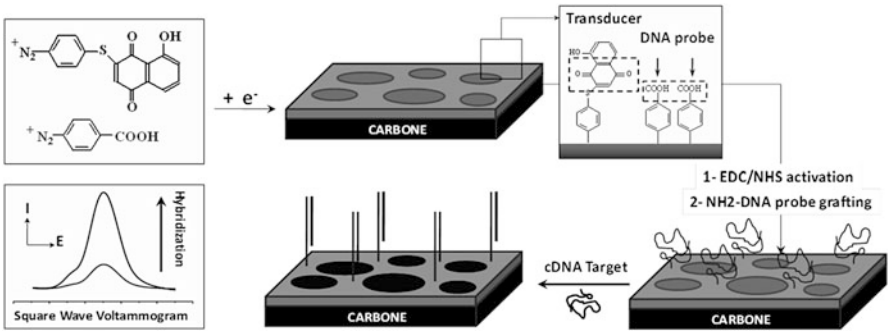

Fig. 8 Schematic principle of one-step electroreduction of electroactive and chemically reactive diazonium salts, followed by DNA grafting [Reprinted from Hai et al. (2014). Copyright 2014 with permission from Elsevier]

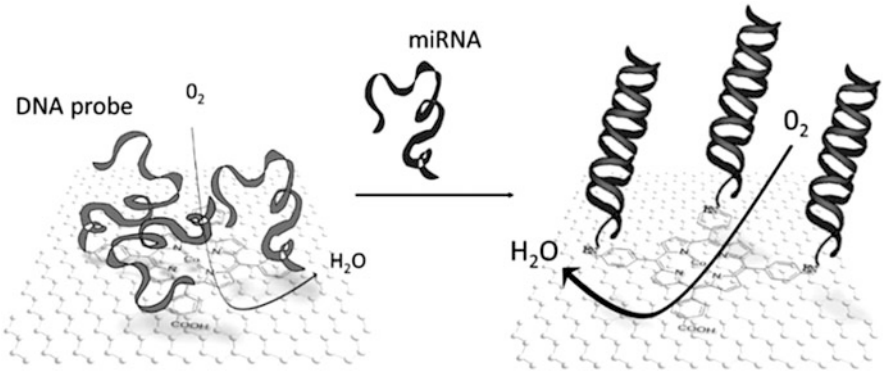

Fig. 9 miRNA detection is based on an increase in the catalytic oxygen reduction current on cobalt porphyrin immobilized on reduced graphene oxide [Reproduced from De Souza et al. (2014)]

impedance detection using sulfonated polyaniline and graphene oxide (GO) composite was reported, relying on steric hindrance changes upon hybridization (Yang et al. 2013). Another original approach by De Souza et al. (2014) described reduced GO modified by carboxylic acid-functionalized cobalt porphyrin. The carboxylic groups were used to covalently graft ODN probes. It was shown that the catalytic oxygen electroreduction on cobalt porphyrin is influenced by hybridization and is favorable compared to non-catalytic amperometric system. Apart from oxygen, no added reagent is necessary. A LoD in the pM range was reached (Fig. 9).

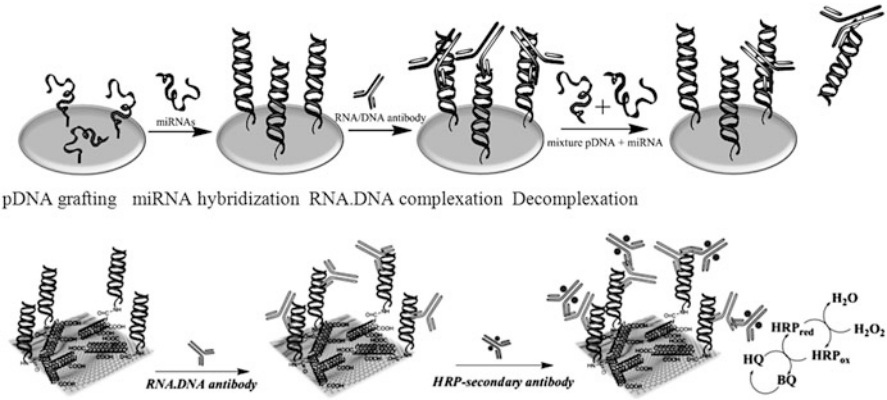

Fig. 10 *Above* Principle of RNA. DNA duplexes immunodetection [Reprinted with permission from Tran et al. (2013a). Copyright 2013 American Chemical Society]. *Below* Schematic representation of the electrochemical ELISA-like immunosensor [Reprinted from Tran et al. (2014). Copyright 2014 with permission from Elsevier]

2.1.11 Antibodies

Antibodies (Ab) directed to RNA/DNA hybrids were developed in the late 1960s, such as anti-poly(A)/poly(dT) and more recently anti-S9.6 (Schwartz and Stollar 1969; Phillips et al. 2013). These Ab are specific to DNA/RNA hybrids but not to their sequence. In a recent work by Tran et al. (2013a), they were applied in an electrochemical system where complexation with a DNA/RNA heteroduplex leads to a measurable current decrease, with a LoD of 10 fM. The Ab can be then dissociated by adding DNA/RNA free in solution, causing a re-increase in the current (signal-on) due to a competitive exchange. This *on–off–on* detection sequence was used as a triple verification of the results (Fig. 10 Above). Taking profit of this original immunological approach, an electrochemical ELISA-like amplification strategy was set up by Tran et al. (2014), using a secondary HRP-Ab. Two miRNA were studied: miR-141 (a prostate biomarker) and miR-29b-1 (a lung cancer biomarker) (Fig. 10 Below).

2.2 Peptide Nucleic Acid (PNA) Probes

A peptide nucleic acid (PNA) is a DNA analog in which the phosphate backbone is replaced by glycine units (Nielsen et al. 1991; Egholm et al. 2003). PNA can therefore be easily synthesized and functionalized using techniques from peptide chemistry, and their backbone is neutral, avoiding electrostatic repulsion upon hybridization, which leads to higher thermal stability (Nielsen and Egholm 1999). Apart from their remarkable biostability (PNAs are resistant to nucleases and proteases and are stable over a wider pH range than DNA), using PNA in place

of DNA in sensors gives more specific and sensitive results. Electrochemical sensors based on PNA probes were extensively reported, following the same transduction scheme than for DNA probes (Singh et al. 2010), using redox indicators added in solution (Wang et al. 1996; Ozkan et al. 2002a, b; Ju and Zhao 2005) or immobilized in a polymer (Le Floch et al. 2005; Kjaellman et al. 2007; Prabhakar et al. 2008) or using Fc-modified PNA probes (Fc–PNA) (Aoki et al. 2000; Aoki and Tao 2007; Baldoli et al. 2006; Li et al. 2008; Gasser and Spiccia 2008), metalated PNA (Joshi et al. 2013; Gross et al. 2012; Nickita et al. 2009; Gasser et al. 2008), or redox intercalators such as methylene blue (MB) (Ozkan et al. 2002a, b; Kara et al. 2002). The direct oxidation of guanine was also investigated (Kerman et al. 2003).

2.2.1 Organometallic Complexes

Derivatization of PNA by electroactive labels is easier than for DNA, therefore extensively reported in the literature. For example, Fc–PNA or cobaltocenium–PNA monomers were synthesized for insertion in various positions in PNA oligomers, not only at the end (Aoki and Tao 2007; Baldoli et al. 2004, 2005, 2006; Maurer et al. 2005; Gasser et al. 2006), for example, for direct electrochemical detection. Practical applications were demonstrated, such as detection of methicillin-resistant *Staphylococcus aureus*, with a LoD in the fM range without PCR amplification (Corrigan et al. 2013). Binary SAMs (of two different Fc–PNA capture probes having a significant difference in their redox potentials) were also reported. Based on changes in peak current and potential, identification of two different DNA sequences on a single electrode was achieved (Hüsken et al. 2010). A non-covalent labeling with Fc was also proposed, using Zr^{4+}. Zr^{4+} is able to interact with both the phosphate groups in DNA and carboxylic group of a derivatized Fc–COOH, so that the redox probe can be attached non-covalently to the DNA, to form a PNA/DNA–Zr–Fc assembly (Fang et al. 2011). In another example, covalent end-labeling of PNA with osmium tetroxide, 2,2′-bipyridine (Os, bipy) was described. Os, bipy interacting with PNA presents a peak potential slightly different from free Os, bipy, allowing analysis in homogenous conditions (Paleček et al. 2009). More complex architectures were also described by Xuan et al. (2012), based on DNA polymerase with a strand displacement activity. The electrochemical detection was realized by taking advantage of the difference in diffusivity between a free Fc–PNA and a Fc–PNA hybridized with a complementary DNA (Fig. 11). A recent review discussed the latest advances on the preparation and utilization of PNA monomers and oligomers containing metal complexes (Gasser et al. 2011).

2.2.2 Conducting Polymers, Redox Polymers, and Oligomers

Conversely to DNA, PNA immobilization and hybridization transduction on conducting polymers were scarcely investigated. One of these works relates the

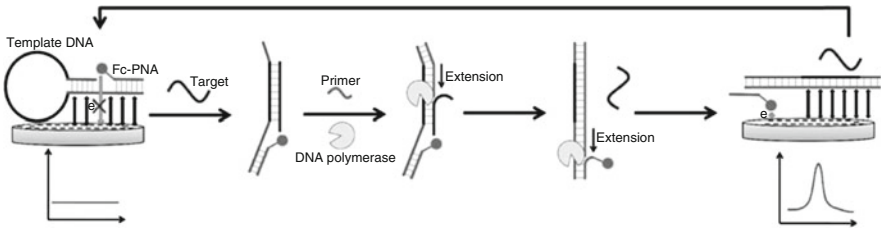

Fig. 11 The mechanism of the signal-amplified electrochemical DNA sensor based on isothermal circular strand displacement polymerization reaction [Reprinted from Xuan et al. (2012). Copyright 2012 with permission from Elsevier]

covalent attachment of PNA probes on a quinone-based electroactive polymer which allows a reagentless, label-free electrochemical detection (Reisberg et al. 2008a). To elucidate the mechanism involved in the transduction process, four hybridization configurations were investigated: PNA/DNA, PNA/PNA, DNA/PNA, and DNA/DNA. It was concluded that steric effects are predominant in the transduction process and that the effect of charges carried on the DNA strands is negligible (Reisberg et al. 2008b). Structural and physicochemical differences between PNA/DNA and DNA/DNA duplexes were also investigated using Fc-conjugated chitosan nanoparticles as electroactive indicator. After hybridization of DNA target on the PNA probe, a nuclease was used to hydrolyze adsorbed DNA and possible mismatch, and then Chi–Fc was added to reveal hybrids (Chi–Fc does not bind on PNA probe but electrostatically binds on PNA/DNA heteroduplex). This method is particularly sensitive to SNPs (Kerman et al. 2008). An electrochemical method for sequence-specific detection of DNA without solid-phase probe immobilization was also reported. The first step is a solution-phase hybridization of Fc–PNA and its complementary DNA sequence. The second step consists of electrochemically probing Fc on a positively charged poly(allylamine hydrochloride) layer; the electrostatic attraction between the positive surface and the negatively charged Fc–PNA/DNA hybrid leads to a much higher electrochemical signal than that of the unhybridized probe Fc–PNA (Luo et al. 2008). Water-soluble Fc-functionalized polythiophene was also used, for the same purpose (Harding-Lepage et al. 2011).

2.2.3 Charge Transport in PNA and PNA/DNA Heteroduplex

Charge transport in PNA was reviewed (Venkatramani et al. 2011). It is dominantly hole mobility through HOMO of individual bases (Paul et al. 2009). CT rates were compared for aminoethylglycine PNA (aeg-PNA, achiral, flexible) and for γ-methylated backbone (γ-PNA, chiral, rigid); it was shown that flexibility increases CT rate (Wierzbinski et al. 2012).

2.2.4 Advantages of Charge Neutrality

PNAs were shown to have significantly higher sensitivity and specificity than DNA (including greater discrimination against SNP) and minimal dependence on ionic strength. These properties are due to the absence of electrostatic repulsion between strands. Another obvious advantage is that DNA hybridization on PNA probe brings negative charges. This was exploited using positively charged redox complexes such as $Co(phen)_3^{3+}$, which accumulate in the charged duplex and therefore allow to electrochemically reveal hybridization (Wang et al. 1996, 1997). This principle was extensively developed afterwards with various electroactive complexes (Kerman et al. 2006; Steichen et al. 2007; Degefa and Kwak 2008; Keighley et al. 2008; Won et al. 2008). Electrochemical melting curves were obtained using this technique, measuring the Fc signal as a function of temperature (Luo and Hsing 2009a, b). The principle was extended to water-soluble Fc-functionalized polythiophene; its polycationic structure increases affinity with DNA and gives a clearer hybridization detection signal (Fang et al. 2008).

SAMs were also investigated for PNA immobilization (Ozkan et al. 2002a), e.g., to make a kind of ion-channel sensor. A mixed SAM of thiolated PNA and 8-amino-1-octanethiol was positively charged due to the protonated amino group. Thus, the ET reaction between an electroactive marker $[Ru(NH_3)_6]^{3+}$ in solution and the electrode is hindered due to electrostatic repulsion, which is decreased after hybridization. A LoD of 10^{-15} M was achieved (Aoki and Umezawa 2002, 2003). More complex strategies were also employed by Shin et al. 2011, using DNA target cleavage by nuclease, whereas the PNA probe remains intact (Fig. 12). $Fe(CN)_6^{3-/4-}$, repulsed by negatively charged DNA but not by neutral PNA, was used as redox probe added in solution.

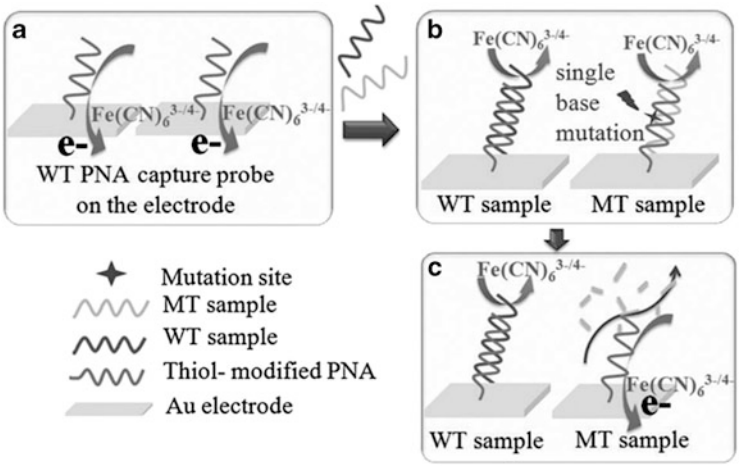

Fig. 12 Cleavage of target DNA by nuclease leading to recovery of free diffusion of the redox mediator. The PNA probe remains intact [From Shin et al. (2011) with permission from The Royal Society of Chemistry]

2.2.5 PNA Binding to Double-Stranded DNA

In spite of the extensive attention paid to ssDNA detection, very few studies focused on direct detection of dsDNA. However, it is possible to use PNA without the need for a denaturation step. Indeed, PNA binds sequence specifically to dsDNA and forms PNA/dsDNA triplexes (Hejazi et al. 2011).

Considering that dsDNA are negatively charged, whereas PNA is not, the transduction principle may be similar to that of ssDNA detection, e.g., with the use of positively charged metal complexes or redox intercalators, with similar LoD of ca. 10^{-12} M (Ahour et al. 2012, 2013).

2.2.6 Conclusion

Among electrochemical approaches, amperometry was extensively used. However, potentiometry and capacitive effects are also pertinent when implemented on semiconductors. For example, impedance spectroscopy was used for the detection of ssDNA using PNA probe immobilized onto Si/SiO_2 chips. Hybridization changes the charge distribution at the oxide/solution interface and significantly shifts the semiconductor's flat-band potential (Macanovic et al. 2004). Potentiometric effects were also investigated. Upon hybridization, it was shown that changes in the charge density at the solution/electrode interface on SAM-modified microelectrodes may be directly transformed into potentiometric signals. The Gouy–Chapman model indicated that the dominant effect comes from electrostatic forces between anionic DNA and the underlying electrode (Goda et al. 2013; Thipmanee et al. 2012). Sensors based on changes in capacitance of electrode-solution interfaces were also investigated (Berggren et al. 1999) often made of interdigitated microelectrodes (Tsouti et al. 2011), with sub-nanomolar LoD (Moreno-Hagelsieb et al. 2007). These results paved the way for the transistor technology in DNA sensors.

3 Transistors

Ion-sensitive field-effect transistor (ISFET) (Bergveld 2003), charge-modulated FET (CM-FET), organic electrochemical transistor (OECT), organic FET (OFET), and electrolyte-gated organic FET (EGOFET) are the most reported architectures used for biodetection (Fig. 13) (Kergoat et al. 2012a; Liao and Yan 2013; Torsi et al. 2013). FETs being very sensitive to changes in surface charges, they are particularly suitable for detection of charged molecules such as DNA (Schöning and Poghossian 2002).

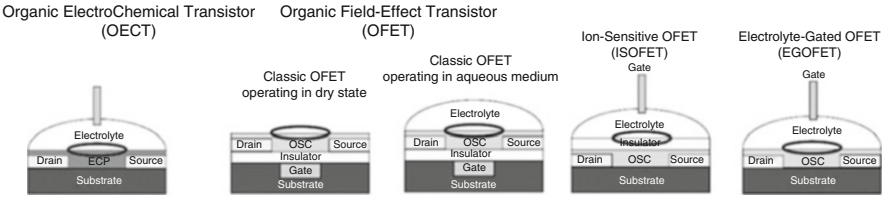

Fig. 13 Transistor architectures reported in the literature as possible biosensors. The *circle* indicates the interface involved in the biodetection [Reproduced from Kergoat et al. (2012a), with permission from Springer]

3.1 DNA Probes

3.1.1 Ion-Sensitive Field-Effect Transistors

ISFETs were investigated for analysis of various biomolecules, among them DNA (Lee et al. 2009). The first successful attempt by Souteyrand et al. 1997 consisted in using ODN strands immobilized onto Si/SiO_2. The ODN layer was used as a gate in an ISFET (Fig. 14 Left), monitoring surface charge when DNA target hybridizes on the surface (Fritz et al. 2002; Uslu et al. 2004; Poghossian et al. 2006). ISFETs were, for example, used by Sakata et al. 2004, for detection of PCR products (Fig. 14 Middle).

3.1.2 Electrochemical Transistors

In OECTs, the source and drain are connected via a conducting polymer, separated from the gate by an electrolyte. The operating principle of OECTs relies on the doping and dedoping of the polymer, which results in modification of its conductivity (Kergoat et al. 2012a). OECTs were described for DNA sensing, for example, using PEDOT–PSS. Label-free DNA detection was obtained by Lin et al. (2011), through the modulation of the surface potential of the gate electrode induced by target hybridization, with a LoD of 10 pM (Fig. 14 Right).

3.1.3 Organic Field-Effect Transistors

Even if changes in $I_d - V_d$ characteristics may come from artifact related to contact resistances at the source–drain electrodes (Yan et al. 2009), it was demonstrated, e.g., with a pentacene-based OFET, that DNA immobilization and hybridization produce an unambiguous doping-induced threshold voltage shift (Zhang and Subramanian 2007; Stoliar et al. 2009; Liu et al. 2012). Using 6,13-bis (triisopropylsilylethynyl) (TIPS) pentacene as the organic semiconductor and an original architecture with a remote sensing area, Lai et al. (2013) described another

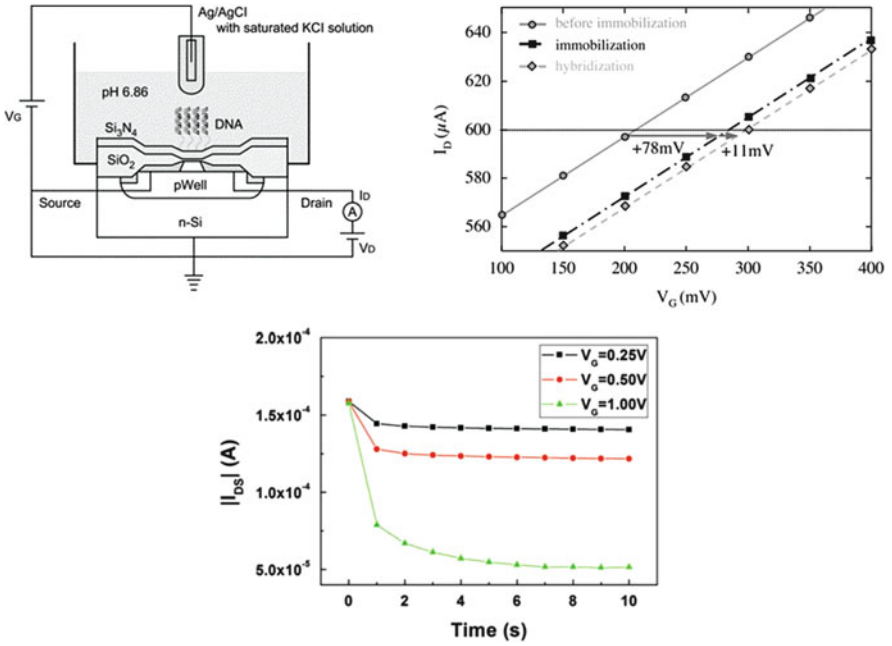

Fig. 14 *Left* Si_3N_4-based ISFET using a ssDNA layer on *top* of the dielectric. A reference electrode is necessary [Reprinted from Sakata et al. (2004). Copyright 2004 with permission from Elsevier]. *Middle* DNA immobilization and hybridization lead to a threshold voltage (V_T) shift [Reprinted from Sakata et al. (2004). Copyright 2004 with permission from Elsevier]. *Right* Time-dependent channel current of an OECT measured after applying different gate voltages. $V_{DS} = -0.1$ V [Reproduced from Lin et al. (2011). Copyright ©2011 WILEY-VCH Verlag GmbH & Co]

ultralow-voltage DNA-OFET. The device shows a sub-nanomolar detection limit and unprecedented selectivity with respect to SNPs (Fig. 15).

3.1.4 Carbon Nanotubes and Graphene in Field-Effect Transistors

CNTs were implemented in FETs (CNTFETs) (Roy et al. 2008; Roy and Gao 2009; Kauffman and Star 2008). Due to the high surface-to-volume ratio, the electrical resistance of nanotubes is extremely sensitive to changes in charge density at their surface.

Hybridization on DNA-functionalized CNTs can therefore be detected by measuring the source–drain current through nanotubes, function of the gate (or reference) potential (Balasubramanian 2010; Balasubramanian et al. 2008; Yanez-Sedeno et al. 2010). There are two classical types of device (Fig. 16) (Allen et al. 2007). The first design uses a single carbon nanotube to act as an electron channel between the source and the drain electrodes (Hahm and Lieber 2004), whereas the second type involves a network of CNT as a collective channel (Patolsky et al. 2006). DNA hybridization using CNTFETs was reported using

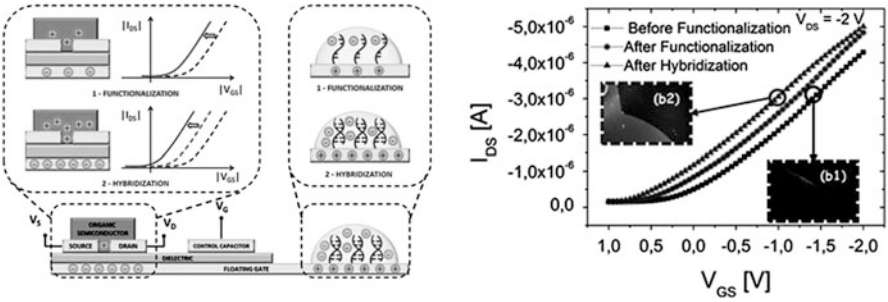

Fig. 15 *Left* Structure and detection mechanism. *Right* Transfer characteristics. [ODN_{target}] = 100 nM. Inserts: fluorescence images of the sensing surface (the target ODN were labeled with a fluorescent dye) [Adapted from Lai et al. (2013). Copyright ©2013 WILEY-VCH Verlag GmbH & Co]

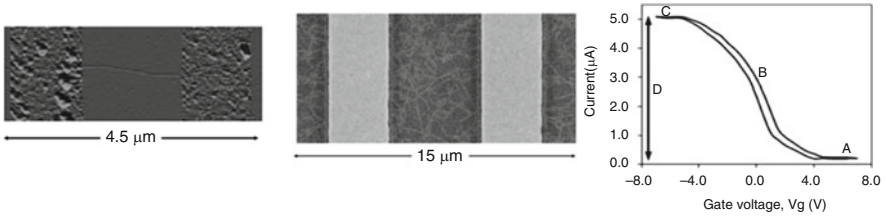

Fig. 16 *Left* AFM picture of a CNTFET with a semiconducting SWNT contacted by source (S) and drain (D), above a SiO_2 insulating layer. *Middle* SEM image of a random *array* of CNT. *Right* Typical CNTFET transfer characteristics (*A* threshold voltage, *B* transconductance, *C* maximum conductance, *D* modulation) [Adapted from Allen et al. (2007). Copyright ©2007 WILEY-VCH Verlag GmbH & Co]

PNA, with LoD as low as 6.8 fM (Maehashi et al. 2004), and improved later (Star et al. 2006). The transduction mechanism is still under discussion, but the role of charges is confirmed.

Compared to CNTs, graphene presents even higher surface-to-volume ratio and conductivity. Graphene-based transistor devices able to detect DNA hybridization were described with LoD in the fM range, attributed to electronic doping induced by target DNA (Fig. 17) (Dong et al. 2010).

3.1.5 Electrolyte-Gated Field-Effect Transistors

In EGOFET, upon polarization of the gate, an electrical double layer of extremely high capacitance is formed, which enables the transistor to be operated at very low potentials (<1 V). A DNA sensor based on an EGOFET was described, based on P3HT and poly[3-(5-carboxypentyl)thiophene-2,5-diyl] (P3PT–COOH) onto which DNA probes were covalently grafted. Clear changes in the output

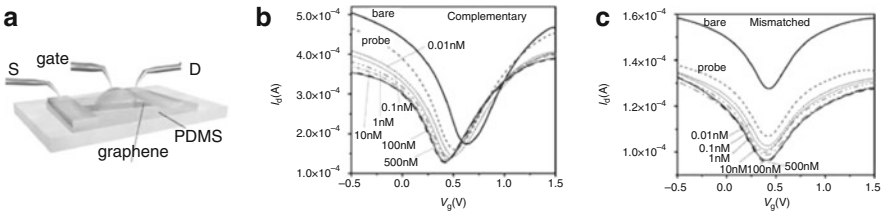

Fig. 17 *Left* (**a**) Schematic illustration of the graphene device operated by liquid gating. *Center* and *Right* Transfer characteristics for the graphene transistors before adding DNA, after immobilization with probe DNA, and after reaction with (**b**) complementary or (**c**) one-base-mismatched DNA molecules with the concentration ranging from 0.01 to 500 nM [Adapted from Dong et al. (2010). Copyright ©2010 WILEY-VCH Verlag GmbH & Co]

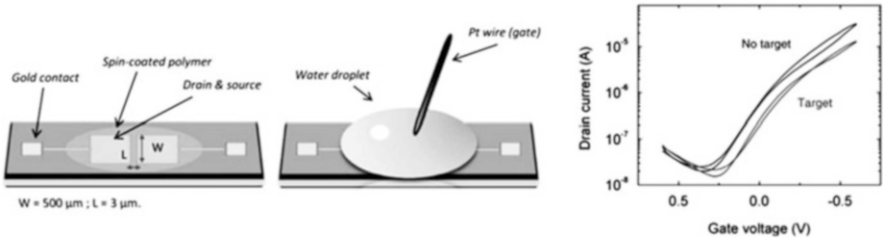

Fig. 18 *Left* P3HT and P3PT–COOH solutions were spin coated between source and drain. For measurements, a water droplet was deposited onto the semiconductor, and a platinum wire dipped into the droplet was used as the gate. *Right Transfer curves* for hybridization with a complementary target and without target [Reprinted from Kergoat et al. (2012b). Copyright 2012 with permission from Elsevier]

characteristic of the device were observed upon DNA immobilization and after DNA hybridization. Results pointed out the importance of the Debye length that can screen negative DNA charges and impede transduction (Fig. 18) (Kergoat et al. 2012b).

3.2 Peptide Nucleic Acid Probes

PNAs are neutral. This constitutes the major advantage of their use in transistors, for which charges play a crucial role in the transduction mechanism.

3.2.1 Ion-Sensitive Field-Effect Transistors

ISFET DNA sensors take advantage of the change in the surface potential upon hybridization of a negatively charged DNA on neutral PNA probes. PNA is

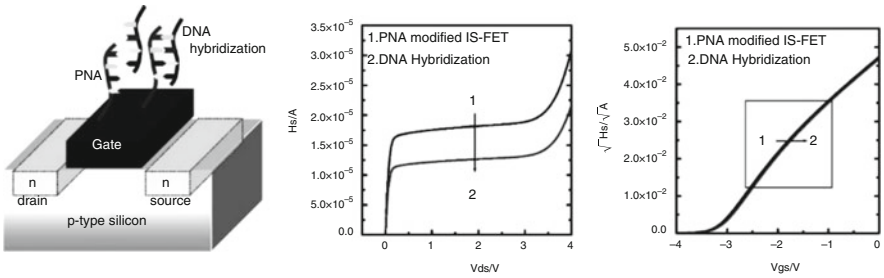

Fig. 19 *Left* Hybridization of PNA-modified ISFET by DNA in solution. The ISFET consists of a p-type silicon substrate with two n-doped regions (source and drain), separated by a short channel that is covered by a silicon nitride gate insulator. *Center* The I_D–V_D characteristics before and after hybridization. *Right* The I_D–V_G characteristics for the change in the V_T before and after hybridization [Adapted with permission from Uno et al. (2007). Copyright 2007 American Chemical Society]

particularly advantageous for ISFET systems because it enables highly specific and selective binding at low ionic strength. They are typically immobilized on the gate electrode. It was shown through the $I-V$ characteristics that the PNA/DNA duplexes induce a positive shift in the threshold voltage, V_T, and a decrease in the saturated drain current, I_D (Fig. 19) (Uno et al. 2007). In another publication, the changes in V_T observed for neutral PNA-probe ISFET were more than ten times greater than those for negatively charged DNA-probe ISFET (Ohtake 2006).

3.2.2 Field-Effect Transistors

FETs using PNA as probe were very scarcely described in the literature. Now, emerging devices use graphene or reduced graphene oxide (RGO) as semiconductor. For example, a PNA/RGO FET having a LoD of ca. 100 fM (one order of magnitude lower than using DNA probe) was described very recently (Cai et al. 2014).

3.2.3 Organic Field-Effect Transistors

An organic thin film transistor based on 5,5′-bis-(7-dodecyl-9H-fluoren-2-yl)-2,2′-bithiophene (DDFTTF) and modified with 15-base PNA strands was used for the selective detection of target DNA sequences (Fig. 20) (Khan et al. 2010). DDFTTF exhibits a stable mobility even in buffer solutions. The binding constant of DNA on the surface-bound PNA probes was determined from the concentration-dependent response (Khan et al. 2012).

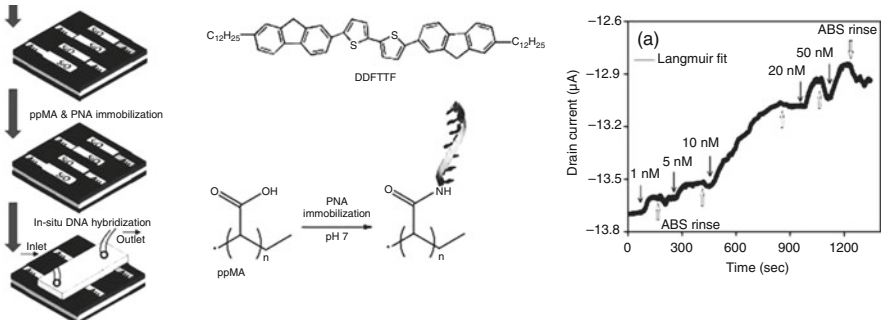

Fig. 20 *Left* Fabrication of the OTFT. *Center* Chemical structure of DDFTTF. Schematics of the surface modification to immobilize the PNA probe [Adapted with permission from Khan et al. (2010). Copyright © 2010 WILEY-VCH Verlag GmbH & Co]. *Right* Titration curves for PNA/DNA hybridization at constant bias ($V_G = -1$ V, $V_{DS} = -0.5$ V). *Solid arrows* indicate the additions of target DNA solutions, and *open arrows* indicate the exchange to buffer solutions [Reprinted from Khan et al. (2012). Copyright 2012, with permission from Elsevier]

3.2.4 Conclusion

The inherent compatibility of FETs with micro-fabrication technology makes them extremely attractive for the industry, due to an easy interface with classical micro-electronic devices. In particular, organic transistors are excellent candidates for disposable sensors due to their potentially low-cost fabrication process, particularly if they are obtained from printing technology. The next step is therefore to integrate them in more elaborated chips able to perform several tasks, from sample collection to signal treatment, so-called lab-on-chips.

4 Lab-on-Chip, Nanowires, and Other Nanometer-Sized Devices

4.1 Lab-on-Chips

Lab-on-chips (LoCs) allow to work on very small volumes of analyte and may integrate pretreatment steps, therefore avoiding tedious manual work (Dutse and Yusof 2011; Njoroge et al. 2011). They generally integrate the same transduction architectures than classical sensors.

4.1.1 Electrochemical Detection

A 20-channel array was reported in the early 2000s for the detection of PCR products, but with a very high LoD of 10^{-6} M (Hashimoto and Ishimori 2001).

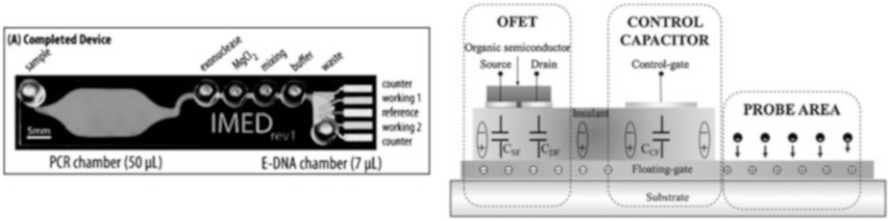

Fig. 21 *Left* Example of electrochemical LoC architecture [Reprinted with permission from Ferguson et al. (2009). Copyright 2009 American Chemical Society]. *Right* Cross section of a floating gate FET sensor, floating gate transistor (M_0), control gate with the role of reference electrode (V_C and C_C), and active area (in contact with solution) [Reprinted from Demelas et al. (2012). Copyright 2012, with permission from Elsevier]

Later, enzyme-amplified transduction was proposed, based on interdigitated gold ultra-microelectrodes functionalized by thiolated ODN (Nebling et al. 2004). A device capable of all preparation steps (addressing of ODN probes at selected electrodes, electrochemical detection, and regeneration) was reported more recently, for the detection of H1N1 and H5N1 influenza PCR samples (Pavlovic et al. 2008). On the same principle, detection of genomic DNA from *Salmonella* was demonstrated by Ferguson et al. (2009), with a very low LoD of 10 aM (Fig. 21 Left).

4.1.2 Field-Effect Transistors

Due to their easy integration, FETs were often implemented in LoCs. Among more classical works, an original architecture was proposed. The device was composed of a control gate and floating gate in electrical contact (but not physical contact) with the detection area where probe DNA are immobilized (Barbaro et al. 2006). The minimum amount of detectable DNA molecules is not limited by the threshold voltage because the control gate is used to apply an offset potential. In addition, the semiconductor is not in contact with a liquid, which improves stability (Fig. 21 Right) (Demelas et al. 2012; Roy and Gao 2009). Despite these examples of lab-on-chip devices for DNA detection, it appears that efforts are still necessary in this domain; FETs are certainly the most pertinent devices for these developments.

4.2 Nanopores and Nanochannels

Nanopores or nanochannels present a diameter similar to ssDNA or dsDNA. Nanopores are generally protein channels embedded in lipid bilayer or apertures in synthetic membranes fabricated in a variety of materials (plastic, glass, or silicon) (Harrell et al. 2006). Upon application of potential difference across the

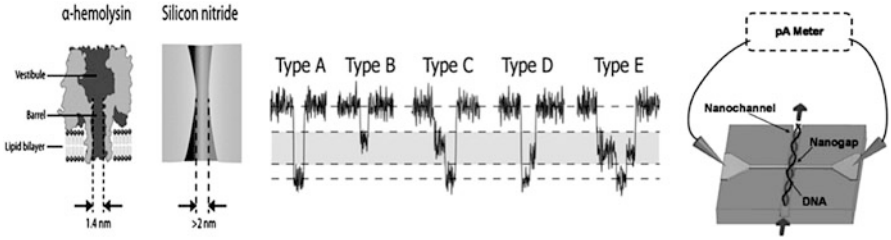

Fig. 22 *Left* 1, an α-HL nanopore and 2, a typical solid-state nanopore in a silicon nitride membrane [Reprinted from Miles et al. (2013). Copyright © 2013, Royal Society of Chemistry]. *Middle* Ionic current recorded as a function of time, during a translocation process. A, direct translocation; B, DNA is captured then exits from the entry; C, DNA is captured in the vestibule before it translocates; D, DNA enters the barrel then retracts from the entrance; E, DNA explores the vestibule, threads into the barrel, retracts back into the vestibule, and exits from the entrance [Reprinted from Maglia et al. (2008). Copyright © 2008, by the National Academy of Sciences, USA]. *Right* Schematic principle of a nanochannel [Reprinted with permission from Liang and Chou (2008). Copyright © 2008 American Chemical Society]

membrane, an ionic current goes through the nanopore (Fig. 22 Left) (Miles et al. 2013), but is blocked during translocation of a DNA strand through the pore (DeBlois and Bean 1977). Initially, biological nanopores were used (Howorka et al. 2001; Howorka and Bayley 2002; Meller et al. 2001), e.g., α-hemolysin (α-HL) which presents a suitable diameter (Fig. 22) (Maglia et al. 2008). The DNA sequences can even be identified by this way (Purnell et al. 2008; Purnell and Schmidt 2009; Stoddart et al. 2009; Butler et al. 2008). Identification of nucleobases is also possible using conducting nanogaps inside nanochannels, able to measure the electrical conductivity perpendicular to the channel (Liang and Chou 2008).

4.3 Nanowires

Gold NWs were described to detect DNA hybridization using traditional cyclic voltammetry (Fang and Kelley 2009). However, NW-based FET sensors are more promising because, for the same reason than for CNTs and graphene, their high surface-to-volume ratio makes them sensitive to minor surface perturbations (e.g., binding of biomolecules). Publications reviewing nanowire-based FETs for DNA sensing are available, considering classical DNA probes (Noor and Krull 2014; Choi et al. 2011) or neutral probes (PNA or other neutral DNA derivatives) (Chen et al. 2013). In the mid-2000s, Patolsky et al. (2006)have shown that DNA hybridization on SiNW leads to conductance changes, with extremely low LoD (Fig. 23, Left). The sensing mechanism is based on changes in charge density at the NW surface after hybridization (field effect) (Gao et al. 2007; Zhang et al. 2009a, 2010; Chen et al. 2011; Stern et al. 2007). P-type and n-type SiNWs were compared by Barbaro et al. (2006) and Li et al. (2004) (Fig. 23 Middle and Right), the results

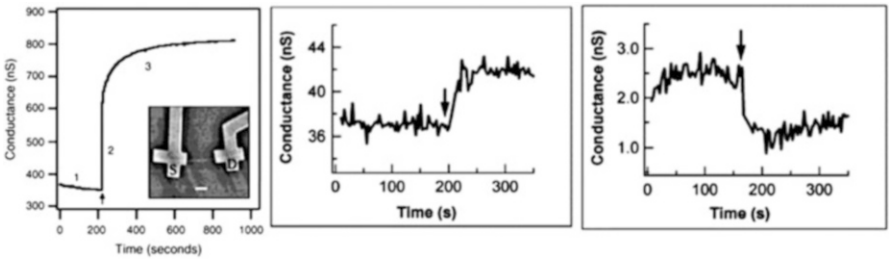

Fig. 23 *Left* DNA hybridization measurements at SiNW functionalized with ODN probes. (**a**) Real-time conductance response to 60 fM DNA. The *inset* shows a SEM image of a typical SiNW device with a source (S) and a drain (D) indicated; scale bar is 1 μm [Reprinted with permission from Patolsky et al. (2006). Copyright © 2006 American Chemical Society]. *Middle* Conductance modified with DNA probes, where the *arrow* indicates the addition of 25 pM complementary DNA for (**b**) for p-type SiNW. *Right* For an n-type SiNW [Reprinted with permission from Li et al. (2004). Copyright © 2004 American Chemical Society]

validating the supposed field-effect mechanism. This mechanism was also validated by controlling the distance between the hybridization sites and the surface. As expected, the sensitivity decreases as the charged DNA moves away from the SiNW surface (Zhang et al. 2008).

4.4 Break Junctions and Nanogaps

Nanogaps were described by Hashioka et al. (2004) for DNA detection, generally based on gold electrodes (used to graft DNA probes) separated by a 40 nm gap.

The current is modulated by the presence of DNA strands in between the two electrodes (Fig. 24, Left and Center). Interestingly, arrays of multi-junctions were achieved by construction of a AuNP film above a classical interdigitated electrode (Fig. 24, Right) (Shiigi et al. 2005). SWNTs were also used for the same goal. Upon hybridization, dsDNA act as conducting channels and increase current.

5 General Conclusion and Perspectives

This chapter dealt with DNA and PNA probes for DNA detection, using most frequently amperometry, less frequently potentiometry, or, based on the transistor effect, either electrochemical or field effect. We also discussed other techniques based on nanopores or nanochannels, for which transduction is not based on hybridization but on size exclusion. These methods were refined to the extreme, to reach limits of detection down to the femtomolar or even atomolar level.

New perspectives will probably come from two directions: technology and particularly lab-on-chips and micro- and nanofluidics from one hand (these points

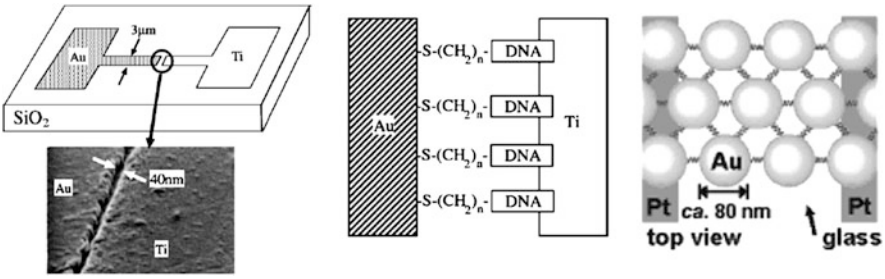

Fig. 24 *Left* and *Center* Gold and titanium electrodes separated by a 40 nm gap, used to electrically detect DNA strands [Reprinted with permission from Hashioka et al. (2004). Copyright 2004, AIP Publishing LLC]. *Right* Schematized top view of a AuNP film with bridging dsDNA [Adapted with permission from Shiigi et al. (2005). Copyright © 2005 American Chemical Society]

have been discussed in this chapter) and chemistry and biochemistry innovations on the other hand. Indeed, chemists and biochemists may probably have to further improve the molecular recognition step, e.g., through the use of xeno-nucleic acids (XNAs) which may have better availability, stability, and recognition properties.

The term XNA was first proposed by Herdewijn and Marliere (2009). Recent reviews gave an extensive overview of existing unnatural nucleic acids, with their particular chemical and biological properties (Pinheiro and Holliger 2012; Wang et al. 2013). Nucleic acid analogs are obtained by modifications of native nucleic acids at the nucleobases, the sugar ring, or the phosphodiester backbone. Many forms are available, such as locked nucleic acids (LNAs), unlocked nucleic acids (UNAs), peptide nucleic acids (PNAs), glycol nucleic acid (GNA), threofuranosyl nucleic acid (TNA), or morpholinos (Fig. 25).

LNA, PNA, and morpholinos can form both duplexes and triplexes and have improved biostability. They have become a versatile tool for DNA and RNA recognition. PNA was largely described previously in this chapter and is not further discussed here. Due to their high affinity for ssDNA and ssRNA, base mismatches in LNA/DNA heteroduplexes are much destabilizing than in classical dsDNA or dsRNA (Briones and Moreno 2012) so that LNA are particularly pertinent for low-LoD DNA or RNA detection (Petersen and Wengel 2003; Jepsen et al. 2004; Veedu and Wengel 2009). This is particularly true for RNA because structural studies have shown that LNA induce A-type (RNA-like) duplex conformations (Vester and Wengel 2004). For this reason, LNA are particularly well suited for miRNA detection and analysis in cancer diagnostics (Stenvang et al. 2008; Chen et al. 2008). Morpholinos, like PNA, are uncharged DNA analogs but are cheaper and easier to synthesize. They are particularly well adapted for surface hybridization applications where high concentration of salt may compromise hybridization detection through surface charge effects (Tercero et al. 2009). Conversely to LNA, unlocked nucleic acid (UNA) is a highly flexible modification which can be used to modulate duplex characteristics. They have hybridization properties and are emerging as versatile modifications for aptamers (Campbell and Wengel 2011;

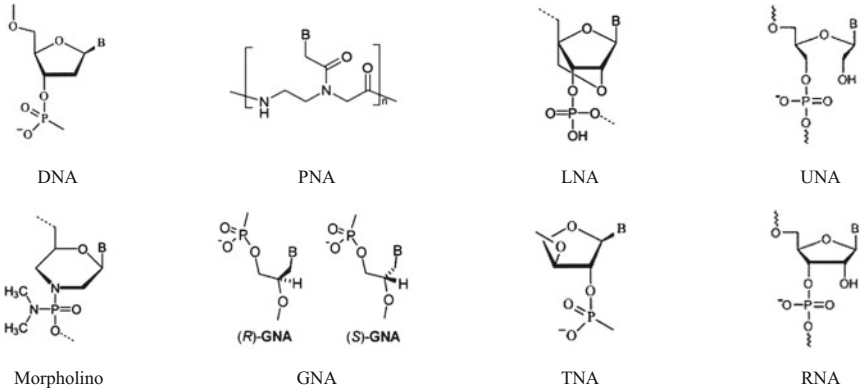

Fig. 25 Structures of deoxyribonucleic acid (DNA), peptide nucleic acid (PNA), locked nucleic acid (LNA), unlocked nucleic acid (UNA), morpholinos, glycol nucleic acid (GNA), threofuranosyl nucleic acid (TNA), and ribonucleic acid (RNA)

Doessing and Vester 2011). Glycol nucleic acid (GNA) is the simplest stable nucleic acid after PNA (Acevedo and Andrews 1996; Zhang et al. 2005). However, neither the R- nor S-GNA conformations can hybridize DNA with an acceptable affinity, which limits their application in DNA or RNA sensors (Meggers and Zhang 2010). At last, TNA, (L)-α-threofuranosyl oligonucleotide, is probably the simplest natural nucleic acid alternative and is capable of cross-pairing with RNA and DNA (Schöning et al. 2001; Herdewijn 2001). As far as the authors know, no electrochemical or FET devices were described in the literature involving UNA, GNA, or TNA yet; it certainly deserves explorations.

At last, even if electrochemical or field-effect transistors have already been proposed for DNA detection, it is obvious that technical improvements are needed to meet the desired requirements in terms of stability and sensitivity to make reliable analytical tools. Particularly, the most promising scientific approaches such as organic electronics, coupled to modern techniques such as roll-to-roll or ink-jet printing, may strongly help the emerging of extremely low-cost and widely distributed DNA sensors for routine analysis, point of care, and, at the end, personal use.

References

Abi A, Ferapontova EE (2013) Electroanalysis of single-nucleotide polymorphism by hairpin DNA architectures. Anal Bioanal Chem 405:3693–3703

Acevedo OL, Andrews RS (1996) Synthesis of propane-2,3-diol combinatorial monomers. Tetrahedron Lett 37:3931–3934

Acevedo DF, Reisberg S, Piro B et al (2008) Fabrication of an interpenetrated network of carbon nanotubes and electroactive polymers to be used in oligonucleotide biosensing. Electrochim Acta 53:4001–4006

Ahour F, Pournaghi-Azar MH, Hejazi MS (2012) An electrochemical approach for direct detection and discrimination of fully match and single base mismatch double-stranded oligonucleotides corresponding to universal region of hepatitis C virus. Anal Methods 4:967–972

Ahour F, Pournaghi-Azar MH et al (2013) Detection and discrimination of recombinant plasmid encoding hepatitis C virus core/E1 gene based on PNA and double-stranded DNA hybridization. Biosens Bioelectron 45:287–291

Allen BL, Kichambare PD, Star A (2007) Carbon nanotube field-effect-transistor-based biosensors. Adv Mater 19:1439–1451

Aoki H, Tao H (2007) Label- and marker-free gene detection based on hybridization-induced conformational flexibility changes in a ferrocene-PNA conjugate probe. Analyst 132:784–791

Aoki H, Umezawa Y (2002) High sensitive ion-channel sensors for detection of oligonucleotides using PNA modified gold electrodes. Electroanalysis 14:1405–1410

Aoki H, Umezawa Y (2003) Trace analysis of an oligonucleotide with a specific sequence using PNA-based ion-channel sensors. Analyst 128:681–685

Aoki H, Buhlmann P, Umezawa Y (2000) Electrochemical detection of a one-base mismatch in an oligonucleotide using ion-channel sensors with self-assembled PNA monolayers. Electroanalysis 12:1272–1276

Balasubramanian K (2010) Challenges in the use of 1D nanostructures for on-chip biosensing and diagnostics: a review. Biosens Bioelectron 26:1195–1204

Balasubramanian K (2012) Label-free indicator-free nucleic acid biosensors using carbon nanotubes. Eng Life Sci 12:121–130

Balasubramanian K, Lee EJH, Weitz RT et al (2008) Carbon nanotube transistors—electrochemical functionalization and device characterization. Phys Status Solidi 205:644–646

Baldoli C, Falciola L, Licandro E et al (2004) A new ferrocene conjugate of a tyrosine PNA monomer: synthesis and electrochemical properties. J Org Chem 689:4791–4802

Baldoli C, Licandro E, Maiorana S et al (2005) Electrochemical activity of new ferrocene-labelled PNA monomers to be applied for DNA detection: effects of the molecular structure and of the solvent. J Electroanal Chem 585:197–205

Baldoli C, Rigamonti C, Maiorana S et al (2006) A new triferrocenyl-tris(hydroxymethyl) aminomethane derivative as a highly sensitive electrochemical marker of biomolecules: application to the labelling of PNA monomers and their electrochemical characterization. Chemistry 12:4091–4100

Barbaro M, Bonfiglio A, Raffo L et al (2006) A CMOS, fully integrated sensor for electronic detection of DNA hybridization. IEEE Electron Device Lett 27:595–597

Berggren C, Stålhandske P, Brundell J et al (1999) A feasibility study of a capacitive biosensor for direct detection of DNA hybridization. Electroanalysis 11:156–160

Bergveld P (2003) Thirty years of ISFETology. What happened in the past 30 years and what may happen in the next 30 years. IEEE Electron Device Lett 88:1–20

Berti F, Lozzi L, Palchetti I et al (2009) Aligned carbon nanotube thin films for DNA electrochemical sensing. Electrochim Acta 54:5035–5041

Boal AK, Barton JK (2005) Electrochemical detection of lesions in DNA. Bioconjugate Chem 16: 312–321

Boon EM, Barton JK (2002) Charge transport in DNA. Curr Opin Struct Biol 12:320–329

Briones C, Moreno M (2012) Applications of peptide nucleic acids (PNAs) and locked nucleic acids (LNAs) in biosensor development. Anal Bioanal Chem 402:3071–3089

Bunimovich YL, Shin YS, Yeo WS et al (2006) Quantitative real-time measurements of DNA hybridization with alkylated nonoxidized silicon nanowires in electrolyte solution. J Am Chem Soc 128:16323–16331

Butler TZ, Pavlenok M, Derrington IM et al (2008) Single-molecule DNA detection with an engineered MspA protein nanopore. Proc Natl Acad Sci USA 105:20647–20652

Cai H, Xu Y, He PG et al (2003) Indicator-free DNA hybridization detection by impedance measurement based on the DNA-doped conducting polymer film formed on the carbon nanotube modified electrode. Electroanalysis 15:1864–1870

Cai B, Wang S, Huang L et al (2014) Ultrasensitive label-free detection of PNA-DNA hybridization by reduced graphene oxide field-effect transistor biosensor. ACS Nano 8:2632–2638
Caliskan A, Erdem A, Karadeniz H (2009) Direct DNA hybridization on the single-walled carbon nanotubes modified sensors detected by voltammetry and electrochemical impedance spectroscopy. Electroanalysis 21:2116–2124
Campbell MA, Wengel J (2011) Locked vs. unlocked nucleic acids (LNA vs. UNA): contrasting structures work towards common therapeutic goals. Chem Soc Rev 40:5680–5689
Chen J, Zhang J, Huang L et al (2008) Hybridization biosensor using 2-nitroacridone as electrochemical indicator for detection of short DNA species of chronic myelogenous leukemia. Biosens Bioelectron 24:349–355
Chen KI, Li BR, Chen YT (2011) Silicon nanowire field-effect transistor-based biosensors for biomedical diagnosis and cellular recording investigation. Nano Today 6:131–154
Chen WY, Chen HC, Yang YS et al (2013) Improved DNA detection by utilizing electrically neutral DNA probe in field-effect transistor measurements as evidenced by surface plasmon resonance imaging. Biosens Bioelectron 41:795–801
Choi S, Goryll M, Sin LYM et al (2011) Microfluidic-based biosensors toward point-of-care detection of nucleic acids and proteins. Microfluid Nanofluid 304:203–260
Corrigan DK, Schulze H, Henihan G et al (2013) Development of a PCR-free electrochemical point of care test for clinical detection of methicillin resistant Staphylococcus aureus (MRSA). Analyst 138:6997–7005
De Souza C, Zrig S, Wang D et al (2014) Electrocatalytic miRNA detection using cobalt porphyrin-modified reduced graphene oxide. Sensors 14:9984–9994
DeBlois RW, Bean CP (1977) Electrokinetic measurements with submicron particles and pores by the resistive pulse technique. J Colloid Interface Sci 61:323–335
Degefa TH, Kwak J (2008) Electrochemical impedance sensing of DNA at PNA self-assembled monolayer. J Electroanal Chem 612:37–41
Demelas M, Lai S, Casula G et al (2012) An organic, charge-modulated field effect transistor for DNA detection. Sensors Actuators B 171:198–203
Doessing H, Vester B (2011) Locked and unlocked nucleosides in functional nucleic acids. Molecules 16:4511–4526
Dong XC, Shi YM, Huang W et al (2010) Electrical detection of DNA hybridization with single-base specificity using transistors based on CVD-grown graphene sheets. Adv Mater 22: 1649–1653
Drummond TG, Hill MG, Barton JK (2003) Electrochemical DNA sensors. Nat Biotechnol 21: 1192–1199
Dutse SW, Yusof NA (2011) Microfluidics-based lab-on-chip systems in DNA-based biosensing: an overview. Sensors 11:5754–5768
Egholm M, Buchardt O, Christensen L et al (2003) PNA hybridizes to complementary oligonucleotides obeying the Watson-Crick hydrogen-bonding rules. Nature 365:566–568
Erdem A, Papakonstantinou P, Murphy H (2006) Direct DNA hybridization at disposable graphite electrodes modified with carbon nanotubes. Anal Chem 78:6656–6659
Fan CH, Plaxco KW, Heeger A (2003) Electrochemical interrogation of conformational changes as a reagentless method for the sequence-specific detection of DNA. Proc Natl Acad Sci USA 100:9134–9137
Fang Z, Kelley SO (2009) Direct electrocatalytic mRNA detection using PNA-nanowire sensors. Anal Chem 81:612–617
Fang B, Jiao S, Li M et al (2008) Label-free electrochemical detection of DNA using ferrocene-containing cationic polythiophene and PNA probes on nanogold modified electrodes. Biosens Bioelectron 23:1175–1179
Fang C, Ji H, Karen WY et al (2011) Electrochemical detection of oligonucleotide by attaching redox probes onto its backbone. Biosens Bioelectron 26:2670–2674
Farjami E, Clima L, Gothelf K et al (2011) "Off−On" electrochemical hairpin-DNA-based genosensor for cancer diagnostics. Anal Chem 83:1594–1602

Ferguson BS, Buchsbaum SF, Swensen JS et al (2009) Integrated microfluidic electrochemical DNA sensor. Anal Chem 81:6503–6505
Fritz J, Cooper EB, Gaudet S et al (2002) Electronic detection of DNA by its intrinsic molecular charge. Proc Natl Acad Sci USA 99:14142–14146
Gao Z, Agarwal A, Trigg AD et al (2007) Silicon nanowire arrays for label-free detection of DNA. Anal Chem 79:3291–3297
Gao L, Lian C, Zhou Y et al (2014) Graphene oxide–DNA based sensors. Biosens Bioelectron 60: 22–29
Gasser G, Spiccia L (2008) Synthesis of a ferrocenyl uracil PNA monomer for insertion into PNA sequences. J Org Chem 693:2478–2482
Gasser G, Belousoff MJ, Bond AM et al (2006) Facile synthesis and detailed characterization of a new ferrocenyl uracil peptide nucleic acid monomer. J Org Chem 71:7565–7573
Gasser G, Hüsken N, Köster SD et al (2008) Synthesis of organometallic PNA oligomers by click chemistry. Chem Commun 31:3675–3677
Gasser G, Sosniak AM, Metzler-Nolte N (2011) Metal-containing peptide nucleic acid conjugates. Dalton Trans 40:7061–7076
Gerard M, Chaubey A, Malhotra BD (2002) Application of conducting polymers to biosensors. Biosens Bioelectron 17:345–359
Goda T, Singi AB, Maeda Y et al (2013) Label-free potentiometry for detecting DNA hybridization using peptide nucleic acid and DNA probes. Sensors 13:2267–2278
Gooding JJ (2008) Advances in interfacial design for electrochemical biosensors and sensors: aryl diazonium salts for modifying carbon and metal electrodes. Electroanalysis 20:573–582
Gross A, Hüsken N, Schur J et al (2012) A ruthenocene–PNA bioconjugate—synthesis, characterization, cytotoxicity, and AAS-detected cellular uptake. Bioconjugate Chem 23:1764–1774
Hahm J, Lieber C (2004) Direct ultrasensitive electrical detection of DNA and DNA sequence variations using nanowire nanosensors. Nano Lett 4:51–55
Hai LV, Reisberg S, Chevillot-Biraud A et al (2014) Simultaneous electroreduction of different diazonium salts for direct electrochemical DNA biosensor development. Electrochim Acta. doi:10.1016/j.electacta2014.01.159
Harding-Lepage P, Peytavi R, Bergeron MG et al (2011) Amplification strategy using aggregates of ferrocene-containing cationic polythiophene for sensitive and specific electrochemical detection of DNA. Anal Chem 83:8086–8092
Harrell CC, Choi Y, Horne LP et al (2006) Resistive-pulse DNA detection with a conical nanopore sensor. Langmuir 22:10837–10843
Hashimoto K, Ishimori Y (2001) Preliminary evaluation of electrochemical PNA array for detection of single base mismatch mutations. Lab Chip 1:61–63
Hashioka S, Saito M, Tamiya E et al (2004) Deoxyribonucleic acid sensing device with 40-nm-gap-electrodes fabricated by low-cost conventional techniques. Appl Phys Lett 85:687–688
Hejazi MS, Pournaghi-Azar MH, Alipour E et al (2011) Development of a novel electrochemical biosensor for detection and discrimination of DNA sequence and single base mutation in dsDNA samples based on PNA-dsDNA hybridization—a new platform technology. Electroanalysis 23:503–511
Herdewijn P (2001) TNA as a potential alternative to natural nucleic acids. Angew Chem Int Ed 40:2249–2251
Herdewijn P, Marliere P (2009) Toward safe genetically modified organisms through the chemical diversification of nucleic acids. Chem Biodivers 6:791–808
Howorka S, Bayley H (2002) Probing distance and electrical potential within a protein pore with tethered DNA. Biophys J 83:3202–3210
Howorka S, Cheley S, Bayley H (2001) Sequence-specific detection of individual DNA strands using engineered nanopores. Nat Biotechnol 19:636–639
Hüsken N, Gębala M, Schuhmann W et al (2010) A single-electrode, dual-potential ferrocene–PNA biosensor for the detection of DNA. ChemBioChem 11:1754–1761

Jepsen JS, Sørensen MD, Wengel J (2004) Locked nucleic acid: a potent nucleic acid analog in therapeutics and biotechnology. Oligonucleotides 14:130–146
Ji H, Yan F, Lei J et al (2012) Ultrasensitive electrochemical detection of nucleic acids by template enhanced hybridization followed with rolling circle amplification. Anal Chem 84:7166–7171
Joshi T, Patra M, Spiccia L et al (2013) Di-heterometalation of thiol-functionalized peptide nucleic acids. Artif DNA PNA XNA 4:11–18
Ju HX, Zhao HT (2005) Electrochemical biosensors for DNA analysis. Front Biosci 10:37–46
Kara P, Kerman K, Ozkan D et al (2002) Label-free and label based electrochemical detection of hybridization by using methylene blue and peptide nucleic acid probes at chitosan modified carbon paste electrodes. Electroanalysis 14:1685–1690
Kauffman DR, Star A (2008) Electronically monitoring biological interactions with carbon nanotube field-effect transistors. Chem Soc Rev 37:1197–1206
Keighley SD, Estrela P, Li P et al (2008) Optimization of label-free DNA detection with electrochemical impedance spectroscopy using PNA probes. Biosens Bioelectron 24:906–911
Kergoat L, Piro B, Berggren M et al (2012a) Advances in organic transistor-based biosensors: from organic electrochemical transistors to electrolyte-gated organic field-effect transistors. Anal Bioanal Chem 402:1813–1826
Kergoat L, Piro B, Berggren M et al (2012b) DNA detection with a water-gated organic field-effect transistor. Org Electron 13:1–6
Kerman K, Ozkan D, Kara P et al (2003) Label-free bioelectronic detection of point mutation by using peptide nucleic acid probes. Electroanalysis 15:667–670
Kerman K, Vestergaard M, Nagatani N et al (2006) Electrochemical genosensor based on peptide nucleic acid-mediated PCR and asymmetric PCR techniques: electrostatic interactions with a metal cation. Anal Chem 78:2182–2189
Kerman K, Saito M, Tamiya E (2008) Electroactive chitosan nanoparticles for the detection of single-nucleotide polymorphisms using peptide nucleic acids. Anal Bioanal Chem 391: 2759–2767
Khan HU, Roberts ME, Johnson O et al (2010) In situ, label-free DNA detection using organic transistor sensors. Adv Mater 22:4452–4456
Khan HU, Roberts ME, Johnson O et al (2012) The effect of pH and DNA concentration on organic thin-film transistor biosensors. Org Electron 13:519–524
Kim E, Kim K, Yang H et al (2003) Enzyme-amplified electrochemical detection of DNA using electrocatalysis of ferrocenyl-tethered dendrimer. Anal Chem 75:5665–5672
Kjaellman T, Peng H, Travas-Sejdic J et al (2007) DNA-sensors based on functionalized conducting polymers and quantum dots. Proc SPIE Int Soc Opt Eng 6416
Korri-Youssoufi H, Garnier F, Srivastava P et al (1997) Toward bioelectronics: specific DNA recognition based on an oligonucleotide-functionalized polypyrrole. J Am Chem Soc 119: 7388–7389
Kouřilová A, Babkina S, Cahová K et al (2005) DNA hybridization on membrane-modified carbon electrodes. Anal Lett 38:2493–2703
Lai S, Demelas M, Casula G et al (2013) Ultra-low voltage, OTFT-based sensor for label-free DNA detection. Adv Mater 25:103–107
Lazerges M, Bedioui F (2013) Analysis of the evolution of the detection limits of electrochemical DNA biosensors. Anal Bioanal Chem 405:3705–3714
Le Floch F, Ho HA, Harding-Lepage P et al (2005) Ferrocene-functionalized cationic polythiophene for label-free electrochemical detection of DNA. Adv Mater 17:1251–1254
Lee CS, Kim SK, Kim M (2009) Ion-sensitive field-effect transistor for biological sensing. Sensors 9:7111–7131
Li Z, Chen Y, Li X et al (2004) Sequence-specific label-free DNA sensors based on silicon nanowires. Nano Lett 4:245–247
Li J, Liu Q, Liu Y et al (2005) DNA biosensor based on chitosan film doped with carbon nanotubes. Anal Biochem 346:107–114

Li D, Yan Y, Wieckowska A et al (2007) Amplified electrochemical detection of DNA through the aggregation of Au nanoparticles on electrodes and the incorporation of methylene blue into the DNA-crosslinked structure. Chem Commun 34:3544–3546

Li J, Chen M, Zhang H et al (2008) Electrochemical and photochemical characterization of novel ferrocenyl–azobenzene labeled PNA monomers for DNA detection. Inorg Chem Commun 11: 392–395

Liang X, Chou SY (2008) Nanogap detector inside nanofluidic channel for fast real-time label-free DNA analysis. Nano Lett 8:1472–1476

Liao C, Yan F (2013) Organic semiconductors in organic thin-film transistor-based chemical and biological sensors. Polym Rev 53:352–406

Lin P, Luo X, Hsing I et al (2011) Organic electrochemical transistors integrated in flexible microfluidic systems and used for label-free DNA sensing. Adv Mater 23:4035–4040

Liu A, Anzai JI (2004) Use of polymeric indicator for electrochemical DNA sensors: poly(4-vinylpyridine) derivative bearing [Os(5,6-dimethyl-1,10-phenanthroline)2Cl]2+. Anal Chem 76:2975–2980

Liu N, Hua Y, Zhang J et al (2012) A label-free, organic transistor-based biosensor by introducing electric bias during DNA immobilization. Org Electron 13:2781–2785

Lucarelli F, Marrazza G, Turner APF et al (2004) Carbon and gold electrodes as electrochemical transducers for DNA hybridisation sensors. Biosens Bioelectron 19:515–530

Luo X, Hsing IM (2009a) Real time electrochemical monitoring of DNA/PNA dissociation by melting curve. Electroanalysis 21:1557–1561

Luo X, Hsing IM (2009b) Immobilization-free multiplex electrochemical DNA and SNP detection. Biosens Bioelectron 25:803–808

Luo X, Lee TMH, Hsing IM (2008) Immobilization-free sequence-specific electrochemical detection of DNA using ferrocene-labeled peptide nucleic acid. Anal Chem 80:7341–7346

Macanovic A, Marquette C, Polychronakos C et al (2004) Impedance-based detection of DNA sequences using a silicon transducer with PNA as the probe layer. Nucleic Acids Res 32:e20

Maehashi K, Matsumoto K, Kerman K et al (2004) Ultrasensitive detection of DNA hybridization using carbon nanotube field-effect transistors. Jpn J Appl Phys 43:L1558–L1560

Maglia G, Restrepo MR, Mikhailova E et al (2008) Enhanced translocation of single DNA molecules through alpha-hemolysin nanopores by manipulation of internal charge. Proc Natl Acad Sci U S A 105:19720–19725

March G, Noel V, Piro B et al (2008) Nanometric layers for direct, signal-on, selective and sensitive electrochemical detection of oligonucleotides hybridization. J Am Chem Soc 130: 15752–15753

Maurer A, Kraatz HB, Metzler-Nolte N (2005) Synthesis and electrochemical characterization of metallocene–PNA oligomers. Eur J Inorg Chem 2005:3207–3210

Meggers E, Zhang L (2010) Synthesis and properties of the simplified nucleic acid glycol nucleic acid. Acc Chem Res 43:1092–1102

Meller A, Nivon L, Branton D (2001) Voltage-driven DNA translocations through a nanopore. Phys Rev Lett 86:3435–3438

Miles BN, Ivanov AP, Wilson KA et al (2013) Single molecule sensing with solid-state nanopores: novel materials, methods, and applications. Chem Soc Rev 42:15–28

Millan KM, Mikkelsen SR (1993) Sequence-selective biosensor for DNA based on electroactive hybridization indicators. Anal Chem 65:2317–2323

Moreno-Hagelsieb L, Foultier B, Laurent G et al (2007) Electrical detection of DNA hybridization: three extraction techniques based on interdigitated Al/Al2O3 capacitors. Biosens Bioelectron 22:2199–2207

Nebling E, Grunwald T, Albers J et al (2004) Electrical detection of viral DNA using ultramicroelectrode arrays. Anal Chem 76:689–696

Nickita N, Gasser G, Bond AM et al (2009) Synthesis, spectroscopic properties and electrochemical oxidation of RuII-polypyridyl complexes attached to a peptide nucleic acid monomer backbone. Eur J Inorg Chem 14:2179–2186

Nielsen PE, Egholm M (1999) Peptide nucleic acids: protocols and applications. Horizon Scientific, Norfolk, UK
Nielsen PE, Egholm M, Berg RH et al (1991) Sequence-selective recognition of DNA by strand displacement with a thymine-substituted polyamide. Science 254:1497–1500
Niu SY, Zhang SS, Wang L et al (2006) Hybridization biosensor using di(1,10-phenanthroline)(imidazo[f]1,10-phenanthroline)cobalt(II) as electrochemical indicator for detection of human immunodeficiency virus DNA. J Electroanal Chem 597:111–118
Njoroge SK, Chen HW, Witek MA et al (2011) Integrated microfluidic systems for DNA analysis. Top Curr Chem 304:203–260
Noor MO, Krull UJ (2014) Silicon nanowires as field-effect transducers for biosensor development: a review. Anal Chim Acta 825:1–25
Odenthal KJ, Gooding JJ (2007) An introduction to electrochemical DNA biosensors. Analyst 132:603–610
Ohtake T (2006) Development of high sensitive DNA sensor by using probe PNA with ISFET electrode. Electrochemistry 74:114–117
Ozkan D, Erdem A, Kara P et al (2002a) Electrochemical detection of hybridization using peptide nucleic acids and methylene blue on self-assembled alkanethiol monolayer modified gold electrodes. Electrochem Commun 4:796–802
Ozkan D, Kara P, Kerman K et al (2002b) DNA and PNA sensing on mercury and carbon electrodes by using methylene blue as an electrochemical label. Bioelectrochemistry 58:119–126
Paleček E, Bartošík M (2012) Electrochemistry of nucleic acids. Chem Rev 112:3427–3481
Paleček E, Jelen F (2002) Electrochemistry of nucleic acids and development of DNA sensors. Crit Rev Anal Chem 32:261–270
Paleček E, Trefulka M, Fojta M (2009) End-labeling of peptide nucleic acid with osmium complex. Voltammetry at carbon and mercury electrodes. Electrochem Commun 11:359–362
Patolsky F, Zheng G, Lieber CM (2006) Nanowire-based biosensors. Anal Chem 78:4260–4269
Paul A, Bezer S, Venkatramani R et al (2009) Role of nucleobase energetics and nucleobase interactions in single-stranded peptide nucleic acid charge transfer. J Am Chem Soc 131:6498–6507
Pavlovic E, Lai RY, Wu TT et al (2008) Microfluidic device architecture for electrochemical patterning and detection of multiple DNA sequences. Langmuir 24:1102–1107
Peng H, Zhang L, Soeller C et al (2009) Conducting polymers for electrochemical DNA sensing. Biomaterials 30:2132–2148
Petersen M, Wengel J (2003) LNA: a versatile tool for therapeutics and genomics. Trends Biotechnol 21:74–81
Pham MC, Piro B, Tran LD et al (2003) Direct electrochemical detection of ODN hybridization on poly(5-hydroxy-1,4-naphthoquinone -co- 5-hydroxy-2-acetic acid-1,4-naphthoquinone) film. Anal Chem 75:6748–6752
Phillips DD, Garboczi DN, Singh K et al (2013) The sub-nanomolar binding of DNA–RNA hybrids by the single-chain Fv fragment of antibody S9.6. J Mol Recognit 26:376–381
Pinheiro VB, Holliger P (2012) The XNA world: progress towards replication and evolution of synthetic genetic polymers. Curr Opin Chem Biol 16:245–252
Piro B, Haccoun J, Pham MC et al (2005) Study of the DNA hybridization transduction behaviour of a quinone-containing electroactive polymer by cyclic voltammetry and electrochemical impedance spectroscopy. J Electroanal Chem 577:155–165
Piro B, Reisberg S, Noel V et al (2007) Investigations of the steric effect on electrochemical transduction in a quinone-based DNA sensor. Biosens Bioelectron 22:3126–3131
Poghossian A, Abouzar MH, Sakkari M et al (2006) Field-effect sensors for monitoring the layer-by-layer adsorption of charged macromolecules. Sensor Actuators B 118:163–170
Prabhakar N, Arora K, Singh H et al (2008) Polyaniline based nucleic acid sensor. J Phys Chem B 112:4808–4816

Purnell RF, Schmidt JJ (2009) Discrimination of single base substitutions in a DNA strand immobilized in a biological nanopore. ACS Nano 3:2533–2538
Purnell RF, Mehta KK, Schmidt JJ (2008) Nucleotide identification and orientation discrimination of DNA homopolymers immobilized in a protein nanopore. Nano Lett 8:3029–3034
Rai V, Toh CS (2013) Electrochemical amplification strategies in DNA nanosensors. Nanosci Nanotechnol Lett 5:613–623
Reisberg S, Piro B, Noel V et al (2005) DNA electrochemical sensor based on conducting polymer: dependence of the signal-on detection on the probe sequence localization. Anal Chem 77:3351–3356
Reisberg S, Piro B, Noel V et al (2006) Selectivity and sensitivity of a reagentless electrochemical DNA sensor studied by square wave voltammetry and fluorescence. Bioelectrochemistry 69:172–179
Reisberg S, Dang LA, Nguyen QA et al (2008a) Label-free DNA electrochemical sensor based on a PNA-functionalized conductive polymer. Talanta 76:206–210
Reisberg S, Piro B, Noel V et al (2008b) Investigation of the charge effect on the electrochemical transduction in a quinone-based DNA sensor. Electrochim Acta 54:346–351
Roy S, Gao Z (2009) Nanostructure-based electrical biosensors. Nano Today 4:318–334
Roy S, Vedala S, Roy AD et al (2008) Direct electrical measurements on single-molecule genomic DNA using single-walled carbon nanotubes. Nano Lett 8:26–30
Sakata T, Kamahori M, Miyahara Y (2004) Immobilization of oligonucleotide probes on Si3N4 surface and its application to genetic field effect transistor. Mater Sci Eng C 24:827–832
Samanta D, Sarkar A (2011) Immobilization of bio-macromolecules on self-assembled monolayers: methods and sensor applications. Chem Soc Rev 40:2567–2592
Schöning MJ, Poghossian A (2002) Recent advances in biologically sensitive field-effect transistors (BioFETs). Analyst 127:1137–1151
Schöning KU, Scholz P, Guntha S et al (2001) Chemical etiology of nucleic acid structure: the α-threofuranosyl-(3′→2′) oligonucleotide system. Science 290:1347–1351
Schwartz EF, Stollar BD (1969) Antibodies to polyadenylate-polyuridylate copolymers as reagents for double strand RNA and DNA-RNA hybrid complexes. Biochem Biophys Res Commun 35:115–120
Shao Y, Wang J, Wu H et al (2010) Graphene based electrochemical sensors and biosensors: a review. Electroanalysis 22:1027–1036
Shiigi H, Tokonami S, Yakabe H et al (2005) Label-free electronic detection of DNA-hybridization on nanogapped gold particle film. J Am Chem Soc 127:3280–3281
Shin S, Won BY, Jung C et al (2011) Electrochemical detection of DNA mutations on a PNA-modified electrode utilizing a single-stranded DNA specific endonuclease. Chem Commun 47:6611–6613
Singh RP, Oh BK, Choi JW (2010) Application of peptide nucleic acid towards development of nanobiosensor arrays. Bioelectrochemistry 79:153–161
Souteyrand E, Cloarec JP, Martin JR et al (1997) Direct detection of the hybridization of synthetic homo-oligomer DNA sequences by field effect. J Phys Chem B 101:2980–2985
Spain E, Keyes TE, Forster RJ (2013) DNA sensor based on vapour polymerized pedot films functionalized with gold nanoparticles. Biosens Bioelectron 41:65–70
Star A, Tu E, Niemann J et al (2006) Label-free detection of DNA hybridization using carbon nanotube field-effect transistors. Proc Natl Acad Sci U S A 103:921–926
Steel AB, Herne TM, Tarlov MJ (1998) Electrochemical quantitation of DNA immobilized on gold. Anal Chem 70:4670–4677
Steel AB, Levicky RL, Herne TM et al (2000) Immobilization of nucleic acids at solid surfaces: effect of oligonucleotide length on layer assembly. Biophys J 79:975–981
Steichen M, Decrem Y, Godfroid E et al (2007) Electrochemical DNA hybridization detection using peptide nucleic acids and [Ru(NH3)6]3+ on gold electrodes. Biosens Bioelectron 22: 2237–2243
Stenvang J, Silahtaroglu AN, Lindow M et al (2008) The utility of LNA in microRNA-based cancer diagnostics and therapeutics. Semin Cancer Biol 18:89–102

Stern E, Wagner R, Sigworth FJ et al (2007) Importance of the Debye screening length on nanowire field effect transistor sensors. Nano Lett 11:3405–3409
Stoddart D, Heron AJ, Mikhailova E et al (2009) Single-nucleotide discrimination in immobilized DNA oligonucleotides with a biological nanopore. Proc Natl Acad Sci U S A 106:7702–7707
Stoliar P, Bystrenov E, Quirog SD et al (2009) DNA adsorption measured with ultra-thin film organic field effect transistors. Biosens Bioelectron 24:2935–2938
Sun X, He P, Liu S et al (1998) Immobilization of single-stranded deoxyribonucleic acid on gold electrode with self-assembled aminoethanethiol monolayer for DNA electrochemical sensor applications. Talanta 47:487–495
Tercero N, Wang K, Gong P et al (2009) Morpholino monolayers: preparation and label-free DNA analysis by surface hybridization. J Am Chem Soc 131:4953–4961
Thipmanee O, Samanman S, Sankoh S et al (2012) Label-free capacitive DNA sensor using immobilized pyrrolidinyl PNA probe: effect of the length and terminating head group of the blocking thiols. Biosens Bioelectron 38:430–435
Torsi L, Magliulo M, Manoli K et al (2013) Organic field-effect transistor sensors: a tutorial review. Chem Soc Rev 42:8612–8628
Tran HV, Piro B, Reisberg S et al (2013a) Antibodies directed to RNA/DNA hybrids: an electrochemical immunosensor for microRNAs detection using graphene-composite electrodes. Anal Chem 85:8469–8474
Tran HV, Piro B, Reisberg S et al (2013b) Label-free and reagentless electrochemical detection of micro RNAs using a conducting polymer nanostructured by carbon nanotubes. Application to prostate cancer biomarker miR-141. Biosens Bioelectron 49:164–169
Tran HV, Piro B, Reisberg S et al (2014) An electrochemical ELISA-like immunosensor for miRNAs detection based on reduced graphene oxide and carbon nanotubes composite. Biosens Bioelectron 62:25–30
Tsouti V, Boutopoulos C, Zergioti I et al (2011) Capacitive microsystems for biological sensing. Biosens Bioelectron 27:1–11
Uno T, Tabata H, Kawai T (2007) Peptide−nucleic acid-modified ion-sensitive field-effect transistor-based biosensor for direct detection of DNA hybridization. Anal Chem 79:52–59
Uslu F, Ingebrandt S, Mayer D et al (2004) Label-free fully electronic nucleic acid detection system based on a field-effect transistor device. Biosens Bioelectron 19:1723–1731
Veedu RN, Wengel J (2009) RNA locked nucleic acid as a novel class of therapeutic agents. Biology 6:321–323
Venkatramani R, Keinan S, Balaeff A et al (2011) Nucleic acid charge transfer: black, white and gray. Coord Chem Rev 255:635–648
Vester B, Wengel J (2004) LNA (locked nucleic acid): high-affinity targeting of complementary RNA and DNA. Biochemistry 43:13233–13241
Wang J (2003) Nanoparticle-based electrochemical DNA detection. Anal Chim Acta 500:247–257
Wang J, Palecek E, Nielsen PE et al (1996) Peptide nucleic Acid probes for sequence-specific DNA biosensors. J Am Chem Soc 118:7667–7670
Wang J, Rivas G, Cai X et al (1997) Detection of point mutation in the p53 gene using a peptide nucleic acid biosensor. Anal Chim Acta 344:111–118
Wang J, Liu G, Polsky R et al (2002) Electrochemical stripping detection of DNA hybridization based on cadmium sulfide nanoparticle tags. Electrochem Commun 4:722–726
Wang J, Kawde AN, Musameh M (2003) Carbon nanotube modified glassy carbon electrodes for amplified label-free electrochemical detection of DNA hybridization. Analyst 128:912–916
Wang Q, Chen L, Long YT et al (2013) Molecular beacons of xeno-nucleic acid for detecting nucleic acid. Theranostics 3:395–408
Wei MY, Guo LH, Famouri P (2011) DNA biosensors based on metallo-intercalator probes and electrocatalytic amplification. Microchim acta 172:247–260
Wierzbinski E, de Leon A, Yin X et al (2012) Effect of backbone flexibility on charge transfer rates in peptide nucleic acid duplexes. J Am Chem Soc 134:9335–9342
Willner I, Katz E, Willner B (1999) Layered biomaterials on electrode supports: routes to electrochemical biosensors, immunosensors and DNA sensors. Sensors Update 5:45–102

Won BY, Yoon HC, Park HG (2008) Enzyme-catalyzed signal amplification for electrochemical DNA detection with a PNA-modified electrode. Analyst 133:100–104
Wong ELS, Gooding JJ (2006) Charge transfer through DNA: a selective electrochemical DNA biosensor. Anal Chem 78:2138–2144
Xuan F, Luo X, Hsing IM (2012) Sensitive immobilization-free electrochemical DNA sensor based on isothermal circular strand displacement polymerization reaction. Biosens Bioelectron 35:230–234
Yan F, Mok SM, Yu JJ et al (2009) Label-free DNA sensor based on organic thin film transistors. Biosens Bioelectron 24:1241–1245
Yanez-Sedeno P, Riu J, Pingarron JM et al (2010) Electrochemical sensing based on carbon nanotubes. Trends Anal Chem 29:939–953
Yang T, Meng L, Wang X et al (2013) Direct electrochemical DNA detection originated from the self-redox signal of sulfonated polyaniline enhanced by graphene oxide in neutral solution. ACS Appl Mater Interfaces 5:10889–10894
Zanoli LM, D'Agata R, Spoto G (2012) Functionalized gold nanoparticles for ultrasensitive DNA detection. Anal Bioanal Chem 402:1759–1771
Zhang QT, Subramanian V (2007) DNA hybridization detection with organic thin film transistors: toward fast and disposable DNA microarray chips. Biosens Bioelectron 22:3182–3187
Zhang Y, Pothukuchy A, Shin W et al (2004) Detection of 103 copies of DNA by an electrochemical enzyme-amplified sandwich assay with ambient O2 as the substrate. Anal Chem 76:4093–4097
Zhang L, Peritz A, Meggers E (2005) A simple glycol nucleic acid. J Am Chem Soc 127: 4174–4175
Zhang J, Song S, Zhang L et al (2006) Sequence-specific detection of femtomolar DNA via a chronocoulometric DNA sensor (CDS): effects of nanoparticle-mediated amplification and nanoscale control of DNA assembly at electrodes. J Am Chem Soc 128:8575–8580
Zhang GJ, Zhang G, Chua JH et al (2008) DNA sensing by silicon nanowire: charge layer distance dependence. Nano Lett 8:1066–1070
Zhang GJ, Chua JH, Chee RE et al (2009a) Label-free direct detection of miRNAs with silicon nanowire biosensors. Biosens Bioelectron 24:2504–2508
Zhang J, Chen JH, Chen RC et al (2009b) Sequence-specific detection of trace DNA via a junction-probe electrochemical sensor employed template-enhanced hybridization strategy. Biosens Bioelectron 25:815–819
Zhang X, Jiao K, Liu S et al (2009c) Readily reusable electrochemical DNA hybridization biosensor based on the interaction of DNA with single-walled carbon nanotubes. Anal Chem 81:6006–6012
Zhang GJ, Zhang L, Huang MJ et al (2010) Silicon nanowire biosensor for highly sensitive and rapid detection of Dengue virus. Sens Actuators B 146:138–144
Zhang QD, Piro B, Noël V et al (2011) Functionalization of single-walled carbon nanotubes for direct and selective electrochemical detection of DNA. Analyst 136:1023–1028
Zhang QD, March G, Noël V et al (2012a) Label-free and reagentless electrochemical detection of PCR fragments using quinone derivative self-assembled monolayer. Biosens Bioelectron 32: 163–168
Zhang QD, Piro B, Noël V et al (2012b) An electroactive conjugated oligomer for a direct electrochemical DNA sensor. Synth Met 162:1496–1502
Zhang QD, Piro B, Ramsay S et al (2012c) Electrochemical investigation of interactions between quinone derivatives and single stranded DNA. Electrochim Acta 85:588–593
Zhou N, Yang T, Jiang C et al (2009) Highly sensitive electrochemical impedance spectroscopic detection of DNA hybridization based on Au nano-CNT/PAN nano films. Talanta 77: 1021–1026

DNA for Non-nucleic Acid Sensing

Vincent Noel, Benoit Piro, and Steeve Reisberg

Contents

Abstract The structure of DNA, encoded on four bases, allows to generate a considerable number of unique markers, even considering very short sequences composed of n nucleotides leading to 4^n different combinations. The possibility of synthesizing DNA sequences in vitro at low cost and in large quantities, coupled with well-known strategies of strand functionalization with groups having optical, magnetic or redox properties, allows to consider DNA not simply as a tool for detection of target nucleotide sequences but as versatile label in many biomolecular recognition event transduction schemes. This ability is strongly enhanced by modern DNA amplification approaches. Furthermore, iterative selection methods (SELEX) have achieved a high level of performance, reliability and sophistication, enabling the use of short DNA sequences also as selective binding element for the detection of an increasing number of analytes ranging from proteins to small organic molecules, such as pollutants and endocrine disruptors. This chapter highlights the progress made in the areas of analytical sciences through the use of

V. Noel (✉) • B. Piro • S. Reisberg
ITODYS, UMR 7086 CNRS, Université Paris Diderot, Sorbonne Paris Cité, 15 rue Jean-Antoine de Baïf, F-75205, Paris Cedex 13, France
e-mail: vincent.noel@univ-paris-diderot.fr

V.A. Erdmann et al. (eds.), *RNA and DNA Diagnostics*, RNA Technologies,
DOI 10.1007/978-3-319-17305-4_4

nucleic acid sequences that act either only as an amplifiable label or both as a recognition element and as a marker.

Keywords Aptamer • Strand displacement amplification (SDA) • Enzyme-assisted amplification • Biosensor • Chiral sensing

1 Introduction

DNA is one of the most studied systems due to its biological role as the carrier of genetic information. The advent of high-speed DNA sequencing techniques pushed the frontiers of knowledge and paved the way for new research fields that generated possibilities to a better understanding of pathologies and develop innovative therapies, i.e. proteomics and transcriptomics. DNA is unique in the living world. From a very simple code of four bases, complementary 2 by 2, single-strand DNAs hybridize to form a double helix. This sequence complementarity has enabled the realization of analytical devices for detecting the presence of nucleic acid sequences. Furthermore, the development of biotechnology to amplify a target sequence via the polymerase chain reaction allows the detection of single DNA copies. The combination of these two advantages has contributed to the development of biosensors and high-performance analytical systems that bear no comparison with other targets of interest, at the centre of which proteins or small organic molecules (endocrine disruptors, neurotransmitters, etc.).

However, beyond genetic information storage, the potential of single-strand DNA has been extremely underutilized. Despite a small number of bases and secondary and tertiary structures known to date, the combined capabilities of (1) in vitro synthesis, (2) functionalization of the ends or one of the intermediate bases and (3) selection of nucleic acid sequence against virtually any target (aptamer) from ethanolamine to whole cell has led the scientific community to expand the scope of the single-strand sequence and to integrate it into countless analytical devices. The advent of iterative selection methods gathered under the name SELEX or "systematic evolution of ligands by exponential enrichment" allows, in a very short time, to today identify receptors that are generally very selective with high affinity for targets of interest in various application fields, from medical diagnostics to environmental control (Klussmann 2006). More recently, the use of enzymes (polymerases, nucleases) having catalytic activity towards nucleic acids has led to the integration of isothermal amplification schemes in nucleic acid sequence detection devices with increased performance. The combination of both the amplification and SELEX methods reaching maturation allows to view the development of ultrasensitive and selective analytical assays for the measurement of protein or small organic molecules from a new angle. These devices are now able

to compete with conventional separative analytical methods while allowing the realization of portable, easy-to-use and multiplexable detection tools.

Besides the nucleic acid sequence itself, which leads to a specific interaction with the targets against which they were selected, the chirality of the sugar phosphate backbone may, in special SELEX conditions, lead to the generation of enantioselective aptamers. The current methods for measuring enantiomeric excess (e.e.) are mainly chromatographic based on chiral columns that use expensive and fragile equipment requiring cumbersome and time-consuming implementation. Hence, the possibility to generate enantioselective receptors coupled to the ability for DNA amplification is an attractive and unique way to develop enantioselective assays that meet the high demand of several major industries involved in enantiomer production, at the centre of which lies the pharmaceutical industry. This possibility of e.e. measurement with versatile receptors (SELEX) that are easily functionalized (transduction) and producible at low cost (synthesizer) is a property of nucleic acid sequences again beyond that of DNA detection.

The other biomolecule family of central interest in medical diagnosis is protein. Indeed, nucleotide-based targets benefit from a large number of available amplification methods, whereas protein-based targets do not. Standard tests for the detection and quantification of proteins are ELISA tests (enzyme-linked immunosorbent assay), based on the specificity of the antibody and the amplification ability of the enzyme labelling secondary antibody (marker). ELISAs are typically relevant at target concentration greater than 10^{-13} M, a concentration range largely insufficient in the light of current demands for early diagnosis, especially with biomarker assays. Several strategies using a nucleotide sequence as a *biobarcode* have dramatically reduced the detection limits of current assays. In this case, DNA is not used for its recognition properties but rather first for the ability to achieve countless distinctive labels (performing parallel assays) and second to amplify the response beyond that which an enzyme can achieve in a standard ELISA.

2 Overview of Toehold-Mediated Strand Displacement and Isothermal Amplification

2.1 Strand Displacement Amplification Strategies

The application field of nucleic acids has recently been extended to the realization of logic circuits, mainly for applications in diagnosis but also, ultimately, for the creation of more complex algorithms. The first examples show their ability to mimic sophisticated operations such as neural network computation (Qian et al. 2011). Many patterns were developed to generate from an *input* sequence the release of nucleotide sequence(s) (*output*) or trigger a programmed self-assembly. They are grouped under the term strand displacement amplification (SDA). The original SDA field of application, i.e. logical operations using at least

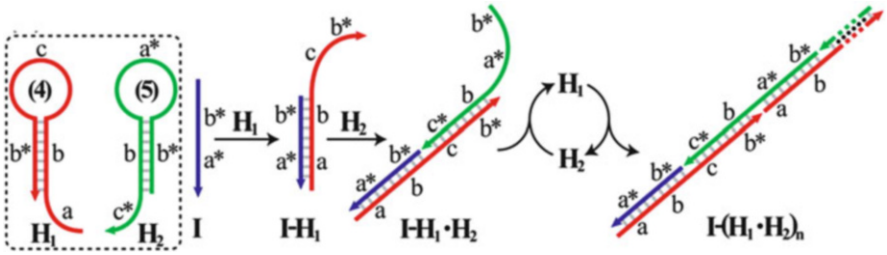

Fig. 1 Hairpin chain reaction (HCR) [Adapted with permission Wang et al. (2014). American Chemical Society]

one DNA sequence as an input trigger for various computing commands, has been surpassed, and SDA is currently developed and adapted for analytical purposes (Jung and Ellington 2014). The main SDA strategies are catalytic hairpin assembly (CHA, Yin et al. 2008), entropy-driven catalysis (EDC, Zhang et al. 2007a) and the hairpin chain reaction (HCR, Dirks and Pierce 2004). Figure 1 presents these major SDA approaches.

While EDC and CHA release strands in solution and hence are poorly compatible to microarray based devices, HCR leads to concatemer formation. Such a DNA superstructure fits to the requirements of solid-state-based detection methods. Moreover, such structures can potentially contain multiple reporters that will be immobilized in one place. Note that one of the main advantages of such SDA strategies is their modularity and ability to be combined to one another or to enzymatic-assisted DNA amplification.

2.2 Isothermal DNA Amplification Methods

The intensive use of enzymes to amplify the presence of nucleotide sequences started with the invention of the polymerase chain reaction (PCR), which allows exponential amplification through multiple temperature cycles. Since then, other approaches working in isothermal conditions have been developed, including the rolling circle amplification (RCA, Fire and Xu 1995), the loop-mediated isothermal amplification (LAMP, Notomi et al. 2000) and the exponential amplification reaction (EXPAR, Van Ness et al. 2003) being the most encountered ones. The possibility of amplification can be advantageously used in the development of bio-analytic systems based on aptamers to drastically decrease the detection limit, thanks to the catalytic activity of nuclease and polymerase enzymes. Indeed, aptamers have many advantages but one major drawback, a sub-micromolar affinity. Aptamers with the highest affinity in the pM to nM range are in reality only selected against proteins. The many possible points of interaction between a protein and a nucleic acid sequence are responsible for such high affinity. However, the detection of proteins by nucleic acids remains uncompetitive in view of the extreme

sophistication of ELISAs. The major advantage is therefore rather in the detection of small molecules for which there are no alternatives. Figure 1 presents the main isothermal amplification methods already described elsewhere (Yan et al. 2014). The major distinction between these techniques is their amplification mode, linear for RCA, exponential for EXPAR and LAMP but also the probability of parasite amplification (no template control), negligible in the case of LAMP, which includes three primers in its operating mode, and higher in the case of RCA and EXPAR.

The main advantage of RCA is that the amplified strand remains anchored to the padlock strand though hybridization. In the case of a multiarray assay format, such properties allow to easily and independently detect many different targets. The main drawback of RCA is the complex primer design. Although this problem is also encountered for EXPAR and LAMP, these approaches allow to amplify at least 10^6–10^9-fold the initial strand quantity, in several minutes for EXPAR and in 1 h for LAMP. The main difference between LAMP and EXPAR is relative to the possible parasite amplification, which is minimized in the case of LAMP due the number of primers used (i.e. two).

3 Nucleic Acids as Amplifiable Antibody Labels for Protein Detection

3.1 Nucleic Acids Amplification: Biological Approach

3.1.1 Strand Displacement Amplification and ELISA Format

Demand for development of analytical devices for the determination of proteins is steadily increasing. The reference technique remains ELISA. The ability to generate antibodies against all possible targets, except those having a too high toxicity, coupled with the use of enzyme as an amplifier enabled this technique to reach sufficient maturity for most diagnostic purposes. However, current demand, particularly for the determination of trace biomarkers, faces an inherent limitation in antibody affinity towards their target. Indeed, an ELISA has acceptable reliability for target concentrations above 10^{-13} mol/L^{-1} (M). However, many substances are present in concentrations between 10^{-13} and 10^{-18} M and require the development of dedicated assays.

For nucleic acids, amplification methods applied to the target nucleotide sequence can increase their concentration to reach quantities compatible with the sensitivity thresholds of conventional measurement techniques. In contrast, for proteins there is no method of amplification. It is therefore necessary to develop approaches to amplify the target/primary antibody recognition event. The possibility of labelling the secondary antibody with a nucleotide sequence and to implement sequence amplification using PCR has been explored (Sano et al. 1992). This approach improves the sensitivity of ELISA tests by a factor of 100–10,000 and has

been widely used for the detection of rare infectious diseases (Guo et al 2006), toxins in food (Kuczius et al. 2009; Zhang et al. 2010) or pollutants in aqueous media (Zhuang and Zhou 2009; Chen and Zhuang 2009). However, PCR requires the implementation of complex protocols that need special instruments and qualified personnel.

The most recent schemes based on nucleic acid amplification incorporate advances in isothermal rolling circle amplification (RCA). RCA extends a DNA strand attached to the antibody by adding circular single-strand DNA as template (Fig. 2). Furthermore, the fact that the elongated strand remains attached to the antibody (no release) enables this approach to be particularly suitable for a microarray detection format (Mullenix et al. 2002; Yang et al. 2007; Zhou et al. 2007). The conventional immuno-PCR transduction scheme is shown in Fig. 2. The strategy is to extend the nucleotide sequence attached to the secondary antibody and to add a complementary DNA strand, often labelled by a fluorophore, after the rinsing steps (Akter et al. 2011, 2012). Most systems work in a heterogeneous pattern particularly suitable for electrochemical detection. Under these conditions, the complementary strand is functionalized with an enzyme capable of generating a

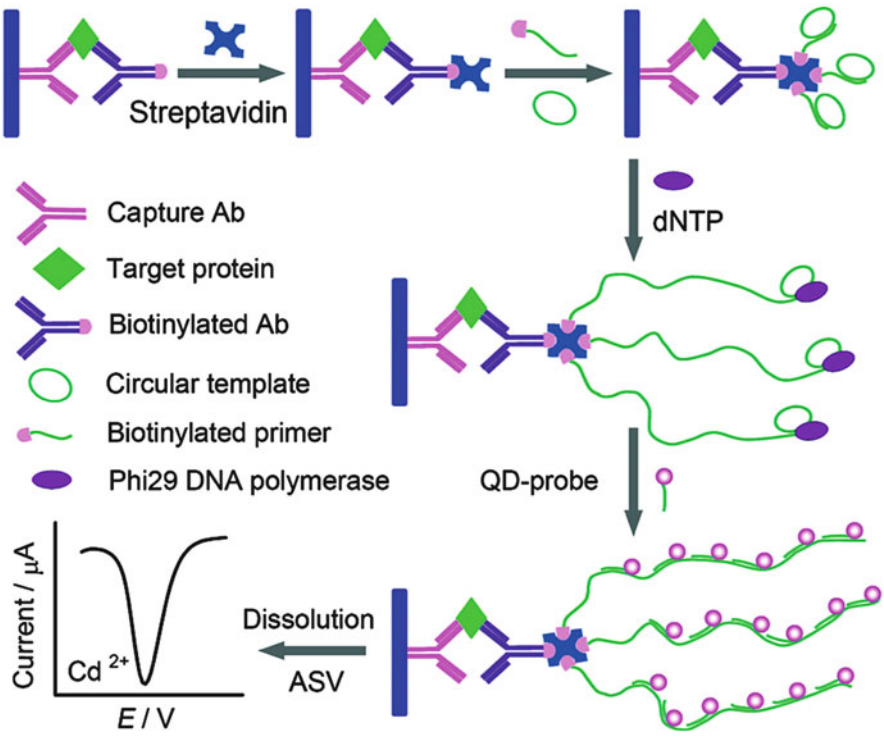

Fig. 2 Schematic representation of the cascade signal strategy for protein detection [Reprinted with permission from Cheng et al. (2010). American Chemical Society]

stream of redox species detected at the surface of the electrode functionalized by the capture antibody. All these approaches can achieve detection limits of the order of 10–100 pg/mL. These values are of the same order of magnitude as those obtained using iPCR, but RCA is still easier to implement than PCR (no need for temperature cycles and detection easily performed in situ, avoiding cross-contamination).

One strategy used recently to improve sensitivity is to work not with a unique detection strand per antibody but with several. Theoretically, the amplification factor is multiplied by the number of DNA strands when amplification methods such as RCA are used. One approach is not to fix the DNA strand covalently to the antibody but to mark it with biotin. The detection antibody is also functionalized with biotin. Thus, in the presence of streptavidin, containing four binding sites, three strands can be immobilized to each captured antibody. The detection limits achieved in these conditions are of the order of 0.1 fg/mL (Xue et al. 2012b; Cheng et al. 2010; Lu et al. 2012). More recently, a strategy to improve detection limits has been developed on the basis of liposome encapsulation capabilities. Each liposome can contain hundreds of RCA initiators. In this approach, the circular template is in solution. After the steps of capturing and flushing, opening of the liposomes and amplification take place in a homogeneous phase leading to better detection limits of the order of 0.1 fg/mL (Ou et al. 2009).

Although the RCA method has the advantage of operating in isothermal conditions, there are many defects very similar to PCR, such as the difficulty of labelling antibodies with DNA, complex and lengthy measurement protocols and problems related to primer design. In addition RCA only allows a linear amplification of the target, unlike PCR that follows exponential amplification. Therefore, the current trend is strongly in line with the coupling of antibodies selectivity and affinity with the LAMP method that allows exponential amplification of the DNA detection sequence.

Some examples of this coupling have recently been published (Ravan and Yazdanparast 2012, 2013; Pourhassan-Moghaddam et al. 2013; Jiang et al. 2012; Focke et al. 2013). Ultimately, it is clear that this method of amplification will be more widely used due to its specificity (very low background noise) and its ability to generate large quantities of product thereby allowing to consider the development of visual reading tests. However, as for RCA and PCR, several problems remain. Besides the difficulty related to primer design, which is expected to be resolved in view of advances in dedicated softwares, DNA grafting onto antibodies is complex and very expensive (low yield, laborious and time-consuming purification steps). Furthermore, the main problem is the poor performance of such amplification methods in a complex biological medium, the only relevant one for protein assay. These negative considerations should not obscure the enormous potential of this approach that combines the selectivity of antibodies and isothermal amplification of nucleic acids to achieve detection sensitivities compatible with the early diagnosis of deadly diseases such as cancer that would allow more effective treatments.

3.1.2 Enzyme-Assisted DNA-Labelled Antibody Amplification

To circumvent the problem of primer design and avoid working with enzymes (cost and stability), an alternative approach was proposed by Mirkin's group (Hill and Mirkin 2006) that uses the large surface/volume ratio of nanoparticles. The number of nucleotide sequences that can be immobilized onto the surface of a nanoparticle of a few nm in radius is of the same order of magnitude as those encapsulated in a liposome. The central idea is shown in Fig. 3. The detection scheme is based on two types of nanoparticles. The first, magnetic, is called the capture nanoparticle and is functionalized with a target-specific primary antibody. The second, the detection nanoparticle, is functionalized both by the secondary antibody and by a large number of identical DNA sequences. Each target has a specific capture nanoparticle/detection nanoparticle couple identified through the sequence of the immobilized DNA. The capture particle thus serves as an amplifier because more than one DNA sequence is available per protein/antibody complex. Furthermore, the ability to generate numerous different DNA sequences allows the detection of multiple targets simultaneously.

DNA chips carrying DNA complementary strand of each DNA-labelled nanoparticle are used. The capture/detection nanoparticle complex, formed exclusively in the presence of the target, is isolated using a magnet. Successive washes are performed to remove any non-specific target binding as well as adsorbed nanoparticles. Then, nanoparticles are released on the chip. Many high-performance systems are based on this principle and differ mainly in their transduction mode (Campolongo et al. 2010; Pei et al. 2013; Adams et al. 2012). While the magnetic nanoparticle is always used, the detection nanoparticle nature is adapted to the transduction mode. Mirkin et al. have developed a clever reading method for their assay that takes advantage of the optical properties of nanoparticles. Their approach allows results to be read with the naked eye, without

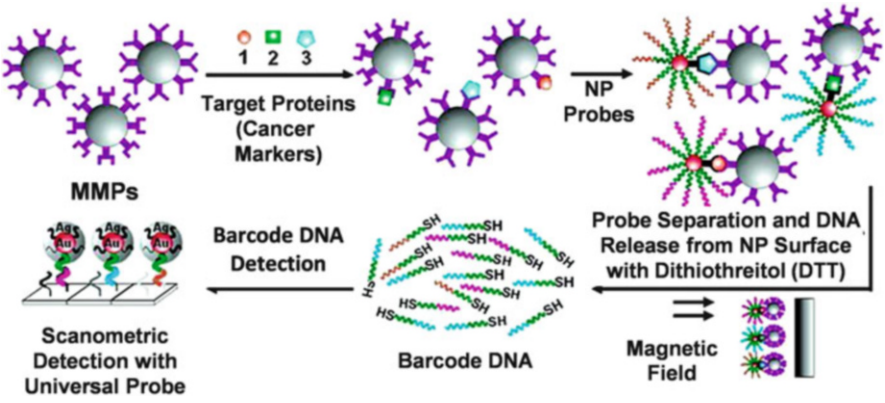

Fig. 3 Biobarcode assay for multiplexed protein detection [Reprinted with permission from Hill and Mirkin (2006). American Chemical Society]

any sophisticated equipment (on-site measurements, low cost of analysis, unskilled personnel, etc.). Indeed, hybridization is carried out and the presence of Au nanoparticles on a spot is revealed using a "silver enhancement" solution containing Ag^+ ions. The Au nanoparticles act as a catalyst in the reduction of the Ag salts in solution, which are then deposited as a shell and lead to a significant increase in the Au nanoparticle mean size (from 30 nm to 100 nm). The appearance of a dark spot indicates the presence of Au nanoparticles and thus of the corresponding target. This approach was used successfully for detection of biomarkers (Stoeva et al. 2006; Goluch et al. 2006; Nam et al. 2002) or viral protein (Yin et al. 2011). There exists the possibility of labelling the complementary strand barcode used to measure the amount of nanoparticles and thus targets by conventional methods, usually optical (fluorescent labelling with fluorescein: Cao et al. 2010; Zhang et al. 2009; chemiluminescence: Peng et al. 2011) but using more of the conductance modulation nanogap (Chang et al. 2007). This amplification approach using nano-objects has achieved sensing devices with detection thresholds 3–4 orders of magnitude below what can be achieved with an ELISA. Such a concentration range is compatible with the concentration of trace protein for which alternatives were currently unknown.

3.2 Nanoparticles for Ultrasensitive Assay Development

The barcode approach can be improved by incorporating an additional amplification step. If the transduction is based on physico-chemical properties of the nanoparticle, it is possible to generate superstructures that will, for one target/antibody complex, lead to a very large number of immobilized nanoparticles (Fig. 4, Zhou et al. 2013). Furthermore, the detection particle carries a nucleotide sequence of versatile structure and can be designed to contain an enzymatic primer. The possibility of combining the barcode approach with an enzymatic amplification, essentially RCA type, is increasingly used (Ou et al. 2009; Xue et al. 2012c; Yan et al. 2012; Zhao et al. 2013a; Cao et al 2011). It would probably be desirable to develop this approach using the LAMP method, but the main advantage of the barcode strategy is the simultaneous detection of multiple targets. However, the LAMP amplification is carried out in the homogeneous phase and therefore not suitable for transfer to microarray.

The most recent barcode approaches combine DNA superstructure generation by SDA into which the input is a sequence carried by the detection nanoparticle (Tang et al. 2012a). Liu et al. used this amplification mode and revealed the target binding by the use of ferrocene-functionalized short sequences that hybridize on the superstructure and then performed an electrochemical detection. A remarkable limit of detection for IgG of 0.1 fg/mL^{-1} was obtained (Fig. 5, Zhang et al. 2012a).

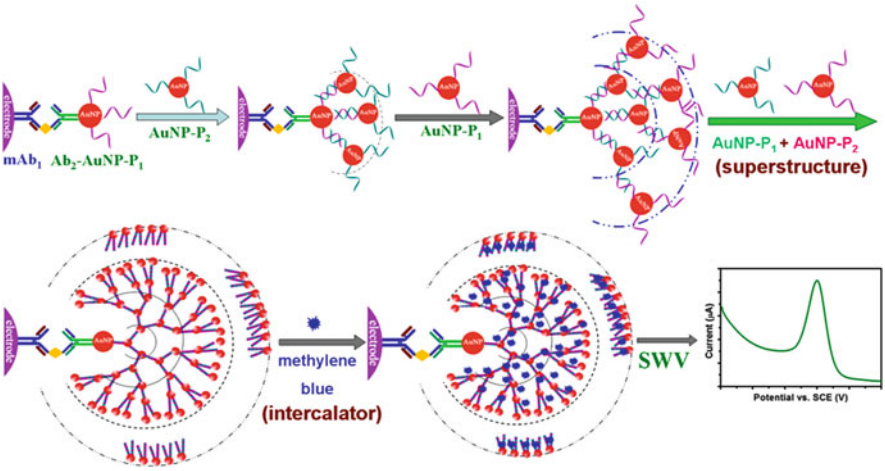

Fig. 4 Dual nanogold-linked complementary bio-barcodes with superstructures for in situ amplified signals of electrochemical immunoassay by using the intercalator molecules. Reproduced by permission of the Royal Society of Chemistry (Zhou et al. 2013)

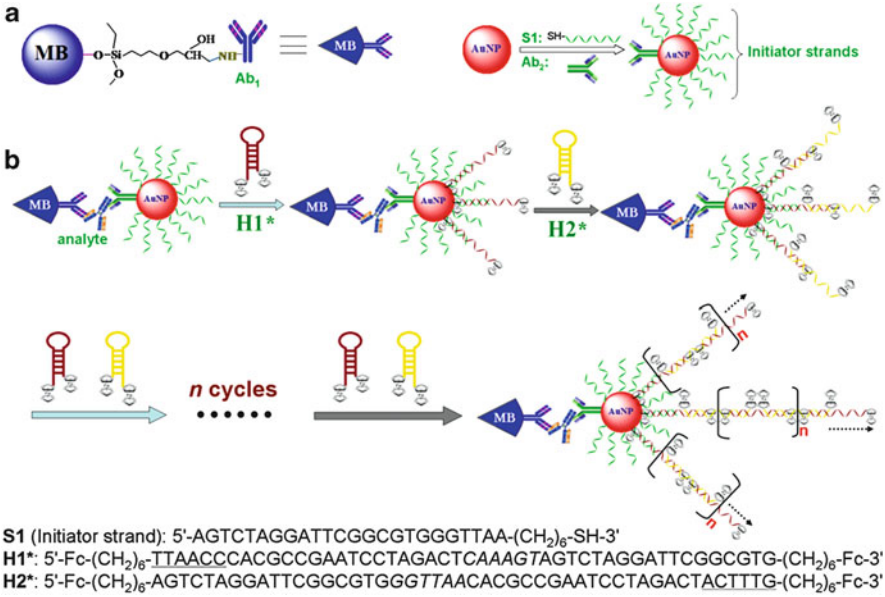

Fig. 5 (**a**) Design and preparation of monoclonal mouse anti-human IgG-functionalized magnetic beads (Ab1-MBs) and polyclonal goat anti-human IgG/initiator strand-conjugated gold nanoparticles (Ab2-S1-AuNPs). (**b**) Schematic depiction of the sandwiched immunoassays with the DNA-based hybridization chain reaction (*MB* magnetic beads, *AuNP* gold nanoparticle with 16 nm in diameter, *S1* DNA initiator strand, *Fc* ferrocenecarboxylic acid) [Reprinted with permission from Zhang et al. (2012a). American Chemical Society]

4 Nucleic Acids for Both Binding and Amplified Detection

4.1 Amplification Strategies and Aptamers

Apart from the protein targets for which pM dissociation constants are sometimes measured, most aptamers have a dissociation constant in the μM range. Detecting trace amounts of target, i.e. below several μM, therefore requires the development of an amplification scheme that may be based on one or more of the following strategies:

- Enzyme mimicking
- Target recycling
- SDA (HCR, EDC, CHA)
- Target-triggered sequence amplification

The number of publications that employ enzymes to amplify recognition aptamer/target is constantly increasing. The objective of this section is therefore not to present an exhaustive list, already published (Jung and Ellington 2014; Wang et al. 2014; Gerasimova and Kolpashchikov 2014), but to present how advances made in the context of nucleotide sequence detection can be cleverly combined with aptamer selectivity.

4.1.1 Mimicking Enzyme

Some aptamers, called *DNAzyme* or *RNAzyme*, have special catalytic activity in the presence of their substrate: essentially, nucleic acid cleavage under target binding, which is often a bidentate cation (Pb^{2+}, Mg^{2+}, Zn^{2+}, etc.). Indeed, most of the nucleic acid activity onset is due to a special conformation change triggered by the presence of a metal cation (Willner et al. 2008). This property is widely used to detect such cations but also as a transducer. Frequently used in detection schemes, a particular *DNAzyme* is a guanine-rich nucleic acid that has a catalytic activity mimicking peroxidises (Travascio et al. 1998). In the presence of alkaline cation, G-quartet structuring of the nucleotide sequence occurs. The hemin (chloro [3,7,12,17-tetramethyl-8,13-divinylporphyrin-2,18-dipropanoato(2−)]iron(III)) is then binded and exhibits high activity towards the conventional oxidation of peroxidase substrates, such as ABTS (2,2′-azino-bis (3-ethylbenzothiazoline-6-sulphonic acid) or luminol. The possibility to have a label capable of providing a flux of detectable species allows to amplify one binding event. Obviously, it is necessary that hemin complexation only occurs in the presence of the target. The most frequently encountered strategy uses a nucleotide sequence comprising a capture sequence (aptamer) coupled to a detection sequence (G-quartet). Formation of G-quartet is possible only if the detection sequence is released by the interaction of the capture sequence with the target (Fig. 6). Somehow, this allosteric activity is very similar to the operation of natural *riboswitch* for which transcription properties

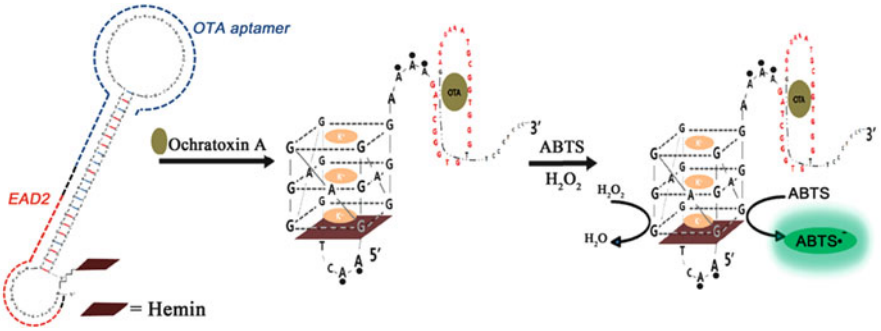

Fig. 6 A schematic cartoon depicts a design of a hemin-conjugated DNA hairpin and its structural change upon recognition of ochratoxin A, which forms an active G-quadruplex [Reproduced by permission of the Royal Society of Chemistry (Lee et al. 2014)]

are effective in the presence of the target that, upon binding, alters the secondary and tertiary RNA structure by interacting only with a short fraction of the total RNA sequence, called the aptamer sequence (Suess 2010).

This approach has been widely used for the detection of ochratoxin A (Lee et al. 2014), ATP (Xu et al. 2011) and thrombin (Yuan et al. 2011). For thrombin, nanoparticles functionalized both by the aptamer sequence and guanine-rich sequences (Yuan et al. 2012) were used in the transduction scheme. Immobilization of a first sequence of anti-thrombin aptamer on an electrode permits the creation of an aptamer/thrombin complex revealed by the addition of the nanoparticles. In the presence of hemin substrate (NADH) and a redox mediator (thionine), the catalytic activity of the many hemins carried by the nanoparticle allows efficient electrochemical detection of the enzymatic product and therefore thus to reach a sensitivity threshold of ca. 0.15 pM. This approach leads to very sensitive target detection, but has several limitations rarely mentioned. The first is the low affinity constant for hemin/aptamère complex formation (above 10^5 Travascio et al. 1998), suggesting a high kinetic dissociation rate that can affect detection. The second concerns the non-zero catalytic activity of non-bonded hemin (free in solution) that gives, in some cases, a strong non-specific response and therefore contributes significantly to the degradation of detection limits. Beyond these aspects, which need to be quantified for each given system, the peroxidise mimicking approach is widely used in more sophisticated transduction principles presented in the following section.

4.1.2 Target Recycling

The amplification of target nucleic acid sequence approaches (PCR, LAMP, etc.) obviously cannot be applied in the case of aptamers as the target is not a nucleotide sequence. However, many detection strategies are based on the use of enzymes to selectively dissociate the aptamer/target complex while releasing an active marker

(redox group, fluorophore, etc), leading to the release of the target to perform a new cycle (complexation/release). For example, the use of a shorter sequence, functionalized at one end by a quantum dot (QD) and the other by a quencher, shows no fluorescence (FRET between the quencher and the QD, Freeman et al. 2012). In the presence of the target (VEGF) and the addition of a short template sequence, the aptamer conformation switches to a G-quartet structure in the presence of the target, activating one of the sequence positions towards exonuclease. Sequence digestion with exonuclease releases both the quencher, leading to an intense fluorescence emission, and also the target, which may then bind again (Fig. 7). At each cycles, fluorescence increases. The same principle has been used for the detection of ATP (Liu et al. 2012).

This idea to couple target recycling and a marker activation has recently been described using a graphene oxide (GO) surface (Lu et al. 2010). In this scheme, a nucleic acid containing a capture sequence (aptamer) and a detection sequence is first immobilized on the surface through weak interactions with GO. In this form, the fluorescence of the label graft at one end of the sequence is quenched. In the presence of target, the aptamer is released from the surface to bind to the target. The sequence is then accessible to exonuclease, which frees both the target and the fluorophore by digestion. At each cycle, the fluorophore concentration in solution increases and hence also florescence emission. This principle has been described for a pseudo-homogeneous format by substituting the GO surface with carbon nanoparticles (Lin et al. 2014). This approach improves the detection limit by ca. two orders of magnitude for the detection of ATP (40 nM for GO and 0.2 nM for C nanoparticles).

Variant detection schemes using polymerases have shown excellent results. The principle is based on target recognition making available a primer polymerase that by its action extends the single-strand sequence in the direction of the target binding pocket and thus leads to its release (Tan et al. 2014; Peng et al. 2014; Cheng et al. 2012). To facilitate release, a Bst polymerase is sometimes used. Liu et al. proposed a detection scheme based on an exonuclease capable of digesting

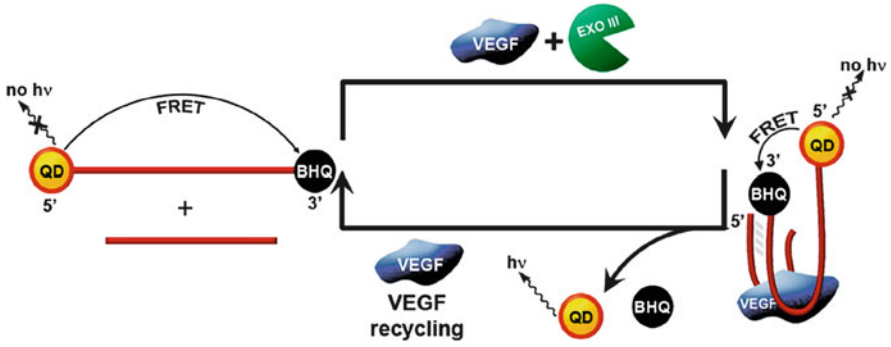

Fig. 7 FRET analysis of VEGF165 by CdSe/ZnS QDs modified with the anti-VEGF aptamer [Reprinted with permission from Freeman et al. (2012). American Chemical Society]

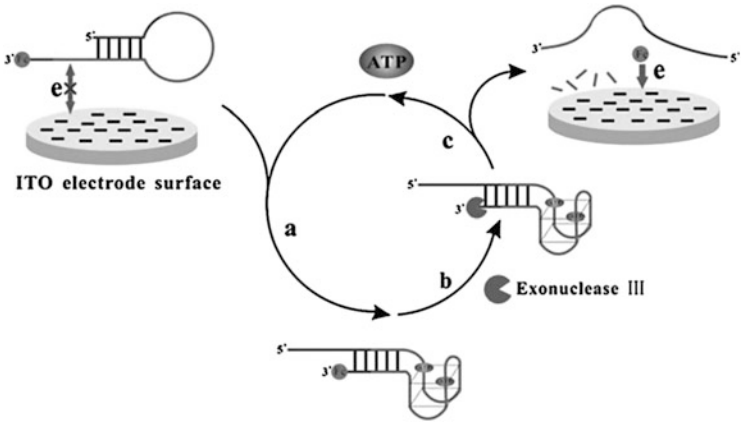

Fig. 8 Principle of the Exo III-aided ATP recycling strategy and its associated homogeneous electrochemical detection [Reproduced by permission of the Royal Society of Chemistry (Liu et al. 2013)]

a ferrocene-terminated aptamer only when the latter forms a complex with its target, here ATP (Liu et al. 2013). The enzymatic activity releases the redox probe. The difference in diffusion coefficient of free ferrocene and ferrocene grafted to the DNA allows to correlate the current value to the amount of target and thereby achieve a sensitivity threshold of 1 nM for ATP (Fig. 8).

4.1.3 Logic Gate Inspired: Strand Displacement Amplification (HCR, EDC, HCA)

The general principle of accessibility of a nucleotide sequence only after target binding can be associated with strategies developed in a DNA circuit, such as strand displacement amplification (SDA) approaches. The idea remains the design of a nucleotide sequence comprising an aptamer portion (capture) and an input portion that triggers construction of a supramolecular DNA structure (DNA detection/amplification). This principle has been successfully implemented using the CHA (Zheng et al. 2012a), EDC (Cheng et al. 2014a, b; Li et al. 2013), and HCR (Zheng et al. 2014; Zhang et al. 2013; Zhao et al. 2013b; Song et al. 2012; Yuan et al. 2013) strategies.

The most studied target is undoubtedly thrombin. Thanks to the identical target and corresponding aptamer sequence, it is possible to compare detection limits achieved depending on the chosen approach (Table 1).

Strand extension by HCR leads to more effective sensing characteristics than by CHA, an advantage already highlighted in the context of nucleic acid detection (Jung and Ellington 2014). Exceptional LODs of 3 (Zhao et al. 2013b) and 80 fM (Yuan et al. 2013) are obtained by using, in addition to HCR, enzyme-modified

Table 1 LOD for thrombin detection as a function of the SDA strategy

SDA	Transduction	LOD	References
CHA	Fluorescence	20 pM	Zheng et al. (2012b)
HCR	SERS	18 pM	Zheng et al. (2014)
HCR	Electrochemical	2 pM	Zhang et al. (2013)
HCR	Electrochemical	80 fM	Yuan et al. (2013)
HCR	Electroluminescence	3 fM	Zhao et al. (2013b)

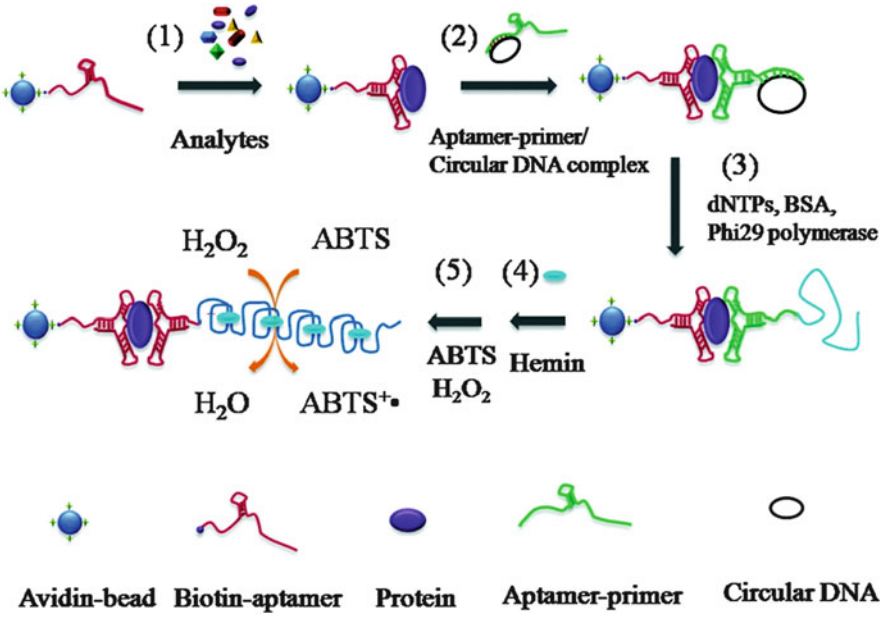

Fig. 9 Schematic representation of the colorimetric assay for protein detection using sandwiched aptamer recognition mechanism and dual signal amplification by RCA and DNAzyme-ABTS reaction: (1) aptamer beads capture the target biomarker in sample solution; (2) the complexes of aptamer-primer/circular DNA templates are subsequently bound to the surface-capture biomarkers on MBs; (3) in the presence of dNTPs and DNA polymerase, *rolling circle* amplification is initiated and generates single-stranded, long, repetitive DNA chains of DNAzyme domains. After incubated with hemin (4), these multiple DNAzyme domains catalysed the oxidation of ABTS, producing a blue-green colorimetric signal, which was used as a transduction reporter (5) [Reprinted with permission from Tang et al. (2012b). American Chemical Society]

complementary sequences of the extended strand that allow further amplification through enzymatic product flow (Fig. 9). The LOD difference between these two examples of ca. one order of magnitude probably comes from transduction mode, i.e. electrochemistry and electroluminescence. In the case of heterogeneous electrochemical detection, it is likely that a significant fraction of product diffuses to the solution and not to the electrode, thereby limiting total amount of detected marker.

4.1.4 Enzyme-Assisted Sensing Amplification

The possibility of using one or more enzymes in the detection scheme provides numerous opportunities for amplification. Very recent studies demonstrate the potential of these approaches for the detection of non-target nucleotide. The use of nicking enzyme alone (Feng et al. 2012; Xue et al. 2014; Zheng et al. 2012b) or in combination with an exonuclease (Xue et al. 2012a) allows to cut a sequence functionalized at each one end by a fluorophore and at the other end by a quencher. The enzyme binding site is located on a complementary strand that hybridizes to the aptamer detection sequence that is only available after target/aptamer complex formation. When the detection sequence is released, fluorophore emission occurs, and another functionalized sequence can hybridize to the aptamer. At each cycle, the fluorescence signal increases (Fig. 10).

This principle may be reproduced identically by directly using the catalytic properties of DNAzymes (Huang et al. 2013, 2014). Target binding triggers a sequence conformation change that allows a short complementary strand to hybridize and to activate the cleavage. The cleavage first induces a release of a short detectable sequence and secondly induces target recycling.

In addition to nucleases, several strategies are based on RCA of a sequence by elongation of a detection sequence that is available only after target binding. Many examples underline the interest to design a sequence containing a detection sequence (RCA padlock formation) available only after target binding on the

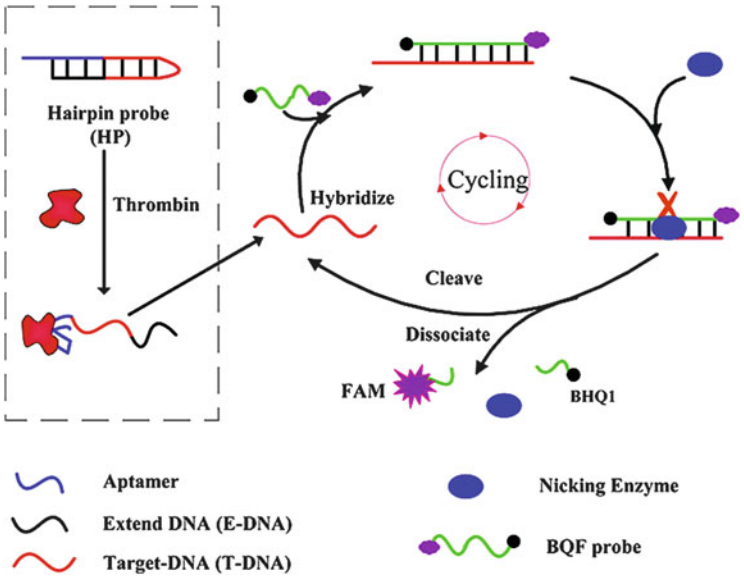

Fig. 10 Schematic representation of homogeneous aptamer and nicking enzyme-assisted fluorescence signal amplification (NEFSA) assay for protein [Reprinted with permission from Xue et al. (2012a) American Chemical Society]

aptamer sequence (Wang et al. 2013a, b; McManus and Li 2013; Cho et al. 2005). In general two strategies have been developed. The first is specific to protein detection for which two aptamers binding to two distinct target domains are known (as in the case for thrombin). In this instance, a first aptamer is immobilized (on a bulk surface or nanoparticle) and the second aptamer contains a cyclic sequence compatible with RCA (Tang et al. 2012). The second approach is more universal and is based on an aptamer conformation change upon target binding that triggers cyclization of the detection sequence and then RCA (Fig. 11). The elongated sequence serves as a support for sensing, either using complementary DNA sequences alone (double-strand intercalators such as methylene blue, Wang et al. 2013b) or fluorophore-labelled ones (Wang et al. 2013b).

The combination of high-affinity aptamers and the HCR method delivers highly sensitive detection limits, e.g. 1.6 fM for the platelet-derived growth factor B chain (fluorophore-labelled detection sequence, Wang et al. 2013b), which is far lower than similar approaches without amplification (electrochemical detection, LOD of ca. 60 pM, Wu et al. 2010). These significant improvements are obtained using linear amplification. The ability to exponentially amplify a nucleotide sequence would permit even lower LODs. This approach is not still developed as such a strategy remains very novel even in the DNA detection field. However, there are some examples that highlight its potential utility. Indeed, LAMP has been coupled to aptamers for detection of ochratoxin A (OChA) using electrochemical detection (Xie et al. 2014). The strategy is based on electrode functionalized by DNA double strands, the anti-OChA aptamer and its immobilized complementary strand. In the presence of the target, a competitive exchange takes place between the complementary strand and the target towards the aptamer. The surfaces are then rinsed and placed in contact with a solution containing the LAMP template in high concentration, which displaces the aptamer already present on the surface and amplifies it. The amount of double-strand DNA present after the amplification cycles is

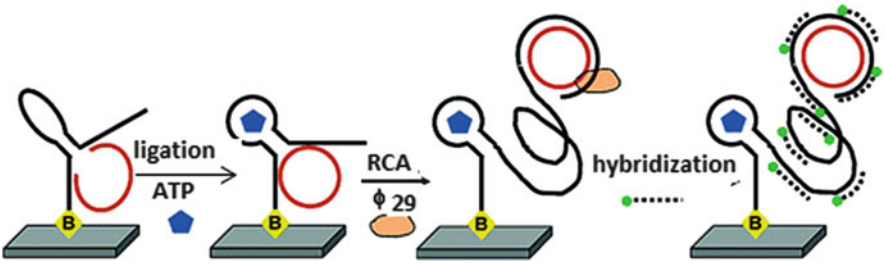

Fig. 11 Deoxyribozyme ligase and substrate. The ligase is shown in *black*; the allosteric, ATP-binding domain is in *black*; and the padlock probe is in *grey*. An *arrow* indicates the ligation junction. (B) Schematic of deoxyribozyme-mediated RCA. The aptazyme labelled with biotin at its 5′ end is immobilized on a streptavidin-coated glass slide. The aptazyme is activated by ATP and ligates a padlock probe. RCA is initiated from the 3′ end of the aptazyme, and the elongated aptazyme is visualized using fluorescent oligonucleotide probes labelled with Cy3 [Reprinted with permission from Cho et al. (2005). American Chemical Society]

probed by using a redox intercalator (methylene blue). The resulting current depends on the amount of unbound MB as an inverse function of double-strand DNA concentration. The number of copies depends on the amount of aptamer remaining on the surface after initial target competitive exchange. Hence, current is an inverse function of the target concentration. This approach has an LOD of 0.3 pM, much better than the best performing alternative strategies based on an electrochemical transduction but using linear amplification (LOD ca. 1 nM, Tong et al. 2012). However, unfortunately transduction is off-type, that is, strong currents are indicative of the absence of target, and has higher probability to generate false positives.

Other exponential amplification strategies such as EXPAR have been combined with aptamer schemes. A very interesting transduction scheme was developed for the detection of lysozyme (Zhang et al. 2012b). In this approach, the target binding causes release of a short sequence initially hybridized to the aptamer. This short sequence is the input for EXPAR. An LOD of 1 fM was obtained, better than other approaches using the same aptamer but combined to linear amplification (LOD 0.52 pM, Zhang et al. 2011). Beyond exceptional LODs obtained using exponential amplification, a large amount of material is produced. This property can be used to develop colorimetric tests suitable for field detection of pathogens, toxins, illicit drugs, etc. (Fig. 12).

The principle is again based on the release of a short sequence initially hybridized to the aptamer and released upon target binding. The released strand serves as an input to the EXPAR, which then exponentially generates *a**/*b** strands. Nanoparticles functionalized by *a* or *b* sequences are added and Au nanoparticle network formation occurs. Plasmon band absorption shifts allowing the sensor response to be seen with the naked eye (appearance of a red colour). The sensitivity of the method is an improvement by four orders of magnitude

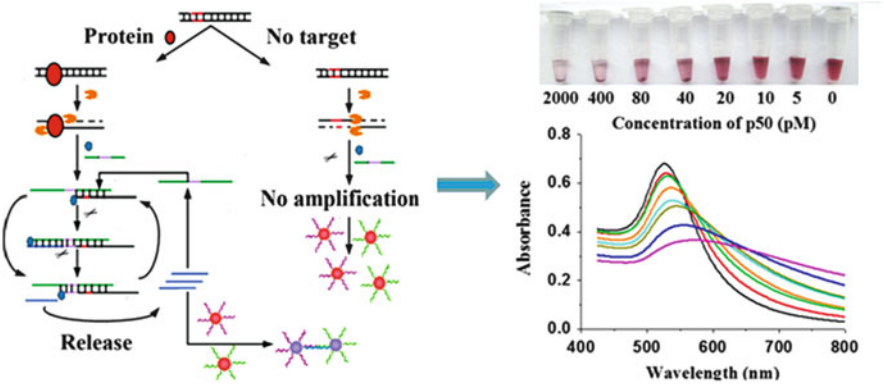

Fig. 12 Schematic illustration of EXPAR-based colorimetric assay for the detection of transcription factors. Reprinted with permission from Zhang et al. (2012b). American Chemical Society

compared to previously published colorimetric tests without amplification and based on luminescence (Ma et al. 2011) or FRET (Heyduk and Heyduk 2002; Wang et al. 2005).

4.2 Chirality and Nucleic Acids

4.2.1 Overview of Use of Aptamers as Chiral Receptors

The chirality of the phosphate backbone is an intrinsic structural property of nucleotides that remains underutilized. The natural state of DNA is the D-enantiomer due to sugar chirality. DNA is readily synthesized as L-enantiomer with conventional technology using L-sugar nucleobases. Early work by Klussmann et al. shows that SELEX can lead to identification of highly enantioselective D-aptamers against an L-target (Klussmann 2006). The strength of the approach is that the L-aptamer recognizes the D-target with equal affinity. SELEX can therefore lead to the production of enantioselective receptors towards each enantiomer of the same target. This ability must be put in the perspective that current analytical approaches developed in the context of enantiomeric excess (e.e.) measurements are mainly separation methods. Chiral stationary phase, mainly composed of oligosaccharides such as cellulose or cyclodextrine are non selective towards the target but efficient to separate L- and D-series species. Aptamers have a double advantage: both selectivity and enantioselectivity that can selectively complex one enantiomer of a unique target, thereby facilitating transduction schemes to analyse enantiomeric mixtures.

Early work using aptamers as chiral selectors is based on affinity chromatography in which the aptamer was grafted onto the stationary phase. McGown et al. were the first to use enantiomers of amino acids (D-tryptophan and D-tyrosine, Kotia et al. 2000), by using affinity electrochromatography (combination of liquid chromatography and capillary electrophoresis). Due to potential for miniaturization, integration and resolution, capillary electrophoresis is a useful separation method for measuring e.e. in combination with aptamers. Indeed, both the low molecular weight of the target compared with that of the aptamer and the fact that the aptamer is charged (polyanion) allow the possibility to discriminate between free and bound target and hence to quantify the enantiomer against which an aptamer has been selected with excellent precision. This was exemplified for the detection of trace D-arginine by Peyrin et al. up to 0.01 % of D-arginine in a mixture of enantiomers (Fig. 13, Ruta et al. 2007). However, capillary electrophoresis has experimental constraints such as high ionic medium, and occasionally the technique is incompatible with the conditions used to conduct SELEX. The need to develop approaches that have wider operating ranges in terms of sample diversity has led to the development of transduction schemes based primarily on aptamer conformational change upon target binding.

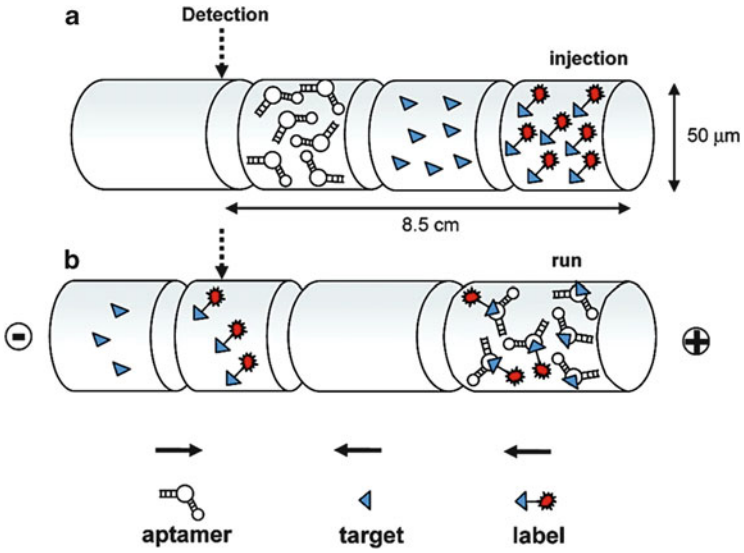

Fig. 13 Principle of the CE-based competitive binding assay using the on-capillary mixing of the different species. *Arrows* indicate the migration direction of the interacting species when the electric field is applied. Reprinted with permission from Ruta et al. (2007). American Chemical Society

4.2.2 Detection Based on Aptamer Conformational Change upon Target Binding

In this respect, one of the most successful approaches is based on fluorescence polarization. A sample containing a fluorophore irradiated with linearly polarized light emits a polarized fluorescence. The degree of fluorescence polarization is quantified by a parameter called fluorescence anisotropy. This measure indicates the degree of freedom of a fluorescent molecule, defined as the ease with which this fluorescent molecule rotates upon itself. If, during a recognition reaction, the fluorophore changes its degrees of freedom, then the change in fluorescence polarization allows to follow and to quantify target binding. It has been reported the use of fluorescence polarization to detect L-tyrosinamide (Ruta et al. 2009). In this work, the anti-(L)-tyrosinamide aptamer was modified at one end by a fluorescein. Upon recognition, the change of aptamer conformation induced an increase in the fluorescence anisotropy. This methodology has also been successfully applied to (L)-argininamide.

4.2.3 Detection Based on Change of Physical Properties upon Target Binding

All these works highlight the strong potential of aptamers to function as chiral receptors. However, detection principles are all based on a significant conformational change of the aptamer upon target binding, which is not always

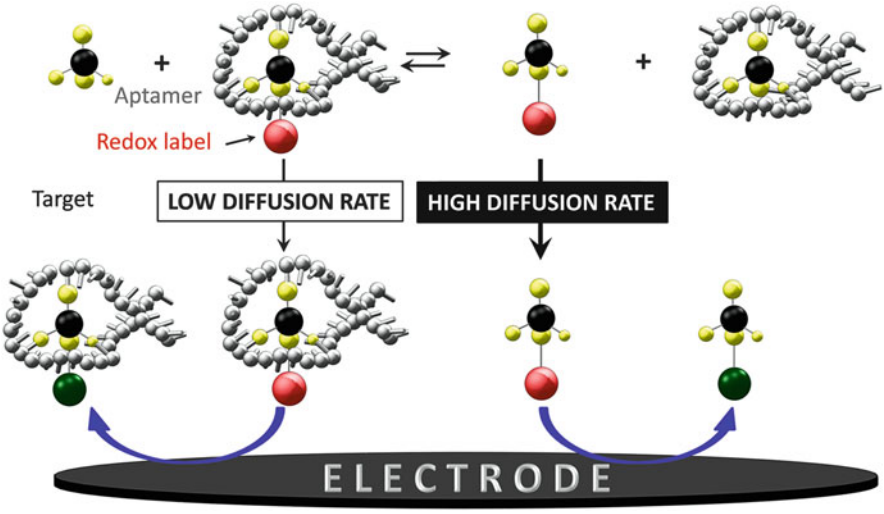

Fig. 14 Enantioselective molecular recognition of trace amounts of L- or D-tyrosinamide [Reprinted with permission from Challier et al. (2012). American Chemical Society]

the case. More recently, a more universal principle was proposed that is applicable to any aptamer/target pair. The principle is to discriminate between the complexed and free fractions of the target on the basis of their transport properties in solution. Indeed, upon binding, the target solution has a molecular weight that artificially increases, decreasing its solution transport characteristics. Such a binding event can then be followed by measuring a current, provided that the target is electroactive. This method has been illustrated using L-tyrosinamide (Challier et al. 2012, 2013), and the principle has been extended to the detection of non-electroactive targets by developing a competitive exchange scheme using a target functionalized with a redox probe (Fig. 14, Moreau et al. 2014). This approach has allowed measurement of e.e. to about 0.1 % in 20 % diluted serum in less than a minute.

At present, although the approach of e.e. measurement using aptamers remains underdeveloped, it is highly likely that this should change substantially taking into account (i) first encouraging results in alternative analytical techniques to chromatography (on a chiral phase) that do not associate target class selectivity to enantioselectivity and (ii) simplicity of aptamer production and selection. This scope would benefit from the use of amplification methods already developed elsewhere and would likely achieve exceptional sensitivities and therefore increased accuracy of e.e. measurement.

5 Conclusion and Outlook

Nucleic acids now play a central role in many analytical devices that address issues beyond DNA detection. Used as markers, they allow the development of high-performance amplification processes but also for accurate identification of any of

the components of a transduction scheme, from antibodies to nanoparticles. These advantages can be combined directly with the molecular recognition properties of aptamers. The majority of examples and approaches are based on the design of sequences containing both a capture portion (aptamer) and a detection portion capable of triggering many processes upon target binding. However, the majority of examples apply a model, an aptamer/target system, for which there is a significant conformational change of the aptamer upon target binding, with the formation of well-identified secondary and tertiary structures (such as hairpin structure, G-quartet, etc.). Much effort is still required to develop more universal patterns that can operate even if the structure of the complex is undetermined or if the conformational change is only minor.

References

Adams M, Jackson SR, Haselton FR et al (2012) Design, synthesis, and characterization of nucleic-acid-functionalized gold surfaces for biomarker detection. Langmuir 28:1068–1082

Akter F, Mie M, Kobatake E (2011) Immuno-rolling circle amplification using a multibinding fusion protein. Anal Biochem 416:174–179

Akter F, Mie M, Grimm S et al (2012) Detection of antigens using a protein−DNA chimera developed by enzymatic covalent bonding with phiX gene A. Anal Chem 84:5040–5046

Campolongo MJ, Tan SJ, Xu J et al (2010) DNA nanomedicine: engineering DNA as a polymer for therapeutic and diagnostic applications. Adv Drug Deliv Rev 62:606–616

Cao C, Dhumpa R, Bang DD et al (2010) Detection of avian influenza virus by fluorescent DNA barcode-based immunoassay with sensitivity comparable to PCR. Analyst 135:337–342

Cao ZJ, Peng QW, Qiu X et al (2011) Highly sensitive chemiluminescence technology for protein detection using aptamer-based rolling circle amplification platform. J Pharm Anal 1:159–165

Challier L, Mavre F, Moreau J et al (2012) Simple and highly enantioselective electrochemical aptamer-based binding assay for trace detection of chiral compounds. Anal Chem 84:5415–5420

Challier L, Miranda-Castro R, Marchal D et al (2013) Kinetic rotating droplet electrochemistry: a simple and versatile method for reaction progress kinetic analysis in microliter volumes. J Am Chem Soc 135:14215–14228

Chang TL, Tsai CY, Sun CC et al (2007) Ultrasensitive electrical detection of protein using nanogap electrodes and nanoparticle-based DNA amplification. Biosens Bioelectron 22:3139–3145

Chen HY, Zhuang HS (2009) Real-time immuno-PCR assay for detecting PCBs in soil samples. Anal Bioanal Chem 394:1205–1211

Cheng W, Yan F, Ding L et al (2010) Cascade signal amplification strategy for subattomolar protein detection by rolling circle amplification and quantum dots tagging. Anal Chem 82:3337–3342

Cheng W, Ding S, Li Q et al (2012) A simple electrochemical aptasensor for ultrasensitive protein detection using cyclic target-induced primer extension. Biosens Bioelectron 36:12–17

Cheng S, Zheng B, Wang M et al (2014a) A target-triggered strand displacement reaction cycle: the design and application in adenosine triphosphate sensing. Anal Biochem 446:69–75

Cheng S, Zheng B, Wang M et al (2014b) Determination of adenosine triphosphate by a target inhibited catalytic cycle based on a strand displacement reaction. Anal Lett 47:478–491

Cho EJ, Yang L, Levy M et al (2005) Using a deoxyribozyme ligase and rolling circle amplification to detect a non-nucleic acid analyte, ATP. J Am Chem Soc 127:2022–2023

Dirks RM, Pierce NA (2004) Triggered amplification by hybridization chain reaction. Proc Natl Acad Sci USA 101:15275–15278
Feng K, Kong R, Wang H et al (2012) A universal amplified strategy for aptasensors: enhancing sensitivity through allostery-triggered enzymatic recycling amplification. Biosens Bioelectron 38:121–125
Fire A, Xu SQ (1995) Rolling replication of short DNA circles. Proc Natl Acad Sci USA 92:4641–4645
Focke F, Haase I, Fischer M (2013) Loop-mediated isothermal amplification (LAMP): methods for plant species identification in food. J Agric Food Chem 61:2943–2949
Freeman R, Girsh J, Jou AF et al (2012) Optical aptasensors for the analysis of the vascular endothelial growth factor (VEGF). Anal Chem 84:6192–6198
Gerasimova YV, Kolpashchikov DM (2014) Enzyme-assisted target recycling (EATR) for nucleic acid detection. Chem Soc Rev 43:6405–6438
Goluch ED, Nam J-M, Georganopoulou DG et al (2006) A bio-barcode assay for on-chip attomolar-sensitivity protein detection. Lab Chip 6:1293–1299
Guo YC, Zhou YF, Zhang XE et al (2006) Phage display mediated immuno-PCR. Nucleic Acids Res 34:e62–e68
Heyduk T, Heyduk E (2002) Molecular beacons for detecting DNA binding proteins. Nat Biotechnol 20:171–176
Hill HD, Mirkin CA (2006) The bio-barcode assay for the detection of protein and nucleic acid targets using DTT-induced ligand exchange. Nat Protoc 1:324–336
Huang Y, Chen J, Zhao S et al (2013) Label-free colorimetric aptasensor based on nicking enzyme assisted signal amplification and DNAzyme amplification for highly sensitive detection of protein. Anal Chem 85:4423–4430
Huang J, He Y, Yang X et al (2014) Split aptazyme-based catalytic molecular beacons for amplified detection of adenosine. Analyst 139:2994–2997
Jiang X, Cheng S, Chen W et al (2012) Comparison of oligonucleotide-labeled antibody probe assays for prostate-specific antigen detection. Anal Biochem 424:1–7
Jung C, Ellington AD (2014) Diagnostic applications of nucleic acid circuits. Acc Chem Res 47:1825–1835
Klussmann S (2006) The aptamer handbook: functional oligonucleotides and their applications. Wiley, Hoboken, NJ
Kotia RB, Li L, McGown LB (2000) Separation of nontarget compounds by DNA aptamers. Anal Chem 72:827–831
Kuczius T, Becker K, Karch H et al (2009) High sensitivity detection of the glial fibrillary acidic protein as indicator for TSE risk material in meat products using an immuno-PCR. Mol Nutr Food Res 53:1329–1335
Lee J, Jeon CH, Ahn SJ et al (2014) Highly stable colorimetric aptamer sensors for detection of ochratoxin A through optimizing the sequence with the covalent conjugation of hemin. Analyst 139:1622–1627
Li Y, Ji X, Song W et al (2013) Design of a sensitive aptasensor based on magnetic microbeads-assisted strand displacement amplification and target recycling. Anal Chim Acta 770:147–152
Lin X, Cui L, Huang Y et al (2014) Carbon nanoparticle-protected aptamers for highly sensitive and selective detection of biomolecules based on nuclease-assisted target recycling signal amplification. Chem Commun 50:7646–7648
Linck L, Reiß E, Bier F et al (2012) Direct labeling rolling circle amplification as a straightforward signal amplification technique for biodetection formats. Anal Methods 4:1215–1220
Liu X, Freeman R, Willner I (2012) Amplified fluorescence aptamer-based sensors using exonuclease III for the regeneration of the analyte. Chem Eur J 18:2207–2211
Liu S, Wang Y, Zhang C et al (2013) Homogeneous electrochemical aptamer-based ATP assay with signal amplification by exonuclease III assisted target recycling. Chem Commun 49:2335–2337

Lu C-H, Li J, Lin M-H et al (2010) Amplified aptamer-based assay through catalytic recycling of the analyte. Angew Chem Int Ed 49:8454–8457
Lu L, Liu B, Zhao Z et al (2012) Ultrasensitive electrochemical immunosensor for HE4 based on rolling circle amplification. Biosens Bioelectron 33:216–221
Ma DL, Xu T, Chan DSH et al (2011) A highly selective, label-free, homogenous luminescent switch-on probe for the detection of nanomolar transcription factor NF-kappaB. Nucleic Acids Res 39:e67–e75
McManus SA, Li Y (2013) Turning a kinase deoxyribozyme into a sensor. J Am Chem Soc 135:7181–7186
Moreau J, Challier L, Lalaoui N et al (2014) Rational design of a redox-labeled chiral target for an enantioselective aptamer-based electrochemical binding assay. Chem Eur J 20:2953–2959
Mullenix MC, Sivakamasundari R, Feaver WJ et al (2002) Rolling circle amplification improves sensitivity in multiplex immunoassays on microspheres. Clin Chem 48:1855–1858
Nam J-M, Park S-J, Mirkin CA (2002) Bio-barcodes based on oligonucleotide-modified nanoparticles. J Am Chem Soc 124:3820–3821
Notomi T, Okayama H, Masubuchi H et al (2000) Loop-mediated isothermal amplification of DNA. Nucleic Acids Res 28:E63
Ou LJ, Liu SJ, Chu X et al (2009) DNA encapsulating liposome based rolling circle amplification immunoassay as a versatile platform for ultrasensitive detection of protein. Anal Chem 81:9664–9673
Pei X, Zhang B, Tang J et al (2013) Sandwich-type immunosensors and immunoassays exploiting nanostructure labels. Anal Chim Acta 758:1–18
Peng Q, Cao Z, Lau C et al (2011) Aptamer-barcode based immunoassay for the instantaneous derivatization chemiluminescence detection of IgE coupled to magnetic beads. Analyst 136:140–147
Peng K, Zhao H, Yuan Y et al (2014) Mediator-free triple-enzyme cascade electrocatalytic aptasensor with exonuclease-assisted target recycling and hybridization chain reaction amplification. Biosens Bioelectron 55:366–371
Pourhassan-Moghaddam M, Rahmati-Yamchi M, Akbarzadeh A et al (2013) Protein detection through different platforms of immuno-loop-mediated isothermal amplification. Nanoscale Res Lett 8:485–496
Qian L, Winfree E, Bruck J (2011) Neural network computation with DNA strand displacement cascades. Nature 475:368–372
Ravan H, Yazdanparast R (2012) Development and evaluation of a loop-mediated isothermal amplification method in conjunction with an enzyme-linked immunosorbent assay for specific detection of Salmonella serogroup D. Anal Chim Acta 733:64–70
Ravan H, Yazdanparast R (2013) Loop region-specific oligonucleotide probes for loop-mediated isothermal amplification-enzyme-linked immunosorbent assay truly minimize the instrument needed for detection process. Anal Biochem 439:102–108
Ruta J, Ravelet C, Baussanne I et al (2007) Aptamer-based enantioselective competitive binding assay for the trace enantiomer detection. Anal Chem 79:4716–4719
Ruta J, Perrier S, Ravelet C et al (2009) Noncompetitive fluorescence polarization aptamer-based assay for small molecule detection. Anal Chem 81:7468–7473
Sano T, Smith CL, Cantor CR (1992) Immuno-PCR: very sensitive antigen detection by means of specific antibody-DNA conjugates. Science 258:120–122
Song W, Zhu K, Cao Z et al (2012) Hybridization chain reaction-based aptameric system for the highly selective and sensitive detection of protein. Analyst 137:1396–1401
Stoeva SI, Lee JS, Smith JE et al (2006) Multiplexed detection of protein cancer markers with biobarcoded nanoparticle probes. J Am Chem Soc 128:8378–8379
Suess B (2010) Riboswitches: new aspects of an old story. RNA Biol 7:65–66
Tan Y, Guo Q, Zhao X et al (2014) Proximity-dependent protein detection based on enzyme-assisted fluorescence signal amplification. Biosens Bioelectron 51:255–260

Tang J, Hou L, Tang D et al (2012a) Hemin/G-quadruplex-based DNAzyme concatamers as electrocatalysts and biolabels for amplified electrochemical immunosensing of IgG1w. Chem Commun 48:8180–8182
Tang L, Liu Y, Ali MM et al (2012b) Colorimetric and ultrasensitive bioassay based on a dual-amplification system using aptamer and DNAzyme. Anal Chem 84:4711–4717
Tong P, Zhao WW, Zhang L et al (2012) Double-probe signal enhancing strategy for toxin aptasensing based on rolling circle amplification. Biosens Bioelectron 33:146–151
Travascio P, Lia Y, Sen D (1998) DNA-enhanced peroxidase activity of a DNA-aptamer-hemin complex. Chem Biol 5:505–517
Van Ness J, Van Ness LK, Galas DJ (2003) Isothermal reactions for the amplification of oligonucleotides. Proc Natl Acad Sci USA 100:4504–4509
Wang JK, Li TX, Guo XY et al (2005) Exonuclease III protection assay with FRET probe for detecting DNA-binding proteins. Nucleic Acids Res 33:e23
Wang F, Freage L, Ron Orbach R et al (2013a) Autonomous replication of nucleic acids by polymerization/nicking enzyme/DNAzyme cascades for the amplified detection of DNA and the aptamer−Cocaine Complex. Anal Chem 85:8196–8203
Wang Q, Zheng H, Gao X et al (2013b) A label-free ultrasensitive electrochemical aptameric recognition system for protein assay based on hyperbranched rolling circle amplification. Chem Commun 49:11418–11420
Wang F, Lu C-H, Willner I (2014) From cascaded catalytic nucleic acids to enzyme-DNA nanostructures: controlling reactivity, sensing, logic operations, and assembly of complex structures. Chem Rev 114:2881–2941
Willner I, Shlyahovsky B, Zayats M et al (2008) DNAzymes for sensing, nanobiotechnology and logic gate applications. Chem Soc Rev 37:1153–1165
Wu ZS, Zhou H, Zhang SB et al (2010) Electrochemical aptameric recognition system for a sensitive protein assay based on specific target binding-induced rolling circle amplification. Anal Chem 82:2282–2289
Xie S, Chai Y, Yuan Y et al (2014) Development of an electrochemical method for Ochratoxin A detection based on aptamer and loop-mediated isothermal amplification. Biosens Bioelectron 55:324–329
Xu J, Cai LL, Kong DM et al (2011) General sensor design strategy based on G-quadruplex-hemin DNAzymes. Anal Lett 44:2582–2592
Xue L, Zhou X, Xing D (2012a) Sensitive and homogeneous protein detection based on target-triggered aptamer hairpin switch and nicking enzyme assisted fluorescence signal amplification. Anal Chem 84:3507–3513
Xue Q, Wang L, Jiang W (2012b) A versatile platform for highly sensitive detection of protein: DNA enriching magnetic nanoparticles based rolling circle amplification immunoassay. Chem Commun 33:3897–4020
Xue Q, Wang Z, Wang L et al (2012c) Sensitive detection of proteins using assembled cascade fluorescent DNA nanotags based on rolling circle amplification. Bioconjug Chem 23:734–739
Xue Q, Zhang G, Wang L et al (2014) Aptamer-based exonuclease protection and enzymatic recycling cleavage amplification homogeneous assay for the highly sensitive detection of thrombin. Analyst 139:3167–3173
Yan J, Su S, He S et al (2012) Nano rolling-circle amplification for enhanced SERS hot spots in protein microarray analysis. Anal Chem 84:9139–9145
Yan L, Zhou J, Zheng Y et al (2014) Isothermal amplified detection of DNA and RNA. Mol BioSyst 10:970–1003
Yang L, Fung CW, Cho EJ et al (2007) Real-time rolling circle amplification for protein detection. Anal Chem 79:3320–3329
Yin P, Choi HMT, Calvert CR et al (2008) Programming biomolecular self-assembly pathways. Nature 451:318–322
Yin H-Q, Jia M-X, Shi L-J et al (2011) Nanoparticle-based bio-barcode assay for the detection of bluetongue virus. J Virol Methods 178:225–228

Yuan Y, Gou X, Yuana R et al (2011) Electrochemical aptasensor based on the dual-amplification of G-quadruplex horseradish peroxidase-mimicking DNAzyme and blocking reagent-horseradish peroxidase. Biosens Bioelectron 26:4236–4240

Yuan Y, Yuan R, Chai Y et al (2012) Hemin/G-quadruplex simultaneously acts as NADH oxidase and HRP-mimicking DNAzyme for simple, sensitive pseudobienzyme electrochemical detection of thrombin. Chem Commun 48:4621–4623

Yuan Y, Chai Y, Yuan R et al (2013) An ultrasensitive electrochemical aptasensor with autonomous assembly of hemin-G-quadruplex DNAzyme nanowires for pseudo triple-enzyme cascade electrocatalytic amplification. Chem Commun 49:7328–7330

Zhang DY, Turberfield AJ, Yurk B et al (2007a) Engineering entropy-driven reactions and networks catalyzed by DNA. Science 5883:1121–1125

Zhang D, Carr DJ, Alocilja EC (2009) Fluorescent bio-barcode DNA assay for the detection of Salmonella enterica serovar Enteritidis. Biosens Bioelectron 24:1377–1381

Zhang L, Ren J, Pan K et al (2010) Detection of gastric carcinoma-associated MG7-Ag by serum immuno-PCR assay in a high-risk Chinese population, with implication for screening. Int J Cancer 126:469–473

Zhang H, Fang C, Zhang S (2011) Ultrasensitive electrochemical analysis of two analytes by using an autonomous DNA machine that works in a two-cycle mode. Chem Eur J 17:7531–7537

Zhang B, Liu B, Tang D et al (2012a) DNA-based hybridization chain reaction for amplified bioelectronic signal and ultrasensitive detection of proteins. Anal Chem 84:5392–5399

Zhang Y, Hu J, Zhang C-Y (2012b) Sensitive detection of transcription factors by isothermal exponential amplification-based colorimetric assay. Anal Chem 84:9544–9549

Zhang J, Chai Y, Yuan R et al (2013) A novel electrochemical aptasensor for thrombin detection based on the hybridization chain reaction with hemin/G-quadruplex DNAzyme-signal amplification. Analyst 138:4558–4564

Zhao B, Yan J, Wang D et al (2013a) Carbon nanotubes multifunctionalized by rolling circle amplification and their application for highly sensitive detection of cancer markers. Small 15:2595–2601

Zhao M, Zhuo Y, Chai Y et al (2013b) Dual signal amplification strategy for the fabrication of an ultrasensitive electrochemiluminescence aptasensor. Analyst 138:6639–6644

Zheng AX, Wang JR, Li J et al (2012a) Enzyme-free fluorescence aptasensor for amplification detection of human thrombin via target-catalyzed hairpin assembly. Biosens Bioelectron 36:217–221

Zheng AX, Wang JR, Li J et al (2012b) Nicking enzyme based homogeneous aptasensors for amplification detection of protein. Chem Commun 48:374–376

Zheng J, Hu Y, Bai J et al (2014) Universal surface-enhanced Raman scattering amplification detector for ultrasensitive detection of multiple target analytes. Anal Chem 86:2205–2212

Zhou L, Ou LJ, Chu X et al (2007) Aptamer-based rolling circle amplification: a platform for electrochemical detection of protein. Anal Chem 79:7492–7500

Zhou J, Zhuang J, Tang J et al (2013) Dual-nanogold-linked bio-barcodes with superstructures for in situ amplified electronic detection of low-abundance proteins. Mol BioSyst 9:622–625

Zhou W, Gong X, Xiang Y et al (2014) Target-triggered quadratic amplification for label-free and sensitive visual detection of cytokines based on hairpin aptamer DNAzyme probes. Anal Chem 86:953–958

Zhuang HS, Zhou C (2009) Determination of anthracene by real-time immune-polymerase chain reaction assay. Anal Chim Acta 633:278–282

Aptamers in Oncotherapy

Darija Muharemagic and Maxim V. Berezovski

Contents

Abstract The ability of oligonucleotide aptamers to bind with high affinity and specificity, as well as their ease of production, has made them great candidates for their use as potential drugs, probes, or delivery agents. In this chapter, we will cover three novel biological applications incorporating the use of aptamers in therapeutics. First, we will discuss the most recent advancements in the use of these short oligonucleotides for targeted delivery of small molecules and biomolecules, such as drugs and microRNAs, in order to achieve tumor suppression. The second focus will be on the use of aptamers to image specific types of cells when coupled with nanoparticles, allowing in vivo detection of tumors, while bypassing the issue of aptamer degradation. Finally, we will discuss the use of aptamers that act upon infectious agents, either to eliminate those that are malignant or to protect the useful ones. Oncolytic viruses are such useful infectious agents and form an emerging cancer treatment featuring tumor-specific replication, leading to cell lysis. One of the biggest setbacks for this type of therapy is viral clearance by neutralizing antibodies. Aptamers can be turned into tools for protecting oncolytic viruses from the immune system and to assist higher specificity in targeting cancerous cells.

D. Muharemagic • M.V. Berezovski (✉)
Department of Chemistry, University of Ottawa, Ottawa, Canada
e-mail: maxim.berezovski@uottawa.ca

V.A. Erdmann et al. (eds.), *RNA and DNA Diagnostics*, RNA Technologies,
DOI 10.1007/978-3-319-17305-4_5

Keywords Aptamers • Targeted delivery • Nanoparticles • Oncolytic viruses • Bacteriostatic aptamers • Nanostructures

1 Introduction

Aptamers are short single-stranded DNA or RNA oligonucleotides[1] selected for their binding to specific targets. They are evolved from a diverse library, consisting of approximately 10^{15} single-stranded oligonucleotides with random sequences, and can be selected to bind to a wide range of targets, such as small molecules (McKeague and Derosa 2012), proteins (Zhang et al. 2006), bacteria (Maeng et al. 2012), and viruses (Labib et al. 2012b). Development of aptamers follows the simple principle of evolution of a desired trait (binding to a target in this case) by applying a selective pressure against those that do not possess this trait. Regardless of the specific technique employed, aptamer selection relies on the presence of a large number of DNA or RNA molecules from which those binding a target are enriched by removal of the molecules that do not bind. Aptamers' complex tertiary structures allow them to bind with high affinity and specificity, which makes them ideal candidates for many purposes and use in various fields, including therapeutics.

To date, pegaptanib (Macugen) is the only aptamer drug commercially available, which is obtained from a modified RNA inhibitor to vascular endothelial growth factor and is used for the treatment of age-related macular degeneration (Group et al. 2006). Nevertheless, pegaptanib is not the only success story for targeting this disease; E10030 and ARC1905 also reached clinical trials, Phase I and III, respectively. Aptamers for other targets and treatments are also undergoing clinical tests. Among them is an aptamer used for the treatment of von Willebrand's disease, a bleeding disorder. It works by binding to the von Willebrand factor in blood and thus induces an antithrombotic effect. An interesting feature of this effect is that it can be reversed, simply by adding a complementary sequence oligonucleotide (Cosmi 2009). Other conditions that have the potential of being treated by these oligonucleotides include carcinomas (Bates et al. 2009), diabetes (Ninichuk et al. 2008), and hemophilia (Waters et al. 2011).

[1] Polypeptides form another class of aptamers whose selection and propagation differs greatly from oligonucleotide aptamers. In this chapter, we will only consider the latter class of aptamers.

2 Aptamers as Delivery Vehicles

2.1 Drug Delivery by DNA Nanostructures

Advancements in computational chemistry have enabled us to predict oligonucleotides' unique secondary and tertiary structures, based on their primary sequences, and to control the folding of DNA and RNA molecules. Therefore, they can be self-assembled in solution with precise architecture and high efficiency. Many researchers have taken advantage of these properties to make an array of different structures, also known as DNA origami, ranging from rectangular, triangular, and circular shapes to smiley faces (Fig. 1) (Aldaye and Sleiman 2007; Rothemund 2006). Several works have also demonstrated that compact three-dimensional nucleic acids are more readily internalized within cells (Hamblin et al. 2012). Charoenphol et al. targeted a well-characterized DNA-based nanostructure that self-assembles into a pyramidal cage using AS1411, an aptamer that binds to a

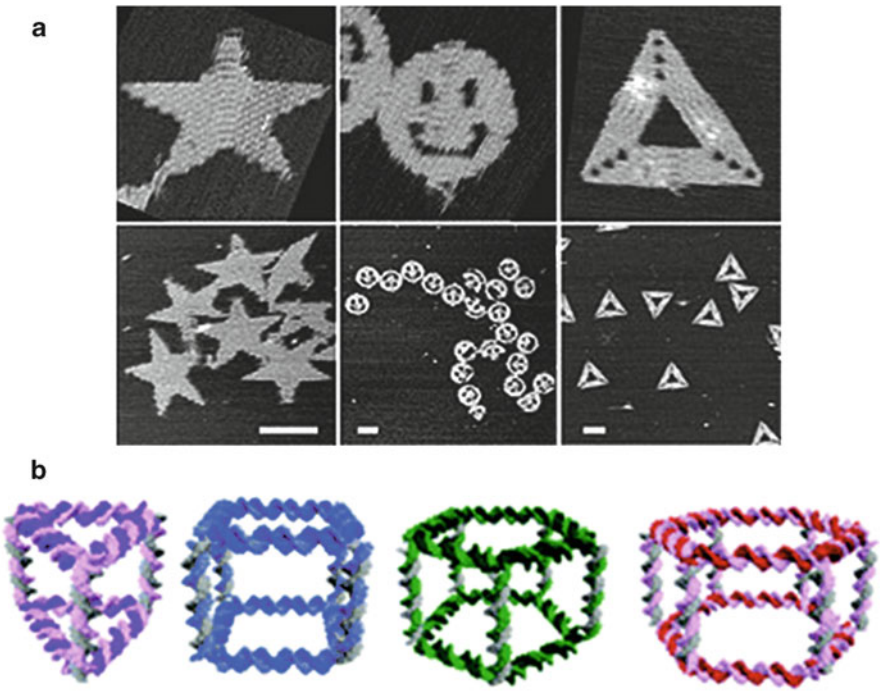

Fig. 1 (**a**) Atomic force microscopy images depicting the design and self-assembly of DNA molecules into different shapes; scale bar 100 nm. Adapted from Macmillan Publishers Ltd.: Nature (Rothemund 2006), copyright 2006. (**b**) Schematic depicting a triangular prism, a cube, pentameric and hexameric prism structures, and their building blocks presented in different colors. Adapted from the American Chemical Society: Journal of the American Chemical Society (Aldaye and Sleiman 2007), copyright 2007

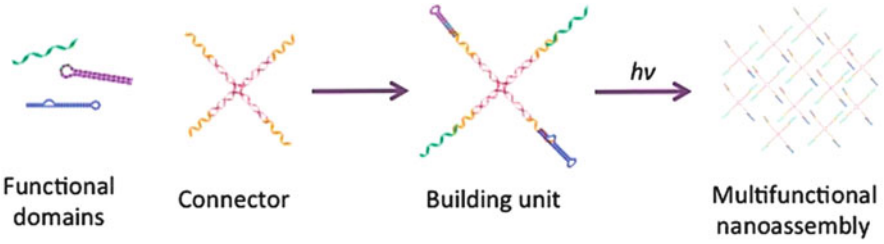

Fig. 2 A schematic of a multifunctional self-assembled nanostructure consisting of functional groups, such as aptamers or antisense oligonucleotides, a connector, and building units. Once assembled, these are photo-cross-linked into a nano-assembly structure

glycoprotein upregulated in several cancer types (Soundararajan et al. 2009). Their experiments showed that uptake of the pyramidal structure was increased when the aptamer was incorporated, suggesting that the uptake was mediated by the aptamer-cell-specific interaction (Charoenphol and Bermudez 2014).

The major benefit of these designs is that different molecular loads can be incorporated and entrapped inside, such as small drugs (Edwardson et al. 2013), proteins (Juul et al. 2013), and nanoparticles (Lau et al. 2014). Furthermore, in order to allow a controlled release of the carried load, aptamers have recently been combined with these structures. Wu et al. demonstrated the concept of these multifunctional molecules by building a nucleic acid nano-assembly, consisting of "connectors" and "building units". Each building unit has three functional groups, targeting aptamers, intercalated doxorubicin, a DNA intercalating anticancer drug, and therapeutic antisense oligonucleotides (Fig. 2). When added to the cells, they observed cytotoxicity, selective for CCRF-CEM cancer cells recognized by the aptamer incorporated inside the construct (Wu et al. 2013).

In order to design a 3D DNA-based structure, researchers have to rely on Watson-Crick base pairing to anneal small building blocks. However, the Tan group has proposed an alternative. They were able to obtain spherical structures, termed nanoflowers (NFs), which are generated from long nucleic acid strands and self-assemble through liquid crystallization (Fig. 3). These strands are formed by rolling circle amplification (RCA), a unidirectional replication of oligonucleotides, where a template and primers are used to make concatemeric DNA, containing multiple copies of the same sequence (Fire and Xu 1995). Furthermore, during the RCA, chemically modified deoxynucleotides were incorporated to obtain multicolored nucleic acids, which facilitated the tracking of these molecules when bound to target cells. Nanoflower structures offer a number of advantages as delivery vehicles: their size is tunable by amplifying different lengths of DNA strands; compacted moieties present a reduced amount of potential nick sites, making these oligonucleotides less susceptible to nuclease degradation (Zhu et al. 2013); and cancer cell-specific aptamers can be seamlessly integrated into the sequence of these long concatemers (Zhao et al. 2012). The efficacy of this technique was tested through delivery of doxorubicin-treated nanoflowers to

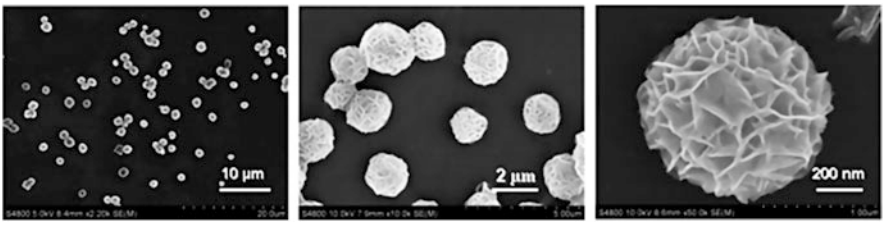

Fig. 3 Scanning electron microscopy images of DNA nanoflowers obtained from rolling circle amplification (RCA). Reproduced from John Wiley and Sons: Angewandte Chemie International Edition (Hu et al. 2014), copyright 2014

different cancer cell types; only cells targeted by the incorporated aptamers exhibited dose-dependent cytotoxicity (Hu et al. 2014).

2.2 Aptamer-siRNA Chimera

Short interfering RNA (siRNA) and microRNA (miRNA) have recently been found to be important gene regulators of most eukaryotic lineages, including fungi, plants, and animals. RNA molecules regulate gene expression through multiple routes, including guided cleavage of mRNA, inhibition of protein translation, or chromatin modifications (Katiyar-Agarwal et al. 2006). This inhibitory function of RNA interference (RNAi) has a tremendous potential in therapeutics, as it allows us to control cellular protein expression. However, when exogenous siRNA is administered, it needs to be uptaken by the desired cells, avoid those cells' endosome, and become incorporated into their RNA-induced silencing complex (RISC); here lie the biggest setbacks of RNAi therapeutics (Perkel 2009). The Rossi group has extensively characterized Dicer substrate interfering RNA (DsiRNA), demonstrating that this type of RNA is more efficient than classical 21-mer siRNAs. It appears that these longer DsiRNA molecules are more readily processed by Dicer into the conventional siRNA or miRNA, which enhances their subsequent association with and activation of RISC (Amarzguioui and Rossi 2008).

The Giangrande group was the first to report successful use of covalent aptamer-siRNA chimera for cell-type-specific delivery in 2006 (McNamara et al. 2006). For this purpose, they used an aptamer developed to bind the prostate-specific membrane antigen (PSMA). This aptamer was linked to the sense strand of a 21-mer siRNA (Fig. 4a), which targets polo-like kinase 1 (PLK1) and B-cell lymphoma 2 (BCL2), two survival genes overexpressed in most tumors. Application of this construct, with a double-stranded siRNA part, both in vitro and with intratumoral administration, resulted in decreased proliferation and increased apoptosis of cells expressing PSMA (McNamara et al. 2006). Several other aptamer-siRNA chimeras ensued using a similar approach (Wullner et al. 2008; Zhou et al. 2008, 2009).

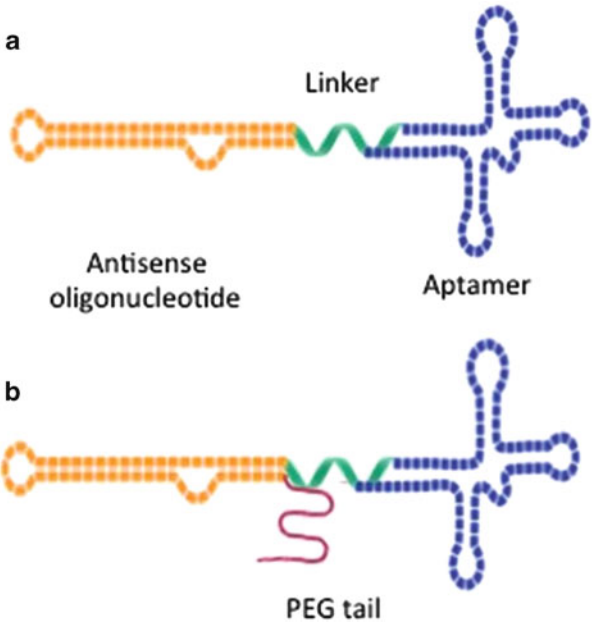

Fig. 4 A general schematic of (**a**) an aptamer-siRNA/aptamer-miRNA chimera linked by an oligonucleotide linker; (**b**) a modified version of the chimera including a 20 kDa polyethylene glycol (PEG) tail

One of the biggest setbacks for nucleic acid therapy is the susceptibility of DNA and RNA to the abundance of nucleases in bodily fluids and thus their short half-lives in the blood. Therefore, Giangrande and colleagues set out to improve their previously developed chimera in order to make it applicable for systemic administration. To this end, 3 years later, the group modified their chimera in a variety of ways, including shortening the aptamer to make its large-scale synthesis more affordable, addition of a 20 kDa polyethylene glycol (PEG) moiety (Fig. 4b) to increase the half-life of the construct from less than 35 min to more than 30 h, and, finally, alteration of the siRNA duplex to favor RISC processing of the correct siRNA guide strand. When injected intraperitoneally, the new generation of the construct was tolerated better and showed less toxicity (Dassie et al. 2009).

Unlike siRNAs, which target and inhibit one specific gene, miRNAs have the ability to produce a more global effect on many different genes. Recently, the de Franciscis group has shown, for the first time, the efficacy of in vivo delivery of miRNA-aptamer chimera (Esposito et al. 2014). For this proof-of-principle study, they used the GL21.T aptamer as a delivery carrier, previously selected and characterized in their laboratory (Cerchia et al. 2012). This aptamer has been found to inhibit Axl tyrosine kinase activity and to interfere with target cell growth and motility (Cerchia et al. 2012; Li et al. 2009). The let-7g miRNA, an inhibitor of high-mobility group AT-hook 2 (HMGA2) (Lee and Dutta 2007) and N-Ras, was used as the gene-silencing part of the chimera (Johnson et al. 2005). When conjugated together, the addition of GL21.T-let construct to Axl-positive cells resulted in a more pronounced silencing of let-7g targets. Finally, for the in vivo evaluation of the conjugate effect, Esposito et al. used immunodeficient mice

bearing Axl-positive and Axl-negative tumors. When treated with a single intravenous injection of GL21.T-let, they observed an increase of let-7g miRNA in Axl-positive cells only, followed by a significant reduction in the targeted tumors after a 2-week administration of the treatment. Therefore, these two studies have shown that aptamers can be used for a safe and targeted delivery of RNAi in vitro and in vivo.

2.3 Nanoparticle-Aptamer Conjugates for Drug Delivery

Nanomaterials became widely used due to their ease of synthesis, as well as their easily tunable size. However, because of their lack of specificity, they often need to be conjugated with other agents that will make their delivery more efficient. A number of research groups have investigated coupling aptamers with such nanomaterials as liposomes (Kim et al. 2011; Willis et al. 1998), micelles (Miyamoto et al. 2007; Wu et al. 2010), single-walled carbon nanotubes (Guo et al. 2011; So et al. 2008), and quantum dots (Kang et al. 2009; Zhang and Johnson 2009) for a number of applications, including detection of small molecules, drug delivery to cells, or imaging of cancer cells. Gold nanoparticles (AuNPs), in particular, have shown great promise for many applications due to their ease of synthesis and stability.

A promising area of aptamer-AuNP conjugates is in the detection of early circulating tumor cells (CTCs). CTCs are cells that have detached from a primary tumor and are circulating in the bloodstream. It has been recognized, as early as in the nineteenth century, that CTCs are responsible for cancer metastasis and the formation of multiple tumors in a single host (Ashworth 1869; Wong 2012). Recently, there has been an emergence of several instruments designed to detect these cells; the period from the detachment of the cells before the tumor metastasis is of utmost importance. The majority of these platforms rely on the capture of CTCs based on their biomarkers or their morphology. For instance, the only currently FDA-approved platform is the CellSearch Assay, which uses antibody-coated magnetic particles to isolate these CTCs. However, the capture efficiency of this assay is not optimal, and many circulating cancer cells go undetected. Therefore, there is a need for an instrument that possesses high specificity and a low limit of detection that will be able to identify these rare circulating cells (Kling 2012).

The Fan research group proposed a technique for detection and isolation of these circulating tumor cells by combining, for the first time, the technology of gold nanoparticles (AuNPs) and aptamers (Fig. 5). The use of these particles allowed them to attach up to 95 aptamers onto each AuNP, which greatly increased their binding affinity to cancer cells. Moreover, they employed a herringbone groove-based micromixer device to achieve a capture efficiency of more than 90 % by processing 1 ml of whole blood, with samples containing as little as 100 cells. This proof-of-principle research opened the door for others to combine nanoparticles and aptamers for the isolation of CTCs (Sheng et al. 2013).

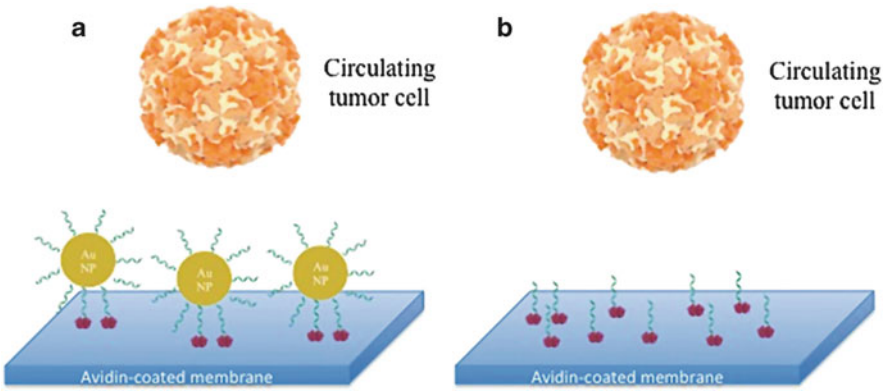

Fig. 5 A schematic of circulating tumor cells (CTCs) captured using a combination of gold nanoparticles (AuNPs) and aptamers in a microfluidic device. (**a**) The use of AuNPs allowed a higher capture efficiency of CTCs when compared to (**b**) the use of aptamer alone

2.4 Nanoparticles for Tumor Imaging

Another important application for nanoparticles is cellular or tissue imaging. For this purpose, many different types of nanoparticles have been used, including silica (Wu et al. 2008), carbon (Fang et al. 2012), and gold (Liu et al. 2013). More recently, superparamagnetic iron oxide nanoparticles (SPIONs) have attracted interest since they can improve the visualization of different tissues in magnetic resonance imaging (MRI), a noninvasive method for three-dimensional imaging of tissues (Wang et al. 2001). SPIONs, in particular, offer several advantages over other contrast agents that can be used for MRI, including lower toxicity and a lower limit of detection (Jalalian et al. 2013). Aptamer coupling to paramagnetic iron nanoparticles was first reported by the Lu group in 2007 and 2008, where they used anti-adenosine and antithrombin aptamers in order to construct cross-linked dextran-coated superparamagnetic iron oxide nanoparticle (CLIO) contrast agents and detect their binding counterparts (Yigit et al. 2007, 2008). Following these proof-of-principle experiments, several other groups have used similar constructs (Fig. 6) to visualize specific tissues, including different types of cancer cells (Jalalian et al. 2013; Kanwar et al. 2011; Yu et al. 2011).

In 2014, You et al. demonstrated the utility of ultrasmall superparamagnetic iron oxide nanoparticles (USPIOs) cross-linked with aptamers targeting vascular endothelial growth factor 165 (VEGF165). The specificity of this magnetic contrast agent was shown by an enzyme-linked immunosorbent assay (ELISA), comparing its binding to VEGF165 versus VEGF121. The USPIO-aptamer conjugated nanoparticle accumulated in the liver tumors of xenografted mice models upon intravenous injection. This enhancement in the delivery of the USPIO to the tumor site augmented imaging contrast and increased the magnetic signal enhancement effect (You et al. 2014). These nanoparticle-aptamer constructs improve imaging of

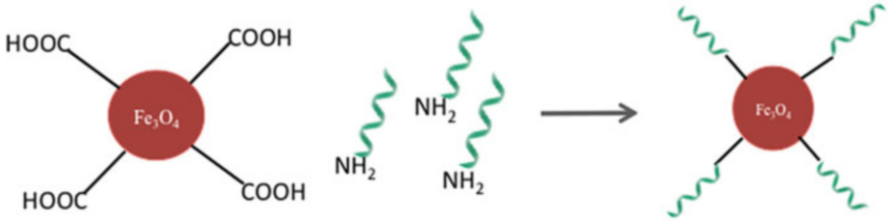

Fig. 6 The general scheme of one of the methods used for the preparation of superparamagnetic iron oxide nanoparticles cross-linked to aptamers. The carboxyl groups of nanoparticles are activated with 1-ethyl-3-(3-dimethylaminopropyl)carbodiimide (EDC) and N-hydroxysuccinimide (NHS) in order to react with a target-specific aptamer

tumors in vivo as they encompass several criteria that define a potent MRI probe, such as high selectivity and affinity, high permeability, as well as low immunogenicity.

3 Aptamers for Infectious Agents

3.1 Inhibition of Infectious Agents

Other than binding their respective targets, aptamers can have other properties, such as modifying the target's function. Viruses are a diverse type of infectious agents, with more than 2,400 identified viral species. Their DNA or RNA genomes are usually packaged in a protein shell, which also carries them to the host organism. Once the host is infected, the virus produces its ubiquitous progeny, leaving the host tissue damaged (Russell and Peng 2007). To date, aptamers have been selected for an array of different viruses, including human immunodeficiency virus (HIV) (D'Atri et al. 2012), rabies virus (Liang et al. 2013), hepatitis C (Shi et al. 2014), and ebola (Binning et al. 2013). Several of these aptamers bind to viruses and prevent their attachment to the cellular membrane, thus inhibiting their infectivity. Jeon et al. have reported one such example where the selected aptamer was able to block the binding of influenza virus to target cell receptors. The binding inhibition was observed in vitro in tissue cultures, where cells treated with the aptamer survived in the presence of the virus. Moreover, intranasal administration of this aptamer treatment in mice resulted in decreased weight loss, as well as a lower amount of virus in their lungs (Jeon et al. 2004).

Furthermore, similar to antibodies, high specificity and affinity of aptamers make them ideal candidates for their use in detection systems. This method has been applied to various types of bacterial pathogens, such as *Escherichia coli* (Bruno et al. 2010), *Staphylococci* (Cao et al. 2009), and *Salmonella* (Yang et al. 2013), for their detection in foods and the environment. Moreover, the Zamay group, in collaboration with our research team, has demonstrated that

aptamers originally developed for the detection of two *Salmonella* species possessed a bacteriostatic effect, paving the way for an excitingly new application of aptamer technology. The aptamers inhibited the formation of bacterial colonies by depolarizing the bacterial membrane (Kolovskaya et al. 2013).

3.2 Oncolytic Viruses

The interest in oncolytic viruses emerged in the 1950s due to their attractive ability to propagate and selectively destroy tumor tissue without having detrimental consequences for normal noncancerous cells (Parato et al. 2005). In 2011, the Bell lab reported the clinical trial results of JX-594, an oncolytic virus developed from a Wyeth strain derived from a poxvirus. Phase I trials, involving 23 patients, consisted of intratumoral injection of JX-594 into liver tumors, which was well tolerated and able to replicate in cancer tissue while not affecting normal cells (Breitbach et al. 2011). However, viral therapy does present some setbacks, as the injected virus can be inactivated inside the host by complement proteins (Ikeda et al. 1999; Wakimoto et al. 2002), reticuloendothelial system (Worgall et al. 1997; Ye et al. 2000), or neutralizing antibodies (nAbs) (Chen et al. 2000; Hirasawa et al. 2003; Lang et al. 2006). Several different approaches have been undertaken in order to deliver the virus more efficiently and evade its clearance. These include the use of immunosuppressive drugs (Kottke et al. 2009), coating of the virus with polymers to evade nAbs (Fisher et al. 2001; Morrison et al. 2008; O'Riordan et al. 1999), and the use of pre-infected T cells or carrier cells that act as delivery vehicles and shielding agents (Coukos et al. 1999; Garcia-Castro et al. 2005; Mader et al. 2009; Power et al. 2007).

Our lab has developed a technology called aptamer-facilitated virus protection (AptaVIP) (Muharemagic et al. 2014). It is based on two types of DNA aptamers: blocking and shielding aptamers (Fig. 7A). Blocking aptamers bind to antigen-binding fragments (Fab) of nAbs and prevent neutralization of a virus (Muharemagic et al. 2012); shielding aptamers bind to the virus and mask it from recognition by nAbs allowing the virus to attach to and infect cancer cells (Labib et al. 2012a). We used DNA aptamers with different affinities to vesicular stomatitis virus (VSV, an oncolytic virus), or to anti-VSV antibodies, selected by two modified SELEX procedures. Analysis of the aptamers with flow cytometry and biosensors demonstrated their ability to prevent nAbs from binding to the virus. This shielding was also shown in vitro using cancer cells; virus-specific antibodies that were incubated with aptamers were not able to bind and completely neutralize the virus (Fig. 7B). We clearly demonstrated that combining these two different types of aptamers resulted in increased shielding and protection of the virus, enabling it to avoid nAbs and infect the cells even in their presence. Moreover, modifying these aptamers in order to obtain multimeric oligonucleotides (dimers and tetramers) caused the highest viral infectivity. The multimers also decreased VSV degradation and agglomeration, which in turn increased the number of

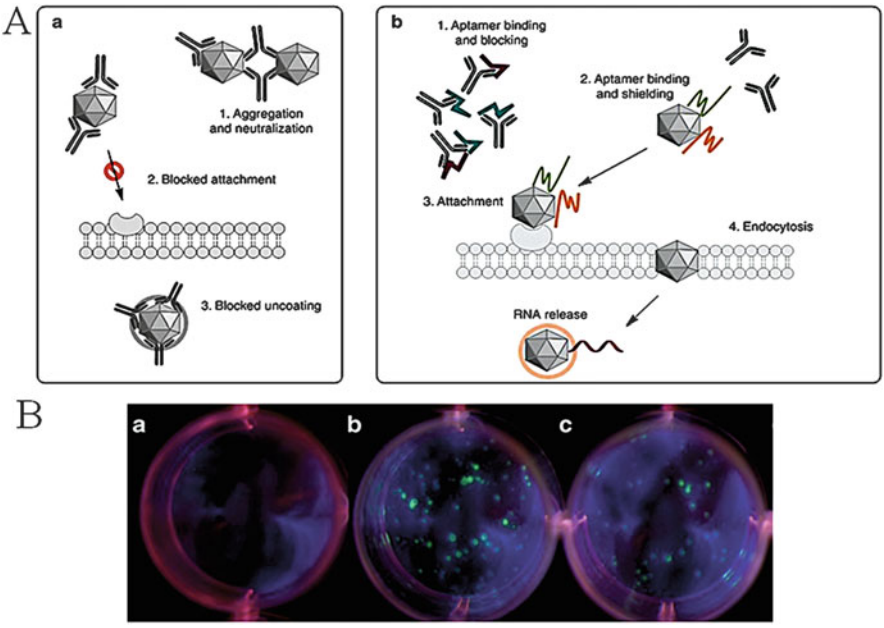

Fig. 7 (**A**) A general schematic of viral clearance and aptamer-facilitated protection of oncolytic viruses from neutralizing antibodies and (**B**) cell-based viral infectivity assay showing cells infected with VSV (a) with nAbs (0 % infectivity), (b) without nAbs (100 % infectivity), and (c) with nAbs and anti-VSV and anti-nAb aptamer pools (61 % infectivity). Adapted from Macmillan Publishers Ltd.: Molecular Therapy – Nucleic Acids (Muharemagic et al. 2014), 2014 freely available under the terms of the Creative Commons Attributions License

individual viral particles. These experiments demonstrated a novel method for protecting oncolytic viruses in order to ensure their more effective delivery in vivo while avoiding antibody neutralization.

4 Conclusion

Aptamers are a relatively new and emerging class of molecules that have the potential to be used for a number of applications. Here, we covered the use of aptamers as delivery vehicles in order to obtain a targeted delivery of therapeutics. Moreover, aptamers can be used in combination with infectious agents, either to prevent their spread or enhance it, as was the case with oncolytic viruses. As clinical trials are currently underway, their outcome will determine the future of aptamers for therapeutical purpose.

References

Aldaye FA, Sleiman HF (2007) Modular access to structurally switchable 3D discrete DNA assemblies. J Am Chem Soc 129:13376–13377

Amarzguioui M, Rossi JJ (2008) Principles of Dicer substrate (D-siRNA) design and function. Methods Mol Biol 442:3–10

Ashworth TR (1869) A case of cancer in which cells similar to those in the tumors were seen in the blood after death. Aust Med J 12:3

Bates PJ, Laber DA, Miller DM et al (2009) Discovery and development of the G-rich oligonucleotide AS1411 as a novel treatment for cancer. Exp Mol Pathol 86:151–164

Binning JM, Wang T, Luthra P et al (2013) Development of RNA aptamers targeting Ebola virus VP35. Biochemistry 52:8406–8419

Breitbach CJ, Burke J, Jonker D et al (2011) Intravenous delivery of a multi-mechanistic cancer-targeted oncolytic poxvirus in humans. Nature 477:99–102

Bruno JG, Carrillo MP, Phillips T et al (2010) A novel screening method for competitive FRET-aptamers applied to E. coli assay development. J Fluoresc 20:1211–1223

Cao X, Li S, Chen L et al (2009) Combining use of a panel of ssDNA aptamers in the detection of *Staphylococcus aureus*. Nucleic Acids Res 37:4621–4628

Cerchia L, Esposito CL, Camorani S et al (2012) Targeting Axl with an high-affinity inhibitory aptamer. Mol Ther 20:2291–2303

Charoenphol P, Bermudez H (2014) Aptamer-targeted DNA nanostructures for therapeutic delivery. Mol Pharm 11:1721–1725

Chen Y, Yu DC, Charlton D et al (2000) Pre-existent adenovirus antibody inhibits systemic toxicity and antitumor activity of CN706 in the nude mouse LNCaP xenograft model: implications and proposals for human therapy. Hum Gene Ther 11:1553–1567

Cosmi B (2009) ARC-1779, a PEGylated aptamer antagonist of von Willebrand factor for potential use as an anticoagulant or antithrombotic agent. Curr Opin Mol Ther 11:322–328

Coukos G, Makrigiannakis A, Kang EH et al (1999) Use of carrier cells to deliver a replication-selective herpes simplex virus-1 mutant for the intraperitoneal therapy of epithelial ovarian cancer. Clin Cancer Res 5:1523–1537

D'Atri V, Oliviero G, Amato J et al (2012) New anti-HIV aptamers based on tetra-end-linked DNA G-quadruplexes: effect of the base sequence on anti-HIV activity. Chem Commun (Camb) 48:9516–9518

Dassie JP, Liu XY, Thomas GS et al (2009) Systemic administration of optimized aptamer-siRNA chimeras promotes regression of PSMA-expressing tumors. Nat Biotechnol 27:839–849

Edwardson TG, Carneiro KM, McLaughlin CK et al (2013) Site-specific positioning of dendritic alkyl chains on DNA cages enables their geometry-dependent self-assembly. Nat Chem 5:868–875

Esposito CL, Cerchia L, Catuogno S et al (2014) Multifunctional aptamer-miRNA conjugates for targeted cancer therapy. Mol Ther 22:1151–1163

Fang Y, Guo S, Li D et al (2012) Easy synthesis and imaging applications of cross-linked green fluorescent hollow carbon nanoparticles. ACS Nano 6:400–409

Fire A, Xu SQ (1995) Rolling replication of short DNA circles. Proc Natl Acad Sci USA 92:4641–4645

Fisher KD, Stallwood Y, Green NK et al (2001) Polymer-coated adenovirus permits efficient retargeting and evades neutralising antibodies. Gene Ther 8:341–348

Garcia-Castro J, Martinez-Palacio J, Lillo R et al (2005) Tumor cells as cellular vehicles to deliver gene therapies to metastatic tumors. Cancer Gene Ther 12:341–349

Group VISiONCT, D'Amico DJ, Masonson HN, Patel M et al (2006) Pegaptanib sodium for neovascular age-related macular degeneration: two-year safety results of the two prospective, multicenter, controlled clinical trials. Ophthalmology 113(992–1001):e6

Guo Z, Ren J, Wang J et al (2011) Single-walled carbon nanotubes based quenching of free FAM-aptamer for selective determination of ochratoxin A. Talanta 85:2517–2521

Hamblin GD, Carneiro KM, Fakhoury JF et al (2012) Rolling circle amplification-templated DNA nanotubes show increased stability and cell penetration ability. J Am Chem Soc 134:2888–2891
Hirasawa K, Nishikawa SG, Norman KL et al (2003) Systemic reovirus therapy of metastatic cancer in immune-competent mice. Cancer Res 63:348–353
Hu R, Zhang X, Zhao Z et al (2014) DNA nanoflowers for multiplexed cellular imaging and traceable targeted drug delivery. Angew Chem 53:5821–5826
Ikeda K, Ichikawa T, Wakimoto H et al (1999) Oncolytic virus therapy of multiple tumors in the brain requires suppression of innate and elicited antiviral responses. Nat Med 5:881–887
Jalalian SH, Taghdisi SM, Shahidi Hamedani N et al (2013) Epirubicin loaded super paramagnetic iron oxide nanoparticle-aptamer bioconjugate for combined colon cancer therapy and imaging in vivo. Eur J Pharm Sci 50:191–197
Jeon SH, Kayhan B, Ben-Yedidia T et al (2004) A DNA aptamer prevents influenza infection by blocking the receptor binding region of the viral hemagglutinin. J Biol Chem 279:48410–48419
Johnson SM, Grosshans H, Shingara J et al (2005) RAS is regulated by the let-7 microRNA family. Cell 120:635–647
Juul S, Iacovelli F, Falconi M et al (2013) Temperature-controlled encapsulation and release of an active enzyme in the cavity of a self-assembled DNA nanocage. ACS Nano 7:9724–9734
Kang WJ, Chae JR, Cho YL et al (2009) Multiplex imaging of single tumor cells using quantum-dot-conjugated aptamers. Small 5:2519–2522
Kanwar JR, Roy K, Kanwar RK (2011) Chimeric aptamers in cancer cell-targeted drug delivery. Crit Rev Biochem Mol Biol 46:459–477
Katiyar-Agarwal S, Morgan R, Dahlbeck D et al (2006) A pathogen-inducible endogenous siRNA in plant immunity. Proc Natl Acad Sci USA 103:18002–18007
Kim YS, Niazi JH, Chae YJ et al (2011) Aptamers-in-liposomes for selective and multiplexed capture of small organic compounds. Macromol Rapid Commun 32:1169–1173
Kling J (2012) Beyond counting tumor cells. Nat Biotechnol 30:578–580
Kolovskaya OS, Savitskaya AG, Zamay TN et al (2013) Development of bacteriostatic DNA aptamers for *Salmonella*. J Med Chem 56:1564–1572
Kottke T, Pulido J, Thompson J et al (2009) Antitumor immunity can be uncoupled from autoimmunity following heat shock protein 70-mediated inflammatory killing of normal pancreas. Cancer Res 69:7767–7774
Labib M, Zamay AS, Muharemagic D et al (2012a) Electrochemical sensing of aptamer-facilitated virus immunoshielding. Anal Chem 84:1677–1686
Labib M, Zamay AS, Muharemagic D et al (2012b) Electrochemical differentiation of epitope-specific aptamers. Anal Chem 84:2548–2556
Lang SI, Giese NA, Rommelaere J et al (2006) Humoral immune responses against minute virus of mice vectors. J Gene Med 8:1141–1150
Lau KL, Hamblin GD, Sleiman HF (2014) Gold nanoparticle 3D-DNA building blocks: high purity preparation and use for modular access to nanoparticle assemblies. Small 10:660–666
Lee YS, Dutta A (2007) The tumor suppressor microRNA let-7 represses the HMGA2 oncogene. Genes Dev 21:1025–1030
Li Y, Ye X, Tan C et al (2009) Axl as a potential therapeutic target in cancer: role of Axl in tumor growth, metastasis and angiogenesis. Oncogene 28:3442–3455
Liang HR, Liu Q, Zheng XX et al (2013) Aptamers targeting rabies virus-infected cells inhibit viral replication both in vitro and in vivo. Virus Res 173:398–403
Liu H, Xu Y, Wen S et al (2013) Targeted tumor computed tomography imaging using low-generation dendrimer-stabilized gold nanoparticles. Chemistry 19:6409–6416
Mader EK, Maeyama Y, Lin Y et al (2009) Mesenchymal stem cell carriers protect oncolytic measles viruses from antibody neutralization in an orthotopic ovarian cancer therapy model. Clin Cancer Res 15:7246–7255

Maeng JS, Kim N, Kim CT et al (2012) Rapid detection of food pathogens using RNA aptamers-immobilized slide. J Nanosci Nanotechnol 12:5138–5142
McKeague M, Derosa MC (2012) Challenges and opportunities for small molecule aptamer development. J Nucleic Acids 2012:748913
McNamara JO II, Andrechek ER, Wang Y et al (2006) Cell type-specific delivery of siRNAs with aptamer-siRNA chimeras. Nat Biotechnol 24:1005–1015
Miyamoto D, Tang Z, Takarada T et al (2007) Turbidimetric detection of ATP using polymeric micelles and DNA aptamers. Chem Commun (Camb) 45:4743–4745
Morrison J, Briggs SS, Green N et al (2008) Virotherapy of ovarian cancer with polymer-cloaked adenovirus retargeted to the epidermal growth factor receptor. Mol Ther 16:244–251
Muharemagic D, Labib M, Ghobadloo SM et al (2012) Anti-Fab aptamers for shielding virus from neutralizing antibodies. J Am Chem Soc 134:17168–17177
Muharemagic D, Zamay A, Ghobadloo SM et al (2014) Aptamer-facilitated protection of oncolytic virus from neutralizing antibodies. Mol Ther Nucleic Acids 3:e167
Ninichuk V, Clauss S, Kulkarni O et al (2008) Late onset of Ccl2 blockade with the Spiegelmer mNOX-E36-3′PEG prevents glomerulosclerosis and improves glomerular filtration rate in db/db mice. Am J Pathol 172:628–637
O'Riordan CR, Lachapelle A, Delgado C et al (1999) PEGylation of adenovirus with retention of infectivity and protection from neutralizing antibody in vitro and in vivo. Hum Gene Ther 10:1349–1358
Parato KA, Senger D, Forsyth PA et al (2005) Recent progress in the battle between oncolytic viruses and tumours. Nat Rev Cancer 5:965–976
Perkel JM (2009) RNAi therapeutics: a two-year update. Science 326:3
Power AT, Wang J, Falls TJ et al (2007) Carrier cell-based delivery of an oncolytic virus circumvents antiviral immunity. Mol Ther 15:123–130
Rothemund PW (2006) Folding DNA to create nanoscale shapes and patterns. Nature 440:297–302
Russell SJ, Peng KW (2007) Viruses as anticancer drugs. Trends Pharmacol Sci 28:326–333
Sheng W, Chen T, Tan W et al (2013) Multivalent DNA nanospheres for enhanced capture of cancer cells in microfluidic devices. ACS Nano 7:7067–7076
Shi S, Yu X, Gao Y et al (2014) Inhibition of hepatitis C virus production by aptamers against the core protein. J Virol 88:1990–1999
So HM, Park DW, Jeon EK et al (2008) Detection and titer estimation of *Escherichia coli* using aptamer-functionalized single-walled carbon-nanotube field-effect transistors. Small 4:197–201
Soundararajan S, Wang L, Sridharan V et al (2009) Plasma membrane nucleolin is a receptor for the anticancer aptamer AS1411 in MV4-11 leukemia cells. Mol Pharmacol 76:984–991
Wakimoto H, Ikeda K, Abe T et al (2002) The complement response against an oncolytic virus is species-specific in its activation pathways. Mol Ther 5:275–282
Wang YX, Hussain SM, Krestin GP (2001) Superparamagnetic iron oxide contrast agents: physicochemical characteristics and applications in MR imaging. Eur Radiol 11:2319–2331
Waters EK, Genga RM, Schwartz MC et al (2011) Aptamer ARC19499 mediates a procoagulant hemostatic effect by inhibiting tissue factor pathway inhibitor. Blood 117:5514–5522
Willis MC, Collins BD, Zhang T et al (1998) Liposome-anchored vascular endothelial growth factor aptamers. Bioconjug Chem 9:573–582
Wong MP (2012) Circulating tumor cells as lung cancer biomarkers. J Thorac Dis 4:631–634
Worgall S, Wolff G, Falck-Pedersen E et al (1997) Innate immune mechanisms dominate elimination of adenoviral vectors following in vivo administration. Hum Gene Ther 8:37–44
Wu P, He X, Wang K et al (2008) Imaging breast cancer cells and tissues using peptide-labeled fluorescent silica nanoparticles. J Nanosci Nanotechnol 8:2483–2487
Wu Y, Sefah K, Liu H et al (2010) DNA aptamer-micelle as an efficient detection/delivery vehicle toward cancer cells. Proc Natl Acad Sci USA 107:5–10

Wu C, Han D, Chen T et al (2013) Building a multifunctional aptamer-based DNA nanoassembly for targeted cancer therapy. J Am Chem Soc 135:18644–18650

Wullner U, Neef I, Eller A et al (2008) Cell-specific induction of apoptosis by rationally designed bivalent aptamer-siRNA transcripts silencing eukaryotic elongation factor 2. Curr Cancer Drug Targets 8:554–565

Yang M, Peng Z, Ning Y et al (2013) Highly specific and cost-efficient detection of *Salmonella* Paratyphi A combining aptamers with single-walled carbon nanotubes. Sensors 13:6865–6881

Ye X, Jerebtsova M, Ray PE (2000) Liver bypass significantly increases the transduction efficiency of recombinant adenoviral vectors in the lung, intestine, and kidney. Hum Gene Ther 11:621–627

Yigit MV, Mazumdar D, Kim HK et al (2007) Smart "turn-on" magnetic resonance contrast agents based on aptamer-functionalized superparamagnetic iron oxide nanoparticles. Chembiochem 8:1675–1678

Yigit MV, Mazumdar D, Lu Y (2008) MRI detection of thrombin with aptamer functionalized superparamagnetic iron oxide nanoparticles. Bioconjug Chem 19:412–417

You XG, Tu R, Peng ML et al (2014) Molecular magnetic resonance probe targeting VEGF165: preparation and in vitro and in vivo evaluation. Contrast Media Mol Imaging 9:349–354

Yu MK, Kim D, Lee IH et al (2011) Image-guided prostate cancer therapy using aptamer-functionalized thermally cross-linked superparamagnetic iron oxide nanoparticles. Small 7:2241–2249

Zhang CY, Johnson LW (2009) Single quantum-dot-based aptameric nanosensor for cocaine. Anal Chem 81:3051–3055

Zhang H, Wang Z, Li XF et al (2006) Ultrasensitive detection of proteins by amplification of affinity aptamers. Angew Chem Int Ed Engl 45:1576–1580

Zhao W, Cui CH, Bose S et al (2012) Bioinspired multivalent DNA network for capture and release of cells. Proc Natl Acad Sci USA 109:19626–19631

Zhou J, Li H, Li S et al (2008) Novel dual inhibitory function aptamer-siRNA delivery system for HIV-1 therapy. Mol Ther 16:1481–1489

Zhou J, Swiderski P, Li H et al (2009) Selection, characterization and application of new RNA HIV gp 120 aptamers for facile delivery of Dicer substrate siRNAs into HIV infected cells. Nucleic Acids Res 37:3094–3109

Zhu G, Hu R, Zhao Z et al (2013) Noncanonical self-assembly of multifunctional DNA nanoflowers for biomedical applications. J Am Chem Soc 135:16438–16445

Genotyping of Single Nucleotide Polymorphisms

Tian Ye, Ran Tong, and Zhiqiang Gao

Contents

Abstract Single nucleotide polymorphisms (SNPs) are the most abundant DNA variations in human genome. Numerous reports have indicated that SNPs are closely associated with diseases such as cardiovascular diseases, different types of cancer, and other genetic diseases. As such, SNPs are currently considered as potentially important cancer biomarkers that may significantly improve cancer diagnosis and prognosis, aid drug development, and offer personalized treatments for cancer patients. The importance of SNPs, especially on the genetic diseases, has urged researchers to develop SNP detection methods for their sensitive and accurate identification in the presence of excessive wild-type (WT) genes. Unlike other DNA assays, the intrinsically subtle difference between WT and mutant genes—a single-base variation—makes it a challenging task to specifically detect low abundant SNPs out of large amounts of coexisting WT genes. To date, many methods have been proposed for SNP detection, and they can be classified into two categories—allele-specific hybridization methods and allele-specific enzymatic methods. A thorough review of the state-of-the-art detection technologies for SNPs will be helpful to researchers in the development of more efficient SNP genotyping technologies. In this article, recent advances in the detection and genotyping of SNPs are summarized, and emerging techniques for SNP genotyping are assessed.

T. Ye • R. Tong • Z. Gao (✉)
Department of Chemistry, National University of Singapore, Singapore 117543, Singapore
e-mail: chmgaoz@nus.edu.sg

V.A. Erdmann et al. (eds.), *RNA and DNA Diagnostics*, RNA Technologies,
DOI 10.1007/978-3-319-17305-4_6

Keywords Single nucleotide polymorphisms • Deoxyribonucleic acid • Biomarkers • Molecular diagnostics • Cancer

1 Introduction

Human Genome Project successfully sequenced the whole human genome of some volunteers (Collins et al. 2003; Venter et al. 2001). During sequencing, a large number of single nucleotide polymorphisms (SNPs) were discovered together with other types of variations (Sachidanandam et al. 2001). Among all kinds of DNA variations, SNPs have the largest amount (Durbin et al. 2010). SNPs are defined as single base pair positions where variable sequences are available (Brookes 1999). The frequency of the variation was estimated to be at least 1 % of the whole allele frequency. The existence of SNPs inspired further projects on the determination of SNPs throughout the whole genome, of which the HapMap and 1,000 Genomes Project are representatives (Frazer et al. 2007; Siva 2008). The 1,000 Genomes Project successfully detected 1.5 million SNPs within populations of human beings, and the phase II of the HapMap project characterized 3.1 million SNPs. By the construction of databases, the data are accessible through the Internet, of which the representative databases are National Center for Biotechnology Information (Pruitt et al. 2005), HapMap (Thorisson et al. 2005), and The Human Genome Variation Database (HGVbase) (Fredman et al. 2004).

The importance of SNPs has many aspects, especially on the pathogenic genetic diseases. It is proved that SNPs are related to diseases such as cardiovascular diseases, different kinds of cancer, and other genetic diseases (Pecoits-Filho et al. 2003; Paynter et al. 2009; Wallace et al. 2008; Onay et al. 2006; Dumur et al. 2003; Tuupanen et al. 2009; Zacharova et al. 2005). The discovery of the relationship between typical SNPs and diseases triggered the improvement of SNP genotyping method. Ideal SNP detection and genotyping should have the following features: rapid and robust sequencing, high automation, promising accuracy, low cost, and so on (Kwok 2001). Based on the knowledge of genotyping, mainly two categories of SNP assays are developed, which are allele-specific hybridization method and allele-specific enzymatic method (Syvanen 2001). Allele-specific enzymatic method is further divided into three branches, namely, the technology based on ligation, primer extension, and enzymatic cleavage (Myakishev et al. 2001; Chen et al. 1998; Nollau and Wagener 1997). In this article, the two categories of SNP genotyping methods are reviewed with typical examples listed in each method, followed by a brief summary.

2 Genotyping of Single Nucleotide Polymorphisms

2.1 Allele-Specific Enzymatic Ligation-Based Genotyping of Single Nucleotide Polymorphisms

The application of ligase to SNP genotyping was first introduced more than 25 years ago (Landegren et al. 1988), after which the importance of enzymatic reaction to SNP detection was gradually noticed by other researchers. The principle of the assay lies in the ligation of two adjacent oligonucleotides which are connected at or near the site of SNPs. After a 30-year development, the ligation-based SNP discrimination has well characterized, and many methods are developed based on different amplification methods, such as polymerase chain reaction (PCR), ligase chain reaction (LCR), and rolling circle amplification (RCA), all of which can significantly increase the sensitivity and accuracy of the results (Lizardi et al. 1998; Wee et al. 2012; Duan et al. 2009). Some ligation-based methods are introduced in the following two sections.

2.1.1 Magnetic Bead-Based Genotyping of Single Nucleotide Polymorphisms

In allele-specific ligation detection, the application of magnetic beads can effectively minimize the noise generated by unreacted reagents, which can further increase the detection power of the assay (Fig. 1) (Shin et al. 2014). By applying such an idea, a multiplexed SNP genotyping method utilizing universal amplification of separated ligation-dependent probes was developed—amplified sequence length polymorphism (ASLP) assay (Shin et al. 2014). Ligation of allele-specific probes, wild-type allele-specific oligonucleotides (ASOW) and mutant allele-specific oligonucleotides (ASOM) with locus-specific probe (LSO) was executed first by DNA ligase, the separation probes, functionalized with biotin, were extended using the ligation product as templates. The double-stranded DNA formed in the previous steps was separated by streptavidin-coated magnetic beads, which were further amplified by PCR, introduced to microarray, and detected. By such an assay, 15 SNPs were discriminated simultaneously.

Another method of separating reacted and unreacted probes by magnetic beads can be achieved by the incorporation of ultrasmall magnetic nanoparticles into oligonucleotides, leveraged on the size-dependent magnetic properties of ferrofluidic nanoparticle probes (FNPs) in ligation reaction to detect SNPs

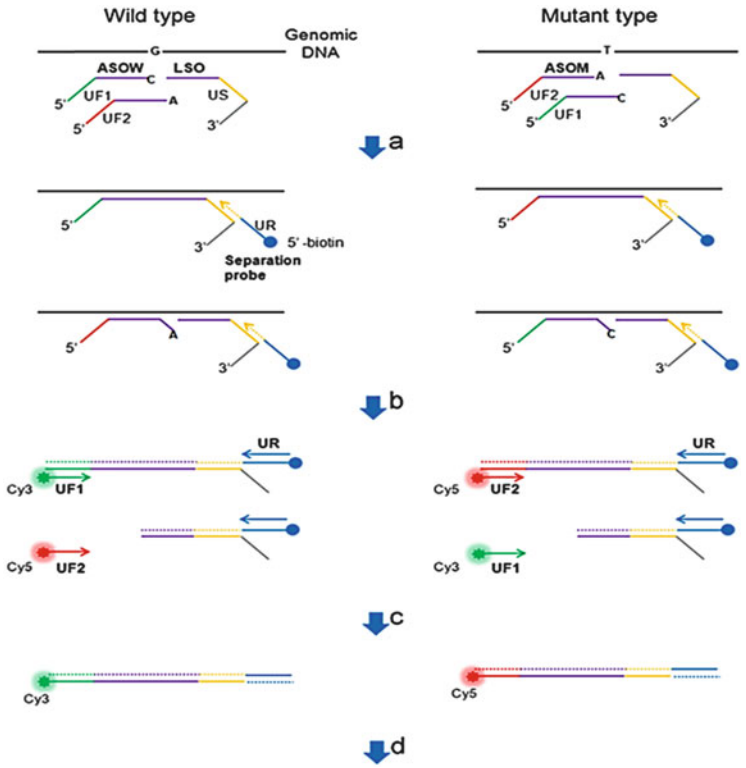

Fig. 1 ASLP technology for multiplexed SNP genotyping (reproduced with permission from Shin et al. 2014)

(Fig. 2) (Shen et al. 2013c). Ligation of two FNP-modified oligonucleotides (FNP-1 and FNP-2) by LCR with perfectly matched target was carried out, after which the aggregated product facilitated by FNP made the reacted nanoparticles easily separated by an external magnetic field. Colorimetric detection, thereafter, could discriminate the SNP by reflecting the concentration of remaining FNPs. In another study, the catalytic properties of horseradish peroxidase and the magnetic separation of magnetic beads were utilized to discriminate SNPs with 1,000-fold excess of wild-type genes (Fig. 3) (Chen et al. 2012). The limit of detection was as low as 1 fM after LCR amplification.

2.1.2 Gold Nanoparticle-Based Genotyping of Single Nucleotide Polymorphisms

Gold nanoparticles (AuNPs) have attracted special attention in SNP detection technology because of their unique optical properties, of which not only the fluorescence but also the quenching of the fluorescence of gold nanoparticles is

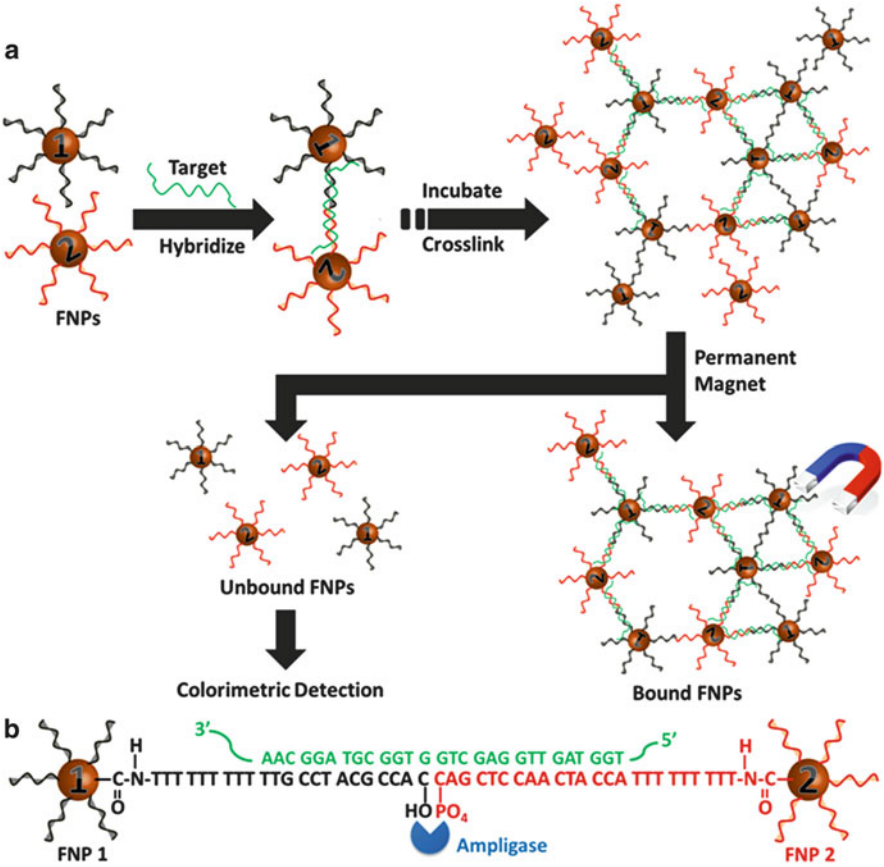

Fig. 2 Principle of the SNP detection assay by FNPs (reproduced with permission from Shen et al. 2013c)

interesting (Wang et al. 2010; Zu et al. 2011). The first report on the colorimetric detection of DNA sequences using nonfunctionalized AuNPs appeared in 2004 (Li and Rothberg 2004). Some selected methods based on the cooperation of AuNPs and allele-specific ligation SNP genotyping are elaborated.

An SNP discrimination chip-based assay applying the optical properties of AuNPs, which is enhanced by silver and the ligation reaction, has been developed (Fig. 4) (Xue et al. 2009). When the perfectly matched target was introduced, capture strand on the chip and the probe on the AuNPs were ligated. Discrimination by the naked eye or flatbed scanner can be executed after a silver attachment and non-stringency wash. One interesting feature of the method is that not only can it detect the SNP at the designed site, but also the discrimination of SNP on the close to the ligation position is still practical.

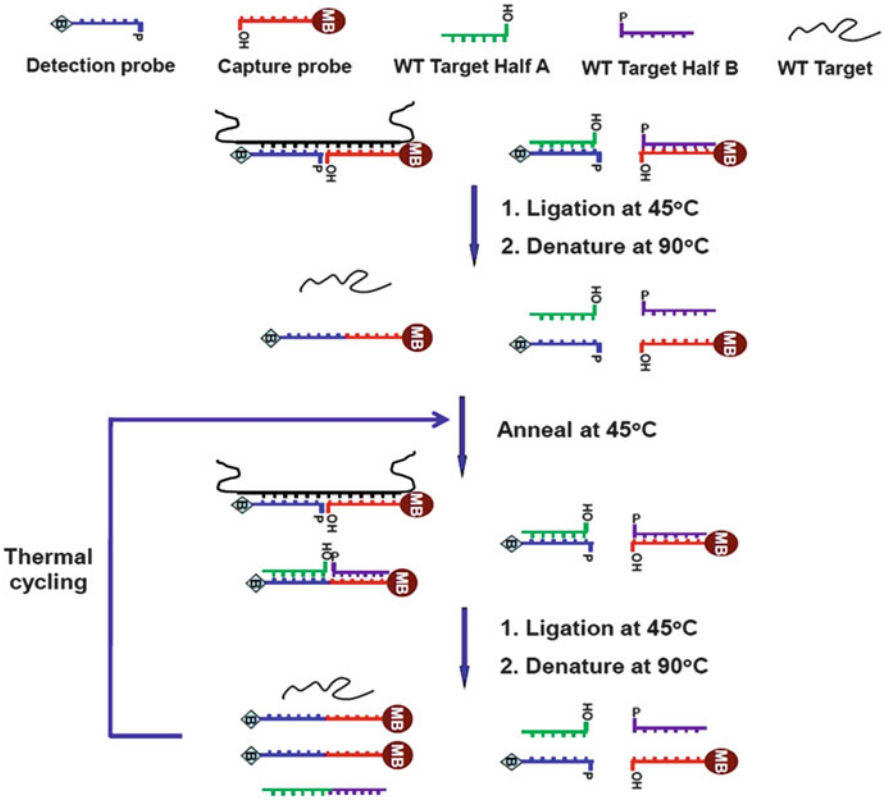

Fig. 3 SNP genotyping assay using magnetic beads (reproduced with permission from Chen et al. 2012)

The detection of SNP with real-time PCR sensitivity utilizing LCR and AuNPs has been developed (Fig. 5) (Shen et al. 2012a, b). The method was controlled by thermal cycle. The hybridization and ligation of the target with two types of AuNP-modified probes happened before raising the denaturing temperature to separate the target and the ligated strand, of which both were templates for the next round LCR reaction. Exponential amplification of ligation product was achieved after the first round of LCR. The irreversible change of the color of the solution from red to gray confirmed the existence of perfectly matched target, whereas the unchanged color indicated the existence of mismatched target. The limit of detection was expected to be 20 aM by theoretical modeling from experimental data (Shen et al. 2012b). Selectivity factor was 1,500 in the detection of wild-type KRAS genes from mutant type.

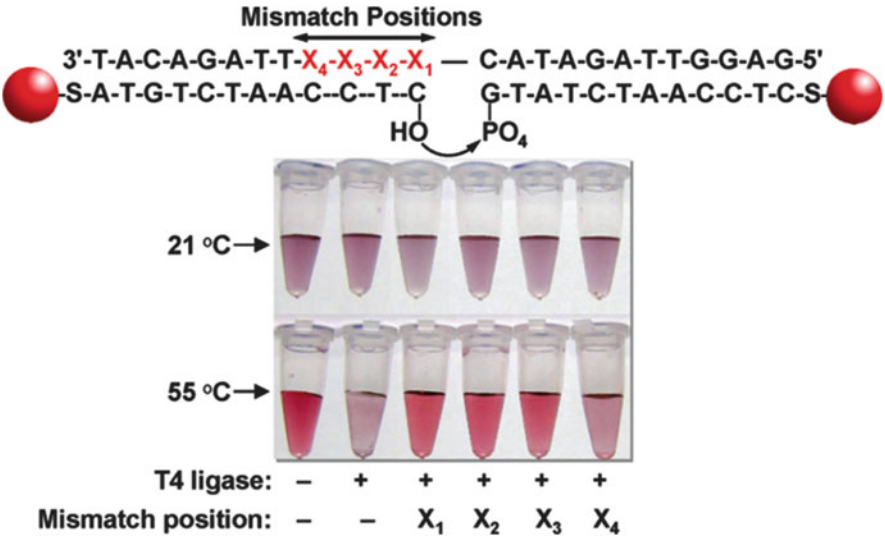

Fig. 4 AuNP-based assay on different SNP positions (reproduced with permission from Xue et al. 2009)

2.2 *Primer Extension-Based Genotyping of Single Nucleotide Polymorphisms*

Most of the SNP genotyping methods are based on known sequences available in order to specifically design the sequence of the probe to achieve the allele-specific discrimination. However, the construction of such a database does not have any references, which means most of the designed detection method for SNP is not applicable. It will be almost impossible to establish a SNP library on a whole-genome scale every time as the Human Genome Project did because of the unaffordable cost. Next-generation sequencing, however, provides the possibility to build the library with a much lower price (Shendurel et al. 2005; Shendurel and Ji 2008). Some representative methods are 454 pyrosequencing, Illumina, SOLiD, and HeliScope (Margulies et al. 2005; Shendurel and Ji 2008; Mardis 2008). Accuracy of the data was further increased by the framework of selection (Depristo et al. 2011; Nielsen et al. 2011). After the whole-genome sequencing, it is not always necessary to perform large-scale SNP detection if only one or few SNPs are of interest in consideration of cost and efficiency. Some methods based on the known library to detect SNPs are illustrated below.

2.2.1 Allele-Specific PCR

Common PCR procedures use the same primers for the extension of targets (Pelt-Verkuil et al. 2008). However, to determine the existence of SNPs, primers with

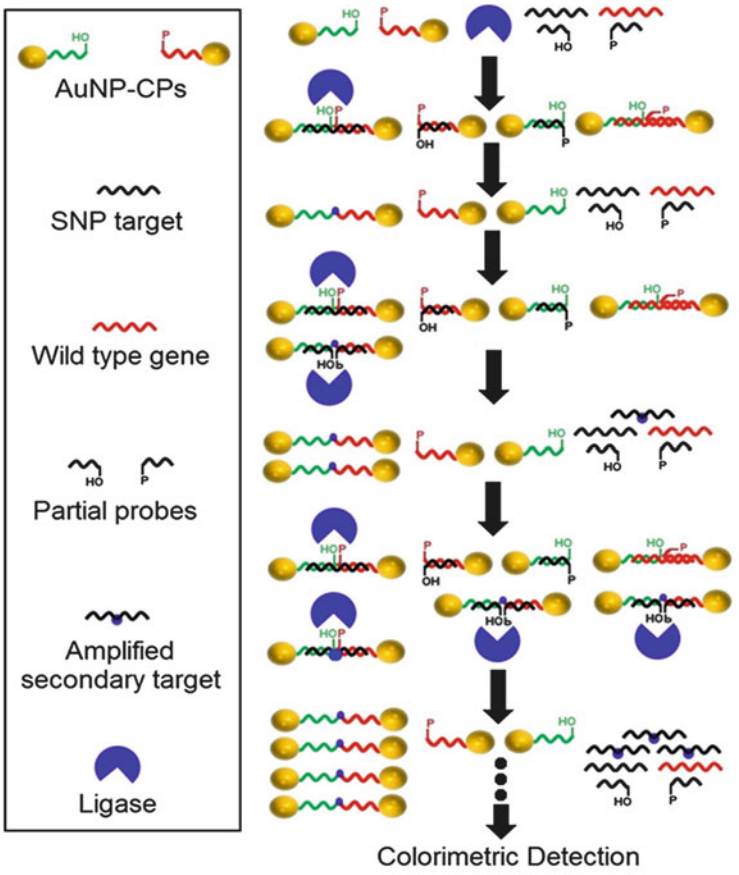

Fig. 5 Representation of SNP detection employing LCR and AuNPs (reproduced with permission from Shen et al. 2012b)

single-base differences at the 3′ end, which is deliberately designed at the SNP site, are utilized so that the extension reaction of PCR can only happen with perfectly matched sequences. Discrimination and genotyping of SNPs can be achieved with specific fluorophore functionalization and gel analysis (Kim and Misra 2007). A SNP assay with similar idea but no reverse primer extension performed is called sequence-specific primer PCR (SSP-PCR) (Hori et al. 2003). In 1989, the first successful application of SNP genotyping by allele-specific PCR was achieved in which a third primer (common primer) was introduced to identify the products with different "allele-specific primers" (Gibbs et al. 1989). High discrimination factor (100:1) and the success in the detection of SNP in low abundance (100-fold mismatched product) proved the robustness and reliability of the method.

As illustrated in Fig. 6, genotyping was successfully performed by combining cationic conjugated polyelectrolytes (CCP) with fluorescent PCR products to

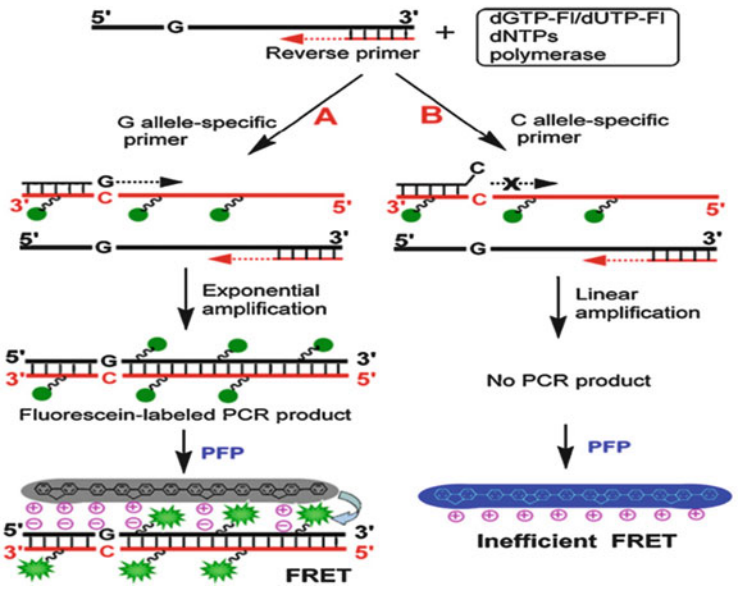

Fig. 6 Schematic illustration of SNP typing by CCP (reproduced with permission from Duan et al. 2009)

enhance the detection power of the assay by the fluorescence resonance energy transfer (FRET) from CCP to the dGTP-FI and dUTP-FI, which can make the intensity of fluorescence increased (Duan et al. 2009). SNP determination was successfully conducted with 50 ng of genome DNA from lung cancer cells. A colorimetric SNP detection scheme based on the optical properties of AuNPs was also reported (Jung et al. 2011). Extension reactions were carried out in four different tubes with all experimental conditions maintained the same, except that the four primers with the only difference at 3′ ends were chemically functionalized with sulfhydryl group (−SH), which promotes the aggregation of PCR product on AuNPs. Red color was observed in the tube containing perfectly matched primer, whereas the rest changed to blue because of the aggregation of AuNPs.

2.2.2 Single-Base Extension

The method of single-base extension (SBE) was initially invented by Goelet et al. as a form of US patent (Goelet et al. 1999). Primers of which the 3′ ends are immediately adjacent to the query site of mutation are designed to hybridize to the target DNA. SBE occurs with the introduction of four dideoxynucleotides, namely, ddATP, ddTTP, ddGTP, and ddCTP, labeling with distinctive reporters. Different detection techniques such as fluorometry, voltammetry, Matrix Assisted Laser Desorption Ionization Time-of-Flight (MALDI-TOF) mass spectrometry, and gel electrophoresis, thereafter, can be conducted to identify the SNPs (Brazill and Kuhr 2002). SNP

detection based on SBE with MALDI-TOF mass spectrometry is one of the examples that has been used to determine SNPs in real targets such as trisomic DNA (Trewick et al. 2011). Application of ribonuclease was also performed (Mengel-Jorgensen et al. 2005). In addition, fluorescence discrimination by the incorporation of graphene oxide can type the SNPs with detection limit of 3 nM (Xu et al. 2013).

Introduction of microfluidic platforms for primers improves the detection by higher automation and multiplex SNP detection. SBE on glass slides (SBE-TAGS) applied this concept to achieve a highly accurate and sensitive assay (Hirschhorn et al. 2000). Two-color SBE reactions to score the SNPs were employed in the configuration of a whole-genome genotyping method (Steemers et al. 2006). Hybridization of targets and primers, immobilized on a BeadArray platform, happened before the execution of SBE during which four types of dideoxynucleotides with two kinds of fluorophores were used. After staining, genotype can be analyzed by the color of the image of the SBE products. Based on the same principle, the employment of gold-coated magnetic nanoparticles functionalized by streptavidin (SA-GMNPs) as the platform for the immobilization of primers was used to discriminate SNPs (Li et al. 2012). After SBE, fluorophore–GMNP complexes were formed which then are "printed" on a glass slide with the aid of an external magnetic field. Discrimination of SNPs was achieved by the comparison of the colors generated by different fluorophores. No purification of the PCR product and no background correction were needed in the assay.

2.3 *Enzymatic Cleavage-Based Genotyping of Single Nucleotide Polymorphisms*

Restriction endonucleases are a class of enzymes that specifically recognize and cleave certain DNA sequences (Roberts 1976; Kessler and Manta 1990). A systemic summary of the classification, function, and potential applications is available (Kessler and Manta 1990). When restriction endonucleases cleave, some of the recognition regions of the endonucleases contain SNPs, or other types of mutations often give rise to unsuccessful cleavage (Kim and Misra 2007). By applying such a strategy, the SNPs within the recognition regions of restriction endonucleases can be determined, of which one of the initial methods was the assay of restriction fragment length polymorphisms (RFLP) and amplified fragment length polymorphisms (Botstein et al. 1980; Nicod and Largiader 2003). However, the drawbacks of these methods are obvious because the restriction endonucleases can only recognize certain sequences of the genome, leaving the majority of SNPs untouched. Restriction endonuclease next-generation sequencing (NGS) can improve the performance of the previous methods by the construction of reducible representation of a genome by the endonucleases and the dedicated design of the assay (Davey et al. 2011). NGS has been applied to genotype whole-genome SNPs, and the results were promising. However, the problem caused by the limitation of

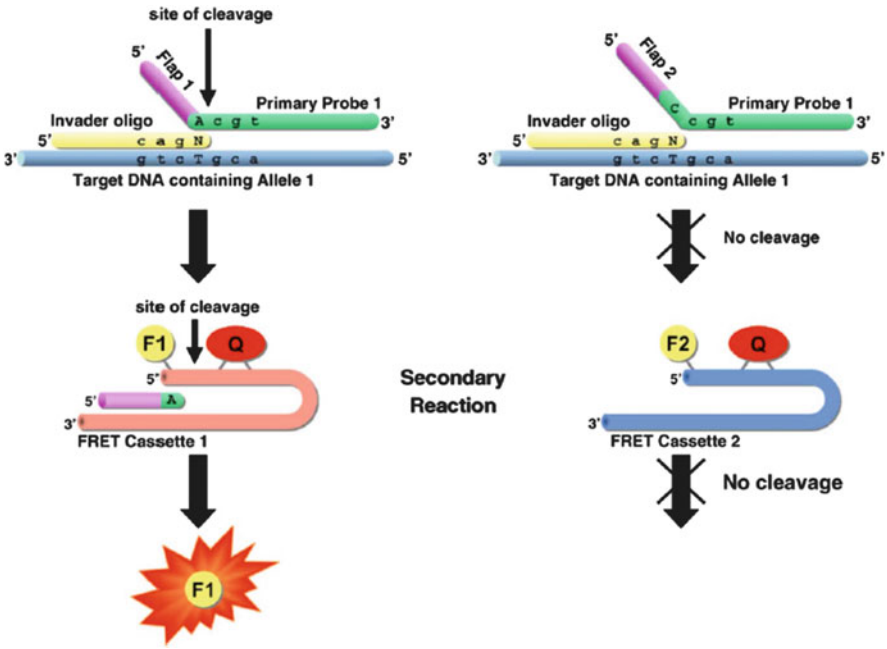

Fig. 7 Principle of invader assay (reproduced with permission from Olivier 2005)

restriction endonucleases may still cause a lower level of SNP detection than other methods (Kim and Misra 2007).

Invader assay is a SNP genotyping method using restriction endonucleases but has a different detection mechanism. The principle of the detection is based on a triplex structure formed among the target DNA sequence, the allele-specific probe, and the invader probe. If the allele-specific probe had perfect match with the target, the restriction endonuclease would cleave off the invader sequence from the triplex structure (Fig. 7) (Gut 2001; Olivier 2005). Detection can be achieved if the free invader probes are labeled. Based on the original method, an enhanced assay in which two invasive reactions were used for the amplification of the target gene has been developed (Hall et al. 2000). The power of amplification was much higher than that of the single invasive detection method (10^7 compared to 3,000–10,000).

2.4 Hybridization-Based Genotyping of Single Nucleotide Polymorphisms

The working principle of the hybridization-based genotyping relies on the detection of subtle differences in stabilities caused by the single-base mismatches, which was

first systemically studied in 1979 (Wallace et al. 1979). Some commercially available approaches are then developed, such as the GeneChip array assay and Qbead technique (Kennedy et al. 2003; Xu et al. 2003). Because hybridization-based genotyping does not require the involvement of complex enzymatic reactions, it is more convenient and easier to be conducted (Mir and Southern 1999; Gao et al. 2013). However, the thermodynamically driven reaction suffered from the problems of sensitivity and specificity (Shen et al. 2013a, b). Much effort has been devoted to overcome the problems on the assay, and some of the improvements are elaborated in the following section.

2.4.1 Molecular Beacon

Molecular beacon (MB) is a stem-loop structure that contains both a fluorophore and a quencher, which diminishes the fluorescence by FRET between them (Tyagi and Kramer 1996). With the stepwise improvement of MBs, many derivatives of MBs are invented, such as the superquencher MBs (Yang et al. 2005), quencher-free MBs (Venkatesan et al. 2008), and the stemless MBs (Gifford et al. 2005). All of the modifications aim at increasing signal-to-noise ratio and specificity. The first application of MBs in SNP genotyping appeared in 1998 in which two MBs labeled with fluorescein and tetramethylrhodamine were employed to selectively detect the wild type and mutant type (Kostrikis et al. 1998). Subsequently, a large variety of applications of MBs were developed. Some representative examples will be elaborated in here.

Base discriminating fluorescent (BDF) oligodeoxyribonucleotides, which are mainly pyrene-functionalized derivatives, can be applied to differentiate SNPs (Ostergaard and Hrdlicka 2011). Research based on this principle was later executed by many groups. The quencher-free MBs were discovered based on the pyrene-modified 2′-deoxynucleotides (Fig. 8) (Seo et al. 2005). When the loop is opened by the target, the fluorescence is quenched through photoinduced electron transfer and π–π interaction, which is mainly attributed to the coupling between the pyrene-labeled bases and the neighboring bases on the nucleotides. Probe A^{PY} was shown to have the best discrimination capacity, and S1 was proven to be suitable as the sequence of the probe. By using deoxyuridine with functionality of 9-fluorenone (FO) or fluorine (FL) as fluorescent probes on the base part, the quencher-free MBs are developed, and some of them showed excellent performance and were regarded as the promising candidates for SNP typing (Lee et al. 2013).

The detection of dual SNPs simultaneously employing two different quantum dot molecular beacon (QD-MB) probes using capillary electrophoresis (CE) for the detection of the SNPs was also reported (Li et al. 2011). The multiple SNP detection was achieved by the application of QDs instead of the normal fluorescence dyes, and CE minimizes the problem of false results which might be observed by the effectively separation of unreacted MB with the MB–target complex. Two QD-MBs hybridized to two SNP sites, which generate distinguishable signals.

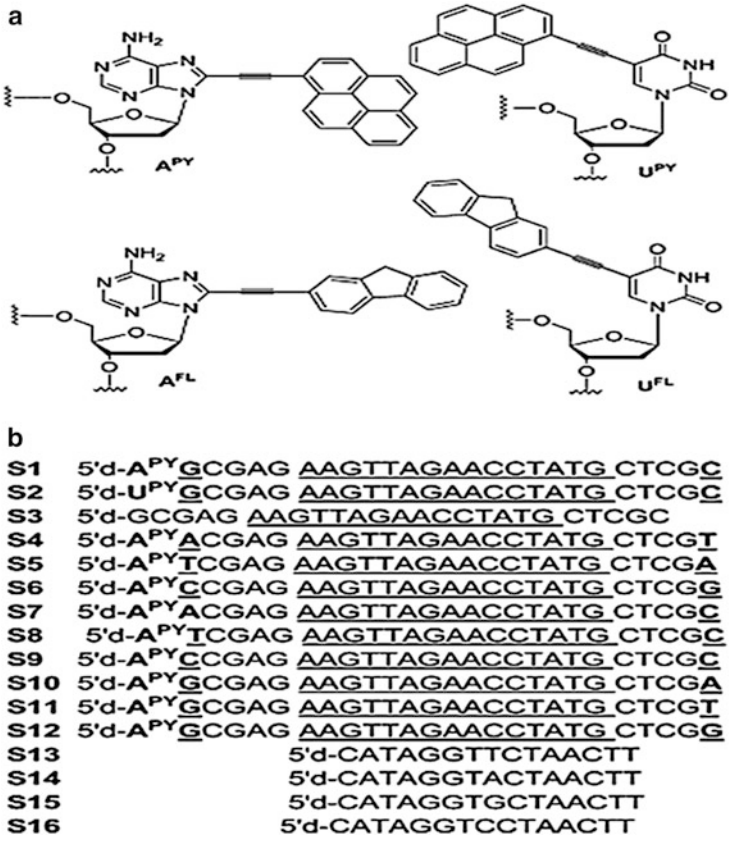

Fig. 8 Structure of fluorescent nucleoside derivatives for the assay (reproduced with permission from Seo et al. 2005)

The detection limit of this method is 14 nM (16.2 pg), an impressive improvement over that of the original method using QD-MBs (8 ng) (Kim et al. 2004).

2.4.2 Y-Shape Junction Probe

Y-shape junction probe is a special case of junction forming probes, which is isothermal and non-PCR based (Knez et al. 2014). The principle of the operation of the probe is template-enhanced hybridization process (TeHyP). The first application of the Y-shape conjugation probe to the detection of SNPs was conducted in 2008 by using the enzymatic cleavage of specific sequences (Nakayama et al. 2008). Afterward, some improvements of the method were achieved.

The effective SNP genotyping strategies of oral cancer by the junction probes with 2′-deoxyinosine nucleoside (dI-nucleotide) substitution on the SNP site using electrochemical detection were attempted (Zhang et al. 2010a). Different stabilities

were obtained when various nucleotides were complementary to the dI-nucleotide in the formation of a three-way junction complex, which can be differentiated by linear sweep voltammetry. Based on the same principle employing the DNA enzyme activity to oxidize 2,2′-azinobis(3-ethylbenzthiazoline-6-sulfonicacid) (ABTS) by hydrogen peroxide to the colored $ABTS^{-}$ radical, SNP discrimination can be achieved by the detectable color change by the naked eye (Tang et al. 2013). Both methods are easily operated, but the detection limits are still relatively high (0.13 pM for the first method and 0.25 nM for the second method).

A point-of-care detection of SNP based on the chameleon NanoCluster Beacon (cNCB) probe, which was divided into NC probe and G-rich probe, was also reported (Yeh et al. 2012). NanoCluster Beacons (NCBs) employed in the research are silver nanoparticles which serve as reporters, which can generate fluorescence with distinctive colors in different proximities of DNA sequences. When the targets were exposed to two parts of the cNCB probes, the Y-shape junction DNA structure was generated. Certain color was obtained when the target was the wild type. When the target had a SNP site within the hybridization region with the cNCB, the frameshift of the third arm caused the color change, which can be detected by the emission spectra or the naked eye. Three signals were obtained when using various bases in the SNP position. The method was further varified by the combination of different nucleotides in SNP sites, and all results were distinguishable, which means it is applicable for SNP typing.

2.4.3 Toehold

Toehold is a short, single-strand overhanging region of a double-stranded nucleotide (Knez et al. 2014). Fast and specific strand displacement reaction (SDR) will happen when an oligonucleotide binds to the toehold, with the replacement of the original “shorter” chain by the totally complementary one (Yan et al. 2014). SNP determination and genotyping based on the toehold-mediated SDR have been systemically studied in recent years.

The application of toehold in SNP detection was first performed in 2010 (Zhang et al. 2010b). Single-stranded DNA probes were initially hybridized with the practically complementary DNA reporter. The sequences, not forming the double-stranded structure with the reporter, were the toehold. The capture probes were connected by DNA origami, which showed red under an atomic force microscope. Streptavidin, generating white-bulge images, was incubated into the reporter as a contrast label to reveal the position of the reporter. When perfectly matched target was employed, complete strand displacement reaction happened, which can be visualized by the disappearance of the streptavidin feature on the DNA origami platform and vice versa, thus achieving genotyping of SNPs.

Optimization was almost necessary for the hybridization-based SNP genotyping in the abovementioned reports, which are tedious, time-consuming, and sometimes highly costing. Toehold exchange probes offer the possibilities for not performing the optimization procedure (Zhang et al. 2012). Three common factors are needed

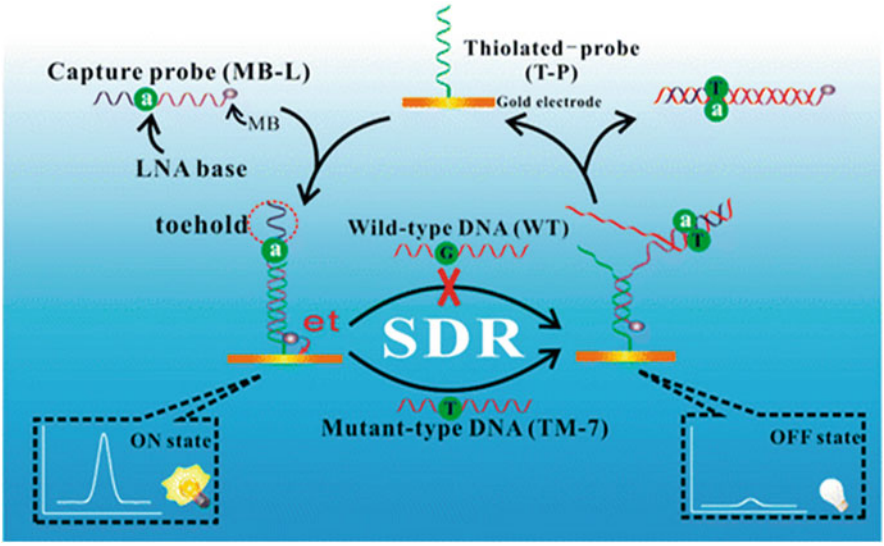

Fig. 9 Principle of SNP detection by toehold-mediated SDR (reproduced with permission from Gao et al. 2014)

for further optimization in previous studies, which are temperature, salinity, and oligonucleotide concentration. However, they did not influence the efficiency and specificity of the probes in a wide range according to the theoretical modeling and actual measurements. The near-optimal SNP discrimination can be maintained from 10 to 37 °C and from 1 to 47 mM Mg^{2+}, and the concentration of target oligonucleotide is from 1 nM to 5 μM. The performance of the probe on the SNP determination was promising with theoretical discrimination factor being as high as 343.

As illustrated in Fig. 9, an on–off switching biosensor based on locked nucleic acid (LNA) and toehold structure was recently proposed (Gao et al. 2014). Thiolated DNA probes (T-P) were first incubated with the capture probes (MB-L) labeled with methylene blue and integrated with LNA at the mismatched point, of which the position optimized the discriminating capability. By replacing the normal nucleotide with LNA, the ability of discrimination between the perfectly matched target and SNP-based target was significantly improved. The current was enhanced with the addition of MB-L by the electron transfer between AuNPs and MB, which is the ON signal. SDR was then initiated by the toehold when the target was introduced. With perfect matching between the MB-L and the target, T-P leaves the system, shifting the signal to OFF. When mismatched template was present, displacement was not executed completely, leaving the signal partially in the ON state. This approach was verified on complex samples such as urine and soil. It was shown that the discrimination ability was very robust permitting the coexistence 6,000-folds of irrelevant genomic DNA.

2.4.4 G-Quadruplex

G-quadruplex is a four-stranded structure assembled from G-rich nucleic acid oligomers (Neidle 2009). The sequence for the uniquely high-ordered DNA structure is mainly connected by Hoogsteen-type base pairing (Hoogsteen 1963). The existence of such a structure in human genome varies, with the occurrence approximately from 300 to 400,000. The morphology of G-quadruplex is diversified, but all are likely to coordinate with metal ions, particularly with high affinities to alkali metals. In fact, potassium ions have a great importance on the sensitivity and specificity of G-quadruplex-based assays (Ren et al. 2012). Coordination of other ions in G-quadruplex is also possible, which makes it possible for the application in genotyping of SNPs.

The first SNP determination strategy was based on the peroxidase-like DNAzyme with the G-quadruplex structure (Kolpashchikov 2008). The DNAzyme was separated into two parts,with four triple G sequences split into a 2 + 2 pattern, which would not be active after the combination with the template DNA and hemin. Each segment was modified by removing the deoxycytidine and connecting a binding arm with a triethylene glycol linker. In the presence of the perfectly matched target with binding arms of the two probes, the formation of G-quadruplex and the acquisition of the enzymatic activity occurred, and the colorless 3-3′-diaminobenzidine tetrahydrochloride was oxidized to a brown compound by hydrogen peroxide. If the mutant type was introduced, no color change was observed. Enabling the distinction by the naked eye, this method has the advantages of simplicity and low cost with relatively promising discrimination power(S/N ~10).

As shown in Fig. 10, a significant improvement was achieved with the incorporation of PCR-like temperature circles into the DNAzyme assay for amplification (Wang et al. 2011b). The probes contained three distinct segments—Domain I, II, and III. The amplification was carried out same as ordinary PCR reactions. At 60 °C, annealing reaction occurred with the Domain III connecting to the target, after which the addition of triple G at the 3′ end of Domain III happened. After the temperature rose at 95 °C, probe and template were separated, and the template was used in the next round of PCR reaction. The addition of hemin generated the G-quadruplex with catalytic reactivity, which was involved in the oxidation of 2,2′-azinobis(3-ethylbenzothiozoline)-6-sulfonic acid (ABTS) with the colorless ABTS change to green $ABTS^{+}$. SNP typing can thus be achieved, but it is necessary to further improve the reaction conditions and probe design by increasing the annealing temperature and incubating competitive probes without G-rich sequences to improve the selectivity of the assay. In principle, shortening the matching sequence can also improve the performance.

Based on the same detection mechanism, the performance of the assay can also be improved by increasing the efficiency of signal amplification (Fig. 11). By utilizing isothermal strand displacement amplification (SDA) twice, better results were obtained (Wang et al. 2011a). Allele discrimination was accomplished by the combination of discrimination probe I and II with the common probe III by ligase. First round of SDA reaction was performed with the 3′ end of probe III as primer.

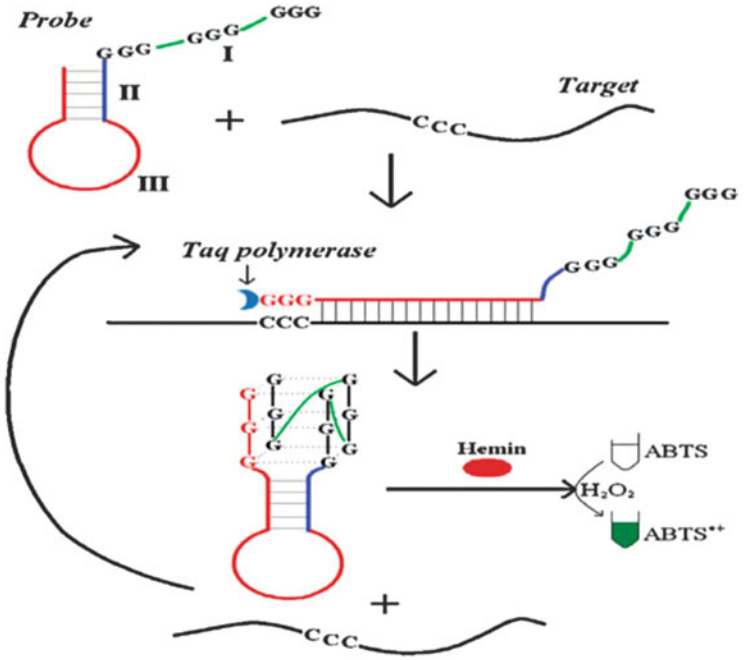

Fig. 10 DNAzyme-mediated SNP genotyping (reproduced with permission from Wang et al. 2011b)

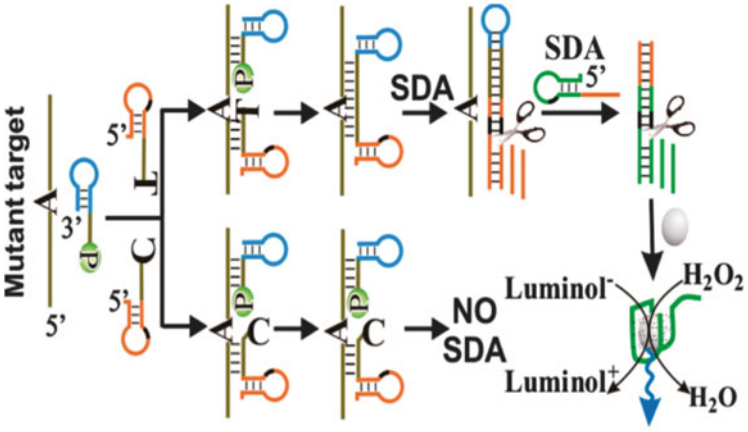

Fig. 11 Discrimination of SNPs by SDA using chemiluminescence (reproduced with permission from Wang et al. 2011a)

The product was further combined with probe IV, of which the product underwent the second round of SDA. The introduction of hemin into the amplicon produced the DNAzyme which triggered a chemiluminescence reaction. The selectivity of

the method is superior to other similar methods with the signal-to-background ratio around 150. Furthermore, the detection limit was 0.1 fM, indicating the procedure can be applied in genotyping SNPs in real-world samples.

3 Conclusions and Future Prospects

SNPs are the most abundant DNA variations in human genome and are closely related to differences in phenotypes and a large number of diseases. Robust, effective, and highly specific SNP genotyping techniques are therefore necessary for the studies of SNPs. Currently, two categories of SNP genotyping techniques—the allele-specific hybridization method and the allele-specific enzymatic method—are widely studied. Enzymatic assays based on ligation, primer extension, and enzymatic cleavage are systemically investigated, and the methodologies are usually more complex than the hybridization methods. However, based on the subtle difference in the stability between the wild-type and mutant genes, the hybridization method is still advantageous because of the comparably simple procedures and relatively low cost. Notwithstanding the current obstacles faced, such as the relatively low discrimination power and higher limit of detection, the hybridization-based SNP genotyping is still a promising way with much attention drawn to the field and promising progress made in recent years.

SNP genotyping technologies have been developed in the past 20 years. Much effort has been spent to the discovery of SNPs on the role they play that may cause certain diseases, such as the Hyperkeratosis Lenticularis Perstans gene variations (Wang and Moult 2001). Modules on the impact of protein that may cause genetic disease by SNP have also been investigated (Bakker et al. 2006). However, the expected destination of the study of SNP genotype should not just stop at the SNP discovery stage when it comes to the study of diseases. The pathogenic mechanism behind the existence of SNPs should be thoroughly investigated in addition to SNP genotyping, thus, enabling the development of molecular diagnostics and personalized therapeutics.

Acknowledgments This work is supported by the Ministry of Education (Grant No. R143000588112).

References

Bakker PIW, McVean G, Sabeti PC et al (2006) A high-resolution HLA and SNP haplotype map for disease association studies in the extended human MHC. Nat Genet 38:1166–1172

Botstein D, White RL, Skolnick M et al (1980) Construction of a genetic linkage map in man using restriction fragment length polymorphisms. Am J Hum Genet 32:314–331

Brazill SA, Kuhr WG (2002) A single base extension technique for the analysis of known mutations utilizing capillary gel electrophoresis with electrochemical detection. Anal Chem 74:3421–3428

Brookes AJ (1999) The essence of SNPs. Gene 234:177–186

Chen X, Livak KJ, Kwok P-Y (1998) A homogeneous, ligase-mediated DNA diagnostic test. Genome Res 8:549–556

Chen X, Ying A, Gao Z (2012) Highly sensitive and selective colorimetric genotyping of single-nucleotide polymorphisms based on enzyme-amplified ligation on magnetic beads. Biosens Bioelectron 36:89–94

Collins FS, Morgan M, Patrinos A (2003) The Human Genome Project: lessons from large-scale biology. Science 300:286–290

Davey JW, Hohenlohe PA, Etter PD et al (2011) Genome-wide genetic marker discovery and genotyping using next-generation sequencing. Nat Rev Genet 12:499–510

DePristo MA, Banks E, Poplin R et al (2011) A framework for variation discovery and genotyping using next-generation DNA sequencing data. Nat Genet 43:491–498

Duan X, Liu L, Wang S (2009) Homogeneous and one-step fluorescent allele-specific PCR for SNP genotyping assays using conjugated polyelectrolytes. Biosens Bioelectron 24:2095–2099

Dumur CI, Dechsukhum C, Ware JL et al (2003) Genome-wide detection of LOH in prostate cancer using human SNP microarray technology. Genomics 81:260–269

Durbin RM, Altshuler DL, Durbin RM et al (2010) A map of human genome variation from population-scale sequencing. Nature 467:1061–1073

Frazer KA, Ballinger DG, Cox DR et al (2007) A second generation human haplotype map of over 3.1 million SNPs. Nature 449:851–861

Fredman D, Munns G, Rios D et al (2004) HGVbase: a curated resource describing human DNA variation and phenotype relationships. Nucleic Acids Res 32:D516–D519

Gao Z, Shen W, Deng H et al (2013) Detection of single-nucleotide polymorphisms based on the formation of an electron-transfer impeding layer on an electrode surface. Chem Commun 49:370–372

Gao ZF, Ling Y, Lu L et al (2014) Detection of single-nucleotide polymorphisms using an ON-OFF switching of regenerated biosensor based on a locked nucleic acid-integrated and toehold-mediated strand displacement reaction. Anal Chem 86:2543–2548

Gibbs RA, Nguyen PN, Caskey CT (1989) Detection of single DNA base differences by competitive oligonucleotide priming. Nucleic Acids Res 17:2437–2448

Gifford LK, Jordan D, Pattanayak V et al (2005) Stemless self-quenching reporter molecules identify target sequences in mRNA. Anal Biochem 347:77–88

Goelet P, Knapp MR, Anderson S (1999) Method for determining nucleotide identity through extension of immobilized primer. Molecular Tool, USA. 37 pp, Cont.-in-part of U.S. 35,888,819

Gut IG (2001) Automation in genotyping of single nucleotide polymorphisms. Hum Mutat 17:475–492

Hall JG, Eis PS, Law SM et al (2000) Sensitive detection of DNA polymorphisms by the serial invasive signal amplification reaction. Proc Natl Acad Sci USA 97:8272–8277

Hirschhorn JN, Sklar P, Lindblad-Toh K et al (2000) SBE-TAGS: an array-based method for efficient single-nucleotide polymorphism genotyping. Proc Natl Acad Sci USA 97:12164–12169

Hoogsteen K (1963) The crystal and molecular structure of a hydrogen-bonded complex between 1-methylthymine and 9-methyladenine. Acta Crystallogr 16:907–916

Hori K, Shin WS, Hemmi C et al (2003) High fidelity SNP genotyping using sequence-specific primer elongation and fluorescence correlation spectroscopy. Curr Pharm Biotechnol 4:477–484

Jung YL, Jung C, Parab H et al (2011) Colorimetric SNP genotyping based on allele-specific PCR by using a thiol-labeled primer. ChemBioChem 12:1387–1390

Kennedy GC, Matsuzaki H, Dong S et al (2003) Large-scale genotyping of complex DNA. Nat Biotechnol 21:1233–1237
Kessler C, Manta V (1990) Specificity of restriction endonucleases and DNA modification methyltransferases – a review (Edition 3). Gene 92:1–248
Kim S, Misra A (2007) SNP genotyping: technologies and biomedical applications. Annu Rev Biomed Eng 9:289–320
Kim JH, Morikis D, Ozkan M (2004) Adaptation of inorganic quantum dots for stable molecular beacons. Sens Actuators B 102:315–319
Knez K, Spasic D, Janssen KPF et al (2014) Emerging technologies for hybridization based single nucleotide polymorphism detection. Analyst 139:353–370
Kolpashchikov DM (2008) Split DNA enzyme for visual single nucleotide polymorphism typing. J Am Chem Soc 130:2934–2935
Kostrikis LG, Tyagi S, Mhlanga MM et al (1998) Molecular beacons: spectral genotyping of human alleles. Science 279:1228–1229
Kwok P-Y (2001) Methods for genotyping single nucleotide polymorphisms. Annu Rev Genomics Hum Genet 2:235–258
Landegren U, Kaiser R, Sanders J et al (1988) A ligase-mediated gene detection technique. Science 241:1077–1080
Lee J, Cho HY, Hwang GT (2013) Highly efficient quencher-free molecular beacon systems containing 2-ethynyldibenzofuran- and 2-ethynyldibenzothiophene-labeled 2′-deoxyuridine units. ChemBioChem 14:1353–1362
Li H, Rothberg L (2004) Colorimetric detection of DNA sequences based on electrostatic interactions with unmodified gold nanoparticles. Proc Natl Acad Sci USA 101:14036–14039
Li Y-Q, Guan L-Y, Wang J-H et al (2011) Simultaneous detection of dual single-base mutations by capillary electrophoresis using quantum dot-molecular beacon probe. Biosens Bioelectron 26:2317–2322
Li S, Liu H, Jia Y et al (2012) A novel SNPs detection method based on gold magnetic nanoparticles array and single base extension. Theranostics 2:967–975
Lizardi PM, Huang X, Zhu Z et al (1998) Mutation detection and single-molecule counting using isothermal rolling-circle amplification. Nat Genet 19:225–232
Mardis ER (2008) Next-generation DNA sequencing methods. Annu Rev Genomics Hum Genet 9:387–402
Margulies M, Egholm M, Altman WE et al (2005) Genome sequencing in microfabricated high-density picolitre reactors. Nature 437:376–380
Mengel-Jorgensen J, Sanchez JJ, Borsting C et al (2005) Typing of multiple single-nucleotide polymorphisms using ribonuclease cleavage of DNA/RNA chimeric single-base extension primers and detection by MALDI-TOF mass spectrometry. Anal Chem 77:5229–5235
Mir KU, Southern EM (1999) Determining the influence of structure on hybridization using oligonucleotide arrays. Nat Biotechnol 17:788–792
Myakishev MV, Khripin Y, Hu S et al (2001) High-throughput SNP genotyping by allele-specific PCR with universal energy-transfer-labeled primers. Genome Res 11:163–169
Nakayama S, Yan L, Sintim HO (2008) Junction probes – sequence specific detection of nucleic acids via template enhanced hybridization processes. J Am Chem Soc 130:12560–12561
Neidle S (2009) The structures of quadruplex nucleic acids and their drug complexes. Curr Opin Struct Biol 19:239–250
Nicod J-C, Largiader CR (2003) SNPs by AFLP (SBA): a rapid SNP isolation strategy for non-model organisms. Nucleic Acids Res 31:e19/11–e19/15
Nielsen R, Paul JS, Albrechtsen A et al (2011) Genotype and SNP calling from next-generation sequencing data. Nat Rev Genet 12:443–451
Nollau P, Wagener C (1997) Methods for detection of point mutations: performance and quality assessment. Clin Chem 43:1114–1128
Olivier M (2005) The invader assay for SNP genotyping. Mutat Res 573:103–110

Onay VU, Briollais L, Knight JA et al (2006) SNP-SNP interactions in breast cancer susceptibility. BMC Cancer 6:114/111–114/116

Ostergaard ME, Hrdlicka PJ (2011) Pyrene-functionalized oligonucleotides and locked nucleic acids (LNAs): tools for fundamental research, diagnostics, and nanotechnology. Chem Soc Rev 40:5771–5788

Paynter NA, Chasman DI, Buring JE (2009) Cardiovascular disease risk prediction with and without knowledge of genetic variation at chromosome 9p21.3. Ann Intern Med 150:65–72

Pecoits-Filho R, Stenvinkel P, Marchlewska A et al (2003) A functional variant of the myeloperoxidase gene is associated with cardiovascular disease in end-stage renal disease patients. Kidney Int Suppl 84:S172–S176

Pelt-Verkuil EV, Belkum AV, Hays JP (2008) PCR primers. Principles and technical aspects of PCR amplification. Springer, Rotterdam, pp 63–90

Pruitt KD, Tatusova T, Maglott DR (2005) NCBI Reference Sequence (RefSeq): a curated non-redundant sequence database of genomes, transcripts and proteins. Nucleic Acids Res 33:D501–D504

Ren J, Wang J, Wang J et al (2012) Contribution of potassium ion and split modes of G-quadruplex to the sensitivity and selectivity of label-free sensor toward DNA detection using fluorescence. Biosens Bioelectron 31:316–322

Roberts RJ (1976) Restriction endonucleases. CRC Crit Rev Biochem 4:123–164

Sachidanandam R, Weissman D, Schmidt SC et al (2001) A map of human genome sequence variation containing 1.42 million single nucleotide polymorphisms. Nature 409:928–933

Seo YJ, Ryu JH, Kim BH (2005) Quencher-free, end-stacking oligonucleotides for probing single-base mismatches in DNA. Org Lett 7:4931–4933

Shen W, Deng H, Gao Z (2012a) Gold nanoparticle-enabled real-time ligation chain reaction for ultrasensitive detection of DNA. J Am Chem Soc 134:14678–14681

Shen W, Deng H, Teo AKL et al (2012b) Colorimetric detection of single-nucleotide polymorphisms with a real-time PCR-like sensitivity. Chem Commun 48:10225–10227

Shen W, Deng H, Ren Y et al (2013a) An electronic sensor array for label-free detection of single-nucleotide polymorphisms. Biosens Bioelectron 43:165–172

Shen W, Deng H, Ren Y et al (2013b) A real-time colorimetric assay for label-free detection of microRNAs down to sub-femtomolar levels. Chem Commun 49:4959–4961

Shen W, Lim CL, Gao Z (2013c) A ferrofluid-based homogeneous assay for highly sensitive and selective detection of single-nucleotide polymorphisms. Chem Commun 49:8114–8116

Shendurel J, Ji H (2008) Next-generation DNA sequencing. Nat Biotechnol 26:1135–1145

Shendurel J, Porreca GJ, Reppas NB et al (2005) Accurate multiplex polony sequencing of an evolved bacterial genome. Science 309:1728–1732

Shin SC, Kim G, Yang H-B et al (2014) Application of the ASLP technology to a novel platform for rapid and noise-free multiplexed SNP genotyping. Biosens Bioelectron 54:687–694

Siva N (2008) 1000 Genomes project. Nat Biotechnol 26:256

Steemers FJ, Chang W, Lee G et al (2006) Whole-genome genotyping with the single-base extension assay. Nat Methods 3:31–33

Syvanen AC (2001) Accessing genetic variation: genotyping single nucleotide polymorphisms. Nat Rev Genet 2:930–942

Tang S, Tong P, Li H et al (2013) The three-way junction DNAzyme based probe for label-free colorimetric detection of DNA. Biosens Bioelectron 41:397–402

Thorisson GA, Smith AV, Krishnan L, Stein LD (2005) The international HapMap project web site. Genome Res 15:1592–1593

Trewick AL, Moustafa JSE-S, de Smith AJ et al (2011) Accurate single-nucleotide polymorphism allele assignment in trisomic or duplicated regions by using a single base-extension assay with MALDI-TOF mass spectrometry. Clin Chem 57:1188–1195

Tuupanen S, Turunen M, Lehtonen R et al (2009) The common colorectal cancer predisposition SNP rs6983267 at chromosome 8q24 confers potential to enhanced Wnt signaling. Nat Genet 41:885–890

Tyagi S, Kramer FR (1996) Molecular beacons: probes that fluoresce upon hybridization. Nat Biotechnol 14:303–308

Venkatesan N, Seo YJ, Kim BH (2008) Quencher-free molecular beacons: a new strategy in fluorescence based nucleic acid analysis. Chem Soc Rev 37:648–663

Venter JC, Adams MD, Myers EW et al (2001) The sequence of the human genome. Science 291:1304–1351

Wallace RB, Shaffer J, Murphy RF et al (1979) Hybridization of synthetic oligodeoxyribonucleotides to phi chi 174 DNA: the effect of single base pair mismatch. Nucleic Acids Res 6:3543–3557

Wallace C, Newhouse SJ, Braund P et al (2008) Genome-wide association study identifies genes for biomarkers of cardiovascular disease: serum urate and dyslipidemia. Am J Hum Genet 82:139–149

Wang Z, Moult J (2001) SNPs, protein structure, and disease. Hum Mutat 17:263–270

Wang H, Li J, Wang Y et al (2010) Combination of DNA ligase reaction and gold nanoparticle-quenched fluorescent oligonucleotides: a simple and efficient approach for fluorescent assaying of single-nucleotide polymorphisms. Anal Chem 82:7684–7690

Wang H-Q, Liu W-Y, Wu Z et al (2011a) Homogeneous label-free genotyping of single nucleotide polymorphism using ligation-mediated strand displacement amplification with DNAzyme-based chemiluminescence detection. Anal Chem 83:1883–1889

Wang N, Kong D-M, Shen H-X (2011b) Amplification of G-quadruplex DNAzymes using PCR-like temperature cycles for specific nucleic acid and single nucleotide polymorphism detection. Chem Commun 47:1728–1730

Wee EJH, Shiddiky MJA, Brown MA et al (2012) eLCR: electrochemical detection of single DNA base changes via ligase chain reaction. Chem Commun 48:12014–12016

Xu H, Sha MY, Wong EY et al (2003) Multiplexed SNP genotyping using the Qbead system: a quantum dot-encoded microsphere-based assay. Nucleic Acids Res 31:e43

Xu H, Yang Q, Li F et al (2013) A graphene-based platform for fluorescent detection of SNPs. Analyst 138:2678–2682

Xue X, Xu W, Wang F et al (2009) Multiplex single-nucleotide polymorphism typing by nanoparticle-coupled DNA-templated reactions. J Am Chem Soc 131:11668–11669

Yan L, Zhou J, Zheng Y et al (2014) Isothermal amplified detection of DNA and RNA. Mol BioSyst 10:970–1003

Yang CJ, Lin H, Tan W (2005) Molecular assembly of superquenchers in signaling molecular interactions. J Am Chem Soc 127:12772–12773

Yeh H-C, Sharma J, Shih I-M et al (2012) A fluorescence light-up Ag nanocluster probe that discriminates single-nucleotide variants by emission color. J Am Chem Soc 134:11550–11558

Zacharova J, Chiasson J-L, Laakso M (2005) The common polymorphisms (single nucleotide genetic polymorphism) [(SNP +45 and SNP +276)] of the adiponectin gene predict the conversion from impaired glucose tolerance to type 2 diabetes: the STOP-NIDDM trial. Diabetes 54:893–899

Zhang J, Wu XY, Chen PP et al (2010a) Electrochemical genotyping and detection of single-nucleotide polymorphisms based on junction-probe containing 2′-deoxyinosine. Chem Commun 46:6986–6988

Zhang Z, Zeng D, Ma H et al (2010b) A DNA-Origami chip platform for label-free SNP genotyping using toehold-mediated strand displacement. Small 6:1854–1858

Zhang DY, Chen SX, Yin P (2012) Optimizing the specificity of nucleic acid hybridization. Nat Chem 4:208–214

Zu Y, Ting AL, Gao Z (2011) Visualizing low-level point mutations: Enzyme-like selectivity offered by nanoparticle probes. Small 7:306–310

Environmentally Responsive and Bright Fluorescent Probes Possessing Dansyl-Modified Oligonucleotides Under Hybridization of DNA and RNA

Yoshio Suzuki and Yasuo Komatsu

Contents

Abstract We synthesized a nonnucleoside amidite block of dansyl fluorophore to prepare dansyl-modified oligonucleotides (ONTs). The fluorescence intensities of the dansyl-ONTs specifically increased in the presence of adjacent guanosine residues but significantly reduced in a dansyl-flipping duplex. These changes were caused by a solvatochromism effect—which was governed by the number of guanine molecules, which are hydrophobic—and the external environment of the dansyl residue. After hybridizing with a guanine-containing target, these dansyl-modified ONTs exhibited a slightly higher melting temperature compared with those of the duplexes containing other base pairs, suggesting some kind of interactions between guanine and dansyl residues. Similar changes in fluorescence intensity were detected upon hybridization of complementary RNAs. Note that the dansyl unit does not require target labeling steps to exert these unique functions. These physicochemical features described here remind that the dansyl amidite

Y. Suzuki
Health Research Institute, National Institute of Advanced Industrial Science and Technology (AIST), Central 6, 1-1-1 Higashi, Tsukuba 305-8566, Japan
e-mail: suzuki-yoshio@aist.go.jp

Y. Komatsu (✉)
Bioproduction Research Institute, National Institute of Advanced Industrial Science and Technology (AIST), 2-17-2-1 Tsukisamu-Higashi, Toyohira-ku, Sapporo 062-8517, Japan
e-mail: komatsu-yasuo@aist.go.jp

V.A. Erdmann et al. (eds.), *RNA and DNA Diagnostics*, RNA Technologies,
DOI 10.1007/978-3-319-17305-4_7

blocks are very useful in the preparation of probes for investigating structural changes in DNA and RNA.

Keywords Fluorescence • DNA • RNA • Molecular probes • Sensor

1 Introduction

The design and synthesis of fluorescence-labeled oligonucleotides (ONTs), which demonstrate strongly enhanced signals upon hybrid formation, are currently a topic of interest. ONTs containing fluorophores are commonly used for real-time analysis of DNA sequences being amplified in a polymerase chain reaction (PCR) as well as for sequencing by hybridization, fluorescence in situ hybridization, fluorescence resonance energy transfer, molecular beacons, TaqMan probes, and DNA chips (Erlich et al. 1991; Mirzabekov 1994; Dumont et al. 2012; Singh et al. 2000; Astakhova et al. 2013; Ke et al. 2012; Tan et al. 2012; Ryazantsev et al. 2012; Benitez et al. 2012; Schulze et al. 2012). They are also commonly used as probes to detect specific DNA or RNA sequences in homogeneous solution, and such measurements are required in various fields such as basic research, drug development, and medical diagnosis. Most of these fluorescent probes were designed on the basis of fluorescence characteristics such as fluorescence resonance energy transfer and excimer formation (Kolpashchikov 2010; Ranasinghe and Brown 2005; Hövelmann et al. 2012; Socher et al. 2012).

The solvatochromic effect of dyes is sensitive to changes in their external environment, and their absorption or fluorescence spectra generally respond to the environment near the dyes, resulting in marked spectral changes (Reichardt 1992; Reichardt et al. 1997). Several solvatochromic dyes have been designed, synthesized, and applied in ion and molecular sensors, electrophotography, solar cells, and nonlinear optical materials (Hisamoto et al. 1998; Arun and Ramaiah 2005; Suzuki and Yokoyama 2007; Pires et al. 2013).

The dansyl fluorophore has recently been reported to induce a solvatochromic effect, and placement of this fluorophore in the hydrophobic regions of molecules induces enhancement of fluorescence, an increase in quantum yield, and a blue shift in fluorescence (Chen and Kernohan 1967; Li et al. 1975; Hoenes et al. 1986). On the basis of these features, dansyl-based oligomers have been developed previously. Dansyl-modified nucleoside phosphoramidites derived from a cytidine derivative or C-8 position of a purine have been used to label these ONTs at internal as well as terminal positions (Misra et al. 2004; Devender et al. 1990; Yamana et al. 1997). In these dansyl-conjugated nucleosides, the base moiety plays a role in forming base pairs with a complementary sequence, which is very useful for designing perfectly matched or mismatched probes. However, the literature contains little information

on the direct interaction of the fluorophore with the base portion, which means that the solvatochromic effect of the dansyl fluorophore has not been exploited.

We first describe here the synthesis of dansyl amidite units (Fig. 4) and the preparation of ONTs, as shown in Fig. 3 (Suzuki et al. 2013). Second, we show that dansyl-modified ONTs can induce changes in fluorescence spectra in response to structural changes in ONTs.

2 Dependence of Fluorescence Properties of Dansyl Carbamate Monomer on Solvent Polarity

Before the investigation of the fluorescent characteristics of ONTs containing dansyl fluorophore, we firstly observed the solvation effect on the fluorescent spectral change of the dansyl fluorophore in a homogeneous solution system. As a monomeric fluorescent compound, ethyl 2-(5-(dimethylamino)naphthalene-1-sulfonamide)ethyl carbamate (compound 5) was synthesized from compound 1 via three steps as shown in Fig. 1, and we have examined the fluorescence spectrum of the dansylcarbamate monomer dissolved in binary solvent mixture ($CHCl_3$: MeOH = 1: 1 v/v, MeOH, MeOH: H_2O = 1: 1 v/v which are mixture of polar and nonpolar solvents).

An increase in fluorescence intensity and blue shifts of the emission maxima were observed with increasing solvent hydrophobicity, as shown in Fig. 2. As a result, the fluorescence intensity of the dansylcarbamate monomer depended on the external environment around the fluorescent dye; in addition, these results indicate that the introduction of the dansyl fluorophore onto ONTs is useful for monitoring duplex formation.

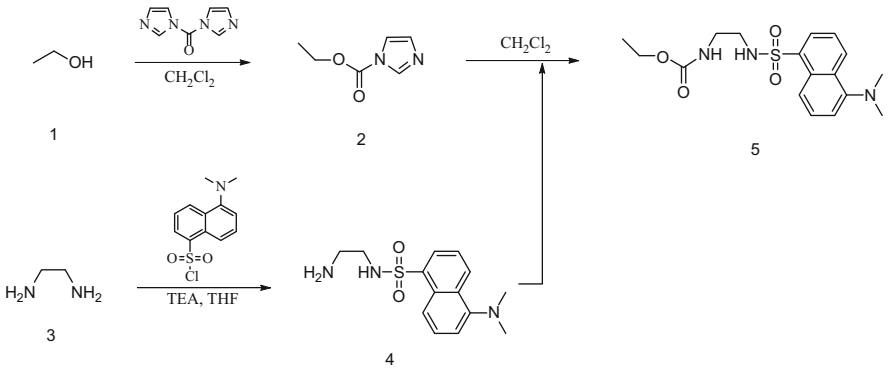

Fig. 1 Method for the synthesis of monomeric dansylcarbamate

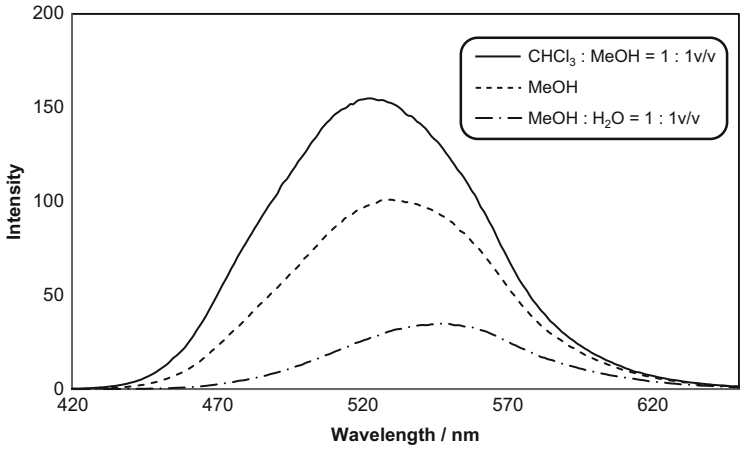

Fig. 2 Fluorescence spectra of dansylcarbamate in various solvents [dansylcarbamate] = 10 μM. Excitation wavelength: 350 nm

3 Synthesis of Phosphoramidite Containing Dansyl Fluorophore and Fluorescent ONTs

A general method for the preparation of dansyl amidite units (D_S-amidite and D_R-amidite) with S- and R-configurations to synthesize fluorescent ONTs (Fig. 3) is outlined in Fig. 4 (Suzuki et al. 2013). Details of the synthetic methods for the preparation of D_S-amidite are as follows: to a solution of compound 6 (3.4 mmol) in 50 mL of dry CH_2Cl_2, N,N′-carbonyldiimidazole (3.7 mmol) was added. The mixture was then stirred for 3 h under an argon atmosphere at room temperature. The solution was washed with water, dried over Na_2SO_4, and then evaporated in vacuo. The product was purified by silica gel column chromatography to give compound 7.

To a solution of compound 4 (1.70 mmol), which was synthesized by the reaction between compound 3 and dansyl chloride as shown in Fig. 1, in 20 mL of dry CH_2Cl_2, compound 7 (2.04 mmol) was added, and the reaction mixture was then stirred for 12 h under an argon atmosphere at room temperature. After removal of the solvent, the product was purified by column chromatography (SiO_2, *n*-hexane:ethylacetate = 2: 3 v/v) to give compound 8.

A solution of compound 8 (0.3 g) in a mixture of acetic acid (10 mL) and water (2.5 mL) was stirred for 6 h at 60 °C. The solvent was evaporated in vacuo, and the residue was dissolved in ethylacetate, washed with water, and then dried over Na_2SO_4. After removal of the solvent, the product was purified by silica gel column chromatography to obtain compound 9.

Compound 9 (1.61 mmol) was dried by addition and evaporation of toluene and pyridine. After addition of 4,4′-dimethoxytrityl chloride (1.93 mmol) and pyridine

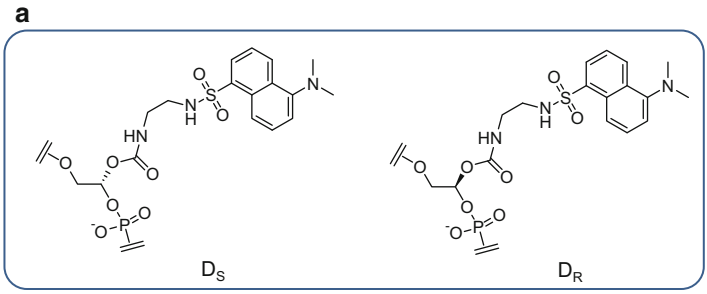

Fig. 3 (**a**) Structure of the dansyl unit (D) in an ONT. (**b**) Sequences of ONTs. Internally dansyl-labeled ONTs (I-D_S) have a complementary sequence with II-X and III. X in II-X indicates dA, dG, dC, or T

(15 mL), the mixture was stirred for 6 h at room temperature under argon atmosphere. The excess amount of 4,4′-dimethoxytrityl chloride was quenched with methanol, and the solvent was evaporated in vacuo. The residue was purified by silica gel column chromatography, and compound 10 was obtained.

Compound 10 (0.95 mmol) was dried by addition and evaporation of toluene and pyridine. After addition of DIEA (2.85 mmol), dry CH_2Cl_2 (10 mL), and 2-cyanoethyl-*N*,*N*,*N*′,*N*′-tetraisopropyl chlorophosphoramidite (1.14 mmol), the reaction mixture was stirred for 6 h at room temperature under argon atmosphere. After complete consumption of starting material, MeOH (2.0 mL) was added, and the solution was washed with water and then dried over Na_2SO_4. After removal of the solvent, the product was purified by silica gel column chromatography to give D_S-amidite.

D_R-amidite was synthesized from compound 11 as described in the method of the above D_S-amidite. The characterization results of all compounds were performed by nuclear magnetic resonance (NMR) and mass spectrometry analyses.

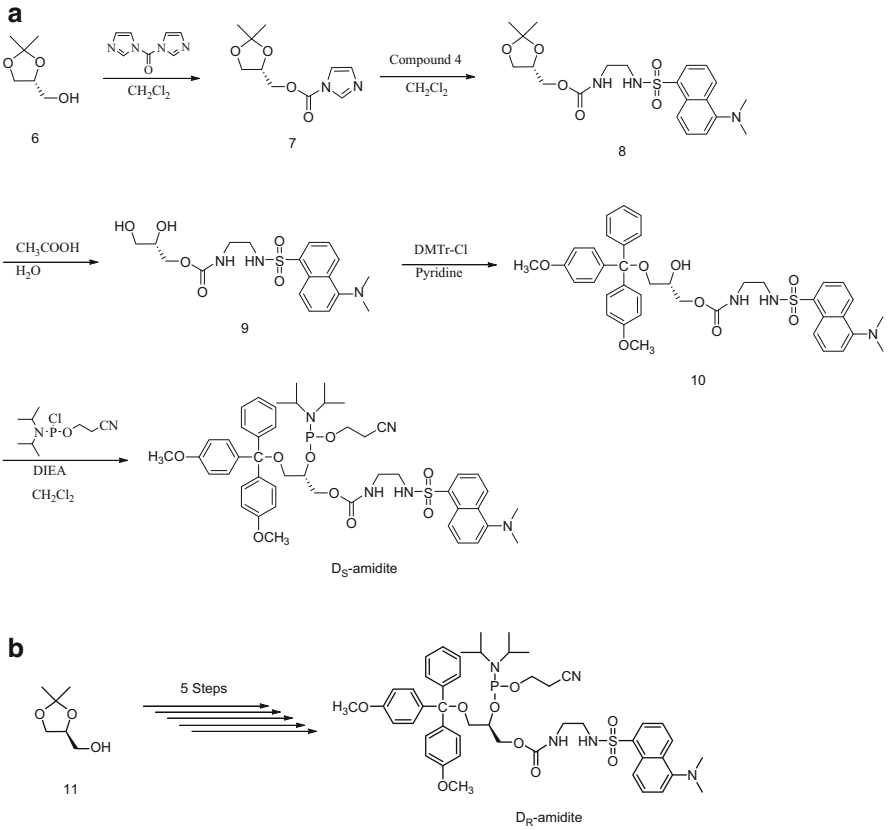

Fig. 4 Method for the synthesis of dansyl-modified phosphoramidite: (*S*)-configuration (**a**) and (*R*)-configuration (**b**)

4 Preparation of Dansyl-Modified ONTs

All ONTs were chemically synthesized via the dimethoxytrityl (DMT)-ON mode using standard phosphoramidite chemistry. Cleavage from the CPG support and deprotection of the ONTs were carried out by incubating the CPG in concentrated ammonium hydroxide (2 mL) at 55 °C for 16 h. After the synthesis, the DMT-ONTs were purified as described in our previous report (Komatsu et al. 2008). A typical HPLC chromatogram and the retention times of the fluorescently labeled oligomers are shown in Fig. 5.

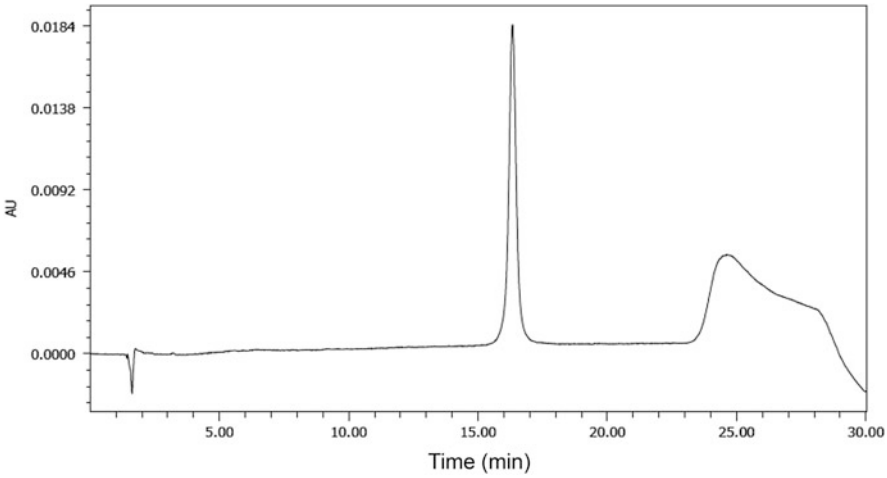

Fig. 5 Reverse-phase HPLC chromatogram for the purification of fluorescent-labeled ONT ($I\text{-}D_S$). $I\text{-}D_s$ was eluted at 16.3 min

5 Fluorescence Properties of Dansyl-Modified ONTs by Duplex Formation

To study the in vitro photophysical properties of internally dansyl-labeled ONTs ($I\text{-}D_S$), we first investigated the excitation and emission spectra of $I\text{-}D_S$ in 250 mM phosphate buffer (pH 7.0) and 10 mM NaCl at 25 °C. Figure 6 shows typical excitation and emission spectra of $I\text{-}D_S$. $I\text{-}D_S$ exhibited an excitation maximum at 350 nm, which was monitored at the emission maximum of 535 nm; in addition, a large Stokes shift (185 nm) was observed. This result is consistent with the typical excitation and emission maxima of the dansyl fluorophore (Chen and Kernohan 1967; Li et al. 1975; Hoenes et al. 1986).

The fluorescence spectra of $I\text{-}D_S$ was measured after hybridization with four complementary 35-base DNA (II-X) with base X (X = dA, dG, dC, or T) opposite the D_S. The duplexes were prepared as follows: the mixture solution containing equimolar amounts (1.5 nmol) of $I\text{-}D_S$ and the target ONT were heated to 90 °C for 5 min, slowly cooled to room temperature, and then maintained at 0 °C for 2 min. The typical fluorescence spectra and relative fluorescence intensities of $I\text{-}D_S$ before and after duplex formation are shown in Fig. 7. The fluorescence intensities of the duplexes between $I\text{-}D_S$ and II-A, -T, and -C slightly increased (1.2- to 1.8-fold) compared with the intensity of a single strand. Note that, however, the $I\text{-}D_S$/II-G duplex exhibited an approximately threefold increase in fluorescence intensity and its emission maximum blue shifted 15 nm. A photograph of the $I\text{-}D_S$ solution before and after duplex formation is shown in Fig. 8. The strongest green emission of base pair $I\text{-}D_S$/II-G was also visually apparent under UV irradiation. This was because the fluorescence intensity of the dansyl fluorophore strongly depends on its neighboring environment and factors such as hydrophobicity and hydrophilicity with

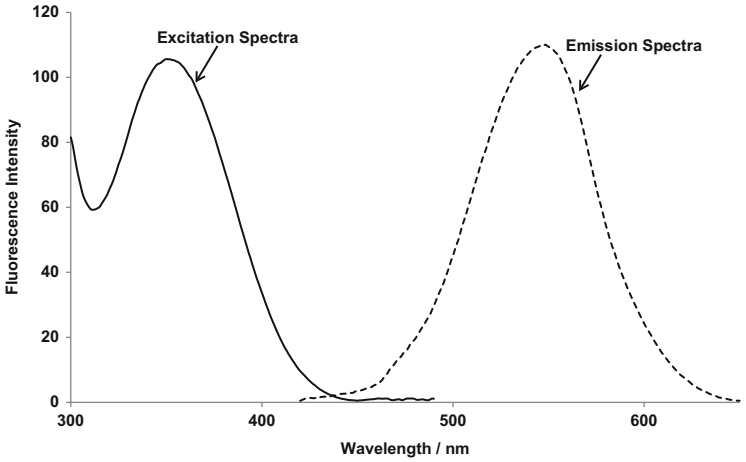

Fig. 6 Excitation and emission spectra of I-D_S [I-D_S] = 500 pmol. Solvent: 250 mM phosphate buffer (pH 7.0), 10 mM NaCl. Excitation wavelength: 350 nm. Monitored wavelength: 545 nm

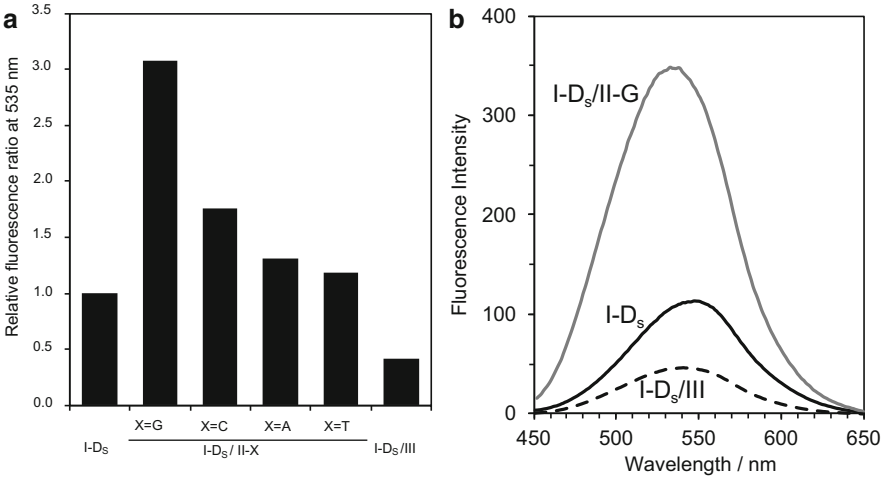

Fig. 7 Relative fluorescence intensities of I-D_S before and after duplex formation (**a**) and typical fluorescence spectra of I-D_S and its duplexes (**b**) [I-D_S] = [II-X] = [III] = 500 pmol. Solvent: 250 mM phosphate buffer (pH 7.0), 10 mM NaCl. Excitation wavelength: 350 nm. The ratio of (fluorescence intensity before and after duplex formation at 535 nm)/(fluorescence intensity before duplex formation at 535 nm) is plotted on the *y*-axis in Fig. 7(**a**)

blue shift of emission maximum. The duplex formation by II-G created the hydrophobic environment around the dansyl fluorophore in I-D_S, resulting in an increase in the fluorescence quantum yield of I-D_S. This result is consistent with that of the monomeric dansylcarbamate study, as shown in Fig. 2; that is, the fluorescence

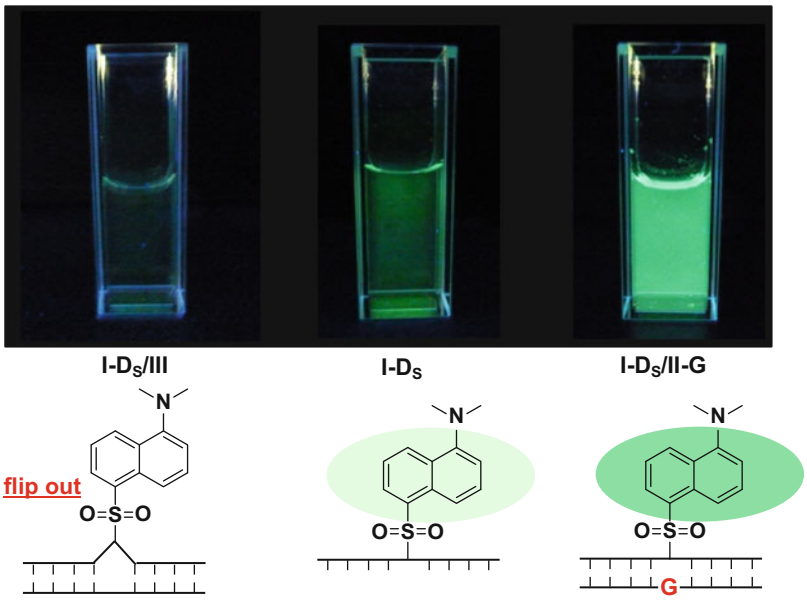

Fig. 8 Photograph of the I-D_S solution before and after duplex formation with II-G or III

enhancement resulting from hybridization with II-G was derived from the solvatochromic effect, indicating that the dansyl fluorophore was transferred into a less polar environment formed by guanosine residues. Importantly, a single-strand I-D_S exhibited only low background fluorescence, which is necessary for the highly sensitive detection of ONTs.

We next examined whether the aforementioned characteristic emission profile was also observed in the DR-unit ONT. Fluorescence analysis indicated that I-D_R exhibited the same fluorescence profile upon hybridization with II-X, as shown in Fig. 9, and confirmed that the isomers exhibited the same fluorescence properties.

To observe the fluorescence patterns of duplexes, we plotted the fluorescence intensities of I-D_S at 535 nm as a function of II-X concentration. I-D_S (500 pmol) in 250 mM phosphate buffer (pH 7.0) and 10 mM NaCl was mixed with various concentrations of targeting ONTs (0–500 pmol). Typical calibration graphs of fluorescence intensity vs. the concentration of target ONTs were prepared until equimolar concentrations of complementary strands were reached, as shown in Fig. 10. Significant enhancement in the fluorescence intensities was consistently observed when II-G concentration was increased; after the equimolar concentration was reached, no further increase in fluorescence intensity was observed.

To examine whether a strong increase in the fluorescence intensity of I-D_S was observed in the case of duplex formation with II-G, the effect of the neighboring base on the fluorescence properties of D_S was investigated using pentamers (D_S-X2, Fig. 11a), where D_S was flanked by 2 X bases (X = A, G, C, or T). Fluorescence measurements at 550 nm of pentamers (D_S-A2, D_S-C2, D_S-T2) with adenylic,

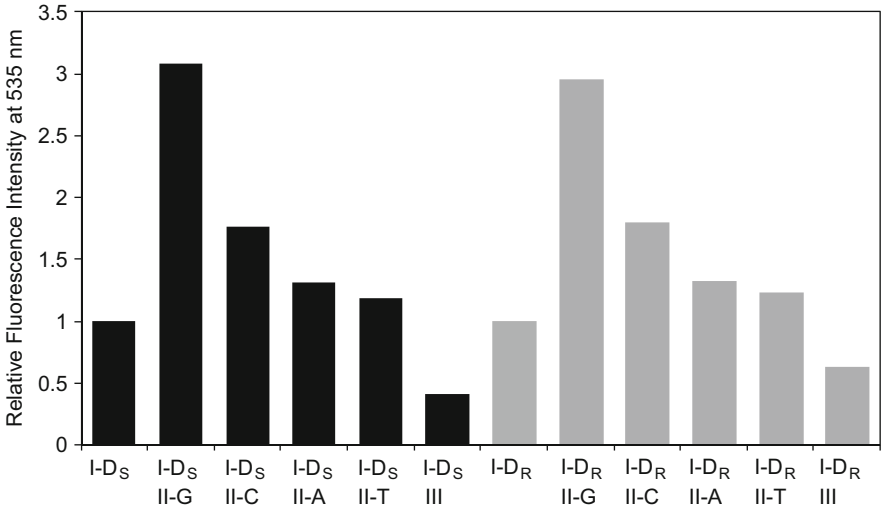

Fig. 9 Relative fluorescence intensities of I-D_S and I-D_R before and after duplex formation at 535 nm [I-Ds] = [I-D_R] = [II-X (X = A, T, G, C)] = [III] = 500 pmol. Solvent: 250 mM phosphate buffer (pH 7.0), 10 mM NaCl. Excitation wavelength: 350 nm. The ratio of (fluorescence intensity before and after duplex formation at 535 nm)/(fluorescence intensity before duplex formation at 535 nm) is plotted on the *y*-axis in Fig. 9

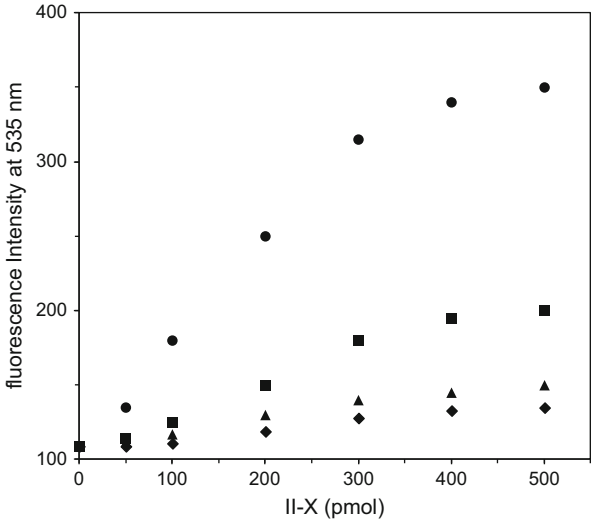

Fig. 10 Fluorescence intensity of I-D_S at 535 nm after duplex formation with various target DNA (II-X) at different concentrations [I-D_S] = 500 pmol. ●: X = G; ■: X = C; ▲: X = A; ◆: X = T. Solvent: 250 mM phosphate buffer (pH 7.0), 10 mM NaCl. Excitation wavelength: 340 nm

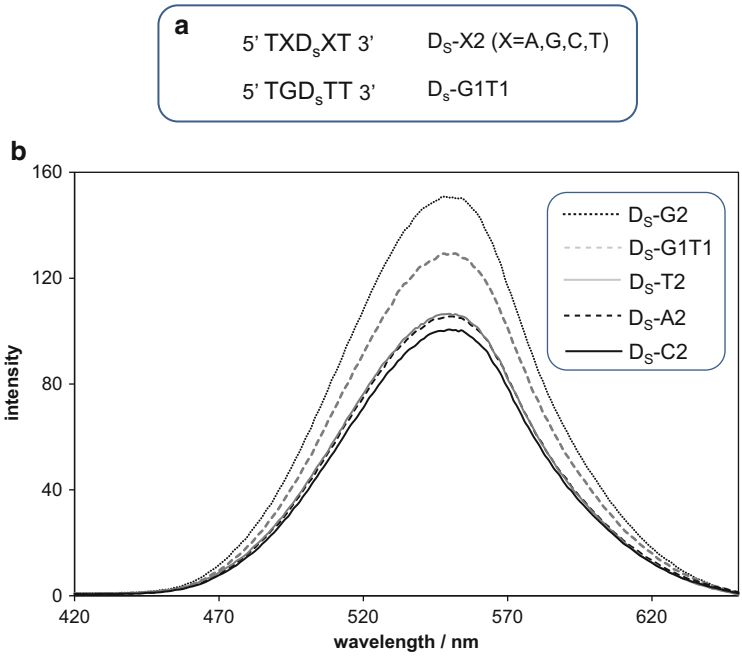

Fig. 11 Sequences of synthesized fluorescent pentamers (**a**) and fluorescence spectra of various fluorescent pentamers (**b**). [Pentamers] = 500 pmol. Solvent: 250 mM phosphate buffer (pH 7.0), 10 mM NaCl. Excitation wavelength: 350 nm

cytidylic, or thymidylic acids adjacent to D_S showed almost equal fluorescence intensities, as shown in Fig. 11b. However, the emission intensities of D_S-G2 increased in comparison with those of other pentamers. The intensity of D_S-G1T1 with a single guanosine fell between those of D_S-G2 and D_S-T2. These results indicate that the fluorescence intensities of the D_S residue could also be enhanced by flanking guanine bases, similar to the enhancement observed for a guanine base on the opposite strand.

To investigate whether the dansyl residue directly interacted with the opposite guanosine, we conducted thermal denaturation studies of I-D_S with II-X. Thermal denaturation experiments of all duplexes (1.5 μM) were conducted in 10 mM sodium cacodylate buffer (pH 7) containing 10 mM NaCl. The solutions were heated at 90 °C for 3 min and then gradually cooled to anneal each duplex. UV absorbance of these duplexes was measured, and the Tm values were calculated from their plots. The spectra of all duplexes exhibited typical sigmoidal curves; the Tm values of each duplex are summarized in Table 1. I-D_S/II-G exhibited a Tm value slightly higher than those of other duplexes, suggesting that direct interaction, such as stacking, might exist between D_S and a guanine base on the opposite strand to form a more stable duplex than those formed with other bases. The Tm values of the duplexes based on I-D_R were approximately the same as those of duplexes based on I-D_S, consistent with the fluorescence spectrometry results.

Table 1 Melting temperatures of the ONT duplexes

Fluorescent DNA	Target DNA	Tm (°C)
I-D_S	II-A	37.1
	II-G	38.5
	II-C	37.3
	II-T	37.1
I-D_R	II-A	37.7
	II-G	38.6
	II-C	37.5
	II-T	37.0

2-Aminopurine is a well-studied probe that increases fluorescence intensity in a base-flipping structure (Holz et al. 1998; Neely et al. 2005). In contrast, the dansyl residue is expected to reduce the emission in an outward-flipped DNA helix because the dansyl fluorophore is transferred into a polar environment through duplex formation. To construct a D_S-flipping structure, we prepared ONT III, which had a sequence without the X base opposite to the D_S residue (Fig. 3). Fluorescence spectra of I-D_S were monitored before and after hybridization with III in an equimolar mixture. As shown in Fig. 7, I-D_S remarkably reduced the emission maximum at 535 nm to a numerical value of 46 from an intensity of 107 in the case of single strand I-D_S. The decrease in fluorescence (I-D_S/III) was observed visually under UV irradiation, as shown in Fig. 8 (left). This result was likely due to the dansyl residue being transferred to a hydrophilic environment because of the D_S-flipping structure.

There are various RNA species, and the importance of their detection has been increasing in the biological and biomedical research fields (Dirks and Tanke 2006; Czaplinski and Singer 2006; Shav-Tal et al. 2004). In particular, microRNAs (miRNAs) of 17–27 nucleotide lengths are known to play important roles in various physiological processes, including cell differentiation and development, by controlling gene expression at the posttranscriptional level (Bartel 2009). To take advantage of the aforementioned DNA study, we examined the fluorescence properties of the D_S residue through hybridization with RNA targets and prepared RNAs of r-II-X (X = A, G, as shown in Fig. 12a) and r-III, whose sequences corresponded with cognate DNAs (II-X and III). The fluorescence spectra of I-D_S were measured in the presence or absence of complementary strands (r-II-X or r-III). A marked enhancement (approximately 3.32-fold) with a 10-nm blue shift was observed in the case of I-D_S/r-II-G (black solid line, Fig. 12), whereas the addition of r-III significantly reduced the fluorescence intensities (0.38-fold) compared with those of single-strand I-D_S, as shown in Fig. 12b, c. This result was consistent with those obtained using DNA targets, and these responses were stronger than those of DNA targets. The D_S unit was confirmed to be effectively sensitive in not only DNA–DNA interaction but also DNA–RNA interaction.

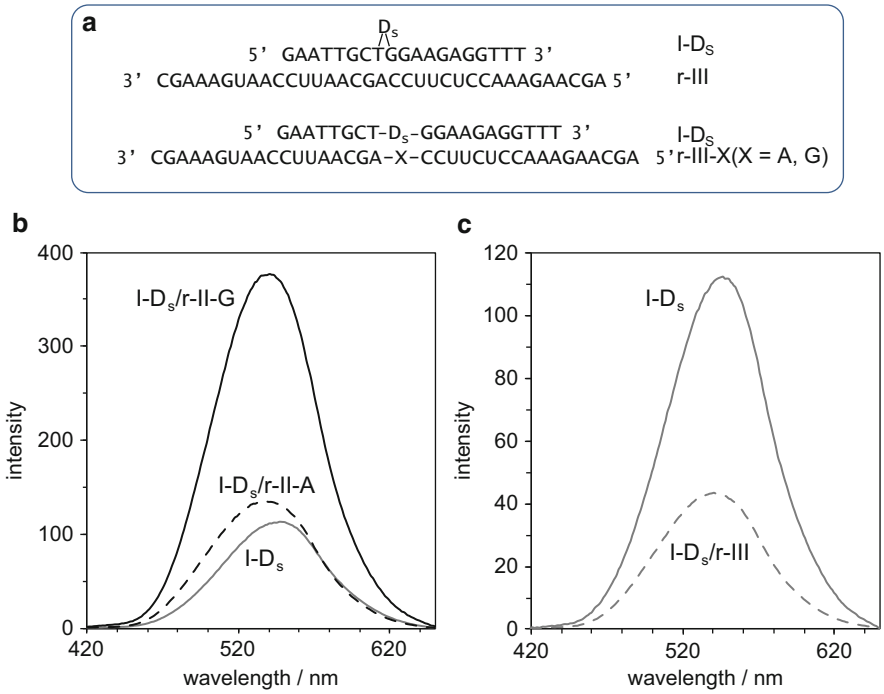

Fig. 12 Sequences of synthesized RNA (X in r-III-X indicates A, G (**a**)) and fluorescence spectra of I-D_S after duplex formation with target RNA. (**b**) I-Ds, gray solid line; I-Ds/r-II-A, dotted line; I-Ds/r-II-G, black solid line. (**c**) I-Ds, gray solid line; I-Ds/r-III, gray dotted line. [I-D_S] = [RNA] = 500 pmol. Solvent: 250 mM phosphate buffer (pH 7.0), 10 mM NaCl. Excitation wavelength: 350 nm

6 Conclusions

In conclusion, we described the synthesis of a dansyl amidite unit that can be introduced into designated sites of ONTs. Because the fluorophore unit has no nucleobase, it can be used to directly evaluate the fluorescence features that result from hybridization with DNA or RNA. The fluorophore characteristically exhibited considerable enhancement in fluorescence intensity upon hybridization with complementary DNA or RNA with a guanosine opposite to the fluorophore. In contrast, the fluorescence intensity was markedly reduced in the dansyl-bulged duplex. We observed that the fluorophore sensitively responds to local structures of polynucleotides, indicating the ability to control the enhancement and reduction of fluorescence. Hence, given the simple structure of the dansyl unit, it can be a useful probe for DNA or RNA detection in various genetic assays.

Acknowledgments We thank Ms. Keiko Kowata (AIST) for her technical assistance and Dr. Eiko Ohtsuka and Dr. Naoshi Kojima (AIST) for their helpful discussions.

References

Arun KT, Ramaiah D (2005) Synthesis and spectroscopic investigations of a few amphiphilic squaraine dyes. J Phys Chem A 109:5571–5578

Astakhova IK, Kumar TS, Campbell MA et al (2013) Branched DNA nanostructures efficiently stabilised and monitored by novel pyrene-perylene 2′-alpha-L-amino-LNA FRET pairs. Chem Commun 49:511–513

Bartel DP (2009) MicroRNAs: target recognition and regulatory functions. Cell 136:215–233

Benitez JJ, Topolancik J, Tian HC et al (2012) Microfluidic extraction, stretching and analysis of human chromosomal DNA from single cells. Lab Chip 12:4848–4854

Chen RF, Kernohan JK (1967) Combination of bovine carbonic anhydrase with a fluorescent sulphonamide. J Biol Chem 242:5813–5823

Czaplinski K, Singer RH (2006) Pathways for mRNA localization in the cytoplasm. Trends Biochem Sci 31:687–693

Devender S, Vijayanti K, Ganesh KN (1990) Oligonucleotides, part 5^{+}: synthesis and fluorescence studies of DNA oligomers $d(AT)_5$ containing adenines covalently linked at C-8 with dansyl fluorophore. Nucleic Acids Res 18:3339–3345

Dirks RW, Tanke HJ (2006) Advances in fluorescent tracking of nucleic acids in living cells. Biotechniques 40:489–496

Dumont SN, Lazar AJ, Bridge JA et al (2012) PAX3/7-FOXO1 fusion status in older rhabdomyosarcoma patient population by fluorescent in situ hybridization. J Canc Res Clin Oncol 138: 213–220

Erlich HA, Gelfond D, Srinsky JJ (1991) Recent advances in polymerase chain reaction. Science 252:1643–1651

Hisamoto H, Tohma H, Yamada T et al (1998) Molecular design, characterization, and application of multi-information dyes for multi-dimensional optical chemical sensing. Molecular design concepts of the dyes and their fundamental spectral characteristics. Anal Chim Acta 373: 271–289

Hoenes G, Houser M, Pfleiderer G (1986) Dynamic total fluorescence and anisotropy decay study of the dansyl fluorophore in model compounds and enzymes. Photochem Photobiol 43: 133–137

Holz B, Klimasauskas S, Serva S et al (1998) 2-Aminopurine as a fluorescent probe for DNA base flipping by methyltransferases. Nucleic Acids Res 26:1076–1083

Hövelmann F, Bethge L, Seitz O (2012) Single labeled DNA FIT probes for avoiding false-positive signaling in the detection of DNA/RNA in qPCR or cell media. ChemBioChem 13:2072–2081

Ke GL, Wang CM, Ge Y et al (2012) L-DNA molecular beacon: a safe, stable, and accurate intracellular nano-thermometer for temperature sensing in living cells. J Am Chem Soc 134: 18908–18911

Kolpashchikov DM (2010) Binary probes for nucleic acid analysis. Chem Rev 110:4709–4723

Komatsu Y, Kojima N, Sugino M et al (2008) Novel amino linkers enabling efficient labeling and convenient purification of amino-modified oligonucleotides. Bioorg Med Chem 16:941–949

Li YH, Chan LM, Tyer L et al (1975) Solvent effects on the fluorescence of 1-(dimethylamino)-5-naphthalenesulfonic acid and related compounds. J Am Chem Soc 97:3118–3126

Mirzabekov AD (1994) DNA sequencing by hybridisation a mega sequencing method and a diagnostic tool? Trends Biotechnol 12:27–32

Misra A, Mishra S, Misra K (2004) Synthesis and fluorescence studies of multiple labeled oligonucleotides containing dansyl fluorophore covalently attached at 2′-terminus of cytidine via carbamate linkage. Bioconjugate Chem 15:638–646

Neely RK, Daujotyte D, Grazulis S et al (2005) Time-resolved fluorescence of 2-aminopurine as a probe of base flipping in M.HhaI–DNA complexes. Nucleic Acids Res 33:6953–6960

Pires PAR, Imran M, Loffredo C et al (2013) Solvatochromism of 2-(N, N-dimethylamino)-7-nitrofluorene and the natural dye β-carotene: application for the determination of solvent dipolarity and polarizability. J Phys Org Chem 26:280–285

Ranasinghe RT, Brown T (2005) Fluorescence based strategies for genetic analysis. Chem Commun 28:5487–5502

Reichardt C (1992) Solvatochromism, thermochromism, piezochromism, halochromism, and chiro-solvatochromism of pyridinium N-phenoxide betaine dyes. Chem Soc Rev 21:147–153

Reichardt C, Asharinf S, Blum A et al (1997) First hyperpolarizability of the heterocyclic sulfonamides for Langmuir−Blodgett films by calculation, solvatochromism, and hyper-rayleigh scattering. J Phys Chem B 101:8967–8974

Ryazantsev DY, Tsybulsky DA, Prokhorenko IA et al (2012) Two-dye and one- or two-quencher DNA probes for real-time PCR assay: synthesis and comparison with a TaqMan™ probe. Anal Bioanal Chem 404:59–68

Schulze H, Barl T, Vase H et al (2012) Enzymatic on-chip enhancement for high resolution genotyping DNA microarrays. Anal Chem 84:5080–5084

Shav-Tal Y, Darzacq X, Shenoy SM et al (2004) Dynamics of single mRNA in nuclei of living cells. Science 304:1797–1800

Singh Y, Pandey A, Dubey KK et al (2000) Fluorescence resonance energy transfer: a diagnostic tool in oligonucleotide therapy. Curr Sci 78:487–492

Socher E, Knoll A, Seitz O (2012) Dual fluorophore PNA FIT-probes−extremely responsive and bright hybridization probes for the sensitive detection of DNA and RNA. Org Biomol Chem 10:7363–7371

Suzuki Y, Yokoyama K (2007) A protein-responsive chromophore based on squaraine and its application to visual protein detection on a gel for SDS-PAGE. Angew Chem Int Ed 46: 4097–4099

Suzuki Y, Kowata K, Komatsu Y (2013) Development of dansyl-modified oligonucleotide probes responding to structural changes of a duplex. Bioorg Med Chem Lett 23:6123–6126

Tan XH, Chen WJ, Lu S et al (2012) Molecular beacon aptamers for direct and universal quantitation of recombinant proteins from cell lysates. Anal Chem 84:8272–8276

Yamana K, Ohashi Y, Nunota K et al (1997) Synthesis, binding and fluorescence properties of oligonucleotide derivatives having a dansyl fluorescence label attached to the 2′-position of a ribonucleoside. Tetrahedron 53:4265–4270

Fluorescent Nucleic Acid Analogues in Research and Clinical Diagnostics

Hanlee Ji and Kira Astakhova

Contents

Abstract The synthesis of modified nucleic acid analogues has dramatically improved genomic research and point-of-care diagnostics. Much of this progress has come from the preparation of artificial DNA and RNA molecules that are used in oligonucleotide probes for nucleic acid recognition. To date, nucleoside, nucleotide, and oligonucleotide analogues, as well as compounds interacting with nucleic acids, are very diverse. They are used for multiple applications in clinical diagnostics, therapy, research on molecular recognition, and studies of human diseases. Information on the target sequence within a genome and robust synthetic technologies together allow preparation of a complementary oligonucleotide sensor prior to detection or while running an assay by an enzymatic reaction.

For this review, we provide a summary of the major enzymatic and nonenzymatic related applications (i.e., molecular assays and diagnostics) of

H. Ji
The Division of Oncology, Stanford School of Medicine, Stanford University, 269 Campus drive, 94305-5151 Stanford, CA, USA

K. Astakhova (✉)
Department of Physics, Chemistry and Pharmacy, Nucleic Acid Center, University of Southern Denmark, Campusvej 55, 5230 Odense M, Denmark
e-mail: ias@sdu.dk

V.A. Erdmann et al. (eds.), *RNA and DNA Diagnostics*, RNA Technologies,
DOI 10.1007/978-3-319-17305-4_8

novel synthetic fluorescent probes. We will discuss fluorophores and their interactions with the nucleic acid complex environment and determine the main parameters of quantitative polymerase-chain reaction (qPCR), Illumina sequencing, fluorescent single-nucleotide polymorphism (SNP) microarray, homogeneous hybridization assays, etc. We also demonstrate that the underlying chemistry of these nucleotide analogues determine a diagnostic assay's performance and its availability and price on the market. Thus, demonstrating the connection between the chemistry of nucleic acid analogues, research, and clinical diagnostics is the main objective of this chapter as well as the hallmark of our collaborative efforts. This review is targeted for a broad audience, including chemists, molecular biologists, and clinical researchers working with various aspects of nucleic acids and their analogues for natural sciences, biomedical research, and clinical applications.

Keywords Clinical science • Diagnostics • Fluorescence • Hybridization assay • Nucleic acids • PCR • Sensor • Sequencing

1 Introduction

Current methods for DNA/RNA diagnostics can be divided in two large categories of assays: (1) enzymatic high-throughput assays and (2) enzyme-free assays that are portable and less expensive (Khan 2014; Lyubchenko et al. 2011; Astakhova 2014; Turner 2013). The former methods typically apply enzymes and state-of-the-art equipment in order to achieve a necessary degree of sensitivity and specificity of diagnostics, e.g., sequencing, polymerase-chain reaction PCR, and microarrays. Due to a high cost of enzymatic techniques which often lack reproducibility and robustness, the development of enzyme-free methods is of increasing interest in industry and academia (Astakhova 2014). Incorporation of chemically modified nucleotide scaffolds into nucleic acids to form ultrabright fluorescent assemblies is an innovative area with great promise for biomedical applications including rapid non-expensive and reliable diagnostics of human diseases. Their intrinsic biorecognition properties combined with advanced properties of modified scaffolds such as locked nucleic acids (LNAs) provide opportunities to develop new nano-materials and sensors for the enzyme-free diagnostic settings (Astakhova and Wengel 2014).

Fluorescence detection is the method most frequently used among nucleic acid assays due to the extraordinary sensitivity (Astakhova and Wengel 2014). Chemical structure and optical properties of the fluorophore determine applicability of a "nucleic acid sensor" and performance (e.g., sensitivity and specificity) of any given assay (Lakowicz 2006). Generally, we distinguish five major classes of fluorescent sensors for nucleic acid research and diagnostics: (1) intercalating dyes, (2) dyes covalently attached to nucleoside triphosphates, (3) terminally labeled fluorescent oligonucleotide probes, (4) fluorescent nucleobase analogues,

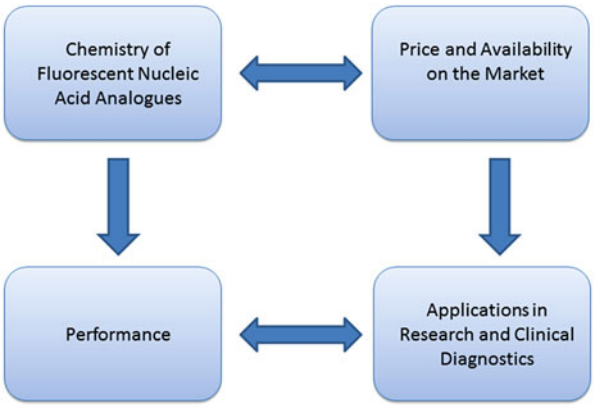

Fig. 1 Connection between the chemistry of fluorescent nucleic acid analogues and their applications in research and clinical diagnostics

and (5) groove binders to double-stranded DNA. We provide an overview of each class with emphasis on their synthesis and applications in clinical research. In the final part of the chapter, we compare all classes of sensors and discuss future perspective of the field. We emphasize advantages of stronger connection between nucleic acid chemistry and clinical sciences in order to benefit both research fields. We also discuss the potential of nucleic acid-based sensors and their diverse configurations and performance (Fig. 1).

2 Intercalating Dyes

This type of dyes can be applied in the detection of nucleic acid hybridization by various methods including PCR, dPCR, and ddPCR described below. Intercalating dyes are flat aromatic molecules which upon binding localize within the nucleobase stack of the double helix (Fig. 2). Typically, dye intercalation results in increased thermal stability of the double helix and altered fluorescence signal of the dye (Glazer and Rye 1992; Berndl and Wagenknecht 2009). Intercalators can be either attached covalently to the nucleic acid sequence or interact with the duplex non-covalently (Rye and Glazer 1995; Karlsen et al. 2012). Non-nucleosidic analogues of nucleic acids such as IPN, UNA, and TINA contain a covalently attached intercalating dye within the oligonucleotide probe which is labeled during oligonucleotide synthesis or postsynthetically (Filichev and Pedersen 2005; El-Sayed et al. 2012; Stadler et al. 2011). The resulting probes were found to be useful in simultaneous targeting and detection of double-stranded DNA in various fashions. Pyrene and (phenylethynyl)pyrenepolyaromatic hydrocarbon dyes attached to TINA within triplex-forming oligonucleotides (TFOs) bind target dsDNA with high affinity, giving increased fluorescence signal. The advantage of TINA and other non-nucleosidic scaffolds is a relatively simple synthetic route. However, the low quantum yield of pyrene and other dyes is additionally decreased by

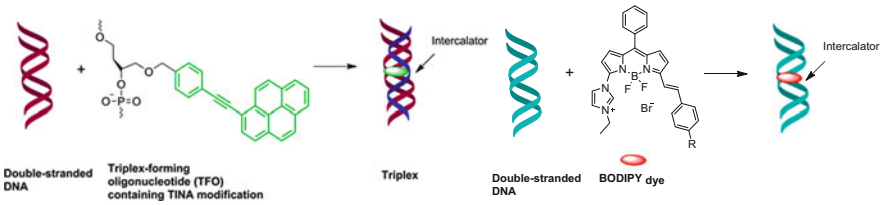

Fig. 2 Representative intercalating dyes TINA and BODIPY binding double-stranded DNA via covalent and non-covalent mode, respectively

nucleobases; this results in the overall decreased sensitivity of the assay (Astakhova and Wengel 2014).

Non-covalently intercalating dyes represent a broad class of organic compounds (e.g., ethidium bromide (EB), perylene bisimide (PBDI), BODIPY, SYBR Green, and the recently introduced EvaGreen dyes), which change fluorescence properties upon intercalation into double-stranded nucleic acids (Xu et al. 2014; Ikeda et al. 2009; Brzezinska et al. 2012; Zhao et al. 2013; Morgan et al. 1979; Ahn et al. 1996; Miotke et al. 2014). The main advantage of this class of dyes is their low cost and higher availability compared to other nucleoside-based sensors due to shorter synthetic route. Intercalating dyes find broad application in detection and quantification of nucleic acids, as well as therapeutics. For example, Xu et al. synthesized a water-soluble PBDI and used it for nuclear intercalation and suppression of cancer cells and tumors (Xu et al. 2014). Previously applied intercalating dyes have the disadvantage of high toxicity (e.g., EB). However, they have been replaced with low toxic analogues such as EvaGreen dye (EG) (Mao et al. 2007).

Assays with intercalating dyes can be used to detect clinically relevant single-nucleotide replacements or polymorphisms (SNPs). High specificity occurs when no double strand is formed. Limiting double-strand formation requires additional design considerations and is not always successful. In spite of that, intercalating dyes are applied in various detection settings incl. qPCR and digital PCR (dPCR) (Cosa et al. 2001). dPCR is an enzyme-based diagnostic method which allows detection and quantification target DNA by individual molecular counting. dPCR partitions DNA analyte into multiple parallel PCR reactions. In the absence of the target DNA, no signal is observed (dPCR usually utilizes terminally labeled TaqMan probes described below). dPCR allows quantification of DNA at the single-molecule level without the need for external standards or controls. AS has been recently demonstrated with intercalating dyes, and integrated technologies using droplets and fluidics have led to a technology referred to as droplet digital PCR (ddPCR) (Pinheiro et al. 2012). In ddPCR, each amplification reaction is performed within microscopic emulsion-based droplets containing at most a few target molecules. As a result, ddPCR allows discrimination of mutant vs. wild-type sequences at a very low mutant abundance. This is of a particular interest for clinical research and diagnostics of diverse cancer biomarkers and viral load determination. In a recent paper, Miotke and coworkers reported detecting cancer mutations even at very low fractions with ddPCR that relied on EvaGreen dye

(Miotke et al. 2014). This was done for a series of target and reference amplicons of different lengths each distinguished and quantified independently (Miotke et al. 2014). The effectiveness of this method has been proved by examining the copy number in the proto-oncogene *FLT3* and the common V600E point mutation in *BRAF* gene. Notably, upon adjustment of applied primers, EG–ddPCR assay is able to detect a mutation comprising less than 1 % of an otherwise wild-type sample, as well as copy number changes from cancers even in the context of significant dilution with normal DNA. The authors underline that using EG dye reduces the overall cost of the ddPCR assay and increases its applicability for diverse target sequences, since no sequence optimization of TaqMan probe is needed (Miotke et al. 2014).

3 Fluorescent Nucleotide Triphosphates

Fluorescent nucleotide triphosphates (FNTPs) allow detection of nucleic acids by enzymatic methods including sequencing, microarrays, qPCR, and microscopy. FNTPs are a class of nucleoside analogues for enzymatic incorporation into oligonucleotides in vitro or in vivo (França et al. 2002; Li et al. 2003; Tsuyama et al. 2013).To prepare an FNTP, the dye can be attached either to the nucleobase or to a hydroxyl group of ribose. After the labeling, the 5′-hydroxyl group is concerted to triphosphate under standard phosphorylation conditions. Since enzymatic reactions and fluorescence detection are commonly employed in molecular assays, FNTPs represent a large sector of the overall modified nucleic acid market. Diverse FNTPs can be purchased individually or as a part of ready-to-use kits. Multiple commercial vendors also provide custom nucleotide triphosphate synthesis starting from the nucleosides made in-house, customer supplied, or purchased if it is commercially available (Fig. 3).

Sequencing and microarray assays are broadly applied in research and clinical diagnostics. Illumina sequencing is based on enzymatic elongation of a complementary strand to target using four FNTPs with specific emission wavelength for each letter (sequencing by synthesis or SBS) (Kim et al. 2011; Flaherty et al. 2012).

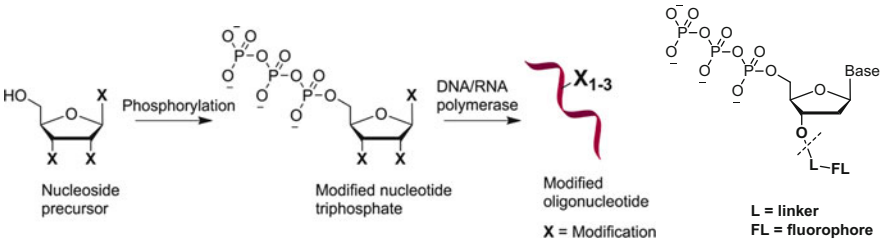

Fig. 3 Custom nucleotide triphosphate synthesis offered by TriLink BioTechnologies; general structure of FNTP terminator applied in Illumina sequencing

Each FNTP serves as a reversible terminator of elongation, and after analysis the fluorescent group is removed from 3′-OH residue allowing the growing chain to continue the elongation (Fig. 3, TINA modification). A similar principle is applied in microarray technology for nucleic acid genotyping provided by Bio-Rad (Kurg et al. 2000; Tebbutt et al. 2005). Genotyping by arrayed primer extension (APEX) is performed after PCR amplification of the target. Subsequently, the amplified target is hybridized to sequence-specific primers immobilized on a glass microarray. The primers are immobilized via 5′-end and are designed to contain a missing nucleotide opposite to SNP specific position at their 3′-end. Elongation with four different FNTPs allows detection of SNP on the 3′-end of the target.

Most gene expression studies have used bulk measurements from heterogeneous cells and tissues, which can obscure information from rare or specific cell types. By analyzing gene expression in individual cells, a more complete picture of the gene expression dynamics within heterogeneous samples can be obtained (Bengtsson et al. 2005; Raj and Tyagi 2010; Narsinh et al. 2011; Di Carlo et al. 2012). This is made possible by the development of high-resolution microscopy that can detect nucleic acids directly within individual cells. In doing this, FNTPs have garnered increase attention from researchers developing new assays. For example, modified nucleotide analogues were used to visualize HIV-1 genome during HIV-1 life cycle (Xu et al. 2013). Viral RNA within individual cells was monitored using 5-ethynyl-2′-deoxyuridine (EU). After entry into the core, the fluorescent azide of the bright Alexa Fluor dye could detect RNA through labeling of the already inserted EU by "click" azide–alkyne conjugation. Using the labeling of HIV-1 particles by this approach in cell culture, it was demonstrated how the amount of the HIV-1 RNA visualized with Alexa Fluor–EU decreases after initial HIV-1 infection of the cells. The authors underline that fluorescent microscopy combined with Alexa Fluor–EU labeling technique may provide previously unavailable quantitative information on viral nucleic acids within the host cells and virions (Xu et al. 2013).

Application in microscopy puts additional requirements to choice of fluorescent dye (Longmire et al. 2008; Gray et al. 2008; Koide et al. 2012; Stracy et al. 2014). The dye has to be photo stable and not toxic if living cells are studied. Moreover, for multiplexing opportunities, broad panel of such dyes with different excitation/emission wavelengths is required. Besides the aforementioned Alexa Fluor dyes, ATTO dyes, rhodamines, and near-IR dyes have been recently introduced, also as functionalized reagents for click chemistry (Salic and Mitchison 2008; Longmire et al. 2008; Gray et al. 2008; Koide et al. 2012; Stracy et al. 2014; Shieh et al. 2014). This opens up exciting opportunities for highly sensitive detection and studies of nucleic acids at previously unachievable resolution.

4 Terminally Labeled Oligonucleotide Probes

Terminal attachment of fluorescent dyes is a convenient method which is often applied in oligonucleotide probe design for in vitro diagnostics (qPCR, sequencing by hybridization, fluorescence in situ hybridization, or FISH) and imaging (Fig. 4).

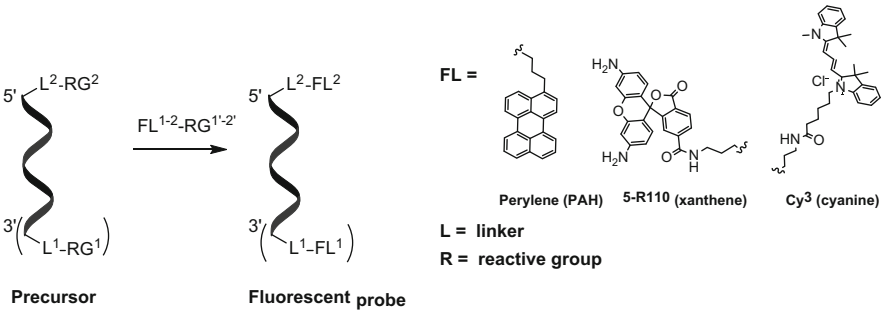

Fig. 4 General synthesis of terminally labeled oligonucleotide probes (single and double labeling)

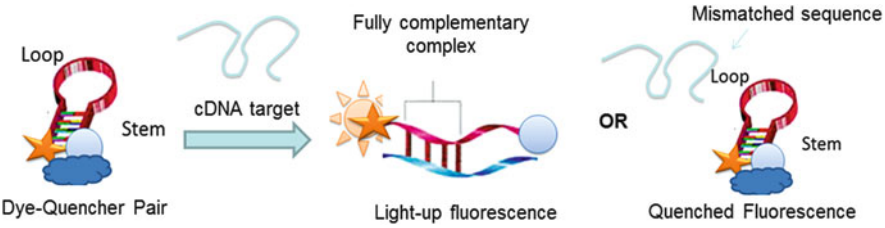

Fig. 5 Detection of SNP in viral cDNA by a molecular beacon (MB)

Chemically unstable fluorophores can be attached after oligonucleotide synthesis by different chemical reactions (Astakhova and Wengel 2013). Usually activated ester or click chemistry can be applied for the terminal attachment of fluorophores to oligonucleotides (Raddatz et al. 2002). Single- and double-labeled probes can be prepared in-house using commercially available reagents and/or kits or obtained from suppliers, although the price can be very high.

The distinctive feature of terminally labeled probes is that a target-binding region contains no fluorophore attached. Therefore, additional design parameters have to be applied to achieve sensitivity of terminally attached dyes to hybridization. An example of terminally labeled probes for nucleic acid diagnostics and research is single-stranded oligonucleotides with a stem–loop structure called **molecular beacons** (MBs; Fig. 5) (Marras et al. 2002). The loop is designed to bind a target sequence, while the stem forms by the hybridization of the arm sequences on either side of the loop sequence. The 5′- and 3′-termini of MBs are typically labeled with a fluorescent dye and its FRET pair forming a second dye or a quencher of fluorescence. Hybridization of a loop to its target forces the opening of MBs and gives increased fluorescence at the certain wavelength, since the fluorophore is moved away from the FRET acceptor/quencher. The main classes of fluorophores incorporated into molecular beacons are shown in Scheme 1. Bright cyanine and xanthene dyes are very often applied in MBs. However, they are rather expensive. Furthermore, some of the dyes are chemically and/or photo unstable.

Polyaromatic hydrocarbons have lower molar extinction values when compared to, e.g., cyanines (ε_{max} 45,000–75,000 vs. 90,000–250,000, respectively) (Lakowicz 2006; Astakhova and Wengel 2014). The high sensitivity of polyaromatic hydrocarbons to the microenvironment's structure and polarity, along with their remarkable photostability, makes them promising dyes in particular for imaging applications.

The major advantage of MBs is the possibility of multiplexing using up to 30 probes in a high-throughput approach (Barreiro et al. 2009). SNP detection using MBs is based on a competition of perfectly matched and mismatched probes for binding to a PCR template, with each probe containing different fluorescent dyes. A short stem sequence (4–8 nt) has been demonstrated as being sufficient for genotyping using MBs. Such short stems could be formed in the presence of magnesium within in vitro settings. Alternatively, MBs are applied in RT-PCR, also with a possibility of multiplexing and quantification. Disadvantages of MBs in SNP sensing are complicated sequence design, false signals due to probe degradation or binding to a mismatched target, and low sensitivity requiring amplification prior to detection (Brown et al. 2000; Kannegård et al. 2013).

The sequence diversity of genomic DNA often results in decreased specificity of standard gene targeting methods that require long oligonucleotide probes. Existing genetic variations such as SNPs and deletions may overlap with target-specific oligonucleotides, decrease the hybridization efficiency of complementary oligonucleotides, and alter fluorescence signaling results. SNPs are of a special importance for detection of viral and cancer-related nucleic acids. Synthetic oligonucleotides containing locked nucleic acids (LNAs) are useful tools in overcoming these obstacles (Koshkin et al. 1998; Hari et al. 2002; Levin et al. 2006; Madsen et al. 2012). LNAs are synthetic nucleic acid analogues with improved biophysical properties compared to natural nucleotides. The bridged rigid structure of ribose in LNA leads to high binding affinity and specificity of LNA containing probes to complimentary targets with the advantage of improved enzymatic stability. LNA units can be combined with terminal labeling in order to improve probe performance or chemically modified to carry, e.g., fluorophore, peptide, etc. Attachment of modifications to 2′-position of 2′-amino-LNA results in their location within the minor groove of duplexes or alternatively within the major groove when the base of the LNA nucleotide is modified (Astakhova and Wengel 2014). Diverse LNA/DNA probes find multiple applications in research and clinical diagnostics, e.g., qPCR, ddPCR, siRNA, imaging, etc. A new application of LNA-modified probes is a so-called LNA/DNA TaqMan assay. This assay applies a short LNA/DNA probe which contains terminally attached fluorophore and a quencher of fluorescence and is complementary to the target of choice. The probe gets cleaved by nuclease after the extension of a sequence-specific primer which results in the release of the fluorophore. Using short, highly specific LNA/DNA probes, the TaqMan assay shows a broad dynamic range, remarkable sensitivity, and applicability to diverse HIV-1 subtypes. As further outlined by the authors, "this approach to Taqman probe design could be explored further for use in diagnosis and monitoring of HIV-1 in resource-limited settings, especially where several subtypes co-circulate,"

owing to the opportunity to create multiplexing settings (Erali and Hillyard 1999; Perrin et al. 2006; Damond et al. 2007; Li et al. 2010).

4.1 Sequencing by Hybridization

Sequencing by hybridization is a nonenzymatic method that uses a DNA microarray (Fig. 6). As a first step, DNA is fluorescently labeled (typically at 5′-termini) and hybridized to an array containing known sequences, typically 18–25 nt long. The hybridization signals from a given spot on the array identify the sequence of the hybridized fragment. The array-bound probes vary by a single-nucleotide variant for all four possible positions (i.e., A, G, T, and C). Thus, patterns of hybridization reveal the sequence of any contiguous portion of the target DNA. Following this principle, Affymetrix developed a GeneChip technology in which multiple arrays of sequence-specific oligonucleotides are packaged in sequencing cartridges.

Sequencing arrays can be applied for sequencing of, e.g., HIV-1 protease and a part of transcriptase while determining drug-resistance-causing SNPs. During the sequencing, cDNA is transcribed into RNA containing fluorescent label and hybridized to the capture on the array. Afterwards, a laser scanner detects the color resulting from binding of RNA to the complementary capture. This array-based sequencing approach requires a known target gene for the design of GeneChip. Therefore, this method is called a "re-sequencing." According to multiple studies, GeneChip technology is less reliable for SNP detection than, e.g., dideoxynucleotide sequencing. Current sequencing arrays cannot detect insertions and deletions, and are suitable only for HIV-1 subtype B. According to Affymetrix, improved microarrays for sequencing other HIV-1 subtypes and for signaling insertions are under development.

Alternatively, an immobilized DNA target can be subjected to hybridization with fluorescently labeled sequence-specific probe(s) followed by detection of fluorescence. For example, Ji and coworkers developed highly efficient microarray for parallel diagnostics of genomic DNA for one or several molecular markers (Ji et al. 2004). Two SNP markers localized to the methylenetetrahydrofolate reductase gene (MTHFR) were selected as targets for proof-of-principle assays. Amplified PCR products from nine genomic DNA specimens were spotted and

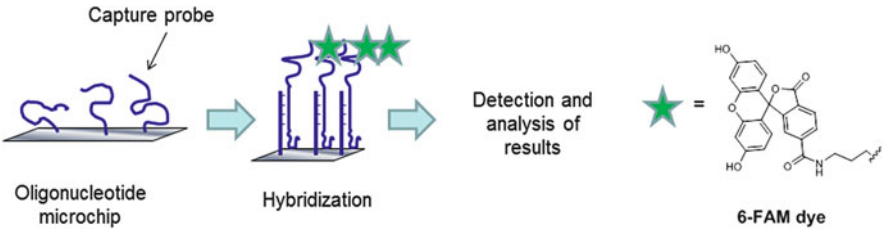

Fig. 6 Re-sequencing using 5′-terminally labeled target cDNA

immobilized onto a poly-l-lysine-coated glass slide to fabricate a microarray then interrogated by hybridization with dual-color probes to determine the SNP genotype of each sample (the applied dyes were Cy3 and Cy5 terminally attached to the probes). The results indicated that the microarray-based method could successfully determine the genotype of 677 and 1298 MTHFR polymorphisms in a full agreement with high-throughput sequencing.

5 Fluorescent Nucleobase Analogues

Fluorescent nucleobase analogues are applied in both enzymatic and enzyme-free diagnostic settings including imaging nucleic acids in cell culture and homogeneous in vitro fluorescence assays.

5.1 Fluorescent Labeling of Nucleobases

Fluorescent labeling of nucleobases provides another tool for developing nucleic acid assays for biomedical research and diagnostic use. A fluorophore of choice can be attached prior to incorporation into oligonucleotides or postsynthetically. Simultaneously, the sugar part of nucleotide can be functionalized as in the case of C5-modified LNA nucleotides (Kumar et al. 2011; Kaura et al. 2014). Several fluorescent nucleobase analogues are now available from commercial suppliers, for example, pyrene-dU and perylene-dU (Fig. 7). Alternatively, a commercially available precursor with a reactive group attached to the base can be used for postsynthetic labeling in a similar fashion as using the aforementioned EU (Fig. 7) (Xu et al. 2013).

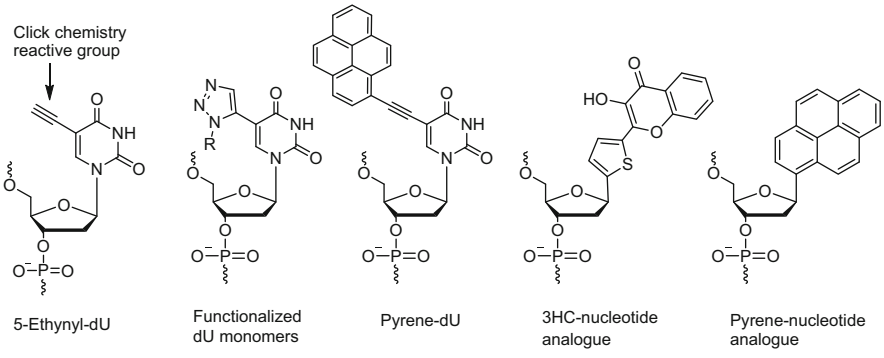

Fig. 7 Representative chemical structures of fluorescent nucleobase analogues and precursors for their synthesis

The aforementioned pyrene and its longer-wavelength analogue perylene are both polyaromatic hydrocarbon dyes that have attractive spectral properties, namely, they form exciplexes and excimers when two molecules are in a close proximity and placed coplanary (Lakowicz 2006). Excimer/exciplex formation results in additional emission band in fluorescence spectrum applicable for, e.g., SNP sensing in vitro (Okamoto et al. 2004) and probing mRNA in cells (Martí et al. 2006). It has been shown that attachment of the pyrene to the five positions of deoxyuridine via alkyne group leads to redshifted absorbance of the pyrene by approx. 50 nm compared to the unsubstituted 1-ethynylpyrene (Malakhov et al. 2000). Furthermore, electronic coupling of the base and the pyrene through triple bond makes the fluorescence of the pyrene sensitive to mismatched targets (Hwang et al. 2004). Finally, being used as a **FRET pair**, perylene and pyrene display emission which is highly dependent on the sequence and spacing between the fluorophores (Skorobogatyi et al. 2006; Wilson et al. 2007).

5.2 Substitution of the Entire Nucleobase with a Fluorescent Molecule

Substitution of the entire nucleobase with a fluorescent molecule is another labeling option; it enables designing sophisticated detection assays and studies of base pairing within nucleic acid complexes (Dziuba et al. 2012). However, fluorescent nucleobase substitutes have relatively low quantum yield due to interaction with nucleobases within the stack and require complicated synthetic route (Lakowicz 2006). In order to overcome the problem of decreased quantum yield, Dziuba and coworkers recently introduced a novel nucleoside analogue based on 3-hydroxychromone (3-HC) fluorophore (Fig. 7) (Dziuba et al. 2012). The nucleoside was synthesized and incorporated into series of oligonucleotide chains following standard phosphoramidite chemistry protocol. In comparison with existing fluorescent nucleoside analogues, this dye demonstrated high environmental-sensitivity switching between two well-resolved fluorescence bands. In labeled DNA, this nucleoside showed no interruption of the duplex structure while exhibiting a high-fluorescence quantum yield. The product probe had up to 50-fold higher fluorescence than 2-aminopurine applied as a standard. Moreover, the emission by novel analogue was highly sensitive to the polarity of the environment. Finally, using this nucleoside, the effect of a viral chaperone protein on DNA base stacking was site-selectively monitored (Dziuba et al. 2012).

Another successful example of a bright fluorescent nucleobase analogue is thiazole orange (TO) attached to oligonucleotides via non-nucleosidic scaffold. The conjugation mode is the most important factor for the TO derivative. Following determined design considerations, TO-labeled probes have a low background fluorescence of the unbound probe and light up of the signal when the TO dye intercalates into the helix replacing a canonical nucleobase. Interestingly, the

fluorescence of the "TO–base" remains low when a base mismatch is positioned in immediate vicinity (Bethge et al. 2010).

Substitution of all four nucleobases of oligonucleotide probes with different fluorophores such as naphthalene, phenanthrene, perylene, and pyrene has been reported (Matray and Kool 1998, 1999; Kim and Kool 2005). The substitution resulted in bright probes which were still able to form complementary complexes. It was also demonstrated that polymerase enzymes can interact and use these nucleoside analogues (Kool 2000; Lai and Kool 2005; Krueger and Kool 2009). This discovery inspired further designing new bases and base pairs as alternative genetic code that vary in shape/size and testing whether they function as normal base pairs.

6 DNA Groove-Binding Dyes

This is another type of DNA binding molecules which has multiple applications in the detection of nucleic acids in vitro. Potentially, this type of dyes can be also used for imaging in cell culture and in vivo. Besides intercalation and terminal attachment, a dye can be incorporated into groove compartments of DNA double helix. For B-type helix, a wide and broad major groove and a smaller minor groove are distinguished (Baraldi et al. 2004; Rohs et al. 2009). Polarity of the grooves and accessibility to nucleobases are also different (Sinkeldam et al. 2008). Positioning of fluorophore within the grooves can be achieved non-covalently (e.g., BOXTO dye) (Strekowski and Wilson 2007; Astakhova et al. 2013a, b) or by covalent internal attachment of the label to the sugar or nucleobase via a relatively short linker (Kumar et al. 2006, 2007a, b, 2009; Kolb et al. 2001; Sletten and Bertozzi 2009; Lallana et al. 2011; Grammel and Hang 2013; Xie et al. 2013). Again, using currently available techniques, the latter can be done either prior to oligonucleotide synthesis or postsynthetically.

The major advantage of internal incorporation of the dyes into oligonucleotide probes is their high ability to sense local microenvironment in the target sequence. In doing this, the choice of a fluorophore becomes a critical factor. The optimal groove-binding fluorophore is highly sensitive to the local microenvironment, stable under conditions of oligonucleotide synthesis or postsynthetic labeling, water soluble, and bright (Lindegaard et al. 2008; Umemoto et al. 2007; Astakhova et al. 2008a, b, 2010, 2012, 2013a, b; Astakhova 2014; Østergaard et al. 2010a, b; Sau and Hrdlicka 2012; Kumar et al. 2013). Notably, the chemistry and length of a linker play an important role for the attachment of groove-binding dyes to oligonucleotides. S. Kumar and coauthors investigated the influence of a linker on binding affinity and optical properties of α-L-LNA/DNA probes containing pyrene (Kumar et al. 2006, 2007a, b, 2009). Optimal performance was observed for C2 and C3 linkers, whereas longer chains resulted in decreased thermal stability of modified duplexes and smaller effect of hybridization on the pyrene's fluorescence.

A plethora of publications have demonstrated the general utility of groove-binding dyes for oligonucleotide probe assays given their unique biophysical and

optical properties. However, these dyes have not been fully utilized, the reason being related to their complicated synthetic routes. They require preparation of a fluorescently labeled phosphoramidite reagent and its further incorporation into the probes (Astakhova and Wengel 2014). Recently, this has been improved by introducing commercially available nucleotide scaffolds for postsynthetic labeling using, e.g., click chemistry or activated ester reactions, also upon enzymatic incorporation of precursors (Sletten and Bertozzi 2009; Lallana et al. 2011; Grammel and Hang 2013; Xie et al. 2013). Several suppliers provide 2′-*O*- and 3′-*O*-alkyne nucleotide analogues suitable for oligonucleotide synthesis and click labeling with a fluorescent azide of choice. Styryl, cyanine, and Nile red derivatives of 2′-*O*-propargyldeoxyuridine showed their utility in the labeling of DNA, also upon enzymatic incorporation of precursor nucleotide (Rubner et al. 2012; Holzhauser et al. 2013; Wenge et al. 2013). In another recent work, ultrabright boron–dipyrromethene (BODIPY) dyes were internally incorporated into oligonucleotide probes by click chemistry (Loudet and Burgess 2007). Having extraordinary high-fluorescence quantum yields and chemical stability and photostability, BODIPY dyes are very promising tools for nucleic acid research and diagnostic in vitro, in cell culture, and in vivo (Loudet and Burgess 2007; Arroyo et al. 2009; Carlson et al. 2013).

In our recent work, we showed that the positioning of fluorophores within minor groove by a relatively short linker using "clickable" 2′-amino-LNA and 2′-*O*-propargyl-dU scaffolds results in bright probes with high sensitivity of fluorescence to hybridization (Figs. 8 and 9) (Jørgensen et al. 2013; Okholm et al. 2014). The

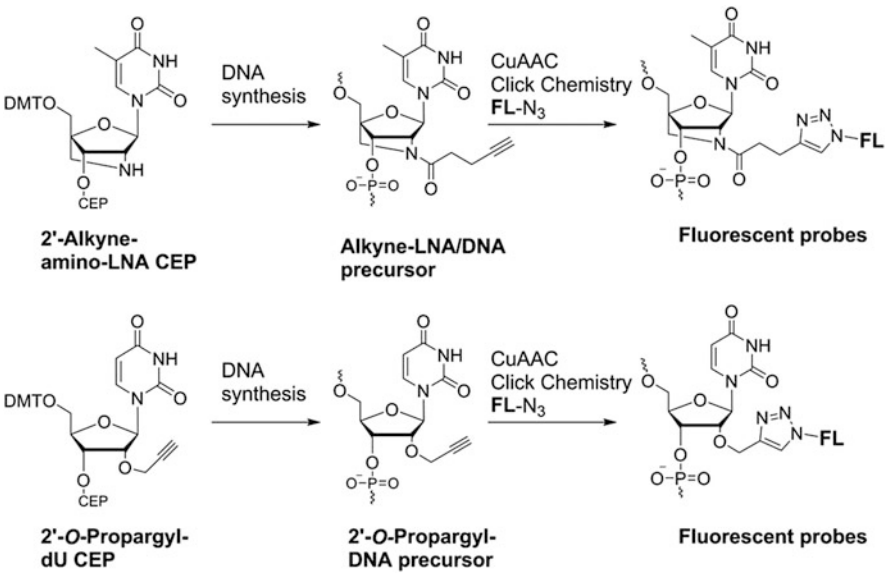

Fig. 8 Postsynthetic CuAAC click chemistry using 2′-alkyne-amino-LNA and 2′-*O*-propargyl-dU scaffolds for generating fluorescent probes; DMT = 4,4′-dimethoxytrityl, CEP = cyanoethoxyphosphoramidite

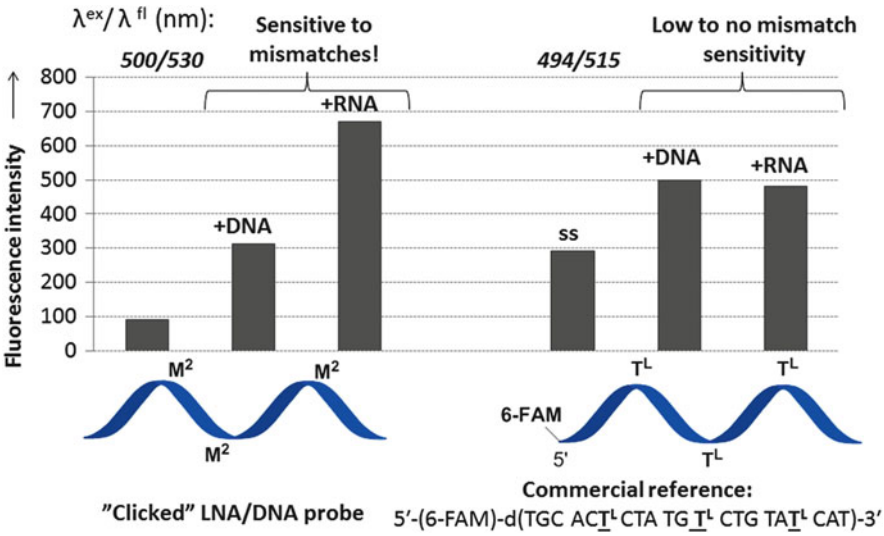

Fig. 9 Fluorescence sensing of complementary DNA/RNA targets compared to commercially available 5′-labeled LNA/DNA probes. $M^2 = 2'$-5-R110 2′-amino-LNA click product; $T^L =$ regular LNA

fluorescence of single-stranded triple-labeled probes was quenched compared to double-stranded complexes and commercial 5′-labeled LNA/DNA analogues. Introducing a quencher within MB design improves the performance of terminally labeled probes. Simultaneously the price of the probe increases fivefold or more, along with decreased photostability and chemical stability, since most quenchers of fluorescence are rather unstable molecules. We also demonstrated the improved sensitivity of the novel probes to SNPs compared to 5′-labeled analogues (Jørgensen et al. 2013; Okholm et al. 2014) (Fig. 8). The background fluorescence of the single strands was reduced while upon formation of complexes with the target miR-7 and circRNA emission increased giving remarkably high quantum yields (Φ_f up to 0.99) and, therefore, low limit of detection values (<5 nM in solution using regular fluorometer). Simple design and robust synthetic route, high yields of the products, effective target binding, and consistent target-specific fluorescence make the novel probes a new robust platform for the detection of natural DNA/RNA sequences.

7 Comparison of Fluorescent Nucleotide Analogues

As the final aspect, we summarize the availability, price, and performance of diverse fluorescent nucleotide analogues and assays in nucleic acid research and diagnostics (Table 1). Most of the discussed substances are currently available on

Table 1 Performance characteristics of fluorescent nucleotides and oligonucleotides in research and diagnostics

Dye/FNTP/Oligo	Availability	Chemical stability/ photostability	Price of probe (USD)	Research applications	Clinical applications	LOD	Accuracy	Multiplexing
Intercalating dyes	+	+	0.08–2	Quantification, studies of nucleic acid interactions	qPCR, ddPCR	Single molecule–100 nM	M–H	–
FNTPs	+	+	4–6	Imaging, studies of nucleic acid interactions, clinical sciences	Sequencing, microarray	Single molecule	M–H	+
Terminally labeled probes (MBs, TaqMan etc.)	+	±	2–20		Sequencing, qPCR, microarray	Single molecule–100 nM	M–H	+
Fluorescent nucleobase analogues	± (limited)	+	0.18–0.25[a]		SNP sensing		H	+
Groove binders	+	+			SNP sensing		H	+

[a]Approximate price is estimated per one assay detecting 0.1–100 nM DNA target by fluorescence based on current prices of reagents from the following commercial suppliers: EvaGreen dye (Biotium); FNTPs (Applied Biosystems); MBs, TaqMan (Sigma-Aldrich, Applied Biosystems); fluorescent nucleobase analogues (phosphoramidite reagents from Glen Research); groove-binding probes (phosphoramidite reagents from Glen Research). Accuracy in three independent assays: H (high) = deviation <1 %; M (medium) = 2–10 %; P (poor) = ≥ 10 %. The price is estimated not taking into account expenses on oligonucleotide synthesis and purification (HPLC/PAGE). For groove-binding modifications, price is estimated per commercially available alkyne–phosphoramidite and postsynthetic labeling by click chemistry

the market and are applied in multiple assays in research and clinical settings. The limit of target detection (LOD) is a crucial parameter and depends on several factors including the brightness of the applied dye, the analyte (i.e., DNA or RNA), the enzymatic requirements if any, and the type of the used optical system (Astakhova 2014; Demchenko 2009). PCR allows detection of individual molecules with any labeling method (Ganzel et al. 2013; Faltin et al. 2013; Weber and Köster 2013; Marshall et al. 2013; Kuroda et al. 2013). The same sensitivity can be now achieved using single-molecule spectroscopy (Han et al. 2013; Kusumi et al. 2014; Shivanandan et al. 2014). In the absence of enzymatic reaction and high-resolution spectroscopy, LOD is approx. 5–200 nM of target sequence using regular fluorometry (Astakhova 2014).

However, accuracy and reproducibility can be decreased when enzymatic reactions are applied in the assay (Eckert and Kunkel 1991). Next, multiplexing is available for all dyes besides intercalators. Overall, based on these data, we conclude that the best performance at lowest price can be now achieved using fluorescent nucleobase analogues and DNA groove-binding dyes (Table 1).

8 Conclusions and Future Direction

As exemplified in this chapter, many molecular assays in nucleic acid research and clinical sciences rely on synthetic nucleic acid analogues containing fluorescent dyes. Over the past three decades, dramatically improved sensitivity and specificity of nucleic acid targeting was achieved by applying enzymatic reactions, not always completely successful due to enzymatic errors. Recent advances in microscopy, chemistry of fluorescent dyes, and bioconjugation allow development of reliable, inexpensive, and robust enzyme-free methods. To fully exploit synthetic nucleosides and nucleotides for these methods, a growing interaction between nucleic acid chemistry and clinical sciences is needed. Increased knowledge, understanding of problems, and increased availability and efficacy of new chemically altered nucleotides seem to be the main objectives of the future fields of nucleic acid research, biotechnology, and clinical diagnostics.

References

Ahn SJ, Costa J, Emanuel JR (1996) PicoGreen quantitation of DNA: effective evaluation of samples pre- or post-PCR. Nucleic Acids Res 24:2623–2625

Arroyo IJ, Hu R, Merino G, Tang BZ, Peña-Cabrera E (2009) The smallest and one of the brightest. Efficient preparation and optical description of the parent borondipyrromethene system. J Org Chem 74(15):5719–5722

Astakhova K (2014) Toward non-enzymatic ultrasensitive identification of single nucleotide polymorphisms by optical methods. Chemosensors 2:193–206

Astakhova IK, Wengel J (2013) Interfacing click chemistry with automated oligonucleotide synthesis for the preparation of fluorescent DNA probes containing internal xanthene and cyanine dyes. Chem Eur J 19:1112–1122

Astakhova IK, Wengel J (2014) Scaffolding along nucleic acid duplexes using 2′-amino-locked nucleic acids. Acc Chem Res 47:1768–1777

Astakhova IV, Korshun VA, Jahn K et al (2008a) Perylene attached to 2′-amino-LNA: synthesis, incorporation into oligonucleotides, and remarkable fluorescence properties in vitro and in cell culture. Bioconjug Chem 19:1995–2007

Astakhova IV, Korshun VA, Wengel J (2008b) Highly fluorescent conjugated pyrenes in nucleic acid probes: (phenylethynyl)pyrenecarbonyl-functionalized locked nucleic acids. Chem Eur J 14:11010–11026

Astakhova IV, Lindegaard D, Korshun VA et al (2010) Novel interstrand communication systems within DNA duplexes based on 1-, 2- and 4-(phenylethynyl)pyrenes attached to 2′-amino-LNA: high-affinity hybridization and fluorescence sensing. Chem Commun 46:8362–8364

Astakhova IK, Samokhina E, Babu BR et al (2012) Novel (phenylethynyl)pyrene–LNA constructs for fluorescence SNP sensing in polymorphic nucleic acid targets. Chembiochem 13:1509–1519

Astakhova IK, Kumar TS, Campbell MA et al (2013a) Branched DNA nanostructures efficiently stabilised and monitored by novel pyrene-perylene 2′-α-L-amino-LNA FRET pairs. Chem Commun 49:511–513

Astakhova IK, Pasternak K, Campbell MA et al (2013b) A locked nucleic acid-based nanocrawler: designed and reversible movement detected by multicolor fluorescence. J Am Chem Soc 135:2423–2426

Baraldi PG, Bovero A, Fruttarolo F et al (2004) DNA minor groove binders as potential antitumor and antimicrobial agents. Med Res Rev 24(4):475–528

Barreiro LB, Henriques R, Mhlanga MM (2009) High-throughput SNP genotyping: combining tag SNPs and molecular beacons. Methods Mol Biol 578:255–276

Bengtsson M, Stahlberg A, Rorsman P et al (2005) Gene expression profiling in single cells from the pancreatic islets of Langerhans reveals lognormal distribution of mRNA levels. Genome Res 15:1388–1392

Berndl S, Wagenknecht H-A (2009) Fluorescent color readout of DNA hybridization with thiazole orange as an artificial DNA base. Angew Chem Int Ed 48:2418–2421

Bethge L, Singha I, Seitz O (2010) Designed thiazole orange nucleotides for the synthesis of single labelled oligonucleotides that fluoresce upon matched hybridization. Org Biomol Chem 8:2439–2448

Brown LJ, Cummins J, Hamilton A et al (2000) Molecular beacons attached to glass beads fluoresce upon hybridisation to target DNA. Chem Commun:621–622

Brzezinska J, Adrych-Rozek K, Jahnz-Wenchmann Z et al (2012) Non-nucleosidic analogs of nucleic acids. J Biotechnol Comput Biol Bionanotechnol 93:391–399

Carlson JCT, Meimetis LG, Hilderbrand SA, Weissleder R (2013) BODIPY–tetrazine derivatives as superbright bioorthogonal turn-on probes. Angew Chem Int Ed 52(27):6917–6920

Cosa G, Focsaneanu KS, McLean JR et al (2001) Photophysical properties of fluorescent DNA-dyes bound to single- and double-stranded DNA in aqueous buffered solution. Photochem Photobiol 73:585–599

Damond F, Roquebert B, Bénard A et al (2007) Human immunodeficiency virus type 1 (HIV-1) plasma load discrepancies between the Roche Cobas Amplicor HIV-1 Monitor version 1.5 and the Roche Cobas AmpliPrep/Cobas TaqMan HIV-1 assays. J Clin Microbiol 45:3436–3438

Demchenko AP (2009) Introduction to fluorescence sensing. Springer, Singapore

Di Carlo D, Tse HT, Gossett DR (2012) Introduction: why analyze single cells? Methods Mol Biol 853:1–10

Dziuba D, Postupalenko VY, Spadafora M et al (2012) A universal nucleoside with strong two-band switchable fluorescence and sensitivity to the environment for investigating DNA interactions. J Am Chem Soc 134:10209–10213

Eckert KA, Kunkel TA (1991) DNA polymerase fidelity and the polymerase chain reaction. PCR Methods Appl 1:17–24

El-Sayed AA, Pedersen EB, Khaireldin NA (2012) Studying the influence of the pyrene intercalator TINA on the stability of DNA i-motifs. Nucleosides Nucleotides Nucleic Acids 31:872–879

Erali M, Hillyard DR (1999) Evaluation of the ultrasensitive Roche Amplicor HIV-1 monitor assay for quantitation of human immunodeficiency virus type 1 RNA. J Clin Microbiol 37:792–795

Faltin B, Zengerle R, von Stetten F (2013) Current methods for fluorescence-based universal sequence-dependent detection of nucleic acids in homogenous assays and clinical applications. Clin Chem 59:1567–1582

Filichev VV, Pedersen EB (2005) Stable and selective formation of Hoogsteen-type triplexes and duplexes using twisted intercalating nucleic acids (TINA) prepared via postsynthetic Sonogashira solid-phase coupling reactions. J Am Chem Soc 127:14849–14858

Flaherty P, Natsoulis G, Muralidharan O et al (2012) Ultrasensitive detection of rare mutations using next-generation targeted resequencing. Nucleic Acids Res 40:e2

França LTC, Carrilho E, Kist TBL (2002) A review of DNA sequencing techniques. Q Rev Biophys 35:169–200

Ganzel C, Douer D, Tallman MS (2013) Postconsolidation maintenance and monitoring in patients with acute promyelocytic leukemia. J Natl Compr Canc Netw 11:1512–1521

Glazer AN, Rye HS (1992) Stable dye-DNA intercalation complexes as reagents for high-sensitivity fluorescence detection. Nature 359:859–861

Grammel M, Hang HC (2013) Chemical reporters for biological discovery. Nat Chem Biol 9:475–484

Gray DC, Wolfe R, Gee BP et al (2008) In vivo imaging of the fine structure of rhodamine-labeled macaque retinal ganglion cells. Invest Ophthalmol Vis Sci 49:467–473

Han R, Li Z, Fan Y, Jiang Y (2013) Recent advances in super-resolution fluorescence imaging and its applications in biology. J Genet Genomics 40:583–595

Hari Y, Obika S, Sasaki M (2002) Effective synthesis of C-nucleosides with 2′-4′-BNA modification. Tetrahedron 58:3051–3063

Holzhauser C, Rubner MM, Wagenknecht H-A (2013) Energy-transfer-based wavelength-shifting DNA probes with “clickable” cyanine dyes. Photochem Photobiol Sci 12(5):722–724

Hwang GT, Seo YJ, Kim SJ, Kim BH (2004) Fluorescent oligonucleotide incorporating 5-(1-ethynylpyrenyl)-2′-deoxyuridine: sequence-specific fluorescence changes upon duplex formation. Tetrahedron Lett 45:3543–3546

Ikeda Y, Iwakiri S, Yoshimori T (2009) Development and characterization of a novel host cell DNA assay using ultra-sensitive fluorescent nucleic acid stain “PicoGreen”. J Pharm Biomed Anal 49:997–1002

Ji M, Hou P, Li S et al (2004) Microarray-based method for genotyping of functional single nucleotide polymorphisms using dual-color fluorescence hybridization. Mutat Res 548:97–105

Jørgensen AS, Gupta P, Wengel J, Astakhova IK (2013) “Clickable” LNA/DNA probes for fluorescence sensing of nucleic acids and autoimmune antibodies. Chem Commun 49 (91):10751–10753

Kannegård KK, Okholm AH, Kjems J et al (2013) A quencher-free molecular beacon design based on pyrene excimer fluorescence using pyrene-labeled UNA (unlocked nucleic acid). Bioorg Med Chem 21:6186–6190

Karlsen KK, Pasternak A, Jensen TB et al (2012) Pyrene-modified unlocked nucleic acids: synthesis, thermodynamic studies, and fluorescent properties. Chembiochem 13:590–601

Kaura M, Kumar P, Hrdlicka PJ (2014) Synthesis, hybridization characteristics and fluorescence properties of oligonucleotides modified with nucleobase-functionalized LNA (Locked Nucleic Acid) adenosine and cytidine monomers. J Org Chem 79:6256–6268

Khan AS (2014) Rapid advances in nucleic acid technologies for detection and diagnostics of pathogens. J Microbiol Exp 1:00009

Kim TW, Kool ET (2005) A series of nonpolar thymidine analogues of increasing size: DNA base pairing and stacking properties. J Org Chem 70:2048–2053
Kim RY, Xu H, Myllykangas S et al (2011) Genetic-based biomarkers and next-generation sequencing: the future of personalized care in colorectal cancer. J Pers Med 8:331–345
Koide Y, Urano Y, Hanaoka K et al (2012) Development of NIR fluorescent dyes based on Si–rhodamine for in vivo Imaging. J Am Chem Soc 134:5029–5031
Kolb HC, Finn MG, Sharpless KB (2001) Click chemistry: diverse chemical Function from a few good reactions. Angew Chem Int Ed Engl 40:2004–2021
Kool ET (2000) Synthetically modified DNAs as substrates for polymerases. Curr Opin Chem Biol 4:602–608
Koshkin A, Rajwanshi VK, Wengel J (1998) Novel convenient syntheses of LNA [2.2.1] bicyclo nucleosides. Tetrahedron Lett 39:4381–4384
Krueger AT, Kool ET (2009) Redesigning the architecture of the base pair: toward biochemical and biological function of new genetic sets. Chem Biol 16:242–248
Kumar TS, Madsen AS, Wengel J, Hrdlicka PJ (2006) Synthesis and hybridization studies of 2′-amino-alpha-L-LNA and tetracyclic locked LNA. J Org Chem 71:4188–4201
Kumar TS, Wengel J, Hrdlicka PJ (2007a) 2′-N-(pyren-1-yl)acetyl-2′-amino-alpha-L-LNA: synthesis and detection of single nucleotide mismatches in DNA and RNA targets. Chembiochem 8:1122–1125
Kumar TS, Wengel J, Hrdlicka PJ (2007b) Pyrene-functionalized 2′-amino-alpha-L-LNA as potential diagnostic probes. Nucleosides Nucleotides Nucleic Acids 26:1407–1409
Kumar TS, Madsen AS, Østergaard ME et al (2009) Functionalized 2′-amino-alpha-L-LNA: directed positioning of intercalators for DNA targeting. J Org Chem 4:1070–1081
Kumar P, Østergaard ME, Hrdlicka PJ (2011) Preparation of C5-functionalized locked nucleic acids (LNAs). Curr Protoc Nucleic Acid Chem 4:43
Kumar TS, Myznikova A, Samokhina E et al (2013) Rapid genotyping using pyrene–perylene locked nucleic acid complexes. Artif DNA PNA XNA 4:58–68
Kurg A, Tõnisson N, Georgiou I et al (2000) Arrayed primer extension: solid-phase four-color DNA resequencing and mutation detection technology. Genet Test 4:1–7
Kuroda N, Tanaka A, Sasaki N et al (2013) Review of renal carcinoma with t(6;11)(p21;q12) with focus on clinical and pathobiological aspects. Histol Histopathol 28:685–690
Kusumi A, Tsunoyama TA, Hirosawa KM et al (2014) Tracking single molecules at work in living cells. Nat Chem Biol 10:524–532
Lai JS, Kool ET (2005) Fluorous' base-pairing effects in a DNA polymerase active site. Chem Eur J 11:2966–2971
Lakowicz JR (2006) Principles of fluorescence spectroscopy, 3rd edn. Springer, Singapore
Lallana E, Riguera R, Fernandez-Megia E (2011) Reliable and efficient procedures for the conjugation of biomolecules through Huisgen azide–alkyne cycloadditions. Angew Chem Int Ed 50:8794–8804
Levin JD, Fiala D, Samala MF et al (2006) Position-dependent effects of locked nucleic acid (LNA) on DNA sequencing and PCR primers. Nucleic Acids Res 34:e142
Li Z, Bai X, Ruparel H, Kim S, Turro NJ, Ju J (2003) A photocleavable fluorescent nucleotide for DNA sequencing and analysis. Proc Natl Acad Sci USA 100:414–419
Li P, Ruel T, Fujimoto K et al (2010) Novel application of Locked Nucleic Acid chemistry for a Taqman assay for measuring diverse human immunodeficiency virus type 1 subtypes. J Virol Methods 170:115–120
Lindegaard D, Madsen AS, Astakhova IV et al (2008) Pyrene-perylene as a FRET pair coupled to the N2′-functionality of 2′-amino-LNA. Bioorg Med Chem 16:94–99
Longmire MR, Ogawa M, Hama Y et al (2008) Determination of optimal rhodamine fluorophore for in vivo optical imaging. Bioconjug Chem 19:1735–1742
Loudet A, Burgess K (2007) BODIPY dyes and their derivatives: syntheses and spectroscopic properties. Chem Rev 107(11):4891–4932

Lyubchenko YL, Shlyakhtenko LS, Ando T (2011) Imaging of nucleic acids with atomic force microscopy. Methods 54:274–283
Madsen AS, Jørgensen AS, Jensen TB et al (2012) Large scale synthesis of 2′-amino-LNA thymine and 5-methylcytosine nucleosides. J Org Chem 77:10718–10728
Malakhov AD, Malakhova EV, Kuznitsova SV et al (2000) Synthesis and fluorescent properties of 5-(1-pyrenylethynyl)-2′-deoxyuridine-containing oligodeoxynucleotides. Rus J Bioorg Chem 16:34–44
Mao F, Leung W-Y, Xin X (2007) Characterization of EvaGreen and the implication of its physicochemical properties for qPCR applications. BMC Biotechnol 7:76
Marras SA, Kramer FR, Tyagi S (2002) Genotyping SNPs with molecular beacons. Methods Mol Biol 212:111–128
Marshall D, Laberge JM, Firetag B et al (2013) The changing face of percutaneous image-guided biopsy: molecular profiling and genomic analysis in current practice. J Vasc Interv Radiol 24:1094–1103
Martí AA, Li X, Jockusch S et al (2006) Pyrene binary probes for unambiguous detection of mRNA using time-resolved fluorescence spectroscopy. Nucleic Acids Res 34:3161–3168
Matray TJ, Kool ET (1998) Selective and stable DNA base pairing without hydrogen bonds. J Am Chem Soc 120:6191–6192
Matray TJ, Kool ET (1999) A specific partner for a basic damage in DNA. Nature 399:704–708
Miotke L, Lau BT, Rumma RT et al (2014) High sensitivity detection and quantitation of DNA copy number and single nucleotide variants with single color droplet digital PCR. Anal Chem 86:2618–2624
Morgan AR, Lee JS, Pulleyblank DE et al (1979) Review: ethidium fluorescence assays. Part 1. Physicochemical studies. Nucleic Acids Res 7:547–56935
Narsinh KH, Sun N, Sanchez-Freire V et al (2011) Single cell transcriptional profiling reveals heterogeneity of human induced pluripotent stem cells. J Clin Invest 121:1217–1221
Okamoto A, Kanatani K, Saito I (2004) Pyrene-labeled base-discriminating fluorescent DNA probes for homogeneous SNP typing. J Am Chem Soc 126:4820–4827
Okholm A, Kjems J, Astakhova K (2014) Fluorescence detection of RNA using rationally designed “clickable” oligonucleotide probes. RCS Adv 4(86):45653–45656
Østergaard ME, Cheguru P, Papasani MR et al (2010a) Glowing LNA—brightly fluorescent probes for detection of nucleic acids in cells. J Am Chem Soc 132:14221–14228
Østergaard ME, Maiti J, Babu BR et al (2010b) Glowing LNA as nucleic acid detection probes—Nucleobase analogs and insights into probe design. Bioorg Med Chem Lett 20:7265–7268
Perrin L, Pawlotsky JM, Bouvier-Alias M et al (2006) Multicenter performance evaluation of a new TaqMan PCR assay for monitoring human immunodeficiency virus RNA load. J Clin Microbiol 44:4371–4375
Pinheiro LB, Coleman VA, Hindson CM et al (2012) Evaluation of a droplet digital polymerase chain reaction format for DNA copy number quantification. Anal Chem 84:1003–1011
Raddatz S, Mueller-Ibeler J, Kluge J et al (2002) Hydrazide oligonucleotides: new chemical modification for chip array attachment and conjugation. Nucleic Acids Res 30:4793–4802
Raj A, Tyagi S (2010) Detection of individual endogenous RNA transcripts in situ using multiple singly labeled probes. Methods Enzymol 472:365–386
Rohs R, West SM, Sosinsky A et al (2009) The role of DNA shape in protein–DNA recognition. Nature 461:1248–1253
Rubner MM, Holzhauser C, Bohländer PR, Wagenknecht H-A (2012) A “clickable” styryl dye for fluorescent DNA labeling by excitonic and energy transfer interactions. Chem Eur J 18 (5):1299–1302
Rye HS, Glazer AN (1995) Interaction of dimeric intercalating dyes with single-stranded DNA. Nucleic Acids Res 23:1215–1222
Salic A, Mitchison TJ (2008) A chemical method for fast and sensitive detection of DNA synthesis in vivo. Proc Natl Acad Sci USA 105:2415–2420

Sau SP, Hrdlicka PJ (2012) C2′-Pyrene-functionalized triazole-linked DNA: universal DNA/RNA hybridization probes. J Org Chem 77:5–16
Shieh P, Siegrist MS, Cullen AJ et al (2014) Imaging bacterial peptidoglycan with near-infrared fluorogenic azide probes. Proc Natl Acad Sci U S A 111:5456–5461
Shivanandan A, Deschout H, Scarselli M et al (2014) Challenges in quantitative single molecule localization microscopy. FEBS Lett 588:3595–3602
Sinkeldam RW, Greco NJ, Tor Y (2008) Polarity of major grooves explored by using an isosteric emissive nucleoside. Chembiochem 9:706–709
Skorobogatyi MV, Malakhov AD, Pchelintseva AA et al (2006) Fluorescent 5-alkynyl-2-′-deoxyuridines: high emission efficiency of a conjugated perylene nucleoside in a DNA duplex. Chembiochem 7:810–816
Sletten EM, Bertozzi CR (2009) Bioorthogonal chemistry: fishing for selectivity in a sea of functionality. Angew Chem Int Ed Engl 48:6974–6998
Stadler AL, Delos Santos JO, Stensrud ES et al (2011) Fluorescent DNA nanotags featuring covalently attached intercalating dyes: synthesis, antibody conjugation, and intracellular imaging. Bioconjug Chem 22:1491–1502
Stracy M, Uphoff S, de Leona FG, Kapanidis AN (2014) In vivo single-molecule imaging of bacterial DNA replication, transcription, and repair. FEBS Lett 588:3585–3594
Strekowski L, Wilson B (2007) Noncovalent interactions with DNA: an overview. Mutat Res 623:3–13
Tebbutt SJ IV, Opushnyev TBW et al (2005) SNP Chart: an integrated platform for visualization and interpretation of microarray genotyping data. Bioinformatics 21:124–127
Tsuyama T, Kishikawa J-I, Han Y-W et al (2013) In vivo fluorescent adenosine 5′-triphosphate (ATP) imaging of drosophila melanogaster and caenorhabditis elegans by using a genetically encoded fluorescent ATP biosensor optimized for low temperatures. Anal Chem 85:7889–7896
Turner APF (2013) Biosensors: sense and sensibility. Chem Soc Rev 42:3184–3196
Umemoto T, Hrdlicka P, Babu BR et al (2007) Sensitive SNP dual-probe assays based on pyrene-functionalized 2′-amino-LNA: lessons to be learned. Chembiochem 8:2240–2248
Web: http://biotium.com/product/evagreen-dye-20x-in-water/. Accessed 24th Aug 2014
Web: http://www.glenresearch.com/Catalog/modifiers.php#branching. Accessed 10th Aug 2014
Web: http://www.jenabioscience.com/cms/en/1/catalog/1380_2opropargyl_ceps.html. Accessed 10th Aug 2014
Web: http://www.lifetechnologies.com/us/en/home/references/molecular-probes-the-handbook/tables/characteristics-of-chromatide-dutp-chromatide-obea-dctp-aha-dutp-and-aha-dctp-labeled-nucleotides.html. Accessed 20th Aug 2014
Web: http://www.sigmaaldrich.com/life-science/custom-oligos/dna-probes/product-lines/molecular-beacons.html. Accessed 24th Aug 2014
Weber T, Köster R (2013) Genetic tools for multicolor imaging in zebra fish larvae. Methods 62:279–291
Wenge U, Ehrenschwender T, Wagenknecht H-A (2013) Synthesis of 2′-O-propargyl nucleoside triphosphates for enzymatic oligonucleotide preparation and “click” modification of DNA with nile red as fluorescent probe. Bioconjug Chem 24(3):301–304
Wilson JN, Gao J, Kool ET (2007) Oligodeoxyfluorosides: strong sequence dependence of fluorescence emission. Tetrahedron 63:3427–3433
Xie R, Hong S, Chen X (2013) Cell-selective metabolic labeling of biomolecules with bioorthogonal functionalities. Curr Opin Chem Biol 17:747–752
Xu H, Franks T, Gibson G et al (2013) Evidence for biphasic uncoating during HIV-1 infection from a novel imaging assay. Retrovirology 10:70
Xu Z, Guo K, Yu J et al (2014) A unique perylene-based DNA Intercalator: localization in cell nuclei and inhibition of cancer cells and tumors. Small 10:4087–4092
Zhao C, Zhang Y, Wang X, Cao J (2013) Development of BODIPY-based fluorescent DNA intercalating probes. J Photochem Photobiol A Chem 264:41–47

Emergent Properties and Functions of Nanoconfined Nucleic Acid Architectures

Allen W. Nicholson, Shiv K. Redhu, Alex Stopar, Lucia Coral, Vincenzo Carnevale, and Matteo Castronovo

Contents

A.W. Nicholson
Department of Biology, Temple University, 1900 North 12th Street, Philadelphia, PA 19122, USA

Department of Chemistry, Temple University, 1901 North 13th Street, Philadelphia, PA 19122, USA

S.K. Redhu
Department of Biology, Temple University, 1900 North 12th Street, Philadelphia, PA 19122, USA

A. Stopar • L. Coral
Ph.D. School of Nanotechnology, University of Trieste, Trieste, Italy

Department of Biological and Medical Sciences, University of Udine, Piazzale Kolbe 4, Udine, Italy

V. Carnevale
Department of Biology, Temple University, 1900 North 12th Street, Philadelphia, PA 19122, USA

Institute for Computational Molecular Science, Temple University, 1925 North 12th Street, Philadelphia, PA 19122, USA

M. Castronovo (✉)
Department of Biology, Temple University, 1900 North 12th Street, Philadelphia, PA 19122, USA

Department of Medical and Biological Sciences, University of Udine, Piazzale Kolbe 2, 33100 Udine, Italy
e-mail: mcastro@temple.edu

V.A. Erdmann et al. (eds.), *RNA and DNA Diagnostics*, RNA Technologies,
DOI 10.1007/978-3-319-17305-4_9

Abstract The facile ability of DNA to self-assemble has enabled the creation of complex architectures with diverse functions on surfaces or in solution. This approach provides a powerful design tool for the development of nanoscale devices with transformative applications in multiple areas, including the detection of complex biomolecules, drug delivery, and in situ biomolecular synthesis. However, little is known of the effect of confinement on the function of complex nucleic acid architectures, which exhibit unanticipated behaviors that presumably reflect high-level molecular crowding. In this chapter, we review selected recent studies that describe the application and atypical behaviors of nanoconfined nucleic acids, in particular with respect to hybridization, denaturation, conformation, stability, and enzyme accessibility. We argue that the novel behavior of dense nucleic acid arrays naturally emerge as a result of immobilization and reduction in spatial degrees of freedom. We summarize by emphasizing the need for basic physical–chemical studies of dense nucleic acid architectures, involving an interplay of experimental and theoretical approaches, in order to effectively guide the successful technological development of nucleic acid nanodevices.

Keywords Atomic force microscopy • Barcoding • Crowding • Denaturation • Detection • DNA • DNA origami • Electrochemistry • Enzymes • Fluorescence • Hybridization • Molecular device • Molecular modeling • Nanoarray • Nanomanipulation • Nanomedicine • Nanotechnology • Nanoscale confinement • Nucleic acids • Nucleases • RNA • Self-assembled monolayers • Self-assembly • Steric hindrance • Surfaces • Theory

1 Introduction

Nucleic acids continue to play an essential role in the current age of nanotechnology, as they provide an important new material in the form of building blocks for artificial nanostructured systems with novel functions and important applications. While it is appreciated that the high level of packing and crowding in nanoconfined systems is similar to that in intracellular environments, a number of hitherto unanticipated effects of confinement on nucleic acids have been recently identified in studies on physical and biochemical processes, including translocation through pores or membranes, recognition by biomolecules, and enzymatic transformation. A number of these effects have been exploited in the development of highly sensitive and discriminatory biomolecular sensing and are beginning to have a transformative impact in the biomedical and clinical arenas. As the other confinement-dependent effects become better characterized, their successful application should quickly follow.

As an example, the development of polymerase chain reactions on surface-bound DNA molecules, in combination with high-throughput fluorescence imaging, has enabled extraordinarily high-throughput DNA sequencing at the single-molecule level (Metzker 2010a). Rapidly evolving solid-state or biological nanopore-based technologies are allowing ultrahigh-throughput DNA sequencing, with commercialization close at hand (Venkatesan and Bashir 2011). Compared to the surface-based technologies, nanopore-based sequencing has an advantage in not requiring (1) DNA immobilization; (2) a surface-localized polymerase reaction, which is prone to errors; and (3) fluorescent imaging, with its attendant costs. Nanopore-based techniques instead rely on the change in ion conductivity of the nanopore during translocation of a nucleic acid strand in a sequence-dependent fashion. Since measurement of ionic current can be multiplexed using engineered nanopore-containing membranes, the method in principle can achieve essentially unlimited throughput. Since the method does not require the labeling or other manipulation of DNA molecules, it is nondestructive to samples, and measurements can be repeated several times or instead applied (at least in principle) to read long sequences (Venkatesan and Bashir 2011). Alternatively, single-molecule electrophoretic approaches hold promise in the analysis of very long DNA molecules. For example, Craighead and coworkers demonstrated the separation of long DNA molecules using a nanofluidic device based on entropic traps (Han and Craighead 2000). In response to an applied electric field, DNA molecules travel across a pattern of alternating thick and thin regions in a microfluidic channel and are forced to repeatedly change their conformations. Within the regions whose thickness is larger than the radius of gyration of DNA, the molecules tend to form spherical shapes, while within the thinner regions, the DNA molecules are deformed. In these regions, the longer DNA molecules have a larger surface area in contact with the boundary (due to a larger radius of gyration) that provide higher probability of escape per unit time, thus providing a greater overall mobility (Han and Craighead 2000). In this regard, Austin and coworkers demonstrated that long DNA filaments fully unfold in nanochannels with cross-sectional widths of about twice the DNA persistence length (Tegenfeldt et al. 2004; Reisner et al. 2005), so as to minimize their conformational free energy. In a subsequent study, Reisner and coworkers used such a nanofluidic-based approach to carry out denaturation mapping of single dsDNA filaments and obtained sequence-specific denaturation fingerprints (Reisner et al. 2010).

Overall, the studies of the emergent properties of nucleic acids under confinement are highly diverse, with implications for biology and medicine (Ke et al. 2008; Akbulut et al. 2010; Gifford et al. 2010; Niemeyer 2010) as well as for other fields such as next-generation information technology (Liu et al. 2000; Seelig et al. 2006; Lund et al. 2010; Franco et al. 2011). For instance, the facile self-assembly and nanomanipulation of nucleic acids hold great promise in the design of innovative, programmable materials, with applications ranging from biosensing to cellular targeting and drug delivery. We believe that the application of nucleic acid-based nanodevices will greatly benefit from a full understanding of the factors that influence nucleic acid function, reflecting the unique nanoscale environment. Little is known about the effects of crowding, steric hindrance, surface interactions, and

molecular order/disorder, which could create unanticipated behaviors, but which also may be exploited to achieve novel functionalities (Minton 2006; Miyoshi and Sugimoto 2008; Lizana et al. 2009; McGuffee and Elcock 2010). For instance, in living cells, nuclear crowding and DNA packing are involved in cell cycle and cell differentiation. In vitro studies demonstrated that crowding shifts binding reactions toward bound states, due to the excluded volume induced by co-solutes (Bancaud et al. 2009). This was confirmed in living cells by Bancaud et al. (2009) who described crowding as a driving force to maintain functional nuclear compartments at a low cellular energy cost (i.e., without requiring the involvement of membranes or other additional structural boundaries).

We summarize in this review several key emergent properties of nucleic acids that derive from nanoscale confinement. The properties specifically relate to nucleic acid behavior with respect to hybridization, denaturation, conformation, stability, and enzyme accessibility. The selected studies highlight several emergent properties and also show the experimental approaches used to detect these properties, including atomic force microscopy, electron microscopy, fluorescence spectroscopy, electrochemistry, and gel electrophoresis. These studies reveal that the behavior and properties of dense, nanoconfined nucleic acid architectures is highly dependent upon density, molecular or supramolecular structure, molecular flexibility, and the types and strengths of weak interactions between adjacent molecules.

2 Novel Sensing Approaches Using Nanoconfined Nucleic Acid Architectures

Nucleic acid nanoengineering pioneered by Nadrian Seeman (Seeman 1982, 1990; Chen and Seeman 1991) takes advantage of the inherent capacity of the molecules to self-assemble in solution by Watson–Crick base pairing, allowing formation of diverse structural motifs, several nanometers in width, such as double-helical and single-helical regions, sticky ends, hairpin loops, bulge loops, junctions, and crossovers (Feldkamp and Niemeyer 2006). With the aid of computer design, this process can be scaled up to form structures several hundred nanometers in width (Feldkamp and Niemeyer 2006; Rothemund 2006; Woo and Rothemund 2011; Ke et al. 2012). The fashioned nanostructures then can be tailored to carry additional fully functional biomolecules, for example via click chemistry or DNA-directed immobilization (Jonkheijm et al. 2008; Niemeyer 2010; Voigt et al. 2010; Meyer and Niemeyer 2011; Douglas et al. 2012; Lavella et al. 2012).

In 2006, Paul Rothemund introduced a novel approach to produce "DNA origami"-dense nanostructures comprising a several-thousand-nucleotide, single-stranded(ss) DNA molecule ("scaffold") that folds into programmable shapes via Watson–Crick hybridization of several, short ssDNA sequences ("staples") (Rothemund 2006). DNA origami can be functionalized further in several ways with different probes, including aptamers, DNA, proteins, antibodies, and gold nanoparticles (Rinker et al. 2008; Kuzyk et al. 2009; Ghosh et al. 2012; Sacca

and Niemeyer 2012). In most of these cases, the probes are linked to selected staples after their incorporation within the scaffold–staple-based nanostructure, formed in a single-step self-assembly process (Meyer and Niemeyer 2011). In combination with atomic force microscopy (AFM), two-dimensional DNA origami has been utilized as nanochips for biosensing applications (Ke et al. 2008; Sacca and Niemeyer 2012). Lindsay, Yan, and coworkers created a DNA origami as an RNA detector, potentially applicable to gene expression analysis at the single-cell level (Ke et al. 2008). The method, however, would be challenging to implement, as RNA detection requires that the nanochips are first immobilized on a surface, then sample-imaged by high-resolution AFM, allowing the enumeration of individual RNA molecules immobilized on their respective nanochip (Ke et al. 2008). In contrast, the combination of fluorescence imaging with self-assembled DNA nanostructures has led to novel approaches that also underscore the impact of fluorescence-based tools on tissue imaging. Initial studies demonstrated that DNA self-assembly can generate materials exhibiting precise spatial positioning of fluorescent labels and possessing exquisite optical properties (Acuna et al. 2012; Kuzyk et al. 2012). For instance, Niemeyer and coworkers realized a supramolecular Forster resonance energy transfer (FRET) system, based on a linear structure, stabilized by several ssDNA staples, that provided a defined distance between a fluorescent protein and a synthetic chromophore (Kukolka et al. 2007). Similarly, Tinnefeld and coworkers exploited DNA origami technology to generate a two-dimensional "molecular breadboard" allowing a programmed spatial arrangement of fluorophores in a grid-like fashion (Stein et al. 2011a, b). This was used to demonstrate alternative energy-transfer pathways dependent upon incorporation of a "jumper" dye at specific positions (Stein et al. 2011b). Intensive parallel development efforts in fluorescence optical imaging have led to super-resolution techniques that validate the proposal that biomarker detection in tissues can be achieved through single-molecule counting (Nanguneri et al. 2012). Besides the diagnostic importance of single-molecule sensitivity, there has been a pressing need to circumvent the current limits to the number of simultaneously localizable biomarkers in cells and tissues. This has spurred the development of super-resolution approaches based on combinations of dyes as "barcodes," allowing multiplexed biomarker imaging (Bates et al. 2007). DNA origami provided a revolutionary approach to this problem: Yin, Shih, and coworkers created up to 216 different biomarker barcodes by the site-specific fluorescent labeling of different self-assembled DNA nanostructures (shaped as rods, several hundred nm in length) linked to antibodies. This was accomplished using four fluorescent dyes corresponding to four different colors. Barcode species were unambiguously decoded using diffraction-limited total internal reflection fluorescence (TIRF) microscopy (Lin et al. 2012). Up to five barcodes with higher spatial information density were demonstrated via construction of super-resolution barcodes, with features spaced by ~40 nm (Lin et al. 2012) (see Fig. 1). This imaging approach, termed DNA-PAINT, relies on the continuous association/dissociation reactions involving the origami-affixed ssDNA molecules and the complementary, fluorescently labeled ssDNA (imager) molecules in solution. The latter molecules are

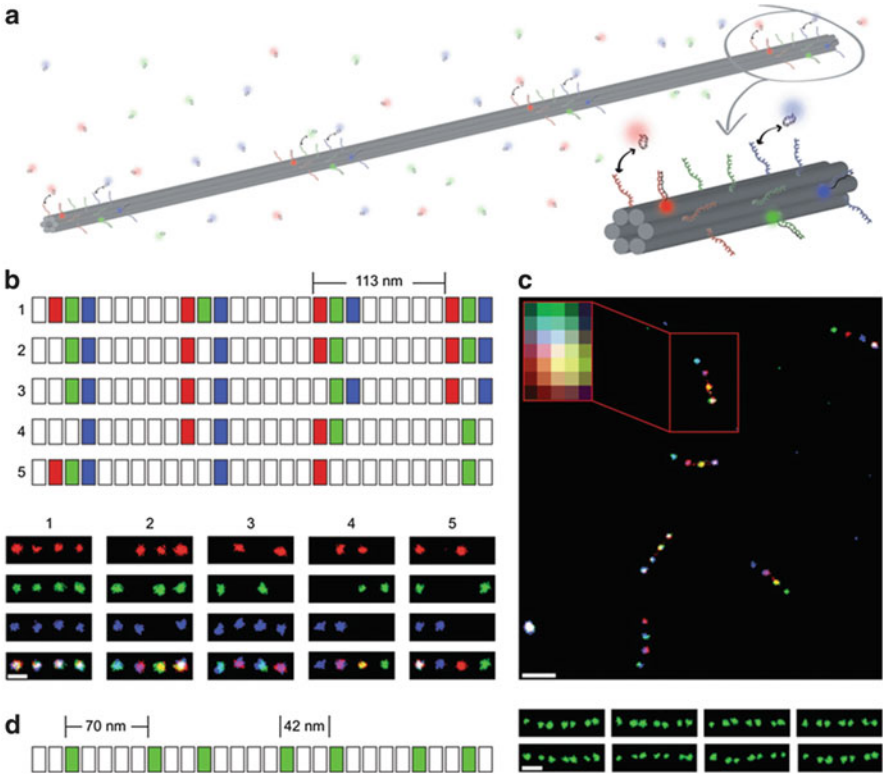

Fig. 1 Submicrometer geometrically encoded fluorescent barcodes self-assembled from DNA. (**a**) Schematic of *barcodes* for DNA-PAINT super-resolution imaging. The 400 nm DNA nanorod consists of four binding zones evenly spaced by ~113 nm. Each zone can be decorated with the desired combination of "docking" sequences for *red*, *green*, or *blue* imager strands. The *orthogonal* imager strands bind transiently to their respective "docking" sites on the nanorod, which creates the necessary "blinking" for super-resolution reconstruction. (**b**) The *top panel* is a segment diagram of the nanorod monomers used to create five barcodes. The *lower panel* comprises super-resolution images of the five *barcodes* shown in separate channels and as superimposed images. Scale bar = 100 nm. (**c**) Super-resolution image showing all five *barcodes* from (**b**) one mixture. The *inset* shows the diffraction-limited image of a barcode. Scale bar = 250 nm. (**d**) An asymmetric barcode that consists of seven binding zones for *green* imager strands spaced at ~70 nm and ~42 nm for longer and shorter distances, respectively. Scale bar = 100 nm [Reprinted from Lin et al. (2012). Copyright © 2012, Rights Managed by Nature Publishing Group]

ubiquitously present during imaging, but are preferentially localized to the corresponding hybridization sites on the origami surface. Transient binding between imager and docking strands produces fluorescence "blinking," allowing stochastic super-resolution imaging (Jungmann et al. 2014). Using the same approach, Yin, Shih, and coworkers demonstrated that super-resolution fluorescence imaging can provide multiplexed detection of multiple proteins in microtubules and mitochondria in a single fixed cell sample, using a single dye. Here,

antibodies linked to specific short ssDNA molecules were used as docking strands, while the complementary imager strands (labeled with the same dye) were exchanged, step-by-step, thus allowing the multiplexed detection of up to four proteins by super-resolution imaging, in a layer-by-layer fashion (Jungmann et al. 2014).

DNA origami technology is not limited to the creation of smart devices for imaging, but also opens up the prospect of nanomachines that can control their shape and perform operations in a programmable manner in biological systems (Krishnan and Simmel 2011; Pinheiro et al. 2011). This has provided the basis for development of novel carriers for the delivery and release of drugs in a cell-specific manner (Walsh et al. 2011; Douglas et al. 2012; Hubbell and Chilkoti 2012; Jiang et al. 2012; Zhao et al. 2012). For instance, Högberg utilized rod-like DNA origami to create precise spatial distribution of ligands at the nanoscale. Thus, ligand spacing can be controlled independently of ligand concentration (Shaw et al. 2014). The device, termed a ligand "nanocaliper," displays precise, programmable ligand arrays. The tested hypothesis is that cell signaling is usually performed using a group of receptors and ligands, and that within the cell membrane, receptors are confined in spatially organized membrane domains, such as lipid rafts. The authors applied nanocalipers to map the relationship between the nanoscale spacing of ligand and cell-surface receptor activation that provided a cellular response. It was determined that the nanoscale distribution of the ligand ephrin-A5 determines signal transduction and cell behavior. Cells stimulated with an ephrin-A5 ligand nanocaliper with 40-nm spacing showed higher levels of activating phosphorylation of the EphA2 receptor and lower invasive properties of the breast cancer cells (MDA-MB-231) than with the cells stimulated with the monomeric ligand or dimeric ligands spaced at 100 nm. In summary, this study demonstrates an unprecedented application of DNA origami for stimulating a cellular response by controlling the "display architecture" of nanoscale-confined cell surface ligands (Shaw et al. 2014).

3 Behavior of Nanoconfined Nucleic Acids from a Theoretical Perspective

Understanding the emergent behavior of nanoconfined nucleic acids can benefit from computational modeling and theoretical approaches. However, the goal of predicting equilibrium average structures and conformational fluctuations of DNA origami designs poses significant challenges, and the currently available models are not yet able to provide accurate descriptions in the most general cases. The task is made particularly challenging by the intrinsic multi-scale nature of the problem. With linear dimensions of the order of tens of nanometers, the peculiar mechanical properties of the origami emerge as a collective behavior involving thousands of nucleobases. At the same time, the energetics of Holliday junctions—the basic

structural feature provided by DNA staples that ultimately constrains the shape of the assembly—is dominated by hydrogen bonding, which is an interaction occurring over a range of tenths of nanometers. Given this wide spectrum of length scales, an entire hierarchy of theoretical descriptions has been put forward to capture different aspects of origami designs. Approaches range from mesoscopic descriptions based on finite-element calculations (CanDo) (Kuzyk et al. 2009), to coarse-grained modeling with nucleobase resolution (Arbona et al. 2012a, b), to all-atom molecular dynamics (MD) simulations (Yoo and Aksimentiev 2013). Below we provide an overview of these methods by proceeding in a top-down fashion, from the method encompassing the major macroscopic features to the method that dwells on the microscopic details. Discussions are necessarily brief and cover only the major tenets and the scope of applicability.

3.1 Finite-Element Modeling

At the heart of this approach is the treatment of DNA origami as bundles of isotropic elastic rods (Kuzyk et al. 2009). In practice, each DNA strand is represented by a set of two-node beams characterized by a stretching, bending, and torsional stiffness. To effectively take into account the additional degrees of freedom provided by nicks in the DNA structure, the corresponding beams are assigned a different set of parameters. Single-stranded DNA connecting double-helical regions is treated as an entropic spring. Finally, each rod is constrained to be in contact with its nearest neighbor at the specific locations of crossover junctions, via a rigid link of zero length. With this approach, free energy computing the structure of the origami amounts to a mechanical perturbation analysis, in which DNA domains are simultaneously relaxed from their initial structure. Specifically, all neighboring rods first are deformed to align the junctions and then crossover constraints are applied. The overall structure is then relaxed iteratively using finite-element approaches that are extensively used in the field of structural mechanics. Although highly successful, this approach involves an unavoidable empiricism in the choice of the model parameters. Stretching, bending, and torsional moduli are chosen so to reproduce the B-form of the DNA double helix, while the scaled parameters for the nicks are tuned to match experimental transmission electron microscopy (TEM) images. Thus, the transferability of these parameters across different origami designs can be ascertained only a posteriori by comparison with results from imaging experiments.

3.2 Coarse-Grained Models

One of the most successful coarse-grained models used to study the self-assembly of DNA origami is the so-called stack of plates (SOP) model (Arbona et al. 2012a,

b). In this representation, a DNA helix is treated as a set of stacked objects with ellipsoidal shape, where each ellipsoid represents a base pair. Clearly, by mimicking the shape of each base pair by an ellipsoid, all the degrees of freedom describing the relative orientation of the two H-bonded bases are necessarily ignored. The rationale is that H-bonded bases are relatively rigid, i.e., fluctuations in their relative positions are small, compared to the length scales deemed significant for this problem. A similarly simplifying assumption is used to describe the sugar–phosphate bonds between bases: the potential that holds together neighboring ellipsoids is quadratic in its displacement from an appropriately chosen equilibrium value (elastic springs). Specific values of the interaction parameters (spring energy and stacking energy) give rise to a helical pattern mimicking the DNA structure. Indeed, the correct trade-off between two driving forces—the spring energy that tends to bring the ellipsoids close to one another and the stacking energy that tends to align them—causes an effective twist along the pseudo-axis of symmetry. To study self-assembly of origami designs, this minimalist model is complemented by appropriate interactions between different strands. Specifically, an interaction of excluded volume between strands is added in such a way that a configuration is rejected that has a negative distance between ellipses belonging to different DNA strands. Moreover, because each phosphate group bears a negative charge, electrostatic interactions between neighboring helices are taken into account via Coulomb-like interactions. To this end, negative charges are placed at the extremities of the ellipsoids, and the effect of counterions is implicitly considered via a Debye-type screening of the Coulombic interaction. It is important to note that this model is a coarse-grained one, i.e., it is completely oblivious of the atomistic structural features ultimately governing the pattern of hydrogen bonds. Most importantly, with this level of granularity, there is no difference between the major and minor grooves and no intrinsic preference between left- and right-handed helices. As for the finite-element model, a fine-tuning of the parameters is needed to reproduce correctly the structure of DNA origami designs.

3.3 All-Atom Molecular Dynamics Simulations

All-atom MD simulations constitute, in general, the most unbiased approach to study the equilibrium properties of a thermodynamic system. Thanks to its ability to relate microscopic interaction energy to macroscopic, thermodynamic observables, MD simulations are the tools of choice to study the behavior of new materials. Indeed, provided that the microscopic interactions have been correctly described and a reasonable starting conformation is available, the information contained in MD trajectories can be effectively exploited to compute the desired ensemble averages. Since the elementary constituents of DNA origami designs, the nucleic acids, have long been studied through MD simulations, the available molecular models (the so-called force fields) are accurate enough to describe realistically these systems. Moreover, computational tools can be used to generate a template of

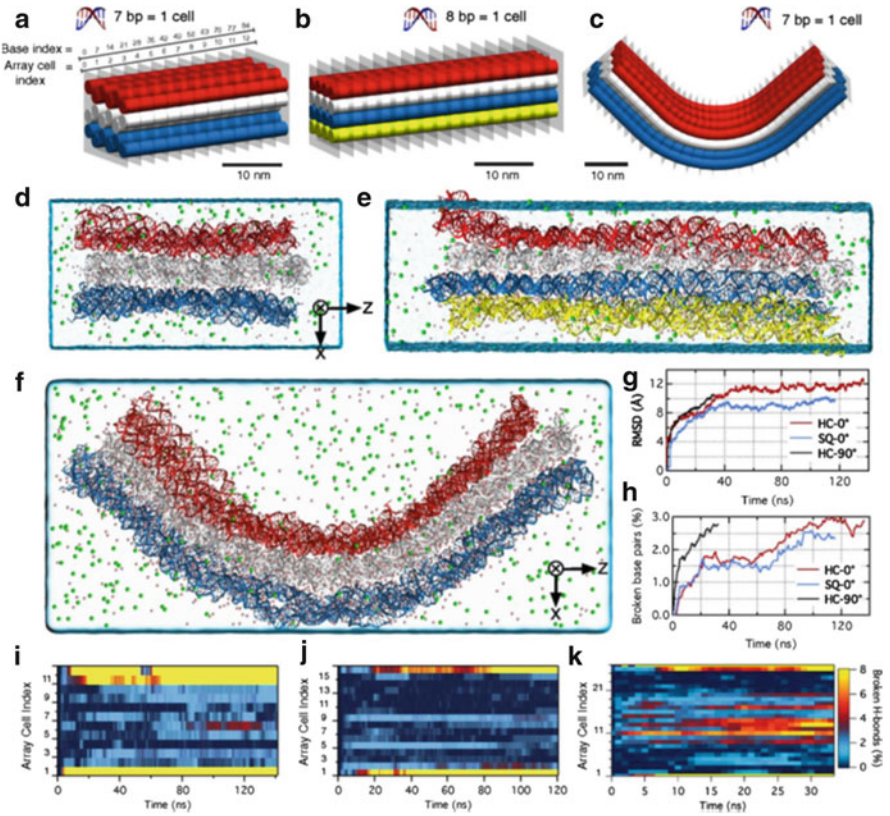

Fig. 2 All-atom MD simulations of DNA origami structures. (**a**–**c**) Schematic representations of the three DNA origami structures investigated in Yoo and Aksimentiev (2013). *Cylinders* represent DNA duplexes. *Cylinders* are connected to one another through crossovers every seven or eight base pairs (*gray* semitransparent planes). (**d**–**f**) Relaxed structures at the end of our production MD runs (Mg^{2+} and Cl^{-} ions) are shown as *pink* and *green* spheres, respectively. The systems contain up to three million atoms. (**g**) Root-mean-square deviation (RMSD) of the DNA atoms from their initial coordinates as a function of the simulated time. (**h**) Fraction of base pairs broken during the MD simulations. (**i**–**k**) Fraction of broken base pairs in individual *array* cells for the three systems [Reprinted with permission from Yoo and Aksimentiev (2013). Copyright © 2013, Rights Managed by Proceedings of the National Academy of Sciences of the USA Publishing Group]

the target design, thereby providing a suitable initial conformation. However, despite the fact that MD simulations appear as a desirable option to study DNA origami designs, to date the only example in literature of an all-atom MD simulation addressed linear designs, involving honeycomb and square lattices and with one of them having a programmed 90° bend (Yoo and Aksimentiev 2013) (see Fig. 2). In particular, the system was modeled using periodic boundary conditions, the CHARMM36 force field for DNA and ions (Huang and MacKerell 2013), and the TIP3P model of water (Jorgensen et al. 1983). Strikingly, trajectories were

collected for millions of atoms, thanks to the availability of high performance computing facilities. Importantly, results from simulations were found to be in good agreement with the experimental data. While these simulations prove the usefulness of all-atom MD simulations to study the equilibrium conformation and the structural dynamics of DNA origami designs, the computational cost of these calculations limit their applicability to the study of fast relaxations occurring over time intervals in the order of hundreds of nanoseconds. This time-scale limitation makes all-atom MD unsuited to study several crucial aspects of DNA origami designs, such as the assembly process, and underscores the need for a true multi-scale theoretical strategy reliant on a combination of all the aforementioned approaches.

4 Behavior of Nanoconfined Nucleic Acids from an Experimental Perspective

As described, DNA self-assembly permits the generation of highly dense nanostructures with architectures reflecting controlled molecular orientations. The obligatory close packing of the DNA structures can strongly influence functionality. Understanding the processes associated with the subsequent addition, removal, or modification of molecular elements is a prerequisite for ensuring the optimal function of the nanostructures in diverse external environments. In this section, we review recent studies that examine the behavior of nucleic acids, using computational and experimental approaches, toward achieving an in-depth understanding of nucleic acid behavior in crowded, highly inhomogeneous systems.

4.1 DNA Hybridization Within Nanoconfined Nucleic Acid Architectures

It is generally accepted that DNA hybridization is hindered in highly dense monolayers (Peterson et al. 2001a). Similarly, the formation of highly dense, self-assembled 3D DNA origami nanostructures is impeded as the number of inter-helix connections (“crossovers”) increases. These structures are formed by the hybridization of short ssDNA staples with multiple segments of the long ssDNA scaffold. The amount of inter-helix connections inevitably increases with nanostructure size and complexity, and the concomitant hindrance of self-assembly reflects the effects of molecular crowding. The study of Yan suggests that crossovers introduce repulsive forces and steric hindrance that impede the action of ssDNA staples on the ssDNA scaffold during self-assembly (Ke et al. 2009). The authors demonstrated that the yield of self-assembly of a 3D DNA cuboid structure (with DNA duplexes arranged in a square lattice) increases by diminishing the

number of crossovers only within the core of the cuboid, thus preserving the desired shape.

Pinheiro et al. (2012) designed a water-soluble DNA nanostructure to determine how steric crowding may influence DNA hybridization. The nanostructure was a planar, rectangular tile comprised of six parallel double helices, joined by helix-spanning, single-stranded oligonucleotides. The tile possessed adjacent, 20-nt overhangs, with one of the overhangs serving as the binding site for the target probe, while the other overhangs functioning as "off-target" probe binding sites. The steric factors evaluated included (1) the site of binding of the target probe in the tile, (2) the presence of DNA flanking the hybridization site, and (3) formation of a double-helical structure between the target probe and other components of the tile. Using real-time fluorescence spectroscopy, the authors found that duplex formation involving the target probe overhang caused enhanced fluorescence, reflecting the ability of the newly formed double helix to displace the dye from its intercalation site within the core of the tile structure. More efficient hybridization was obtained when the target probe was flanked by blunt-ended duplexes or was located at an outermost (edge) position. In the latter case, the target probe would be flanked by only a single off-target probe. When the target probe is located at inner positions, the kinetics of hybridization are largely insensitive to whether the flanking off-target probes are single or double stranded. Additional experiments showed that the hybridization rate dramatically decreases when the target probe is bent (kinked), rendering the hybridization site less accessible from solution. The authors argue that observed differences in kinetics primarily reflect differences in the frequency of productive collisions and that the slower hybridization kinetics reflects an impaired nucleation step. In summary, this study has demonstrated the significant impact of accessibility within the context of highly dense DNA tiles.

Bombelli et al. used short DNA oligonucleotides to create hexagonal DNA nanostructures that were grafted onto phospholipid bilayers (Bombelli et al. 2009). It was shown that changing the grafting density could affect hybridization kinetics. Thus, DNA hybridization to the nanostructures grafted onto phospholipid membranes at low density was faster than seen in solution, but was slower on the more densely grafted membranes, due to molecular crowding on the membranes.

The impact of crowding on DNA hybridization to self-assembled DNA monolayers was (DNA SAMs) examined by Ricci et al. (2007). An electrochemical probe was employed to detect oligonucleotide binding in a process that repositioned a redox-sensitive probe further away from the gold surface, thereby reducing the faradic current. Measurements of the faradic current as a function of probe density yielded non-monotonic behavior: (1) When the surface electrochemical DNA probe density was reduced from 10^{12} molecules/cm^2, signal suppression decreased in an essentially monotonic manner. This is consistent with previous observations on the behavior of surface-affixed DNA, in which hybridization efficiency is inversely proportional to the surface probe density (Steel et al. 2000; Peterson et al. 2001b; Castelino et al. 2005). (2) However, for densities $>10^{12}$ molecules/cm^2, corresponding to a mean spatial separation of <10 nm, the faradic current

suppression dramatically increased, attaining a limiting value of 70 % of the initial value (Ricci et al. 2007). At high density, the equilibration time for the reaction is ~40 min, which is two- or eightfold higher than the equilibration time measured at medium or low density, respectively.

Based on these observations, it has been argued that signal suppression at high probe density reflects an inhibition of subsequent collisions with neighboring probes after target hybridization at a given probe, which in turn implies that densely packed probe molecules exhibit, on average, a vertical configuration (Ricci et al. 2007). Thus, for high-density electrochemical DNA probe surfaces, faradic current suppression reflects the sensitivity of the configurational structure of the E-DNA probe toward surface density. These findings are consistent with independent observations that densely packed DNA surface assemblies exhibit limited hybridization capability (Peterson et al. 2001b; Castelino et al. 2005), reaching >50 % in ssDNA monolayers with densities ~2–3 $\times 10^{12}$ molecules/cm^2. Finally, the observation that bending of the electrochemical probe DNA causes a reduction in nucleation capability of the initial probe–target interaction reflects the findings of Pinheiro and coworkers on the influence of DNA bending on hybridization efficiency (Pinheiro et al. 2012) (see also above).

A series of investigations examined DNA self-assembly on flat gold surfaces (Peled et al. 2008) or gold nanoparticles (Peled et al. 2010) and assessed the effect of density on the stability of the short (15 or 26 bp) duplex structures. The change in density of surface-bound ssDNA molecules involved in the self-assembly process was monitored using radiolabeled ssDNA, either as the surface-attached probe or as the added substrate. DNA binding and duplex stability was assessed by phosphorimaging, allowing an absolute determination of the probe surface density. Peled and coworkers also measured duplex stability as a function of DNA density on gold nanoparticles (Peled et al. 2010). The two studies provided complementary results in showing that for 15 bp or 26 bp dsDNA on a flat surface or a 26 bp dsDNA on gold nanoparticles of differing diameters (5 and 10 nm), DNA duplex denaturation efficiency is essentially linearly related to the attached DNA density, reaching ~80 % at maximum density (~4 $\times 10^{13}$ molecules/cm^2) for the gold nanoparticles. In contrast, a longer (50 bp) DNA does not undergo significant denaturation. The authors argue that for the 50-bp duplex, the energy of formation of a new thiol–gold bond is insufficient to compensate for the energy required to separate the two strands. These results do not support the mechanism where duplex denaturation is promoted by interactions between the surface and the ssDNA bases (exposed, e.g., by duplex "breathing"). If such a mechanism were operative, the denaturation process would be favored at low densities, where the adsorption energy between the surface and dissociated ssDNA strands would compensate for the energy required for duplex dissociation (Chen et al. 2009).

Crowding-induced denaturation can occur with shorter duplexes at densities $<10^{13}$ molecules/cm^2 (Peled et al. 2008). Thus, in Ricci et al. (2007) (see also above), a 5-bp stem can "unzip" upon hybridization, allowing formation of a ≥27-bp duplex. This may explain the stepwise change in faradic suppression, reflecting the ability of several stems per unit area to change their conformation, allowing

hybridization with much longer complementary strands that are fewer in number. The model of Peled and coworkers also suggests that "stretching" of surface-bound ssDNA molecules in response to electrostatic repulsion at high densities can facilitate access of additional DNA molecules to the monolayer.

The functionality of nucleic acids in spatially confined, self-assembled monolayers (SAMs) has been investigated by Mirmomtaz et al. (2008). Here, spatially confined DNA arrays were created by an AFM-based technique termed nanografting (Hu et al. 2005; Castronovo et al. 2008, 2011; Mirmomtaz et al. 2008; Staii et al. 2008; Bano et al. 2009; Sanavio et al. 2010; Liang et al. 2011; Parisse et al. 2012). Nanografting is performed by an AFM tip that is scanned at a relatively high load (a few to several tens of nN) over the desired area in a solution containing the thiolated nucleic acid. Due to tip-induced mechanical perturbations, the preadsorbed thiol molecules that form the "protective" SAM undergo local exchange with the thiolated nucleic acid molecules in solution. Surface patterns of DNA can be generated with different shapes and lateral widths, ranging between a few tens of nm to several microns and of varying density. Using this approach, Mirmomtaz et al. (2008) showed that the topographic height of a highly dense ssDNA monolayer obtained by nanografting is greater than that of the corresponding monolayer obtained by passive self-assembly. Thus, at the same ssDNA concentration, ssDNA molecules are incorporated in a nanografted patch more efficiently than in the corresponding SAM. Thus, in the nanopatch, ssDNAs acquire a mostly stretched conformation.

Mirmomtaz et al. (2008) also demonstrated that hybridization behavior and efficiency in nanografted patches is qualitatively different than that for ssDNA SAMs. At high density, the maximum amount of duplexes formed in a nanografted patch is approximately 50 %, and that denaturation is less pronounced in a nanopatch than in the SAMs studied by Peled et al. (2008). The AFM study provided a maximum density estimation for nanopatches of about ~10^{13} molecules/cm^2.

To account for DNA reactivity within nanografted patches, Bosco (Bosco et al. 2012) combined AFM nanografting and compressibility experiments with coarse-grained computational simulation. The study provided a compressibility dependence on density for ssDNA and dsDNA and, importantly, provided calibrated AFM-based and numerical tools for characterizing DNA nanostructures that are too small for accurate examination by optical and spectroscopic approaches. These studies support a nanografting process in which the "combing" action of the AFM tip creates ssDNA matrices with homogeneous spatial distributions. Moreover, the level of physical interaction between adjacent DNA molecules is reduced, compared to spontaneously formed self-assembled monolayers. In the latter case, the structural mobility of ssDNA molecules is reduced, perhaps affording a greater interaction with the surface.

Josephs and Ye (2013) studied crowding and homogeneity of DNA monolayers using high-resolution AFM microscopy and single-molecule imaging of DNA probes, tethered by a hexanethiol linker to the gold surface. In one method ("insertion"), the gold surface is initially passivated by treatment with 6-mercaptohexanol

and then exposed to the thiolated DNA that preferentially attaches to the surface at defect sites in the passivated surface. In the second method ("backfilling"), the gold surface is first exposed to thiolated DNA and then immersed in a solution of 6-mercaptoethanol, which occupies the remaining sites and "lifts" the DNA off of the surface (Levicky et al. 1998; Park et al. 2004). The achieved single-molecule sensitivity allowed the application of spatial statistics that provided direct evidence that DNA on surfaces prepared by backfilling have a tendency to form aggregates. In contrast, the insertion method yields surfaces that are more uniform at the molecular scale. The findings of Josephs and coworkers also provided a rationale for the effectiveness of nanografting in enabling the formation of highly dense monolayer patches, with a homogeneous spatial distribution of DNA molecules.

Liang et al. (2011) found that highly dense, self-assembled monolayers of ssDNA on a gold surface share the same AFM-measured height as nanografted patches of the same molecule in the absence of a backfilling thiol. However, the hybridization-induced change in height of a ssDNA nanopatch upon hybridization is ~four-fold greater than that for the corresponding SAM. The height change is reversed upon hybrid dissociation, and the hybridization can be repeated to provide the same topographic change, thus indicating the conserved structural distinction of the patch and the self-assembled monolayer.

4.2 *Enzymatic Reactions Within Nanoconfined Nucleic Acid Architectures*

The enzymatic processing of surface-attached nucleic acids is an active area of investigation and has multiple implications for biosensing and biotechnology (Eid et al. 2009; Metzker 2010b; Zhou et al. 2011; Heyman et al. 2012). For instance, the enzymatic processing of DNA in situ has been utilized for cloning and sequencing on solid supports, enabling unprecedented high-throughput capability (Metzker 2010b). These applications require a reaction environment that provides maximal reaction efficiency, allowing nucleases to process their substrates in bulk while minimizing inhibition or side reactions imposed by crowding and steric hindrance (Carmon et al. 2002; Buxboim et al. 2008; McCalla et al. 2009). Castronovo and coworkers studied the action of the restriction enzyme DpnII (recognition sequence, 5′–^GATC–3′), on surface-bound dsDNA nanopatches created by nanografting (Castronovo et al. 2008). By measuring the extent of cleavage as a function of packing density for a 44 bp dsDNA, a specific density threshold was identified above which the reaction is inhibited. Access of *Dpn*II (a homodimer) to the monolayer (density $\sim 1 \times 10^{12}$ molecules/cm^2) is fully inhibited when the average dsDNA–dsDNA distance <10 nm, which also corresponds to the diameter of the DpnII holoenzyme. This result, also supported by other studies (Bar and Bar-Ziv 2009; McCalla et al. 2009; Palanisamy et al. 2010), indicates that accessibility of protein binding sites in dsDNA molecules confined in self-assembled

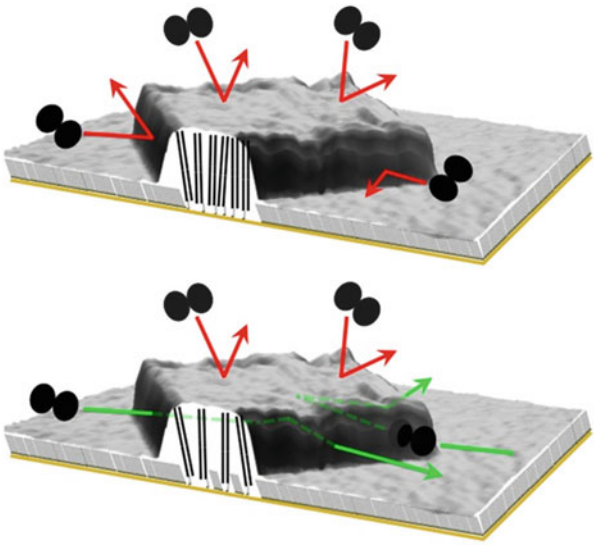

Fig. 3 Two-dimensional enzyme diffusion in nanografted DNA surface matrices [See also Castronovo et al. (2011)]

nanostructures critically depends on the steric constraints imposed by the molecular density. In contrast to previous studies demonstrating that macromolecular crowding significantly affects the speed of endonuclease processing on DNA substrates (Sasaki et al. 2007), this work provides a demonstration that the enzymatic processing is either fully allowed or fully inhibited as a function of molecular density.

Castronovo and coworkers investigated the enzymatic reactivity of dsDNA within the context of specific nanografted patterns and showed that dsDNA confinement has quantifiable effects on enzyme diffusion and access to target sites within the surface-bound nanostructures (Castronovo et al. 2011). Here, DpnII was shown to have essentially no access to a low-density dsDNA nanopatch, containing the DpnII recognition site that is surrounded by a nanografted "fence" of highly dense dsDNA lacking the recognition site. This situation is maintained regardless of the total contact area between the inner low-density patch and solution, which can be as large as several square microns. The study indicated that the enzyme (as others in the same family) only can gain access to its recognition sequence from the nanopatch "sidewalls," rather than from the larger, topmost face of the patch. The enzyme is predicted to diffuse within the two-dimensional matrix to locate its target sites (see illustrative Fig. 3).

The accessibility of ssDNA and dsDNA toward the sequence-nonspecific DNase I was studied using an electrochemical biosensor (Biagiotti et al. 2012). The processing of the ssDNA probes, followed using an electrochemical reporter, is fully efficient at lower probe densities ($\sim 1 \times 10^{11}$ molecules/cm^2), but monotonically decreases at higher densities (2.5×10^{12} molecules/cm^2) to a final efficiency of 50 %. However, the enzymatic digestion of the surface-bound dsDNA was limited to 60 % even at the lowest densities investigated ($<1 \times 10^{11}$ molecules/

cm^2). Thus, a significant fraction of the immobilized dsDNA is inaccessible to DNase, regardless of surface density.

Compared to surface-bound DNA monolayers, water-soluble DNA nanostructures are highly ordered systems that either consist of a limited number of short DNA molecules or are larger two- or three-dimensional shapes, comprising several thousands of nucleotides. Keum and Bermudez investigated the reactivity of a DNA tetrahedron toward a sequence-specific endonuclease (Keum and Bermudez 2009). The action of DdeI restriction endonuclease (recognition sequence C^TNAG) was examined as a function of cleavage site placement within the DNA tetrahedron. One tetrahedron (T1) had the restriction site located in the center of one of the edges, while the second tetrahedron (T2) had the site adjacent to one of the vertexes. The DNA tetrahedrons as initially formed contained several nicks along the DNA duplex segments, thereby conferring flexibility. Both structures exhibited significant reactivity toward DdeI. Treatment of T1 and T2 with DNA ligase increased the rigidity of the nanostructures, and treatment of the ligated nanostructures with DdeI revealed that endonuclease action is inhibited only for the ligated T2 nanostructure (Keum and Bermudez 2009). The authors suggest that the presence of certain structural motifs, such as the presence of rigid segments connected by short linkers that provide small radius of curvature at vertexes, could play an essential role toward the formation of nuclease-resistant DNA-based nanostructures, potentially useful in drug delivery applications.

Nuclease action in nanostructured DNA systems is sensitive to salt concentration. Seferos et al. showed that, although high salt concentrations can cause DNA denaturation, it also can inhibit enzymatic cleavage. The group compared the effect of DNase I on dsDNA in solution and on dsDNA attached to water-soluble gold nanoparticles (AuNPs) and found that the latter showed a ~four-fold longer half-life than the former (Seferos et al. 2009). The results also showed that the overall cleavage kinetics were slower, although enzyme association was faster with the AuNPs. This effect was due to high local salt concentration, as monovalent cations can inhibit DNase I by displacing Mg^{2+} and Ca^{2+} ions. When a salt-tolerant mutant of DNase I was used, the enzymatic action on molecular DNA was recovered.

Given the thrust to develop applications in drug delivery or in vivo biosensing, the fate of DNA origami in cell lysates or in the presence of specific nucleases has been investigated. Castro et al. found that the incubation of different 3D DNA nanostructures with exo- or endonucleases provides disparate results (Castro et al. 2011). However, compared to a circular dsDNA plasmid, the DNA nanostructures are more resistant to DNase I action. Meldrum examined the behavior and stability of triangular, rectangular, and cuboidal DNA nanostructures in mammalian cell lysates (Mei et al. 2011). While the DNA origami structures were apparently unaffected by incubation in the cell lysates at different temperatures, with no strong interactions with cellular components as noted by nondenaturing gel electrophoresis, the plasmid DNA was shown to interact with one or more lysate proteins of unspecified identities. In addition, a rectangular DNA nanostructure, functionalized with ssDNA overhangs that can bind a short ssRNA, was shown to retain its functionality after incubation in cell lysates. Meldrum argues that the

enhanced resistance of the DNA nanoassemblies in the presence of the myriad cell components reflects the high charge density and molecular rigidity of the assemblies, which hinders protein engagement, perhaps due to preventing conformational changes required for recognition.

With the new knowledge of the stability of nanoconfined DNA structures, biocompatible carriers were designed that could deliver a siRNA molecule into a xenografted tumor. This approach provided a nearly fourfold increase in siRNA half-life (Lee et al. 2012). Also, DNA origami containing intercalated doxorubicin molecules allowed increased drug internalization in cultured mammalian cells and a concomitant strong reversal of drug resistance in doxorubicin-resistant cancer cell lines (Jiang et al. 2012).

5 Conclusions and Prospects

Nucleic acid nanotechnology is now an established, interdisciplinary field of research whose rapid development reflects the productive collaborations of researchers in the physical sciences, materials science, computer science, biology, and medicine. We believe that the integration of surface science has the potential to provide a transformative effect on successful development and application. Experimental and theoretical studies on surface-supported nanosystems such as self-assembled monolayers and nanopatches will continue to provide fundamental information on the function and behavior of nucleic acids in confined environments. Indeed, a number of unanticipated behaviors of nucleic acid architectures reflect nanoscale confinement. Nucleic acid function in this milieu is dependent on the local density, molecular flexibility, as well as the network of weak interactions involving adjacent nucleic acid molecules, the surface, and the surrounding solution. These factors significantly affect accessibility, molecular crowding, and hydration associated with the processes of hybridization, denaturation, conformational state, and ligand accessibility. A better understanding of these fundamental behaviors and properties will allow significant advances in nucleic acid nanotechnology and will better inform the design of nanostructures with unprecedented functionalities for effective applications in nanomedicine, including diagnostics and drug delivery. The complexity of biomolecular environments, including the bloodstream, tissues, and intracellular environments of cells, demands no less than the robust, reproducible function of a properly designed nucleic acid nanosensor or nanodevice.

Acknowledgments Studies in the authors' laboratories were supported in part by the College of Science and Technology of Temple University (A.W.N., S.K.R., V.C., and M.C.), the NIH (RO1-GM56772) (A.W.N), and the European Research Council (Grant ERC Ideas 2010 n. 269051-Monalisa's Quidproquo) (A.S., L.C., and M.C.).

Competing Financial Interests The authors declare no competing financial interests.

References

Acuna GP, Möller FM, Holzmeister P et al (2012) Fluorescence enhancement at docking sites of DNA-directed self-assembled nanoantennas. Science 338:506–510

Akbulut O, Yu AA, Stellacci F (2010) Fabrication of biomolecular devices via supramolecular contact-based approaches. Chem Soc Rev 39:30–37

Arbona JM, Aimé J-P, Elezgaray J (2012a) Folding of small origamis. J Chem Phys 136:065102

Arbona JM, Aimé J-P, Elezgaray J (2012b) Modeling the mechanical properties of DNA nanostructures. Phys Rev E 86:051912

Bancaud A, Huet S, Daigle N et al (2009) Molecular crowding affects diffusion and binding of nuclear proteins in heterochromatin and reveals the fractal organization of chromatin. EMBO J 28:3785–3798

Bano F, Fruk L, Sanavio B et al (2009) Toward multiprotein nanoarrays using nanografting and DNA directed immobilization of proteins. Nano Lett 9:2614–2618

Bar M, Bar-Ziv RH (2009) Spatially resolved DNA brushes on a chip: gene activation by enzymatic cascade. Nano Lett 9:4462–4466

Bates M, Huang B, Dempsey GT et al (2007) Multicolor super-resolution imaging with photoswitchable fluorescent probes. Science 317:1749–1753

Biagiotti V, Porchetta A, Desiderati S et al (2012) Probe accessibility effects on the performance of electrochemical biosensors employing DNA monolayers. Anal Bioanal Chem 402:413–421

Bombelli FB, Betti F, Gambinossi F et al (2009) Closed nanoconstructs assembled by step-by-step ssDNA coupling assisted by phospholipid membranes. Soft Matter 5:1639–1645

Bosco A, Bano F, Parisse P et al (2012) Hybridization in nanostructured DNA monolayers probed by AFM: theory versus experiment. Nanoscale 4:1734–1741

Buxboim A, Daube SS, Bar-Ziv R (2008) Synthetic gene brushes: a structure-function relationship. Mol Syst Biol 4:1–8

Carmon A, Vision TJ, Mitchell SE et al (2002) Solid-phase PCR in microwells: effects of linker length and composition on tethering hybridization, and extension. Biotechniques 32:410–420

Castelino K, Kannan B, Majumdar A (2005) Characterization of grafting density and binding efficiency of DNA and proteins on gold surfaces. Langmuir 21:1956–1961

Castro CE, Kilchherr F, Kim D-N et al (2011) A primer to scaffolded DNA origami. Nat Methods 8:221–229

Castronovo M, Radovic S, Grunwald C et al (2008) Control of steric hindrance on restriction enzyme reactions with surface-bound DNA nanostructures. Nano Lett 8:4140–4145

Castronovo M, Lucesoli A, Parisse P et al (2011) Two-dimensional enzyme diffusion in laterally confined DNA monolayers. Nat Commun 2:1–10

Chen J, Seeman NC (1991) Synthesis from DNA of a molecule with the connectivity of a cube. Nature 350:631–633

Chen C, Wang W, Ge J et al (2009) Kinetics and thermodynamics of DNA hybridization on gold nanoparticles. Nucleic Acids Res 37:3756–3765

Douglas SM, Bachelet I, Church GM (2012) A logic-gated nanorobot for targeted transport of molecular payloads. Science 335:831–834

Eid J, Fehr A, Gray J et al (2009) Real-time DNA sequencing from single polymerase molecules. Science 323:133–138

Feldkamp U, Niemeyer CM (2006) Rational design of DNA nanoarchitectures. Angew Chem Int Ed 45:1856–1876

Franco E, Friedrichs E, Kim J et al (2011) Timing molecular motion and production with a synthetic transcriptional clock. Proc Natl Acad Sci USA 108:E784–E793

Ghosh D, Lee Y, Thomas S et al (2012) M13-templated magnetic nanoparticles for targeted in vivo imaging of prostate cancer. Nat Nanotechnol 7:677–682

Gifford LK, Sendroiu IE, Corn RM et al (2010) Attomole detection of mesophilic DNA polymerase products by nanoparticle-enhanced surface plasmon resonance imaging on glassified gold surfaces. J Am Chem Soc 132:9265–9267

Han J, Craighead HG (2000) Separation of long DNA molecules in a microfabricated entropic trap array. Science 288:1026–1029
Heyman Y, Buxboim A, Wolf SG et al (2012) Cell-free protein synthesis and assembly on a biochip. Nat Nanotechnol 7:374–378
Hu Y, Das A, Hecht MH et al (2005) Nanografting de novo proteins onto gold surfaces. Langmuir 21:9103–9109
Huang J, MacKerell AD (2013) CHARMM36 all-atom additive protein force field: validation based on comparison to NMR data. J Comput Chem 34:2135–2145
Hubbell JA, Chilkoti A (2012) Nanomaterials for drug delivery. Science 337:303–305
Jiang Q, Song C, Nangreave J et al (2012) DNA origami as a carrier for circumvention of drug resistance. J Am Chem Soc 134:13396–13403
Jonkheijm P, Weinrich D, Schröder H et al (2008) Chemical strategies for generating protein biochips. Angew Chem Int Ed 47:9618–9647
Jorgensen WL, Chandrasekhar J, Madura JD et al (1983) Comparison of simple potential functions for simulating liquid water. J Chem Phys 79:926–935
Josephs EA, Ye T (2013) Nanoscale spatial distribution of thiolated DNA on model nucleic acid sensor surfaces. ACS Nano 7:3653–3660
Jungmann R, Avendano MS, Woehrstein JB et al (2014) Multiplexed 3D cellular super-resolution imaging with DNA-PAINT and exchange-PAINT. Nat Methods 11:313–318
Ke YG, Lindsay S, Chang Y et al (2008) Self-assembled water-soluble nucleic acid probe tiles for label-free RNA hybridization assays. Science 319:180–183
Ke Y, Douglas SM, Liu M et al (2009) Multilayer DNA origami packed on a square lattice. J Am Chem Soc 131:15903–15908
Ke Y, Ong LL, Shih WM et al (2012) Three-dimensional structures self-assembled from DNA bricks. Science 338:1177–1183
Keum J-W, Bermudez H (2009) Enhanced resistance of DNA nanostructures to enzymatic digestion. Chem Commun 7036–7038
Krishnan Y, Simmel FC (2011) Nucleic acid based molecular devices. Angew Chem Int Ed 50: 3124–3156
Kukolka F, Schoeps O, Woggon U et al (2007) DNA-directed assembly of supramolecular fluorescent protein energy transfer systems. Bioconjug Chem 18:621–627
Kuzyk A, Laitinen KT, Torma P (2009) DNA origami as a nanoscale template for protein assembly. Nanotechnology 20:1–5
Kuzyk A, Schreiber R, Fan Z et al (2012) DNA-based self-assembly of chiral plasmonic nanostructures with tailored optical response. Nature 483:311–314
Lavella GJ, Jadhav AD, Maharbiz MM (2012) A synthetic chemomechanical machine driven by ligand–receptor bonding. Nano Lett 12:4983–4987
Lee H, Lytton-Jean AKR, Chen Y et al (2012) Molecularly self-assembled nucleic acid nanoparticles for targeted in vivo siRNA delivery. Nat Nanotechnol 7:389–393
Levicky R, Herne TM, Tarlov MJ et al (1998) Using self-assembly to control the structure of DNA monolayers on gold: a neutron reflectivity study. J Am Chem Soc 120:9787–9792
Liang J, Castronovo M, Scoles G (2011) DNA as invisible ink for AFM nanolithography. J Am Chem Soc 134:39–42
Lin C, Jungmann R, Leifer AM et al (2012) Submicrometre geometrically encoded fluorescent barcodes self-assembled from DNA. Nat Chem 4:832–839
Liu QH, Wang LM, Frutos AG et al (2000) DNA computing on surfaces. Nature 403:175–179
Lizana L, Konkoli Z, Bauer B et al (2009) Controlling chemistry by geometry in nanoscale systems. Annu Rev Phys Chem 60:449–468
Lund K, Manzo AJ, Dabby N et al (2010) Molecular robots guided by prescriptive landscapes. Nature 465:206–210
McCalla SE, Luryi AL, Tripathi A (2009) Steric effects and mass-transfer limitations surrounding amplification reactions on immobilized long and clinically relevant DNA templates. Langmuir 25:6168–6175

McGuffee SR, Elcock AH (2010) Diffusion, crowding & protein stability in a dynamic molecular model of the bacterial cytoplasm. PLoS Comput Biol 6:1–18
Mei Q, Wei X, Su F et al (2011) Stability of DNA origami nanoarrays in cell lysate. Nano Lett 11: 1477–1482
Metzker ML (2010) Sequencing technologies—the next generation. Nat Rev Genet 11:31–46
Meyer R, Niemeyer CM (2011) Orthogonal protein decoration of DNA nanostructures. Small 7: 3211–3218
Minton AP (2006) How can biochemical reactions within cells differ from those in test tubes? J Cell Sci 119:2863–2869
Mirmomtaz E, Castronovo M, Grunwald C et al (2008) Quantitative study of the effect of coverage on the hybridization efficiency of surface-bound DNA nanostructures. Nano Lett 8:4134–4139
Miyoshi D, Sugimoto N (2008) Molecular crowding effects on structure and stability of DNA. Target DNA Part 1(90):1040–1051
Nanguneri S, Flottmann B, Horstmann H et al (2012) Three-dimensional, tomographic super-resolution fluorescence imaging of serially sectioned thick samples. PLoS One 7:e38098
Niemeyer CM (2010) Semisynthetic DNA-protein conjugates for biosensing and nanofabrication. Angew Chem Int Ed 49:1200–1216
Palanisamy R, Connolly AR, Trau M (2010) Considerations of solid-phase DNA amplification. Bioconjug Chem 21:690–695
Parisse P, Vindigni A, Scoles G et al (2012) In vitro enzyme comparative kinetics: unwinding of surface-bound DNA nanostructures by RecQ and RecQ1. J Phys Chem Lett 3:3532–3537
Park S, Brown KA, Hamad-Schifferli K (2004) Changes in oligonucleotide conformation on nanoparticle surfaces by modification with mercaptohexanol. Nano Lett 4:1925–1929
Peled D, Daube SS, Naaman R (2008) Selective enzymatic labeling to detect packing-induced denaturation of double-stranded DNA at interfaces. Langmuir 24:11842–11846
Peled D, Naaman R, Daube SS (2010) Packed DNA denatures on gold nanoparticles. J Phys Chem B 114:8581–8584
Peterson AW, Heaton RJ, Georgiadis RM (2001) The effect of surface probe density on DNA hybridization. Nucleic Acids Res 29:5163–5168
Pinheiro AV, Han D, Shih WM et al (2011) Challenges and opportunities for structural DNA nanotechnology. Nat Nanotechnol 6:763–772
Pinheiro AV, Nangreave J, Jiang S et al (2012) Steric crowding and the kinetics of DNA hybridization within a DNA nanostructure system. ACS Nano 6:5521–5530
Reisner W, Morton KJ, Riehn R et al (2005) Statics and dynamics of single DNA molecules confined in nanochannels. Phys Rev Lett 94:196101
Reisner W, Larsen NB, Silahtaroglu A et al (2010) Single-molecule denaturation mapping of DNA in nanofluidic channels. Proc Natl Acad Sci USA 107:13294–13299
Ricci F, Lai RY, Heeger AJ et al (2007) Effect of molecular crowding on the response of an electrochemical DNA sensor. Langmuir 23:6827–6834
Rinker S, Ke Y, Liu Y et al (2008) Self-assembled DNA nanostructures for distance-dependent multivalent ligand-protein binding. Nat Nanotechnol 3:418–422
Rothemund PWK (2006) Folding DNA to create nanoscale shapes and patterns. Nature 440: 297–302
Sacca B, Niemeyer CM (2012) DNA origami: the art of folding DNA. Angew Chem Int Ed 51: 58–66
Sanavio B, Scaini D, Grunwald C et al (2010) Oriented immobilization of prion protein demonstrated via precise interfacial nanostructure measurements. ACS Nano 4:6607–6616
Sasaki Y, Miyoshi D, Sugimoto N (2007) Regulation of DNA nucleases by molecular crowding. Nucleic Acids Res 35:4086–4093
Seelig G, Soloveichik D, Zhang DY et al (2006) Enzyme-free nucleic acid logic circuits. Science 314:1585–1588
Seeman NC (1982) Nucleic acid junctions and lattices. J Theor Biol 99:237–247

Seeman NC (1990) De novo design of sequences for nucleic acid structural engineering. J Biomol Struct Dyn 8:573–581
Seferos DS, Prigodich AE, Giljohann DA et al (2009) Polyvalent DNA nanoparticle conjugates stabilize nucleic acids. Nano Lett 9:308–311
Shaw A, Lundin V, Petrova E et al (2014) Spatial control of membrane receptor function using ligand nanocalipers. Nat Methods 11:841–846
Staii C, Wood DW, Scoles G (2008) Ligand-induced structural changes in maltose binding proteins measured by atomic force microscopy. Nano Lett 8:2503–2509
Steel AB, Levicky RL, Herne TM et al (2000) Immobilization of nucleic acids at solid surfaces: effect of oligonucleotide length on layer assembly. Biophys J 79:975–981
Stein IH, Schueller V, Boehm P et al (2011a) Single-molecule FRET ruler based on rigid DNA origami blocks. Chemphyschem 12:689–695
Stein IH, Steinhauer C, Tinnefeld P (2011b) Single-molecule four-color FRET visualizes energy-transfer paths on DNA origami. J Am Chem Soc 133:4193–4195
Tegenfeldt JO, Prinz C, Cao H et al (2004) The dynamics of genomic-length DNA molecules in 100-nm channels. Proc Natl Acad Sci USA 101:10979–10983
Venkatesan BM, Bashir R (2011) Nanopore sensors for nucleic acid analysis. Nat Nanotechnol 6: 615–624
Voigt NV, Torring T, Rotaru A et al (2010) Single-molecule chemical reactions on DNA origami. Nat Nanotechnol 5:200–203
Walsh AS, Yin H, Erben CM et al (2011) DNA cage delivery to mammalian cells. ACS Nano 5: 5427–5432
Woo S, Rothemund PWK (2011) Programmable molecular recognition based on the geometry of DNA nanostructures. Nat Chem 3:620–627
Yoo J, Aksimentiev A (2013) In situ structure and dynamics of DNA origami determined through molecular dynamics simulations. Proc Natl Acad Sci USA 110:20099–20104
Zhao Y-X, Shaw A, Zeng X et al (2012) DNA origami delivery system for cancer therapy with tunable release properties. ACS Nano 6:8684–8691
Zhou W-J, Chen Y, Corn RM (2011) Ultrasensitive microarray detection of short RNA sequences with enzymatically modified nanoparticles and surface plasmon resonance imaging measurements. Anal Chem 83:3897–3902

RNA and DNA Diagnostics on Microspheres: Current and Emerging Methods

Anna Weis, Fang Liang, Jing Gao, Ross T. Barnard, and Simon Corrie

Contents

A. Weis • F. Liang • J. Gao
School of Chemistry and Molecular Biosciences, The University of Queensland, St. Lucia, Brisbane, QLD 4072, Australia

R.T. Barnard (✉)
School of Chemistry and Molecular Biosciences, The University of Queensland, St. Lucia, Brisbane, QLD 4072, Australia

Australian Infectious Diseases Research Centre, The University of Queensland, St. Lucia, Brisbane, QLD 4072, Australia
e-mail: rossbarnard@uq.edu.au

S. Corrie
Australian Institute for Bioengineering and Nanotechnology, The University of Queensland, St. Lucia, Brisbane, QLD 4072, Australia

Australian Infectious Diseases Research Centre, The University of Queensland, St. Lucia, Brisbane, QLD 4072, Australia

ARC Centre of Excellence in Convergent Bio-Nano Science and Technology, Monash University, Parkville 3052, VIC, Australia

V.A. Erdmann et al. (eds.), *RNA and DNA Diagnostics*, RNA Technologies,
DOI 10.1007/978-3-319-17305-4_10

Abstract Emerging infections and rapidly evolving pathogens are a challenge to conventional nucleic acid-based diagnostic tests. Current nucleic acid-based diagnosis is limited in the spectrum of analytes that can be simultaneously detected. This can potentially be addressed by single-tube multiplexing or multiple-well multiplexing (where multiplexing is defined as using a mixture of reagents, capable of detecting multiple diagnostic targets in a single tube or in highly parallel arrays). The number of organisms that can be targeted in a single tube by the current gold standard in clinical laboratories [quantitative real-time polymerase chain reaction (qPCR)] is limited by the number of resolvable fluorophores. The demand for multiplex technologies has led to the development of various high-throughput assays and broad-spectrum formats. In this article, current microsphere-mediated formats, their clinical applications and established microsphere-based diagnostics are reviewed. We then discuss some novel microsphere-integrated techniques and their future prospects in clinical diagnostics. We differentiate between innovations in the molecular reactions with microspheres and novel microsphere encoding strategies to increase multiplexing capacities.

Keywords Microsphere • PCR • Multiplex • Diagnostic • RNA • DNA • Flow cytometry

1 Introduction

1.1 The Need for Multiplex Technologies

Polymerase chain reaction (PCR) remains the most widely used tool of nucleic acid diagnostics. Ongoing PCR improvements aim to meet the current need for microbial and viral detection, genetic disease screening, gene expression profiling and SNP genotyping.

The evolution of the traditional end-point PCR to quantitative real-time PCR (qPCR) addressed the requirement for quantitative analysis and enables the monitoring of PCR product accumulation (Mullis and Faloona 1987; VanGuilder et al. 2008).

The wide use of qPCR has led to specific guidelines assuring consistency of nomenclature, understanding and comparability of assay results between laboratories (Bustin et al. 2009).

Rapid quantitative nucleic acid detection without post-PCR processing (VanGuilder et al. 2008) has become vital for microbiological identifications in the clinical laboratory, such as *Escherichia coli* (Huijsdens et al. 2002), *Neisseria* species, influenza A (Whiley and Sloots 2005), adenovirus (Kuypers et al. 2006), HIV (Cobb et al. 2011) and many other targets. Especially in viral diseases, the

identification of specific subtypes and viral load determination are crucial for disease diagnostic and monitoring. In the case of human papillomavirus (HPV), qPCR is used to monitor viral load (Weissenborn et al. 2010); however, coinfections and the variety of beta-HPV types challenge qPCR assays (de Koning et al. 2009). Similar challenges apply to viruses such as human adenovirus, where multiple types exist and complicate the identification by qPCR. Antiviral therapies for adenovirus, reviewed elsewhere (Ganzenmueller and Heim 2012), herpes simplex virus (HSV) (Bhullar et al. 2014) and human immunodeficiency virus-1 (HIV-1) (Cobb et al. 2011) are relying on viral load monitoring by qPCR.

Further modifications of the real-time PCR system target the fluorogenic capacity to improve assay accuracy, analytical sensitivity and throughput. The TaqMan® real-time PCR addresses the limitation of the single-fluorophore strategy of SYBR Green qPCR (Heid et al. 1996; Reynisson et al. 2006; Zipper et al. 2004). Combining the TaqMan® method with the high sensitivity of a nested PCR has led to quantitative nested real-time PCR assay, for example, detection of low-level infection with varicella zoster virus (VZV) (Takahashi et al. 2013).

Comparison of mono- and multiplex assays can show higher analytical sensitivity of the multiplex method, for example, in bluetongue virus RNA (Vandenbussche et al. 2010). Moreover, multiplex diagnostics can provide a broad-spectrum analysis of patient samples (Sugita et al. 2008), including pathogen identifications, which might not be included in standard assays, resulting in earlier identification of the genus of a pathogen and, potentially, the faster administration of the correct antibiotic or antiviral treatment (Barnard et al. 2011). High levels of multiplexing can also reduce assay costs and turnaround times.

Driven by emerging infections and complex diseases, novel diagnostics need a wider capability to detect variation at the inter- and intraspecies levels. Multiple targets within one pathogen (e.g. pathogenesis or susceptibility markers) as well as multiple pathogen detection have been demonstrated to benefit patient outcome significantly and to reduce the length of hospital stays (Webster and Kumar 2014). Emerging and drug-resistant pathogens spread quickly, such as the H274Y mutation in influenza A (Meijer et al. 2009) and antibiotic-resistant bacterial pathogens in complex diseases such as sepsis (Mayr et al. 2014). These require rapid identification, triage and treatment, which can be met by multiplexing.

The ability of pathogens, such as viruses, to adapt to new vectors (e.g. adaptation to different mosquito vectors) necessitates continuous adaption of diagnostic designs and extension of current standard assays to detect the spread of viruses into unexpected locations (Hanson and Craig 1995; Romi et al. 2006; Barnard et al. 2011).

The emergence of new strains or vectors remains a challenge to in-house or commercially available assays. The so-called “dropout” describes the failure of assays to detect target sequences as a result of mutation, reassortment or recombination (Whiley et al. 2008). Increasing the number of targets within one species, as well as across multiple species, can decrease the number of “dropouts” (Whiley et al. 2008) and increase the diagnostic sensitivity and range.

Benefits arise from single-tube assays, which reduce the required sample size, reduce handling and cross-contamination risk, maximise throughput and provide a broader assay application (Ginocchio and St George 2009). A multiplex approach also benefits SNP genotyping (Iannone et al. 2003) and can be used as a pathogen discovery tool, exemplified by the virus discovery work by Wang et al. (2003). However, newer approaches, such as the PrimRglo method (Lai et al. 2012), represent a push towards much greater "multiplexing" in nucleic acid detection.

1.2 Current Formats

To realise the multiplex approach, several different formats of real-time qPCR have been utilised. These include melting curve analysis on traditional SYBR Green reaction (Jothikumar and Griffiths 2002), parallel real-time reactions in multiple tubes combined with melt-curve analysis to identify multiple viruses (Sugita et al. 2008) or PCR primer tail extensions followed by melt-curve analysis to distinguish between viral serotypes, combined with fluorophore detection (Lo et al. 2007) (Fig. 1).

1.2.1 Assay Formats on Fluorophore-Encoded Microspheres

Although the aforementioned methods expand the multiplex capability to a certain extent, the combination of microspheres with traditional nucleic acid diagnostic formats facilitates a much broader "detection spectrum". Microsphere-mediated multiplexing has been integrated into hybridisation, primer extension, oligonucleotide ligations and cleavage reactions (Table 1). However, these assays are primarily based on fluorophore-encoded microspheres, also referred to as optical encoding. Capture oligonucleotide sequences are used to distinguish between PCR products, and each reaction takes place on, or is captured on, a unique, colour-encoded microsphere population (Fig. 2).

The broad application of fluorophore-encoded microspheres combined with nucleic acid formats has been influenced by the availability of commercial microsphere sets. Noteworthy are the xMAP™ and xTAG™ technologies from Luminex Corporation (Austin, TX, USA), which allow distinction of up to 500 channels (MagPlex) or 150 channels (MagPlex-TAG) in a single reaction and coupling to nucleic acid or protein assays (Luminex Corporation 2013) (Table 2).

Based on the relative number of citations of microsphere-mediated technologies, Luminex Corporation dominates the microsphere "citation space" with more than 66 %, followed by BD Cytometric Bead Array with 31 % (Franklin Lakes, NJ, USA) (Fig. 3).The percentages shown here are the mean of the percentages found from the Google Scholar (25,772 citations found) and the University of Queensland databases (7,388 citations found). The percentage of total citations citing xMAP

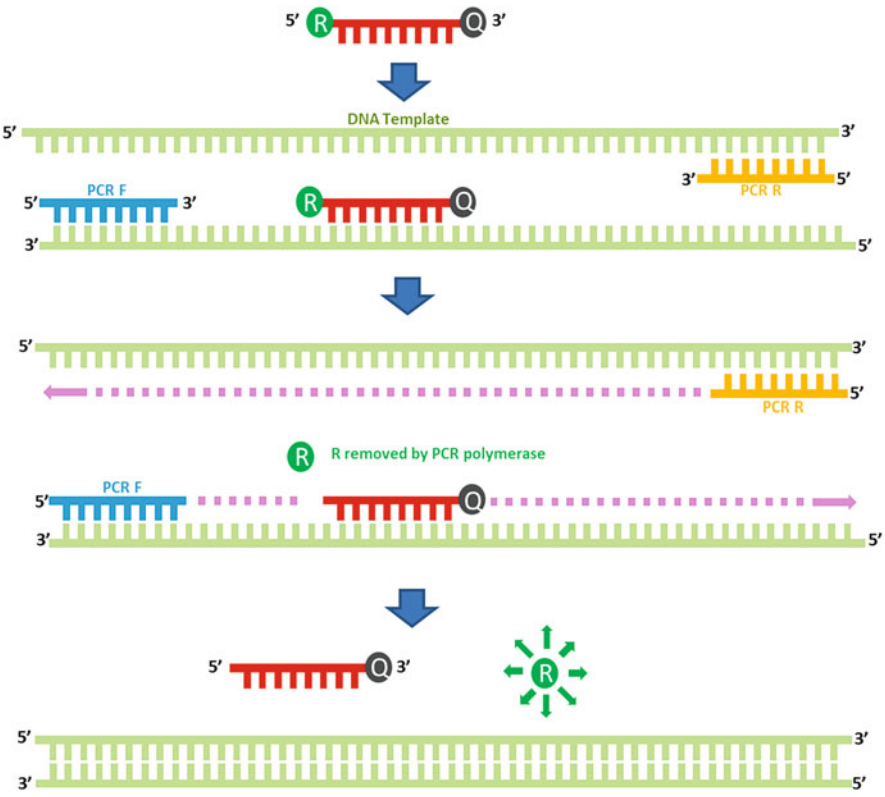

Fig. 1 Schematic representation of the TaqMan® probe real-time PCR system. This system depends on the fluorogenic-labelled probes and the 5′ nuclease activity of Taq DNA polymerase. A target product-specific oligonucleotide (shown in *red*) is designed with a reporter fluorescent dye on the 5′-end (labelled R and shown in *dark green*) and a quencher dye on the 3′-end (labelled Q and shown in *black*). When the probe is intact, the fluorescence of the reporter dye is absorbed by the proximal quencher. When the target DNA template (shown in *light green*) is denatured to single strand, the probe can anneal to the sequence of both primer sites and is cleaved by Taq DNA polymerase along with extension of primer. The reporter dye is freed from the quencher which increases the fluorescent signal

was 64.02 % from the Google Scholar database and 69.3 % from the University database.

A new generation of multiplex hybridisation formats is now available for SNP (single-nucleotide polymorphism) detection. These include GoldenGate™, SNPlex™ (Applied Biosciences by Life Technologies Carlsbad, CA, USA) and qBead™ assays (Luminex Corporation, Austin, TX, USA). Several companies provide ready-to-go diagnostic assays, for example, the xTAG™ (Luminex Corporation Austin, TX, USA), ResPlex II v2.0 (Qiagen, Venlo, Limburg, Netherlands) or MultiCode-PLx (EraGen Biosciences, Madison, WI, USA) respiratory virus diagnostic panel, which have been compared elsewhere (Balada-Llasat et al. 2011).

Table 1 Examples of multiplex nucleic acid assays on microspheres

Method	Platform	Description	Target	Advantage	Disadvantage	References
Allele-specific hybridisation (ASH)	PCR	Initial PCR step followed by hybridisation and flow cytometer read-out, specific probe design (can contain single base pair mismatch), multiplex potential depends on fluorophore coating of microspheres	DNA, RNA	Simple, analytical sensitivity	Specific probe design and optimisation required	Ahn and Walt (2005), Colinas et al. (2000), Fang et al. (2013, 2014), Hadd et al. (2004), Rockenbauer et al. (2005), Trajanoski and Fidler (2012)
Allele-specific primer extension (ASPE)	PCR	dNTPs or ddNTPs used for primer extension, fluorophore labelling of microsphere by tag/anti-tag strategy, flow cytometer read-out, multiplex potential limited by fluorophore coating of microspheres	SNP	High accuracy	Optimisation required	Bortolin (2009), Cai et al. (2000), Lin et al. (2008), Ye et al. (2001), Zhu et al. (2006)
Single base chain extension (SBCE)	PCR	Two-colour fluorophore system, SNP detection by ddNTP[a] fluorogenic label coupled to microsphere, flow cytometer read-out [a]Phycoerythrin (PE) fluorophore labelling of ddNTPs requires post-polymerase reaction for capture probe binding	SNP	High accuracy, minimal optimisation	Locus-specific primer design required	Chen et al. (2000), Deshpande et al. (2005), Taylor et al. (2001)
Oligonucleotide ligation assay (OLA)	PCR	Specific probe to target SNP by PCR and one pair of capturing probes (hybridises to target DNA, hybridises to cDNA–microsphere-coupled sequence), flow cytometer read-out, multiplex potential limited by microsphere fluorophore coatings	SNP	Flexibility in sequence design, sensitivity	Requires multiple probes	Bruse et al. (2008), Iannone et al. (2003)
Invasive cleavage reaction	Hybridisation	Upstream and probe oligonucleotides coupled to microspheres, flow cytometer read-out, multiplex potential limited by fluorophore coating of microspheres	SNP	No initial PCR amplification necessary	Requires initial coupling of microspheres, large sample volume, time consuming, validation of multiplex potential pending	Rao et al. (2003)

[a]Both methods terminate chain extension using ddNTPs and thereby enable SNP identification

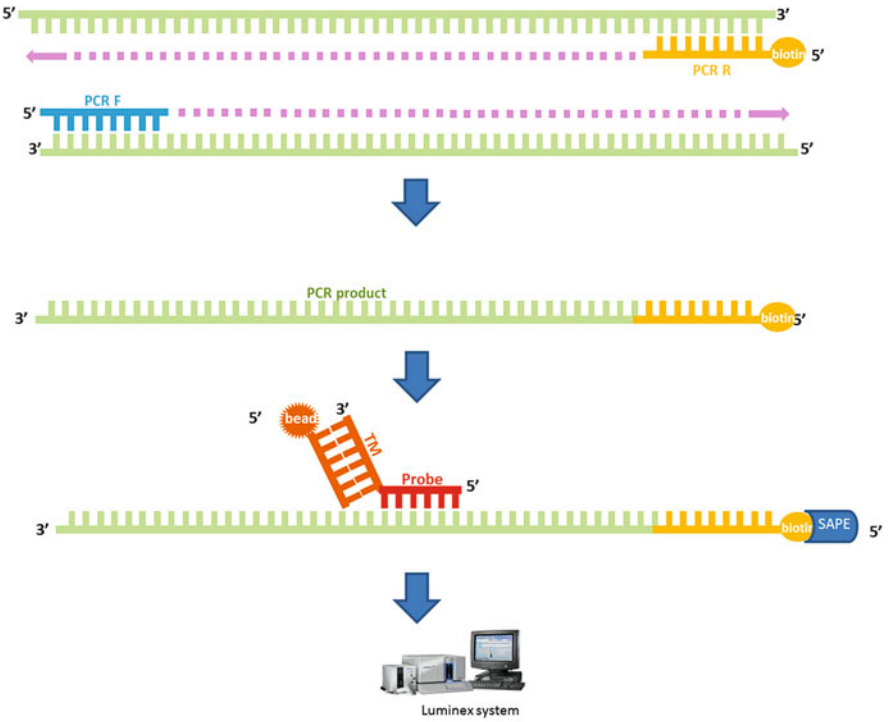

Fig. 2 Schematic representation of a regular microsphere-based PCR system. This system depends on the biotin-labelled PCR reverse primer (shown in *yellow*) and a gene-specific probe (shown in *red*) that binds to the microsphere via a universal sequence (shown in *dark yellow*) tagged to the probe's 5 primed end. After a regular PCR reaction, all PCR amplicons have a biotin group on the reverse strands. Target-specific probes are then hybridised to these reverse strands at the hybridisation temperature. After incubation with streptavidin, these complexes between probe and single-stranded PCR product plus streptavidin-PE are ready for flow cytometry analysis while holding the temperature at the optimal hybridisation temperature

Although commercial microspheres are readily available, the fixed design of the microsphere encodings or limited versatility in assay designs leads to in-house assay development of multiplex-microsphere diagnostics, including microsphere encoding. Frequently this includes the Luminex xMAP™ strategy, due to the optimised colour code which allows high multiplex potential (Table 1), although new approaches focus on novel encoding strategies for microspheres.

1.2.2 Encoding Methods for Microspheres

The encoding methods can be categorised as optical encoding (such as fluorophore dyes), graphical encoding (consisting of barcode strategies), physical encoding (alterations in size, shape or microsphere material) and spectrometric chemical

Table 2 Common microsphere-based technologies

Technology	Corporation	Numbers of analytes per well	Reading instruments	Software	Bead internal colouring system
xMap	Luminex	Up to 500	Dedicated instruments (MAGPIX, LX100/200)	Dedicated (Luminex xPONENT software)	Two fluorescent dyes mixed, one size, polystyrene, carboxylated
Cytometric bead array (CBA)	BD biosciences	Up to 30	Any multiuse flow cytometer equipped with 488 nm or 532 nm and 633 nm lasers	FCAP array multiplex analysis software	Single fluorescent dye, polystyrene (sulfhydrylated added with DTT)
FlowCytomix multiple analyte detection system http://www.ebioscience.com/application/multiplexing.htm	Affymetrix eBioscience	Up to 20	Most traditional flow cytometers including single laser instruments	Free	Single fluorescent dye, two sizes, pre-coated with a specific antibody
AimPlex http://www.yslbio.com/products	YSL Bioprocess Development Co.	Up to 24	Any multiuse flow cytometer		Bead size and fluorescence intensity
Parallume™ optical encoding technology http://www.parallume.com/beads.html	Parallume™		Dedicated multiplex assay reader system (MARS)	Dedicated MARSoft	Optically encoded agarose
Cyto-Plex™ carboxylated microspheres	Thermo Scientific	12	Most multiuse flow cytometer		Single fluorescent dye, two sizes, polystyrene, carboxylated

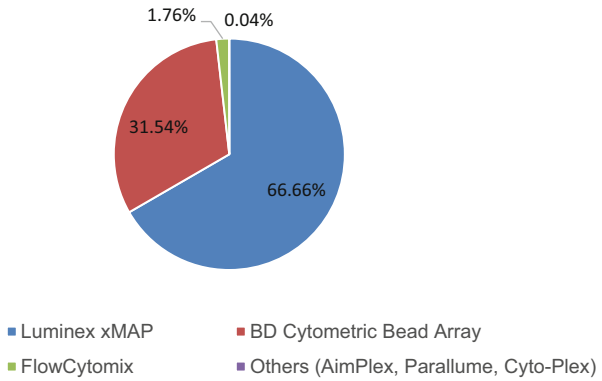

Fig. 3 This data is from searches of the University of Queensland Library and the Google Scholar databases, in July 2014, using the key words "multiplex Luminex", "multiplex cytometric bead array" and "multiplex flowcytomix". These searches capture largely protein-based assays on microspheres, but are broadly indicative of the platform usage likely to be transferred to nucleic acid assays

encoding [such as nuclear magnetic resonance (NMR) or mass spectrometry (MS)] (Table 3).

However, a new generation of encoded microspheres focuses on "encoding hybrids". Encoding hybrids combine two or multiple encoding strategies and create multiplex ability beyond the traditional fluorophore encoding. An example is the colour-barcoded magnetic microspheres, based on the so-called M-Ink system. Herein the M-Ink is tuned by an external magnetic field, which is possible by the use of a magnetic material called superparamagnetic colloidal nanocrystal clusters (CNCs). This structure allows the tuning of different M-Ink "colours" by magnetic field changes. This process allows colour barcoding by physical and optical encoding modifications and reaches a multiplex capacity of 8^{10} distinguishable colours (Lee et al. 2010).

Another example of hybrid encodings has been designed for fluorescence resonance energy transfer (FRET) bioassays. Combining polystyrene (PS) microspheres encoded firstly with CdSe/ZnS luminescent quantum dots (QDs) and secondly modified by peptides creates strong emitting microspheres. Additional gold nanoparticle (Au-NP) encoding enables the use of QD–PS microspheres as FRET probes. Originally FRET probes were based on acceptor/donor properties of molecular fluorophore; however, these properties now can be addressed by Au-NP–QD–PS microspheres (Quach et al. 2011). Nevertheless, confirmation in nucleic acid assays is pending. Further assay improvements are also required for the sandwich-based, bio-barcoded nucleic acid detection assay, which consists of gold nanoparticles and microsphere application (Nam et al. 2004).

Table 3 Examples of encoding methods for microspheres

Microsphere encoding	Method	Description	Application	References
Fluorophore encoding in polystyrene beads	Optical encoding	Uniform encoding for spectral identification, for example, polystyrene beads doped with red and orange fluorescent dyes. Can be combined with a fluorescent label on analytes (e.g. Cy3)	DNA, RNA, protein	Anderson and Taitt (2008), Fang et al. (2013, 2014)
Quantum-dot (QD) encoding	Optical encoding	Uniform surface encoding of synthetic/polymeric microspheres using quantum dots, can be combined with bioconjugated fluorescent probes; QD can be used to create QD patterns also referred to as QD barcode	DNA, RNA	Han et al. (2001), Ma et al. (2007), Medintz et al. (2005), Thiollet et al. (2012), Wang et al. (2013), Yu et al. (2012)
Barcode-encoded hydrogel microspheres	Graphical encoding	Barcode structure based on partial polymerisation of microparticle surface consistent of a pattern of holes; hydrogel microparticles consistent of poly(ethylene glycol) and multiple probe strips	DNA, RNA, protein	Appleyard et al. (2011a, b), Chapin et al. (2011)
Magnetic mesoporous hollow carbon microspheres	Physical encoding	Physical modification of microspheres by designing a mesoporous carbon nanostructure consistent of sacrificed/consumed inorganic core (Fe_3O_4) and carbonisation of organic shell (polydopamine core–shell calcination)	Protein	Cheng et al. (2014)
Covalently colour-encoded mesoporous silica microspheres	Chemical encoding	Microsphere populations individually loaded with covalently attached fluorophores, with a separate chemical pathway available for probe attachment. Chemistry is stable enough to withstand multiple rounds of DNA or peptide synthesis	DNA, RNA, proteins, peptides	Miller et al. (2005), Corrie et al. (2011)
Hollow mesoporous silica microspheres (HSMs)	Physical encoding	Microsphere consists of ordered mesoporous silica to enlarge binding surface, such as internal space within the shell, and mesopores increase substrate diffusion; secondary use of nanoporous gold (NPG) onto glass electrode allows sandwich immunoassay[a]	Protein	Wu et al. (2012), Yu et al. (2011)
Colour-barcoded magnetic microspheres	Physical encoding/ optical encoding (**Hybrid encoding**)	Magnetic field-controlled colour barcode printing by modifying the superparamagnetic colloidal nanocrystal cluster	DNA, RNA	Lee et al. (2010)
Magnetic barcode encoding	Spectrometric chemical encoding	Complementary capture DNA-modified polymer microparticles coated with magnetic nanoprobes (MNPs), nuclear magnetic resonance (NMR) read-out	DNA, RNA	Liong et al. (2013)

[a]There is increasing application of gold nanoparticles and nanoporous gold for biosensing and RNA/DNA diagnostics; however, the physical properties and applications are reviewed elsewhere (Carlos et al. 2014; Fritzsche and Taton 2003; Heuer-Jungemann et al. 2013; Hu et al. 2008; Liu et al. 2013; Polak et al. 2013; Yang et al. 2013; Zhu et al. 2011)

2 Examples of Diagnostic Assays on the Microsphere Platform

Oligonucleotide-associated microspheres are usually used following a PCR reaction as a detection method or between PCR and sequencing as a separation tool. With the advantage of extremely high multiplexing capability, many detection/diagnostic panels have been developed and applied in fields including broad bacteria, broad virus, respiratory virus, bio-threat, food-borne, multidrug resistance.

2.1 Transcript Profiling

Collection of information on project-specific genes with efficiency and high throughput has been expedited by the publication of few hundred whole human genomes. One aim of this kind of study is the realisation of providing personal healthcare on the basis of well-studied predictive transcriptional markers. Regarding this area, many research tools have been developed including DNA microarrays, quantitative RNA sequencing, microfluidics PCR (Zimmermann et al. 2008), Luminex system (Dunbar 2006), NanoString technology (Reis et al. 2011), oligonucleotide-based cantilever arrays (Zhang et al. 2006) and AmpliSeq-based RNA sequencing (Zhang et al. 2014). The accuracy of these methods depends on the final analysis techniques: fluorophore-based liquid/solid microsphere microarray can provide SNP or short oligonucleotide fragment level information, while sequencing can produce complete information regarding genes of interest; in the latter case, the role of beads is in selecting and immobilising target genes from enriched amplicons (Zhang et al. 2014).

2.2 Bacteria/Virus Genotyping

Microsphere techniques are now widely applied to genotyping of bacteria or viruses, and these techniques have their own advantages over direct sequencing, although the latter is considered a gold standard in bacterial or viral genotyping (Gharizadeh et al. 2005).

In one report regarding human papillomavirus (HPV) detection, a microsphere-based multiplex genotyping method (digene HPV Genotyping LQ Test, QIAGEN, Germany) showed higher concordance than the results of using PNA-based methods (PANArray HPV Genotyping Chip, Panagene, Korea) with a pool of 508 clinical specimens (Park et al. 2014). This report also verified that the microsphere-based genotyping method is superior to sequencing when determining

multiple HPV genotypes existing in one subject, since low concentrations of DNA may lead to less sequencing accuracy (Park et al. 2014). In another study, Luminex Mebgen HPV assay was considered superior compared with other commercially available HPV tests such as Hybrid Capture™ 2 (HC2) test from Qiagen, the Linear Array™ HPV genotyping test/line-blot assay and the Amplicor™ HPV test from Roche (Ozaki et al. 2014). Besides commercialised panels, in-house customised SNP detection panels have been widely adopted during research (Bortolin et al. 2004; Zhu et al. 2014).

2.3 *Bacteria/Virus Pathogen Detection*

Most hybridisation-based platforms have high potential multiplex limits but are weak for high-throughput testing (Boonham et al. 2007). Nonetheless, these emerging techniques are preferable to traditional TaqMan™ methods in true multiplex detection or genotyping. One of these platforms, the Luminex microsphere system, has been applied in clinical pathogen diagnostics and genotyping (Liu et al. 2011; Mahony et al. 2007). A recent study described the identification of all nine pospiviroids known so far in one single tube using Luminex xMAP technology (van Brunschot et al. 2014). In another study, a group of six human enteric viruses from environmental water were successfully identified with specificity and sensitivity using the same approach (Hamza et al. 2014). In another area, liquid microsphere microarray was used in sensitive detection of anthrax and its relative pathogens. In the report, two genes from nine anthrax core pathogens were selected and analysed in one reaction (Schweighardt et al. 2014). Another study utilised a 15-plex PCR, followed by hybridisation onto oligonucleotide probes conjugated onto microspheres, to detect several species of pathogenic bacteria and some of their serotypes (Zhao et al. 2013). These platforms have also been applied to fungus diagnostics (Kozel and Wickes 2014). One common limitation mentioned in all these reports is the multiplex PCR reaction, which can be difficult to balance between specificity and sensitivity.

In addition, current multiplexed array methods are still based on known bacteria/virus sequence, while parallel next-generation sequencing can provide unknown sequence information and screen new genotypes (Barnard et al. 2011; Boonham et al. 2014).

2.4 *Antibiotic Resistance Analysis*

Nucleotide-coupled Luminex beads have been used as probes targeting eight beta-lactam antibiotic resistance genes from four bacterial species (Lu et al. 2014). Because the traditional multiplex RT-PCR followed by Tm analyses would not be specific enough when dealing with several resistance genes existing in a single

isolate (Tm peaks are hard to distinguish), liquid bead microarray assays were applied here. The Luminex platform results were consistent with the results generated by the earlier methods and were claimed to be the first to apply microsphere-based methods to determine bacterial antibiotic resistance genes.

3 Emerging Formats on Microspheres

3.1 Emerging Formats on Fluorophore-Encoded Microspheres

Continuous improvements of real-time PCR-based strategies aim to address the unmet clinical need for multiplexing. Therefore, emerging approaches combine

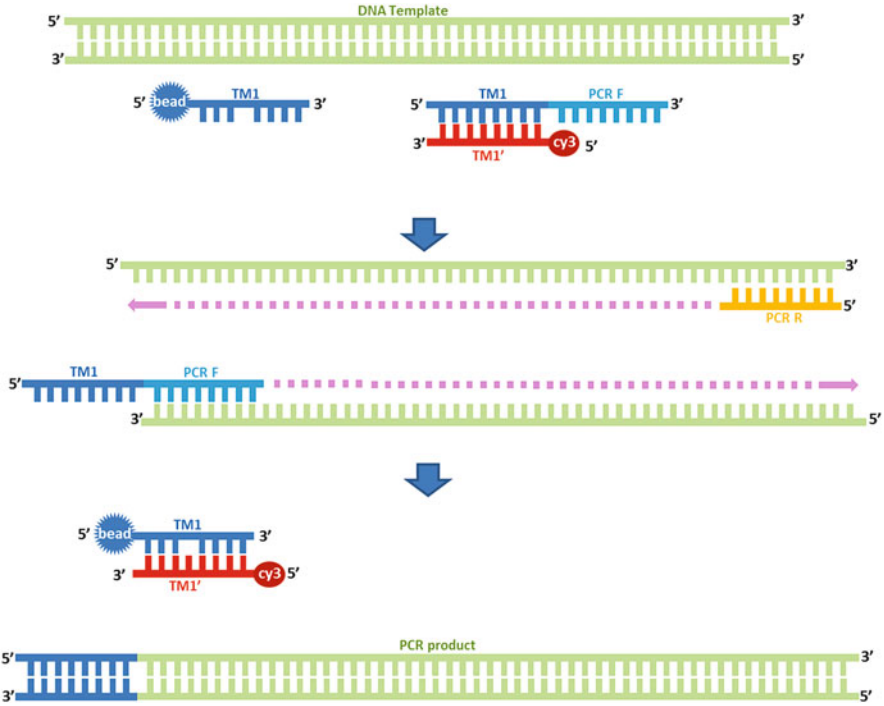

Fig. 4 Schematic representation of multiplex-microsphere-quantitative PCR system (PrimRglo). In this system, fluorescent signal detection relies on the hybridisation between the "forward" oligonucleotide probe, which has a fluorescence reporter attached at its 5′-end (labelled Tm1' in *red*) and reporter reverse oligonucleotide coupled to microbeads (labelled Tm1 in *blue*). As PCR progresses, the PCR forward primers are sequestered into the replicated PCR product. With the consumption of PCR forward primers, annealing between the reporter forward probe and the reverse probe coupled onto microbeads is favoured. The number of microbeads carrying fluorescent signal from the reporter dye can be measured in a Luminex machine or equivalent device

quantitative real-time PCR with microsphere-mediated multiplexing. For example, the PrimRglo qPCR strategy integrated microspheres, and is known as a multiplex-microsphere qPCR format for nucleic acid detection (Fang et al. 2013) (Fig. 4). The format depends on primer consumption during the reaction and allows either end-point analysis in a flow cytometer/Luminex machine or the monitoring of the increasing fluorophore signal on the microspheres as the PCR reaction proceeds. These combinations of traditional nucleic acid formats with microspheres have increased over the last decade (Table 1) and will result in more microsphere-mediated assays.

3.2 Emerging Encoding Strategies for Microspheres

Emerging approaches target the encoding of the microsphere itself. This promises extension of multiplexing capabilities based on the microsphere coding, independent of novel assay design.

The emergence of "hybrid-encoded" microspheres shows particular promise. The described colour-barcoded magnetic microspheres (Lee et al. 2010) have already outgrown the traditional fluorophore-encoded microspheres. Compared to the standard Luminex xMAP™ technique, which allows a colour encoding of up to 150 channels, or the 500 channel detections theoretically possible under application of the MagPlex™ microspheres, the "hybrid encoding" promises detection of up to 8^{10} colours (Lee et al. 2010). This may be many more channels than is usable in a diagnostic setting, because the practical challenge is the design of functioning multiplex assays that could utilise such a large number of codings.

Combining technologies in microscale (microspheres) and nanotechnology is becoming more important to meet new levels of multiplex capacity and assay improvements, such as decreases in assay costs and time consumption, and enable portable diagnostics. For example, the magnetic barcode encoding of microspheres provides a platform for rapid *Mycobacterium tuberculosis* nucleic acid detection out of clinical samples (Liong et al. 2013). Multiplex improvements are addressed by combining quantum-dot encoding and microspheres as novel optical encoding strategy (Ma et al. 2007; Thiollet et al. 2012). QD is also emerging in the area of "encoding hybrids", for example, the QD- and gold nanoparticle-encoded polystyrene microspheres (Quach et al. 2011). Quantum dot nanocrystal applications and physics have been reviewed by others (Zhu et al. 2011).

The use of gold nanoparticles (Au-NPs) is already established in the field of nucleic acid detection. Au-NP-based formats are already applied in bacterial detection, such as *Salmonella* (Liu et al. 2013), and in the field of biosensing to detect single-nucleotide mutations within DNA sequences (Polak et al. 2013). The value of Au-NP, also in the application as oligonucleotide-linked biosensor, is

founded by its physical properties, which are reviewed elsewhere (Heuer-Jungemann et al. 2013; Zhu et al. 2011).

However, the emergence of Au-NP combined with microsphere techniques promises high levels of multiplexing and novel nucleic acid assays. The indirect application of Au-NP in microsphere assays for protein detection has been published (Wu et al. 2012), as well as the direct application of Au-NP in nucleic acid detection (Nam et al. 2004); however, improvements in these strategies are needed. Addressing "hybrid" microspheres, Au-NP coating of glass microspheres has been reported (Gadomska et al. 2013), and other "hybrids" in nucleic acid diagnostics are to be expected.

4 Future Directions

The fast developing world of nucleic acid diagnostics demands higher-throughput capabilities for clinical samples, broader detection spectra and new approaches and formats in disease identification, addressed by multiplexing.

The emergence of microsphere-mediated multiplex formats is already showing a strong influence on nucleic acid diagnostic research and clinical applications. Microsphere-mediated nucleic acid detection is already the core of new generation sequencing formats (Margulies et al. 2005). The emerging microsphere-mediated formats, such as hydrolysis probes (Schrader and Whitman 2013), as well as new formats combining the strengths of traditional assays (Table 1) with multiplexing ability will become more widely available.

Nanotechnology will be integrated into microsphere formats and possibly replace standard fluorophore encoding of microspheres; QD and Au nanoparticles show particular promise for nucleic acid diagnostics (Azzazy et al. 2006). "Hybrid encoding" will develop and will be integrated into microsphere-based diagnostic assays.

New platforms for multiplex assays will emerge, and more reactions will be carried out using chips, microplates, microspheres, nanowires and "ready-to-go" point-of-care devices. The design of nanowires will challenge the application of microspheres as a multiplex platform. Nanowires can be linked to oligonucleotides and do not require labelling. The potential of nanowires promises highly parallel detections and has already been adapted to immunodetection (Stern et al. 2007) and nucleic acid hybridisations (Bunimovich et al. 2006; Gao et al. 2007; Zhang et al. 2008, 2010). It is to be expected that nanowires and chip-based assays will compete with microsphere usage, but will also inspire new generation microsphere formats and "hybrid" formats, which will potentially combine the advantages of both nanowire and microsphere technologies.

In conclusion, the demand for wider applications of microspheres in front-line diagnostics will increase over the next decade. There will be extensive innovations and integration with new chemistries and the use of novel microsphere labelling technologies. The current gold-standard qPCR will undergo microsphere

extensions. These new formats will go some way towards addressing the necessary change in diagnostic paradigms and meet the emerging challenges in detection, well beyond the point of traditional pathogen identification by narrowly focused, reactive, rather than anticipatory assays.

References

Ahn S, Walt DR (2005) Detection of Salmonella spp. using microsphere-based, fiber-optic DNA microarrays. Anal Chem 77:5041–5047

Anderson GP, Taitt CR (2008) Amplification of microsphere-based microarrays using catalyzed reporter deposition. Biosens Bioelectron 24:324–328

Appleyard DC, Chapin SC, Doyle PS (2011a) Multiplexed protein quantification with barcoded hydrogel microparticles. Anal Chem 83:193–199

Appleyard DC, Chapin SC, Srinivas RL et al (2011b) Bar-coded hydrogel microparticles for protein detection: synthesis, assay and scanning. Nat Protoc 6:1761–1774

Azzazy HM, Mansour MM, Kazmierczak SC (2006) Nanodiagnostics: a new frontier for clinical laboratory medicine. Clin Chem 52:1238–1246

Balada-Llasat JM, LaRue H, Kelly C et al (2011) Evaluation of commercial ResPlex II v2.0, MultiCode-PLx, and xTAG respiratory viral panels for the diagnosis of respiratory viral infections in adults. J Clin Virol 50:42–45

Barnard RT, Hall RA, Gould EA (2011) Expecting the unexpected: nucleic acid-based diagnosis and discovery of emerging viruses. Expert Rev Mol Diagn 11:409–423

Bhullar SS, Chandak NH, Purohit HJ et al (2014) Determination of viral load by quantitative real-time PCR in herpes simplex encephalitis patients. Intervirology 57:1–7

Boonham N, Tomlinson J, Mumford R (2007) Microarrays for rapid identification of plant viruses. Annu Rev Phytopathol 45:307–328

Boonham N, Kreuze J, Winter S et al (2014) Methods in virus diagnostics: from ELISA to next generation sequencing. Virus Res 186:20–31

Bortolin S (2009) Multiplex genotyping for thrombophilia-associated SNPs by universal bead arrays. Methods Mol Biol 496:59–72

Bortolin S, Wells P, Janeczko R et al (2004) Analytical validation of the tag-it high-throughput microsphere-based universal array genotyping platform: application to the multiplex detection of a panel of thrombophilia-associated single-nucleotide polymorphisms. Clin Chem 50:2028–2036

Bruse S, Moreau M, Azaro M et al (2008) Improvements to bead-based oligonucleotide ligation SNP genotyping assays. Biotechniques 45:559–571

Bunimovich YL, Shin YS, Yeo WS et al (2006) Quantitative real-time measurements of DNA hybridization with alkylated nonoxidized silicon nanowires in electrolyte solution. J Am Chem Soc 128:16323–16331

Bustin SA, Benes V, Garson JA et al (2009) The MIQE guidelines: minimum information for publication of quantitative real-time PCR experiments. Clin Chem 55:611–622

Cai H, White PS, Torney D et al (2000) Flow cytometry-based minisequencing: a new platform for high-throughput single-nucleotide polymorphism scoring. Genomics 66:135–143

Carlos FF, Flores O, Doria G et al (2014) Characterization of genomic SNP via colorimetric detection using a single gold nanoprobe. Anal Biochem 465:1–5

Chapin SC, Appleyard DC, Pregibon DC et al (2011) Rapid microRNA profiling on encoded gel microparticles. Angew Chem Int Ed Engl 50:2289–2293

Chen J, Iannone MA, Li MS et al (2000) A microsphere-based assay for multiplexed single nucleotide polymorphism analysis using single base chain extension. Genome Res 10:549–557

Cheng G, Zhou MD, Zheng SY (2014) Facile synthesis of magnetic mesoporous hollow carbon microspheres for rapid capture of low-concentration peptides. ACS Appl Mater Interfaces 6 (15):12719–12728
Cobb BR, Vaks JE, Do T et al (2011) Evolution in the sensitivity of quantitative HIV-1 viral load tests. J Clin Virol 52(1):S77–S82
Colinas RJ, Bellisario R, Pass KA (2000) Multiplexed genotyping of beta-globin variants from PCR-amplified newborn blood spot DNA by hybridization with allele-specific oligodeoxynucleotides coupled to an array of fluorescent microspheres. Clin Chem 46:996–998
Corrie SR, Feng Q, Blair T et al (2011) Multiplatform comparison of multiplexed bead arrays using HPV genotyping as a test case. Cytometry A 79(9):713–719
de Koning MN, Weissenborn SJ, Abeni D et al (2009) Prevalence and associated factors of betapapillomavirus infections in individuals without cutaneous squamous cell carcinoma. J Gen Virol 90:1611–1621
Deshpande A, Valdez Y, Nolan JP (2005) Multiplexed SNP genotyping using primer single-base extension (SBE) and microsphere arrays. Curr Protoc Cytom Chapter 13:Unit 13 4
Dunbar SA (2006) Applications of Luminex® xMAP™ technology for rapid, high-throughput multiplexed nucleic acid detection. Clin Chim Acta 363:71–82
Fang L, Lai R, Arora N et al (2013) Multiplex-microsphere-quantitative polymerase chain reaction: nucleic acid amplification and detection on microspheres. Anal Biochem 432:23–30
Fang L, Weis A, Wong LK et al (2014) Application of the PrimRglo assay chemistry to multiplexed bead assays. Curr Protoc Cytom 69:13.13.1–13.13.10
Fritzsche W, Taton TA (2003) Metal nanoparticles as labels for heterogeneous, chip-based DNA detection. Nanotechnology 14:R63–R73
Gadomska KM, Lechner SJ, Spatz JP (2013) Gold-nanoparticle-decorated glass microspheres. Part Part Syst Charact 30:940–944
Ganzenmueller T, Heim A (2012) Adenoviral load diagnostics by quantitative polymerase chain reaction: techniques and application. Rev Med Virol 22:194–208
Gao Z, Agarwal A, Trigg AD et al (2007) Silicon nanowire arrays for label-free detection of DNA. Anal Chem 79:3291–3297
Gharizadeh B, Oggionni M, Zheng B et al (2005) Type-specific multiple sequencing primers: a novel strategy for reliable and rapid genotyping of human papillomaviruses by pyrosequencing technology. J Mol Diagn 7:198–205
Ginocchio CC, St George K (2009) Likelihood that an unsubtypeable influenza A virus result obtained with the Luminex xTAG respiratory virus panel is indicative of infection with novel A/H1N1 (swine-like) influenza virus. J Clin Microbiol 47:2347–2348
Hadd AG, Laosinchai-Wolf W, Novak CR et al (2004) Microsphere bead arrays and sequence validation of 5/7/9T genotypes for multiplex screening of cystic fibrosis polymorphisms. J Mol Diagn 6:348–355
Hamza IA, Jurzik L, Wilhelm M (2014) Development of a Luminex assay for the simultaneous detection of human enteric viruses in sewage and river water. J Virol Methods 204:65–72
Han M, Gao X, Su JZ et al (2001) Quantum-dot-tagged microbeads for multiplexed optical coding of biomolecules. Nat Biotechnol 19:631–635
Hanson SM, Craig GB Jr (1995) Aedes albopictus (Diptera: Culicidae) eggs: field survivorship during northern Indiana winters. J Med Entomol 32:599–604
Heid CA, Stevens J, Livak KJ et al (1996) Real time quantitative PCR. Genome Res 6:986–994
Heuer-Jungemann A, Harimech PK, Brown T et al (2013) Gold nanoparticles and fluorescently-labelled DNA as a platform for biological sensing. Nanoscale 5:9503–9510
Hu K, Lan D, Li X et al (2008) Electrochemical DNA biosensor based on nanoporous gold electrode and multifunctional encoded DNA-Au bio bar codes. Anal Chem 80:9124–9130
Huijsdens XW, Linskens RK, Mak M et al (2002) Quantification of bacteria adherent to gastrointestinal mucosa by real-time PCR. J Clin Microbiol 40:4423–4427
Iannone MA, Taylor JD, Chen J et al (2003) Microsphere-based single nucleotide polymorphism genotyping. Methods Mol Biol 226:123–134

Jothikumar N, Griffiths MW (2002) Rapid detection of Escherichia coli O157:H7 with multiplex real-time PCR assays. Appl Environ Microbiol 68:3169–3171
Kozel TR, Wickes B (2014) Fungal diagnostics. Cold Spring Harb Perspect Med 4:a019299
Kuypers J, Wright N, Ferrenberg J et al (2006) Comparison of real-time PCR assays with fluorescent-antibody assays for diagnosis of respiratory virus infections in children. J Clin Microbiol 44:2382–2388
Lai R, Fang L, Pearson D et al (2012) PrimRglo: a multiplexable quantitative real-time polymerase chain reaction system for nucleic acid detection. Anal Biochem 422:89–95
Lee H, Kim J, Kim H et al (2010) Colour-barcoded magnetic microparticles for multiplexed bioassays. Nat Mater 9:745–749
Lin YC, Sheng WH, Chang SC et al (2008) Application of a microsphere-based array for rapid identification of Acinetobacter spp. with distinct antimicrobial susceptibilities. J Clin Microbiol 46:612–617
Liong M, Hoang AN, Chung J et al (2013) Magnetic barcode assay for genetic detection of pathogens. Nat Commun 4:1752
Liu J, Kang G, Houpt E et al (2011) Multiplex reverse transcription PCR Luminex assay for detection and quantitation of viral agents of gastroenteritis. J Clin Virol 50:308–313
Liu CC, Yeung CY, Chen PH et al (2013) Salmonella detection using 16S ribosomal DNA/RNA probe-gold nanoparticles and lateral flow immunoassay. Food Chem 141:2526–2532
Lo CL, Yip SP, Cheng PK et al (2007) One-step rapid reverse transcription-PCR assay for detecting and typing dengue viruses with GC tail and induced fluorescence resonance energy transfer techniques for melting temperature and color multiplexing. Clin Chem 53:594–599
Lu X, Nie S, Xia C et al (2014) A rapid two-step algorithm detects and identifies clinical macrolide and beta-lactam antibiotic resistance in clinical bacterial isolates. J Microbiol Methods 102:26–31
LuminexCorporation (2013) Perform assays more efficiently and cost effectively with xMAP® and xTAG® Technologies. http://www.luminexcorp.com/TechnologiesScience/. 2014
Ma Q, Wang X, Li Y et al (2007) Multicolor quantum dot-encoded microspheres for the detection of biomolecules. Talanta 72:1446–1452
Mahony J, Chong S, Merante F et al (2007) Development of a respiratory virus panel test for detection of twenty human respiratory viruses by use of multiplex PCR and a fluid microbead-based assay. J Clin Microbiol 45:2965–2970
Margulies M, Egholm M, Altman WE et al (2005) Genome sequencing in microfabricated high-density picolitre reactors. Nature 437:376–380
Mayr FB, Yende S, Angus DC (2014) Epidemiology of severe sepsis. Virulence 5:4–11
Medintz IL, Uyeda HT, Goldman ER et al (2005) Quantum dot bioconjugates for imaging, labelling and sensing. Nat Mater 4:435–446
Meijer A, Lackenby A, Hungnes O et al (2009) Oseltamivir-resistant influenza virus A (H1N1), Europe, 2007-08 season. Emerg Infect Dis 15:552–560
Miller CR, Vogel R, Surawski PP et al (2005) Biomolecular screening with novel organosilica microspheres. Chem Commun (Camb) 38:4783–4785
Mullis KB, Faloona FA (1987) Specific synthesis of DNA in vitro via a polymerase-catalyzed chain reaction. Methods Enzymol 155:335–350
Nam JM, Stoeva SI, Mirkin CA (2004) Bio-bar-code-based DNA detection with PCR-like sensitivity. J Am Chem Soc 126:5932–5933
Ozaki S, Kato K, Abe Y et al (2014) Analytical performance of newly developed multiplex human papillomavirus genotyping assay using Luminex xMAP technology (Mebgen HPV Kit). J Virol Methods 204:73–80
Park KS, Kim J-Y, Ki C-S et al (2014) Comparison of the digene HPV genotyping LQ Test and the PANArray HPV genotyping chip for detection of high-risk or probable high-risk human papillomavirus genotypes. Ann Lab Med 34:279–285
Polak P, Zalevsky Z, Shefi O (2013) Gold nanoparticles-based biosensing of single nucleotide DNA mutations. Int J Biol Macromol 59:134–137

Quach AD, Crivat G, Tarr MA et al (2011) Gold nanoparticle-quantum dot-polystyrene microspheres as fluorescence resonance energy transfer probes for bioassays. J Am Chem Soc 133:2028–2030

Rao KV, Stevens PW, Hall JG et al (2003) Genotyping single nucleotide polymorphisms directly from genomic DNA by invasive cleavage reaction on microspheres. Nucleic Acids Res 31:e66

Reis PP, Kamel-Reid S, Waldron L et al (2011) mRNA transcript quantification in archival samples using multiplexed, color-coded probes. BMC Biotechnol 11:46

Reynisson E, Josefsen MH, Krause M et al (2006) Evaluation of probe chemistries and platforms to improve the detection limit of real-time PCR. J Microbiol Methods 66:206–216

Rockenbauer E, Petersen K, Vogel U et al (2005) SNP genotyping using microsphere-linked PNA and flow cytometric detection. Cytometry A 64:80–86

Romi R, Severini F, Toma L (2006) Cold acclimation and overwintering of female Aedes albopictus in Roma. J Am Mosq Control Assoc 22:149–151

Schrader B, Whitman DF (2013) Hydrolysis probes. U.S. Patent number 2013/0085078A1

Schweighardt AJ, Battaglia A, Wallace MM (2014) Detection of anthrax and other pathogens using a unique liquid array technology. J Forensic Sci 59:15–33

Stern E, Klemic JF, Routenberg DA et al (2007) Label-free immunodetection with CMOS-compatible semiconducting nanowires. Nature 445:519–522

Sugita S, Shimizu N, Watanabe K et al (2008) Use of multiplex PCR and real-time PCR to detect human herpes virus genome in ocular fluids of patients with uveitis. Br J Ophthalmol 92:928–932

Takahashi T, Tamura M, Takasu T (2013) Diagnostic value of a "wide-range" quantitative nested real-time PCR assay for varicella zoster virus myelitis. J Med Virol 85:2042–2055

Taylor JD, Briley D, Nguyen Q et al (2001) Flow cytometric platform for high-throughput single nucleotide polymorphism analysis. Biotechniques 30(3):661–666, 668–669

Thiollet S, Higson S, White N et al (2012) Investigation and development of quantum dot-encoded microsphere bioconjugates for DNA detection by flow cytometry. J Fluoresc 22:685–697

Trajanoski D, Fidler SJ (2012) HLA typing using bead-based methods. Methods Mol Biol 882:47–65

van Brunschot SL, Bergervoet JHW, Pagendam DE et al (2014) A bead-based suspension array for the multiplexed detection of begomoviruses and their whitefly vectors. J Virol Methods 198:86

Van Guilder HD, Vrana KE, Freeman WM (2008) Twenty-five years of quantitative PCR for gene expression analysis. Biotechniques 44:619–626

Vandenbussche F, Vandemeulebroucke E, De Clercq K (2010) Simultaneous detection of bluetongue virus RNA, internal control GAPDH mRNA, and external control synthetic RNA by multiplex real-time PCR. Methods Mol Biol 630:97–108

Wang D, Urisman A, Liu YT et al (2003) Viral discovery and sequence recovery using DNA microarrays. PLoS Biol 1:E2

Wang G, Leng Y, Dou H et al (2013) Highly efficient preparation of multiscaled quantum dot barcodes for multiplexed hepatitis B detection. ACS Nano 7:471–481

Webster M, Kumar VS (2014) Losing the MRSA label. Clin Chem 60:903–905

Weissenborn SJ, Wieland U, Junk M et al (2010) Quantification of beta-human papillomavirus DNA by real-time PCR. Nat Protoc 5:1–13

Whiley DM, Sloots TP (2005) A 5′-nuclease real-time reverse transcriptase-polymerase chain reaction assay for the detection of a broad range of influenza A subtypes, including H5N1. Diagn Microbiol Infect Dis 53:335–337

Whiley DM, Lambert SB, Bialasiewicz S et al (2008) False-negative results in nucleic acid amplification tests-do we need to routinely use two genetic targets in all assays to overcome problems caused by sequence variation? Crit Rev Microbiol 34:71–76

Wu D, Li R, Wang H et al (2012) Hollow mesoporous silica microspheres as sensitive labels for immunoassay of prostate-specific antigen. Analyst 137:608–613

Yang AK, Lu H, Wu SY et al (2013) Detection of Panton-Valentine Leukocidin DNA from methicillin-resistant Staphylococcus aureus by resistive pulse sensing and loop-mediated isothermal amplification with gold nanoparticles. Anal Chim Acta 782:46–53

Ye F, Li MS, Taylor JD et al (2001) Fluorescent microsphere-based readout technology for multiplexed human single nucleotide polymorphism analysis and bacterial identification. Hum Mutat 17:305–316

Yu J, Ge L, Liu S et al (2011) Facile and scalable synthesis of a novel rigid artificial superoxide dismutase based on modified hollow mesoporous silica microspheres. Biosens Bioelectron 26:1936–1941

Yu HW, Kim IS, Niessner R et al (2012) Multiplex competitive microbead-based flow cytometric immunoassay using quantum dot fluorescent labels. Anal Chim Acta 750:191–198

Zhang J, Lang H, Huber F et al (2006) Rapid and label-free nanomechanical detection of biomarker transcripts in human RNA. Nat Nanotechnol 1:214–220

Zhang GJ, Zhang G, Chua JH et al (2008) DNA sensing by silicon nanowire: charge layer distance dependence. Nano Lett 8:1066–1070

Zhang G, Chua HJ, Chee RE et al (2010) Sensor for detection of nucleic acid, vol WO2010059126A1. Agency Of Science, Technology and Research, Bci (Biochip Innovations), Simems, Washington, DC

Zhang JD, Schindler T, Küng E et al (2014) Highly sensitive amplicon-based transcript quantification by semiconductor sequencing. BMC Genomics 15:565–565

Zhao J, Kang L, Hu R et al (2013) Rapid oligonucleotide suspension array-based multiplex detection of bacterial pathogens. Foodborne Pathog Dis 10:896–903

Zhu Y, Hein DW, Doll MA et al (2006) Simultaneous determination of 7 N-acetyltransferase-2 single-nucleotide variations by allele-specific primer extension assay. Clin Chem 52:1033–1039

Zhu S, Fischer T, Wan W et al (2011) Luminescence amplification strategies integrated with microparticle and nanoparticle platforms. Top Curr Chem 300:51–91

Zhu Z, He J, Zeng T et al (2014) A multiplexer liquid chip technology for detecting single nucleotide polymorphisms from metabolism of anti-thrombotic drugs in dried blood spots on filter paper. Acta Biochim Biophys Sin 46:522

Zimmermann BG, Grill S, Holzgreve W et al (2008) Digital PCR: a powerful new tool for noninvasive prenatal diagnosis? Prenat Diagn 28:1087–1093

Zipper H, Brunner H, Bernhagen J et al (2004) Investigations on DNA intercalation and surface binding by SYBR Green I, its structure determination and methodological implications. Nucleic Acids Res 32:e103

DNA and RNA Electronic Properties for Molecular Modifications and Environmental State Diagnostics

Irena Kratochvílová

Contents

Abstract The main goal of this chapter is to show how specific DNA and RNA modifications and defects change the molecular electronic properties and how electronic state measurements can be used for oligonucleotide modifications and defect sensing. We also show that specific electronic states in DNA/Hg complexes play an important role in sensing the Hg presence in the environment. This chapter encompasses different concepts and methods showing the coherence between the structure, composition, and electronic properties of DNA and RNA.

Keywords Charge transport through DNA/RNA • DNA sensors • STM • Fluorescence spectroscopy

I. Kratochvílová (✉)
Physical Properties of Biomaterials Research Group, Institute of Physics Academy of Sciences of the CR, Na Slovance 2, 18221 Prague 8, Czech Republic
e-mail: krat@fzu.cz

V.A. Erdmann et al. (eds.), *RNA and DNA Diagnostics*, RNA Technologies,
DOI 10.1007/978-3-319-17305-4_11

1 Introduction

Oligonucleotides, carrying the genetic code of all living species, have recently become a center of great attention on the part of chemists and physicists, one of the reasons being their potential use in nanoelectronic devices, both as a template for assembling nanocircuits and as an active element of such circuits. Charge migration along oligonucleotides has attracted scientific interest for more than 50 years (Taniguchi and Kawai 2006).

The ability of oligonucleotides to mediate charge transfer is the basis of novel molecular devices and plays a role in the processes of sensing and/or repair of molecular damage. Charge transfer along or through these molecules has been investigated by various experimental techniques for over a decade, sometimes with contradictory results (Wagenknecht 2005). Oligonucleotides conduct electric charge via various mechanisms (depending on many parameters) and their characterization and understanding is a very important and complicated task.

The prevailing DNA architecture, the double helix, has well stacked nearly parallel bases with overlapping π-electron systems. Such π-electron systems may be good candidates for long-distance and one-dimensional (linear) charge transport. Unlike the π-electrons, which can form extended states, water molecules and counter ions create localized states of electrons, resulting in the hopping mechanism of conduction, with the inclusion of the electron–phonon interactions. The DNA molecule contains electronic states that have an extended character and in which the electrons easily carry a ballistic current, and localized states of electrons mediating the hopping mechanism of conduction. These two rather complementary pictures of conduction, π-electron overlap and hopping through energetically near states, may fit together (Giese 2002; Genereux et al. 2011).

The high charge transfer rate between elaborated donor–acceptor pairs in DNA has triggered a series of direct electrical transfer measurements. As far as the biological importance of oligonucleotide charge transfer is concerned, Barton and co-workers found that the repair of a damaged base is controlled from a remote site via long-distance charge transfer–DNA charge transfer can serve as an antenna for DNA damage, allowing proteins to monitor oxidation events that occur far away and respond to them quickly. The extent of delocalization and the character of electronic states in DNA are believed to play an essential role in probing the electronic properties of a substrate during DNA repair; even its subtle deviations from normal DNA could probably be detected with different charge–carrier mobility. Specifically, detection of the oxidative damage in the regulation of tumor-suppressor genes such as p53 can be controlled by charge transfer. It has also been shown that the conductance of DNA is important for the functioning of enzymatic activity with possible biological consequences (Pamela et al. 2012; Wagenknecht 2005).

Rapid and sensitive detection of a very low concentration of specific DNA sequences using DNA microarrays or DNA sensors has become an important topic of investigation (Rasheed and Sandhyarani 2014). In general, the sensing

surface of a DNA sensor consists of an immobilized single-stranded oligonucleotide that binds to its complementary target DNA sequence via hybridization. The hybridization process is then converted into a readable signal by the appropriate transducers such as electrochemical, optical, or mass-sensitive elements that can generate readable current, light signals or frequency, respectively. Biomolecules can easily be conjugated with gold nanoparticles without losing their biochemical activity. Gold nanoparticles are used for signal amplification in several biosensors taking advantage of their unique optical and electrical properties. Changes in current–voltage characteristics are reported as one of the sensitive detection strategies for the DNA hybridization event. Current–voltage characteristics can be measured using scanning tunneling microscopy, and the gold nanoparticles on the sensor surface give characteristic shape to the current–voltage plots.

As far as the charge transfer mechanism of hybrid DNA/RNA duplexes is concerned, detailed study was made by Kratochvílová et al. (2013). The temperature dependence of steady-state fluorescence spectroscopy, time-resolved fluorescence spectroscopy, melting temperature measurements, and theoretical approaches within molecular dynamics (MD) and Density Functional Theory (DFT) were applied to DNA/DNA and DNA/RNA complexes and it was proposed how the short distance charge transfer efficiency in oligonucleotides is affected by the molecular structure, temperature stability of the systems, chain flexibility, holes, base interactions, and charge distributions.

One of the most promising approaches to modifying DNA charge transfer properties is to form metal–DNA complex systems. Specifically, DNA/Hg complexes play an important role in probing DNA defects or the presence of Hg in the environment (Matsui et al. 2007; Wang et al. 2005). An important way of characterizing the DNA/Hg complexes is to investigate the manner in which the electric charge is transferred through them.

2 Methods of Characterization of the DNA and RNA Electronic Properties

Historically, three basic experimental approaches have been applied to investigate conduction through molecules:

1. Studying transport in thick molecular films and devices, such as organic thin-film transistors or light-emitting diodes (Kratochvílová et al. 2008).
2. Isolated molecules are positioned between two electrical contacts. This experimental setup is very difficult to implement and especially hard to verify (Fig. 1) (Wagenknecht 2005).
3. Spectroscopic techniques are employed to probe the relationships between the structural dynamics and charge transfer efficiency in oligonucleotides containing a donor–acceptor pair (typically photo excited 2-amino-purine and guanine pair) (Kratochvílová et al. 2013; Genereux et al. 2011).

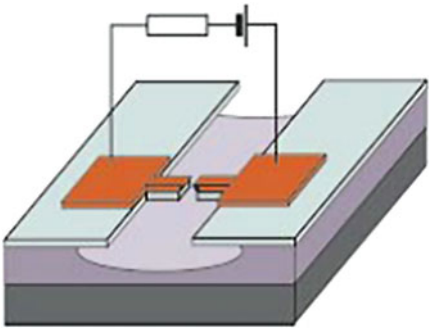

Fig. 1 The optimal experimental setup for investigation of charge transport through molecules is positioning of isolated molecules between two electrical contacts: voltage–current characteristics can be measured directly (Porath et al. 2000)

2.1 Oligonucleotides Between Two Electrical Contacts

Attempts to infer DNA electron transfer from fluorescence quenching measurements of DNA strands doped with donor and acceptor molecules have spurred intense debate over the question of whether or not this important biomolecule is able to conduct electrical charges. The first electrical transport measurements of micrometer-long DNA ropes, followed by large numbers of DNA molecules, have indicated that DNA behaves as a good linear conductor (Porath et al. 2000; Taniguchi and Kawai 2006).

The Scanning Tunneling Microscope (STM) has already been proven (Kratochvílová et al. 2008) as a very suitable tool for investigating ordered monolayer films, making it possible to contact one or more molecules and obtain images of the structural characteristics of the film. The experiments have also been used to investigate the room-temperature electronic properties of 12 base-pair $d(GC)_{12}$–$d(GC)_{12}$ DNA molecules attached to the gold surface by a thiol link (Kratochvílová et al. 2008). The STM experiments offer a novel way of probing the electronic properties of biomolecules on surfaces at the atomic level.

In previous studies (Kratochvílová et al. 2008, 2010) the STM measurements were performed with the NTEGRA Prima NT MDT system. Both topographic and spectroscopic data were obtained using freshly cut Pt/Ir tips. Using STM, the topography of the samples was observed for a set point of low voltage of ~10 mV and relatively high current of ~0.5 nA, and therefore at quite a small tip–sample distance. The topographic images showed a considerable difference between the bare gold substrates and the samples with DNA molecules. In the case of molecular layers, specific surface patterns were observed. The occurrence of these patterns was attributed to the corrosion of the bottom gold layers arising from the reaction of the thiol groups with the gold atoms, forming dissolvable complexes. The orientation of DNA molecules at the gold surface was investigated by variable angle spectroscopic ellipsometry working in the rotating analyzer mode. The thicknesses of both layers and the optical constants of the DNA layer were determined using a direct fitting procedure applied to the experimental ellipsometric data. For 32-nucleotide-long DNA molecules that were used for the experiment, this length

corresponds to the average distance between the neighboring bases of about 0.3 nm, which in turn corresponds to the base–base stacking distance intermediate between the B- and A-DNA forms.

STM experiments were carried out for pairs of samples on one chip that were measured so that each of the studied duplex was compared with all the others. The position of the tip above the samples was controlled by comparing the histograms of the decay constants and the breakpoints of the current/tip distance curves measured for various DNA samples. When the tip is very close to the molecules (defined by the set point value) at very low voltages, the number of the molecules contributing to the total current is low. The current–voltage characteristics were recorded for various feedback voltage and current set points, i.e., for different initial sample–tip distances. In all experiments, the STM tip acted as the electrical contact on the "top" side of the assembled monolayer of the DNA molecules, whereas the supporting gold substrate acted as the other, "bottom" contact. The distance between the top of the molecules and the STM tip for all the set points was estimated as 2.5–4 Å.

2.2 *Fluorescence Spectroscopy*

In Kratochvílová et al. (2013, 2014) and Wagenknecht (2005), fluorescence spectroscopy was used to probe the charge transfer efficiency in DNA/DNA (Fig. 2) duplexes and RNA/DNA hybrids and in DNA/DNA with a mismatched (T–T) base pair and DNA with T–Hg(II)–T (containing the T–T mismatched pair bridged by Hg). For this purpose the temperature dependence of steady-state fluorescence and UV-VIS spectroscopy were measured. In all measurements, 2-aminopurine (Ap) representing an optically excited fluorescent redox probe was introduced into the DNA chain as a hole donor. The charge developed upon excitation and transferred from Ap to the redox counterpart was trapped by the hole acceptor G. The fluorescence of DNA/DNA duplexes and RNA/DNA hybrids was measured at a temperature scale ranging from 10 to 40 °C; DNA/DNA with the mismatched (T–T) base pair and DNA with T–Hg(II)–T (containing the T–T mismatched pair bridged by Hg) fluorescence was measured in the interval from 10 to 40 °C. The fluorescence spectroscopy was measured with Fluoro log Horiba JY using double monochromators for excitation and emission. The steady-state emission spectra were obtained by exciting at 320 nm; the excitation spectra were measured at 365 nm. The excitation in time-resolved fluorescence spectroscopy was performed at 329 nm with a laser diode and a pulse duration <1 ns, and the fluorescence was recorded at the Ap maximum, 365 nm (Kratochvílová et al. 2013).

Integrals of fluorescence emission spectra over wavelengths were expressed (at each relevant temperature point) for redox-active (Φ_G) and redox-inactive duplexes (Φ_I). Importantly, the fluorescence of redox-active duplexes was always lower compared to redox-inactive duplexes. This decrease was attributed to the

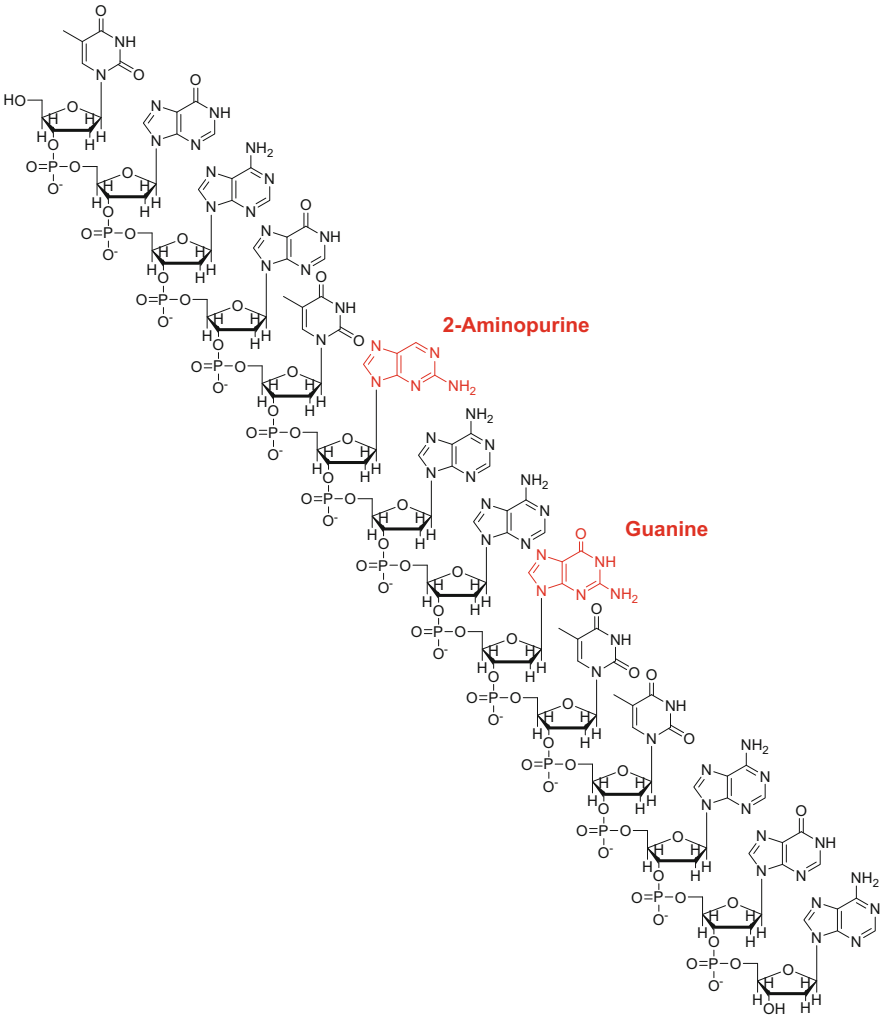

Fig. 2 The chemical structure of a DNA/DNA redox-active duplex for optical spectroscopy measurements—the hole acceptor is guanine and the hole donor is 2-aminopurine (Kratochvílová et al. 2013, 2014). DNA/DNA is composed of two DNA strands, where the donor–acceptor pairs, 2-aminopurine (Ap)-guanine (G), are separated by two or three bases

quenching caused by the charge transfer. The quenching efficiencies were calculated as $F_q = 1 - \Phi_G/\Phi_I$ (Figs. 4 and 6). A higher F_q value corresponds to higher charge transfer through the part of the molecular chain between Ap and G.

The emission of photo excited Ap was monitored over a 120-ns time regime using the single photon counting method (TCSPC, Fluorocube Horiba JY) for redox-inactive and redox-active oligonucleotides (Kratochvílová et al. 2013). The decay of the time-resolved fluorescence of photoexcited Ap was fitted in a three-

exponential fashion, yielding three lifetimes and three amplitudes. The different lifetimes corresponded to different modes and/or efficiencies of fluorescence quenching, which can be related to different conformers. Overall, higher fluorescence quenching in fluorescence spectroscopy indicates better charge transfer through the chain (of corresponding lengths).

2.3 *Theoretical Modeling: Molecular Dynamics Simulations, DFT Quantum Mechanics Calculations*

Molecular dynamics (MD) calculations were carried out in order to model the global structural changes and dynamical behavior of the oligonucleotides. Density functional theory (DFT) quantum mechanics calculations were then performed in time evolution, as had been modeled by the molecular dynamics simulations in order to map the time progress of the electronic and structural factors that may impact the charge–carrier transport in the studied molecules.

In Kratochvílová et al. (2008, 2010), three double-stranded 32-mer oligonucleotides were studied: the canonical standard double strands, DNA double strands with three mismatched base pairs, and double strands with three central pairs of nitrogenous bases replaced by methyl groups.

MD simulations started for molecular models with the sugar–phosphate backbone in the fiber conformation as furnished by the AMBER program. Prior to the MD simulations, a six-step equilibration was carried out when the solvent geometry was relaxed and the DNA geometry kept rigid, after which both solvent and DNA geometries were relaxed and, finally, a heating/equilibration simulation was performed at a constant volume with rigid DNA and temperature increased from 0 to 300 K. The actual molecular simulation was run for 10 ns using the periodic boundary conditions at a temperature of 300 K and a cutoff at 10 Å.

In the study by Kratochvílová et al. (2010), molecular models for quantum mechanics calculations included only the central part of the DNA duplexes that the MD simulations had shown to be the most flexible. Electronic characteristics of each molecular model were calculated for six coordinate sets that were extracted from the MD simulations at 0, 1, 2, 3, 4, and 5 ns. In order to examine the electronic structure of DNA under various structural and solvation conditions, each coordinate set of each model was considered at three levels of solvation: one non-hydrated ("isolated") system and two systems containing 50 and 110 water molecules, respectively. All DFT calculations were performed directly using the molecular geometries from the molecular dynamics calculations as single-point calculations without any further structure optimization. The quantum chemical calculations were performed using the Gaussian 03 software package. The 6-31G* polarized double-ζ basis sets together with M05-2x functional designed for the study of weak interactions and π–π interacting systems were used in the DFT calculations.

3 Mechanisms of Charge Transfer Through Oligonucleotides: Environmental State Diagnostics

The STM measurements presented in previous studies (Kratochvílová et al. 2008, 2010) show a sequence-dependent manner of charge transfer through the duplex with GC-rich double strands having the largest conductivity. The STM data also show that any disruption of the canonical W–C base pairing or introduction of chemical modification to the DNA backbone or removal of the three bases from the middle of the 32 pair-containing samples (abasic samples) lead to lower conductivity; single-stranded DNA always displays lower conductivity than duplexes. A decrease of the conductivity in the sample with three mismatched base pairs relative to the sample with all W–C pairs may seem large considering the preserved vertical π-stacking and overall stability of the mismatched sample; both properties are comparable in both samples as revealed by analysis of the Raman spectra and suggested by molecular dynamics simulations. A possible explanation may be offered by the Density Functional Theory (DFT) calculations showing that the mismatched pairs constitute isolated electronic states requiring greater activation energy and their HOMO orbitals are less uniformly dispersed than regularly ordered W–C base pairs, further diminishing the charge transport probability. The abasic samples still had lower conductivity than the mismatched sample, but the decrease from mismatched to abasic sample conductivity was moderate. It is perhaps surprising, especially considering the complete removal of several base pairs that had dramatic consequences for the duplex stability and structural regularity demonstrated clearly by the Raman experiments: while samples with three non-W–C base pairs were only slightly less stable than the canonical duplexes and melted in a cooperative way, the structural regularity and thermal stability of abasic duplexes was strongly affected (Fig. 3).

The DFT calculations show that water orbitals strongly influence the charge transport for all the models. For the W–C-paired and mismatched models alike, the HOMO orbitals are localized on the bases and the water orbitals increase the charge transport probability. The lower conductivity and transport probability of the mismatched model can be explained by its less uniformly dispersed HOMO orbitals. The abasic samples still had lower conductivity than the mismatched sample, but the decrease from mismatch to abasic was moderate. We assume that water is solely responsible for the charge transport across the abasic lesion because only its orbitals can bridge the distant bases flanking the abasic site. Design of particular DNA sequences with chain or base modifications and/or non-canonical base pairing, enabling partial hydration of the interior of the duplexes, can be envisioned for future use of molecular wires of defined conductivity.

Using fluorescence spectroscopy, charge transfer properties of DNA/DNA double strands and DNA/RNA double strands were compared (Kratochvílová et al. 2010)—Fig. 4. Conformationally more flexible RNA/DNA hybrids have larger inter-strand stacking, more delocalized HOMO orbitals, more delocalized charge and holes, and better electronic coupling, which all means better conditions

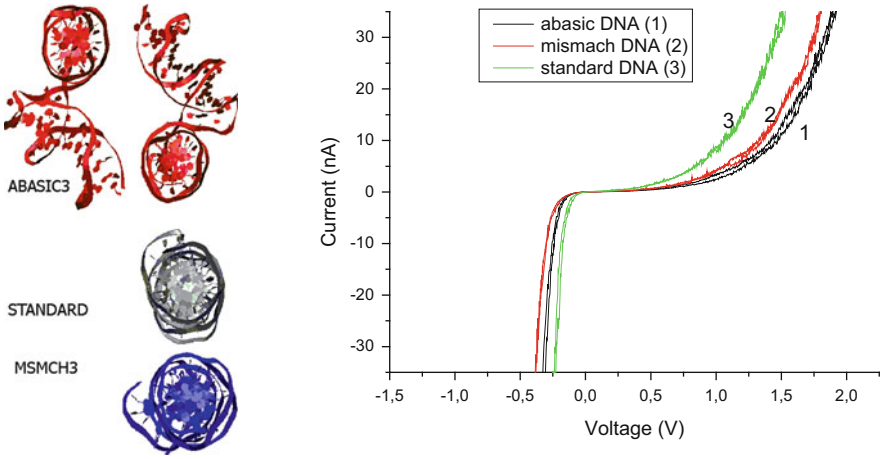

Fig. 3 *Left*: The projections show views along the molecular axis after 10 ns of MD simulations. The abasic (ABASIC3) molecule is shown twice from the "top" and "bottom" to emphasize that both of its ends are well-preserved B-type double helices and that only the central region is highly disordered. Standard and mismatched samples stay practically ordered after 10 ns (Kratochvílová et al. 2010). *Right*: Typical STM current/voltage—$I(V)$ curves of a DNA 32-mer oligonucleotide double strands: abasic (*black*), mismatch GC (*red*), standard (*green*). The STM set point was 0.1 nA and 0.1 V, the $I(V)$ curves were measured in both voltage directions

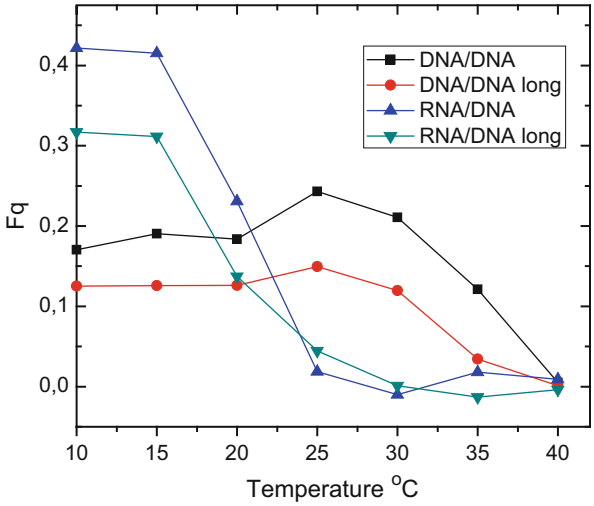

Fig. 4 Temperature-dependent yield of the fluorescence quenching efficiencies F_q. Fluorescence emission intensities were measured at temperatures ranging from 10 to 40 °C for DNA/DNA and RNA/DNA duplexes with various distance (2–3 adenosine units) between the donor and the acceptor. All studied duplexes had higher overall quenching of fluorescence (indicating better charge transfer properties) for the hybrid RNA/DNA rather than the DNA/DNA sequences of corresponding lengths. Importantly, the reduction of redox-active fluorescence as compared to redox-inactive fluorescence confirmed the donor–acceptor charge transfer for DNA/DNA and RNA/DNA. At the same time, a longer distance between the Ap and G led in all cases to smaller charge transfer yield—this effect also confirmed the donor–acceptor charge transfer (Kratochvílová et al. 2013)

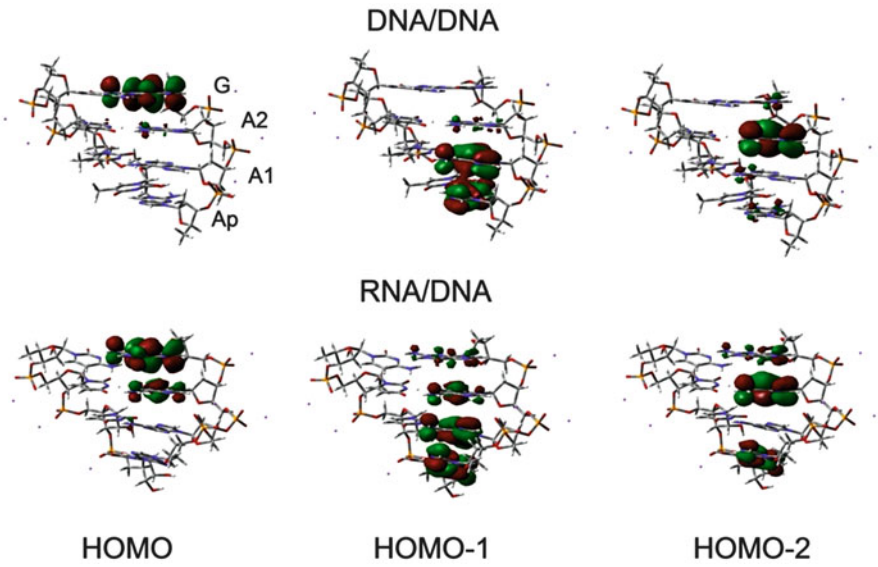

Fig. 5 Spatial distribution of the highest occupied molecular orbitals (HOMO) calculated in DNA/DNA and RNA/DNA model duplexes ordered according to their energies. The orbitals were localized at the purine-rich ApAAG strand. The HOMO orbital was dominantly localized at G, HOMO-1 at Ap and neighboring A, and HOMO-2 at A next to the G base. The oligonucleotide sequences were set according to Table 1. The hydrogen atoms were added and each model was augmented with six Na^+ ions coordinated to the backbone phosphates (Kratochvílová et al. 2013)

for charge transfer. Enhanced mobility of the bases within the RNA/DNA hybrids gives the bases greater access to conformations and thus increases the probability of achieving conditions for charge transfer. The larger conformational flexibility of the hybrid duplexes also causes larger delocalization of the holes that have a strong impact on the charge transfer process. The electronic overlap between bases within the hole is even larger, because the hole is formed in response to a need for electron donation. As a consequence of all these effects, the charge in RNA/DNA hybrids becomes more delocalized. In this case, the charge is more effectively transferred coherently. However, for temperatures above 20 °C, due to the very specific properties of RNA/DNA hybrids (inter-strand stacking, more delocalized HOMO orbitals, more delocalized charge and holes, better electronic coupling, conformational flexibility), the system setting is destroyed (in relation to the melting procedure) and the charge transfer ability of the hybrids falls down. In contrast, DNA/DNA duplexes do not possess such a conformationally flexible chain as RNA/DNA hybrids, more localized HOMO orbitals, localized charge and holes, and they display worse electronic coupling. Under these conditions, there is high probability that the DNA/DNA charge transfer could be more incoherent than the charge transfer through RNA/DNA. The DNA/DNA charge transfer efficiency changes with temperature in a different way: charge transfer is increasing with

Table 1 The DNA/DNA and RNA/DNA duplexes for optical spectroscopy measurements

Sample description	Sequence
DNA/DNA redox active	5´-d(TIA ITAp AAG TTA IA)-3´
	3´-d(ACT CAT TTC AAT CT)-5´
DNA/DNA redox inactive	5´-d(TIA ITAp AAI TTA IA)-3´
	3´-d(ACT CAT TTC AAT CT)-5´
RNA/DNA redox active	5´-d(TIA ITAp AAG TTA IA)-3´
	3´-r(ACU CAU UUC AAU CU)-5´
RNA/DNA redox inactive	5´-d(TIA ITAp AAI TTA IA)-3´
	3´-r(ACU CAU UUC AAU CU)-5´
DNA/DNA long redox active	5´-d(TIA ITAp AAAG TTA IA)-3´
	3´-d(ACT CAT TTTC AAT CT)-5´
DNA/DNA long redox inactive	5´-d(TIA ITAp AAAI TTA IA)-3´
	3´-d(ACT CAT TTTC AAT CT)-5´
RNA/DNA long redox active	5´-d(TIA ITAp AAAG TTA IA)-3´
	3´-r(ACU CAU UUUC AAU CU)-5´
RNA/DNA long redox inactive	5´-d(TIA ITAp AAAI TTA IA)-3´
	3´-r(ACU CAU UUUC AAU CU)-5´

In the redox active duplexes, the hole acceptor was guanine (G) and the hole donor was 2-aminopurine (Ap). In the redox inactive duplexes, G was replaced by redox-inactive inosine (I). Other symbols indicate normal nucleic acid bases in the oligonucleotide sequences

temperature up to the melting point, where the chain charge transfer efficiency of the destroyed duplex falls down.

As far as DNA double strands with incorporated Hg are concerned (Figs. 5 and 6), the highest overall quenching of fluorescence (and therefore the highest rate of charge transfer) at low temperatures was obtained for the DNA mismatch with Hg. Mismatched DNA without Hg had lower quenching than standard DNA duplexes.

For all the DNA/DNA systems under study (Fig. 6) the charge transfer yield increased with temperature up to a breaking point that was specific for each type of samples. Fluorescence spectroscopy measurements (fluorescence quenching and excitation band intensity) indicated that temperature caused weakening of mutual base interactions and thus activated the charge transfer. For temperatures above the breaking point, the charge transfer rapidly decreased. Temperature at the breaking point of a mismatched DNA duplex increased after adding Hg to the solution. Calculations indicated that the changes in charge transfer were likely owing to the differences in local geometry (overlap of bases) than due to the electronic structure. The models showed that Hg orbitals did not contribute to the HOMO and HOMO-1 orbitals, and therefore they could not directly influence the charge transport properties.

At low temperatures, the charge transfer conditions were poorest for most structurally disordered DNA T–T. On the contrary, for DNA T–Hg(II)–T, the bases between the donor and acceptor were in such positions that the bases' overlap

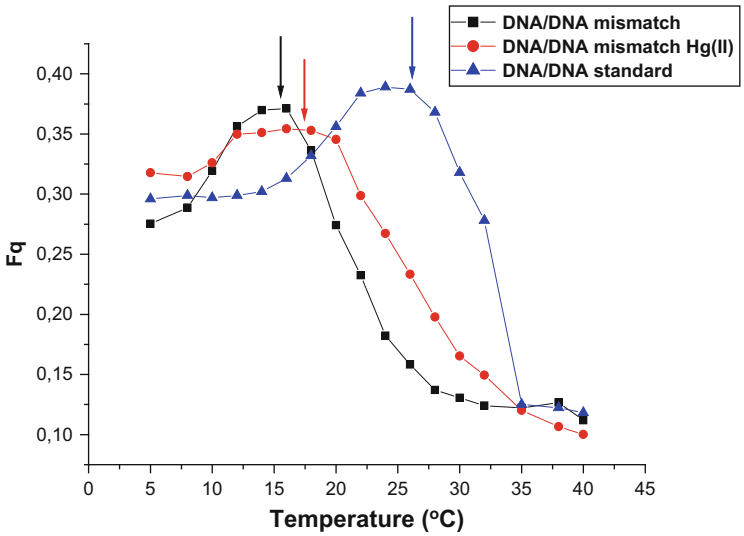

Fig. 6 Temperature dependence of the quenching efficiency (F_q) for DNA T–T, DNA T–Hg(II)–T and standard DNA. Higher F_q value corresponds to higher charge transfer through the part of the DNA chain between Ap and G. The *arrows* above the curves show the duplex melting temperature T_m obtained from UV melting experiments (Kratochvílová et al. 2014)

was most favorable for charge transfer. Rising temperature generally improved charge transfer in all the cases—owing to sufficient thermal motions, bases adopted suitable positions more frequently. For standard DNA, the temperature-enhanced dynamics enabled such overlap of bases that charge transfer closely under the break point was best from all the systems under study. However, with increasing temperature, Hg bound to the T–Hg(II)–T system eventually limited the thermal motion by which the charge transfer was otherwise facilitated, thereby reducing the charge transfer. In all cases, as a consequence of conformational changes associated with melting of the duplexes, the charge transfer efficiency declined at temperatures above the break points. **T–Hg(II)–T formation stabilized the whole system and improved resistance of the mismatched DNA to melting. DNA/Hg complexes play an important role in the sensing of defects in DNA or presence of Hg in the environment (Guo et al. 2009)—change of melting point and charge transfer efficiency in Hg bridged DNA double strands is very sensitive probe for Hg presence in the solutions.**

Two extreme mechanisms of charge transport in DNA may be considered. The prevailing DNA architecture, anti-parallel double helix, has well-stacked bases with overlapping π-electron systems, and it is widely assumed that nearly parallel bases with overlapping π-electrons have highly delocalized molecular orbitals that are good candidates for long-distance, one-dimensional (linear) charge transport (Pamela et al. 2012; Wagenknecht 2005). The second possible charge transport mechanism in DNA is charge hopping, which presumes localized molecular orbitals and no significant electronic overlap between adjacent base pairs. Unlike

π-electrons that can form extended molecular orbitals, the DNA backbone, water molecules, and counterions in the solvation shell create localized states resulting in charge conduction by the phonon-assisted (thermally activated) hopping. There is one phenomenon that is important for charge transport in organic molecules: a polaron. A polaron is a radical charge self-trapped by a structural distortion of its containing medium. A polaron may migrate by tunneling or by phonon-assisted (thermally activated) hopping. The electronic overlap between bases within the polaron is larger, because it is formed in response to a need for electron donation. As a consequence, the charge becomes delocalized within the base pairs in a polaron-like distortion and its transport therein might appear to occur by a super-exchange mechanism. Structural fluctuations of base pairs transferred to their π-stack interactions have experimentally been shown to influence charge transfer of DNA duplexes (Wagenknecht 2005; Kratochvílová et al. 2010).

Regardless of its exact mechanism, charge transfer through the DNA duplex strongly depends on the base composition. Preferential trapping of charge in the isolated guanine base, or more markedly at the GG steps, has been confirmed by several studies (Wagenknecht 2005; Tang et al. 2006; Kratochvílová et al. 2010). One-electron oxidation was mostly observed at the GG steps in the mixed GG/A/T sequences with the proposed charge transfer mechanism by phonon-assisted polaron hopping. Introduction of mismatches, non-Watson–Crick base pairs, to a DNA duplex changes its electrical properties. All observations demonstrate that charge transfer characteristics of a DNA duplex are able to reveal the presence of mismatches in the sequence, which may help elucidate the possible mechanisms of mismatch identification both in the cell and in technological applications.

4 Practical Applications: Oligonucleotides Charge Transfer-Based Sensors

A simple and robust DNA sensor has been developed for the detection of *BRCA1* (Breast cancer 1) DNA sequences (Rasheed and Sandhyarani 2014). *BRCA1* is a human gene that is expressed in the cells of breast and other tissues, where it helps repair damaged DNA or destroys cells if the DNA cannot be repaired. Certain variations of the *BRCA1* gene may lead to an increased risk of breast cancer with hereditary breast–ovarian cancer syndrome. Researchers have identified hundreds of mutations in the *BRCA1* gene that are associated with an increased risk of cancer. Mutations in the *BRCA1* gene are responsible for ~40 % of inherited breast cancers and more than 80 % of inherited breast and ovarian cancers. Rasheed and Sandhyarani (2014) described development of a sensitive and simple DNA biosensor for the low concentration detection of *BRCA1* DNA sequences. This DNA sensor was based on a "sandwich" detection strategy, which involved immobilization of DNA on a gold electrode surface (Scheme 1). Initially, the capture DNA probe (DNA-c) was immobilized on the cleaned gold electrode surface by dipping

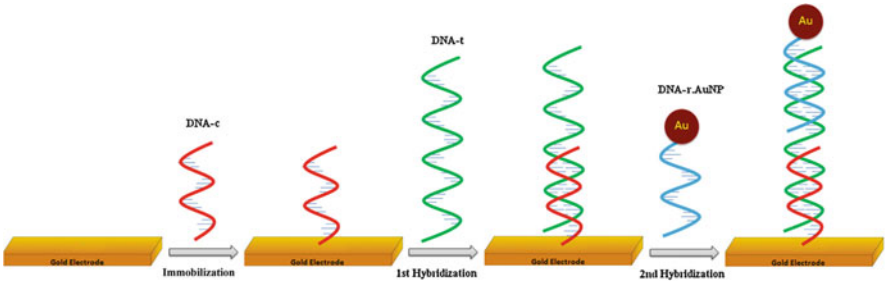

Scheme 1 Schematic representations of the various stages of sensor fabrication and DNA hybridization related to BRCA 1. Initially, the capture DNA probe (DNA-c) was immobilized on the cleaned gold electrode surface by dipping the electrode in 1 M DNA-c probe solution in 0.1 M phosphate buffer. The resulting electrode was cleaned and then immersed into a solution containing the target DNA (DNA-t) in 0.3 M NaCl PBS buffer for 2 h. The complementary portions of the DNA-t were hybridized with DNA-c on the surface, leaving the remaining portion for the hybridization with DNA-r. After that, the hybridization with DNA-r AuNP was achieved. The resulting electrode was denoted as the Au/DNA-c|DNA-t|DNA-r.AuNP electrode (Rasheed and Sandhyarani 2014)

the electrode in 1 M DNA-c probe solution in 0.1 M phosphate buffer. The resulting electrode was cleaned and then immersed into a solution containing target DNA (DNA-t) in 0.3 M NaCl PBS buffer for 2 h. The complementary portions of the DNA-t were hybridized with DNA-c on the surface, leaving the remaining portion for the hybridization with DNA-r. After that, the hybridization with DNA-r AuNP was achieved. The resulting electrode was denoted as the Au/DNA-c|DNA-t|DNA-r.AuNP electrode (Rasheed and Sandhyarani 2014).

Such a hybridization process significantly enhanced the signal-to-noise ratio, leading to reliable detection of femtomolar concentrations of the DNA targets. In the absence of target DNA, the sandwich complexes do not form, leaving the surface-confined capture probe DNA unhybridized. One major advantage of the sandwich-type sensor is that no modification is required for the target *BRCA1* DNA sequence. Hybridization was monitored as a function of DNA-t concentration using I–V measurements. The sensor surface was characterized by scanning electron microscopy (SEM) and energy dispersive X-ray spectroscopy (EDS) with SU-6600 field emission scanning electron microscopy (FESEM, Hitachi, Japan) during each stage of the modifications.

SEM and STM measurements indicated that the Au nanostructures and the DNA hybridization are well constructed. The detection limit of the sandwich-type DNA sensor using STM I–V and normal I–V methods was evaluated. This DNA sensor could detect up to 1 fM *BRCA1* DNA and exhibited excellent selectivity against non-complementary sequences and three-base mismatch complementary sequences. It showed good reproducibility, stability, and reusability. It is expected that the sensor could find applications in cancer biomarker detection in the early stages of cancer, where the concentration of biomarkers is very low (Rasheed and Sandhyarani 2014).

References

Genereux JC, Wuerth SM, Barton JK (2011) Single-step charge transport through DNA over long Distances. J Am Chem Soc 133:3863–3868

Giese B (2002) Long-distance electron transfer through DNA. Annu Rev Biochem 71:51–70

Guo L et al (2009) Highly sensitive fluorescent sensor for mercury ion based on photoinduced charge transfer between fluorophore and π-stacked T–Hg(II)–T base pairs. Talanta 79:775–779

Kratochvílová I, Král K, Bunček M et al (2008) Conductivity of natural and modified DNA measured by scanning tunneling microscopy. The effect of sequence, charge and stacking. Biophys Chem 138:3–10

Kratochvílová I, Todorciuc T, Král K et al (2010) Charge transport in DNA oligonucleotides with various base-pairing patterns. J Phys Chem B 114:5196–5205

Kratochvílová I, Vala M, Weiter M et al (2013) Charge transfer through DNA/DNA duplexes and DNA/RNA hybrids: complex theoretical and experimental studies. Biophys Chem 180:127–134

Kratochvílová B, Golan M, Vala M et al (2014) Theoretical and experimental study of charge transfer through DNA: impact of mercury mediated T-Hg-T base pair. J Phys Chem B 22:5374–5381

Matsui T, Shigeta Y, Hirao K (2007) Multiple proton-transfer reactions in DNA base pairs by coordination of Pt complex. J Phys Chem B 111:1176–1181

Pamela A, Sontz PA, Muren NB et al (2012) DNA charge transport for sensing and signaling. Acc Chem Res 45:1792–1800

Porath D, Bezryadin A, Vries S et al (2000) Direct measurement of electrical transport through DNA molecules. Nature 403:635–638

Rasheed PA, Sandhyarani N (2014) Femtomolar level detection of BRCA1 gene using a gold nanoparticle labeled sandwich type DNA sensor. Colloids Surf B Biointerfaces 117:7–13

Tang YL, He F, Yu MH (2006) A reversible and highly selective fluorescent sensor for mercury (II) using poly (thiophene)s that contain thymine moieties. Macromol Rapid Commun 27:389–392

Taniguchi M, Kawai T (2006) Review. DNA Electronics Phys E 33:1–12

Wagenknecht HA (2005) Charge transfer process in DNA: from mechanism to application. Germany, ISBN: 978-3-527-31085-2

Wang Z, Zhang DQ, Zhu DB (2005) A sensitive and selective "turn on" fluorescent chemosensor for Hg(II) ion based on a new pyrene-thymine dyad. Anal Chim Acta 549:10–13

Mechanochemical Sensing

Prakash Shrestha, Shankar Mandal, and Hanbin Mao

Contents

Abstract In this chapter, we discuss a new sensing strategy that exploits mechanochemical principles of biological molecules, DNA in particular. Mechanochemical coupling reflects the interaction between chemical bonds in a molecule and mechanical stress experienced by the molecule. It is a key subject in the newly emerged field, mechanochemistry, which has led to a number of exotic applications in materials chemistry. However, the potential of the mechanochemical principles in the chemical sensing has not been fully recognized and exploited. Using force-based single-molecule techniques, such as optical tweezers, magnetic tweezers, or AFM, the tension in individual DNA templates can be followed in a mechanochemical sensing setup. When the template recognizes an analyte, the accompanied change in the tension of the template can be monitored in real time. This chapter discusses the general principle of the mechanochemical sensing, the pros and cons of this new sensing scheme, as well as future prospects for this strategy.

P. Shrestha • S. Mandal • H. Mao (✉)
Department of Chemistry and Biochemistry, Kent State University, Kent, OH 44242, USA
e-mail: hmao@kent.edu

V.A. Erdmann et al. (eds.), *RNA and DNA Diagnostics*, RNA Technologies,
DOI 10.1007/978-3-319-17305-4_12

Keywords Mechanochemical sensing • DNA nanotechnology • Mechanical affinity • Single-molecule methods • Mechanoanalytical chemistry

1 Introduction to Mechanobiology and Mechanochemistry

Mechanobiology and mechanochemistry are two emerging interdisciplinary subjects that investigate the coupling of mechanical force or work with biology and chemistry processes, respectively (Keller and Bustamante 2000; Schnitzer et al. 2000; Mavroidis et al. 2004; Beyer and Clausen-Schaumann 2005; Liao et al. 2005; Vogel and Sheetz 2006; Gennerich and Vale 2009; Weder 2009; Black et al. 2011; Craig 2012; May and Moore 2013). While the former discipline deals with the mechanical effect on macroscopic biological processes such as deformation of a tissue or an organ, the latter is focused on the mechanical effect on microscopic processes, such as formation or breaking of chemical bonding (covalent or non-covalent), that may sustain various mechanobiological effects.

Mechanochemical phenomena are universal in nature. At the level of tissues, muscles generate force as a result of conformational change in interacting proteins such as myosin and actin (Rayment et al. 1993; Svoboda and Block 1994; Visscher et al. 1999). The organization of cellular matrix influences the micromechanical properties of cells, which has been shown to play an important role in various diseases including cancers (Lord et al. 1988). Inside cells, the load force of motor proteins such as DNA and RNA polymerases (Wang et al. 1998; Davenport et al. 2000; Wuite et al. 2000) helps new bond formation in the DNA and RNA syntheses, respectively. Applications by using mechanochemical effects are ample. Mechanical unfolding of biomacromolecules is one example. By applying a mechanical force in a range of piconewtons along a specific direction, a biomacromolecule, protein, for example, can be unfolded as a result of breaking of secondary and/or higher-order structures in the molecule. With higher forces in the range of nanonewtons, even covalent bonds can be broken (Rief et al. 1997). On the other hand, reformation of non-covalent bonds occurs when mechanical force is reduced. In polymers, special chemical groups have been exploited to modulate the mechanical properties of the material (White et al. 2001; Caruso et al. 2009; Weder 2009; Black et al. 2011; Kean and Craig 2012; Kean et al. 2013; May and Moore 2013).

Many sensing mechanisms in our body are mechanochemical in nature. The interdependence of intracellular chemical and mechanical properties has been studied by using magnetic tweezers and fluorescence microscopy (Shekhar et al. 2012). Primary cilia that protrude from the surface of epithelial cell are specialized mechanosensory organelles. It is demonstrated of having important roles in cellular signaling, fluid shear sensing, and communication of cells with extracellular matrix. For example, the nephrons inside the kidney consist of those primary cilia of 200 nm in diameter and 10 μm in length. The bending nature of the cilium with the fluid flow in the nephron has been discussed to mechanochemically influence the intracellular release of calcium. Inhibition of this response through an IFT (Tg737/IFT88) mutation results in the development of cystic kidney. The role

of primary cilia as a fluid shear stress mechanosensor in the cardiovascular system has also been demonstrated (Alaiwi et al. 2009).

2 Mechanochemical Sensing

To detect biological analyte, a biosensor employs two major components: a recognition unit and a signal transduction unit. The recognition elements often rely on chemical interactions, such as intermolecular forces, to specifically recognize an analyte. This recognition event is then transformed into a detectable signal, which includes electrical and spectroscopic signals such as fluorescence. The transformation usually occurs in the signal transduction unit in the sensor. To serve as an effective mechanochemical sensor, the signal transduction unit must exploit mechanical signals, such as mechanical work, tension in a recognition template, or pressure in a system (Fig. 1). As demonstrated in the first-in-class mechanochemical sensor (Koirala et al. 2011b), mechanical tension or spatial change, the latter of which is a variable closely coupled to the tension of the template, has been measured. Since force has little interference from the environment, the mechanochemical sensor has high signal-to-noise ratio.

Another important advantage in the mechanochemical sensing is that the target recognition and signal transduction are tightly coupled without the requirement of additional components. The mechanochemical coupling allows a change in the mechanical property of a template as it recognizes a target through chemical interactions. Therefore, two separate units in a traditional sensor can now be combined into a single unit. This not only simplifies the sensing scheme but also improves the performance of the sensor, since the noise present in extra components of a sensing scheme can be avoided.

Notwithstanding these inherent advantages of mechanochemical sensing and rapid development in mechanochemistry, biomimetic sensing exploiting mechanochemical effects is rare and sporadic.

We found few literatures about mechanochemical sensing in which mechanical manipulation was exploited to bring chemical changes with a detectable signal. It has been described that the chemical reaction between a copper complex and CdSe quantum dots is only possible by mechanical grinding. They used this mechanochemical reaction

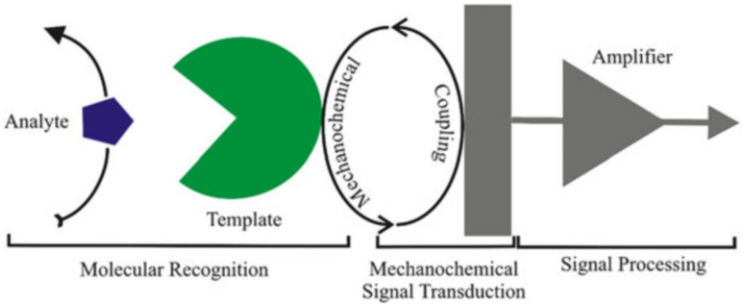

Fig. 1 Schematic of the basic steps involved in the mechanochemical sensing

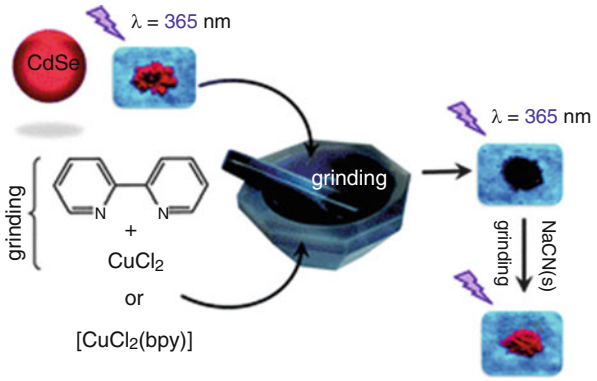

Fig. 2 Manual grinding of $CuCl_2$, 2,2′-bipyridine and hydrophobic CdSe QDs creates a selective and fast turn-on fluorescence sensor for detection of nanogram quantities of solid cyanide salts by the naked eye. Using a fluorescence detector, this simple sensor detects 100 ppm of NaCN in sand (Maldonado et al. 2011)

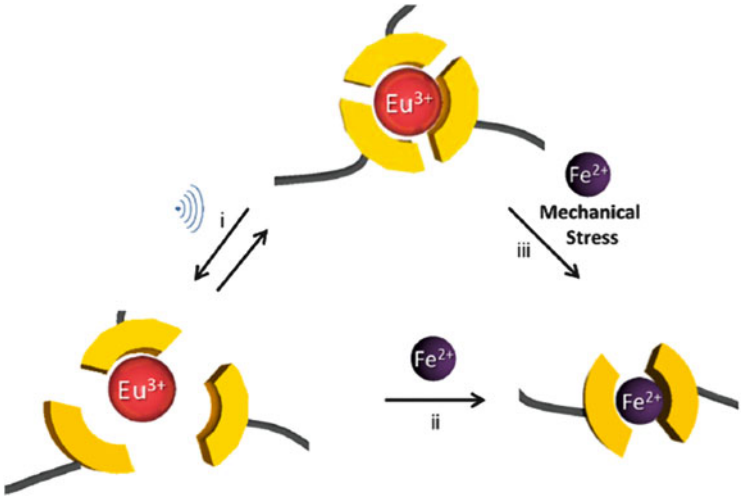

Fig. 3 (i) Reversible dissociation reaction of the Eu^{3+}-ligand complexes in $[Eu(BKB)_{1.5}](ClO_4)_3$ upon ultrasonication of these metallopolymers. Irreversible metal exchange with Fe^{2+} ions in films of $[Eu(BKB)_{1.5}](ClO_4)_3$ imbibed with a $Fe(ClO_4)_2$ solution as a result of (ii) ultrasonication or (iii) application of other mechanical forces (Balkenende et al. 2014)

to detect the cyanide ion. The visualization detection approach has shown high selectivity in that only cyanide ion could enhance the quenched fluorescence of QD in the presence of copper complex (Fig. 2) (Maldonado et al. 2011).

In another example, it has recently been reported that mechanochemical transduction can also be achieved in metallosupramolecular polymers. They demonstrated both reversible and irreversible reactions to form mechanically responsive materials and exchange of metal ions in the metallosupramolecular complex (Fig. 3) (Balkenende et al. 2014).

3 Basic Components of Mechanochemical Sensing

Although these sensing schemes use mechanical manipulations, they do not fully exploit mechanochemical coupling processes. In fact, the detection and the recognition are still decoupled. The measurement of the mechanical signal is critical for mechanochemical sensing that employs mechanochemical coupling principles. However, it is rather challenging to evaluate mechanical property at the molecular level. With the advent of single-molecule techniques such as atomic force microscope (AFM) (Binnig et al. 1986), optical tweezers (Ashkin et al. 1986), and magnetic tweezers (Strick et al. 1996), this task of mechanical force evaluation becomes feasible.

3.1 Instrumentation for the Force Measurement

The development of scanning tunneling microscope (STM) by *Binnig* and *Rohrer* was recognized for the Nobel Prize in 1986 (Binnig and Rohrer 1983). AFM was developed based on the STM (Binnig et al. 1986). After decades of development, AFM has been known as one of the best tools for nanoscale imaging and measurements, as well as mechanically manipulating at piconewton–nanonewton scale. An AFM instrument consists of a microfabricated cantilever with a highly delicate tip that can be composed of a few atoms. In the application of single-molecule force spectroscopy, a molecule is first tethered between the cantilever tip and surface of a substrate as shown in Fig. 4a. With the movement of the substrate controlled by a

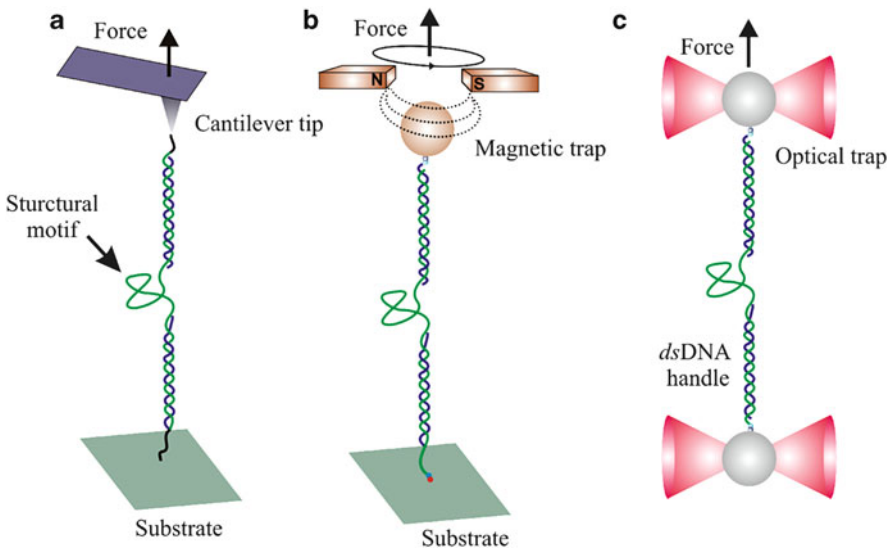

Fig. 4 Schematic of the force-based single-molecule techniques, (**a**) optical tweezers, (**b**) magnetic tweezers, and (**c**) atomic force microscopy (AFM), showing the folded structure of interest is sandwiched between two long dsDNA handles for mechanical manipulation

piezoelectric device, the tension in the molecule varies, which is measured by the deflection of the cantilever. The spatial resolution at nanometer scale and mechanical resolution at piconewton scale empower AFM as one of the best methods to investigate the biochemical interactions at the single-molecule level.

Magnetic tweezers is the most recently developed single-molecule force spectroscopy technique. A molecule is tethered between a magnetically trapped microparticle and the surface of a substrate (Fig. 4b). The unique capability of this method allows the investigation of the torque on a molecule by rotating the magnetic particle. It has much better force resolution comparing to other methods. However, a major disadvantage is associated with an indirect measurement of force.

Optical tweezers were first developed in 1986 (Ashkin et al. 1986) and improved later (Smith et al. 1996; Visscher et al. 1999). This method uses laser beams to trap dielectric microparticles (Fig. 4c). In dual-beam optical tweezers (Luchette et al. 2007; Mao and Luchette 2008), the molecule of interest is tethered between two optically trapped beads by using affinity interactions. This instrument has a better force resolution (10^{-13} to 10^{-10} N) comparing to the AFM (10^{-11} to 10^{-7} N). Its sub-nanometer spatial resolution permits to study DNA molecules at the single base-pair level. However, the possible laser-induced damage of biomolecules is a major disadvantage for this method.

Different chemical interactions present different mechanical properties. For most non-covalent interactions in recognition events, the mechanical stability is in piconewton range. Whereas AFM can reach nanonewton forces easily, its capability to detect and apply piconewtons force is limited. Magnetic tweezers, on the other hand, can reach sub-piconewton force; however, its spatial resolution is often not comparable with optical tweezers. Therefore, optical tweezers become ideal for force detection in the mechanochemical sensing.

3.2 Recognition Platforms Used for Mechanochemical Sensing

The mechanical stress can induce the breakage or formation of chemical bonds in a molecular structure. With the interaction between a ligand and a receptor, the mechanical tension in a receptor molecule varies with the binding of the ligand. Such a mechanochemical transduction is the basis of mechanochemical sensing, and hence the signal can be either mechanical or chemical. In the following sections, various platforms for the mechanochemical sensing strategy are discussed.

3.2.1 Polymer Templates

A variety of different recognition elements can be employed in the mechanochemical sensing. Although elemental compositions are similar in small molecules and

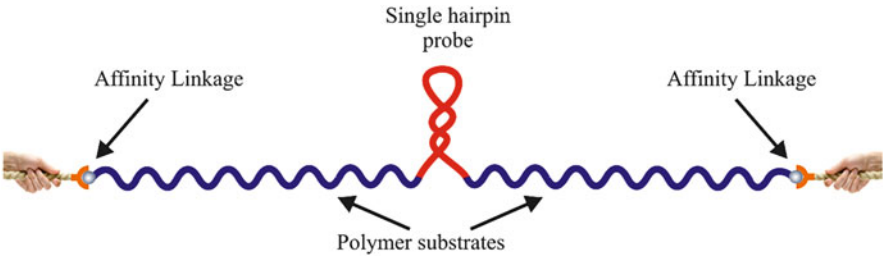

Fig. 5 Schematic of the single-molecule probe inside a biopolymer template for mechanical manipulation. Pulling hands are shown to represent mechanical manipulation of the single molecule

macromolecules, the chain-like property of a polymer endows it special mechanical features such as elasticity and stiffness. Thanks to the significant technical advances from the past few decades, mechanical manipulation of macromolecules becomes common in many laboratories. Therefore, it is possible to measure mechanical signals from the change of structural conformation in various macromolecules.

Biopolymers such as DNA, RNA, and proteins are commonly used as templates for mechanochemical sensing. These biopolymers show high specificity and strong affinities with a variety of analytes, which include metal ions, small molecule ligands, and other macromolecules. In all the force-based single-molecule techniques introduced above, the biopolymers are tethered between two surfaces by virtue of affinity linkages such as antibody–antigen interactions (Fig. 5). By moving the two surfaces approaching to or away from each other, the tension of the biopolymer changes. When an analyte interacts with the biopolymer, the variation of the tension differs, which signifies the detection of the analyte.

3.2.2 DNA Nanostructure as a Mechanochemical Sensing Platform

As described in the previous section, the versatility of a mechanochemical sensor lies in the fact that either DNA, RNA, or protein can serve as recognition elements. Proteins and RNAs are expensive to prepare and difficult to maintain their stability due to their intolerance to conditions such as heat or their susceptibility to numerous enzymes (protease and RNAse for proteins and RNAs, respectively). DNA molecules, on the other hand, are easy to prepare and recalcitrant to harsh conditions with respect to proteins and RNAs. For practical sensor development in which cost and durability are major concerns, DNA molecules become the material of choice to serve as recognition templates.

By virtue of methods such as SELEX (Tuerk and Gold 1990), DNA aptamers can be selected to specifically recognize a variety of analytes ranging from small molecules, biomacromolecules, to whole cells (Sefah et al. 2010). Secondary structures such as hairpins (Woodside et al. 2006), G-quadruplex (Yu et al. 2009) and i-motif (Dhakal et al. 2010) form in DNA aptamers. These non-B DNA

structures interact with ligands through numerous non-covalent interactions, resulting in strong affinity that can approach nanomolar in dissociation constant, which is equal to or better than those of antibody–antigen pairs employed in many sensing schemes. The tight binding between a DNA aptamer and a ligand warrants superior detection limit in the biosensing.

Recent rapid development in DNA nanotechnology (Niemeyer 1997; Seeman 2003, 2005; Calderone and Liu 2004; Simmel and Dittmer 2005; Alberti et al. 2006; Fazio et al. 2008; Pinheiro et al. 2011; Krishnan and Bathe 2012; Michelotti et al. 2012) is instrumental for the design of biosensors that use DNA as a template (Drummond et al. 2003; Kolpashchikov and Stojanovic 2005; Rosi and Mirkin 2005; Modi et al. 2009; Wang et al. 2009, 2010; Silverman 2010; Porchetta et al. 2012; Wilner and Willner 2012; Xing et al. 2012; Chandran et al. 2013). For example, the toehold strategy (Fritz et al. 2000; Beissenhirtz and Willner 2006; Zhang and Winfree 2009; Zhang and Seelig 2011) has allowed many clever methods for signal amplification, which significantly decreases detection limit. On the other hand, self-assembled DNA nanostructures (Mao et al. 2000; Rothemund 2006; Douglas et al. 2009; Han et al. 2011; Wei et al. 2012) have provided a potent template with increased throughput (Dirks and Pierce 2004; Lin et al. 2007; Douglas et al. 2012). DNA origami is such an example (Rothemund 2006). In this nanoassembly, a long *ss*DNA template with thousands of nucleotides is annealed in the presence of short DNA staples. These DNA staples are designed to crosslink different regions in the *ss*DNA template so that desired geometry can be achieved. This nanoassembly serves as a template upon which multiple sensing elements, aptamers, for example, can be precisely assembled (Douglas et al. 2012). In analogy, such a template can be considered as a mainframe of a computer in which different USB communication ports are available. According to different tasks, each USB port can host a specific device (recognition element, Fig. 6).

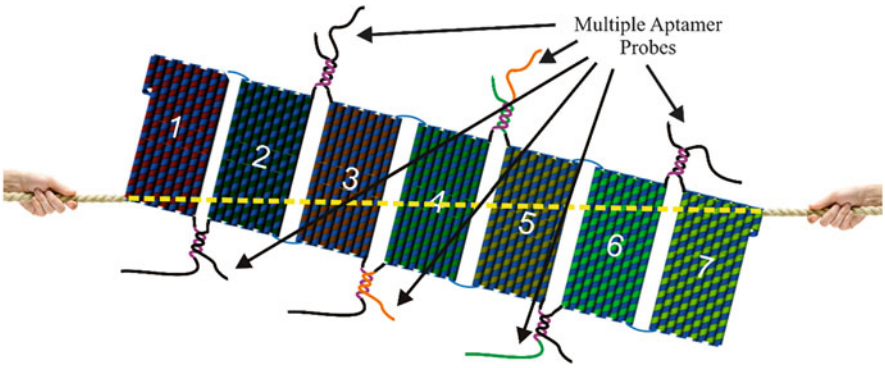

Fig. 6 DNA nanostructure as a template; single-molecule DNA construct integrated with seven DNA origami nanotiles consisting of multiple aptamer probes. Numerals are used to represent the number of origami tiles

3.2.3 Cell as a Template

The biological cell is a complex machinery that performs a variety of functions such as the synthesis, the storage and transport of molecules, the genetic expression, and the recognition and transduction of signals (Bao and Suresh 2003). Similar to engineering materials, cells also undergo deformation when subjected to mechanical stress or geometrical constrains. The deformation characteristics of cells are highly important to predict their biological and structural functions. The deformability of cells is largely determined by the mechanical and chemical environments including cell–cell and cell–extracellular matrix interactions (Zhu et al. 2000). Due to these mechanical properties, we anticipate cells can also be used as mechanochemical probe to recognize various structural motifs either inside or outside cells.

4 Single-Molecule Mechanochemical Sensing

It is known that the size or the amount of materials to be detected scales with the size of a template. To increase the sensitivity of detection, therefore, small template is preferred. If a single-molecule template can be used, detection of individual analyte molecules is expected. The high-resolution instrumentation described above has facilitated the characterization of many single-molecule interactions. This property also implies that mechanochemical sensing using force-based detection has the inherent single-molecule detection limit, which is the ultimate mass detection limit in biosensing.

Due to its universal nature, mechanical force can be used to describe many chemical processes such as the breakage of existing bonds and formation of new bonds. The strength of covalent or non-covalent bonds has been defined by bond energy: the amount of energy required to break one mole of a compound into its constituent atoms. Since non-covalent binding process in biosensing is a dynamic and reversible process, a thermodynamic quantity, dissociation constant (K_d), has been used to represent the reversibility of binding. Given the nature of thermodynamic parameters, however, neither bond energy nor K_d contains mechanical or kinetic information. To describe transient mechanochemical coupling used in the mechanochemical sensing, these variables are therefore not appropriate.

To better delineate the kinetic and mechanical information of a binding, the concept of mechanical affinity was proposed (Koirala et al. 2013). For a ligand–receptor complex, the mechanical affinity (W_{affinity}) is defined as the work to dissociate a ligand–receptor complex, which is equivalent to the difference between the work of dissociating a receptor–ligand complex by unfolding the receptor ($W_{\text{complex-unfold}}$) and that to unfold the free receptor ($W_{\text{receptor-unfold}}$).

$$W_{\text{affinity}} = W_{\text{complex-unfold}} - W_{\text{receptor-unfold}}$$

The mechanical affinity accounts for the kinetics of a binding process. Therefore, it is a more general parameter to describe the binding quantitatively. For a fast dissociation process, the relative movement between the ligand and receptor results in larger dissipation of friction heat. Thus, mechanical affinity increases as the dissociation of the ligand–receptor requires increased work. This leads to high rupture force given the similar change in the distance between folded and unfolded states of receptors. Such a prediction has been experimentally verified in single-molecule force spectroscopy experiments (Clausen-Schaumann et al. 2000). The chemical affinity ($\Delta G_{\text{affinity}}$) can be retrieved from the mechanical affinity by using Jarzynski's nonequilibrium theorem (Jarzynski 1997).

$$\Delta G_{\text{affinity}} = -k_{\text{B}}T \ln \sum_{i=1}^{N} \frac{1}{N} \exp\left(-\frac{W_{\text{affinity},i}}{k_{\text{B}}T}\right)$$

Where N is the total number of measurements, k_{B} is the Boltzmann constant, and T is absolute temperature. A unique feature of force-based single-molecule method is that the dissociation constant (K_d) of a ligand–receptor complex can be retrieved easily without measuring the binding probability at different concentrations of either a ligand or a receptor (Koirala et al. 2011a).

The mechanical affinity allows a binding event to be characterized through its rupture under the mechanical force. Such a mechanochemical coupling process has been exploited in recent examples of single-molecule mechanochemical sensing (SMMS) described in the next section.

5 Examples of Single-Molecule Mechanochemical Sensing

5.1 Detection of Single-Nucleotide Polymorphism (SNP) and Small Molecule (ATP) Using a Single-DNA Molecule Template

Single-nucleotide polymorphism (SNP) is a common genetic variation in human genome with an average occurrence of ~1/1,000 base pairs. A mechanochemical sensing strategy has been demonstrated by using the stochastic behavior of a single-molecule probe to detect SNP sequences in a microfluidic platform (Fig. 7a–h) (Koirala et al. 2011b). The SNP probe contains a hairpin that recognizes specific DNA sequences. The hairpin is sandwiched between two dsDNA handles, which are tethered to two optically trapped beads via digoxigenin (Dig)–antiDig antibody and biotin–streptavidin linkages, respectively. The tethered SNP probe was placed inside a microfluidic device with interconnected channels (Fig. 7d). This design allows desired buffers in separate channels while keeping free movement of the

SNP probe between channels. The detection relies on on–off mechanical signals of a single-DNA template that recognizes SNP, which are recorded by laser tweezers. Before sensing, the tethered DNA construct was repeatedly stretched and relaxed in the buffer channel without SNP target, which allowed unfolding and refolding of the hairpin in the SNP probe, respectively, in force–extension (*F–X*) curves (Fig. 7e). However, folding/unfolding features were not observed in the *F–X* curves of the SNP probe in the target channel, which indicates the binding of the SNP target (Fig. 7g). Hoppings between folded, or "on," and unfolded, or "off," states of the hairpin are also observed in real time in the constant force mode (Fig. 7f). When the SNP probe was moved to the channel that contains a complementary SNP target, 19-nt ODN (Fig. 7c), with 1 μM concentration, hopping immediately ceased, and the hairpin populated in its unfolded state (Fig. 7f, bottom panel). This system has the capacity to detect as low as 100 pM of an SNP target associated with coronary diseases within half an hour without any amplification steps (Fig. 7h). The mechanical signal with little endogenous background noise warrants superior sensitivity for this approach. One disadvantage associated with single-probe sensing is restricted throughput as one sensing event can be monitored at a time. However, this microfluidic mechanochemical strategy can function as a highly sensitive generic biosensor after incorporation of specific recognition element such as an aptamer.

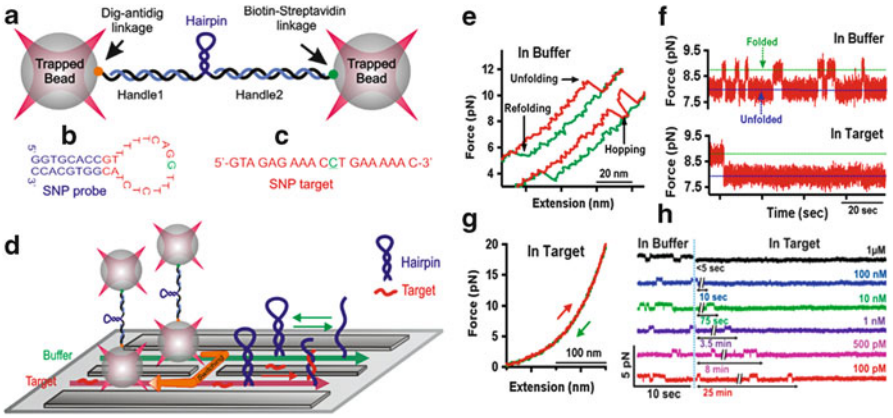

Fig. 7 Schematic of mechanochemical sensing strategy for detection of SNP by DNA hairpin. (**a**) A hairpin contains an SNP probe that recognizes specific SNP target (DNA sequences) that is sandwiched between two dsDNA handles, which are tethered to two optically trapped beads. (**b**) Hairpin used for the sensing strategy. (**c**) A wild-type SNP target. (**d**) Sensing mechanism for the SNP probe. (**e**) Typical force–extension (*F–X*) curves during the mechanical stretching (*red*) and relaxing (*green*) of the SNP probe in the buffer channel. (**f**) Force vs. time traces observed for the SNP probe at fixed optical trap positions in the buffer (*top*) and the target (*bottom channel*) solutions. (**g**) *F–X* curves of the SNP probe in the target channel where folding/unfolding features were not observed. (**h**) Hopping traces for SNP probe with different target concentrations. The *vertical dotted line* indicates the transfer of the SNP probe from the buffer to the target channel. *Double-headed arrows* depict the average time observed before the hopping ceases to the unfolded hairpin state, which indicates the binding of the SNP to the hairpin

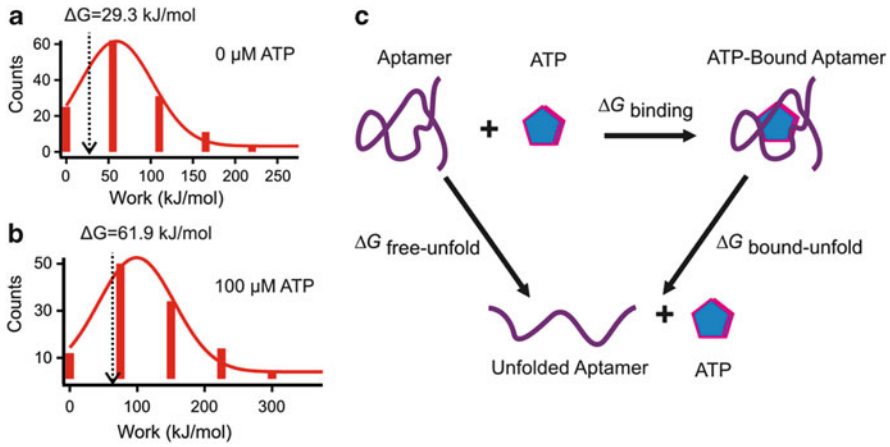

Fig. 8 Histograms of the work done to unfold the free aptamer (**a**) and ATP-bound aptamer (**b**). Dotted arrows show the work equivalent to the change in free energy of unfolding (ΔG_{unfold}). Hess-like cycle of the aptamer–ATP binding process used for the calculation of the $\Delta G_{\text{binding}}$ and the determination of the dissociation constant (**c**)

DNA aptamer can be used as a basic biosensing platform to evaluate the binding constant (K_d) between an aptamer and a small molecule such as ATP using laser tweezers (Yangyuoru et al. 2012). This technique offers a significant advantage to determine the dissociation constant (K_d) for aptamer–ligand interactions at the single-molecule level from only one ligand concentration (Nguyen et al. 2011). In comparison, conventional techniques such as electrochemical detection, fluorescence, colorimetric, and capillary electrophoresis require a series of experiment with varying ligand or aptamer concentrations for the same K_d measurement. Histograms for the work revealed that the average work done to unfold the free aptamer (Fig. 8a) is less than that for the ATP-bound aptamer (Fig. 8b), which confirms that the mechanical stability of the aptamer is enhanced after ligand binding. Comparison of the change in free energy of unfolding (ΔG_{unfold}) between these two aptamers yields a ΔG of -33 ± 4 kJ/mol for the binding. By applying a Hess-like cycle (Fig. 8c) at room temperature, they obtained a dissociation constant (K_d) of 2.0 ± 0.2 μM, by the equation $\Delta G_{\text{binding}} = -RT \ln K_d$. Such a value is consistent with the capillary electrophoresis (CE) measurement (2.4 ± 0.4 μM) as well as the literature value 6.0 ± 3.0 μM.

5.2 *Multiplex Mechanochemical Biosensing Based on DNA Origami Nanoassembly*

2D and 3D DNA origami nanostructures were used as expanded single-molecule platforms in a new mechanochemical sensing strategy with increased throughput.

As a proof of concept, 7-tile 2D DNA origami nanoassembly has been synthesized, which is tethered between two optically trapped beads through two dsDNA handles modified with a terminal digoxigenin and biotin, respectively (Fig. 9a) (Koirala et al. 2014). The seven interconnected origami tiles comprise six sensing probes that are located as two complementary DNA strands between neighboring DNA tiles to further lock these tiles. One DNA strand in the locking DNA contains an aptamer-based target recognition element that can change its conformation upon binding with a specific target, thereby unlocking the tiles (Fig. 9b). A portion of the typical force–extension curves of the 7-tile nanoassembly showed $\leq$6 force-induced unlocking events in the absence of the target molecule (PDGF) as depicted by arrowheads (Fig. 9c). Binding of the target to any of these probes facilitated the formation of the secondary structure of the aptamer, which leads to mechanochemical rearrangement (unlocking) of the origami tiles. When PDGF (50 nM) was incubated with the sensor prior to the pulling experiment, no unfolding features

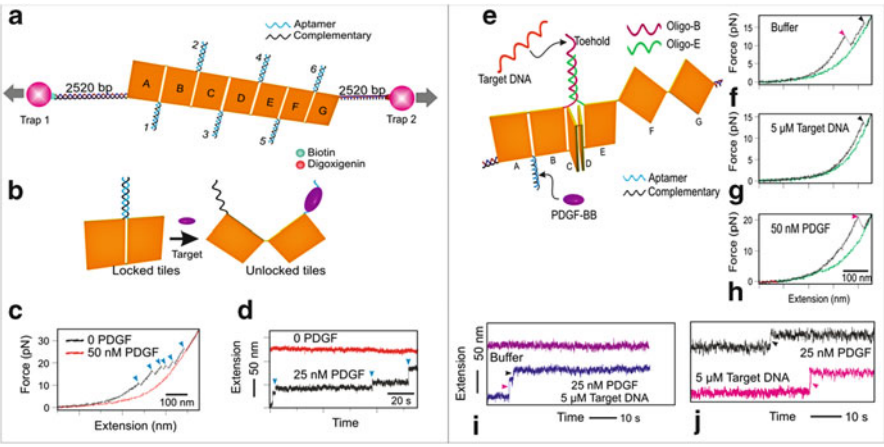

Fig. 9 Multiplex mechanochemical biosensing in optical tweezers using DNA origami nanostructures. (**a**) Schematic of a 7-tile 2D DNA origami nanoassembly is tethered between two optically trapped beads through two dsDNA handles modified with terminal digoxigenin and biotin. The adjacent tiles are locked (marked 1–6) by an aptamer DNA (*blue*) and its complementary strand (*black*). (**b**) Illustration of the tile unlocking due to the target binding to an aptamer lock. (**c**) Representative force–extension (*F–X*) curves of the 7-tile DNA nanoassembly in the absence (*gray*) and presence (*red*) of 50 nM PDGF. The force-induced unlocking events (*arrowheads*) were absent in the solution containing the PDGF. (**d**) Real-time observation of the target recognition events in the constant force (8 pN). Without PDGF, no recognition events were observed, whereas switching to the target solution, the binding of the target unlocked the tiles, leading to the extension jumps (*arrowheads*). (**e**) Schematic of the sensing platform using 3D origami nanoassembly. The lock between tiles A and B contains a PDGF aptamer, whereas that between the tiles B and E consists of a toehold DNA strand. All other tiles remain unlocked. (**f–h**) Typical *F–X* curves in the buffer, target DNA and PDGF solutions, respectively. (**i** and **j**) Real-time detection of multiple targets in the constant force mode. In target-free solution, the sensor showed no extension jumps. When both targets were present, two extension jumps consistent with the breaking of the two locks were observed. However, in the solution that contains only one target, one extension jump was observed

were observed as locks had been disintegrated by binding of the PDGF to the aptamer (Fig. 9c, red trace).

Next, constant force mode experiment (8 pN) was performed with and without PDGF to observe the real-time target recognition events. Without PDGF, no recognition events were observed. Upon switching to the target solution (25 nM PDGF), the binding of the target unlocked the tiles, leading to the extension jumps (arrowheads in Fig. 9d). Using these platforms, they estimated a detection limit of 10 pM (3σ) within 10 min for binding of PDGF to at least one probe. This provides a strong support that the multiple recognition probes can effectively improve the detection by lowering the detection limit while significantly reducing detection time compared to a mechanochemical sensor that contains only one recognition element.

To demonstrate multiplexing capability of the mechanochemical sensing platform, they synthesized a DNA origami nanostructure comprising multiple recognition elements (Fig. 9e). The lock between tiles A and B contains a PDGF aptamer sequence, whereas that between the tiles B and E consists of a toehold DNA strand. All other tiles remain unlocked. During the ramping force mode, the F–X curves showed two features in the target-free solution that correspond to the force-induced unlocking of the tiles between A–B and B–E, respectively (Fig. 9f). In the presence of one target, one unlocking event was observed (Fig. 9g and h). In the ramping force detection mode, unlocking events were not observed in the presence of both targets (50 nm PDGF and 5 μm target DNA).

During their demonstration of real-time detection of multiple targets in the constant force mode (8 pN), the sensor showed no extension jumps in a target-free solution. When both targets were present, two extension jumps consistent with the breaking of the two locks were observed (Fig. 9i). However, in the solution that contains only one target, one extension jump was observed (Fig. 9j).

These findings well established the capability of multiplex SMMS in the DNA origami template. With the incorporation of more tiles and the full use of each tile, this mechanochemical sensing strategy is rather flexible to detect many different targets. By tapping into the rapid development of versatile DNA origami nanostructures, this mechanochemical platform is anticipated to offer a long-sought solution for single-molecule sensing with improved throughput.

6 Conclusions and Prospects

The chemical transformations brought by light (photochemistry) and heat (thermochemistry) have been investigated for centuries. In spite of its long history, mechanically induced chemical transformations, known as mechanochemistry, have been esoteric until recently. As an intrinsic phenomenon involved in various physiological activities, mechanical transformation has become a key element in the understanding of biochemical events. In addition, mechanical processes are vital for materials scientists to develop the methods and probe the mechanisms of

mechanically induced assembly–disassembly of polymers, metallosupramolecular polymers, etc. With the emergence of force-based single-molecule methods such as AFM, magnetic tweezers, and optical tweezers, it becomes routine to measure piconewton force, which facilitates the exploitation of mechanochemical coupling in macromolecules for the development of new sensors. Here, we have shown examples of using DNA templates to perform SMMS on a variety of small molecule and macromolecule analytes. We anticipate the sensing platform can be expanded to other macromolecules such as RNA and proteins, as well as cells. As a new type of the sensing strategy with the capability of the ultimate detection limit, single molecules, we foresee a rapid application of this method in the new field of mechanoanalytical chemistry (Koirala et al. 2014) in general and mechanochemical biosensing in particular.

Acknowledgment HM thanks NSF (CHE-1026532) for funding this research.

References

Alaiwi WAA, Lo ST, Nauli SM (2009) Primary cilia: highly sophisticated biological sensors. Sensors 9:7003–7020

Alberti P, Bourdoncle A, Sacca B et al (2006) DNA nanomachines and nanostructures involving quadruplexes. Org Biomol Chem 4:3383–3391

Ashkin A, Dziedzic JM, Bjorkholm JE et al (1986) Observation of a single-beam gradient force optical trap for dielectric particles. Opt Lett 11:288–290

Balkenende DWR, Coulibaly S, Balog S et al (2014) Mechanochemistry with metallosupramolecular polymers. J Am Chem Soc 136:10493–10498

Bao G, Suresh S (2003) Cell and molecular mechanics of biological materials. Nat Mater 2:715–725

Beissenhirtz MK, Willner I (2006) DNA-based machines. Org Biomol Chem 4:3392–3401

Beyer MK, Clausen-Schaumann H (2005) Mechanochemistry: the mechanical activation of covalent bonds. Chem Rev 105:2921–2948

Binnig G, Rohrer H (1983) Scanning tunneling microscopy. Surf Sci 126:236–244

Binnig G, Quate CF, Gerber C (1986) Atomic force microscope. Phys Rev Lett 56:930–933

Black AL, Lenhardt JM, Craig SL (2011) From molecular mechanochemistry to stress-responsive materials. J Mater Chem 21:1655–1663

Calderone CT, Liu DR (2004) Nucleic-acid-templated synthesis as a model system for ancient translation. Curr Opin Chem Biol 8:645–653

Caruso MM, Davis DA, Shen Q et al (2009) Mechanically-induced chemical changes in polymeric materials. Chem Rev 109:5755–5798

Chandran H, Rangnekar A, Shetty G et al (2013) An autonomously self-assembling dendritic DNA nanostructure for target DNA detection. Biotechnol J 8:221–227

Clausen-Schaumann H, Seitz M, Krautbauer R et al (2000) Force spectroscopy with single bio-molecules. Curr Opin Chem Biol 4:524–530

Craig SL (2012) Mechanochemistry: a tour of force. Nature 487:176–177

Davenport RJ, Wuite GJL, Landick R et al (2000) Single-molecule study of transcriptional pausing and arrest by E-coli RNA polymerase. Science 287:2497–2500

Dhakal S, Schonhoft JD, Koirala D et al (2010) Coexistence of an ILPR i-motif and a partially folded structure with comparable mechanical stability revealed at the single-molecule level. J Am Chem Soc 132:8991–8997

Dirks RM, Pierce NA (2004) Triggered amplification by hybridization chain reaction. Proc Natl Acad Sci USA 101:15275–15278
Douglas SM, Dietz H, Liedl T et al (2009) Self-assembly of DNA into nanoscale three-dimensional shapes. Nature 459:414–418
Douglas SM, Bachelet I, Church GM (2012) A logic-gated nanorobot for targeted transport of molecular payloads. Science 335:831–834
Drummond TG, Hill MG, Barton JK (2003) Electrochemical DNA sensors. Nat Biotechnol 21:1192–1199
Fazio T, Visnapuu M-L, Wind S et al (2008) DNA curtains and nanoscale curtain rods: high-throughput tools for single molecule imaging. Langmuir 24:10524–10531
Fritz J, Baller MK, Lang HP et al (2000) Translating biomolecular recognition into nanomechanics. Science 288:316–318
Gennerich A, Vale RD (2009) Walking the walk: how kinesin and dynein coordinate their steps. Curr Opin Cell Biol 21:59–67
Han D, Pal S, Nangreave J et al (2011) DNA origami with complex curvatures in three-dimensional space. Science 332:342–346
Jarzynski C (1997) Nonequilibrium equality for free energy differences. Phys Rev Lett 78:2690–2693
Kean ZS, Craig SL (2012) Mechanochemical remodeling of synthetic polymers. Polymer 53:1035–1048
Kean ZS, Niu Z, Hewage GB et al (2013) Stress-responsive polymers containing cyclobutane core mechanophores: reactivity and mechanistic insights. J Am Chem Soc 135:13598–13604
Keller D, Bustamante C (2000) The mechanochemistry of molecular motors. Biophys J 78:541–556
Koirala D, Dhakal S, Ashbridge B et al (2011a) A single-molecule platform for investigation of interactions between G-quadruplexes and small-molecule ligands. Nat Chem 3:782–787
Koirala D, Yu Z, Dhakal S et al (2011b) Detection of single nucleotide polymorphism using tension-dependent stochastic behavior of a single-molecule template. J Am Chem Soc 133:9988–9991
Koirala D, Yangyuoru PM, Mao H (2013) Mechanical affinity as a new metrics to evaluate binding events. Rev Anal Chem 32:197–208
Koirala D, Shrestha P, Emura T et al (2014) Single-molecule mechanochemical sensing using DNA origami nanostructures. Angew Chem Int Ed Engl 53:8137–8141
Kolpashchikov DM, Stojanovic MN (2005) Boolean control of aptamer binding states. J Am Chem Soc 127:11348–11351
Krishnan Y, Bathe M (2012) Designer nucleic acids to probe and program the cell. Trends Cell Biol 22:624–633
Liao J-C, Jeong Y-J, Kim D-E et al (2005) Mechanochemistry of T7 DNA Helicase. J Mol Biol 350:452–475
Lin C, Liu Y, Yan H (2007) Self-assembled combinatorial encoding nanoarrays for multiplexed biosensing. Nano Lett 7:507–512
Lord JM, Bunc CM, Brown G (1988) The role of protein phosphorylation in control of cell growth and differentiation. Br J Cancer 58:549–555
Luchette P, Abiy N, Mao H (2007) Microanalysis of clouding process at the single droplet level. Sens Actuators B Chem 128:154–160
Maldonado CR, Touceda-Varela A, Jones AC et al (2011) A turn-on fluorescence sensor for cyanide from mechanochemical reactions between quantum dots and copper complexes. Chem Commun 47:11700–11702
Mao H, Luchette P (2008) An integrated laser-tweezers instrument for microanalysis of individual protein aggregates. Sens Actuators B 129:764–771
Mao C, LaBean TH, Reif JH et al (2000) Logical computation using algorithmic self-assembly of DNA triple-crossover molecules. Nature 407:493–496

Mavroidis C, Dubey A, Yarmush ML (2004) Molecular machines. Annu Rev Biophys Biomed Eng 6:363–395
May PA, Moore JS (2013) Polymer mechanochemistry: techniques to generate molecular force via elongational flows. Chem Soc Rev 42:7497–7506
Michelotti N, Johnson-Buck A, Manzo AJ et al (2012) Beyond DNA origami: the unfolding prospects of nucleic acid nanotechnology. WIREs Nanomed Nanobiotechnol 4:139–152
Modi S, Swetha MG, Goswami D et al (2009) A DNA nanomachine that maps spatial and temporal pH changes inside living cells. Nat Nanotechnol 4:325–330
Nguyen T-H, Steinbock LJ, Butt H-J et al (2011) Measuring single small molecule binding via rupture forces of a split aptamer. J Am Chem Soc 133:2025–2027
Niemeyer CM (1997) DNA as a material for nanotechnology. Angew Chem Int Ed 36:585–587
Pinheiro AV, Han D, Shih WM et al (2011) Challenges and opportunities for structural DNA nanotechnology. Nat Nanotechnol 6:763–772
Porchetta A, Vallée-Bélisle A, Plaxco KW et al (2012) Using distal-site mutations and allosteric inhibition to tune, extend, and narrow the useful dynamic range of aptamer-based sensors. J Am Chem Soc 134:20601–20604
Rayment I, Holden HM, Whittaker M et al (1993) Structure of the actin-myosin complex and its implications for muscle contraction. Science 261:58–65
Rief M, Oesterhelt F, Heymann B et al (1997) Single molecule force spectroscopy on polysaccharides by atomic force microscopy. Science 275:1295–1297
Rosi NL, Mirkin CA (2005) Nanostructures in biodiagnostics. Chem Rev 105:1547–1562
Rothemund PWK (2006) Folding DNA to create nanoscale shapes and patterns. Nature 440:297–302
Schnitzer MJ, Visscher K, Block SM (2000) Force production by single kinesin motors. Nat Cell Biol 2:718–723
Seeman NC (2003) DNA in a material world. Nature 421:427–431
Seeman NC (2005) From genes to machines: DNA nanomechanical devices. Trends Biochem Sci 30:119–125
Sefah K, Shangguan D, Xiong X et al (2010) Development of DNA aptamers using Cell-SELEX. Nat Protocols 5:1169–1185
Shekhar S, Cambi A, Figdor CG et al (2012) A method for spatially resolved local intracellular mechanochemical sensing and organelle manipulation. Biophys J 103:395–404
Silverman SK (2010) DNA as a versatile chemical component for catalysis, encoding, and stereocontrol. Angew Chem Int Ed 49:7180–7201
Simmel FC, Dittmer WU (2005) DNA nanodevices. Small 1:284–299
Smith SB, Cui YJ, Bustamante C (1996) Overstretching B-DNA: the elastic response of individual double-stranded and single-stranded DNA molecules. Science 271:795–799
Strick TR, Allemand J-F, Bensimon D et al (1996) The elasticity of a single supercoiled DNA molecule. Science 271:1835–1837
Svoboda K, Block SM (1994) Force and velocity measured for single kinesin molecules. Cell 77:773–784
Tuerk C, Gold L (1990) Systematic evolution of ligands by exponential enrichment—RNA ligands to bacteriophage-T4 DNA-polymerase. Science 249:505–510
Visscher K, Schnitzer MJ, Block SM (1999) Single kinesin molecules studied with a molecular force clamp. Nature 400:184–189
Vogel V, Sheetz M (2006) Local force and geometry sensing regulate cell functions. Nat Rev Mol Cell Biol 7:265–275
Wang MD, Schnitzer MJ, Yin H et al (1998) Force and velocity measured for single molecules of RNA polymerase. Science 282:902–907
Wang H, Yang R, Yang L et al (2009) Nucleic acid conjugated nanomaterials for enhanced molecular recognition. ACS Nano 3:2451–2460
Wang X, Lou X, Wang Y et al (2010) QDs-DNA nanosensor for the detection of hepatitis B virus DNA and the single-base mutants. Biosens Bioelectron 25:1934–1940

Weder C (2009) Mechanochemistry: polymers react to stress. Nature 459:45–46
Wei B, Dai M, Yin P (2012) Complex shapes self-assembled from single-stranded DNA tiles. Nature 485:623–626
White SR, Sottos NR, Geubelle PH et al (2001) Autonomic healing of polymer composites. Nature 409:794–797
Wilner OI, Willner I (2012) Functionalized DNA nanostructures. Chem Rev 112:2528–2556
Woodside MT, Anthony PC, Behnke-Parks WM et al (2006) Direct measurement of the full, sequence-dependent folding landscape of a nucleic acid. Science 314:1001–1004
Wuite GJL, Smith SB, Young M et al (2000) Single-molecule studies of the effect of template tension on T7 DNA polymerase activity. Nature 404:103–106
Xing H, Wong NY, Xiang Y et al (2012) DNA aptamer functionalized nanomaterials for intracellular analysis, cancer cell imaging and drug delivery. Curr Opin Chem Biol 16:429–435
Yangyuoru PM, Dhakal S, Yu Z et al (2012) Single-molecule measurements of the binding between small molecules and DNA aptamers. Anal Chem 84:5298–5303
Yu Z, Schonhoft JD, Dhakal S et al (2009) ILPR G-quadruplexes formed in seconds demonstrate high mechanical stabilities. J Am Chem Soc 131:1876–1882
Zhang DY, Seelig G (2011) Dynamic DNA nanotechnology using strand-displacement reactions. Nat Chem 3:103–113
Zhang DY, Winfree E (2009) Control of DNA strand displacement kinetics using toehold exchange. J Am Chem Soc 131:17303–17314
Zhu C, Bao G, Wang N (2000) Cell mechanics: mechanical response, cell adhesion, and molecular deformation. Annu Rev Biomed Eng 2:189–226

Microarrays as Research Tools and Diagnostic Devices

Karin Lemuth and Steffen Rupp

Contents

Abstract Molecular diagnostics comprises a main analytical division in clinical laboratory diagnostics. The analysis of RNA or DNA helps to diagnose infectious diseases and identify genetic determined disorders or even cancer. Starting from mono-parametric tests within the last years, technologies have evolved that allow for the detection of many parameters in parallel, e.g., by using multiplex nucleic acid amplification techniques, microarrays, or next-generation sequencing technologies. The introduction of closed-tube systems as well as lab-on-a-chip devices further resulted in a higher automation degree with a reduced contamination risk. These applications complement or even stepwise replace classical methods in

K. Lemuth
Robert Bosch GmbH, Corporate Sector Research Microsystem Technologies, Robert Bosch Platz 1, 70839 Gerlingen, Germany

S. Rupp (✉)
Fraunhofer Institut für Grenzflächen- und Bioverfahrenstechnik, Nobelstr. 12, 70569 Stuttgart, Germany

Institut für Grenzflächenverfahrenstechnik und Plasmatechnologie, Universität Stuttgart, Nobelstr. 12, 70569 Stuttgart, Germany
e-mail: Steffen.Rupp@igb.fraunhofer.de

V.A. Erdmann et al. (eds.), *RNA and DNA Diagnostics*, RNA Technologies,
DOI 10.1007/978-3-319-17305-4_13

clinical microbiology like virus cultures, resistance determination, microscopic and metabolic analyses, as well as biochemical or immunohistochemical assays. In addition, novel diagnostic markers appear, like noncoding RNAs and miRNAs providing additional room for novel biomarkers.

This article provides an overview of microarrays as diagnostics devices and research tools. Introduced in 1995 for transcription analysis, microarrays are used today to detect several different biomolecules like DNA, RNA, miRNA, and proteins among others. Mainly used in research, some microarrays also found their way to clinical diagnostics. Further, closed lab-on-a-chip devices that use DNA microarrays as detection tools are discussed, and additionally, an outlook toward applications of next-generation sequencing tools in diagnostics will be given.

Keywords DNA microarray • Lab-on-a-chip • Molecular diagnostics • Next-generation sequencing

1 Introduction

With their pioneering work, Schena and colleagues published a completely outstanding method in molecular technologies in 1995 (Schena et al. 1995). First used for multiparametric transcriptional profiling, the technology rapidly developed toward a tool for the detection of all kinds of biological targets (DNA, RNA, proteins, cells, nucleic acids, carbohydrates, etc.) or their modifications (methylation, phosphorylation, etc.) within the last 20 years. The principle is simple. The biological interaction of molecules, e.g., the interaction of complementary bases of nucleic acids, antibody–antigen interactions, or the interaction of carbohydrates with lectins, represents the basic principle of microarray technology. As an example, in the following, the basic principles of a DNA microarray is described: to detect target molecules, e.g., mRNA or genomic DNA; oligonucleotides complementary to the respective target molecule are immobilized on solid supports like glass, nylon, other polymers, or silicon in an ordered manner—the microarray. These oligonucleotides may correspond to all open reading frames of an organism to allow transcriptional profiling. From the sample of interest, e.g., RNA is extracted and labeled using nucleic acid polymerizing enzymes (e.g., reverse transcriptase, T7 polymerases to generate cDNA) and fluorescently labeled nucleotides. Hybridization to the microarray leads to a specific molecular interaction at the location where the complementary strand is immobilized. Readout using a fluorescence scanner with a photomultiplier tube or imaging with a CCD camera will give the information if the target molecule is present in the analyzed sample or not (Pollack 2009) (Fig. 1). Next to the direct labeling, also indirect labeling techniques can be used. Biotin-labeled nucleotides are incorporated during PCR und afterwards detected using streptavidin or antibody conjugates. One of the first examples was published shortly after the work by Schena et al. (1995) which started the

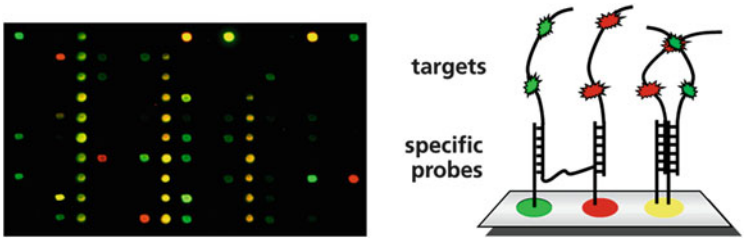

Fig. 1 Basic principle of a DNA microarray. On the *left side,* the readout of a diagnostic microarray is shown using *two-color labeling*, representing two samples to be compared, used, e.g., in transcriptional profiling. Cy3- and Cy5-labeled target cDNAs are hybridized to their specific probes on the *array* as indicated on the *left side*. The schematic overview on the *right* side shows a typical hybridization using a competitive *two-color* (Cy3 and Cy5) hybridization in transcriptional profiling experiments. Targets present only in one sample result in either *green* or *red* signals, and targets present equally in both samples result in a *yellow* signal. The ratio between the *red* and *green* signal gives the difference in mRNA levels in the different samples

commercialization of nucleic acid microarrays by Affymetrix, USA (Wodicka et al. 1997). Another example is the colorimetric Silverquant® technology used by Eppendorf for their DualChip® microarrays. Biotin-labeled nucleotides are used in the PCR reaction. Gold-coupled antibodies against biotin are added after hybridization. The colorimetric reaction is started by adding silver nitrate and a reducing agent. This leads to silver precipitation at the gold particles. Another labeling technology uses a streptavidin–horseradish peroxidase conjugate for colorimetric detection (Rubtsova et al. 2010).

2 DNA Microarrays as Research Tools

2.1 Microarray Development

Microarray technology has revolutionized both DNA and RNA research. In contrast to most classical biological assays, microarrays enable the parallel analysis of several tens of thousands of analytes. For the analysis of nucleic acids, the application possibilities range from a focused set of multiple transcriptional units for transcriptional profiling or genomic fragments for analysis of copy number or genetic variation up to entire genomes and beyond. The availability of complete genomic sequences was the keystone for the development and use of genome-wide technologies, like array technologies. In the past century, the sequencing of entire genomes has been a major effort both in academic and in commercial research. The first sequenced eukaryotic genome was the genome of *Saccharomyces cerevisiae*, the second completely sequenced genome at all, in 1996. Before 2,000, genome sequencing was a daunting task. In total, the number of sequenced organisms was rather small, including 38 bacteria, 1 fungus (*S. cerevisiae*), 2 invertebrates

(*Caenorhabditis elegans* and *Drosophila melanogaster*), and 1 plant (*Arabidopsis thaliana*), all with relatively small and simple genomes. Only 5 years after the first eukaryotic genome was presented, a first draft of the human genomic sequence was published (Lander et al. 2001; Venter et al. 2001). The human draft sequence, although a landmark, was still rather imperfect. It covered only 90 % of the euchromatic genome and was interrupted by 250,000 gaps. About 10 years later, the catalogue of sequenced organisms included already over 16,000 projects, including more than 10,000 microbial organisms and close to 1,700 vertebrate organisms of completed or ongoing sequencing project of organisms (status Sept 2012) (Pruitt et al. 2012). The major reason for this explosion in genome sequencing is due to the development of an additional revolutionizing technology at the beginning of the twenty-first century, generally termed next-generation sequencing (NGS) (Margulies et al. 2005) to which we refer in a later paragraph of this article. At the last NCBI update (October 2013), the number in public archives again increased to 24,788 prokaryotic registered genome projects representing 4,528 different species; 14,311 of them have assembled genomes either complete (2,670) or draft (11,641), and the remainder either do not have submitted sequence data yet or have only raw sequence reads uploaded to the Sequence Reads Archive (Kodama et al. 2012). Sequencing is not restricted to individual organisms any more but includes also microbial communities, like samples from the mid-ocean and environmental remediation sites and human samples from the gut and skin (Grice et al. 2009; Gill et al. 2006). Remarkably, partial genome sequences have even been obtained from several extinct species, including the woolly mammoth and the Neanderthal (Green et al. 2010). In addition populations of one species are sequenced, like in the 100 K Genome Project for microbial pathogens (Timme et al. 2012) and the 1,000 Genomes Project for humans (Genomes Project Consortium et al. 2012). This will enable completely new approaches to medical research and diagnostics, including the development of diagnostic microarrays.

In parallel to the completion of the first genomic sequences, DNA microarray technology has been developed as mentioned above. Pioneering experiments were focused on expression profiling using model organisms like *S. cerevisiae* to monitor changes of transcriptional activity of every known or annotated gene in a single experiment. For *S. cerevisiae*, the first genome-wide transcriptional analyses indeed appeared shortly after completion of the genomic sequence (DeRisi et al. 1997; Hauser et al. 1998; Wodicka et al. 1997). On the nucleic acid level, this set the start for genome-wide analyses of organisms based on the knowledge of their genomes. *S. cerevisiae* as one of the major model organisms was the key in developing both the biochemical and bioinformatic methods necessary for transcriptional profiling. Today, thousands of transcription profiles have been generated from almost all sequenced species. Besides the knowledge of the genome, ways to generate and analyze the data are a prerequisite for transcriptomics. An overview of data analysis methods, however, is beyond the scope of this chapter. Several books on microarray technology and data analysis have been written which introduce perfectly into these topics (Bremer et al. 2010; Dufva 2009). Microarray fabrication, which has been shortly introduced above, will be discussed in the following in more details.

2.2 DNA Microarray Fabrication

There are three main ways to manufacture DNA microarrays: light-directed synthesis (photolithography), piezoelectric ink-jet printing, and robot spotting (Hughes et al. 2001; Tan et al. 2003; Dufva 2009). For photolithography, premade masks or digital micromirror devices are used. Premade masks are used by the Affymetrix platform. For every nucleotide (nt) added to the growing strand on the solid support, a mask covering regions on the microarray where no base addition should take place is applied. Previous nucleotide blocking groups are removed by a photosensitive reaction after UV light-induced deprotection, and the extension by one further nucleotide can take place. The technology is rather expensive due to mask costs. Every array design needs its own set of masks. Usually, probes are 20–25 nt in length, and 22–40 probes per gene are synthesized. Another photolithography technology is used by NimbleGen: single-nucleotide extension is performed by light-mediated inactivation of a photolabile protective group and afterward a base addition. This is similar to the Affymetrix technology. However, NimbleGen uses micromirror devices that can lead the light needed for inactivation of protective groups to every desired spot on the microarray. Therefore, there is no need for masks anymore which makes this technology much cheaper. Another technology for making microarrays is the piezoelectric ink-jet printing technology, also called HP technology deduced from HP printing technology. The Agilent sure print technology is an example for an industrial platform. They produce cDNA or oligonucleotide microarrays. cDNA is spotted directly, oligonucleotides are synthesized base-by-base in repetitive print layers using standard phosphoramidite chemistry (https://www.chem.agilent.com/Library/technicaloverviews/Public/5988-8171en.pdf). The most widely used technology for microarray production especially in the field of research institutions and universities is the robot spotting technology: e.g., proteins, PCR products or oligonucleotides are spotted on a solid glass support using split or solid pins. Using split pins, DNA is fed in by capillary forces and deposited at defined locations on the microarray using robot technology. Usually, PCR products up to 1 kb and oligonucleotides between 20 and 100 nts in length are printed. This technology is affordable and therefore often used in individual research labs. Next to these classical technologies, also semiconductor-based systems have been developed. For example, CombiMatrix uses such a system for the production of their microarrays. Thousands of platinum microelectrodes can be addressed simultaneously to synthesize individual oligonucleotides by digitally controlled synthesis. The activation of a microelectrode leads to the production of an acid by an electrochemical reaction. This leads to the deprotection of the growing oligonucleotide strand activating it for the next synthesis step. The possibility to individually address thousands of microelectrodes in parallel allows the comfortable production of individual microarrays (Ghindilis et al. 2007). Over 12,000 oligos are synthesized in parallel as 50 mers.

Not only natural DNA has been used as probes or capture molecules on DNA microarray systems. In order to reduce cross-reactivity and to increase interaction with the targets in the sample applied, nonnatural variants have been used as

capture molecules, including L-DNA (Hauser et al. 2006) and PNA variants (Sforza et al. 2014). L-DNA probes have the great advantage that they interact with the exact same kinetics with its antiparallel L-DNA strand, like the D-DNA duplex. Thus, all the knowledge gained with D-DNA-microarrays can be used for the L-DNA equivalent. To bind to targets like RNA, DNA, or even peptides/epitopes or chemical molecules, the so-called ZIP-code arrays are used. The probes used in ZIP-code arrays are fusions in which the targets are bound in solution using, e.g., natural D-DNA oligomer complementary to the target DNA/RNA which is fused to an L-DNA. This L-DNA oligomer addresses an immobilized complementary L-DNA oligonucleotide on the microarray surface, which allows a literally background-free hybridization on the arrays. However, the price for synthesizing L-DNA oligomers is rather high, hampering further development. P-DNAs, synthetic nucleic acid analogues based on a pseudopeptide backbone instead of a phosphodiester backbone, show excellent sequence-specific recognition properties and are less susceptible to changes in ionic strength. Since they are not charged, repulsion between the negatively charged backbone present in DNA duplexes is missing resulting in higher affinities as shown by the higher melting curves of PNA/DNA or PNA/RNA duplexes if compared to their natural counterparts (Brandt and Hoheisel 2004; Jacob et al. 2004; Sforza et al. 2014).

Next to these planar array systems, bead-based systems have been developed like random bead arrays or suspension arrays. The beads are marked with different amounts of fluorescent dye or another barcoding technology and are individually identifiable. After coupling, e.g., oligonucleotides to such beads, a specific binding event can be detected. For example Illumina has developed a bead array technology, where they use either planar silicon slides or fiber-optic bundles. Silicon wafers or optical fibers are etched such that the individual beads can fit into the resulting three micron-sized wells. After the binding event, the beads are subsequently identified. This technology uses fluorescently labeled primers http://www.ncbi.nlm.nih.gov/projects/genome/probe/doc/TechBeadArray.shtml. Similar to this, suspension arrays also use optically differentiable beads that are coupled to the interesting biomolecule which can be, e.g., oligonucleotides or antibodies. The hybridization reaction with fluorescently labeled substrates takes place in solution, and a subsequent FACS (fluorescence-activated cell sorting) sorting process allows the identification of the binding process. An example is the Luminex xMAP technology (http://www.luminexcorp.com/TechnologiesScience/xMAPTechnology/).

DNA microarrays have been widely used as research tool in the lab, and according to this, a huge amount of literature has been published in this field. Microarrays addressing specific targets like proteins, carbohydrates, tissue, or cells have been developed as well, but will not be reviewed here. Many reviews exist that deal with topics like whole-genome expression analysis (over 2,200 reviews in PubMed with the search strings “microarray” and “expression analysis”), cancer research (Chibon 2013; Daigo et al. 2013; Ho et al. 2013; Sato-Otsubo et al. 2012; Tiwari 2012), molecular karyotyping (Dhillon et al. 2014), chromosomal microarray analysis (Brady and Vermeesch 2012), phylogenetics/microbiome (Nikolaki

and Tsiamis 2013), or gene regulation via ChIP-chip (Falk 2010; Powell et al. 2013). DNA microarrays have been used to study heart diseases (Phan et al. 2012), aspects in dermatology (Villasenor-Park and Ortega-Loayza 2013), or mental disorders like autism (Carter and Scherer 2013) and many others. A more detailed overview focusing on applications in clinical microbiology has been given by Miller et al. (Miller and Tang 2009). In the following section, a more detailed overview of a few selected research-driven microarrays is given.

2.3 Microarrays in Infection Biology

The past century brought the availability of vaccines and antibiotics, leading to a dramatic fall in mortalities caused by infectious diseases. Nevertheless, today again nearly 25 % of the annual deaths worldwide are directly related to pathogens (Morens et al. 2004). This can be attributed to the appearance of new diseases like HIV, SARS, West Nile Virus, or the recent Ebola outbreak, but also to an increase of resistance to antibiotics in pathogens thought to be defeated, like *Mycobacterium tuberculosis* or *Staphylococcus* and *Enterococcus* strains. In addition, the progress in medical care results in a large proportion of temporarily or lifelong immune-deficient patients and consequently in an increase in opportunistic infections often resulting in sepsis, requiring fast and accurate diagnosis to save patient lives. Approximately 1,415 species have been identified as known to be pathogenic to humans, including 538 bacteria and 307 fungi (Cleaveland et al. 2001), indicating the multiparametric problem of identification of the disease-causing pathogen.

DNA microarrays have emerged as a viable platform for the detection of pathogenic organisms. Microbial detection arrays both with regard to cost and application range are in between low cost, narrowly focused assays like multiplex PCR and the more expensive, broad-spectrum technologies like high-throughput sequencing. Pathogen detection arrays have been used primarily in a research context; however, several groups have developed arrays for clinical diagnostics, food safety testing, environmental monitoring, and biodefense. Statistical algorithms that enable data analysis and provide easily interpretable results are absolutely required for an applicable detection array.

One of the first microarrays designed for a wide range of pathogens was the ViroChip (Wang et al. 2002). An updated version was published shortly thereafter (Wang et al. 2003). This array, fabricated by robotic spotting of 70-mer oligos, contained initially 1,600 probes derived from 140 viral genomes available at that time. Since the probes were designed against conserved sequences common to a taxonomic family, it could be used to identify novel viruses within the same family. The ViroChip, therefore, could contribute to characterizing the novel coronavirus responsible for the SARS outbreak in 2003 (Ksiazek et al. 2003). Also today the ViroChip is still used in clinical studies. Its utility for detection of viruses in acute respiratory tract infections in children could be shown in a clinical study of more

than 200 children, showing superior performances with regard to sensitivity and specificity profile and expanded spectrum for detection of viruses if compared to serologic or PCR-based detection methods (Chiu et al. 2008). The latest version of the array is now based on the Agilent ink-jet platform (Chen et al. 2011).

One of the most comprehensive arrays has been described by Gardener et al. (Gardner et al. 2010), based on NimbleGen technology platform. In this report, a pan-Microbial Detection Array (MDA) to detect all known viruses (including phages), bacteria, and plasmids at that time is described including a novel statistical analysis method to identify mixtures of organisms from complex samples hybridized to the array. On this array, family specific probes were selected for all sequenced viral and bacterial complete genomes. The probes on the array were designed to tolerate sequence variations which will allow the detection of divergent species provided that some homology to sequenced organisms is given, as described for the ViroChip. Using this comprehensive chip in blinded testing on spiked samples and in clinical fecal, serum, and respiratory samples, the chip was able to correctly identify multiple species or strains as confirmed by PCR.

In addition, many different arrays focusing on defined pathogens or families of pathogens as well as resistance patterns have been described.

To detect fungal infections, especially in intensive care units in hospitals where they have emerged as a major cause of morbidity and mortality in immune-compromised patients, a diagnostic microarray for the rapid and simultaneous identification of the 12 most common pathogenic *Candida* and *Aspergillus* species has been developed. Oligonucleotide probes were designed based on sequence variations of the internal transcribed spacer (ITS) regions using a universal PCR amplifying the fungal ITS target region. The array was validated by using 21 clinical isolates as blinded samples (Leinberger et al. 2005).

Arrays for detecting resistance determinants like lactamases have been established as well. For example, Leinberger et al. described an extended-spectrum beta-lactamases detection array able to detect resistance mechanisms based on the TEM, SHV, or CTX-M type conferring resistance to beta-lactam antibiotics in gram-negative bacteria (Leinberger et al. 2010). The activity of these enzymes against beta-lactam antibiotics and their resistance against inhibitors can be influenced by genetic variation at the single-nucleotide level. The array is described to consist of 618 probes that cover mutations responsible for 156 amino acid substitutions. The validity of the DNA microarray was demonstrated with 60 blinded clinical isolates, which were collected during clinical routines. The chip was characterized successfully with regard to its resolution, phenotype–genotype correlation, and ability to resolve mixed genotypes.

Also resistance mechanisms of emerging pathogens like *Acinetobacter baumannii* can be detected using arrays. Dally et al. have developed a microarray that can be used to detect 91 target sequences associated with antibiotic resistance within 4 h from a bacterial culture (Dally et al. 2013). The array was validated with 60 multidrug-resistant strains of *A. baumannii* in a blinded, prospective study and compared to results determined by the VITEK2 system, based on phenotypic susceptibility. This array is able to detect all relevant resistance determinants of

A. baumannii in parallel. Thus, it enables fast results in order to initiate adequate anti-infective therapy for critically ill patients and can be used for epidemiologic surveillance.

2.4 Microarray-Based Gene Expression Profiling in Cancer

Transcriptional profiling rapidly expanded to research on all types of human cancers, starting already before the initial draft of the human genome was published in 2001. Breast cancer has been one of the most intensively studied human cancers, with regard to microarray-based gene expression profiling for cancer classification, prognosis, and prediction. One of the reasons for this, besides the high frequency of breast cancer in the population, is the observation that although approximately 60 % of all patients with early breast cancer receive some form of chemotherapy, only a minority will benefit from it (Schmidt et al. 2009). Therefore, reliable prognostic and predictive markers are needed to guide the selection of the most appropriate adjuvant therapies for individual patients with breast cancer. Microarrays actually contributed significantly to a change in the understanding of breast cancer as a heterogenous group of complex tumors instead of a single group. Pioneering work by Perou and colleagues rediscovered the large heterogeneity of breast cancer tumors on a molecular level (Perou et al. 2000). The demonstration that ER-positive and ER-negative tumor cells are fundamentally different in their expression profiles led to the suggestion to use microarray-based multigene prognostic classifiers, known as gene signatures or diagnostic signatures, as a prognostic/predictive marker panel for therapy decisions. In the last decade, several groups have embarked in the identification of gene signatures for breast cancer diagnostics with the goal to predict if chemotherapy can be omitted in early-stage breast cancer or select the most appropriate treatment. One of the first prognostic signatures consisted of 70 genes enabling the identification of good prognosis patients with a minimal risk of developing of metastases within the next 5 years (van 't Veer et al. 2002). This 70-gene signature has been validated in several clinical trials, in general using fresh biopsy tissue for preparation of the transcriptional profiles during the last years and is now commercially available via Agendia as MammaPrint® (using Microarrays based on Agilent technology) for guided therapy of early-stage breast cancer (Exner et al. 2014). In parallel, a gene signature consisting of 16 diagnostic genes (and 5 controls) was established, based on qRT-PCR (Oncotype DX) (Paik et al. 2004). This assay also underwent several clinical trials and was recently positively evaluated for economic impact on patient management (Nerich et al. 2014). Several other assays have been developed, which are nicely reviewed by Colombo et al. and by Zanotti et al. (Colombo et al. 2011; Zanotti et al. 2014).

In summary, this shows how within the last 15–20 years the development of microarrays enabled the successful setup of multigene assays, designed to support physicians and patients in clinical decision-making in early-stage breast cancer.

2.5 Detection of Small Noncoding RNAs and Their Precursors

Noncoding RNAs, especially microRNAs, have been described in the last decade as key developmental regulators (Bushati and Cohen 2007). Therefore, considerable efforts have been made to unravel the function of miRNAs and use them as diagnostic markers, especially in cancer (Jansson and Lund 2012; Zhang et al. 2014) but also in other diseases, including neurodegenerative diseases (Gandhi et al. 2013), cardiovascular diseases (Ellis et al. 2013), and infectious diseases (Shrivastava et al. 2013). Detection of small noncoding RNAs like microRNAs is a challenge, since they are very short in their mature form, containing neither cap nor poly (A) tails naturally and in addition to the mature form exist in a pri-form and a preform which are processed and transported out of the nucleus by a complex sequence of events as reviewed nicely by Bartel (Bartel 2004). Several systems have been described which enable microRNA detection on a microarray platform. For example, Agilent has developed such a platform including a special labeling technology which enables the detection of miRNAs for tissue or formalin-fixed biopsy material (D'Andrade and Fulmer-Smentek 2012). The profiling of different miRNA maturation levels in parallel is important for a comprehensive cancer classification (O'Hara et al. 2008). Therefore, it is desirable to distinguish between mature, pri- and preforms. Since the mature miRNA is also part of the preforms the available microarray systems in general are not able to distinguish between pre-mature and mature miRNAs without costly size exclusion or approximate data analysis. However, using a ZIP-code array system together with a defined labeling approach, a system enabling the distinction between pre-miRNAs and their mature form was described recently by Weishaupt et al. (Weishaupt et al. 2013). By labeling all forms of miRNAs with a poly(A) tail, they can distinguish between miRNA containing still a precursor sequence and a mature miRNA containing the poly(A) tail in direct proximity to the mature sequence. This is done by using primer extension reactions in combination with two distinct ZIP-code primers hybridizing to the mature miRNA targeted and the specific complementary ZIP on the array. The two ZIP-code primers are used for two distinct labeling reactions containing (1) only unlabeled dTTP together with Cy3-dUTP in the labeling reaction allowing for the detection of the mature form and (2) unlabeled dATP, dCTP, dGTP, and dTTP together with Cy3-dATP in the labeling reaction for the detection of the precursor form as shown in Fig. 2. Combining both labeling reactions on one array, we can now identify via the specific complementary ZIP code the amount of both the premature and mature miRNA. This is possible because the precursor miRNA is the only species which is able to carry labeled dATP, since the poly(A) tail directly following the mature form does not allow the integration of dATP into the mature form (for labeling reaction see Fig. 2), and the mature miRNA is the only species which is able to contain Cy3-dUTP via the poly (A) tail. The label reaction has to be performed separately to achieve this and is mixed on one array for readout. Using a set of well-defined, evaluated ZIP-code primers a quantitative readout could be demonstrated.

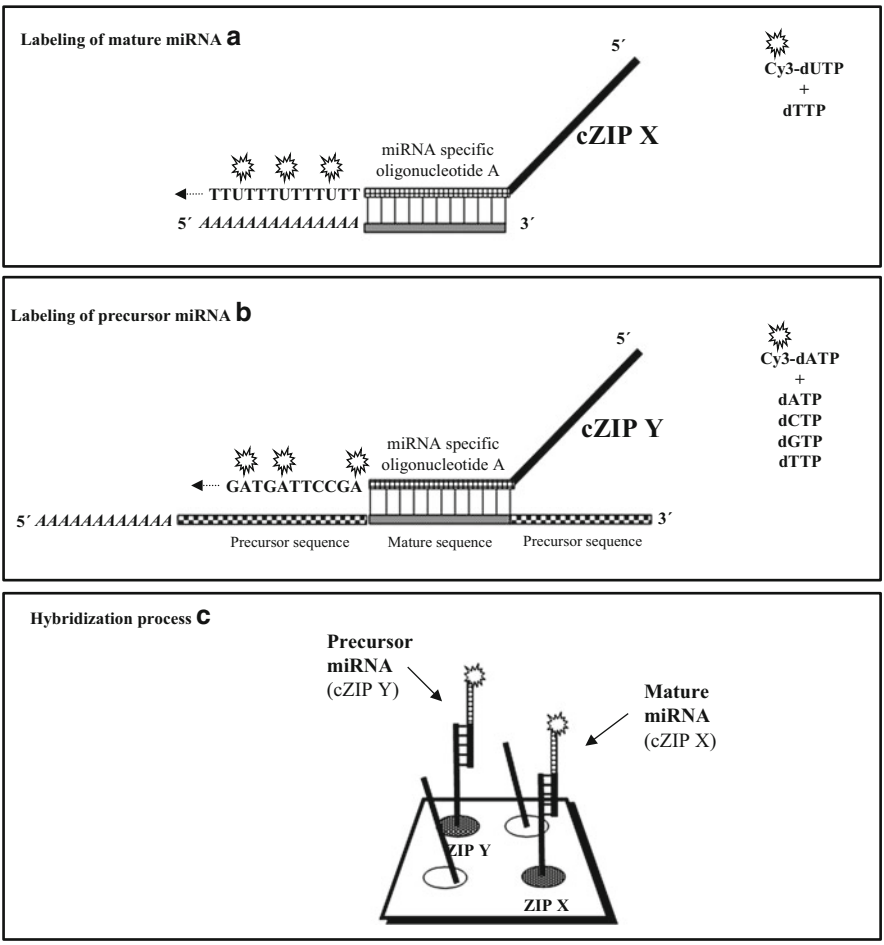

Fig. 2 Principle of the ZIP-code miRNA array for the differentiation of mature (**a**) and precursor miRNA (**b**) forms (Weishaupt et al. 2013). miRNA-specific cZIP-primer with an identical part complementary to the mature miRNA sequence and an individual cZIP-part are used in individual labeling reactions for every miRNA analyzed. Mature miRNA (**a**) is labeled with Cy3-dUTP in the presence of unlabeled dTTP; precursor miRNA is labeled with Cy3-dATP in the presence of all four unlabeled dNTPs. Differentiation takes place during the hybridization process (**c**) where the individual cZIP codes hybridize to their corresponding counterparts on the *array*

3 DNA Microarrays: Already in the Clinical Laboratory?

There are many commercially available DNA microarray platforms for research applications as introduced in Sect. 1. However, arrays that are used for diagnostic purposes in the clinics are rare. DNA microarray-based systems often face problems like reproducibility, sensitivity, ease of use, and the contamination risk.

However, there are several examples of DNA microarrays that made it into diagnostics. One example is the Amplichip®CYP450 from Roche, based on the Affymetrix system. It is the first microarray-based pharmacokinetic test cleared for clinical use. An excerpt from their homepage: "The AmpliChip CYP450 Test provides comprehensive detection of gene variations—including deletions and duplications—for the CYP2D6 and CYP2C19 genes, which play a major role in the metabolism of an estimated 25 % of all prescription drugs. It is intended to be an aid to clinicians in determining therapeutic strategy and treatment dose for therapeutics metabolized by the CYP2D6 or CYP2C19 gene product" (http://www.roche.com/products/product-details.htm?type=product&id=17).

The FDA-cleared 70-gene MammaPrint profile commercially available from Agendia as described above is one of the examples for a transcriptional profiling array that allows predicting the risk of metastasis formation for breast cancer. Biopsy- or formalin-embedded tissue is analyzed by expression analysis. Agendia also has several other cancer tests in their portfolio, e.g., for colon cancer recurrence or mutation analysis assays for EGFR, KRAS, BRAF, and PIK3CA to select appropriate patients for therapy (http://www.agendia.com/managed-care/). The ViroChip described above is an example of a diagnostic device for respiratory diseases, which however is not commercialized as such by a company but used as a research tool. Nevertheless, several commercial products are or were available for detection of (partially) overlapping panels of respiratory viruses, based on microarrays as the identification method (Miller and Tang 2009). These products include the ResPlex II assay from Qiagen (Valencia, CA); the MultiCode-PLx RVP from EraGen Biosciences (Madison, WI); the Infiniti RVP from AutoGenomics, Inc. (Carlsbad, CA); the Ngen respiratory virus ASR assay from Nanogen (San Diego, CA); and the xTAG RVP from Luminex Molecular Diagnostics (Toronto, Canada).

Randox also offers DNA microarrays in the field of molecular diagnostics (http://www.randox.com/evidence.php). Assay kits are provided for cardiac risk prediction, familial hypercholesterolemia, KRAS/BRAF/PIK3CA assay, respiratory multiplex array, or a multiplex array for sexually transmitted diseases. A convenient-to-use array system is offered by Euroimmun Medizinische Labordiagnostika AG. The company uses the so-called BIOCHIP technology. Small DNA microarray glass plates are adhered to plastic EUROArray object slides. The hybridization is performed in a standardized manner using the TITERPLANE® technology. CE-IVD certified assays, e.g., for autoimmune diseases (e.g., detection of rheumatic disease-associated alleles of human leukocyte antigen B27 (HLA-B27) or detection of psoriasis-associated alleles of HLA-Cw6) or an assay for the detection of human papilloma virus (HPV) types, are provided (http://www.euroimmun.de/index.php?id=startseite). Greiner Bio One International AG also offers CE-IVD certified microarray test kits. Their oCheck® product line comprises DNA microarrays for the diagnostic of 24 different HPV types or 20 periodontal pathogens and even a DNA microarray for the identification of animal species for food control. An open array platform for the development of multiparametric tests for research and diagnostics is offered by Alere. The

ArrayTube system consists of a custom microarray integrated into a microreaction tube. Parallelization is allowed by the ArrayStrip system. Here, the assays are available in a microplate-compatible format. Several assay types can be implemented like nucleic acid as well as protein- and peptide-based arrays. An overview of relevant publications is given on their website (http://alere-technologies.com/en/science-technologies/publications.html).

3.1 Lab-on-a-Chip Devices: Applicable for Multiparametric Tests with Need for Fast Information

There are several manual steps in diagnostics with DNA microarrays from sample to result like nucleic acid extraction, amplification or reverse transcription, labeling, hybridization, data readout, and data analysis. Each step is a potential risk for contamination and mistakes. One possibility to overcome these limitations is automation by using so-called micro total analysis systems (μTAS) or lab-on-a-chip devices (LoC) that allow for a complete sample preparation, analysis, and readout in a single closed device. In such microfluidic devices μ-, nano-, or even picoliter volumes are transported through micrometer-sized channels and are filtered, mixed, further processed, and detected. Fluid transport is often pressure-driven but alternatively also induced by electroosmotic flow or capillary forces. Complete automation harbors several advantages like getting by with smaller sample volumes, diminished contamination risk, faster assay processing due to small diffusion ways, efficient thermodynamics, and favorable surface-to-volume ratio as well as multiplex- and high-throughput capabilities. The implementation of complete processes from sample to result in LoC devices, however, is complex. First, one has to implement single functional units that in the end have to be combined to run in concert in one complete process. Challenges next to others are the choice of the material that has to be compatible to all assay steps, the assembly process, and the modification of the biological assay for maximal compatibility. Many research institutions are working on the development of LoC devices. Reviewing these, however, is beyond the scope of this review. The focus lies on array-based LoC devices that found or may find their way into the clinical routine laboratory.

Several companies are working on LoC devices for nucleic acid analytics; some of them use DNA microarrays as detection system, like Curetis, a company in Holzgerlingen, Germany, that uses a patented special array technology in a LoC device. Cell lysis is done in a separate processing unit. All other steps (purification, amplification, and detection) are then performed in a single cartridge. The Curetis technology can be used to diagnose infections. CE-certified cartridges are offered for the detection of pathogens and resistance markers for pneumonia (Unyvero™ P50) and implant and tissue infections (Unyvero™ i60 ITI). FDA clearance is aspired. Another complete solution with array-based detection is developed by

Nanosphere. Their Verigene system allows for the simple testing of nucleic acid and protein on a single platform (http://www.nanosphere.us/technology). For the detection of DNA or RNA targets, nanoparticle probe technology is used. Automated nucleic acid extraction and PCR amplification from a clinical sample take place on the Verigene® Processor SP. Eluted nucleic acids are transferred automatically into a Verigene Test Cartridge for hybridization of target DNA to capture oligonucleotides on a microarray. Detection is realized by specific mediator oligonucleotides and gold nanoparticle probe; the signal amplification of hybridized probes is done via a silver staining process. Automated qualitative analysis of results is performed on the Verigene Reader. Diseases like bacterial infections or cardiac tests are addressed. Rheonix (http://www.rheonix.com/technology/technology-overview.php) develops the Encompass platform. Disposable cards with onboard reagents and a low-density microarray- or qPCR-based detection system are the heart of the system. The company states that every user-designed or future FDA-cleared test can be run in their card due to the high flexibility of the system. Product development programs for infectious diseases, pharmacogenomics, and environmental applications are in progress.

Next to DNA microarray-based detection in LoC devices one can find quantitative real-time PCR, pH-mediated detection, or NGS technologies as readout strategy. Cepheid (http://www.cepheid.com/us/) has developed an integrated benchtop analyzer (GeneXpert) for the detection of several pathogens and resistance markers. They have a microfluidic cartridge where ultrasonic lysis and multiplex rapid real-time PCR technique are realized. The company has CE-certified cartridges for the detection of, e.g., *Clostridium difficile* (*C. difficile*), methicillin-resistant *Staphylococcus aureus* (MRSA), or norovirus and FDA-approved tests for, e. g., MRSA or tuberculosis. Focus Diagnostics (http://www.focusdx.com/3m-integrated-cycler/ud-intl) developed the 3M™ Integrated Cycler for a disk-based qPCR-based analytical system. 96 samples can be run in parallel. Assays are offered for the detection of viral-caused infections like dengue fever, influenza, and infectious mononucleosis (Epstein–Barr virus) or for the detection of bacteria like *Bordetella* species or *C. difficile*. Idaho Technologies [now BioFire (Biomerieux)] develops a product series based on the FilmArray® (Poritz et al. 2011). This novel diagnostic platform combines automated sample preparation, nucleic acid extraction, and PCR-based detection of multiple targets from a single unprocessed sample in 1 h. It combines nesting and multiplexing of the PCR (referred to here as nested multiplex or "nmPCR") together with DNA melting curve analysis to detect and distinguish multiple pathogens simultaneously. The FilmArray and the FilmArray Respiratory Panel (RP) pouch have since received FDA clearance for use as an in vitro diagnostic (IVD) device. Advanced Liquid Logic (http://www.liquid-logic.com/technology) which was acquired by Illumina in July 2013 has a digital microfluidic technology that is based on the use of electrowetting to precisely manipulate droplets on a surface. For electrowetting, a voltage is applied between a droplet and an insulated electrode that can cause the droplet to spread on the surface and allows the precise manipulation of droplets within a sealed microfluidic LoC. Illumina is mainly interested to deliver the simplest and most efficient sample-to-answer next-generation

sequencing (NGS) workflow (press release). DNA Electronics (http://dnae.co.uk/technology/overview/) develops electronic-based microchip solutions for DNA and RNA detection. An ion-sensitive field effect transistor (ISFET) is used for genotyping or semiconductor-based sequencing. Whenever DNA or RNA is amplified, a H+ ion is released that can be detected by the ISFET. Therefore, specific hybridization events can be detected. Addressed healthcare applications are in the field of personalized medicine and infection screening. Another sensor technology is developed by GeneFluidics. The technology enables quantification of nucleic acids and proteins on a single platform with electrochemical detection. High sensitivity even in unamplified, unpurified biological samples is advertised. Results are delivered within 1 h. Sensor surfaces are functionalized by antibodies or DNA. After the binding event and washing steps, a secondary antibody with HRP (reporter enzyme binding) is applied. Signals occurring during enzymatic conversion of HRP substrate are proportional to the analyte concentration (http://www.genefluidics.com/technology). HandyLab, acquired by BD in 2009, developed disposable cartridges with onboard dry reagents and patented real-time microfluidic PCR technology. Cartridges could be run in a benchtop instrument that integrated heating, mechanical valves for fluid control, and fluorescent detection. FDA-approved tests were available for MRSA, *C. difficile*, and group B *Streptococci*. These tests and one further test (vancomycin-resistant *Enterococci*) were approved for use in Europe. Another interesting and completely different system is the lab-in-a-tube system (Liat™ system) by IQuum (http://www.iquum.com/products/technology.shtml). All assay reagents are prepacked in tube segments separated by peelable seals in the Liat. The Liat is compressed by sample processing actuators of the Liat analyzer so that reagents are selectively released from tube segments, the sample is moved from one segment to another, and reaction conditions are controlled. You can start with a variety of sample matrices, including whole blood, plasma, urine, and swab samples. All required assay processes, including reagent preparation, nucleic acid purification, amplification, and real-time detection, are performed by the analyzer in 20 min–1 h, depending on the assay. Rapid PCR amplification and real-time detection are integrated. Products are the Liat™ Influenza A/2009 H1N1 Assay (research use only), a fully automated sample-to-result detection of viral RNA in 26 min that received FDA Emergency Use Authorization in 2009 (since expired), and the Liat™ Influenza A/B Assay (IVD product). Assays for HIV, CMV, influenza subtypes, and dengue are in the product pipeline.

4 Next-Generation Sequencing: The End of the DNA Microarray Era?

After 30 years of Sanger sequencing, within 3 years between 2005 and 2007, three different novel commercially available sequencing approaches have been introduced: the pyrosequencing technology by 454 Life Sciences, later acquired by

Roche, the ligation-based short-read sequencing technology by Applied Biosystems (SOLiD), and the Solexa short-read sequencing system that uses bridge amplification and sequencing by reversible dye terminators, later acquired by Illumina. The discussion of these impressive technological approaches summed up as next-generation sequencing (NGS) approaches is not in the scope of this review. A nice overview is given, e. g., in (Voelkerding et al. 2009). Since then, several other high-throughput sequencing technologies have been developed. One example is the semiconductor-based nonoptical sequencing system by Ion Torrent/Life Technologies. A pH-shift occurring during incorporation of desoxy-nucleotides in the growing strand is monitored by an ion-sensitive field effect transistor (Rothberg et al. 2011). Today, even single molecule sequencing is possible (Pacific Biosciences; http://www.pacificbiosciences.com/), and technologies are being developed that could allow the sequencing of whole genomes through nanopores within the shortest time (announced e. g. by Oxford Nanopore Technologies; https://www.nanoporetech.com/).

Nearly every DNA-based array platform has been mirrored to sequencing-based technological procedures. With the enormous high-throughput capabilities of NGS technology, whole-genome approaches if affordable can be performed, including transcription analysis [RNAseq, reviewed in (Mutz et al. 2013)], targeted genomic or even whole-genome re-sequencing (Ng et al. 2009, 2010; Tsuji 2010), comparison of genomes, mapping of DNA-binding proteins and chromatin analysis, epigenetics [reviewed in (Capell and Berger 2013; Mensaert et al. 2014)], methylation analysis [reviewed in (Olkhov-Mitsel and Bapat 2012)], or meta-genomics [reviewed in (Cox et al. 2013; Kim et al. 2013; Miller et al. 2013)].

Interestingly, a combination of microarrays and next-generation sequencing has been established. In order to focus on the most relevant part of the human genome for SNP detection, exome sequencing can be performed instead of using genotyping arrays. In exome sequencing, all coding sequences of the human genome are sequenced to identify variants between individuals. Approximately 180,000 exons comprising 30 million base pairs are reported which constitute about 1 % of the human genome (Directors ABo 2012). Focusing on mutations in the exons which are much more likely to cause an effect, the sequencing effort can be reduced by two orders of magnitude, if the exons can be enriched efficiently. Several enrichment methods are described (Lin et al. 2012). One of them uses DNA microarrays containing all complementary sequences of exons. For example, Nimble Gene developed a so-called Sequence Capture Human Exome 2.1 M Array to enrich all ~180,000 coding exons (Choi et al. 2009). Exome sequencing can be used as an approach to identify unknown causal genes for rare Mendelian disorders (Ng et al. 2009, 2010). The advantage of the sequencing technology is that it does not require any preexisting knowledge—one gets every mutation present—and not only the SNPs represented on the array. The challenge in this case is the specific sequence enrichment and to generate the know-how about the effect of the individual SNPs detected or their combination on human well-being. The first company making exome sequencing available for diagnostic purposes is Ambry. They introduced the Clinical Diagnostic Exome™. The company also offers more

than 300 highly specialized genetic tests (http://www.ambrygen.com/clinical-diagnostics).

Focusing on single genes, in diagnostics today, Sanger sequencing is used for the identification of rare variants. NGS has the capacity to replace Sanger sequencing by targeted genomic NGS (Sikkema-Raddatz et al. 2013). Using this approach, only subsets of genes that are known to be important and involved in a special disease are sequenced. Sikkema-Raddatz et al. constructed a targeted enrichment kit that includes 48 genes associated with hereditary cardiomyopathies and demonstrated that targeted NGS of a disease-specific subset of genes is equal to the quality of Sanger sequencing using the Illumina MiSeq sequencer (Sikkema-Raddatz et al. 2013). They state that it can therefore be reliably implemented as a stand-alone diagnostic test. *Illumina* offers the MiSeqDx Cystic Fibrosis (CF) 139-Variant Assay that detects 139 clinically relevant *CFTR* (*CF-transmembrane conductance regulator*) variants and the MiSeqDx Cystic Fibrosis Clinical Sequencing Assay that accurately captures all variants in the protein-coding regions and intron/exon boundaries of *CFTR* (Grosu et al. 2014). These are the first FDA-cleared NGS-based assays and kits for in vitro diagnostic use on the MiSeqDx instrument (http://www.illumina.com/clinical/diagnostics.ilmn).

Currently, NGS technologies are getting cheaper and easier to handle and also might be the molecular assay of choice in the future in the clinic. Clinical diagnostics requires easy-to-handle experimental procedures, robustness, accuracy, sensitivity, and comparable or lower costs compared to existing diagnostic approaches. Although, recent developments in NGS have led to small instruments that allow flexible throughput and short run times, current drawbacks of NGS approaches are their high investment and running cost, elaborate library preparation, and complex data analysis. Detached from these shortcomings, with the possibilities of NGS, novel diagnostic scales are thinkable not only for diagnostics of cancer, mitochondrial disorders, or hereditary diseases where the assay time is in general not critical but also for assays in clinical microbiology like the detection of MRSA or sepsis causative organisms. Within the scientific community, workshops and symposiums are held everywhere dealing with the topic how NGS can be validly used for clinical diagnostics. The FDA also looks deeper into this subject and performs public workshops that focus on the evaluation of the use of NGS technologies for clinical diagnostics (e.g., Ultra High Throughput Sequencing for Clinical Diagnostic Applications—Approaches to Assess Analytical Validity: Report from the Public Meeting (June 23, 2011), http://www.fda.gov/MedicalDevices/NewsEvents/WorkshopsConferences/ucm284442.htm and Public Workshop—Advancing Regulatory Science for High Throughput Sequencing Devices for Microbial Identification and Detection of Antimicrobial Resistance Markers, April 1, 2014, http://www.fda.gov/MedicalDevices/NewsEvents/WorkshopsConferences/ucm386967.htm). These activities indicate a strong competition of this new technology in the field of diagnostics.

5 Conclusions and Outlook

Microarrays have been developed and are used to detect or analyze a wide range of target molecules. A great portfolio of excellent research has been done in the field not only dealing with the molecular interaction but also with data analysis or automation of assay steps. Although developed nearly 20 years ago, the technology until now didn't really find its way into routine clinical laboratory diagnostics. Only a few arrays are used for such applications as described above. As the main reasons for this, the high complexity of the technology, missing robustness, accuracy, and sensitivity are discussed. Microarray procedures require many complex, often manual, steps that are prone to errors and need skilled staff and expensive equipment for processing. One way to overcome these shortcomings might be automation of the process steps using LoC devices that allow for a convenient and reproducible processing of patient samples with minimized risk for handling errors or contamination. Diagnostic assays beginning from sample preparation up to and including data readout and processing can be easily performed using such systems. This might be the most promising path for microarrays to find their way into clinical laboratory diagnostics at a larger scale.

Nevertheless, NGS has a high potential to revolutionize the diagnostic market within the next decades. As an open technology, it clearly competes with array-based systems where you only get what you screen for. The cheaper and the more comfortable the sequencing systems get, including data storage, analysis, and interpretation, the sooner they will replace array-based systems. However, for the detection of exactly defined genetic disorders, in clinical microbiology, and for the detection of a limited set of molecular markers, e.g., on a transcriptional level for cancer diagnostics, array technology still will for the foreseeable future be a valuable diagnostic tool to aid in therapy.

Acknowledgments We would like to acknowledge Dr. Jan Weile, HDZ-NRW, for critical reading of the manuscript and Dr. Sonja Weishaupt for contributing to the figures. This review was made possible partially through the BMBF-funded project FYI-Chip #13EZ1113.

References

Bartel DP (2004) MicroRNAs: genomics, biogenesis, mechanism, and function. Cell 116:281–297

Brady PD, Vermeesch JR (2012) Genomic microarrays: a technology overview. Prenat Diagn 32: 336–343

Brandt O, Hoheisel JD (2004) Peptide nucleic acids on microarrays and other biosensors. Trends Biotechnol 22:617–622

Bremer M, Himelblau E, Madlung A (2010) Introduction to the statistical analysis of two-color microarray data. Methods Mol Biol 620:287–313

Bushati N, Cohen SM (2007) microRNA functions. Annu Rev Cell Dev Biol 23:175–205

Capell BC, Berger SL (2013) Genome-wide epigenetics. J Invest Dermatol 133:e9

Carter MT, Scherer SW (2013) Autism spectrum disorder in the genetics clinic: a review. Clin Genet 83:399–407
Chen EC, Miller SA, DeRisi JL et al (2011) Using a pan-viral microarray assay (Virochip) to screen clinical samples for viral pathogens. J Vis Exp (50):pi 2536
Chibon F (2013) Cancer gene expression signatures—the rise and fall? Eur J Cancer 49: 2000–2009
Chiu CY, Urisman A, Greenhow TL et al (2008) Utility of DNA microarrays for detection of viruses in acute respiratory tract infections in children. J Pediatr 153:76–83
Choi M, Scholl UI, Ji W et al (2009) Genetic diagnosis by whole exome capture and massively parallel DNA sequencing. Proc Natl Acad Sci USA 106:19096–19101
Cleaveland S, Laurenson MK, Taylor LH (2001) Diseases of humans and their domestic mammals: pathogen characteristics, host range and the risk of emergence. Philos Trans R Soc Lond B Biol Sci 356:991–999
Colombo PE, Milanezi F, Weigelt B et al (2011) Microarrays in the 2010s: the contribution of microarray-based gene expression profiling to breast cancer classification, prognostication and prediction. Breast Cancer Res 13:212
Cox MJ, Cookson WO, Moffatt MF (2013) Sequencing the human microbiome in health and disease. Hum Mol Genet 22:R88–R94
D'Andrade PN, Fulmer-Smentek S (2012) Agilent microRNA microarray profiling system. Methods Mol Biol 822:85–102
Daigo Y, Takano A, Teramoto K et al (2013) A systematic approach to the development of novel therapeutics for lung cancer using genomic analyses. Clin Pharmacol Ther 94:218–223
Dally S, Lemuth K, Kaase M et al (2013) DNA microarray for genotyping antibiotic resistance determinants in Acinetobacter baumannii clinical isolates. Antimicrob Agents Chemother 57: 4761–4768
DeRisi JL, Iyer VR, Brown PO (1997) Exploring the metabolic and genetic control of gene expression on a genomic scale. Science 278:680–686
Dhillon RK, Hillman SC, Morris RK et al (2014) Additional information from chromosomal microarray analysis (CMA) over conventional karyotyping when diagnosing chromosomal abnormalities in miscarriage: a systematic review and meta-analysis. BJOG 121:11–21
Directors ABo (2012) Points to consider in the clinical application of genomic sequencing. Genet Med 14:759–761
Dufva M (2009) Introduction to microarray technology. Methods Mol Biol 529:1–22
Ellis KL, Cameron VA, Troughton RW et al (2013) Circulating microRNAs as candidate markers to distinguish heart failure in breathless patients. Eur J Heart Fail 15:1138–1147
Exner R, Bago-Horvath Z, Bartsch R et al (2014) The multigene signature MammaPrint impacts on multidisciplinary team decisions in ER(+), HER2(−) early breast cancer. Br J Cancer 111: 837–842
Falk J (2010) Using ChIP-based technologies to identify epigenetic modifications in disease-relevant cells. IDrugs 13:169–174
Gandhi R, Healy B, Gholipour T et al (2013) Circulating microRNAs as biomarkers for disease staging in multiple sclerosis. Ann Neurol 73:729–740
Gardner SN, Jaing CJ, McLoughlin KS et al (2010) A microbial detection array (MDA) for viral and bacterial detection. BMC Genomics 11:668
Genomes Project Consortium, Abecasis GR, Auton A et al (2012) An integrated map of genetic variation from 1,092 human genomes. Nature 491:56–65
Ghindilis AL, Smith MW, Schwarzkopf KR et al (2007) CombiMatrix oligonucleotide arrays: genotyping and gene expression assays employing electrochemical detection. Biosens Bioelectron 22:1853–1860
Gill SR, Pop M, Deboy RT et al (2006) Metagenomic analysis of the human distal gut microbiome. Science 312:1355–1359
Green RE, Krause J, Briggs AW et al (2010) A draft sequence of the Neandertal genome. Science 328:710–722

Grice EA, Kong HH, Conlan S et al (2009) Topographical and temporal diversity of the human skin microbiome. Science 324:1190–1192
Grosu DS, Hague L, Chelliserry M et al (2014) Clinical investigational studies for validation of a next-generation sequencing in vitro diagnostic device for cystic fibrosis testing. Expert Rev Mol Diagn 14:605–622
Hauser NC, Vingron M, Scheideler M et al (1998) Transcriptional profiling on all open reading frames of Saccharomyces cerevisiae. Yeast 14:1209–1221
Hauser NC, Martinez R, Jacob A et al (2006) Utilising the left-helical conformation of L-DNA for analysing different marker types on a single universal microarray platform. Nucleic Acids Res 34:5101–5111
Ho CC, Mun KS, Naidu R (2013) SNP array technology: an array of hope in breast cancer research. Malays J Pathol 35:33–43
Hughes TR, Mao M, Jones AR et al (2001) Expression profiling using microarrays fabricated by an ink-jet oligonucleotide synthesizer. Nat Biotechnol 19:342–347
Jacob A, Brandt O, Stephan A et al (2004) Peptide nucleic acid microarrays. Methods Mol Biol 283:283–293
Jansson MD, Lund AH (2012) MicroRNA and cancer. Mol Oncol 6:590–610
Kim M, Lee KH, Yoon SW et al (2013) Analytical tools and databases for metagenomics in the next-generation sequencing era. Genomics Inform 11(3):102–113
Kodama Y, Shumway M, Leinonen R et al (2012) The sequence read archive: explosive growth of sequencing data. Nucleic Acids Res 40(Database issue):D54–D56
Ksiazek TG, Erdman D, Goldsmith CS et al (2003) A novel coronavirus associated with severe acute respiratory syndrome. N Engl J Med 348(20):1953–1966
Lander ES, Linton LM, Birren B et al (2001) Initial sequencing and analysis of the human genome. Nature 409(6822):860–921
Leinberger DM, Schumacher U, Autenrieth IB et al (2005) Development of a DNA microarray for detection and identification of fungal pathogens involved in invasive mycoses. J Clin Microbiol 43:4943–4953
Leinberger DM, Grimm V, Rubtsova M et al (2010) Integrated detection of extended-spectrum-beta-lactam resistance by DNA microarray-based genotyping of TEM, SHV, and CTX-M genes. J Clin Microbiol 48:460–471
Lin X, Tang W, Ahmad S et al (2012) Applications of targeted gene capture and next-generation sequencing technologies in studies of human deafness and other genetic disabilities. Hear Res 288:67–76
Margulies M, Egholm M, Altman WE et al (2005) Genome sequencing in microfabricated high-density picolitre reactors. Nature 437:376–380
Mensaert K, Denil S, Trooskens G et al (2014) Next-generation technologies and data analytical approaches for epigenomics. Environ Mol Mutagen 55:155–170
Miller MB, Tang YW (2009) Basic concepts of microarrays and potential applications in clinical microbiology. Clin Microbiol Rev 22:611–633
Miller RR, Montoya V, Gardy JL et al (2013) Metagenomics for pathogen detection in public health. Genome Med 5:81
Morens DM, Folkers GK, Fauci AS (2004) The challenge of emerging and re-emerging infectious diseases. Nature 430:242–249
Mutz KO, Heilkenbrinker A, Lonne M et al (2013) Transcriptome analysis using next-generation sequencing. Curr Opin Biotechnol 24:22–30
Nerich V, Curtit E, Bazan F et al (2014) Economic assessment of the routine use of Oncotype DX assay for early breast cancer in Franche-Comte region. Bull Cancer 101:681–689
Ng SB, Turner EH, Robertson PD et al (2009) Targeted capture and massively parallel sequencing of 12 human exomes. Nature 461:272–276
Ng SB, Buckingham KJ, Lee C et al (2010) Exome sequencing identifies the cause of a Mendelian disorder. Nat Genet 42:30–35

Nikolaki S, Tsiamis G (2013) Microbial diversity in the era of omic technologies. Biomed Res Int 2013:958719
O'Hara AJ, Vahrson W, Dittmer DP (2008) Gene alteration and precursor and mature microRNA transcription changes contribute to the miRNA signature of primary effusion lymphoma. Blood 111:2347–2353
Olkhov-Mitsel E, Bapat B (2012) Strategies for discovery and validation of methylated and hydroxymethylated DNA biomarkers. Cancer Med 1:237–260
Paik S, Shak S, Tang G et al (2004) A multigene assay to predict recurrence of tamoxifen-treated, node-negative breast cancer. N Engl J Med 351:2817–2826
Perou CM, Sorlie T, Eisen MB et al (2000) Molecular portraits of human breast tumours. Nature 406:747–752
Phan JH, Quo CF, Wang MD (2012) Cardiovascular genomics: a biomarker identification pipeline. IEEE Trans Inf Technol Biomed 16:809–822
Pollack JR (2009) DNA microarray technology. Introduction. Methods Mol Biol 556:1–6
Poritz MA, Blaschke AJ, Byington CL et al (2011) FilmArray, an automated nested multiplex PCR system for multi-pathogen detection: development and application to respiratory tract infection. PLoS One 6:e26047
Powell JR, Bennett M, Waters R et al (2013) Functional genome-wide analysis: a technical review, its developments and its relevance to cancer research. Recent Pat DNA Gene Seq 7:157–166
Pruitt KD, Tatusova T, Brown GR et al (2012) NCBI Reference Sequences (RefSeq): current status, new features and genome annotation policy. Nucleic Acids Res 40(Database issue): D130–D135
Rothberg JM, Hinz W, Rearick TM et al (2011) An integrated semiconductor device enabling non-optical genome sequencing. Nature 475:348–352
Rubtsova MY, Ulyashova MM, Edelstein MV et al (2010) Oligonucleotide microarrays with horseradish peroxidase-based detection for the identification of extended-spectrum beta-lactamases. Biosens Bioelectron 26:1252–1260
Sato-Otsubo A, Sanada M, Ogawa S (2012) Single-nucleotide polymorphism array karyotyping in clinical practice: where, when, and how? Semin Oncol 39:13–25
Schena M, Shalon D, Davis RW et al (1995) Quantitative monitoring of gene expression patterns with a complementary DNA microarray. Science 270:467–470
Schmidt M, Victor A, Bratzel D et al (2009) Long-term outcome prediction by clinicopathological risk classification algorithms in node-negative breast cancer--comparison between Adjuvant!, St Gallen, and a novel risk algorithm used in the prospective randomized Node-Negative-Breast Cancer-3 (NNBC-3) trial. Ann Oncol 20:258–264
Sforza S, Tedeschi T, Bencivenni M et al (2014) Use of peptide nucleic acids (PNAs) for genotyping by solution and surface methods. Methods Mol Biol 1050:143–157
Shrivastava S, Mukherjee A, Ray RB (2013) Hepatitis C virus infection, microRNA and liver disease progression. World J Hepatol 5:479–486
Sikkema-Raddatz B, Johansson LF, de Boer EN et al (2013) Targeted next-generation sequencing can replace Sanger sequencing in clinical diagnostics. Hum Mutat 34:1035–1042
Tan PK, Downey TJ, Spitznagel EL Jr et al (2003) Evaluation of gene expression measurements from commercial microarray platforms. Nucleic Acids Res 31:5676–5684
Timme RE, Allard MW, Luo Y et al (2012) Draft genome sequences of 21 Salmonella enterica serovar enteritidis strains. J Bacteriol 194:5994–5995
Tiwari M (2012) Microarrays and cancer diagnosis. J Cancer Res Ther 8:3–10
Tsuji S (2010) Genetics of neurodegenerative diseases: insights from high-throughput resequencing. Hum Mol Genet 19:R65–R70
van 't Veer LJ, Dai H, van de Vijver MJ et al (2002) Gene expression profiling predicts clinical outcome of breast cancer. Nature 415:530–536
Venter JC, Adams MD, Myers EW et al (2001) The sequence of the human genome. Science 291: 1304–1351

Villasenor-Park J, Ortega-Loayza AG (2013) Microarray technique, analysis, and applications in dermatology. J Invest Dermatol 13:e7

Voelkerding KV, Dames SA, Durtschi JD (2009) Next-generation sequencing: from basic research to diagnostics. Clin Chem 55:641–658

Wang D, Coscoy L, Zylberberg M et al (2002) Microarray-based detection and genotyping of viral pathogens. Proc Natl Acad Sci USA 99:15687–15692

Wang D, Urisman A, Liu YT et al (2003) Viral discovery and sequence recovery using DNA microarrays. PLoS Biol 1(2):E2

Weishaupt SU, Rupp S, Lemuth K (2013) Simultaneous detection of different MicroRNA types using the ZIP-code array system. J Nucleic Acids 2013:496425

Wodicka L, Dong H, Mittmann M et al (1997) Genome-wide expression monitoring in Saccharomyces cerevisiae. Nat Biotechnol 15:1359–1367

Zanotti L, Bottini A, Rossi C et al (2014) Diagnostic tests based on gene expression profile in breast cancer: from background to clinical use. Tumour Biol 35:8461–8470

Zhang W, Liu J, Wang G (2014) The role of microRNAs in human breast cancer progression. Tumour Biol 35:6235–6244

Quadruplex Priming Amplification (QPA) for Nucleic Acid Diagnostics

Besik Kankia

Contents

Abstract Due to its incredible sensitivity, polymerase chain reaction (PCR) is a method of choice for nucleic acid diagnostics. However, PCR is a complex reaction due to (1) limited yield of product DNA (PCR plateau), (2) temperature cycling, and (3) complicated quantification methods. We have developed quadruplex priming amplification (QPA) to greatly simplify nucleic acid amplification and real-time quantification assays. The method relies on specifically designed guanine-rich primers, which after polymerase elongation are capable of spontaneous dissociation from target sites and forming DNA quadruplex. The quadruplex is characterized by

B. Kankia (✉)
Department of Chemistry and Biochemistry, The Ohio State University, 43210 Columbus, OH, USA

Institute of Biophysics, Ilia State University, 0162 Tbilisi, Republic of Georgia
e-mail: kankia.1@osu.edu

V.A. Erdmann et al. (eds.), *RNA and DNA Diagnostics*, RNA Technologies,
DOI 10.1007/978-3-319-17305-4_14

significantly more favorable thermodynamics than the corresponding DNA duplexes. As a result, target sequences are accessible for the next round of priming, and DNA amplification proceeds under isothermal conditions with improved product yield. In addition, the quadruplex formation is accompanied by an increase in intrinsic fluorescence of the primers, allowing simple and accurate detection of product DNA. The chapter discusses the thermodynamic and optical principles of QPA and its application in nucleic acid diagnostics.

Keywords DNA quadruplexes • Intrinsic fluorescence • Isothermal amplification • Quadruplex priming amplification

1 Introduction

Polymerase chain reaction (PCR) is one of the most widespread techniques used for detection of pathogenic microorganisms and genetic diseases. PCR relies on thermal cycling, consisting of repeated temperature changes for DNA unfolding, primer annealing, and enzymatic elongation of the DNA template. The key idea that made PCR applicable to a large variety of problems was the use of thermostable DNA polymerases to amplify a piece of DNA by in vitro enzymatic replication carried out in a single closed tube. Another key component of PCR is primers or short DNA fragments containing sequences complementary to the target region within DNA templates. DNA polymerase binds to this double-stranded region and initiates the replication process. As PCR progresses, the newly generated DNA is used as a template for replication, setting up a chain reaction with an exponential amplification pattern, which plateaus around low nanomolar concentrations of product DNA. Real-time PCR (RT-PCR), which detects and quantifies product molecules within PCR reaction vessels, is a most powerful tool for DNA quantification. However, current RT-PCR quantification systems use FRET (Förster Resonance Energy Transfer)-based detection mechanisms, which require costly synthesis and considerable effort to design.

2 Shortcomings of PCR

There are three fundamental shortcomings of PCR: (1) the need for thermal cycling, (2) the PCR plateau, and (3) complicated detection mechanisms.

Thermal Cycling Thermal cycling requiring expensive instrumentation is not compatible with point-of-care (POC) diagnostics. Several isothermal methods using polymerase activity have been developed (for a review, see Niemz et al. 2011); they are grouped in Table 1 based on the mechanism used to eliminate thermal cycling. All methods, with the exception of quadruplex priming

Table 1 Isothermal methods of DNA amplification based on polymerase activity

Mechanism	Method	Extra components	Product	Machine	Energy
(1) Release of PBS	QPA	None	DNA	None	ΔG of Q[a]
	HAD	2 (helicase; SSB)	Short DNA	Helicase	ATP
	RPA	2 (recombinase; SSB)	Short DNA	Recombinase	ATP
(2) Producing primer/PBS complex by nicking enzymes (NE)[b]	SDA	3 (NE; 2 bump. primer)	DNA	NE	None
	EXPAR	3 (NE; 2 DNA probes)	Short DNA	NE	Diffusion
	BAD AMP	1 (NE)	Short DNA	NE	None
(3) Amplification of circular targets	RCA	None[c]	HMW DNA	None	None
	RAM	1 (ligase)	HMW DNA	Ligase	ATP
(4) RNA amplification	TMA	2 (RT-pol; RNase H)	RNA	RNA pol	ATP
	NASBA	2 (RT-pol; RNase H)	RNA	RNA pol	ATP
	SMART	1 (RNA pol)	RNA	RNA pol	ATP
(5) Loop priming with bumper primers	LAMP	4–6 (total primers)	HMW DNA	None	None
	CPA	4–5 (total primers)	HMW DNA	None	None
	Smart-AMP	5 (total primers)	HMW DNA	None	None

QPA quadruplex priming amplification, *HAD* helicase-dependent amplification, *RPA* recombinase polymerase amplification, *SDA* strand displacement amplification, *EXPAR* exponential amplification reaction, *BAD AMP* beacon-assisted detection amplification, *RCA* rolling circle amplification, *RAM* ramification amplification, *TMA* transcription-mediated amplification, *NASBA* nucleic acid sequence-based amplification, *SMART* signal-mediated amplification of RNA technology, *LAMP* loop-mediated amplification, *CPA* cross-priming amplification, *Smart-AMP* smart amplification, *SSB* single-stranded binding protein, *HMW* high-molecular weight DNA

[a]Free energy of quadruplex formation

[b]NE approach also includes nicking enzyme amplification reaction (NEAR), nicking enzyme-mediated amplification (NEMA), and isothermal chain amplification (ICA)

[c]Requires circular DNA

amplification (QPA), are based on complicated mechanisms and use extra protein and DNA components.

The PCR Plateau Conventional PCR reaches a plateau at low nanomolar concentrations of product. One of the most important factors limiting the yield of the specific product is the competition between primer binding and self-annealing of the product. At the initial stage of PCR, product molecules are at low enough

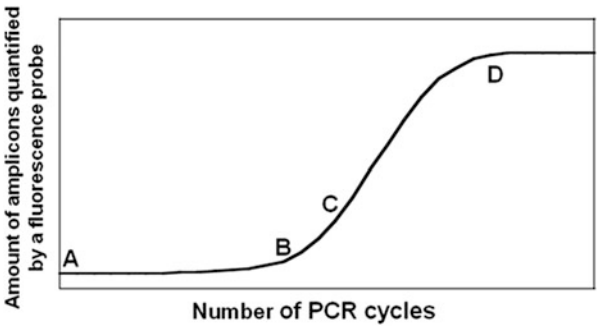

Fig. 1 A typical RT-PCR curve

concentrations that product self-annealing does not compete with primer binding, and amplification proceeds at an exponential rate (AC segment, Fig. 1). (Note: the AB segment in Fig. 1 corresponds to the exponential phase undetectable by fluorescence measurements.) However, with accumulation of product DNA, self-annealing becomes dominant, PCR slows down (CD segment), and eventually DNA amplification ceases (plateau, Fig. 1). Thus, an amplification system that eliminates product self-annealing could greatly improve PCR efficiency. In addition, RT-PCR quantification methods are based on the fact that the amount of product DNA detected is directly proportional to the initial amount of sample DNA during the exponential growth phase only. Since the fluorescence signal during the initial cycles is too weak to be distinguished from the background fluorescence (AB segment), only a narrow window of the exponential growth phase (2–4 cycles) is used for quantification (BC segment). Thus, product DNA quantification in RT-PCR would benefit from a longer exponential phase (Edwards and Logan 2009; Pfaffl et al. 2009).

RT-PCR Quantification Mechanisms Currently, four main techniques are used to monitor real-time PCR (Lee et al. 2009): molecular beacons (Tyagi et al. 1998, Tyagi and Kramer 1996), TaqMan (Holland et al. 1991), Scorpion probes (Whitcombe et al. 1999), and SYBR Green. However, only the first three are specific to the amplified product. Although SYBR Green is inexpensive, sensitive, and easy to use, it also binds to any double-stranded DNA including nonspecific products or primer dimers. All specific probe molecules have similar disadvantages which include (1) the requirement for two external and costly tags (fluorophore and quencher); (2) the contribution of two separate functions in the probes: recognition and reporting (fluorescence), which makes the assay very expensive when several targets are tested; (3) the use of separate binding sites for primer and probe sequences, which introduces another component (probe oligonucleotide) to an already complex reaction and adds additional design limitations due to the need to avoid interactions between the probe and primers; and (4) the use of bimolecular probe-primer system, which makes the reaction entropically unfavorable, slowing down hybridization and complicating product detection at exponential growth. Reporting is much faster and more efficient with a monomolecular probe-primer system as proposed here (Whitcombe et al. 1999).

3 Basic Principle of QPA

Due to their base-pairing properties, nucleic acid sequences can be programmed to form specific structures under certain solution conditions. For example, in the presence of certain metal ions (e.g., K^+), short guanine (G)-rich sequences fold into a structure known as a G-quartet or quadruplex (Fig. 2). Quadruplexes are highly stable and possess intrinsic optical properties (i.e., absorb light at 300 nm) that distinguish them from other secondary structures (Kankia 2004, 2006). We have developed straightforward real-time assays, which exploit this unique quadruplex signature to study restriction endonucleases (Kankia 2006), nucleic acid chaperone proteins (Kankia 2004), or DNA polymerases (Taylor et al. 2013). Briefly, when G-rich sequences with the potential to form a quadruplex are incorporated into DNA substrates, they are initially in the quenched state. Upon enzymatic activity (i.e., cleavage, strand exchange, or polymerase extension), the released sequence folds into a quadruplex and becomes visible when monitored by absorption or fluorescence spectroscopy. We also discovered that the free energy of DNA quadruplexes can be used to drive unfavorable (endergonic) reactions of nucleic acids (e.g., isothermal PCR) (Kankia 2011). The key aspect of these

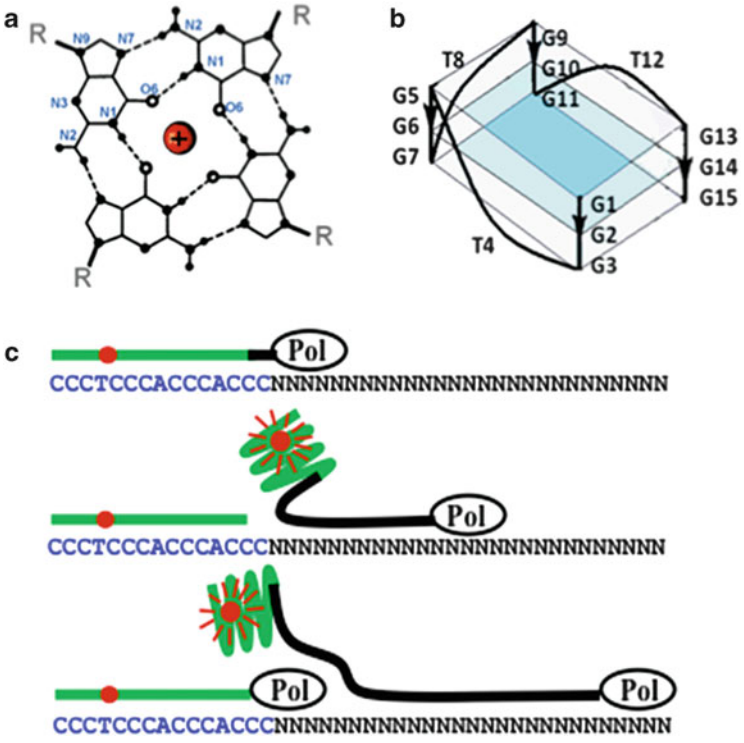

Fig. 2 G-quartet (**a**), GGGTGGGTGGGTGGG (G3T) quadruplex (**b**), and QPA mechanism (**c**)

reactions is that quadruplex structures form with significantly more favorable thermodynamics than corresponding DNA duplexes. Initially G3T (GGGTGGGTGGGTGGG) or G truncated version is incorporated within a DNA duplex. Upon interaction with an initiator (i.e., DNA polymerase, restriction endonucleases, or a binding partner), G3T self-dissociates from the complement and folds into a quadruplex. Thus, the energy of quadruplex formation can be used to drive polymerase-based amplification at constant temperature.

QPA uses the favorable free energy of quadruplex formation to drive PCR (Fig. 2c). Before elongation, the primers form perfect duplexes with the target sequence since they are missing a few guanine residues critical for quadruplex formation. Upon elongation, the 5′-end of each product DNA spontaneously forms in a quadruplex, and its complementary sequence (target) is fully accessible to the incoming primer.

4 Unique Properties of GGGTGGGTGGGTGGG

Any DNA amplification method, including QPA, involves multistep reactions with characteristic bottlenecks at each step. The strength of any method depends on its ability to avoid these bottlenecks. For instance, in PCR, the bottlenecks are avoided by temperature cycling, which unfolds DNA duplexes and favors priming over DNA self-annealing at initial stages of amplification. The PCR primers have different nucleotide sequences but respond to the (1) temperature changes, (2) cation type and concentration, and (3) polymerase activity similarly due to same secondary structure and thermodynamic properties. Thus, PCR uses a nonspecific way (all primers and amplicons are equal upon folding/unfolding) to avoid the bottlenecks, which makes it impractical in specific amplification reactions. Employing quadruplex primers cardinally changes the situation and allows the design of specific amplification schemes where obstacles are overcome by different properties of G3T. The thermodynamic and optical studies of DNA oligonucleotides discussed below reveal the strong potential of quadruplex-based technology in polymerase-based DNA amplification.

4.1 The G3T Quadruplex Is More Stable than Its Corresponding Duplex

To ensure that in the presence of K^+ ions G3T-ds15 (Fig. 3a) initially anneals to its complementary strand, the sequences were annealed in the presence of CsCl followed by later KCl addition. The heating curve (Fig. 3b) reveals two separate transitions with midpoints at 60 °C and ~93 °C (Kankia 2011). The transition at

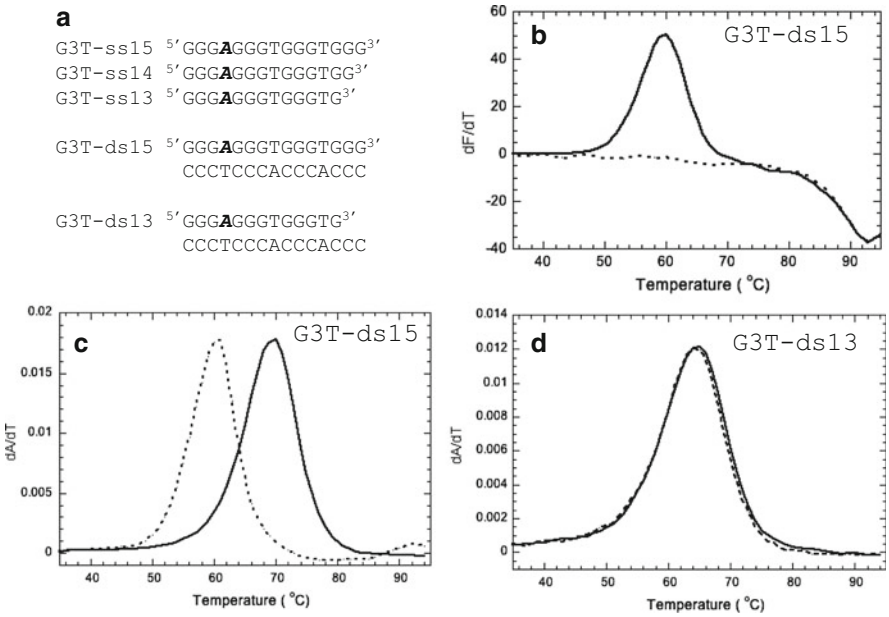

Fig. 3 Base sequences ($A = 2$AP, 2-aminopurine) (**a**); fluorescence melting of G3T-ds15 in 15 mM KCl, 35 mM CsCl, and 2 mM $MgCl_2$ (**b**); UV melting curves of G3T-ds15 (**c**); and G3T-ds13 (**d**). *Solid* and *dashed lines* in panels (**c**) and (**d**) correspond to measurements in 50 mM CsCl, 2 mM $MgCl_2$, and in 15 mM KCl, 35 mM CsCl, and 2 mM $MgCl_2$, respectively

60 °C corresponds to duplex unfolding, which is accompanied by an increase in fluorescence due to quadruplex formation of released G3T-ss15. The second transition at ~95 °C corresponds to the melting of the quadruplex, and it is completely reversible during the cooling process (dashed curve, Fig. 3b). However, no duplex refolding was observed, which clearly indicates that the quadruplex stays folded at lower temperatures in the presence of the complementary strand. Interestingly, the duplex melting temperature (~60 °C, Fig. 3b) is significantly lower than the $T_m = 70$ °C of the same duplex predicted from nearest-neighbor analysis of equilibrium unfolding (Zuker 2003). UV unfolding experiments in the presence and absence of K^+ ions allow comparative analysis. In the presence of K^+ ions, G3T-ds15 unfolds at 60 °C (dashed curve, Fig. 3c), which is in excellent agreement with results of the fluorescence measurements shown in Fig. 3b. In the absence of K^+ ions, the duplex is significantly more stable and unfolds at 70 °C (solid curve, Fig. 3c), as predicted from nearest-neighbor analysis of equilibrium unfolding (Zuker 2003). In the presence of K^+, unfolding of the duplex is a nonequilibrium process due to quadruplex formation of the released strands, which significantly destabilize the duplex (Kankia 2011). Figure 3d demonstrates unfolding of G3T-ds13 in the presence (dashed curve) and absence of K^+ ions (solid curve). Since G3T-ss13 is not able to form a quadruplex, G3T-ds13 duplex melting profiles

are identical in the presence and absence of K^+ ions with $T_m = 65$ °C. As expected, in the presence of Cs^+ ions, the longer duplex, G3T-ds15, is more stable than the shorter duplex, G3T-ds13. However, in the presence of K^+, the opposite is true: the shorter duplex is ~5 °C more stable than the longer one. This unusual result illustrates the driving force for isothermal QPA; at appropriate temperatures, the primer is more stable than its elongated version, which facilitates primer dissociation and the next priming round without the need for thermal denaturation.

As shown from temperature unfolding/refolding experiments (Fig. 3b), the quadruplex stays folded at lower temperatures even in the presence of the complementary strand. We also performed melting experiments using a monomolecular hairpin where GT3 and its complement are connected by a T4 loop. In this construct, quadruplex invasion by the complement is favored by minimizing the entropic barrier of duplex formation. Even in this most favorable monomolecular construct for duplex formation, the complementary strand is not able to invade the quadruplex (data not shown). Thus, due to its thermodynamic stability, the monomolecular G3T quadruplex remains folded even in the presence of the complementary strand.

4.2 Guanine Truncation Inhibits Quadruplex Formation

Since terminal guanines at the 3′-end of G3T play a key role in QPA, their role in quadruplex formation is well documented: deletion of a single guanine at the 3′-end strongly destabilizes the quadruplex (T_m drops by ~50 °C) and deletion of another guanine completely inhibits quadruplex formation (Johnson et al. 2013; Kankia 2011).

4.3 G3T Represents an Efficient Molecular Switch to Turn On Intrinsically Fluorescent Nucleotide Analogs

Fluorescent nucleotide analogs for amplicon quantification are highly desired since they can be readily incorporated into oligonucleotides during solid-phase synthesis. There are several suitable base analogs, such as 2-aminopurine (2AP), 3-methyl isoxanthopterin (3MI), and 6-methylisoxanthopterin (6MI), with high quantum yield (Hawkins 2007, 2008; Hawkins et al. 1997; Law et al. 1996; McLaughlin et al. 1988). Although these fluorescent bases have the potential to be sensitive probes, their fluorescence is significantly quenched upon incorporation into oligonucleotides, which makes them impractical in RT-PCR (Kourentzi et al. 2003; Marti et al. 2006). In contrast, we have shown that fluorescent base analogs incorporated at loop positions of quadruplexes demonstrate a remarkable increase

in fluorescence due to becoming fully accessible to solvent upon quadruplex formation. This allows a simple and very effective quantification method (Johnson et al. 2013; Kankia 2011). Thus, QPA (1) decreases the cost of quantification, (2) makes detection very sensitive and fast (due to its monomolecular nature), and (3) simplifies the reaction mixture by eliminating probe molecules (i.e., TaqMan).

5 Separate Steps of QPA

5.1 *Nucleotide Incorporation Opposite Template 2AP, 6MI, and 3MI*

Since fluorescent nucleotides are part of QPA primers, they must be replicated to create a full-length PBS in newly generated amplicons. The ability of *Taq* polymerase to discriminate between natural and fluorescent nucleotides has been investigated using QPA-based assays (Taylor et al. 2013). The study demonstrates good tolerance of 2AP by DNA polymerases and no significant incorporation of any nucleotides opposite of 6MI or 3MI. Based on these studies, two types of primers with intrinsic fluorescent nucleotides were designed: (1) 2AP-containing, in which the PBS can be completely replicated (left panel, Fig. 4), and (2) 3MI- and 6MI-containing, where the PBS will only be partially replicated (3MI and 6MI are used to terminate replication at the 5′-end of the primer) (right panel, Fig. 4).

5.2 *Linear QPA with a Short PBS*

The simplest version of QPA requires DNA polymerase to add only one or two guanines to the primer. To determine the optimal reaction temperature for linear QPA using a short PBS, two different systems shown in Fig. 4 were studied

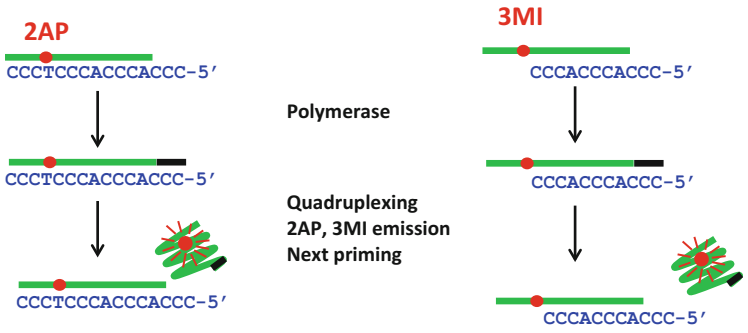

Fig. 4 Schemes of linear QPA using a 15-nt template (*left*) and a 11-nt template (*right*)

(Gogichaishvili et al. 2014a; Taylor et al. 2013). The temperature dependence of QPA rates closely correlates with the melting behavior of the complexes and is probably determined by the thermal stabilities of the primer/template complexes before and after elongation (Taylor et al. 2013). Taken together, the study demonstrated that linear QPA results in robust isothermal amplification over essentially the entire temperature range suitable for all thermophilic DNA polymerases (50–80 °C).

5.3 Quadruplex Unfolding by Polymerases

Exponential QPA requires that the polymerase is able to unfold and replicate the quadruplex sequence in order to create a primer-binding site in newly generated amplicons. The ability of *Bst* and *Taq* polymerases to unfold the quadruplex has been investigated (Partskhaladze et al. 2015). The data, collected at sufficiently high concentration of K^+ ions (25 mM KCl, 25 nmM CsCl, and 2 mM $MgCl_2$ at 72 °C), shows a very good unfolding rate, 5–10 per minute by both polymerases. Additional studies also revealed that the quadruplex unfolding rate is strongly dependent on reaction temperature and K^+ concentration. However, even at 62 °C and 100 mM K^+, we observed measurable unfolding activity. Thus, DNA polymerases are able to unfold and replicate this very stable DNA quadruplex (Partskhaladze et al. 2015).

6 QPA-Based Diagnostic Tools

Introduction of quadruplex primers in polymerase-based reactions not only simplifies signal amplification and makes it isothermal but it allows developing of different diagnostic tools based on QPA. In addition, QPA can be easily adopted to different DNA extracting methods or combined with different assays.

In the assays, discussed below, two different approaches are used: single-tube approach, in which all reaction components are mixed together, and magnetic bead approach, which requires separation of recognition and amplification processes. In the latter, sample (i.e., patient DNA) is immobilized to magnetic beads, processed, and moved to QPA recognition and amplification buffers. The probe molecules (Fig. 5) contain pathogen complements and a universal QPA construct. If the sample contains pathogen 1, Probe 1 will hybridize to it and will be transported to the adjacent solution containing the universal amplification buffer (Fig. 5). In this example, the sample DNA hybridizes to three Probe 1 molecules and not to Probe 2. QPA occurs only in chamber 2. Thus, this magnetic bead approach allows for multiple diagnoses using a single fluorescence signal and can be easily adapted to nucleic acid extraction cassettes (Bordelon et al. 2011).

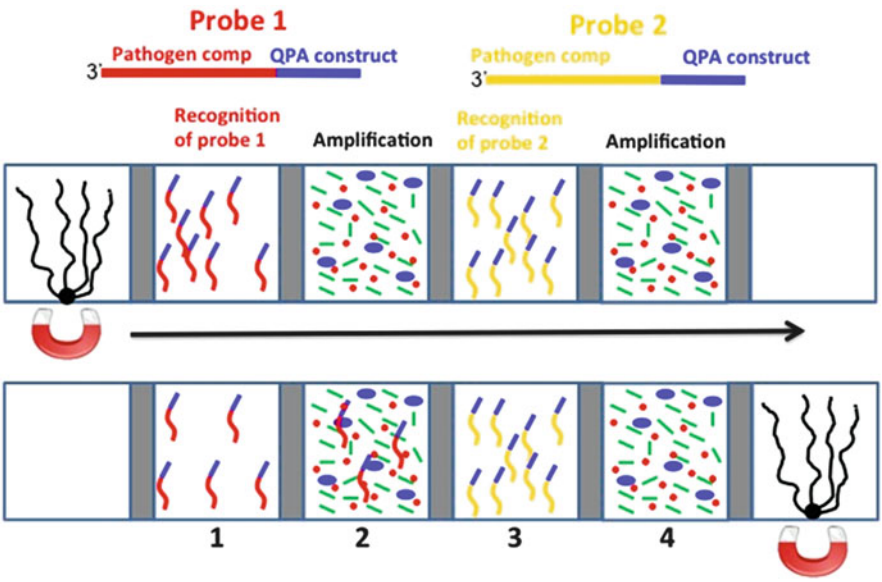

Fig. 5 Magnetic bead approach for multi-well diagnostics based on QPA. Probes specific for two disease targets are shown at the *top*. The two panels show the sample chambers before (*top*) and after (*bottom*) the movement of the sample through the chambers. Washing steps are not shown. In this approach, sample (i.e., patient DNA or any other biomarker) is immobilized to magnetic beads, processed, and moved to QPA recognition (chambers 1 and 3) and amplification buffers (chambers 2 and 4). The probe molecules contain pathogen complements (*red* and *yellow*) and a universal QPA construct (*blue*). If the sample contains pathogen 1, Probe 1 in chamber 1 will hybridize to it and will be transported to the adjacent solution containing the universal amplification buffer (chamber 2). In this example, the sample DNA (*black*) hybridizes to three Probe 1 molecules and not to Probe 2. Exponential QPA occurs only in chamber 2. Thus, this magnetic bead approach allows for multiple diagnoses using a single fluorescence signal and can be easily adapted to nucleic acid extraction cassette

6.1 Linear QPA

Linear amplification has an advantage to be less prone to false signal or background activity, which is a common problem of exponential systems. Specifically, in exponential systems, any false signal is exponentially amplified since amplicons or product molecules are used as templates in the following cycles. Thus, even a few false signals at early stage of amplification can affect the final count.

Recently, the linear QPA was used to detect mRNA from surrogate patient sample matrices (Adams et al. 2014). The complete assay includes (1) extracting of mRNA biomarkers from a complex sample on the surface of a magnetic bead, (2) binding the magnetic bead-captured mRNA biomarkers with QPA template sequences using a QPA probe or mRNA–QPA interface reagent, and (3) delivering the QPA probe in the QPA amplification and detection solution. If the specific mRNA biomarkers are present, the QPA probes are delivered to the QPA

amplification solution, and the signal is detected. The assay was found to maintain >90 % of the maximum signal over a 4 °C range of operational temperatures (64–68 °C). QPA had a dynamic range spanning four orders of magnitude, with a limit of detection of ~20 pM template molecules using a highly controlled heating and optical system and a limit of detection of ~250 pM using a less optimal water bath and plate reader. These results demonstrate that this integrated approach has potential as a simple and effective mRNA biomarker extraction and detection assay for use in limited resource settings (Adams et al. 2014).

6.2 QPA Combined with Nicking Enzyme

Under this strategy, which is suitable for both single-tube and magnetic bead approaches, two linear processes, linear QPA and linear nicking amplification (LNA), were combined (Gogichaishvili et al. 2014b). LNA is based on the work of Galass and coworkers (Van Ness et al. 2003) and can amplify short oligonucleotides by means of DNA polymerase and nicking endonuclease activities. Figure 6 describes the mechanism of QPA-LNA. After probe hybridization to the pathogen DNA and formation of the binding site of the nicking endonuclease, linear process of QPA-PBS (CCCACCCACCC) production is initiated, which is accompanied by light emission upon QPA. As the concentration of QPA-PBS molecules, product of LNA, is steadily increased, the light emission accelerates and becomes semi-exponential. This strategy allowed us to increase sensitivity of the linear QPA

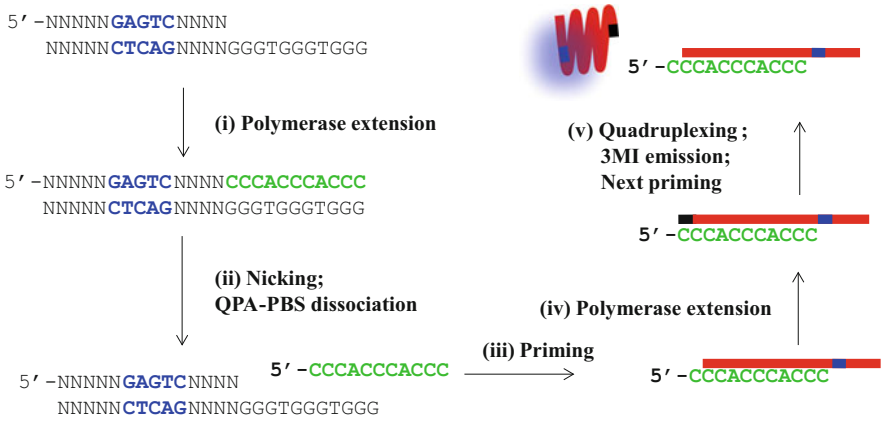

Fig. 6 Diagram of QPA-LNA after hybridization of the probe molecule (lower strand) to the pathogen (upper strand) and initial Nt.*Bst*NBI nicking. (i) Polymerase extends pathogen and creates QPA-PBS (*green*); (ii) Nt.*Bst*NBI nicks the upper strand and QPA-PBS dissociates. At this moment, QPA-PBS producing "machines" are made and number of the machines equal to number of pathogens; (iii) QPA-PBS binds to QPA primer; (iv) polymerase adds missing guanine (*black*); (v) elongated primer dissociates, emits light, and next primer binds to QPA-PBS

by three orders of magnitude and detect as low as 10 fM target molecules (Gogichaishvili et al. 2014b).

6.3 *Two-Primer Exponential QPA for Magnetic Bead Approach*

The assay is designed for the magnetic bead approach and its schematic is shown in Fig. 7 (Partskhaladze et al. 2015). In this design, two kinds of primers are used: (1) QPA primer, which is capable of self-dissociation and determines isothermal nature of QPA, and (2) usual primer, so-called second primer, which is not capable of self-dissociation; however, it is separated from PBS by polymerase displacement activity. As a result, the reaction in Fig. 2b is truly isothermal. Initially, QPA primer binds to the probe (Fig. 7b, step i) and initiates its replication (step ii). After spontaneous quadruplex formation, the next QPA priming occurs (step iii), which is accompanied by displacement of the first amplicon (step iv). The displaced strand contains a freely available PBS for the second primer. The primer binds (step v) and replicates the amplicon, including the quadruplex at the 5′-end (step vi). After another step of amplification, a short duplex containing primer-binding sites for both primers is created, and the reaction becomes exponential (right panel, Fig. 7b). The assay allows detection of attomolar targets and demonstrates 10^{10}-fold amplification in less than 40 min (Partskhaladze et al. 2015).

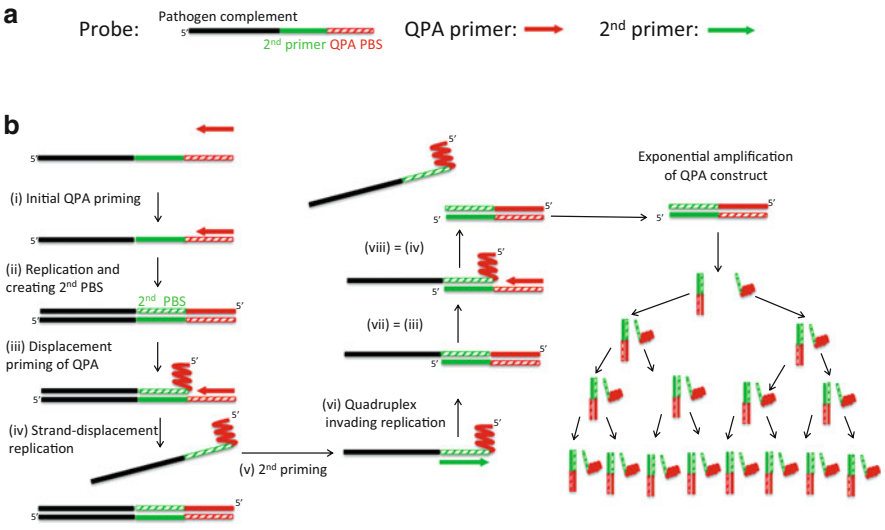

Fig. 7 Scheme of exponential QPA. (**a**) The probe molecule for magnetic bead approach for multi-well diagnostics, which contains three separate segments: pathogen complement (*black*), second primer (*green*), and QPA-PBS (*dashed red*). (**b**) The scheme showing the details of exponential QPA

6.4 QPA Combined with Peroxidase DNAzyme Activity

In the presence of hemin, monomolecular quadruplexes can form a peroxidase-like DNAzyme, which is able to produce a colorimetric signal (Cheng et al. 2009; Travascio et al. 1999). Since QPA produces the monomolecular G3T quadruplex, it can be easily combined to peroxidase DNAzyme activity. This approach was used in the recent paper that uses 59-nt long exponential construct for exponential QPA (Loh et al. 2014). The paper demonstrates that the assay can be used only in qualitative detection of the target sequences. One of the reasons, which did not allow quantitative estimations, should be the selection of the 59-nt long construct with both quadruplex-forming sequence and its complement. As a result, significant amount of quadruplexes can be incorporated in the DNA duplexes decreasing efficiency of the combined assay. Combination of peroxidase DNAzyme activity with linear QPA (Gogichaishvili et al. 2014a; Taylor et al. 2013), which is producing quadruplexes without any attachment, has better potential. Similarly to QPA-LNA, it might increase sensitivity of the linear QPA. Moreover, the peroxidase DNAzyme activity can be combined with QPA-LNA that will create three linear processes running in parallel that can create rapid and very sensitive colorimetric signal.

Acknowledgments This work was funded by a grant (DI/23/7-230/12) from Shota Rustaveli National Science Foundation (Republic of Georgia) and a grant from the Bill & Melinda Gates Foundation through the Grand Challenges in Global Health initiative.

References

Adams NM, Wang KK, Caprioli AC et al (2014) Quadruplex priming amplification for the detection of mRNA from surrogate patient samples. Analyst 139:1644–1652

Bordelon H, Adams NM, Klemm AS et al (2011) Development of a low-resource RNA extraction cassette based on surface tension valves. ACS Appl Mater Interfaces 3:2161–2168

Cheng X, Liu X, Bing T et al (2009) General peroxidase activity of G-quadruplex-hemin complexes and its application in ligand screening. Biochemistry 48:7817–7823

Edwards KJ, Logan JMJ (2009) Peforming real-time PCR. In: Logan J et al (eds) Real-time PCR. Caister Academic, Norfolk, pp 85–93

Gogichaishvili S, Johnson J, Gvarjaladze D et al (2014a) Isothermal amplification of DNA using quadruplex primers with fluorescent pteridine base analogue 3-methyl isoxanthopterin. Biopolymers 101:583–590

Gogichaishvili S, Lomidze L, Kankia B (2014b) Quadruplex priming amplification combined with nicking enzyme for diagnostics. Anal Biochem 466:44–48

Hawkins ME (2007) Synthesis, purification and sample experiment for fluorescent pteridine-containing DNA: tools for studying DNA interactive systems. Nat Protoc 2:1013–1021

Hawkins ME (2008) Fluorescent pteridine probes for nucleic acid analysis. Methods Enzymol 450:201–231

Hawkins ME, Pfleiderer W, Balis FM et al (1997) Fluorescence properties of pteridine nucleoside analogs as monomers and incorporated into oligonucleotides. Anal Biochem 244:86–95

Holland PM, Abramson RD, Watson R et al (1991) Detection of specific polymerase chain reaction product by utilizing the 5′—3′ exonuclease activity of Thermus aquaticus DNA polymerase. Proc Natl Acad Sci U S A 88:7276–7280
Johnson J, Okyere R, Joseph A et al (2013) Quadruplex formation as a molecular switch to turn on intrinsically fluorescent nucleotide analogs. Nucleic Acids Res 41:220–228
Kankia BI (2004) Optical absorption assay for strand-exchange reactions in unlabeled nucleic acids. Nucleic Acids Res 32:e154
Kankia BI (2006) A real-time assay for monitoring nucleic acid cleavage by quadruplex formation. Nucleic Acids Res 34:e141
Kankia BI (2011) Self-dissociative primers for nucleic acid amplification and detection based on DNA quadruplexes with intrinsic fluorescence. Anal Biochem 409:59–65
Kourentzi KD, Fox GE, Willson RC (2003) Hybridization-responsive fluorescent DNA probes containing the adenine analog 2-aminopurine. Anal Biochem 322:124–126
Law SM, Eritja R, Goodman MF et al (1996) Spectroscopic and calorimetric characterizations of DNA duplexes containing 2-aminopurine. Biochemistry 35:12329–12337
Lee MA, Squirrell DJ, Leslie DL et al (2009) Homogeneous fluorescent chemistries for real-time PCR. In: Logan J et al (eds) Real-time PCR. Caister Academic, Norfolk, pp 23–45
Loh Q, Omar N, Glokler J et al (2014) IQPA: isothermal nucleic acid amplification-based immunoassay using DNAzyme as the reporter system. Anal Biochem 463:67–69
Marti AA, Jockusch S, Li Z et al (2006) Molecular beacons with intrinsically fluorescent nucleotides. Nucleic Acids Res 34:e50
McLaughlin LW, Leong T, Benseler F et al (1988) A new approach to the synthesis of a protected 2-aminopurine derivative and its incorporation into oligodeoxynucleotides containing the Eco RI and Bam HI recognition sites. Nucleic Acids Res 16:5631–5644
Niemz A, Ferguson TM, Boyle DS (2011) Point-of-care nucleic acid testing for infectious diseases. Trends Biotechnol 29:240–520
Partskhaladze T, Taylor A, Lomidze L et al (2015) Exponential quadruplex priming amplification for DNA-based isothermal diagnostics. Biopolymers 103:88–95
Pfaffl MW, Vandesompele J, Kubitsa M (2009) Data analysis software. In: Logan J et al (eds) Real-time PCR. Caister Academic, Norfolk, pp 65–83
Taylor A, Joseph A, Okyere R et al (2013) Isothermal quadruplex priming amplification for DNA-based diagnostics. Biophys Chem 171:1–8
Travascio P, Bennet AJ, Wang DY et al (1999) A ribozyme and a catalytic DNA with peroxidase activity: active sites versus cofactor-binding sites. Chem Biol 6:779–787
Tyagi S, Kramer FR (1996) Molecular beacons: probes that fluoresce upon hybridization. Nat Biotechnol 14:303–308
Tyagi S, Bratu DP, Kramer FR (1998) Multicolor molecular beacons for allele discrimination. Nat Biotechnol 16:49–53
Van Ness J, Van Ness LK, Galas DJ (2003) Isothermal reactions for the amplification of oligonucleotides. Proc Natl Acad Sci U S A 100:4504–4509
Whitcombe D, Theaker J, Guy SP et al (1999) Detection of PCR products using self-probing amplicons and fluorescence. Nat Biotechnol 17:804–807
Zuker M (2003) Mfold web server for nucleic acid folding and hybridization prediction. Nucleic Acids Res 31:3406–3415

Single-Molecule Strategies for DNA and RNA Diagnostics

D.Cibran Perez-Gonzalez and J.Carlos Penedo

Contents

Abstract Since the discovery of the DNA structure more than 60 years ago, the use of fluorescence tools for molecular diagnostics of nucleic acids has experienced an astonishing growth. In particular, during the last decade, the development of specific techniques to detect and analyse the structure and dynamics of nucleic

D.C. Perez-Gonzalez
SUPA School of Physics and Astronomy, University of St Andrews, North Haugh, St Andrews KY16 9SS, Scotland

J.C. Penedo (✉)
SUPA School of Physics and Astronomy, University of St Andrews, North Haugh, St Andrews KY16 9SS, Scotland

Biomedical Science Research Complex, University of St Andrews, North Haugh, St Andrews KY16 9ST, Scotland
e-mail: jcp10@st-andrews.ac.uk

V.A. Erdmann et al. (eds.), *RNA and DNA Diagnostics*, RNA Technologies,
DOI 10.1007/978-3-319-17305-4_15

acids at single-molecule level has revolutionised the field, and now it is possible to sequence a complete genome in record-breaking time and to get insights into structure and function of nucleic acids with an unprecedented level of detail. In this chapter, we start by reviewing the basic concepts regarding state-of-the-art single-molecule diagnostics of nucleic acids, and we describe in detail the most recent advances on the field, ranging from DNA sequencing and nucleic acid-based sensing to the analysis of functional RNAs involved in gene regulation and catalysis. The final sections are devoted to explore the latest RNA aptamers for imaging live cells and the next generation of hybrid technologies based on real-time manipulation of their structure and dynamics one at a time.

Keywords Branched DNA • Fluorescence resonance energy transfer (FRET) • Single-molecule microscopy • Ribozymes • Riboswitches • RNA aptamers • Live cell imaging

1 Introduction

Since the discovery of the double-helix DNA structure, our understanding of the structural diversity of nucleic acids (RNA and DNA) and its link to biological function has experienced a stunning growth. In addition to the well-known double-helix structure, nucleic acids can be found in single-stranded form, as triplexes, and in a variety of branched structures adopting multiple conformations responding to different biological needs. Many crucial biological processes such as replication, recombination and DNA repair require the opening of the double helix and the formation of transient structures, either to have access to the encoded genetic information or to repair damaged DNA. For instance, DNA Holliday junctions, replication forks and DNA flaps arise as intermediate states during DNA processing by highly specialised protein machineries. More recently, the formation of stable guanine quadruplexes, in both RNA and DNA sequences, has been reported in guanine-rich nucleic acid sequences. Although initially regarded as exotic forms of single-stranded DNA, the confirmation of their existence in vivo (Biffi et al. 2013) and their potential role in crucial processes such as gene regulation and telomere maintenance has triggered the need to develop novel technologies that can sense these structures with high specificity and affinity. Here, it is important not only to report the presence of the guanine quadruplex structure but also discriminate between the different conformers in which a given G-quadruplex (GQ) sequence can be present. The potential of GQs and GQ–ligands as therapeutic targets has also become highly promising in many areas related to human health. For instance, the role of GQ sequences as molecular targets to induce death in cancer cells has recently been reported (McLuckie et al. 2013).

In the last decades, the RNA world has also experienced its own revolution with the discovery that RNA function goes beyond exclusively acting as a passive

transporter of genetic information. The discovery of non-coding RNA sequences with catalytic activity, the so-called ribozymes, in the early 1980s (Guerrier-Takada et al. 1983; Kruger et al. 1982) demolished a conceptual barrier, and the relevance of RNA as an active element participating in many crucial processes including gene silencing, gene regulation, metabolite sensing and immune response continues to expand. For instance, the discovery in 2002 of a small RNA sequence (riboswitch) that senses coenzyme B12 to regulate downstream expression (Nahvi et al. 2002) constituted the first example of a gene regulation mechanism purely performed by RNA and marked the starting of a new field where the formation of these regulatory RNA–ligand complexes could be explored as antibiotic targets.

The application of fluorescence-based techniques to diagnose the structure and presence of this huge diversity of nucleic structures has become very attractive because of their high sensitivity and the simplicity of the assays, which normally only require a relatively inexpensive fluorimeter that is available in most laboratories. Moreover, they enable real-time continuous probing, and because a fluorophore provides a range of observables (emission intensity, fluorescence lifetime and polarisation), assays in different formats can be tailored and optimised for each particular system. Lastly, the possibility of detecting each of these observables from a single fluorescent molecule, as opposed to the average fluorescence signal from an ensemble of many molecules, constitutes not only the ultimate limit of diagnostic and sensing, but it has also allowed an understanding of how RNA and DNA structures are dynamically processed (McCluskey et al. 2014). In particular, the field of nucleic acid research has greatly benefited in the last decade by allowing the detection and analysis of the structure and dynamics of nucleic acids in real time. Since its first implementation, the single-molecule DNA/RNA field has rapidly expanded, and there is a continuously growing library of techniques based on single-molecule fluorescence (SMF) (Joo et al. 2008). The majority of single-molecule techniques are based on the detection of the light emitted by fluorophores acting as highly sensitive reporters of the surrounding medium. In this chapter, we will describe the application of SMF to diagnose the structure and function on nucleic acids, with special focus on surface-immobilised and freely diffusing techniques. The use of fluorescence resonance energy transfer (FRET) as a diagnostic tool based on changes in molecular distances across the nucleic acid structure has become extensively used in vitro and in vivo assays, and as such, it will be discussed in detail. We will also report the most recent advances on the field ranging from DNA sequencing and nucleic acid-based sensing to the analysis of functional RNAs involved in gene regulation and catalysis. The last section of the chapter is devoted to in vivo RNA imaging using RNA aptamers and to hybrid technologies, where the combination of FRET with force mechanical manipulation is emerging as the state-of-the-art technique to fully understand the function of nucleic acids.

2 Single-Molecule Techniques for Nucleic Acid Diagnostics

The detection of single fluorescent molecules was demonstrated for the first time using pentacene molecules hosted on a crystal matrix at liquid helium temperatures (Moerner and Kador 1989). Advances in single-molecule techniques, mostly due to significant improvements in fluorescence detection technology, allowed a few years later the first measurements of spatially isolated molecules at room temperature (Betzig and Chichester 1993). Shortly after, the use of the total internal reflection (TIR) microscopy brought the first measurements in aqueous solution and provided a means for the detection of biological samples at single-molecule level (Fig. 1a) (Funatsu et al. 1995). More recently, the combination of TIR with FRET made possible to study the conformational changes in nucleic acids using DNA strands labelled at specific positions with a single donor and a single acceptor (Ha et al. 1996). The continuous improvements that single-molecule techniques have experienced in the last decade have consolidated it as one of the most powerful methods for the study of biophysical processes. The main benefit that single-molecule technique provides, when compared to ensemble techniques, is the possibility to observe isolated and non-synchronised samples in real time, representing the ultimate sensitivity limit in molecular diagnosis (Joo et al. 2008).

SMF can be done for either freely diffusing molecules or for specimens immobilised on a glass or quartz microscope slide. Freely diffusing molecules can be observed in solution with the use of confocal microscopy, whilst surface-

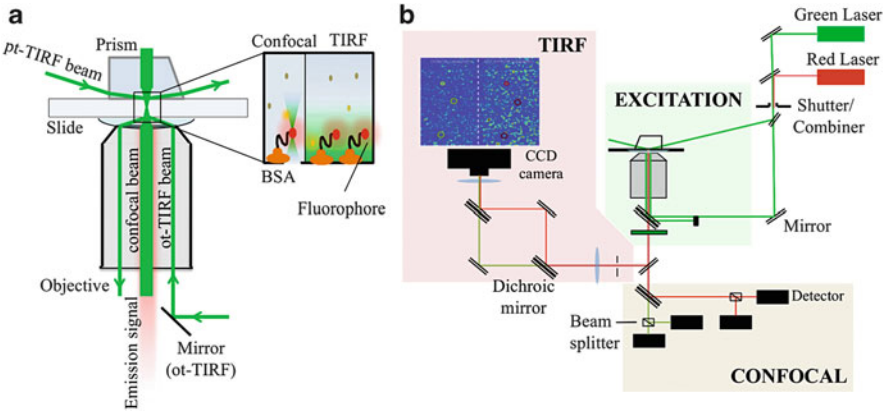

Fig. 1 Schematic diagram for single-molecule TIR and confocal microscopy. (**a**) Diagram for single-molecule confocal and TIR microscopy showing the prism-based (pTIR) and objective-based (oTIR) variants. (Inset) The intensity of the evanescent wave decays exponentially with the distance, illuminating a little volume of sample with a penetration depth of ~150 nm. (**b**) Excitation and emission pathways for TIR and confocal FRET assays. In pTIR, the prism directs the beam to the slide, whilst in oTIR and confocal, the excitation occurs through the objective. (*Left*) A dichroic mirror splits the fluorescence signal into two components, which are collected on a CCD camera. (*Bottom*) Schematics for the confocal detection, where the emissions of donor and acceptor are collected on different avalanche photodiodes

immobilised techniques use either confocal or wide-field excitation. Both confocal and wide-field techniques limit the excitation volume within the sample to reduce the background and provide a better signal-to-noise ratio (Fig. 1b). The reduction of the illuminated region to a small volume (~fL) is critical to detect the low number of photons emitted from a single dye above a background, which is mostly contributed from solvent Raman bands, scattering light and impurities in the medium. In this chapter, we will focus on how to apply two different but complementary single-molecule techniques for nucleic acid diagnosis: (1) single-molecule studies on freely diffusing molecules, which allow measurements of fast events on the sub-millisecond timescale and below, and (2) single-molecule studies of surface-immobilised molecules, which enable to monitor dynamics for long periods of time (up to seconds) with millisecond resolution.

In addition to advances in instrumentation, the widespread use of SMF techniques has been made possible thanks to parallel improvements in nucleic acid synthesis and site-specific labelling of DNA and RNA with fluorescent markers. Solid-phase synthesis and post-synthetic labelling are the two main methods used for this purpose. During solid-phase synthesis, the dye is incorporated in the nucleic acid sequence using fluorescently labelled phosphoramidites. Post-synthetic labelling uses normally a *N*-hydroxysuccinimidyl ester (NHS) derivative of the dye that reacts with a base modified with a primary amino group inserted at specific positions of the nucleic acid sequence (McCluskey et al. 2014). More recently, other chemical reactive groups have been developed to increase the labelling flexibility. This includes the coupling of maleimide ester derivatives of the dye to thiol-modified nucleobases and the use of click chemistry reagents. The purification of the nucleic acid to separate labelled from non-labelled sequences and also unreacted dye can be carried out using native or denaturing polyacrylamide gel electrophoresis (PAGE) or HPLC methods. The development of these labelling and purification methods has facilitated the wider use of SMF techniques and their application in FRET-based and multicolour assays. Another important factor contributing to the success of SMF in biological systems of increasing complexity has been the development of a variety of dye libraries covering from the near ultraviolet to the near infrared with improved photophysical properties (i.e. improved photostability, higher quantum yield). To further increase the observation time window, different oxygen scavenger systems (i.e. glucose oxidase/glucose catalase) and triplet-state quenchers, such as β-mercaptoethanol and trolox, are now commonly used in single-molecule measurements (Aitken et al. 2008; Benesch and Benesch 1953; Zheng et al. 2014). Oxygen scavenger systems allow to slow down the photobleaching rate of the fluorophore, thus enabling the observation of dynamic events up to several seconds. Triplet-state quenchers minimise the influence of blinking events that result in the temporary loss of the fluorescence emission, thus compromising the interpretation of dynamic fluctuations in single-molecule measurements.

2.1 *Surface-Immobilised Molecules: Total Internal Reflection Fluorescence Microscopy*

2.1.1 Surface Immobilisation Methods

Surface immobilisation methods combined with wide-field TIR illumination and CCD detection offer the possibility of observing single molecules for long periods of time with millisecond time resolution. They also provide a way to control the density of molecules within the field of view, which is important when building statistical data that are representative of the underlying mechanism. Early single-molecule experiments based on surface-immobilised samples in aqueous solution used polyacrylamide or agarose gels to confine the sample in a certain volume. The pores formed within the gel trap the molecules and allow their study over a long period of time; however, the slow diffusion of the nucleic acids across the gel and the difficulties for changing solution conditions required to explore additional immobilisation methods. Subsequent experiments used a combination of the strong interaction between biotin and streptavidin to specifically attach the sample to the microscope slide. In this method, quartz slides (wide-field) or coverslips (confocal) are coated with a first layer of biotin-labelled bovine serum albumin protein (BSA), and subsequently, neutravidin is added to the slide to form a second layer to which a biotin-modified RNA or DNA sample can be added to form a stable complex (Fig. 2a). The interaction between neutravidin and biotin is one of the strongest interactions known in nature, with an affinity in the picomolar range and, importantly, with a very slow off rate, thus ensuring the nucleic acid structure will remain anchored to the slide for a long time. Moreover, the interaction is very stable to temperature, pH variations and moderate denaturing conditions, allowing a variety of biologically relevant conditions to be tested without affecting the immobilisation strategy (Kurzban et al. 1991).

In addition, non-specific interactions with negatively charged glass and quartz surfaces present in some avidin proteins can be minimised by using neutravidin because of its lower p*I* (6.3). Because of its robustness and slow dissociation rate, the neutravidin/biotin system is becoming the standard tool for the non-covalent immobilisation of nucleic acids in single-molecule microscopy.

The study of protein–DNA or protein–RNA interactions needs an initial step involving the passivation of the surface with aminosilane and poly(ethylene glycol) (PEG) to prevent any non-specific protein–surface interaction. For these assays, the slide surface is coated with a mixture of biotinylated and non-biotinylated PEG to control the final density of molecules (Fig. 2b) (Chandradoss et al. 2014). Although BSA/neutravidin and PEG methods are by far the most commonly used immobilisation methods in the study of nucleic acid structure and dynamics, it is always crucial to confirm that the observed behaviour is not altered by the nearby surface. Encapsulation of the nucleic acid inside lipid vesicles has become in recent years an alternative method that completely avoids surface artefacts (Fig. 2c) (Okumus et al. 2004). Encapsulation-based methods also offer several possibilities

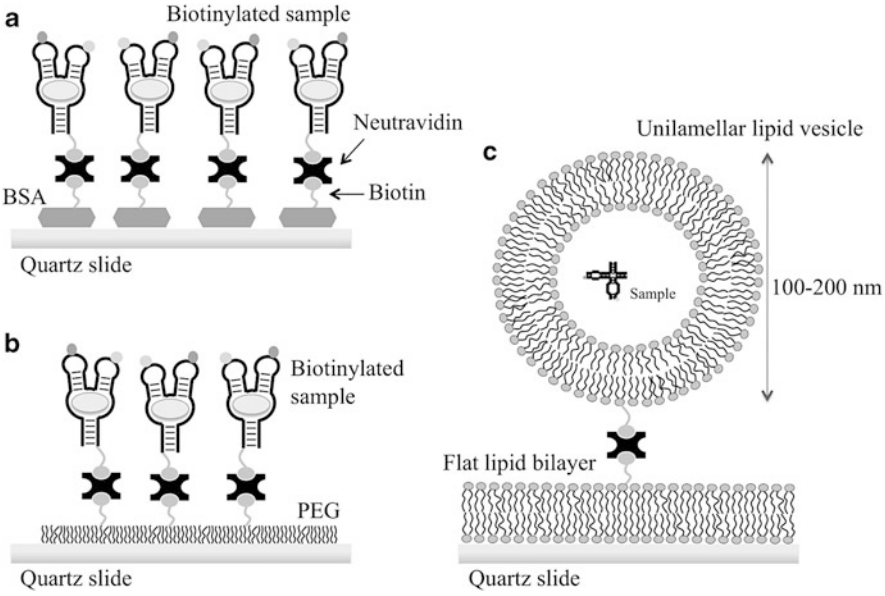

Fig. 2 Surface immobilisation methods for single-molecule fluorescence techniques. (**a**) Surface immobilisation with the use of biotinylated bovine serum albumin (BSA) and neutravidin. Nucleic acid molecules labelled with biotin can bind one of the three free binding sites of the neutravidin. The resulting concentration of the sample is usually on the order of nM or pM. (**b**) The study of protein–DNA or protein–RNA interactions requires another passivation treatment with aminosilane and poly(ethylene glycol) (PEG) to prevent non-specific interactions between the protein and the slide surface. The slide is coated using 1–2 % biotinylated PEG and non-biotinylated PEG. Once the slide is prepared, first, neutravidin and then the sample can be flushed into the sample chamber. (**c**) Schematics of lipid encapsulation. The vesicles require a passivation either with a flat lipid bilayer or PEG to prevent its rupture on contact with the quartz surface. In the formation of the vesicle, only a small amount of lipids are biotinylated (<0.5 %), and those are the ones that can be tethered to the slide through the biotin–streptavidin interaction

for real-time exchange of solution conditions. This includes the insertion of nanopores in the lipid membrane using the intrinsic ability of the bacterial toxin α-haemolysin (α-HL) to assemble into channels that communicate both sides of the lipid bilayer or by tailoring the lipid composition of the vesicle so that transient pores can be formed at room temperature [i.e. DMPC vesicles (Roy et al. 2008)]. Encapsulation is normally achieved by preparing the vesicles by the extrusion method (McCluskey et al. 2014) in the presence of a concentration of nucleic acid enough to maximise the presence of single occupied vesicles whilst minimising significant trapping of multiple DNA or RNA structures within the confined volume. By the extrusion method, highly homogeneous vesicles with diameters ranging from 50 nm to 500 nm and carrying a small percentage of biotinylated lipids can be easily prepared and purified from non-encapsulated DNA or RNA using size exclusion chromatography. It is important to note that lipid vesicles in contact with bare glass or quartz will burst open and release their

contents. However, this well-known liposome property has been used to generate a passive 2-D lipid bilayer in direct contact with the glass/quartz from empty vesicles carrying a small percentage (<0.1 %) of biotinylated lipids. In single-molecule microscopy, the function of this layer is dual: (1) prevent the bursting of lipid vesicles carrying encapsulated molecules and (2) provide spatially separated biotinylated groups inserted in the 2-D bilayer to which neutravidin can bind.

The surface immobilisation methods described above can be used with either wide-field or confocal techniques. In wide-field mode, TIR illumination is normally used to create an evanescent wave within the sample with a penetration depth limited to ~100 nm, thus reducing the excitation volume and providing a signal-to-noise ratio suitable for single-molecule detection. In Sect. 2.1.2, we detailed the basic principles of how single-molecule TIR microscopy can be applied to investigate the function and structure of nucleic acids.

2.1.2 Total Internal Reflection Fluorescence

When light travels from one medium with higher refractive index to another with a lower index, there is a critical angle for which the light is refracted at 90°. Above this angle, total internal reflection takes place, where most part of the light is reflected and an evanescent wave is generated on the other side of the interface. The critical angle can be calculated from the Snell's law (Eq. 1):

$$\frac{\sin\theta_1}{\sin\theta_2} = \frac{n_2}{n_1} \tag{1}$$

where θ_1 and θ_2 represent the incident and the refractive angles, respectively, and n is the refractive index of each medium. In a TIR-based setup, a laser beam is coupled into the sample chamber at an angle greater than the critical angle to create an evanescent wave within the sample. This technique uses the evanescent wave as a wide-field excitation method, where the intensity decays exponentially with the distance.

Two main types of microscopes based on this technique can be distinguished depending on how the evanescent wave is generated: prism-based and objective-based (Fig. 1a). In prism-based TIR, a prism directs the beam to the slide and illuminates the side of the quartz slide in contact with the prism and opposite to the microscope objective. In objective-based total internal reflection fluorescence (TIRF), the excitation beam is focused onto the back focal place of the objective and directed to the slide through one side of the objective to achieve the critical angle condition. In this case, excitation and detection take place on the same side of the slide, and this normally increases the background levels resulting in a lower signal-to-noise ratio.

In the first years of smTIR, nucleic acid structures such as ribozymes (Zhuang et al. 2000) served as testing platforms to explore the potential of smTIR to reveal the intricate mechanisms of folding and catalysis, and in many ways, it can be

considered that both fields benefit from each other. Since then, the application of single-molecule TIR microscopy in biology has been continuously growing, and once again, nucleic acids have been used as test systems for the implementation of more complex single-molecule techniques such as those involving multicolour detection (Hohng et al. 2004) and mechanical manipulation (Hohng et al. 2007). As recent examples, the application of smTIR techniques has greatly contributed to understand RNA-based gene regulation mechanisms in bacteria, to dissect ligand-binding process in RNA aptamers (Heppell et al. 2011) and to decipher the function and structure of guanine quadruplexes (Lee et al. 2005a, b). In the following sections of this chapter, we will describe in detail not only the techniques but also the insights that they have provided regarding the function, structure and dynamics of many of the above-mentioned nucleic acid systems.

2.2 *Fluorescence Resonance Energy Transfer*

Fluorescence resonance energy transfer (FRET) is a technique based on the non-radiative transfer of energy between two fluorescent dyes, a donor (D) and an acceptor (A), that are very close to one another (Fig. 3a) (Stryer 1978). FRET can be used as a powerful spectroscopic technique to measure distances between the two chromophores in the range from 10 Å to 100 Å, which is a relevant distance range in

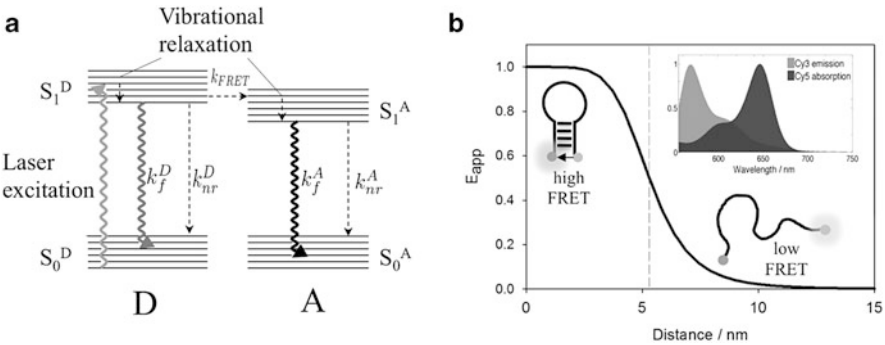

Fig. 3 Single-molecule FRET assays for nucleic acid characterisation. (**a**) Jablonski diagram illustrating the FRET process. On the left, a donor molecule (D) absorbs a photon to reach its first excited electronic state, S_1^D. Then, the molecule relaxes via fluorescence radiative emission (k_f), via non-radiative processes (k_{nr}), or undergoes resonance energy transfer (k_{FRET}) to the acceptor (A). The acceptor, on its excited state S_1^A, can also relax through radiative or non-radiative processes and return to its ground state, S_0^A. (**b**) FRET efficiency as a function of distance, r, between the widely used FRET pair Cy3 (donor) and Cy5 (acceptor). E_{app} depends inversely on the sixth power of the separation between both dyes (r^6) making it useful for the study of structure and dynamics of nucleic acids when the inter-dye distance varies between 1 and 10 nm. *Right inset*: Emission spectra of Cy3 and absorption spectra of Cy5. The pair of dyes needs to have significant overlap between both spectra and be close enough to show FRET

many biological processes involving nucleic acids. The transfer of resonant energy implies a weak Coulombic interaction between the oscillating dipole moments of both dyes and requires a significant overlap between the donor emission and the acceptor absorption spectra (Fig. 3b). The energy transfer depends inversely on the sixth power of the distance between the fluorophores. Thus, the distance between donor and acceptor, r, can be estimated from the efficiency of the FRET process (E_{app}). This is normally achieved by calculating the relative emission of the acceptor with respect to the total fluorescence emission (D + A) (Eq. 2):

$$E_{app} = \frac{F_A}{F_A + F_D} = \frac{R_0^6}{R_0^6 + r^6} \tag{2}$$

R_0 is the Förster radius and represents the distance that corresponds to a 50 % transfer efficiency. This term can be calculated using Eq. (3):

$$R_0^6 = \frac{9,000 \ \ln 10 \kappa^2 Q_D}{128 \pi^5 N n^4} \int_0^\infty F_D(\lambda) \varepsilon_A(\lambda) \lambda^4 d\lambda \tag{3}$$

where κ^2 is a dipole orientation factor (assumed to be 2/3 for anisotropic orientation of the dyes), Q_D is the quantum yield of the donor in the absence of acceptor, n is the refractive index of the medium, N is Avogadro's number and the integral represents the overlap between donor emission and acceptor excitation spectra. This integral includes the normalised donor fluorescence intensity, F_D, and the extinction coefficient of the acceptor at the same wavelength, ε_A. Thus, the FRET efficiency depends on the distance, spectral overlap and relative orientation between the molecular dipoles of both dyes.

Although ensemble-averaging FRET techniques have been used as a molecular ruler to investigate the structure of nucleic acids for more than 30 years, it was not until they were applied at single-molecule level (smFRET) that their full potential was revealed. In common with single-molecule techniques in general, smFRET allows to follow the interactions, dynamics and conformational changes of nucleic acids on a timescale that includes most of the biologically relevant processes, ranging from milliseconds to minutes. Moreover, it enables to quantify the relative populations of different structural conformers that, otherwise, will be hidden in conventional ensemble FRET because of averaging among many molecules. The data obtained from smFRET measurements are commonly shown as time-dependent donor and acceptor intensity trajectories, together with the resulting FRET trace corresponding to the single D–A pair present in the DNA or RNA structure. In the absence of photophysical artefacts, anticorrelated variations in the intensity trajectories of the donor and acceptor molecules are interpreted as evidence for dynamic switching between different structural conformers (Fig. 4a). From each single-molecule FRET trajectory, two types of data can be extracted: (1) the number of different conformers present at equilibrium and their contribution

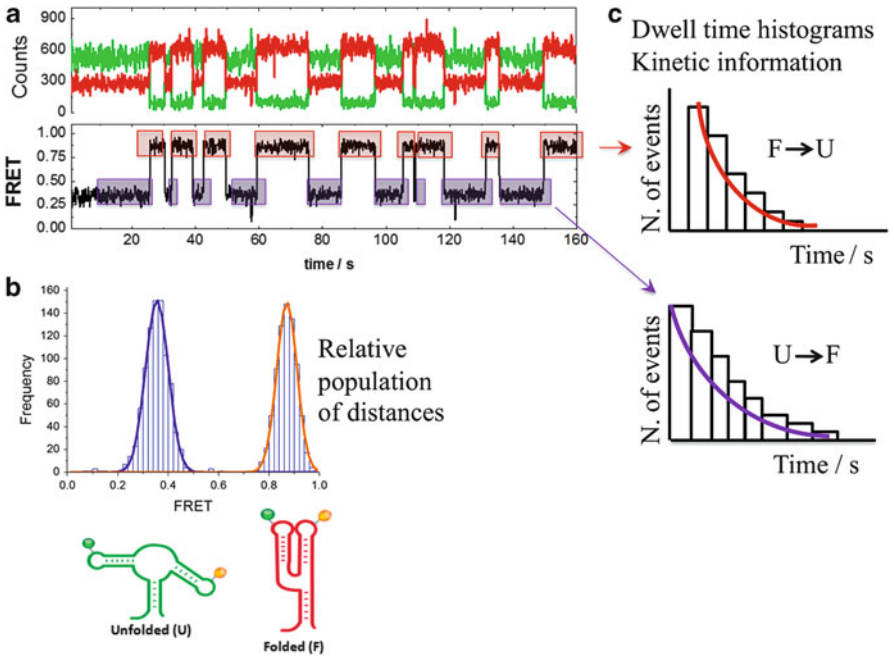

Fig. 4 Data analysis for single-molecule FRET assays. (**a**) Single-molecule FRET trace for a doubly labelled nucleic acid. The detected signal is represented as a function of time and shows the anticorrelated fluorescence intensities of the donor (*green*) and acceptor (*red*). (*Bottom graph*) FRET efficiency, E_{app}, obtained from the upper trace. E_{app} can be calculated from the donor and acceptor intensities using Eq. (2) (see main text). The trace shows a dynamic switching between low-FRET (unfolded) and high-FRET (folded) conformations. (**b**) smFRET histograms representing FRET populations. The histogram is built from the average E_{app} value of the first ten frames of each trace. (**c**) Dwell time histogram for the study of the interconversion dynamics. The distribution can be fitted to a mono- or multi-exponential decay $I(t) = \sum_n a_n \cdot e^{-t/\tau_n}$, where τ_n represents the lifetime of the correspondent conformer

and (2) the kinetic rates associated to the individual transition from one conformer to another. By accumulating these values for many molecules, appropriate steady-state FRET histograms showing the relative structural populations present in solution can be generated (Fig. 4b). Using the same FRET trajectories, rate histograms representing the underlying interconversion dynamics can be built with enough statistics to accurately reveal intricate folding and catalytic mechanisms (Fig. 4c) (Zhuang et al. 2000).

In the last few years, a wide range of dyes is commercially available for single-molecule techniques, covering the spectral range from UV to IR. Some of the most commonly used are the Alexa Fluor, cyanine and ATTO dye families. The photophysical properties of these chromophores need to meet some very specific criteria to be adequate for smFRET applications: (1) They need to have a good separation of their emission spectra (low or negligible crosstalk), have a substantial

Table 1 Spectroscopic properties for some of the most common fluorescent dyes used in single-molecule fluorescence techniques

	Dye	Absorption max. (nm)	Emission max. (nm)	Molar ext. coefficient (M^{-1} cm^{-1})	FRET donors	FRET acceptors
Near-UV	IAEDANS	336	490	5,700		Fluorescein Alexa 488
	Alexa Fluor 350	346	442	35,000		Alexa 488
Visible	Alexa Fluor 488	495	519	73,000	IAEDANS Alexa 350	Alexa 555 Alexa 647
	Fluorescein	496	516	89,000	IAEDANS	Cy3
	Cy3	550	570	150,000	Fluorescein	ATTO 647N Cy5
	Alexa Fluor 555	555	565	155,000	Alexa 488	Alexa 647
	ATTO 647N	644	669	150,000	Cy3	
	Cy5	649	670	250,000	Cy3	Cy7
	Alexa Fluor 647	650	668	270,000	Alexa 488 Alexa 555	
	Cy5.5	675	694	250,000	Cy3 Cy5	Cy7
Near-IR	Cy7	747	776	200,000	Cy5 Cy5.5	

spectral overlap between donor emission and acceptor absorption spectra (determines the R_0 value), have similar quantum yields (no significant change in total fluorescence intensity) and, very importantly, be commercially available with reactive groups for site-specific attachment to nucleic acids. In Table 1, we list the most widely used fluorophores for smFRET applications together with their photophysical properties.

2.3 Single-Molecule Fluorescence Detection of Freely Diffusing Nucleic Acids

2.3.1 Fluorescence Correlation Spectroscopy

Single-molecule fluorescence correlation spectroscopy (smFCS) is an elegant alternative to surface-immobilised methods to investigate the interconversion dynamics and distribution of structural populations of nucleic acids in solution. FCS was initially established in the 1970s (Magde et al. 1972), but it was not until the 1990s that significant technical improvements made possible its wider application in biologically relevant systems (Rigler et al. 1993). smFCS measures small

fluorescence intensity fluctuations from molecules transiting through a confocal observation volume on the order of a femtolitre and in timescales ranging from 10^{-7} to 10^{2} s. smFCS provides information about diffusion coefficients, variations in molecular brightness and concentration, intramolecular conformational dynamics and association rates in a variety of biomolecular process such as host–ligand association and protein–protein and protein–nucleic acid interactions. In recent years, smFCS has been combined with a range of other techniques such as dual-colour cross-correlation methods, two-focus cross-correlation, laser scanning microscopy, TIRF, two-photon microscopy and stimulated emission depletion (STED), and the reader is referred to excellent reviews on the field for more specific information (Enderlein et al. 2004; Kim et al. 2007a, b). smFCS correlates the fluorescence emission signal from a single molecule diffusing across the excitation volume in a certain time t with the same signal at a time $(t + \Delta t)$. This correlation, which is represented by the autocorrelation function (Eq. 4), can be described as the degree of self-similarity of the signal in time. The autocorrelation function can then be fitted to different models depending on the specific mechanism under study to get the values of diffusion times, brightness and molecular dynamics contributing to the observed fluctuations in the fluorescence signal.

$$G(\tau) = \frac{\langle \delta F(t) \delta F(t+\tau) \rangle}{\langle F(t) \rangle^2} \tag{4}$$

In the autocorrelation function, $\delta F(t) = F(t) - \langle F(t) \rangle$ represents the fluctuation around an average intensity. Although smFCS has provided a wealth of information regarding hybridisation rates and the mechanisms of nucleic acid self-assembly, for FCS to be useful in the study of conformational dynamics in nucleic acids, the fluctuations in intensity of the fluorescence probe have to depend on the conformation of the nucleic acid polymer. The most common approach is to label the nucleic acid with a fluorophore that is directly excited and also with either a quencher species or a FRET acceptor. Thus, fluctuations in the emission signal of the fluorophore are a direct consequence of distance changes between the fluorophore and the quencher or the acceptor tag. The analysis and interpretation of the autocorrelation (single-colour) or cross-correlation (two-colour) curves depend on the timescale of the conformational dynamics compared to the residence time of the molecule in the confocal volume, which is characterised by $\tau_D = r_0^2/4D$. Experimentally, the simplest case is when the diffusion time and the timescale of the conformational fluctuations are well separated. For small biomolecules, the diffusion coefficient D is ~10^{-9} to 10^{-10} m^2 s^{-1}, and the residence time in the confocal volume is in the region of 100 μs. Thus, fluctuations in fluorescence signal due to conformational changes taking place between 1 and 10 μs can be easily separated from the diffusion component. For instance, relaxation times in the microsecond regime were monitored for DNA hairpins containing a poly(dT)$_5$ loop with a short dC–dG stem (Kim et al. 2006). Biopolymers showing dynamics at longer timescales that overlap with the diffusion time have also been studied using different

modifications to the basic smFCS technique. The description of these techniques is beyond the scope of this chapter, but readers are referred to excellent reviews and book chapters on the field for further information (Gurunathan and Levitus 2008; Jung and Van Orden 2005; Wallace et al. 2000).

2.3.2 Multiparameter Fluorescence Detection

Multiparameter fluorescence detection (smMFD) shares some common features with the smFCS techniques described previously in terms of targeting freely diffusing samples and using point detectors. However, smMFD methods use time-correlated single-photon counting (TCSPC) techniques to characterise the nucleic acid structure using simultaneously the complete set of fluorescence observables available (Sisamakis et al. 2010). For a nucleic acid structure labelled with a FRET pair, this entire set of fluorescence variables constitutes an 8-D parameter space that includes anisotropy, lifetime, intensity (stoichiometry), detection time, excitation and emission wavelength, fluorophore quantum yield and distance between fluorophores. Briefly, in smMFD, a pulsed laser excites the molecules labelled with donor and acceptor fluorophores when they pass through a small sample volume at the focal spot of the laser. This makes possible the simultaneous recording of various fluorescence parameters such as fluorescence lifetime, emission intensity and anisotropy of donor and acceptor. The detection of more than one parameter at the same time provides a means to represent and analyse the data using multidimensional histograms and allows to filter 'true' FRET events, induced by a change in molecular conformation, from those originating due to poor labelling, mostly lack of acceptor, and from variations in the quantum yield and rotational freedom of each dye. If uncorrected, these effects may lead to incorrect interpretations, particularly at low FRET efficiencies where the lack of acceptor dye may be interpreted as a very large distance. Thus, smMFD offers the possibility to test assumptions that are often considered to be valid a priori when using other single-molecule FRET techniques. For instance, local quenching of the donor and acceptor that may affect the R_0 value, differences in the mobility of the dyes that compromise the assumption of a 2/3 value for the orientation factor (κ^2) and the influence of the linker in the behaviour of the dye (Kühnemuth and Seidel 2001; Sisamakis et al. 2010).

It is beyond the aim of this chapter to describe the basis of smMFD and TCSPC techniques, but very detailed analysis of the methods and mathematic models has been reported by some of the pioneering groups on the field (Kudryavtsev et al. 2007; Sisamakis et al. 2010). The potential of this technique was demonstrated on different MFD–FRET assays. Some examples are the observation of the structure of the enzyme–substrate complex for the HIV-1 reverse transcriptase (Rothwell et al. 2003), the structural dynamics of the exocytose-related protein syntaxin-1 (Margittai et al. 2003) and the accurate determination of intramolecular distances within various branched DNA structures (Sabir et al. 2011; Wozniak et al. 2008).

2.3.3 Alternating-Laser Excitation

Alternating-laser excitation (ALEX), also known as pulsed interleaved excitation (PIE), allows to study simultaneously the structure and dynamics of nucleic acids labelled with a FRET pair and shares with MFD the ability to filter artefacts on the FRET reading caused by partial labelling. ALEX can be used either in combination with TIR for surface-immobilised nucleic acids or with confocal microscopy for freely diffusing molecules. Both cases need two different lasers to alternatively excite donor and acceptor on a nanosecond, microsecond or millisecond timescale, each one with different technical characteristics. In addition, ALEX is suitable for multicolour analysis and can incorporate a third and a fourth laser. The observation of more than two fluorophores within the same molecule enables to measure more inter-dye distances and create a structural model based on distance mapping. ALEX results are presented as two-dimensional histograms where it is possible to distinguish different populations according to their FRET efficiency and donor–acceptor stoichiometry. Thus, direct excitation of the donor and acceptor provides a way to isolate conformers and discriminate those species labelled only with donor or acceptor from those singly labelled (Lee et al. 2005a, b). The details of ALEX and its multiple variations (ns-ALEX, μs-ALEX, ms-ALEX) have been described by Hohlbein et al. (2014) and Kapanidis et al. (2005).

3 Single-Molecule Sequencing of Nucleic Acids: Zero-Mode Waveguides

The requirement to work in the picomolar range (50–500 pM) to achieve a good spatial separation that allows to identify isolated single molecules has constituted for a long time a significant barrier for the wider application of these techniques. Indeed, many enzymatic processes and most biological interactions require higher concentrations of substrate and/or interacting partners. This barrier known as the ‘concentration problem’ has recently been overcome by two different approaches: (1) encapsulation of reagents into a nanocontainer (i.e. lipid vesicle) to increase the effective concentration (see Sect. 2.1.1) and (2) the use of zero-mode waveguides (ZMW), which is described in this section.

The development of single-molecule technologies for DNA sequencing exemplifies how ZMWs have allowed the field to access important biological systems well beyond the concentration limit. To perform its function, the DNA polymerase requires micromolar to millimolar concentrations of fluorescent-labelled nucleotides. For this to be viable at single-molecule level, the excitation volume had to be reduced to the zeptolitre range in order to reach millimolar concentrations of the sample whilst still monitoring only one dye in that volume (Dulin et al. 2013). ZMWs consist of an array of nanoscale holes in a metal film deposited on a fused silica or quartz substrate. Hole dimensions can vary from a few tens to around 300 nm in diameter and 100 nm

in depth. In the study of the DNA polymerisation, each hole might contain one single polymerase immobilised at the bottom, whilst the majority of dye-labelled nucleotides remain outside the nanopore with occasional diffusion of single nucleotides inside the nanopore region. Wide-field excitation can be used in the real-time sequencing study of a DNA strand by following the addition of the four distinct deoxyribonucleoside triphosphates labelled with four different dyes (Eid et al. 2009). The attachment of the dye to the end of the phosphate chain allows the addition of a new labelled nucleotide in the adjacent position. Hence, real-time sequencing requires the use of dyes placed on the third phosphate group of the nucleotide. The little volume illuminated allows the selective observation of single nucleotides whilst they are added to the growing strand. In this step, dyes are easily removed and diffuse out of the ZMW, so they no longer contribute to the collected fluorescent signal. Since the detection signal corresponds to fluorescent pulses of the dyes, the different duration of these pulses could be associated to the enzymatic mechanism. Therefore, in addition to the DNA sequence, ZMWs can also provide information about the kinetics of the process (Eid et al. 2009).

4 Single-Molecule Studies of Branched DNA

4.1 Guanine Quadruplexes

Guanine-rich DNA or RNA sequences can adopt a wide variety of four-stranded structures called G-quadruplexes. Their formation can be usually predicted by the presence of the motif sequence $G \geq 3 N_{1-7} G \geq 3 N_{1-7} G \geq 3 N_{1-7} G \geq 3$, where N can be any base (Maizels and Gray 2013). The primary unit is the G-quartet, a square planar assembly of four guanine bases. G-quartets can form stacks that are mainly stabilised by monovalent cations, such as Na^+ and K^+. These cations interact with the oxygen atoms of the bases to counteract the negative electrostatic potential at the centre of the quartet (Vummidi et al. 2013).

G-quadruplexes have been investigated for a wide range of DNA sequences in vitro (Burge et al. 2006). One of those sequences is found in the human telomeres, which carry an overhang of 100–200 nucleotides formed by TTAGGG repeats that can adopt G-quadruplex structures, and they have attracted considerable interest since the early 1990s. Later studies revealed some other genomic sequences that adopt G-quadruplex architectures, such as the non-coding region of the gene C9orf72, involved in frontotemporal dementia and amyotrophic lateral sclerosis (Haeusler et al. 2014); the promoter of the bcl-2 oncogene, which acts as an apoptosis inhibitor (Dai et al. 2006); c-kit (Rankin et al. 2005), c-MYC (Siddiqui-Jain et al. 2002) and Ras family proto-oncogenes (HRAS, KRAS and NRAS), involved in cellular growth (Cogoi and Xodo 2006; Membrino et al. 2010); and the hypoxia-inducible factor 1 (HIF-1), which regulates the transcription of over 60 genes involved in cellular homeostasis (Armond et al. 2005; Brooks et al. 2010; Verma et al. 2008).

Some of the earliest single-molecule FRET studies on the structure of G-quadruplexes were performed on the human telomere (htelo) sequence $(TTAGGG)_n$ and revealed an extreme conformational diversity (Fig. 5a) (Ying et al. 2003). These smFRET experiments were performed at various temperatures and at different sodium and potassium salt concentrations for freely diffusing and surface-immobilised molecules (Lee et al. 2005a, b). Statistical analysis of the interconversion rates using single-molecule histograms revealed the presence of several distinct structural populations. Based on their FRET values, these populations were mostly associated to one unfolded and two folded states of the G-quadruplex. The two long-lived folded structures that correspond to the most relevant species at physiological conditions were assigned to parallel and antiparallel conformations of the G-quadruplex coexisting in equilibrium. smFRET analysis of the influence of monovalent ions revealed that lower concentration of potassium salts is required to stabilise the folded states when compared to the sodium counterparts. In this study, it was also demonstrated that K^+ stabilises the antiparallel state, observed as an increase of the high-FRET population. The htelo G-quadruplex unfolds upon increasing the temperature at low K^+ concentrations, whilst at physiological concentrations of K^+ (100 mM), the folded state is stable even at 37 °C. The conformational heterogeneity observed for the htelo sequence by smFRET and the presence of additional mixed parallel and antiparallel

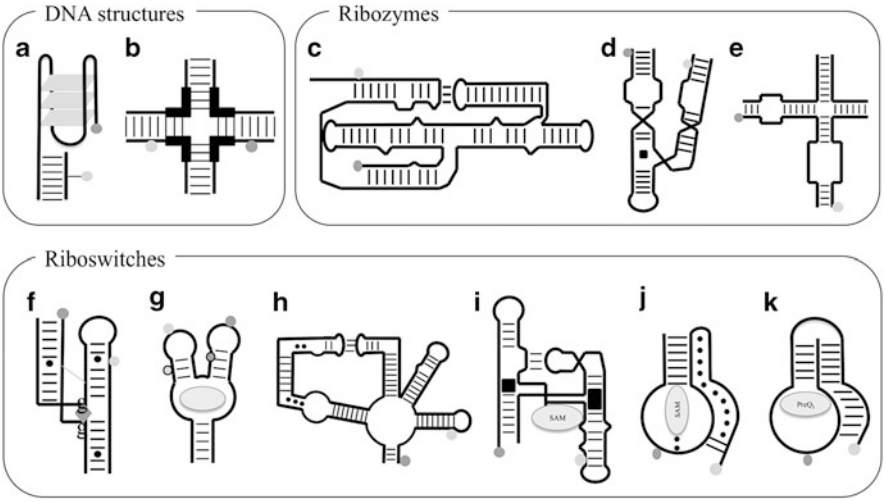

Fig. 5 Schematics of FRET assays on nucleic acid structures. Summary of the most widely studied nucleic acid structures by smFRET. Donor (*light grey*) and acceptor (*dark grey*) groups are shown. (**a**) Guanine quadruplex. (**b**) Holliday junction. (**c–e**) Three different ribozymes, small non-coding RNA fragments with catalytic activity: (**c**) Varkud satellite (VS) ribozyme, (**d**) hammerhead ribozyme and (**e**) natural form of the hairpin ribozyme. (**f–k**) Various structures of riboswitches that sense different metabolites: (**f**) cyclic di-GMP, (**g**) purine (guanine, which riboswitch is represented with circled dyes, and adenine, represented with non-circled dyes), (**h**) lysine, (**i**) SAM-I, (**j**) SAM-II and (**k**) Pre-Q1

conformations were recently confirmed by nuclear magnetic resonance (NMR) spectroscopy (Ambrus et al. 2006; Dai et al. 2007; Shirude and Balasubramanian 2008) and X-ray crystallography (Parkinson et al. 2002). More recently, two G-quadruplex sequences (kit-1 and kit-2) identified in the c-kit promoter region were studied by smFRET in freely diffusing conditions and encapsulated in lipid vesicles (Shirude et al. 2007). kit-1 is positioned between −87 and −109 bp upstream of the transcription start site and was shown to fold into a quadruplex in vitro (Rankin et al. 2005). kit-2 is positioned between −140 and −160 bp upstream of the transcription initiation site and was also shown to form a G-quadruplex structure by NMR and CD spectroscopy (Fernando et al. 2006). These studies confirmed that kit-1 and kit-2 can fold into non-duplex states within a natural extended DNA duplex (Shirude et al. 2007). Importantly, dynamic fluctuations in the c-kit quadruplexes were rare, even in single-stranded form, which is in contrast with the dynamics observed for the htelo sequence. Based on this difference, it was suggested that the dynamic behaviour of intramolecular DNA quadruplexes could be a property of each sequence and vary significantly between different quadruplexes. Moreover, the observation by smFRET of folded G-quadruplexes within the c-kit promoter not only challenges the general view that G- and C-rich sequences form very stable duplex sequences but also suggests a natural function for these motifs involving changes in DNA topology (Dai et al. 2007; Shirude and Balasubramanian 2008).

4.2 Holliday Junctions

DNA is not restricted to a static duplex or G-quadruplex organisation, and indeed, it can also adopt highly dynamic structures as exemplified by the branched architecture of the Holliday junction (HJ) (Holliday 1964). HJs are four-way DNA junctions that act as intermediates in the homologous recombination pathway, which involves the exchange of nucleotide sequences between two identical or very similar dsDNA molecules to repair DNA breaks in one of the duplexes, using the other duplex as a template. Movement of the crossover junction along the DNA is termed branch migration and, whether spontaneous or mediated by proteins, is a key step in various genetic processes. HJs can potentially adopt three structures: open, parallel and antiparallel. The four helical arms in the open form adopt a square shape, but only in the parallel form the two strands that have been exchanged are crossed (Liu and West 2004). smFRET studies on the HJ were carried out to investigate the formation and interconversion of these structures upon addition of Mg^{2+}. It is well known that metal ions, and in particular Mg^{2+}, can play a critical role in defining the most stable conformation of many DNA and RNA structures, but how they modulate HJ dynamics was poorly understood. Initial smFRET measurements in nonmigrating HJs with donor and acceptor molecules placed at the end of two arms of the Holliday junction (Fig. 5b) showed the presence of two conformers of the antiparallel structure and revealed that the open structure acts as an intermediate between these two conformers (McKinney et al. 2003). In contrast,

the parallel conformations were not observed, and their presence was determined to be insignificant (Joo et al. 2004; McKinney et al. 2004). These studies demonstrated the power of smFRET to investigate in real time the structural dynamics of a complex system such as the HJ.

More recently, smFRET was applied to migratable HJs to investigate the branch migration mechanism (Karymov et al. 2005). It was found that branch migration takes place in a stepwise fashion with the overall kinetics depending on the concentration of Mg^{2+} ions. In contrast to early models suggesting a parallel orientation of exchanging strands (Sigal and Alberts 1972), these smFRET studies demonstrated that migratable HJs dynamically fluctuate between a conformation favourable to migration (open conformation) and a folded conformer where migration is hindered. Importantly, it was confirmed that Mg^{2+} induces folding of the HJ in one of the folded conformations, thus terminating the branch migration phase. Additional studies also revealed that stepwise switching between migration and folding phases can be affected by irregularities (i.e. mismatches, nicked HJs) (Palets et al. 2010) and how certain sequences can modulate the junction dynamics and thus influence the branch migration rate (Karymov et al. 2008).

Lastly, the presence of four different arms in the Holliday junction makes it an attractive scaffold for the study of nucleic acid dynamics using multicolour FRET techniques. Four-colour FRET measurements on surface-immobilised HJ molecules were first reported by Lee et al. (2010). Here, each dye was attached to one of the four helices that conform the Holliday junction. The excitation of four different dyes allowed the observation of six intramolecular distances and their relative changes within a single nucleic acid structure, thus paving for the analysis of more sophisticated nucleic acid systems and protein–DNA/protein–RNA complexes.

5 Single-Molecule Analysis of Catalytic RNA

For many years, RNA was considered as a rather passive carrier of the genetic information to the ribosome for the production of proteins. However, this widely accepted notion changed when Thomas Cech (Kruger et al. 1982) and Sidney Altman (Guerrier-Takada et al. 1983) reported that certain RNA sequences exhibit catalytic properties similar to those previously thought to be exclusive of the protein world. The discovery of these ribonucleic acid enzymes, so-called ribozymes, fuelled the ‘RNA world hypothesis’. If RNA molecules can carry genetic information and also perform catalysis, then protein-based processes could have evolved from this into more modern biological systems. Thus, it is possible that RNA catalysis could have played a critical role for the development of early life on Earth. Naturally occurring ribozymes are normally classified according to their size. Large ribozymes (>300 nt) include the self-splicing group I and group II introns (Lilley 2005; Tremblay et al. 2009) and RNAse P (Kazantsev and Pace 2006). Another mechanistically distinct class of ribozymes with a much smaller size includes the hammerhead, hairpin, hepatitis delta virus (HDV) and Varkud

satellite (VS) ribozymes (reviewed in Lilley 2005). All these small ribozymes perform a self-cleaving transesterification reaction, generating a hydroxyl and cyclic phosphate termini that can be used to perform the reverse reaction. In the last few years, two additional ribozymes have been added to this group: the *glmS* ribozyme (Ferré-D'Amaré 2010), which also acts as a regulatory element, and the twister ribozyme (Roth et al. 2014). A common feature shared by all these catalytic RNAs is the requirement to form a very specific 3-D structure to support catalysis (Lilley 2005). This process, known as RNA folding, involves a very complex interplay between the self-recognition capabilities of RNA molecules and the effect of diffuse mono- and divalent metal ions shielding the electrostatic repulsion of the negatively charged phosphate groups. Thus, the catalytic activity of a particular ribozyme is strongly linked to its folding state and dynamics, which can be exceptionally well explored using smFRET techniques (Zhuang et al. 2002). Various excellent reviews have been done recently on single-molecule ribozyme analysis (Cochrane and Strobel 2008; Ditzler et al. 2007; Zhuang 2005). Moreover, it is important to note that although DNA does not appear to perform catalysis in nature, single-stranded DNA can be engineered to perform metal-dependent catalysis in a similar manner as metalloproteins, as it has been shown at single-molecule level for the 8-17 DNAzyme (Kim et al. 2007a, b). Here, we will focus on a detailed description of the hairpin ribozyme folding and function because it is the most studied ribozyme at single-molecule level and exemplifies how the application of smFRET has contributed to unravel the folding and catalytic steps of a small catalytic RNA. Recently, smFRET has been also applied to investigate the folding of the VS (Fig. 5c) (Pereira et al. 2008) and the hammerhead ribozymes (Fig. 5d) (McDowell et al. 2010).

5.1 Hairpin Ribozyme

Hairpin ribozymes are small catalytic RNA motifs found in the satellite RNAs of arabis mosaic virus (arMV), tobacco ringspot virus (TRsV) and chicory yellow mottle virus (CYMoV) that catalyse the self-cleaving reaction and ligation of its own backbone (Bajaj and Hammann 2014). The hairpin ribozyme consists of a four-way RNA junction with two internal loops (loop A and loop B) on adjacent helices (Fig. 5e). The formation of the active site strongly depends on the docking interaction between these two loops, which induces a 10^5 increase in the cleavage rate. A minimal form lacking the two helices with no loops still has catalytic activity, although the transition between open and folded state requires much higher concentrations of Mg^{2+} (Tan et al. 2003). The folding and catalytic activities of both hairpin ribozymes have been extensively characterised using biochemical assays and also at single-molecule level. Here, the power of the technique to uncover short-lived transient states, minor subpopulations and molecular heterogeneity was exploited to provide a complete picture of the reaction pathway. By labelling the termini of the two stems carrying the interacting loops, three distinct FRET

populations were found in the minimal form of the hairpin ribozyme using either a TIR or a scanning confocal microscope (Zhuang et al. 2002). These populations were assigned to the catalytically inactive undocked state, the docked conformation where both loops are brought into close contact, and an intermediate state where the substrate is not bound. As previously suggested by biochemical studies, cleavage was only observed in the docked state. Interestingly, for such a simple RNA enzyme, analysis of the rates for loop–loop docking and undocking revealed a very complex dynamic behaviour with a single docking rate (~0.008 s^{-1}) but up to four docking rates with values ranging from 0.005 s^{-1} to 3 s^{-1}, leading to a complex cleavage kinetics. Surprisingly, it was found that ribozyme molecules tend to repeatedly remain in the docked state for a similar time, providing one of the first evidence for 'memory effects' in individual molecules (Zhuang et al. 2002). It was reasoned that the presence of a broad range of undocking rates and the observed memory effects could arise from slightly different configurations of loops A and B the docked state that exhibits a low interconversion dynamics. This explanation was further supported by NMR studies, which showed evidence for metastable conformations of loops A and B (Butcher et al. 1999).

In a later study, the folding and function of the natural form of the hairpin ribozyme containing a four-way DNA junction was compared to the minimal form using smFRET (Tan et al. 2003). In the absence of the interacting loops, the four-way junction exhibited a Mg^{2+}-dependent interconversion dynamics between a distal (U_D) and a proximal state (U_P) that corresponds to the antiparallel conformation of the junction. Importantly, these studies on the natural form of the hairpin ribozyme demonstrated that the ribozyme inherits the intrinsic dynamics of the four-way DNA junction and rapidly fluctuates between the U_D and U_P states and confirmed that the U_P state is an obligatory intermediate in the folding pathway of the ribozyme towards the catalytically active form. These studies were critical to confirm that the dynamic heterogeneity of the hairpin ribozyme is linked to the docking process between the two loops, as the four-way junction lacking the loops exhibited a much lower level of heterogeneity. Thus, the intrinsic dynamics of the four-way junction acts as a 'folding enhancer' to promote the active encounter between both loops, allowing a three orders of magnitude increase in the folding rate of the natural ribozyme. Similar 'folding enhancers' have also been observed for other small catalytic RNAs such as the hammerhead ribozyme, in which the interaction between the two loops at stems P1 and P2 was shown to be critical to support catalysis at physiological concentrations of Mg^{2+} ions (Penedo et al. 2004).

In two different studies, the equilibrium between cleavage and ligation was investigated using ribozyme constructs where the 2′-deoxynucleotide placed at the −1 position of the active site to prevent cleavage was replaced by the wild-type nucleotide (Tan et al. 2003). The two catalytically active hairpin structures were engineered in such way that cleavage would lead to products of different lengths and therefore stability (Wilson et al. 2007). In both studies, the authors took advantage of the different dynamics exhibited by intact ribozyme and the four-way junction resulting from cleavage to monitor the catalytic step. Natural ribozyme molecules were labelled with the FRET pair at the end of the arms A and B that

carry the loops. Real-time addition of Mg^{2+} induced loop–loop docking characterised by a high and stable FRET value. Subsequent cleavage and rapid release into solution of a short 3 bp product was monitored by the appearance of rapid transitions between high- and low-FRET states typical of the four-way junction (Tan et al. 2003). Statistical analysis of a series of cleavage reactions gave a cleavage rate of ~1 min^{-1}. To be able to record multiple cycles of cleavage and ligation, the length of the A arm was increased to 7 bp to favour the retention of the cleavage product, which can therefore serve as substrate for ligation (Nahas et al. 2004). Upon addition of Mg^{2+} ions, these ribozymes exhibited cyclic switching between two dynamic regimes: a stable high-FRET docked state (ligated form) and a second regime with fast fluctuations between high- and low-FRET states corresponding to the cleaved form. From these experiments it was determined that the cleavage/ligation equilibrium is significantly biased towards ligation ($K = k_L/k_c = 34$). In the natural context of the (−) strand of the tobacco ringspot virus satellite RNA, such shift towards ligation might be important to maintain the integrity of the circular (−) strand whilst serving as a template for the synthesis of the (+) strand (Wilson et al. 2005).

In another smFRET study, Okumus et al. (2004) introduced the use of lipid vesicles to investigate whether the dynamic heterogeneity observed for the hairpin ribozyme could be induced by non-specific interactions with the surface in which they were immobilised. The results using vesicle encapsulation were identical to those reported for ribozymes immobilised using biotin–streptavidin, thus confirming that the observed heterogeneity is intrinsic to the RNA.

6 Single-Molecule Analysis of Regulatory RNA

For a primitive RNA world to be viable, in addition to catalysis, RNA should also be able to perform regulatory functions. A decade ago, a second RNA revolution confirming this aspect took place when it was found that indeed certain non-coding messenger RNA sequences (mRNA) were able to use feedback regulatory mechanisms to control gene expression without the requirement of any helper protein (Mironov et al. 2002; Nahvi et al. 2002; Winkler et al. 2002a, b). These regulatory RNAs, so-called riboswitches, are found in the 5′-untranslated region (5′-UTR) of mRNA in bacteria and sense small metabolites to regulate the expression of genes normally associated to the transport, biosynthesis or degradation of the cognate metabolite (Blouin et al. 2009a, b). Riboswitches are composed of two domains: an aptamer domain and an expression platform. The aptamer is the most conserved part through evolution as it is involved in ligand detection, whilst the expression platform can vary in sequence and structure. The majority of aptamer domains investigated have revealed a tight association to the cognate ligand, where almost every functional group of the ligand interacts with a specific region of the RNA aptamer to ensure a very high ligand-binding specificity. Importantly, formation of the RNA–ligand complex has a direct influence on the structure of the downstream

expression platform, which is used to regulate gene expression by folding into various secondary motifs that are mutually exclusive (Blouin et al. 2009a, b; Winkler and Breaker 2003).

To date, more than 20 classes of riboswitches have been reported for different types of ligands, including adenine (Mandal and Breaker 2004), guanine (Batey et al. 2004), lysine (Grundy et al. 2003), flavin mononucleotide (FMN) (Winkler et al. 2002a, b), adenosylcobalamin (AdCo) (Nahvi et al. 2002), thiamine pyrophosphate (TPP) (Winkler et al. 2002a, b), glycine (Mandal et al. 2004), S-adenosylmethionine (SAM) (Winkler et al. 2003), 9-glucosamine-6-phosphate (*glmS*) (Jansen et al. 2006) and pre-queuosine1 (Pre-Q1) (Roth et al. 2007). Riboswitches can regulate gene expression by different mechanisms such as modulating the formation of Rho-independent transcriptional terminators, controlling mRNA splicing and mRNA stability or sequestering the Shine–Dalgarno sequences required for translation initiation (Bastet et al. 2011; Lemay et al. 2011). Riboswitches have attracted considerable interest as targets for antibacterial drug development (Blount and Breaker 2006; Deigan and Ferré-D'Amaré 2011; Mulhbacher et al. 2010; Winkler and Breaker 2005). Several recent reviews have summarised the architectures and regulatory pathways for many riboswitch structures (Montange and Batey 2008; Serganov and Nudler 2013).

Since the first smFRET study reporting the folding pathway of the adenine riboswitch aptamer domain (Lemay et al. 2006), the application of these techniques to other metabolite-sensing mRNAs has experienced a stunning growth. smFRET studies have now been reported for the aptamer domains of S-adenosylmethionine (SAM-I) (Eschbach et al. 2012; Heppell et al. 2011), SAM-II (Haller et al. 2011a, b), Pre-Q1 (Suddala et al. 2013), c-di-GMP riboswitches (Wood et al. 2012), lysine (Fiegland et al. 2012) and thiamine pyrophosphate (TPP) (Haller et al. 2013) (Fig. 5f–k). The majority of these studies have focused on elucidating how the riboswitch harnesses the interplay between RNA folding and ligand recognition to control the gene regulation process. The emerging picture arising from the application of these fluorescence techniques to investigate riboswitch dynamics, both at ensemble and single-molecule level, has been recently the focus on several excellent reviews (Haller et al. 2011a, b; Heppell et al. 2009; Karunatilaka and Rueda 2009; Lemay et al. 2009; McCluskey et al. 2014; Savinov et al. 2014; St-Pierre et al. 2014). In this chapter, we will use the aptamer domain of the adenine-sensing riboswitch as a model system to describe how smFRET techniques can use to unravel the complex dynamic behaviour of these regulatory mRNAs.

6.1 SmFRET Characterisation of Purine-Sensing Riboswitches

Adenine- and guanine-sensing aptamer domains shared a common junction architecture comprising three helical domains (P1–P2–P3) (Serganov et al. 2004). Loops

positioned at the end of stems P2 and P3 have been shown by X-ray crystallography and biochemical methods to be crucial for the function of the aptamer domain (Allnér et al. 2013; Delfosse et al. 2010; Serganov et al. 2004). Very importantly, these crystal structures have shown a very compact ligand-bound state hold together by tertiary interactions and with the ligand directly involved in a Watson–Crick base pair with the uracil nucleotide at position 65. The importance of this nucleotide in ligand specificity has been confirmed by replacing U65 by C, which converts the aptamer domain into a guanine-responsive motif (Lemay and Lafontaine 2007; Mandal and Breaker 2004; Mulhbacher and Lafontaine 2007; Tremblay et al. 2011).

The formation of the loop–loop interaction in the aptamer domain of the adenine riboswitch was studied by smFRET using a surface immobilisation approach (Lemay et al. 2006). Here, using the information provided by the crystal structure, donor and acceptor FRET labels were placed in loops P2 and P3 at locations that did not alter the aptamer ability to fold and bind the ligand. To perform this orthogonal labelling, the aptamer sequence was divided into two separate strands, each of them individually labelled with either the donor or the acceptor and subsequently ligated using T4 RNA ligase (Lemay et al. 2006, 2009). The folding of the aptamer domain was analysed as a function of Mg^{2+} ions at 50 ms time resolution. The predominant low-FRET ($E_{app} \sim 0.25$) population in the absence of ions (unfolded state, U) shifted to very high-FRET ($E_{app} \sim 0.9$) (docked state, D) population at saturating concentrations of Mg^{2+} ions (>5 mM Mg^{2+}). This population was assigned to the formation of the loop–loop interaction between stems P2 and P3 that brings in close proximity the FRET pair resulting in a high FRET efficiency. Strikingly, using a high time resolution (16 ms EMCCD integration time), an intermediate state (I) with a FRET value between those of the U and D states was detected at subsaturating concentrations of Mg^{2+} ions. Analysis of >800 traces confirmed that most aptamer molecules transit from the U to D state through this intermediate conformation. Although the exact nature of this I state has not yet been determined, it has been suggested that may result from the stacking of P1 and P3 helices as observed in the crystal structure (Gilbert and Batey 2006). Information regarding the role of the ligand in the folding process was also obtained from these smFRET studies. In the absence of ligand, the folding and unfolding rates showed a high degree of heterogeneity (~100-fold), reminiscent of that observed for the hairpin ribozyme (Tan et al. 2003). However, upon addition of the ligand, the dynamic heterogeneity for both processes, U → D and D → U, decreased significantly. A detailed analysis of the interconversion relates revealed a ~2-fold acceleration of the folding rate, suggesting that the ligand actively participates in the formation of the loop–loop interaction and in the folding process of the core of the riboswitch aptamer domain.

6.2 SmFRET Combined with Chemical Denaturation

Although the use of chemical denaturants such as guanidinium chloride and urea is a common method in smFRET studies of protein folding (Schuler and Hofmann

2013), only a handful of single-molecule studies have reported their application to investigate RNA folding processes (Bokinsky et al. 2003; Holmstrom and Nesbitt 2014; Karunatilaka and Rueda 2009). This is a surprising difference if we take into account that the applicability of urea to provide new insights into the thermodynamics of RNA folding and the nature of the rate-limiting step has already been demonstrated at the ensemble level (Sosnick and Pan 2003; Treiber et al. 1998). A recent study used the aptamer domain of the adenine riboswitch to investigate the folding and ligand recognition mechanisms using the competing interplay between folding agents (i.e. Mg^{2+}, ligand) and unfolding agents such as urea (Dalgarno et al. 2013). The authors separately analysed the influence of increasing concentrations of urea on the docking and undocking rates of surface-immobilised adenine aptamers at saturating (~2 mM) and subsaturating (~100 μM) concentrations of divalent metal ions in the presence and absence of adenine ligand.

From the analysis of the undocking rates, with and without ligand added, as a function of urea concentration, it was possible to (1) quantify the degree of aptamer stabilisation due to ligand-binding and (2) differentiate ligand-bound docked states (D_{LB}) from ligand-free aptamers (D_{LF}) even when both states exhibit identical values of FRET efficiency ($E_{app} \sim 0.9$) (Dalgarno et al. 2013). The ability to differentiate these states was based on the fact that the formation of the aptamer–ligand complex strongly protects the D_{LB} state against urea-induced denaturation. It was found that ligand-bound aptamers exhibited in average a 50-fold longer lifetime ($k_{undock} \sim 0.045 \pm 0.003\ s^{-1}$), in the presence of 5 M urea than ligand-free states ($k_{undock} \sim 2.1 \pm 0.1\ s^{-1}$). This 50-fold stabilisation of the docked state due to ligand binding agrees well with values reported by single-molecule force manipulation (Greenleaf et al. 2008). At lower concentrations of urea, the smFRET trajectories displayed a combination of fast and slow undocking events from an identical FRET value ($E_{app} \sim 0.9$) to an $E_{app} \sim 0.3$ corresponding to the undocked state. This work provided the first experimental evidence for the use of denaturants in single-molecule FRET studies to differentiate otherwise identical states in terms of FRET efficiency, purely from their different stability against urea-induced denaturation.

Similarly, the analysis of the docking rates in the presence of urea, with and without adenine ligand, provided additional insights into the fine mechanistic details of the aptamer–ligand interaction. It was found that increasing concentrations of urea decelerate the docking rate (k_{dock}) of the aptamer in the absence of ligand and this was taken as evidence for a trap-free rate-limiting step in the folding of the ligand-free aptamer. Moreover, the relative decrease in the folding rate in the presence of urea (~2- to 3-fold) was independent on the concentration of Mg^{2+} ions (Dalgarno et al. 2013). In contrast, in the presence of ligand, the influence of urea on the docking rate was strongly dependent on the concentration of Mg^{2+} ions and varies from 2-fold at saturating Mg^{2+} ions (>2 mM) to ~8-fold at concentrations <100 μM. These results were taken as evidence for a ligand-induced switching in the rate-limiting step for aptamer folding. At saturating concentrations of Mg^{2+} ions, the rate-limiting step for ligand-free and ligand-bound aptamers is similar and involves the formation of native tertiary contacts between both loops. This is

similar to the rate-limiting step proposed for the docking process of the hairpin ribozyme (Bokinsky et al. 2003). In contrast, ligand binding to the aptamer at subsaturating concentrations of Mg^{2+} ions, in which the loop–loop is not efficiently stabilised, requires the interaction with specifically trapped Mg^{2+} ions to further progress to the native state. Such requirement for specific positioning of divalent metal ions along the aptamer structure agrees with the observation of up to five trapped Mg^{2+} ions in the crystal structures of the ligand-bound aptamer domain (Serganov et al. 2004). In summary, this study exemplifies how balancing the competing effect of folding and unfolding agents constitutes a more powerful approach to uncover mechanistic detail of RNA folding and RNA–ligand interactions that otherwise will remain hidden and to manipulate the RNA folding landscape.

7 In Situ Generated Fluorescent RNA Aptamers for Live Cell Diagnostics

Fluorescence imaging in living cells has been mostly confined to the use of fluorescent proteins such as the green fluorescent protein (GFP) and its derivatives (Chalfie et al. 1994; Lippincott-Schwartz and Patterson 2003). GFP contains a small chromophore, the 4-hydroxybenzylidene imidazolinone (HBI) (Fig. 6c), residing inside the barrel-like structure of the native protein, thus reducing the contribution of non-radiative processes and increasing its overall brightness. However, in 2011, the Jaffrey lab (Paige et al. 2011) reported an RNA sequence, the Spinach aptamer, which mimics the GFP fluorescent properties, thus opening new avenues for imaging tagged RNAs in living cells. The 98-nt Spinach aptamer (Fig. 6a) senses the 3,4-difluoro-4-hydroxybenzylidene imidazolinone (DFHBI) (Fig. 6e), an analogue of the GFP fluorophore that exists as a nonfluorescent species in free solution and switches to an emissive form upon binding to the RNA aptamer.

The Spinach RNA aptamer was identified by systematic evolution of ligands by exponential enrichment (SELEX) (Ellington and Szostak 1990) using a library of 5×10^{13} RNA molecules and searching for RNA sequences initially optimised to bind 3,5-dimethoxy-4-hydroxybenzylidene imidazolinone (DMHBI) (Fig. 6d). The emission spectra of the aptamer–DMHBI complex showed an emission peak at 529 nm and an excitation maximum at 398 nm. The brightness of the complex was 12 % relative to GFP and the dissociation constant value was 464 nM (Paige et al. 2011). In order to generate RNA–ligand complexes that mimic more enhanced GFP (EGFP) than GFP, RNA sequences were optimised to bind the DFHBI, which is exclusively in the phenolate form of a GFP-like fluorophore because the fluorine residues reduce the pK_a. The RNA–DFHBI complex (Spinach aptamer) showed a marked quantum yield of 0.72 which is 20 % higher than EGFP (Paige et al. 2011). The ability of the Spinach aptamer to be used as an in situ RNA tagging method was demonstrated by fusing it to the 3′ end of 5S, a small non-coding RNA that associates with the large ribosomal subunits, and transfecting it into human

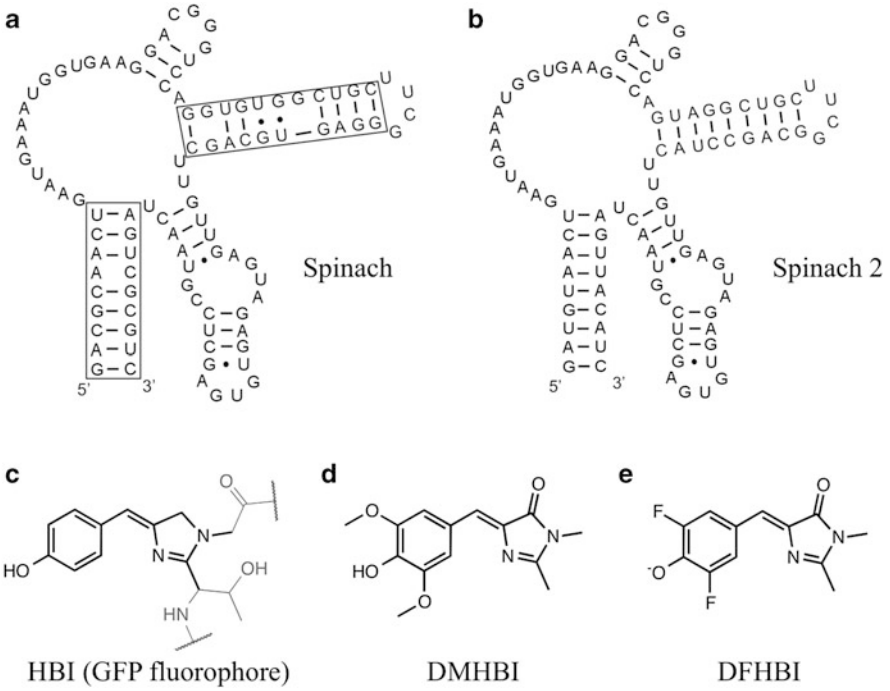

Fig. 6 Schematics of the RNA Spinach aptamers as well as the HBI fluorophore and two of its derivatives. (**a**) Sequence of the Spinach RNA, an aptamer that senses an analogue, DMHBI or DFHBI, of the GFP fluorophore. (**b**) Sequence of the Spinach 2 aptamer, which has been designed to improve the thermostability and the folding efficiency. (**c**) GFP chromophore, HBI, formed after an autocatalytic cyclization and oxidation of the three-residue sequence Ser^{65}–Tyr^{66}–Gly^{67}. This compound exists as a nonfluorescent species when free in solution and switches to an emissive form upon binding to the Spinach RNA. (**d**) DMHBI, derivative of the GFP chromophore. (**e**) DFHBI, derivative of HBI with improved emission. The fluorines reduce the pK_a of the compound, and therefore, it is only present on its phenolate (anionic) form at neutral pH

embryonic kidney (HEK) 293 T cells. 5S–Spinach complex was detected with a distribution similar to that of endogenous 5S, thus confirming its applicability for in vivo imaging of RNA sequences. Interestingly, in vitro and in vivo measurements of Spinach–DFHBI complexes showed that its brightness is only 80 % of that of GFP and 53 % of that of EGFP (Strack et al. 2013). Later studies confirmed that the RNA–DFHBI complex has a propensity to misfold in live cells, and a second version of the RNA sequence (Spinach 2) was engineered with improved thermostability and folding efficiency, particularly when fused to other RNA sequences (Fig. 6b) (Strack et al. 2013).

A recent single-molecule study on the Spinach aptamer has shed some light into the photophysical properties of the RNA–ligand complex. This study explains its reduced fluorescence under cellular and high-resolution imaging conditions compared to what should be expected base on its brightness (Han et al. 2013). Using surface-immobilised Spinach aptamers and 5 μM concentration of DFHBI, it was found that the fluorescence of the Spinach aptamer rapidly decays to ~5 % of its

initial value within 2 s. However, in contrast to GFP, which it is known to undergo photoconversion to long-lived dark states and/or irreversible photobleaching (Dickson et al. 1997; Patterson et al. 1997), the emission of the Spinach aptamer spontaneously recovered to ~95 % of the initial value following a period without light. This suggested that the fast loss of emission is a light-induced process, most likely involving its reversible conversion to a nonfluorescent state. The reversibility of this process was independent on the excitation power, but it depended strongly on the concentration of DFHBI. The fluorescence recovery rate increased from 0.08 s^{-1} to 2 s^{-1} as the concentration of DFHBI varied from 1 μM to 200 μM. Insights into the molecular basis for the observed reversible transition of DFHBI to a dark state were obtained by monitoring the variations in the absorption spectrum following illumination at 405 nm. At these conditions, a decrease in the absorption spectrum and a red shift were observed. These features are similar to those involved in the photoisomerization process of photoswitchable proteins (Andresen et al. 2007) and are spectroscopic hallmarks of molecular changes in the configuration of the chromophore. Based on this evidence, it was proposed that DFHBI might undergo a light-induced *cis*/*trans* isomerization process leading to a dark state, similar to that observed in other fluorescent probes (i.e. cyanine dyes) (Dempsey et al. 2009; Weiss 1999). Although this needs further studies, a model was proposed to explain the behaviour of the 'green RNA' complex. According to this model, under illumination, the bound DFHBI dye undergoes a photoisomerization step that results in fast dissociation and subsequent binding of a new DFHBI molecule that restores the fluorescence. Although this model provides an explanation to the observed fluorescence decay of DFHBI induced by light, it is not possible at this stage to completely rule out that this effect may also relate, at least partially, to the previously mentioned propensity of the Spinach RNA sequence to misfold. Additional information on the photophysics of the Spinach 2 aptamer will contribute to clarify this aspect.

Independently on the exact functional mechanism of these 'green RNAs', it is clear that they fill a current gap in live cell imaging with far-reaching applications. For instance, it has been recently reported the use of Spinach aptamer in fusions with other small-molecule sensing RNA aptamers to detect intracellular levels of adenosine 5′-diphosphate (ADP) and S-adenosylmethionine (SAM) in *Escherichia coli* (Paige et al. 2012). Because RNA aptamers can be engineered relatively easily against a broad variety of biomolecules (Cho et al. 2009), fused Spinach RNA constructs should enable to image essentially any small-molecule target in living cells.

8 From Sensing to Manipulating Nucleic Acids: Single-Molecule Hybrid Technologies

The development of single-molecule techniques to investigate biomolecular processes has traditionally followed two almost independent routes: (1) single-molecule mechanical manipulation and (2) single-molecule fluorescence detection

(Monico et al. 2013). In recent years, it has become clear that the combination of both into hybrid techniques will provide a much more powerful approach to investigate biological systems by enabling not only to detect (fluorescence) but also to disrupt (mechanical manipulation) the nucleic acid sequence. In the context of nucleic acid diagnostics, the combination of single-molecule fluorescence with force-based manipulation methods using either atomic force microscopy (AFM) or optical (OT)/magnetic (MT) traps represents an emerging field that has already delivered insights into nucleic acid function with an unprecedented level of detail. It is beyond the scope of this chapter to describe in detail the technical aspects of combining both single-molecule fields, but the reader is referred to recent reports by the Block and Ha labs (Fazal and Block 2011; Ha 2014).

Early attempts in the development of these hybrid techniques combined optical traps and smFRET to investigate the hybridization and mechanical properties of double-stranded DNA (Lang et al. 2003). In order to separate the two strands, the optical trap applies piconewton forces, and the rupture event can be followed by the loss of FRET signal between two dyes positioned in each strand. A later study from Hohng et al. (2007) provided a tool to observe conformational changes in nucleic acids with the use of subpiconewton forces. The hybrid technique that combines confocal and force spectroscopy was applied to investigate the effect of weak forces on the conformational landscape of immobilised Holliday junctions (HJ). By merging smFRET and OT, it was possible to gently stretch the Holliday junction along different directions and monitor the influence of this mechanical manipulation along specific distance vectors using smFRET. By probing the dynamics of the HJ in response to stretching forces oriented along different directions, it was possible to map the structure and location of the transition states along the HJ conformational landscape. This work clearly demonstrated that unlike DNA or RNA hairpins, where high forces (~15 pN) are required to induce mechanical distortions, much lower forces are needed to probe by smFRET the conformational changes and the accompanying energy barriers in a variety of biologically relevant nucleic acid structures, on their own and in complex interactions with small molecules and proteins.

9 Future Perspectives

In the last decade, it has become clear that the application of single-molecule techniques to investigate the structure and function of nucleic acids provides information at an unprecedented level of detail. Many of these single-molecule diagnostic methods have now reached a mature state, and as a result, commercial equipment is now available in many biophysics and molecular biology laboratories. However, the field still faces many challenges, and further technical developments in many areas are awaiting. Additional methods to overcome the concentration limit barrier so weaker interactions can be measured, without the need for the costly and time-consuming fabrication of zero-mode waveguides, are needed. By opening

the field to micromolar range concentrations of fluorescent species, aptamer-based fluorescence sensing and high-throughput screening will become more accessible. Another important area in the context of nucleic acid research is to exploit the applicability of single-molecule fluorescence technologies to investigate co-transcriptional processes. Although this area has been explored using mechanical-based sensing of the nascent RNA, the application of smFRET methods is still clearly underdeveloped. Such techniques will be extremely valuable to understand the folding and function of non-coding regulatory mRNAs in a closer context to that taking place in vivo.

Acknowledgements We would like to thank EPSRC, BBSRC, Wellcome Trust and the University of St Andrews for supporting this work, and we also wish to thank all members of JCP lab for critical reading of the manuscript.

References

Aitken CE, Marshall RA, Puglisi JD (2008) An oxygen scavenging system for improvement of dye stability in single-molecule fluorescence experiments. Biophys J 94:1826–1835

Allnér O, Nilsson L, Villa A (2013) Loop-loop interaction in an adenine-sensing riboswitch: a molecular dynamics study. RNA 19:916–926

Ambrus A, Chen D, Dai J et al (2006) Human telomeric sequence forms a hybrid-type intramolecular G-quadruplex structure with mixed parallel/antiparallel strands in potassium solution. Nucleic Acids Res 34:2723–2735

Andresen M, Stiel AC, Trowitzsch S et al (2007) Structural basis for reversible photoswitching in Dronpa. Proc Natl Acad Sci USA 104:13005–13009

Armond R, Wood S, Sun D et al (2005) Evidence for the presence of a guanine quadruplex forming region within a polypurine tract of the hypoxia inducible factor 1alpha promoter. Biochemistry 44:16341–16350

Bajaj P, Hammann C (2014) Characterization of hairpin ribozyme reactions. Methods Mol Biol 1103:97–111

Bastet L, Dubé A, Massé E et al (2011) New insights into riboswitch regulation mechanisms. Mol Microbiol 80:1148–1154

Batey RT, Gilbert SD, Montange RK (2004) Structure of a natural guanine-responsive riboswitch complexed with the metabolite hypoxanthine. Nature 432:411–415

Benesch RE, Benesch R (1953) Enzymatic removal of oxygen for polarography and related methods. Science 118:447–448

Betzig E, Chichester RJ (1993) Single molecules observed by near-field scanning optical microscopy. Science 262:1422–1425

Biffi G, Tannahill D, McCafferty J et al (2013) Quantitative visualization of DNA G-quadruplex structures in human cells. Nat Chem 5:182–186

Blouin S, Craggs TD, Lafontaine DA et al (2009a) Functional studies of DNA-protein interactions using FRET techniques. Methods Mol Biol 543:475–502

Blouin S, Mulhbacher J, Penedo JC et al (2009b) Riboswitches: ancient and promising genetic regulators. ChemBioChem 10:400–416

Blount KF, Breaker RR (2006) Riboswitches as antibacterial drug targets. Nat Biotechnol 24:1558–1564

Bokinsky G, Rueda D, Misra VK et al (2003) Single-molecule transition-state analysis of RNA folding. Proc Natl Acad Sci USA 100:9302–9307

Brooks TA, Kendrick A, Hurley L (2010) Making sense of G-quadruplex and i-motif functions in oncogene promoters. FEBS J 277:3459–3469
Burge S, Parkinson GN, Hazel P et al (2006) Quadruplex DNA: sequence, topology and structure. Nucleic Acids Res 34:5402–5415
Butcher SE, Allain FHT, Feigon J (1999) Solution structure of the loop B domain from the hairpin ribozyme. Nat Struct Biol 6:212–216
Chalfie M, Tu Y, Euskirchen G et al (1994) Green fluorescent protein as a marker for gene expression. Science 263:802–805
Chandradoss SD, Haagsma AC, Lee YK et al (2014) Surface passivation for single-molecule protein studies. J Vis Exp 86:1–8
Cho EJ, Lee JW, Ellington AD (2009) Applications of aptamers as sensors. Annu Rev Anal Chem 2:241–264
Cochrane JC, Strobel SA (2008) Catalytic strategies of self-cleaving ribozymes. Acc Chem Res 41:1027–1035
Cogoi S, Xodo LE (2006) G-quadruplex formation within the promoter of the KRAS proto-oncogene and its effect on transcription. Nucleic Acids Res 34:2536–2549
Dai J, Dexheimer TS, Chen D et al (2006) An intramolecular G-quadruplex structure with mixed parallel/antiparallel G-strands formed in the human BCL-2 promoter region in solution. J Am Chem Soc 128:1096–1098
Dai J, Carver M, Punchihewa C et al (2007) Structure of the hybrid-2 type intramolecular human telomeric G-quadruplex in K+ solution: insights into structure polymorphism of the human telomeric sequence. Nucleic Acids Res 35:4927–4940
Dalgarno PA, Bordello J, Morris R et al (2013) Single-molecule chemical denaturation of riboswitches. Nucleic Acids Res 41:4253–4265
Deigan KE, Ferré-D'Amaré AR (2011) Riboswitches: discovery of drugs that target bacterial gene-regulatory RNAs. Acc Chem Res 44:1329–1338
Delfosse V, Bouchard P, Bonneau E et al (2010) Riboswitch structure: an internal residue mimicking the purine ligand. Nucleic Acids Res 38:32057–32068
Dempsey GT, Bates M, Kowtoniuk WE et al (2009) Photoswitching mechanism of cyanine dyes. J Am Chem Soc 131:18192–18193
Dickson RM, Cubitt AB, Tsien RY et al (1997) On/off blinking and switching behaviour of single molecules of green fluorescent protein. Nature 388:355–358
Ditzler MA, Alemán EA, Rueda D et al (2007) Focus on function: single molecule RNA enzymology. Biopolymers 87:302–316
Dulin D, Lipfert J, Moolman MC et al (2013) Studying genomic processes at the single-molecule level: introducing the tools and applications. Nat Rev Genet 14:9–22
Eid J, Fehr A, Gray J et al (2009) Real-time DNA sequencing from single polymerase molecules. Science 323:133–138
Ellington AD, Szostak JW (1990) In vitro selection of RNA molecules that bind specific ligands. Nature 346:818–822
Enderlein J, Gregor I, Patra D et al (2004) Art and artefacts of fluorescence correlation spectroscopy. Curr Pharmaceut Biotech 5:155–161
Eschbach SH, St-Pierre P, Penedo JC et al (2012) Folding of the SAM-I riboswitch: a tale with a twist. RNA Biol 9:535–541
Fazal FM, Block SM (2011) Optical tweezers study life under tension. Nat Photon 5:318–321
Fernando H, Reszka AP, Huppert J et al (2006) A conserved quadruplex motif located in a transcription activation site of the human c-kit oncogene. Biochemistry 45:7854–7860
Ferré-D'Amaré AR (2010) The *glmS* ribozyme: use of a small molecule coenzyme by a gene-regulatory RNA. Q Rev Biophys 43:423–447
Fiegland LR, Garst AD, Batey RT et al (2012) Single-molecule studies of the lysine riboswitch reveal effector-dependent conformational dynamics of the aptamer domain. Biochemistry 51:9223–9233

Funatsu T, Harada Y, Tokunaga M et al (1995) Imaging of single fluorescent molecules and individual ATP turnovers by single myosin molecules in aqueous solution. Nature 374:555–559

Gilbert SD, Batey RT (2006) Riboswitches: fold and function. Chem Biol 13:805–807

Greenleaf WJ, Frieda KL, Foster DA et al (2008) Direct observation of hierarchical folding in single riboswitch aptamers. Science 319:630–633

Grundy FJ, Lehman SC, Henkin TM (2003) The L box regulon: lysine sensing by leader RNAs of bacterial lysine biosynthesis genes. Proc Natl Acad Sci USA 100:12057–12062

Guerrier-Takada C, Gardiner K, Marsh T et al (1983) The RNA moiety of ribonuclease P is the catalytic subunit of the enzyme. Cell 35:849–857

Gurunathan K, Levitus M (2008) Applications of fluorescence correlation spectroscopy to the study of nucleic acid conformational dynamics. Prog Nucleic Acid Res Mol Biol 82:33–69

Ha T (2014) Single-molecule methods leap ahead. Nat Methods 11:1015–1018

Ha T, Enderle T, Ogletree DF et al (1996) Probing the interaction between two single molecules: fluorescence resonance energy transfer between a single donor and a single acceptor. Proc Natl Acad Sci USA 95:6264–6268

Haeusler AR, Donnelly CJ, Periz G et al (2014) C9orf72 nucleotide repeat structures initiate molecular cascades of disease. Nature 507:195–200

Haller A, Rieder U, Aigner M et al (2011a) Conformational capture of the SAM-II riboswitch. Nat Chem Biol 7:393–400

Haller A, Soulière MF, Micura R (2011b) The dynamic nature of RNA as key to understanding riboswitch mechanisms. Acc Chem Res 44:1339–1348

Haller A, Altman RB, Soulière MF et al (2013) Folding and ligand recognition of the TPP riboswitch aptamer at single-molecule resolution. Proc Natl Acad Sci USA 110:4188–4193

Han KY, Leslie BJ, Fei J et al (2013) Understanding the photophysics of the Spinach-DFHBI RNA aptamer-fluorogen complex to improve live-cell RNA imaging. J Am Chem Soc 135:19033–19038

Heppell B, Mulhbacher J, Penedo JC et al (2009) Application of fluorescence measurements for characterization of riboswitch-ligand interactions. Methods Mol Biol 540:25–37

Heppell B, Blouin S, Dussault AM et al (2011) Molecular insights into the ligand-controlled organization of the SAM-I riboswitch. Nat Chem Biol 7:384–392

Hohlbein J, Craggs TD, Cordes T (2014) Alternating-laser excitation: single-molecule FRET and beyond. Chem Soc Rev 43:1156–1171

Hohng S, Joo C, Ha T (2004) Single-molecule three-color FRET. Biophys J 87:1328–1337

Hohng S, Zhou R, Nahas MK et al (2007) Fluorescence-force spectroscopy maps two-dimensional reaction landscape of the Holliday junction. Science 318:279–283

Holliday R (1964) A mechanism for gene conversion in fungi. Genet Res Camb 5:282–304

Holmstrom ED, Nesbitt DJ (2014) Single-molecule fluorescence resonance energy transfer studies of the human telomerase RNA pseudoknot: temperature-/urea-dependent folding kinetics and thermodynamics. J Phys Chem B 118:3853–3863

Jansen JA, McCarthy TJ, Soukup GA et al (2006) Backbone and nucleobase contacts to glucosamine-6-phosphate in the *glmS* ribozyme. Nat Struct Mol Biol 13:517–523

Joo C, McKinney SA, Lilley DMJ et al (2004) Exploring rare conformational species and ionic effects in DNA Holliday junctions using single-molecule spectroscopy. J Mol Biol 341:739–751

Joo C, Balci H, Ishitsuka Y et al (2008) Advances in single-molecule fluorescence methods for molecular biology. Annu Rev Biochem 77:51–76

Jung J, Van Orden A (2005) Folding and unfolding kinetics of DNA hairpins in flowing solution by multiparameter fluorescence correlation spectroscopy. J Phys Chem B 109:3648–3657

Kapanidis AN, Laurence TA, Lee NK et al (2005) Alternating-laser excitation of single molecules. Acc Chem Res 38:523–533

Karunatilaka KS, Rueda D (2009) Single-molecule fluorescence studies of RNA: a decade's progress. Chem Phys Lett 476:1–10

Karymov MA, Daniel D, Sankey OF et al (2005) Holliday junction dynamics and branch migration: single-molecule analysis. Proc Natl Acad Sci USA 102:8186–8191
Karymov MA, Bogdanov A, Lyubchenko YL (2008) Single molecule fluorescence analysis of branch migration of Holliday junctions: effect of DNA sequence. Biophys J 95:1239–1247
Kazantsev AV, Pace NR (2006) Bacterial RNase P: a new view of an ancient enzyme. Nat Rev Microbiol 4:729–740
Kim J, Doose S, Neuweiler H et al (2006) The initial step of DNA hairpin folding: a kinetic analysis using fluorescence correlation spectroscopy. Nucleic Acids Res 34:2516–2527
Kim SA, Heinze KG, Schwille P (2007a) Fluorescence correlation spectroscopy in living cells. Nat Methods 4:963–973
Kim HK, Rasnik I, Liu J et al (2007b) Dissecting metal ion-dependent folding and catalysis of a single DNAzyme. Nat Chem Biol 3:763–768
Kruger K, Grabowski PJ, Zaug AJ et al (1982) Self-splicing RNA: autoexcision and autocyclization of the ribosomal RNA intervening sequence of tetrahymena. Cell 31:147–157
Kudryavtsev V, Felekyan S, Wozniak AK et al (2007) Monitoring dynamic systems with multiparameter fluorescence imaging. Anal Bioanal Chem 387:71–82
Kühnemuth R, Seidel CAM (2001) Principles of single molecule multiparameter fluorescence spectroscopy. Single Mol 2:251–254
Kurzban G, Bayer E, Wilchek M et al (1991) The quaternary structure of streptavidin in urea. J Biol Chem 266:14470–14477
Lang MJ, Fordyce PM, Block SM (2003) Combined optical trapping and single-molecule fluorescence. J Biol 2:6
Lee JY, Okumus B, Kim DS, Ha T (2005a) Extreme conformational diversity in human telomeric DNA. Proc Natl Acad Sci USA 102:18938–18943
Lee NK, Kapanidis AN, Wang Y et al (2005b) Accurate FRET measurements within single diffusing biomolecules using alternating-laser excitation. Biophys J 88:2939–2953
Lee J, Lee S, Ragunathan K et al (2010) Single-molecule four-color FRET. Angew Chem 122:10118–10121
Lemay JF, Lafontaine DA (2007) Core requirements of the adenine riboswitch aptamer for ligand binding. RNA 13:339–350
Lemay JF, Penedo JC, Tremblay R et al (2006) Folding of the adenine riboswitch. Chem Biol 13:857–868
Lemay JF, Penedo JC, Mulhbacher J et al (2009) Molecular basis of RNA-mediated gene regulation on the adenine riboswitch by single-molecule approaches. Methods Mol Biol 540:65–76
Lemay JF, Desnoyers G, Blouin S et al (2011) Comparative study between transcriptionally- and translationally-acting adenine riboswitches reveals key differences in riboswitch regulatory mechanisms. PLoS Genet 7:e1001278
Lilley DMJ (2005) Structure, folding and mechanisms of ribozymes. Curr Opin Struct Biol 15:313–323
Lippincott-Schwartz J, Patterson GH (2003) Development and use of fluorescent protein markers in living cells. Science 300:87–91
Liu Y, West SC (2004) Happy Hollidays: 40th anniversary of the Holliday junction. Nat Rev Mol Cell Biol 5:937–944
Magde D, Webb WW, Elson E (1972) Thermodynamic fluctuations in a reacting system–Measurement by fluorescence correlation spectroscopy. Phys Rev Lett 29:705–708
Maizels N, Gray LT (2013) The G4 genome. PLoS Genet 9:e1003468
Mandal M, Breaker RR (2004) Adenine riboswitches and gene activation by disruption of a transcription terminator. Nat Struct Mol Biol 11:29–35
Mandal M, Lee M, Barrick JE et al (2004) A glycine-dependent riboswitch that uses cooperative binding to control gene expression. Science 306:275–279

Margittai M, Widengren J, Schweinberger E et al (2003) Single-molecule fluorescence resonance energy transfer reveals a dynamic equilibrium between closed and open conformations of syntaxin 1. Proc Natl Acad Sci USA 100:15516–15521
McCluskey K, Shaw E, Lafontaine DA et al (2014) Single-molecule fluorescence of nucleic acids. Methods Mol Biol 1076:759–791
McDowell SE, Jun JM, Walter NG (2010) Long-range tertiary interactions in single hammerhead ribozymes bias motional sampling toward catalytically active conformations. RNA 16:2414–2426
McKinney SA, Déclais AC, Lilley DMJ, Ha T (2003) Structural dynamics of individual Holliday junctions. Nat Struct Biol 10(2):93–97
McKinney SA, Tan E, Wilson TJ et al (2004) Single-molecule studies of DNA and RNA four-way junctions. Biochem Soc Trans 32:41–45
McLuckie KIE, Di Antonio M, Zecchini H et al (2013) G-quadruplex DNA as a molecular target for induced synthetic lethality in cancer cells. J Am Chem Soc 135:9640–9643
Membrino A, Paramasivam M, Cogoi S et al (2010) Cellular uptake and binding of guanidine-modified phthalocyanines to KRAS/HRAS G-quadruplexes. Chem Commun 46:625–627
Mironov AS, Gusarov I, Rafikov R et al (2002) Sensing small molecules by nascent RNA: a mechanism to control transcription in bacteria. Cell 111:747–756
Moerner WE, Kador L (1989) Optical detection and spectroscopy of single molecules in a solid. Phys Rev Lett 62:2535–2538
Monico C, Capitanio M, Belcastro G et al (2013) Optical methods to study protein-DNA interactions in vitro and in living cells at the single-molecule level. Int J Mol Sci 14:3961–3992
Montange RK, Batey RT (2008) Riboswitches: emerging themes in RNA structure and function. Annu Rev Biophys 37:117–133
Mulhbacher J, Lafontaine DA (2007) Ligand recognition determinants of guanine riboswitches. Nucleic Acids Res 35:5568–5580
Mulhbacher J, St-Pierre P, Lafontaine DA (2010) Therapeutic applications of ribozymes and riboswitches. Curr Opin Pharmacol 10:551–556
Nahas MK, Wilson TJ, Hohng S et al (2004) Observation of internal cleavage and ligation reactions of a ribozyme. Nat Struct Mol Biol 11:1107–1113
Nahvi A, Sudarsan N, Ebert MS et al (2002) Genetic control by a metabolite binding mRNA. Chem Biol 9:1043–1049
Okumus B, Wilson TJ, Lilley DMJ et al (2004) Vesicle encapsulation studies reveal that single molecule ribozyme heterogeneities are intrinsic. Biophys J 87:2798–2806
Paige JS, Wu KY, Jaffrey SR (2011) RNA mimics of green fluorescent protein. Science 333:642–646
Paige JS, Nguyen-Duc T, Song W et al (2012) Fluorescence imaging of cellular metabolites with RNA. Science 335:1194
Palets D, Lushnikov AY, Karymov MA et al (2010) Effect of single-strand break on branch migration and folding dynamics of Holliday junctions. Biophys J 99:1916–1924
Parkinson GN, Lee MPH, Neidle S (2002) Crystal structure of parallel quadruplexes from human telomeric DNA. Nature 417:876–880
Patterson GH, Knobel SM, Sharif WD et al (1997) Use of the green fluorescent protein and its mutants in quantitative fluorescence microscopy. Biophys J 73:2782–2790
Penedo JC, Wilson TJ, Jayasena SD et al (2004) Folding of the natural hammerhead ribozyme is enhanced by interaction of auxiliary elements. RNA 10:880–888
Pereira MJB, Nikolova EN, Hiley SL et al (2008) Single VS ribozyme molecules reveal dynamic and hierarchical folding toward catalysis. J Mol Biol 382:496–509
Rankin S, Peszka AP, Huppert J et al (2005) Putative DNA quadruplex formation within the human c-kit oncogene. J Am Chem Soc 127:10584–10589
Rigler R, Mets U, Windengren J, Kask P (1993) Fluorescence correlation spectroscopy with high count rate and low background: analysis of translational diffusion. Eur Biophys J 22:169–175

Roth A, Winkler WC, Regulski EE et al (2007) A riboswitch selective for the queuosine precursor preQ$_1$ contains an unusually small aptamer domain. Nat Struct Mol Biol 14:308–317
Roth A, Weinberg Z, Chen AG et al (2014) A widespread self-cleaving ribozyme class is revealed by bioinformatics. Nat Chem Biol 10:56–60
Rothwell PJ, Berger S, Kensch O et al (2003) Multiparameter single-molecule fluorescence spectroscopy reveals heterogeneity of HIV-1 reverse transcriptase:primer/template complexes. Proc Natl Acad Sci USA 100:1655–1660
Roy R, Hohng S, Ha T (2008) A practical guide to single-molecule FRET. Nat Methods 5:507–516
Sabir T, Schröder GF, Toulmin A et al (2011) Global structure of forked DNA in solution revealed by high-resolution single-molecule FRET. J Am Chem Soc 133:1188–1191
Savinov A, Perez CF, Block SM (2014) Single-molecule studies of riboswitch folding. Biochim Biophys Acta 1839:1030–1045
Schuler B, Hofmann H (2013) Single-molecule spectroscopy of protein folding dynamics—expanding scope and timescales. Curr Opin Struct Biol 23:36–47
Serganov A, Nudler E (2013) A decade of riboswitches. Cell 152:17–24
Serganov A, Yuan YR, Pikovskaya O et al (2004) Structural basis for discriminative regulation of gene expression by adenine- and guanine-sensing mRNAs. Chem Biol 11:1729–1741
Shirude PS, Balasubramanian S (2008) Single molecule conformational analysis of DNA G-quadruplexes. Biochimie 90:1197–1206
Shirude PS, Okumus B, Ying L et al (2007) Single-molecule conformational analysis of G-quadruplex formation in the promoter DNA duplex of the proto-oncogene c-kit. J Am Chem Soc 129:7484–7485
Siddiqui-Jain A, Grand CL, Bearss DJ et al (2002) Direct evidence for a G-quadruplex in a promoter region and its targeting with a small molecule to repress c-MYC transcription. Proc Natl Acad Sci USA 99:11593–11598
Sigal N, Alberts B (1972) Genetic recombination: the nature of a crossed strand-exchange between two homologous DNA molecules. J Mol Biol 71:789–792
Sisamakis E, Valeri A, Kalinin S et al (2010) Accurate single-molecule FRET studies using multiparameter fluorescence detection. Methods Enzymol 475:455–514
Sosnick TR, Pan T (2003) RNA folding: models and perspectives. Curr Opin Struct Biol 13:309–316
St-Pierre P, McCluskey K, Shaw E et al (2014) Fluorescence tools to investigate riboswitch structural dynamics. Biochim Biophys Acta 1839:1005–1019
Strack RL, Disney MD, Jaffrey SR (2013) A superfolding Spinach2 reveals the dynamic nature of trinucleotide repeat-containing RNA. Nat Methods 10:1219–1224
Stryer L (1978) Fluorescence energy transfer as a spectroscopic ruler. Annu Rev Biochem 47:819–846
Suddala KC, Rinaldi AJ, Feng J et al (2013) Single transcriptional and translational preQ1 riboswitches adopt similar pre-folded ensembles that follow distinct folding pathways into the same ligand-bound structure. Nucleic Acids Res 41:10462–10475
Tan E, Wilson TJ, Nahas MK et al (2003) A four-way junction accelerates hairpin ribozyme folding via a discrete intermediate. Proc Natl Acad Sci USA 100:9308–9313
Treiber DK, Rook MS, Zarrinkar PP et al (1998) Kinetic intermediates trapped by native interactions in RNA folding. Science 279:1943–1946
Tremblay R, Mulhbacher J, Blouin S et al (2009) Natural functional nucleic acids: ribozymes and riboswitches. In: Yingfu L, Lu Y (eds) Functional nucleic acids for analytical applications. Springer, New York, NY, pp 11–46
Tremblay R, Lemay JF, Blouin S et al (2011) Constitutive regulatory activity of an evolutionarily excluded riboswitch variant. J Biol Chem 286:27406–27415
Verma A, Halder K, Halder R et al (2008) Genome-wide computational and expression analyses reveal G-quadruplex DNA motifs as conserved cis-regulatory elements in human and related species. J Med Chem 51:5641–5649

Vummidi BR, Alzeer J, Luedtke NW (2013) Fluorescent probes for G-quadruplex structures. ChemBioChem 14:540–558
Wallace MI, Ying JM, Balasubramanian S et al (2000) FRET fluctuation spectroscopy: exploring the conformational dynamics of a DNA hairpin loop. J Phys Chem B 104:11551–11555
Weiss S (1999) Fluorescence spectroscopy of single biomolecules. Science 283:1676–1683
Wilson TJ, Nahas M, Ha T et al (2005) Folding and catalysis of the hairpin ribozyme. Biochem Soc Trans 33:461–465
Wilson TJ, Nahas M, Araki L et al (2007) RNA folding and the origins of catalytic activity in the hairpin ribozyme. Blood Cell Mol Dis 38:8–14
Winkler WC, Breaker RR (2003) Genetic control by metabolite-binding riboswitches. ChemBioChem 4:1024–1032
Winkler WC, Breaker RR (2005) Regulation of bacterial gene expression by riboswitches. Annu Rev Microbiol 59:487–517
Winkler WC, Cohen-Chalamish S, Breaker RR (2002a) An mRNA structure that controls gene expression by binding FMN. Proc Natl Acad Sci 99:15908–15913
Winkler WC, Nahvi A, Breaker RR (2002b) Thiamine derivatives bind messenger RNAs directly to regulate bacterial gene expression. Nature 419:952–956
Winkler WC, Nahvi A, Sudarsan N et al (2003) An mRNA structure that controls gene expression by binding S-adenosylmethionine. Nat Struct Biol 10:701–707
Wood S, Ferré-D'Amaré AR, Rueda D (2012) Allosteric tertiary interactions pre-organize the c-di-GMP riboswitch and accelerate ligand binding. ACS Chem Biol 7:920–927
Wozniak AK, Schröder GF, Grubmüller H et al (2008) Single-molecule FRET measures bends and kinks in DNA. Proc Natl Acad Sci USA 105:18337–18342
Ying L, Green JJ, Li H et al (2003) Studies on the structure and dynamics of the human telomeric G quadruplex by single-molecule fluorescence resonance energy transfer. Proc Natl Acad Sci USA 100:14629–14634
Zheng Q, Juette MF, Jockusch S et al (2014) Ultra-stable organic fluorophores for single-molecule research. Chem Soc Rev 43:1044–1056
Zhuang X (2005) Single-molecule RNA science. Annu Rev Biophys Biomol Struct 34:399–414
Zhuang X, Bartley LE, Babcock HP et al (2000) A single-molecule study of RNA catalysis and folding. Science 288:2048–2051
Zhuang X, Kim H, Pereira MJB et al (2002) Correlating structural dynamics and function in single ribozyme molecules. Science 296:1473–1476

Detection and Assessment of MicroRNA Expression in Human Disease

Adam Mitchell, Amanda Marie James, Tamas Alexy, Gang Bao, and Charles D. Searles

Contents

Abstract MicroRNAs (miRNAs) are noncoding RNAs that posttranscriptionally suppress gene expression through sequence-specific interaction with the 3′ untranslated region (3′UTR) of target mRNAs. By modulating gene networks, miRNAs have been shown to regulate many aspects of cellular homeostasis and physiology, including differentiation, growth, proliferation, and apoptosis. The discovery of extracellular miRNA in blood and other body fluids has prompted investigation into their ability to serve as biomarkers for human disease. Further, many miRNAs have been implicated in the underlying pathophysiology of human disease, and there is substantial opportunity to develop novel molecular

A. Mitchell • A.M. James • T. Alexy
Division of Cardiology, Emory University School of Medicine, Atlanta, GA, USA

G. Bao
Department of Biomedical Engineering, Georgia Institute of Technology and Emory University, Atlanta, GA, USA

C.D. Searles (✉)
Division of Cardiology, Emory University School of Medicine, Atlanta, GA, USA

Section of Cardiology, Atlanta VA Medical Center, 1670 Clairmont Road, Decatur, GA 30033, USA
e-mail: csearle@emory.edu

V.A. Erdmann et al. (eds.), *RNA and DNA Diagnostics*, RNA Technologies,
DOI 10.1007/978-3-319-17305-4_16

therapeutics through manipulation of these miRNAs. Here, we review the evidence for the use of miRNAs as diagnostic and therapeutic targets in human disease. We also describe the advantages and limitations for current miRNA profiling strategies.

Keywords MicroRNA • IsomiR • Biomarker • qRT-PCR • Northern • Microarray • Next-generation sequencing • Molecular beacons

1 Introduction

MicroRNAs (miRNAs) are short (~19–23 nucleotides), highly conserved, noncoding RNAs that repress translation or induce degradation of specific messenger RNA (mRNA) molecules (Bartel 2004; Dennis 2002; Guo et al. 2010). To date, there are 1,881 annotated human miRNAs in miRBase (Kozomara and Griffiths-Jones 2014), which is the repository for miRNA sequences from all plant and animal species. The discovery of miRNAs and their function has substantially increased our appreciation for the complexity of gene regulation in health and disease, and miRNAs are increasingly being recognized as novel diagnostic and therapeutic targets for human disease.

2 miRNAs: Regulators of Gene Networks

2.1 miRNA Function

Targeting of mRNA occurs through base pairing of the miRNA seed sequence, defined as nucleotides 2–8 of the 5′ end, to a complementary sequence in the mRNA (Bartel 2009). Since miRNA-mediated gene suppression typically requires pairing of only 7–8 nucleotides, a single miRNA can regulate the expression of hundreds of mRNAs (Lim et al. 2005), and a given target mRNA can be regulated by multiple miRNAs (Friedman et al. 2009). These features are key to the ability of miRNAs to influence entire gene networks, thereby impacting many aspects of development, physiology, and pathology (Kloosterman and Plasterk 2006; Sayed and Abdellatif 2011). In fact, over 60 % of coding genes in humans are computationally predicted to be targeted by miRNAs (Friedman et al. 2009). Adding to the breadth and complexity of miRNA-mediated gene regulation is the finding that, through targeting transcription factors, miRNAs can indirectly regulate the expression of other miRNAs (Matkovich et al. 2013).

2.2 miRNA Biogenesis

miRNAs may be transcribed from various genomic loci, including introns or exons of noncoding genes, introns of coding genes, or intergenic regions (van Rooij 2011). Also, through variations in miRNA processing, a single miRNA genomic locus can

generate multiple mature miRNAs, which are otherwise known as isomiRs. The canonical miRNA biosynthetic pathway begins in the nucleus where primary miRNA transcripts (pri-miRNAs) are generated, most often by RNA polymerase II but occasionally by RNA polymerase III (Borchert et al. 2006). The hairpin structure of a pri-miRNA includes a double-stranded stem (roughly 33 base pairs) that contains the mature miRNA sequence, a single-stranded loop at one end of the stem, and two single-stranded 5′ and 3′ flanking regions at the other end of the stem (Ha and Kim 2014; Winter et al. 2009). In the nucleus, the 5′ and 3′ flanking regions of the pri-miRNA stem are cleaved by the Microprocessor complex, consisting of an RNase II enzyme, Drosha, and its cofactor, DGCR8 (also known as Pasha). The resulting product is termed the pre-miRNA, which varies in length between 60 and 70 nucleotides (Finnegan and Pasquinelli 2013). The pre-miRNA is exported from the nucleus to the cytoplasm by Exportin-5-Ran-GTP (Lund et al. 2004). In the cytoplasm, a second RNase, Dicer, and a double-stranded RNA-binding protein, TRBP, cleave the pre-miRNA terminal loop to produce a transient double-stranded miRNA with a length equal to that of the mature miRNA. This double-stranded molecule separates into two complimentary mature miRNAs, labeled 5p or 3p, depending on whether they originated from the 5′ or 3′ end of the primary transcript. One of the miRNAs becomes a functional "guide" strand, which complexes with the Argonaute-2 (Ago2) protein and is incorporated into the RNA-induced silencing complex (RISC). The other mature miRNA is referred to as the passenger strand (often denoted with a *) (Ha and Kim 2014), which is degraded. Mature miRNAs incorporated in the RISC guide the complex to specific mRNA sequences, thereby leading to degradation, translational repression, or deadenylation of the target mRNA (Filipowicz et al. 2008; Krol et al. 2010).

As a result of genomic duplications, many miRNAs share similar seed sequences, and miRNAs with identical seed sequences are referred to as a "miRNA family" (Ha and Kim 2014). In general, seed sequences are highly conserved; slight variations in seed sequence can lead to the suppression of completely different groups of targets (Kim et al. 2013). While miRNA biogenesis is often portrayed as a linear, uniform process, further investigation has revealed multiple layers of regulation and alternative pathways that appear to be miRNA specific (Winter et al. 2009). A detailed review of the alternative synthetic pathways and regulatory mechanisms involved is beyond the scope of this chapter and has been recently reviewed elsewhere (Finnegan and Pasquinelli 2013; Ha and Kim 2014).

2.3 Intracellular and Extracellular miRNAs

miRNAs are found within all cells and tissues, where they function as important modulators of cell differentiation (Chen et al. 2004, 2006), organ development (Carrington and Ambros 2003), homeostasis, and physiology (Kloosterman and Plasterk 2006). Efforts to comprehensively describe miRNA profiles in human and animal tissues (Landgraf et al. 2007; Liang et al. 2007) have revealed that some miRNAs are tissue specific, while others are widely and more uniformly expressed

(Liang et al. 2007). Intracellular abundance of miRNAs varies broadly, from only a few molecules per cell to greater than 10,000 molecules per cell (Liang et al. 2007). Repositories of miRNA expression profiles in healthy and diseased human tissues can be found at mirna.org or mirnabodymap.org.

The identification of stable, extracellular miRNAs was surprising given the known presence of highly active RNases in serum, plasma, and other body fluids (Kamm and Smith 1972). Extracellular miRNAs are remarkably stable, even if the sample has been left at room temperature for a prolonged period of time or has been exposed to multiple freeze/thaw cycles (Chen et al. 2008; Mitchell et al. 2008). Circulating miRNAs are protected from RNases through encapsulation within cell-derived membranous vesicles or by binding to circulating proteins or lipoproteins. Cell-derived membranous vesicles include exosomes, microparticles, and apoptotic bodies (Huang et al. 2013; Kosaka et al. 2010; Valadi et al. 2007). Interestingly, the miRNA profiles of circulating microvesicles are different from the contents of their maternal cells, implying an organized and regulated system for packaging and exporting particular miRNAs (Hunter et al. 2008). While little is known about the underlying mechanisms that govern this process, there is evidence that miRNA content within microvesicles changes in response to cell activation or systemic disease and that these conditions may affect the ability of cells to load miRNAs into the microvesicles (Alexy et al. 2014; Diehl et al. 2012; Finn et al. 2013). Importantly, neighboring cells can take up circulating microvesicles, resulting in the intercellular transfer of miRNAs and other bioactive molecules (Turchinovich et al. 2013). In a manner similar to paracrine signaling, transferred miRNAs may then influence gene expression and phenotype of the recipient cells (Hergenreider et al. 2012; Jansen et al. 2013; Zernecke et al. 2009).

It has been suggested that the majority of extracellular miRNAs in plasma, serum, or cell culture media are mostly non-encapsulated (Arroyo et al. 2011; Creemers et al. 2012; Turchinovich et al. 2011) and bound to extracellular proteins or lipoproteins (Arroyo et al. 2011; Vickers et al. 2011). Non-encapsulated miRNAs appear to be primarily associated with Argonaute proteins, the same proteins to which they are bound intracellularly (Arroyo et al. 2011). Lipoproteins, including high-density lipoprotein (HDL) and low-density lipoprotein (LDL), have also been shown to bind and transport miRNAs in the circulation (Vickers et al. 2011), although lipoprotein-bound miRNAs may represent a relatively low proportion of the total circulating miRNA pool. Whereas the ability of protein-bound extracellular miRNAs to function as intercellular communicators has not been well studied, lipoprotein-bound miRNAs do not appear to be efficiently transferred to recipient cells, and their role in intercellular communication appears be limited (Wagner et al. 2013). Despite uncertainty whether the majority of circulating miRNAs are encapsulated or non-encapsulated, it has become clear that the extracellular localization of miRNAs is miRNA dependent. Some miRNAs are predominantly found in microvesicles, while others are primarily bound to circulating Ago-2 (Arroyo et al. 2011). The distinct extracellular transport modalities of miRNA likely represent different cellular export mechanisms (Wang et al. 2010b) that are influenced by the cell type and the activating stimulus or disease state (Finn et al. 2013; Jansen et al. 2013).

2.4 Importance of miRNAs in Disease

High conservation of miRNA sequences across species is indicative of their biological significance. miRNAs are clearly important for development, as demonstrated by studies in which deletion of specific miRNAs or the miRNA synthetic machinery results in severe developmental defects and/or nonviability (Harfe et al. 2005; Thai et al. 2007; Yang et al. 2005; Zhao et al. 2007). The discovery of disease-specific miRNA signatures in tissues (Volinia et al. 2006), along with the identification of stable extracellular miRNAs, has prompted the search for circulating miRNA profiles that might be utilized as noninvasive biomarkers of disease (Mitchell et al. 2008; Weber et al. 2010). Indeed, unique circulating miRNA profiles have been shown to be associated with a variety of human disorders, including, but not limited to, cancer (Calin and Croce 2006; Lu et al. 2005; Mitchell et al. 2008; Schultz et al. 2014; Schwarzenbach et al. 2014), cardiovascular disease (Creemers et al. 2012; Fichtlscherer et al. 2011; Gupta et al. 2010), rheumatologic disease (Kloosterman and Plasterk 2006; Wang et al. 2010a), liver disease (Pirola et al. 2014; Wang et al. 2009), and neurologic disease (Leidinger et al. 2013). Furthermore, accumulating evidence suggests that circulating extracellular miRNAs are not only passive markers of disease, but that they are also biologically active mediators of cell-to-cell communication implicated in the underlying pathophysiology (Valadi et al. 2007; Zhu and Fan 2011).

miRNA expression can be manipulated in vivo, which has led to the development of miRNA-based pharmacotherapies (van Rooij et al. 2012). Antagomirs (antimiRs, blockmirs) are synthetic oligonucleotides with complementary sequence to mature miRNAs and are capable of binding to and inhibiting the function of a given miRNA (Krutzfeldt et al. 2005). Another strategy for modulating miRNA levels is miRNA mimicry, in which synthetic oligonucleotides are modified to enhance stability and cellular uptake and delivered to mimic the function of endogenous miRNAs (Bader et al. 2010). Off-target effects of miRNA mimics in tissues in which they are not normally expressed remain a challenge, and adeno-associated viral vectors have been suggested as tissue-specific miRNA delivery vehicles (Kota et al. 2009). Animal models suggest that manipulation of miRNA levels can mitigate disease, demonstrating the potential for novel, miRNA-based therapeutics (Hinkel et al. 2013; Hu et al. 2010; Jansen et al. 2013; Lanford et al. 2010; Son et al. 2013). The development of human miRNA-based drugs is underway, and there has been early success using this approach to treat hepatitis C in clinical trials (Janssen et al. 2013).

Overall, miRNAs are important modulators of gene expression that become dysregulated in many human diseases. The development of improved strategies to detect and study these molecules is becoming increasingly important, which will aid in identifying novel biomarkers, uncovering new disease mechanisms, and guiding novel therapeutic approaches.

3 miRNA Profiling

3.1 Sample Preparation

Sample preparation and proper RNA extraction techniques are crucial, but often overlooked, aspects of high-quality miRNA profiling. Variations in sample collection methods can influence subsequent assessment of miRNA levels. For example, patient fasting status, phlebotomy technique, hemolysis, cell contamination, and anticoagulants such as heparin have all been identified as factors that influence miRNA detection in serum and plasma (Moldovan et al. 2014). Furthermore, serum and plasma have similar miRNA profiles for some miRNAs, but not for all (Wang et al. 2012). There is concern that, when preparing a serum sample, the clotting process activates platelets, thereby inducing miRNA release in platelet microvesicles and altering miRNA levels in serum (Wang et al. 2012).

Kits for RNA isolation are commercially available, including some that isolate total RNA and others that preferentially enrich for small RNAs. The method by which RNA is extracted is not trivial—one paper was recently retracted because results were confounded by the selective loss of low-GC-content miRNAs during standard TRIzol RNA extraction (2012). Qualitative and quantitative assessment of miRNA isolation may also be challenging. For many profiling studies, RNA is extracted from tissues that have low-abundance miRNA, such as serum and plasma. Because miRNA levels tend to be below the threshold of accurate detection by spectrophotometry, some groups have used the Agilent Bioanalyzer to assess quantity and quality of isolated miRNAs.

3.2 Techniques to Detect and Quantify miRNA

The short length, high degree of sequence homology between closely related miRNAs, varying GC content, and relatively low abundance of miRNAs in some cells/tissues are all factors that impede accurate miRNA detection. Here we will review several of the most common techniques available for miRNA quantification.

3.2.1 Northern Blot Analysis

Northern blot analysis has been a widely used method for miRNA quantification. miRNA is isolated from cells or tissues, fractionated by gel electrophoresis, and then transferred to a membrane. miRNA molecules are fixed to the membrane by either UV cross-linking or baking. Labeled, miRNA-specific probes are hybridized to the membrane, and miRNA abundance is assessed by the signal intensity of bound probe.

Radiolabeled miRNA-specific probes can be generated using the StarFire system from Integrated DNA Technologies (IDT), in which a DNA polymerase is used to add 10 α-^{32}P-dA residues to the 3′ end of a synthetic oligonucleotide probe. Alternatively, predesigned fluorescently labeled, locked nucleic acid (LNA)-enhanced probes can be purchased from Exiqon (miRCURY). As probe specificity is determined by sequence homology and position of the base mismatches, the short length and high sequence similarity of miRNAs make it challenging to generate probes that are highly specific. Through incorporation of a class of nucleic acid analogs, LNA technology improves miRNA probe specificity by increasing the melting temperature (T_m) and binding affinity of the probe. LNA probes can also be 3′ end-labeled with γ-^{32}P-ATP or tagged at the 5′ and/or 3′ end with digoxigenin or biotin. After hybridization to miRNA, the tagged probes are detected by the reaction of a chemiluminescent enzyme that has been attached to anti-digoxigenin monoclonal antibody or streptavidin. In general, radiolabeled poly(A) probes produce stronger signals compared to non-radiolabeled LNA probes (van Rooij 2011).

The main advantage of Northern blot analysis is its ability to assess miRNA size, in particular the ability to distinguish mature and precursor forms of miRNAs in a sample. However, the Northern blot protocol has low throughput, is time consuming, and requires a relatively large amount of RNA (8–10 μg). Despite improvements in detection specificity provided by LNA technology, probe cross-reactivity with miRNA family members with high sequence homology remains a concern.

3.2.2 qRT-PCR

Quantitative reverse transcriptase–polymerase chain reaction (qRT-PCR) or real-time PCR is the most commonly used method for assessing miRNA abundance and has the advantage of being a familiar, readily available technique in many laboratories. In qRT-PCR, a cDNA template is first generated by reverse transcription of the isolated RNA/miRNA, followed by PCR. However, since mature miRNAs are short transcripts of only 19–23 nucleotides, quantification using traditional qRT-PCR methods is challenging. In particular, cDNA produced by reverse transcription of a mature miRNA is not long enough for subsequent specific binding of two PCR primers. PCR primers, which are typically 22–25 nt in length, require a cDNA template that is at least 50 base pairs (bp) in length. Therefore, mature miRNAs must first be extended prior to the RT reaction. There are two main methods to increase the length of miRNA for reverse transcription: (1) miRNA extension with a hairpin-loop primer and (2) miRNA extension by polyadenylation.

The hairpin-loop RT primer (Life Technologies, TaqMan PCR assays) has a 3′ overhang that specifically binds to a few bases in the miRNA template, as well as a double-stranded stem and a loop. This primer serves two purposes: it extends the miRNA of interest to a longer template for RT and its loop structure provides a binding sequence for a universal primer. The RT reaction using the hairpin-loop primer is specific for the miRNA of interest; it will not reverse transcribe other miRNAs or mRNAs. The resulting cDNA is then subjected to PCR using one

miRNA-specific primer and a second, universal primer. While this assay is generally more difficult to design, the structure of the RT and PCR primers reduces nonspecific amplification of the pre- and pri-miRNAs. Also, the specificity of the RT primer is helpful in the detection of miRNAs with low abundance. A major disadvantage of this method for miRNA reverse transcription is the requirement for a separate RT reaction for each miRNA of interest, so screening a sample for expression levels of multiple miRNAs can be labor intensive.

Reverse transcription after miRNA polyadenylation is very similar to a regular RT reaction with oligo-dT primers. In the case of miRNA reverse transcription, an additional polyadenylation step has to be performed that adds a tail of adenines (As) to all miRNAs in the sample. Reverse transcription of the polyadenylated miRNA involves a universal oligo-dT RT primer with a special 3′ anchor and a universal tag sequence in the 5′ end. Using the QIAGEN miScript PCR system or Exiqon's miRCURY system, polyadenylation and reverse transcription can be performed simultaneously in the same tube, producing cDNAs from all miRNAs in the sample. The subsequent PCR uses a forward primer specific to the miRNA-specific sequence and a universal reverse primer that binds to the oligo-dT end of the cDNA. SYBR Green is typically used to quantify the PCR product of this cDNA. Since the RT reaction is not miRNA specific, this method has the advantage of being relatively cost-efficient; the cDNA generated from a single RT reaction can be used as a template to assess expression levels of any miRNA, pre-miRNA, and mRNA of interest. Also, the use of SYBR Green with this qRT-PCR method allows a melting curve analysis, indicating purity of the product. The disadvantage of this method is its reduced specificity compared to the method that uses the hairpin-loop RT primer. Also, since all RNA/miRNA transcripts in the sample are polyadenylated and reverse transcribed, accurate detection of low-abundance miRNAs may be challenging.

Two methods for the assessment of PCR product are available: one uses a DNA intercalating dye, such as SYBR Green described above; the other uses a nonspecific short fluorescent DNA probe that has a fluorophore and a quencher attached. SYBR Green has a very high affinity for double-stranded DNA. During the amplification and synthesis of DNA during PCR, SYBR Green intercalates into the double-stranded DNA product and fluoresces—the intensity of fluorescent signal is directly proportional to the amount of cDNA. In the other method of PCR product detection, the short DNA probe with fluorophore–quencher combination binds to the template DNA, and the fluorophore is quenched when the probe is bound. During the PCR reaction, exonuclease activity of DNA polymerase degrades the probe while the polymerase also extends the primers and synthesizes the nascent strand. Degradation of the probe separates fluorophore from quencher and fluorescence is emitted. The registered fluorescence intensity is directly proportional to the amount of DNA in the sample.

LNA technology, as discussed above, has been utilized to improve primer sensitivity and specificity (e.g., Exiqon's miRCURY LNA Universal RT microRNA PCR kit). Incorporation of LNAs increases primer T_m and binding affinity. This approach requires as little as 1 pg of total RNA to perform

qRT-PCR (Moldovan et al. 2014). Preamplification kits are also available for samples in which low amounts of cDNA are produced after reverse transcription. For example, Megaplex from Applied Biosystems can be used to increase template availability for PCR. Finally, several companies also offer array-based, high-throughput qRT-PCR options. TaqMan Low Density Arrays (Applied Biosystems), miRNome panels (Exiqon), or miScript miRNA PCR Arrays (QIAGEN) allow users to select from pre-plated miRNA panels. These assay panels can also be custom designed to suit the users' preferences.

Whereas the use of various small nucleolar RNAs (e.g., RNU48, RNU6b, RNU444, RNU43) to normalize for technical and biological variation in qRT-PCR data obtained from cells or tissues is well established, normalization of data obtained for extracellular miRNAs has proven to be a challenging issue. For extracellular miRNAs, several normalization strategies have been developed and used, although each has drawbacks. Technical variation can occur between samples as a result of differences in RNA extraction efficiency, reverse transcription, or the presence of PCR inhibitors. A common method employed to normalize for technical variation between samples is to "spike in" an exogenous miRNA that does not have homology with human miRNAs, such as cel-miR-39 from *C. elegans*. During RNA isolation, after endogenous RNases have been denatured, a known concentration of exogenous miRNA is added to the isolate and subsequently assessed by qRT-PCR. After PCR, technical variation is controlled for by normalizing the value for the miRNA of interest to that of the spike-in miRNA.

Ideally, to control for biological variation in qRT-PCR assessment of extracellular miRNAs, a known invariant endogenous small RNA should be used. Unfortunately, no universally invariant miRNA has been discovered to serve this function, especially in body fluids like serum and plasma (Moldovan et al. 2014). Invariant miRNAs in a given dataset can be identified using software, such as geNorm or Normfinder that identifies the best "normalizer" in the dataset. Alternatively, statistically based methods that utilize global measures of miRNA expression can be used, including mean normalization, which was recently shown to be highly effective (Mestdagh et al. 2009). Unfortunately both of these methods rely on having a large dataset and are not suitable for smaller experiments. A third option is to generate a separate standard curve for each PCR reaction by assessing serial dilutions of a known amount of template cDNA. Unknown samples can then be fit to the standard curve for absolute quantification. However, this process requires performing multiple PCRs for the assessment of one miRNA, which is time consuming and uses substantial quantities of PCR reagents.

In summary, qRT-PCR is the most sensitive method for miRNA detection, and it is an established method in many laboratories. Throughput is improving, especially with the array-based options that are commercially available. However, this method may not be able to distinguish between closely related miRNAs that might have only one or two bases different in their sequence. If the qRT-PCR is not performed with standard curve, it can only provide information on relative changes in miRNA expression, not absolute differences in miRNA abundance. Otherwise, with the

exception of normalization issues for extracellular miRNAs, data analysis is relatively straightforward.

3.2.3 miRNA Microarray

Microarrays allow for parallel analysis of a large number of predefined miRNAs through probe hybridization. Multiple platforms for microarrays are available, all varying slightly in their chemistry, labeling, and probe design. Basically, miRNA is isolated and then labeled, usually by using T4 RNA ligase, which attaches one or two fluorophore-labeled nucleotides to the 3′ end of the miRNA. Either synthetic oligonucleotides or cDNAs are used as capture probes. Perhaps the greatest challenge for microarrays is that, based on their sequence, miRNA melting temperatures can vary widely between 45 °C and 74 °C (van Rooij 2011). This variation means that the binding affinities of the miRNA probes will differ at a given temperature; thus, absolute quantification of miRNA abundance is not possible. However, probe designs can be modified in such a way as to equalize annealing temperatures thereby making array binding more homogeneous (Moldovan et al. 2014; van Rooij 2011).

The Affymetrix GeneChip miRNA array version 4.0 covers all miRNAs in miRBase for 203 organisms. After RNA isolation, a poly(A) tail is added to the 3′ end of the miRNA followed by ligation of a biotinylated 3DNA dendrimer. The biotin-labeled miRNA is hybridized to the capture probes on the chip, and binding is detected by streptavidin–phycoerythrin fluorescence. This experiment requires 100 ng of total RNA. Agilent oligonucleotide microarrays offer up-to-date coverage of human, mouse, and rat miRNAs that also require at least 100 ng of total RNA per sample. The Agilent protocol uses RNA dephosphorylation and ligation of Cyanine 3-pCp, followed by hybridization and detection. Results generally correlate well with qRT-PCR data (Ach et al. 2008). Exiqon's miRCURY LNA microRNA arrays offer good coverage of human, mouse, and rat miRNAs from miRBase. It has 3,100 capture probes, including 146 viral miRNAs. This platform requires as little as 30 ng of input RNA. As discussed, the incorporation of LNAs helps to standardize hybridization conditions. This array includes 52 "spike-in" control miRNAs for normalization. Exiqon claims their system provides higher sensitivity and specificity as a result of LNA technology.

Microarrays offer a high-throughput, comprehensive option for miRNA profiling at a reasonable price. Several customizable platforms are available, and microarray-based miRNA profiling is a suitable alternative to other high-throughput methods. However, this method has several drawbacks. The wide range in miRNA expression levels in a particular sample limits the ability of microarrays to detect transcripts at relatively low abundance (low sensitivity). Similar to the methods above, microarrays only probe previously annotated miRNAs, so detection of novel miRNAs or miRNA variants (isomiRs) is not possible. Absolute quantification of miRNA abundance using microarrays is difficult due to variability in probe hybridization efficiency, and the lack of specificity

limits the ability of microarrays to distinguish mature miRNAs from precursors. Most platforms require at least 100 ng of input material, which may pose a problem for miRNA profiling of some tissues. Microarray data analysis is not as straightforward as qRT-PCR, and inter-platform variability remains an issue (Callari et al. 2012). Changes in miRNA expression detected by microarray should be validated by Northern or qRT-PCR analysis. Continued improvements to microarray reproducibility, sensitivity, specificity, and inter-platform variability are being made (Pradervand et al. 2010), but as RNA sequencing technology becomes cheaper and more accessible, microarray-based miRNA profiling is likely to be utilized less.

3.2.4 Deep Sequencing

Next-generation sequencing (NGS) uses a massive number of parallel sequencing reactions to produce millions of sequence reads that are then mapped back to the genome of interest and quantified with advanced bioinformatics. Multiple miRNA sequencing platforms are now available through Illumina, Life Technologies, or Exiqon, among others. Total RNA or purified small RNA is isolated, and adapters are ligated onto the 3′ and 5′ ends of the fragmented products. A reverse transcriptase reaction generates cDNA libraries, and PCR is performed on an immobilized surface or beads (Moldovan et al. 2014). Expression levels are quantified based on the number of reads that map to a particular region. Sequence mapping, normalization, and downstream analysis require advanced bioinformatics software and expertise.

NGS is a highly sensitive and specific method for miRNA quantification. It is unique in that it is unbiased, offering the ability to detect novel miRNAs and to distinguish between very closely related miRNAs or isomiRs. NGS also characterizes other small RNAs that have not been well characterized thus far, but could just as well be biologically relevant species. NGS is able to measure absolute abundance of each transcript over a large range of expression (6–7 log fold range) (Moldovan et al. 2014). NGS requires relatively small amounts of starting material, with current technology able to generate high-quality data from as little as 10 ng of miRNA. These features highlight the advantages of NGS over other miRNA profiling methods, but NGS is the most expensive method for profiling. Furthermore, due to the very large amounts of data that are generated by NGS, it requires a significant amount of bioinformatics and biostatistical support. As with microRNA microarrays, results should be validated by Northern or qRT-PCR analysis.

3.2.5 Molecular Beacons

Molecular beacons are oligonucleotide (DNA or RNA) probes that have become an increasingly important tool for RNA detection both in vitro and in living cells. From their inception, molecular beacons have been used to determine the expression

levels of RNA transcripts, but they also have the specificity to identify splice variants and single-nucleotide polymorphisms. Our group has performed extensive studies on molecular beacon design, molecular beacon hybridization assays, and cellular imaging of mRNA molecules. Compared to other methods for assessing RNA transcript expression, such as qRT-PCR, the molecular beacon-based approach is potentially simpler, faster, more cost-effective, and more specific.

Molecular beacons are single-stranded DNA or RNA molecules labeled with a reporter fluorophore at one end and a quencher at the other end (Tyagi and Kramer 1996). In the absence of a complementary target, they are designed to form a stem–loop hairpin structure that results in quenching of the fluorophore's fluorescence (Tyagi et al. 1998; Tyagi and Kramer 1996; Vet et al. 1999). Hybridization of the molecular beacon's loop sequence with target nucleic acid opens the hairpin and physically separates the fluorophore from the quencher, allowing a fluorescence signal to be emitted upon excitation, which can be assessed in a standard fluorescence plate reader. In theory, the molecular beacon elicits a signal only upon direct hybridization to the complementary RNA sequence. This enables a molecular beacon to function as a sensitive and specific probe with a high signal-to-background-noise ratio (Bao et al. 2009; Guo et al. 2012; Nitin and Bao 2008; Nitin et al. 2004; Santangelo et al. 2004, 2006; Tsourkas et al. 2002, 2003). In addition, RNA abundance is directly correlated with molecular beacon fluorescence.

Since sequences for mature forms of miRNAs are also present in miRNA precursor forms (i.e., pri- and pre-miRNAs), miRNA detection methods that are not able to readily distinguish between different miRNA forms (i.e., qRT-PCR, miRNA microarray) tend to report falsely high values for miRNA abundance. Recently, our group demonstrated that molecular beacons can readily distinguish mature and pre-miRNAs and reliably quantify their expression in the same sample (Baker et al. 2012). Molecular beacons can also distinguish between miRNA family members with similar sequences (Baker et al. 2012). LNA backbone chemistry may be incorporated into molecular beacon design to enhance affinity of the molecular beacon for target miRNA. Profiling of multiple miRNAs and pre-miRNAs in one sample can be accomplished through multiplex assays that utilize molecular beacons containing fluorophores with nonoverlapping spectra. Furthermore, molecular beacon-based assays can be performed in one step without the need for reverse transcription (RT) or amplification steps, and excess probe does not have to be removed prior to measurement.

Overall, molecular beacons are highly specific in their ability to detect both mature and precursor forms of miRNA in a biological sample as well as in their ability to distinguish miRNAs or isomiRs with one or two nucleotide differences in their sequences. However, the sensitivity of the current molecular beacon-based assays for miRNA quantification is modest compared to other methods that utilize signal amplification steps (e.g., qRT-PCR). It remains a challenge to use molecular beacons to profile miRNA expression in biological samples that have low miRNA abundance, such as body fluids. Furthermore, this method for miRNA profiling is currently still rather novel, and optimization of molecular beacon design for each

miRNA and pre-miRNA target is required, which can be costly. As use of this method becomes more widespread and molecular beacons for specific miRNAs or groups of related miRNAs are developed, this method could be a valuable tool for miRNA profiling.

4 Discussion

While enthusiasm for the clinical application of miRNA profiles as biomarkers for human disease is high, technical issues with miRNA profiling remain, particularly in regard to standardization of sample collection/processing and reproducibility of miRNA assessment assays. Causes for inconsistencies in miRNA profiles exist throughout miRNA profiling process, from pre-analysis steps such as sample preparation to variations in one of the several steps between RNA isolation and data analysis. In fact, a recent quality control study of several miRNA profiling platforms concluded that, while each method has strengths and weaknesses, the average validation rate for differentially expressed miRNAs was only 54% between any two platform combinations (Mestdagh et al. 2014). The advantages and limitations for various miRNA profiling methods are summarized in Table 1.

Several features of miRNA expression present challenges for accurate and specific quantification of miRNA abundance and could contribute to inter-assay variability (Guo and Chen 2014; Roy-Chaudhuri et al. 2014). These features include their short length, the high degree of homology between closely related miRNAs, the possibility of slight variations at the 5′ and 3′ ends due to imprecise processing (isomiRs), and the coexistence of mature and precursor forms of miRNAs in the same sample. For example, Lee et al. have demonstrated dramatic discrepancies in the assessment of miRNA abundance due to differences in

Table 1 Characteristics of miRNA profiling methods

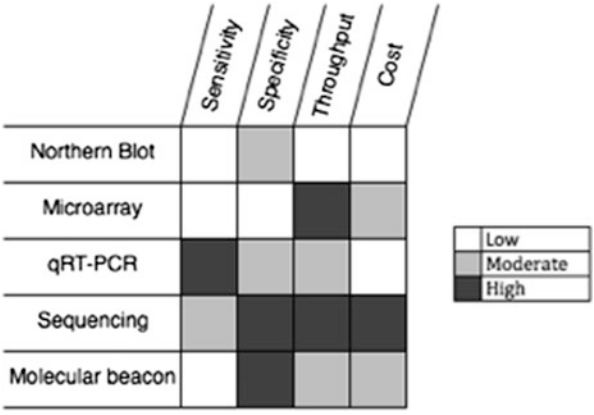

processing at the 3′ end of specific miRNAs, an issue that influences multiple miRNA detection methodologies (Lee et al. 2010). Regardless of the method used to detect and quantify miRNA, the full repertoire of miRNA variability and its biological consequences must be taken into account if appropriate conclusions are to be drawn. As more details emerge about the biology of the intra- and extracellular expression of miRNAs, our understanding of the importance of miRNA profiling in the diagnosis and management of human disease will certainly be enhanced, and methods used to accurately assess miRNA profiles should continue to be refined.

Acknowledgments This work was supported by a VA Merit Award (I01 BX000704 to CDS) and the National Heart Lung and Blood Institute of the National Institutes of Health as a Program of Excellence in Nanotechnology (HHSN268201000043C to GB) and a NHLBI R01 Award (HL 109559 to CDS).

References

(2012) Retraction notice to: cell adhesion-dependent control of microRNA decay. Mol Cell 43:1005–1014; September 16, 2011. Mol Cell 46:896

Ach RA, Wang H, Curry B (2008) Measuring microRNAs: comparisons of microarray and quantitative PCR measurements, and of different total RNA prep methods. BMC Biotechnol 8:69

Alexy T, Rooney K, Weber M et al (2014) TNF-alpha alters the release and transfer of microparticle-encapsulated miRNAs from endothelial cells. Physiol Genomics 46:833–840

Arroyo JD, Chevillet JR, Kroh EM et al (2011) Argonaute2 complexes carry a population of circulating microRNAs independent of vesicles in human plasma. Proc Natl Acad Sci U S A 108:5003–5008

Bader AG, Brown D, Winkler M (2010) The promise of microRNA replacement therapy. Cancer Res 70:7027–7030

Baker MB, Bao G, Searles CD (2012) In vitro quantification of specific microRNA using molecular beacons. Nucleic Acids Res 40:e13

Bao G, Rhee WJ, Tsourkas A (2009) Fluorescent probes for live-cell RNA detection. Annu Rev Biomed Eng 11:25–47

Bartel DP (2004) MicroRNAs: genomics, biogenesis, mechanism, and function. Cell 116:281–297

Bartel DP (2009) MicroRNAs: target recognition and regulatory functions. Cell 136:215–233

Borchert GM, Lanier W, Davidson BL (2006) RNA polymerase III transcribes human microRNAs. Nat Struct Mol Biol 13:1097–1101

Calin GA, Croce CM (2006) MicroRNA signatures in human cancers. Nat Rev Cancer 6:857–866

Callari M, Dugo M, Musella V et al (2012) Comparison of microarray platforms for measuring differential microRNA expression in paired normal/cancer colon tissues. PLoS One 7:e45105

Carrington JC, Ambros V (2003) Role of microRNAs in plant and animal development. Science 301:336–338

Chen CZ, Li L, Lodish HF et al (2004) MicroRNAs modulate hematopoietic lineage differentiation. Science 303:83–86

Chen JF, Mandel EM, Thomson JM et al (2006) The role of microRNA-1 and microRNA-133 in skeletal muscle proliferation and differentiation. Nat Genet 38:228–233

Chen X, Ba Y, Ma L et al (2008) Characterization of microRNAs in serum: a novel class of biomarkers for diagnosis of cancer and other diseases. Cell Res 18:997–1006

Creemers EE, Tijsen AJ, Pinto YM (2012) Circulating microRNAs: novel biomarkers and extracellular communicators in cardiovascular disease? Circ Res 110:483–495
Dennis C (2002) The brave new world of RNA. Nature 418:122–124
Diehl P, Fricke A, Sander L et al (2012) Microparticles: major transport vehicles for distinct microRNAs in circulation. Cardiovasc Res 93:633–644
Fichtlscherer S, Zeiher AM, Dimmeler S (2011) Circulating microRNAs: biomarkers or mediators of cardiovascular diseases? Arterioscler Thromb Vasc Biol 31:2383–2390
Filipowicz W, Bhattacharyya SN, Sonenberg N (2008) Mechanisms of post-transcriptional regulation by microRNAs: are the answers in sight? Nat Rev Genet 9:102–114
Finn NA, Eapen D, Manocha P et al (2013) Coronary heart disease alters intercellular communication by modifying microparticle-mediated microRNA transport. FEBS Lett 587:3456–3463
Finnegan EF, Pasquinelli AE (2013) MicroRNA biogenesis: regulating the regulators. Crit Rev Biochem Mol Biol 48:51–68
Friedman RC, Farh KK, Burge CB et al (2009) Most mammalian mRNAs are conserved targets of microRNAs. Genome Res 19:92–105
Guo L, Chen F (2014) A challenge for miRNA: multiple isomiRs in miRNAomics. Gene 544:1–7
Guo H, Ingolia NT, Weissman JS et al (2010) Mammalian microRNAs predominantly act to decrease target mRNA levels. Nature 466:835–840
Guo J, Ju J, Turro NJ (2012) Fluorescent hybridization probes for nucleic acid detection. Anal Bioanal Chem 402:3115–3125
Gupta SK, Bang C, Thum T (2010) Circulating microRNAs as biomarkers and potential paracrine mediators of cardiovascular disease. Circ Cardiovasc Genet 3:484–488
Ha M, Kim VN (2014) Regulation of microRNA biogenesis. Nat Rev Mol Cell Biol 15:509–524
Harfe BD, McManus MT, Mansfield JH et al (2005) The RNaseIII enzyme Dicer is required for morphogenesis but not patterning of the vertebrate limb. Proc Natl Acad Sci U S A 102:10898–10903
Hergenreider E, Heydt S, Treguer K et al (2012) Atheroprotective communication between endothelial cells and smooth muscle cells through miRNAs. Nat Cell Biol 14:249–256
Hinkel R, Penzkofer D, Zuhlke S et al (2013) Inhibition of microRNA-92a protects against ischemia/reperfusion injury in a large-animal model. Circulation 128:1066–1075
Hu S, Huang M, Li Z et al (2010) MicroRNA-210 as a novel therapy for treatment of ischemic heart disease. Circulation 122:S124–S131
Huang X, Yuan T, Tschannen M et al (2013) Characterization of human plasma-derived exosomal RNAs by deep sequencing. BMC Genomics 14:319
Hunter MP, Ismail N, Zhang X et al (2008) Detection of microRNA expression in human peripheral blood microvesicles. PLoS One 3:e3694
Jansen F, Yang X, Hoelscher M et al (2013) Endothelial microparticle-mediated transfer of MicroRNA-126 promotes vascular endothelial cell repair via SPRED1 and is abrogated in glucose-damaged endothelial microparticles. Circulation 128:2026–2038
Janssen HL, Reesink HW, Lawitz EJ et al (2013) Treatment of HCV infection by targeting microRNA. N Engl J Med 368:1685–1694
Kamm RC, Smith AG (1972) Ribonuclease activity in human plasma. Clin Biochem 5:198–200
Kim YK, Wee G, Park J et al (2013) TALEN-based knockout library for human microRNAs. Nat Struct Mol Biol 20:1458–1464
Kloosterman WP, Plasterk RH (2006) The diverse functions of microRNAs in animal development and disease. Dev Cell 11:441–450
Kosaka N, Iguchi H, Yoshioka Y et al (2010) Secretory mechanisms and intercellular transfer of microRNAs in living cells. J Biol Chem 285:17442–17452
Kota J, Chivukula RR, O'Donnell KA et al (2009) Therapeutic microRNA delivery suppresses tumorigenesis in a murine liver cancer model. Cell 137:1005–1017
Kozomara A, Griffiths-Jones S (2014) miRBase: annotating high confidence microRNAs using deep sequencing data. Nucleic Acids Res 42:D68–D73

Krol J, Loedige I, Filipowicz W (2010) The widespread regulation of microRNA biogenesis, function and decay. Nat Rev Genet 11:597–610
Krutzfeldt J, Rajewsky N, Braich R et al (2005) Silencing of microRNAs in vivo with 'antagomirs'. Nature 438:685–689
Landgraf P, Rusu M, Sheridan R et al (2007) A mammalian microRNA expression atlas based on small RNA library sequencing. Cell 129:1401–1414
Lanford RE, Hildebrandt-Eriksen ES, Petri A et al (2010) Therapeutic silencing of microRNA-122 in primates with chronic hepatitis C virus infection. Science 327:198–201
Lee LW, Zhang S, Etheridge A et al (2010) Complexity of the microRNA repertoire revealed by next-generation sequencing. RNA 16:2170–2180
Leidinger P, Backes C, Deutscher S et al (2013) A blood based 12-miRNA signature of Alzheimer disease patients. Genome Biol 14:R78
Liang Y, Ridzon D, Wong L et al (2007) Characterization of microRNA expression profiles in normal human tissues. BMC Genomics 8:166
Lim LP, Lau NC, Garrett-Engele P et al (2005) Microarray analysis shows that some microRNAs downregulate large numbers of target mRNAs. Nature 433:769–773
Lu J, Getz G, Miska EA et al (2005) MicroRNA expression profiles classify human cancers. Nature 435:834–838
Lund E, Guttinger S, Calado A et al (2004) Nuclear export of microRNA precursors. Science 303:95–98
Matkovich SJ, Hu Y, Dorn GW II (2013) Regulation of cardiac microRNAs by cardiac microRNAs. Circ Res 113:62–71
Mestdagh P, Van Vlierberghe P, De Weer A et al (2009) A novel and universal method for microRNA RT-qPCR data normalization. Genome Biol 10:R64
Mestdagh P, Hartmann N, Baeriswyl L et al (2014) Evaluation of quantitative miRNA expression platforms in the microRNA quality control (miRQC) study. Nat Methods 11:809–815
Mitchell PS, Parkin RK, Kroh EM et al (2008) Circulating microRNAs as stable blood-based markers for cancer detection. Proc Natl Acad Sci U S A 105:10513–10518
Moldovan L, Batte KE, Trgovcich J et al (2014) Methodological challenges in utilizing miRNAs as circulating biomarkers. J Cell Mol Med 18:371–390
Nitin N, Bao G (2008) NLS peptide conjugated molecular beacons for visualizing nuclear RNA in living cells. Bioconjug Chem 19:2205–2211
Nitin N, Santangelo PJ, Kim G et al (2004) Peptide-linked molecular beacons for efficient delivery and rapid mRNA detection in living cells. Nucleic Acids Res 32:e58
Pirola CJ, Fernandez Gianotti T, Castano GO et al (2014) Circulating microRNA signature in non-alcoholic fatty liver disease: from serum non-coding RNAs to liver histology and disease pathogenesis. Gut. doi:10.1136/gutjnl-2014-306996. [Epub ahead of print]
Pradervand S, Weber J, Lemoine F et al (2010) Concordance among digital gene expression, microarrays, and qPCR when measuring differential expression of microRNAs. Biotechniques 48:219–222
Roy-Chaudhuri B, Valdmanis PN, Zhang Y et al (2014) Regulation of microRNA-mediated gene silencing by microRNA precursors. Nat Struct Mol Biol 21:825–832
Santangelo PJ, Nix B, Tsourkas A et al (2004) Dual FRET molecular beacons for mRNA detection in living cells. Nucleic Acids Res 32:e57
Santangelo P, Nitin N, Bao G (2006) Nanostructured probes for RNA detection in living cells. Ann Biomed Eng 34:39–50
Sayed D, Abdellatif M (2011) MicroRNAs in development and disease. Physiol Rev 91:827–887
Schultz NA, Dehlendorff C, Jensen BV et al (2014) MicroRNA biomarkers in whole blood for detection of pancreatic cancer. JAMA 311:392–404
Schwarzenbach H, Nishida N, Calin GA et al (2014) Clinical relevance of circulating cell-free microRNAs in cancer. Nat Rev Clin Oncol 11:145–156

Son DJ, Kumar S, Takabe W et al (2013) The atypical mechanosensitive microRNA-712 derived from pre-ribosomal RNA induces endothelial inflammation and atherosclerosis. Nat Commun 4:3000

Thai TH, Calado DP, Casola S et al (2007) Regulation of the germinal center response by microRNA-155. Science 316:604–608

Tsourkas A, Behlke MA, Bao G (2002) Structure-function relationships of shared-stem and conventional molecular beacons. Nucleic Acids Res 30:4208–4215

Tsourkas A, Behlke MA, Xu Y et al (2003) Spectroscopic features of dual fluorescence/luminescence resonance energy-transfer molecular beacons. Anal Chem 75:3697–3703

Turchinovich A, Weiz L, Langheinz A et al (2011) Characterization of extracellular circulating microRNA. Nucleic Acids Res 39:7223–7233

Turchinovich A, Samatov TR, Tonevitsky AG et al (2013) Circulating miRNAs: cell-cell communication function? Front Genet 4:119

Tyagi S, Kramer FR (1996) Molecular beacons: probes that fluoresce upon hybridization. Nat Biotechnol 14:303–308

Tyagi S, Bratu DP, Kramer FR (1998) Multicolor molecular beacons for allele discrimination. Nat Biotechnol 16:49–53

Valadi H, Ekstrom K, Bossios A et al (2007) Exosome-mediated transfer of mRNAs and microRNAs is a novel mechanism of genetic exchange between cells. Nat Cell Biol 9:654–659

van Rooij E (2011) The art of microRNA research. Circ Res 108:219–234

van Rooij E, Purcell AL, Levin AA (2012) Developing microRNA therapeutics. Circ Res 110:496–507

Vet JA, Majithia AR, Marras SA et al (1999) Multiplex detection of four pathogenic retroviruses using molecular beacons. Proc Natl Acad Sci U S A 96:6394–6399

Vickers KC, Palmisano BT, Shoucri BM et al (2011) MicroRNAs are transported in plasma and delivered to recipient cells by high-density lipoproteins. Nat Cell Biol 13:423–433

Volinia S, Calin GA, Liu CG et al (2006) A microRNA expression signature of human solid tumors defines cancer gene targets. Proc Natl Acad Sci U S A 103:2257–2261

Wagner J, Riwanto M, Besler C et al (2013) Characterization of levels and cellular transfer of circulating lipoprotein-bound microRNAs. Arterioscler Thromb Vasc Biol 33:1392–1400

Wang K, Zhang S, Marzolf B et al (2009) Circulating microRNAs, potential biomarkers for drug-induced liver injury. Proc Natl Acad Sci U S A 106:4402–4407

Wang G, Tam LS, Li EK et al (2010a) Serum and urinary cell-free MiR-146a and MiR-155 in patients with systemic lupus erythematosus. J Rheumatol 37:2516–2522

Wang K, Zhang S, Weber J et al (2010b) Export of microRNAs and microRNA-protective protein by mammalian cells. Nucleic Acids Res 38:7248–7259

Wang K, Yuan Y, Cho JH et al (2012) Comparing the MicroRNA spectrum between serum and plasma. PLoS One 7:e41561

Weber JA, Baxter DH, Zhang S et al (2010) The microRNA spectrum in 12 body fluids. Clin Chem 56:1733–1741

Winter J, Jung S, Keller S et al (2009) Many roads to maturity: microRNA biogenesis pathways and their regulation. Nat Cell Biol 11:228–234

Yang WJ, Yang DD, Na S et al (2005) Dicer is required for embryonic angiogenesis during mouse development. J Biol Chem 280:9330–9335

Zernecke A, Bidzhekov K, Noels H et al (2009) Delivery of microRNA-126 by apoptotic bodies induces CXCL12-dependent vascular protection. Sci Signal 2:ra81

Zhao Y, Ransom JF, Li A et al (2007) Dysregulation of cardiogenesis, cardiac conduction, and cell cycle in mice lacking miRNA-1-2. Cell 129:303–317

Zhu H, Fan GC (2011) Extracellular/circulating microRNAs and their potential role in cardiovascular disease. Am J Cardiovasc Dis 1:138–149